



**HAL**  
open science

# Reliability of reinforced concrete structures : Case of slabs subjected to impact

Fidaa Kassem

► **To cite this version:**

Fidaa Kassem. Reliability of reinforced concrete structures : Case of slabs subjected to impact. Civil Engineering. INSA de Lyon, 2015. English. NNT : 2015ISAL0096 . tel-01339833

**HAL Id: tel-01339833**

**<https://theses.hal.science/tel-01339833>**

Submitted on 30 Jun 2016

**HAL** is a multi-disciplinary open access archive for the deposit and dissemination of scientific research documents, whether they are published or not. The documents may come from teaching and research institutions in France or abroad, or from public or private research centers.

L'archive ouverte pluridisciplinaire **HAL**, est destinée au dépôt et à la diffusion de documents scientifiques de niveau recherche, publiés ou non, émanant des établissements d'enseignement et de recherche français ou étrangers, des laboratoires publics ou privés.

Thèse

# Reliability of reinforced concrete structures: Case of slabs subjected to impact

Présentée devant  
L'Institut National des Sciences Appliquées de Lyon

Pour obtenir  
Le grade de docteur

Formation doctorale :  
Génie Civil  
École doctorale : Mécanique, Energétique, Génie Civil, Acoustique (MEGA)

Par  
**Fidaa KASSEM**  
(Ingénieur)

Soutenue le 04 Novembre 2015 devant la Commission d'examen

## Jury

---

Examineur	<b>Laurence CURTIL</b>	Professeur (Université Claude Bernard Lyon1)
Rapporteur	<b>Fabrice GATUINGT</b>	Professeur (CNRS) (Université Paris Saclay)
Rapporteur	<b>Abdellatif KHAMLICHI</b>	Professeur (Faculté des Sciences de Tétouan)
Examineur	<b>Elias BOU-SAID</b>	Ingénieur (R&D EGIS France, IOSIS Industries)
Co-directeur	<b>David BERTRAND</b>	MCF (INSA de Lyon)
Directeur	<b>Ali LIMAM</b>	Professeur (INSA de Lyon)

Laboratoire de Génie Civil et d'Ingénierie Environnementale (LGCIE)

*INSA Direction de la Recherche - Ecoles Doctorales – Quinquennal 2011-2015*

SIGLE	ECOLE DOCTORALE	NOM ET COORDONNEES DU RESPONSABLE
<b>CHIMIE</b>	<b>CHIMIE DE LYON</b> <a href="http://www.edchimie-lyon.fr">http://www.edchimie-lyon.fr</a> Sec : Renée EL MELHEM Bat Blaise Pascal 3 <sup>e</sup> etage 04 72 43 80 46 Insa : R. GOURDON <a href="mailto:secretariat@edchimie-lyon.fr">secretariat@edchimie-lyon.fr</a>	<b>M. Jean Marc LANCELIN</b> Université de Lyon – Collège Doctoral Bât ESCPE 43 bd du 11 novembre 1918 69622 VILLEURBANNE Cedex Tél : 04.72.43 13 95 <a href="mailto:directeur@edchimie-lyon.fr">directeur@edchimie-lyon.fr</a>
<b>E.E.A.</b>	<b>ELECTRONIQUE, ELECTROTECHNIQUE, AUTOMATIQUE</b> <a href="http://edeea.ec-lyon.fr">http://edeea.ec-lyon.fr</a> Sec : M.C. HAVGOUDOUKIAN <a href="mailto:Ecole-doctorale.eea@ec-lyon.fr">Ecole-doctorale.eea@ec-lyon.fr</a>	<b>M. Gérard SCORLETTI</b> Ecole Centrale de Lyon 36 avenue Guy de Collongue 69134 ECULLY Tél : 04.72.18 60.97 Fax : 04 78 43 37 17 <a href="mailto:Gerard.scorletti@ec-lyon.fr">Gerard.scorletti@ec-lyon.fr</a>
<b>E2M2</b>	<b>EVOLUTION, ECOSYSTEME, MICROBIOLOGIE, MODELISATION</b> <a href="http://e2m2.universite-lyon.fr">http://e2m2.universite-lyon.fr</a> Sec : Safia AIT CHALAL Bat Atrium- UCB Lyon 1 04.72.44.83.62 Insa : S. REVERCHON <a href="mailto:Safia.ait-chalal@univ-lyon1.fr">Safia.ait-chalal@univ-lyon1.fr</a>	<b>M. Fabrice CORDEY</b> Laboratoire de Géologie de Lyon Université Claude Bernard Lyon 1 Bât Géode – Bureau 225 43 bd du 11 novembre 1918 69622 VILLEURBANNE Cédex Tél : 04.72.44.83.74 <a href="mailto:Sylvie.reverchon-pescheux@insa-lyon.fr">Sylvie.reverchon-pescheux@insa-lyon.fr</a> <a href="mailto:fabrice.cordey@univ-lyon1.fr">fabrice.cordey@univ-lyon1.fr</a>
<b>EDISS</b>	<b>INTERDISCIPLINAIRE SCIENCES-SANTÉ</b> <a href="http://www.ediss-lyon.fr">http://www.ediss-lyon.fr</a> Sec : Safia AIT CHALAL Bat Atrium – UCB Lyon 1 04 72 44 83 62 Insa : <a href="mailto:Safia.ait-chalal@univ-lyon1.fr">Safia.ait-chalal@univ-lyon1.fr</a>	<b>Mme Emmanuelle CANET-SOULAS</b> INSERM U1060, CarMeN lab, Univ. Lyon 1 Bâtiment IMBL 11 avenue Jean Capelle INSA de Lyon 696621 Villeurbanne Tél : 04.72.11.90.13 <a href="mailto:Emmanuelle.canet@univ-lyon1.fr">Emmanuelle.canet@univ-lyon1.fr</a>
<b>INFOMATHS</b>	<b>INFORMATIQUE ET MATHÉMATIQUES</b> <a href="http://infomaths.univ-lyon1.fr">http://infomaths.univ-lyon1.fr</a> Sec : Renée EL MELHEM Bat Blaise Pascal 3 <sup>e</sup> etage <a href="mailto:infomaths@univ-lyon1.fr">infomaths@univ-lyon1.fr</a>	<b>Mme Sylvie CALABRETTO</b> LIRIS – INSA de Lyon Bat Blaise Pascal 7 avenue Jean Capelle 69622 VILLEURBANNE Cedex Tél : 04.72. 43. 80. 46 Fax 04 72 43 16 87 <a href="mailto:Sylvie.calabretto@insa-lyon.fr">Sylvie.calabretto@insa-lyon.fr</a>
<b>Matériaux</b>	<b>MATERIAUX DE LYON</b> <a href="http://ed34.universite-lyon.fr">http://ed34.universite-lyon.fr</a> Sec : M. LABOUNE PM : 71.70 –Fax : 87.12 Bat. Direction 1 <sup>er</sup> et. <a href="mailto:Ed.materiaux@insa-lyon.fr">Ed.materiaux@insa-lyon.fr</a>	<b>M. Jean-Yves BUFFIERE</b> INSA de Lyon MATEIS Bâtiment Saint Exupéry 7 avenue Jean Capelle 69621 VILLEURBANNE Cedex Tél : 04.72.43 71.70 Fax 04 72 43 85 28 <a href="mailto:Ed.materiaux@insa-lyon.fr">Ed.materiaux@insa-lyon.fr</a>
<b>MEGA</b>	<b>MECANIQUE, ENERGETIQUE, GENIE CIVIL, ACOUSTIQUE</b> <a href="http://mega.universite-lyon.fr">http://mega.universite-lyon.fr</a> Sec : M. LABOUNE PM : 71.70 –Fax : 87.12 Bat. Direction 1 <sup>er</sup> et. <a href="mailto:mega@insa-lyon.fr">mega@insa-lyon.fr</a>	<b>M. Philippe BOISSE</b> INSA de Lyon Laboratoire LAMCOS Bâtiment Jacquard 25 bis avenue Jean Capelle 69621 VILLEURBANNE Cedex Tél : 04.72 .43.71.70 Fax : 04 72 43 72 37 <a href="mailto:Philippe.boisse@insa-lyon.fr">Philippe.boisse@insa-lyon.fr</a>
<b>ScSo</b>	<b>ScSo*</b> <a href="http://recherche.univ-lyon2.fr/scso/">http://recherche.univ-lyon2.fr/scso/</a> Sec : Viviane POLSINELLI Brigitte DUBOIS Insa : J.Y. TOUSSAINT <a href="mailto:viviane.polsinelli@univ-lyon2.fr">viviane.polsinelli@univ-lyon2.fr</a>	<b>Mme Isabelle VON BUELTZINGLOEWEN</b> Université Lyon 2 86 rue Pasteur 69365 LYON Cedex 07 Tél : 04.78.77.23.86 Fax : 04.37.28.04.48 <a href="mailto:isavonb@dbmail.com">isavonb@dbmail.com</a>

\*ScSo : Histoire, Géographie, Aménagement, Urbanisme, Archéologie, Science politique, Sociologie, Anthropologie

# Dedication

To all my beloved ones

# Abstract

Reinforced concrete (RC) structures are subjected to several sources of uncertainties that highly affect their response. These uncertainties are related to the structure geometry, material properties and the loads applied. The lack of knowledge on the potential load, as well as the uncertainties related to the structure features shows that the design of RC structures could be made in a reliability framework. This latter allows propagating uncertainties in the deterministic analysis. However, in order to compute failure probability according to one or several failure criteria mechanical and stochastic models have to be coupled, which can be very time consuming and in some cases impossible. Indeed, either the complexity of the deterministic model considered implies important computing time (from minutes to hours) or reliability methods evaluating failure probability require a too large number of simulations of the deterministic model.

The platform OpenTURNS is used to perform the reliability analysis of three different structures considered in the present study and propagate uncertainties in their physical models. OpenTURNS can be linked to any external software using the generic wrapper. Therefore, OpenTURNS is coupled to CASTEM to study the reliability of a RC multifiber cantilever beam subjected to a concentrated load at the free end, to Abaqus to study the reliability of RC slabs which are subjected to accidental impacts, and to ASTER to study the reliability of a prestressed concrete containment building.

Among structures considered in this study, only the physical problem of reinforced concrete (RC) slabs subjected to impact is investigated in detail. The design of such type of structures is generally carried out under static or pseudo-static loading. In the case of dynamic loads such as impacts, the force applied on the structural member is often assessed from energetic approaches and then, for the sake of simplicity, an equivalent pseudo-static loading is considered for its design. However, in some particular cases, the dynamic response of the structure cannot be simplified to a quasi-static response. The transient dynamic analysis has to be performed accounting for the main physical processes involved. Thus accurate models are needed to describe and to predict the capacity of the RC member and in particular the impact force.

This study focuses on RC slabs impacted by adropped object impact during handling operations within nuclear plant buildings. When a dropped object impacts a RC slab, damage can arise at the impact zone depending on the impact energy and the relative masses of the colliding bodies. An optimal design requires taking into account the potential development of nonlinearities due to the material damage (concrete cracking, steel yielding, etc.).

The aim of this study is to address the issue of reliability computational effort. Two strategies are proposed for the application of impacted RC slabs. The first one consists in using deterministic analytical models which predict accurately the response of the slab. In general, the analytical model assumptions are constraining and only few slab configurations can be studied. The objective is to reduce the computational cost to the minimum and to explore as far as possible how to use these types of analytical models. In the opposite case, when finite element models are needed, the second strategy consists in reducing the number of simulations needed to assess failure probability or substituting the finite element model by a meta-model less expensive in computational time.

The first part of this study describes the behavior of reinforced concrete slabs subjected to impact and determines the failure modes of slabs according to their characteristics and impact conditions. In

this study only low velocities are considered. Then two deterministic models are used and evaluated: a 3D finite element model simulated with the commercial code “Abaqus/Explicit” and an analytical mass-spring model. For the simulation based on finite element method (FEM), the RC slab and the impactor are fully modeled. The steel is modeled as an elasto-plastic material with hardening and, the concrete behavior is described by the damaged plasticity model. The model is validated with experiments carried out on several RC slabs under drop-weight loads at Heriot-Watt University by Chen and May [34]. As an alternative modeling, a simplified analytical model of the slab is used. The model consists in a two degrees of freedom mass-spring system which accounts for potential viscous damping. The first (resp. the second) spring represents the stiffness of the slab (resp. the contact). A frequency decrease approach is used to describe the degradation of RC slabs stiffness. The natural frequency of the slab is updated as a function of the maximal displacement reached during the loading.

Next, a reliability analysis of reinforced concrete slabs under low velocity impact is performed. Firstly, the choice of random variable inputs and their distributions, failure criteria and probabilistic methods are discussed. In the case where the nonlinear behavior of materials is considered in the model, the failure criterion is defined according to the maximum displacement of the slab at the impact point. Finally, the probabilistic method dedicated to assess failure probability is chosen. This latter has to be adapted in order to reduce the computational cost and keeping a good accuracy. The Monte Carlo and importance sampling methods are coupled with the mass-spring model, while FORM is used with the finite element model.

The two strategies used to reduce the computational cost of a reliability analysis are compared in order to verify their efficiency to calculate the probability of failure. Finally, a parametric study is performed to identify the influence of deterministic model parameters on the calculation of failure probability (dimensions of slabs, impact velocity and mass, boundary conditions, impact point, reinforcement density). This study helps to locate the most critical impact points for the slab design, and illustrate how to optimize the design of reinforced concrete slabs under impact in terms of material choice, concrete properties and ratio of reinforcement.

**Keywords:** RC structures, RC slabs, impact at low velocity, dynamic, material nonlinear behaviors, deterministic approaches, reliability approaches, failure probability.

# Résumé

Dans le domaine du génie civil, le dimensionnement des structures en béton armé est essentiellement basé sur des démarches déterministes. Cependant, les informations fournies par des analyses déterministes sont insuffisantes pour étudier la variabilité de la réponse de la dalle. En outre, la réponse des structures en béton armé sont fortement influencés par de nombreuses sources d'incertitudes. Le manque de connaissance des charges appliquées ainsi que les incertitudes liées à la géométrie de la dalle et les caractéristiques des matériaux nécessitent donc l'utilisation d'une approche fiabiliste qui permet la propagation de ces incertitudes dans les analyses déterministes. De nombreuses méthodes basées sur la théorie des probabilités ont été développées, elles permettent d'une part de calculer la probabilité de défaillance des structures et, d'autre part, d'étudier l'influence de la variabilité des variables de conception sur le comportement de la structure étudiée. L'approche fiabiliste est basée sur le principe de couplage mécano-fiabiliste qui consiste à coupler un modèle stochastique, contenant les caractéristiques probabilistes des variables aléatoires d'entrée, et un modèle déterministe, permettant d'obtenir une estimation quantitative des variables de sortie ainsi que d'évaluer les fonctions de performance qui décrivent les états défaillants de la structure étudiée. Cependant un couplage mécano-fiabiliste peut être très exigeant en temps de calcul, soit à cause des modèles déterministes dont un seul lancement peut être de l'ordre de quelques minutes à quelques heures en fonction de son degré de complexité, soit à cause des méthodes d'évaluation de la probabilité de défaillance qui exigent parfois un nombre d'appels très important au modèle déterministe.

Dans cette étude, il est proposé de s'appuyer sur la plateforme généraliste de traitements des incertitudes OpenTURNS, développé par EDF R&D, EADS et la société PHIMECA pour effectuer les analyses fiabilistes. Cette plateforme open source, permet de nombreuses méthodes de traitement des incertitudes, Monte Carlo, Cumul Quadratique, méthodes de fiabilité FORM/SORM, tirage d'importance, ..., qui méritent d'être testées dans le cadre d'applications du génie civil. Cette plateforme possède une interface qui facilite le couplage avec n'importe quel logiciel externe. Dans le cadre de cette thèse, la méthodologie propre aux problématiques des ouvrages du génie civil est développée et validée tout d'abord sur un cas simple de structures en béton armé. Le cas d'une poutre encastrée en béton armée est proposé. Le système est modélisé sous CASTEM par une approche aux éléments finis de type multifibre. Puis la fiabilité d'une dalle en béton armé impactée par une masse rigide à faible vitesse est étudiée en couplant OpenTURNS à Abaqus. Enfin, une enceinte de confinement en béton précontrainte modélisée sous ASTER est étudiée d'un point de vue probabiliste.

Parmi les structures considérées dans cette étude, seul le problème physique des dalles en béton armé soumises à impact est examiné en détail. Le problème d'impact fait partie des problèmes dynamiques nonlinéaires les plus difficiles parce qu'il pose le problème du contact accompagné par une variation temporelle des vitesses. Le comportement d'une dalle en béton armé soumise à impact est très complexe. Sa réponse peut s'exprimer en deux termes: la réponse globale et la réponse locale. Le cas où l'impacteur a une vitesse initiale importante, la dalle a une réponse locale caractérisée par un endommagement qui se localise près de la zone d'impact où la pénétration, la perforation et l'écaillage ont lieu. Avec une vitesse initiale faible, la réponse globale se caractérise par la fissuration progressive des faces comprimée et tendue, l'endommagement est lié à une réponse en mode de

cisaillement ou en flexion. La conception de ce type de structures est généralement effectuée sous des charges statiques ou pseudo-statiques. Dans le cas de charges dynamiques tels que les impacts, la force appliquée à la structure est souvent évaluée à partir des approches énergétiques et une charge statique équivalente est considérée dans sa conception pour simplifier le problème. Cependant dans certains cas spécifiques, la réponse dynamique de la structure ne peut pas être simplifiée à une réponse quasi-statique. Une analyse dynamique doit être effectuée en tenant compte des principaux phénomènes physiques impliqués. Ainsi des modèles précis sont nécessaires pour décrire et prédire la performance d'une structure en béton armé, notamment lorsqu'elle est soumise à une force d'impact.

Cette étude porte sur des dalles en béton armé qui peuvent être soumises à une chute de colis dans les centrales nucléaires, ce qui peut conduire à un endommagement dans la zone d'impact. Lorsqu'une dalle en béton armé est soumise à un impact, l'endommagement peut se localiser à la zone d'impact et varie en fonction de l'énergie cinétique d'impact et des masses relatives des corps entrant en collision. Dans ce cas, un dimensionnement optimal nécessite la prise en compte de la charge d'impact lors de la conception, ainsi que le développement des nonlinéarités dues aux comportements des matériaux (fissurations du béton, plastification des aciers, etc.). L'objectif de cette étude est de proposer des solutions pour diminuer le temps de calcul d'une analyse fiable en utilisant deux stratégies dans le cas des dalles impactées. La première stratégie consiste à utiliser des modèles analytiques qui permettent de prédire avec précision la réponse mécanique de la dalle et qui sont moins coûteux en temps de calcul. L'idée directrice est de créer des modèles économiques en temps de calcul permettant de tester facilement plusieurs configurations de dalle. La deuxième stratégie consiste à réduire le nombre d'appels au modèle déterministe, surtout dans le cas des modèles par éléments finis, en utilisant des méthodes probabilistes d'approximation ou des méthodes qui permettent de substituer le modèle par éléments finis par un modèle approximé qu'on appelle méta-modèle.

La première partie de cette étude présente le comportement des dalles en béton armé lorsqu'elles sont soumises à impact et détermine les modes de rupture des dalles en fonction de leurs caractéristiques et des conditions d'impact. Ensuite deux modèles déterministes sont utilisés et évalués afin d'étudier les phénomènes dynamiques appliqués aux dalles en béton armé sous impact: un modèle par éléments finis en 3D modélisé sous Abaqus qui permet une grande souplesse en terme de modélisation et un modèle simplifié de type masse-ressort amorti à deux degrés de liberté qui permet de prendre en compte les principaux phénomènes physiques impliqués. Pour le modèle par éléments finis, la dalle avec son ferrailage ainsi que l'impacteur sont entièrement modélisés. L'acier est modélisé à l'aide d'une loi de comportement élasto-plastique avec écrouissage, alors que le comportement du béton est décrit par le modèle élasto-plastique endommageable (concrete damage plasticity) qui est intégré dans Abaqus. La complexité du modèle par éléments finis se situe au niveau des nonlinéarités liées d'une part à la gestion du contact et d'autre part aux comportements des matériaux, ce qui entraîne une augmentation forte en terme du temps de calcul. Ce modèle est validé avec des essais expérimentaux réalisés à l'université Heriot-Watt par Chen et May sur plusieurs dalles en béton armé soumises à une chute d'une masse rigide [34]. Une alternative intéressante est proposée dans cette étude en considérant un modèle simplifié basé sur la modélisation de la structure réelle par un système masse-ressort amorti à deux degrés de liberté. Ce modèle simplifié prend en compte les nonlinéarités du béton armé par une approche de « chute en fréquence » (i.e. la rigidité structurelle). Ce système décrit l'interaction entre la dalle et l'impacteur dont leurs masses interagissent par l'intermédiaire de deux ressorts et prend en compte l'amortissement visqueux lors de la résolution par l'intermédiaire de deux amortisseurs en parallèle avec les ressorts.

L'étape suivante consiste à étudier la fiabilité des dalles en béton armé soumises à l'impact d'une masse à faible vitesse en évaluant la probabilité de défaillance. Le calcul de cette probabilité s'appuie tout d'abord sur le choix des variables d'entrée, des critères de défaillance ainsi que des méthodes probabilistes à coupler avec les modèles déterministes. Les variables d'entrée sont modélisées en tant que des variables aléatoires dont il faut définir leurs lois de distributions. Le choix des critères de

défaillance est aussi essentiel dans une étude fiabiliste, un seul critère de défaillance est étudié dans le cas où le comportement nonlinéaire des matériaux est considéré dans le modèle. Le critère est lié au déplacement maximal que peut subir la dalle au point d'impact. Le seuil de déplacement est choisi de façon à ne pas avoir de plastification dans les armatures ou au moment de l'apparition des fissures dans le béton. La dernière étape à considérer dans une étude fiabiliste nécessite à bien choisir la méthode probabiliste à utiliser pour calculer la probabilité de défaillance, elle doit être adaptée au type du modèle déterministe et pour des temps de calcul optimisés. Dans cette étude, nous avons couplé les méthodes Monte Carlo et simulation d'importance avec le modèle de type masse-ressort. FORM est utilisée avec le modèle par éléments finis, ce qui permet un nombre d'appels réduit au modèle par éléments finis.

Les deux stratégies utilisées pour réduire le temps de calcul d'une étude fiabiliste sont comparées afin de vérifier l'efficacité de chacune pour calculer la probabilité de défaillance. Enfin, une étude paramétrique est réalisée afin d'étudier l'effet des paramètres d'entrées des modèles déterministes sur le calcul de la probabilité de défaillance. Nous avons choisi dans cette étude de considérer les paramètres liés aux dimensions de la dalle, la vitesse d'impact, les conditions aux limites de la dalle, la position du point d'impact et le taux de ferrailage. Cette étude permet de localiser les points d'impact les plus défavorables pour la réponse de la structure, et d'illustrer les moyens d'optimiser le dimensionnement des dalles en béton armé sous impact en termes de choix des matériaux, caractéristiques du béton et pourcentage d'armatures.

**Mots-clés:** Structures en béton armé, dalles en béton armé, impact à faible vitesse, dynamique, comportement nonlinéaire des matériaux, approches déterministes, approches fiabilistes, probabilité de défaillance.

# Contents

<b>Dedication</b>	<b>ii</b>
<b>Contents</b>	<b>viii</b>
<b>Nomenclature</b>	<b>xiii</b>
<b>List of Figures</b>	<b>xvi</b>
<b>List of Tables</b>	<b>xxii</b>
<b>1 Introduction</b>	<b>1</b>
1.1 Background . . . . .	1
1.2 Research motivation . . . . .	2
1.3 Study scope and objectives . . . . .	3
1.4 Thesis contents . . . . .	6
<b>2 Reinforced concrete slabs behavior under impact: Dynamic response and literature review</b>	<b>8</b>
2.1 Introduction . . . . .	8
2.2 Reinforced concrete slabs behavior under impact . . . . .	10
2.2.1 Impact dynamics . . . . .	10
2.2.2 Types of impact . . . . .	12
2.2.3 Failure modes . . . . .	16
2.2.4 Energy considerations . . . . .	18
2.3 Methods to determine the response of RC slabs under impact . . . . .	20
2.3.1 Experimental approaches . . . . .	20
2.3.1.1 Zineddin and Krauthammer tests . . . . .	20
2.3.1.2 Chen and May tests . . . . .	23
2.3.1.3 Hrynyk tests . . . . .	25
2.3.2 Analytical approaches . . . . .	28
2.3.2.1 Tonello model . . . . .	29
2.3.2.2 CEB model . . . . .	29
2.3.2.3 Abrate model . . . . .	29
2.3.2.4 Delhomme <i>et al.</i> model . . . . .	31
2.3.2.5 Yigit and Christoforou model . . . . .	31
2.3.3 Finite element approaches . . . . .	32
2.3.3.1 Berthet-Rambaud <i>et al.</i> model . . . . .	33
2.3.3.2 Mokhatar and Abdullah model . . . . .	35
2.3.3.3 Trivedi and Singh model . . . . .	35
2.4 Mechanical behavior of concrete . . . . .	38

2.4.1	Uniaxial compression . . . . .	39
2.4.2	Uniaxial tension . . . . .	43
2.4.2.1	Uniaxial tensile stress-strain curve . . . . .	43
2.4.2.2	Uniaxial stress-crack opening curve . . . . .	46
2.5	Mechanical behavior of steel . . . . .	48
2.5.1	Uniaxial tension . . . . .	48
2.5.2	Idealizations . . . . .	49
2.5.3	Steel-concrete bond . . . . .	50
2.6	Conclusion . . . . .	51
<b>3</b>	<b>Deterministic analysis: Software and steps</b>	<b>53</b>
3.1	Introduction . . . . .	53
3.2	Finite element analysis . . . . .	53
3.3	Choice of commercial FE software . . . . .	54
3.4	Components of an Abaqus analysis model . . . . .	55
3.5	Configuring analysis . . . . .	57
3.6	Material properties . . . . .	58
3.6.1	Concrete constitutive model . . . . .	58
3.6.2	Concrete damage plasticity model (CDP) . . . . .	59
3.6.2.1	Plastic flow and yield surface . . . . .	60
3.6.2.2	Stress-strain curve for uniaxial compression . . . . .	61
3.6.2.3	Stress-strain curve for uniaxial tension . . . . .	62
3.6.2.4	Damages . . . . .	63
3.6.3	Constitutive model of reinforcing steel . . . . .	65
3.7	Finite elements . . . . .	65
3.8	Contact modeling between slab and impactor . . . . .	66
3.9	Constraints . . . . .	67
3.9.1	Approaches to represent steel in RC numerical analysis . . . . .	67
3.9.2	Tie constraint . . . . .	69
3.10	Output . . . . .	70
<b>4</b>	<b>Reliability analysis: principles and methods</b>	<b>71</b>
4.1	Introduction to reliability . . . . .	71
4.2	Principles of structural reliability analysis . . . . .	72
4.3	Uncertainty sources . . . . .	73
4.3.1	Physical uncertainties . . . . .	73
4.3.2	Measurement uncertainties . . . . .	74
4.3.3	Statistical uncertainties . . . . .	74
4.3.4	Model uncertainties . . . . .	74
4.3.5	Other uncertainties . . . . .	74
4.4	Reliability approach . . . . .	74
4.4.1	Modeling of uncertainty . . . . .	75
4.4.1.1	Joint probability density function . . . . .	77
4.4.1.2	Covariance and correlation . . . . .	77
4.4.2	Variable of interest . . . . .	78
4.4.2.1	Dispersion analysis . . . . .	79
4.4.2.2	Distribution analysis . . . . .	79
4.4.3	Probability of failure . . . . .	80
4.4.3.1	Limit states . . . . .	81
4.4.3.2	Approximation methods . . . . .	81

4.4.3.3	Simulation methods . . . . .	84
4.4.3.4	Response surface methods . . . . .	88
4.4.3.5	Comparison of methods according to some reviews in the literature	89
4.5	Sensitivity analysis . . . . .	90
4.6	Statistical descriptions of random variables . . . . .	91
4.6.1	Concrete properties . . . . .	91
4.6.1.1	Compressive strength of concrete . . . . .	91
4.6.1.2	Tensile strength of concrete . . . . .	93
4.6.1.3	Young's Modulus . . . . .	94
4.6.2	Steel properties . . . . .	95
4.6.2.1	Yield strength of steel . . . . .	95
4.6.2.2	Modulus of elasticity . . . . .	97
4.6.3	Dimensions . . . . .	97
4.7	Conclusion . . . . .	98
<b>5</b>	<b>Deterministic models of RC slab</b>	<b>100</b>
5.1	Introduction . . . . .	100
5.2	FEM of Chen and May slabs . . . . .	101
5.2.1	Creating model . . . . .	101
5.2.2	Creating parts . . . . .	101
5.2.2.1	Part of slab . . . . .	101
5.2.2.2	Part of reinforcement . . . . .	102
5.2.2.3	Part of impactor . . . . .	103
5.2.2.4	Part of support . . . . .	103
5.2.3	Creating materials . . . . .	104
5.2.3.1	Identification of constitutive parameters for CDP model . . . . .	105
5.2.3.2	Identification of parameters for reinforcing steel stress-strain curve .	107
5.2.4	Defining and assigning section properties . . . . .	108
5.2.5	Defining the assembly . . . . .	108
5.2.6	Meshing the model . . . . .	109
5.2.6.1	Slab . . . . .	110
5.2.6.2	Impactor . . . . .	115
5.2.7	Configuring analysis . . . . .	115
5.2.8	Applying loads, boundary and initial conditions to the model . . . . .	116
5.2.9	Creating interaction and constraints . . . . .	116
5.2.10	Output requests . . . . .	118
5.2.11	Creating an analysis job . . . . .	118
5.3	Discussion of results of Chen and May slabs FEM . . . . .	118
5.3.1	Comparison of mesh types . . . . .	118
5.3.2	Comparison of contact algorithms . . . . .	119
5.3.3	Mesh sensitivity . . . . .	120
5.3.4	Choice of materials behavior . . . . .	122
5.3.5	Validation of model for other slabs . . . . .	122
5.4	Deterministic models of the slab in nuclear plant . . . . .	129
5.4.1	Finite element model (FEM) . . . . .	129
5.4.2	Mass-spring models (MSM) . . . . .	133
5.4.2.1	Mass-spring model without damping . . . . .	134
5.4.2.2	Mass-spring model with damping . . . . .	134
5.4.2.3	Identification of MSM parameters . . . . .	135
5.5	Discussion of results of deterministic models of the slab in nuclear plant . . . . .	138

5.5.1	Comparison of FEM and MSM results . . . . .	138
<b>6</b>	<b>Structural reliability: application to RC structures</b>	<b>142</b>
6.1	Introduction . . . . .	142
6.2	Application to RC beams . . . . .	143
6.2.1	Deterministic model . . . . .	143
6.2.2	Probabilistic model . . . . .	143
6.2.3	Failure criteria . . . . .	145
6.2.4	Discussion of results of beam reliability . . . . .	146
6.2.4.1	Sensitivity analysis . . . . .	146
6.2.4.2	Distribution analysis . . . . .	148
6.2.4.3	Comparison of probabilistic methods . . . . .	149
6.2.4.4	Metamodeling . . . . .	162
6.2.4.5	Conclusion remarks . . . . .	164
6.3	Application to RC slab subjected to impact - Elastic behavior . . . . .	165
6.3.1	Deterministic models . . . . .	165
6.3.1.1	Finite element model . . . . .	165
6.3.1.2	Model based on plate theory (PT) . . . . .	166
6.3.1.3	Mass-spring model . . . . .	167
6.3.2	Probabilistic model . . . . .	167
6.3.3	Failure criteria . . . . .	167
6.3.4	Discussion of results of slab reliability (elastic behavior) . . . . .	169
6.3.4.1	Comparison of deterministic models . . . . .	169
6.3.4.2	Comparison of probabilistic methods . . . . .	170
6.3.4.3	Comparison of failure criteria . . . . .	171
6.3.4.4	Parametric study . . . . .	171
6.3.5	Conclusion remarks . . . . .	176
6.4	Application to RC slab subjected to impact - Nonlinear behavior . . . . .	176
6.4.1	Deterministic models . . . . .	176
6.4.2	Probabilistic model . . . . .	176
6.4.2.1	Concrete properties . . . . .	177
6.4.2.2	Steel properties . . . . .	177
6.4.2.3	Dimensions . . . . .	178
6.4.3	Failure criterion . . . . .	178
6.4.4	Discussion of results of slab reliability (Nonlinear behavior) . . . . .	179
6.4.4.1	Comparison of strategies . . . . .	179
6.4.4.2	Parametric study . . . . .	179
6.4.5	Conclusion remarks . . . . .	187
6.5	Application to containment building of nuclear power plant . . . . .	187
6.5.1	Deterministic model . . . . .	189
6.5.1.1	FE software . . . . .	190
6.5.1.2	Material properties and behaviors . . . . .	191
6.5.1.3	Boundary conditions and loading . . . . .	191
6.5.1.4	Mesh . . . . .	192
6.5.1.5	Delayed strains in concrete . . . . .	192
6.5.2	Probabilistic model . . . . .	193
6.5.3	Failure criteria . . . . .	194
6.5.4	Discussion of results of containment building reliability . . . . .	195
6.5.4.1	Deterministic output variable . . . . .	195
6.5.4.2	Dispersion analysis . . . . .	195

6.5.4.3	Distribution analysis . . . . .	196
6.5.4.4	Failure probability . . . . .	198
6.5.4.5	Sensitivity analysis . . . . .	201
6.5.4.6	Convergence? . . . . .	202
6.5.4.7	Conclusion remarks . . . . .	203
<b>7</b>	<b>Conclusions and perspectives</b>	<b>205</b>
7.1	Conclusions . . . . .	205
7.2	Perspectives . . . . .	206
	<b>Bibliography</b>	<b>208</b>
<b>A</b>	<b>Probability distributions in OpenTRUNS 13.2</b>	<b>219</b>
<b>B</b>	<b>MSM results - comparison with FEM results</b>	<b>223</b>
B.1	Impact kinetic energy . . . . .	223
B.2	Impactor velocity . . . . .	230
B.3	Impactor mass . . . . .	237
B.4	Steel diameter . . . . .	244
B.5	Concrete density . . . . .	252
B.6	Slab thickness . . . . .	261

# Nomenclature

$\bar{\sigma}_c$	Effective stress of concrete in compression
$\bar{\sigma}_{max}$	Maximum principal effective stress
$\bar{\sigma}_t$	Effective stress of concrete in tension
$\bar{S}_i$	Mechanical elasticity of variable $X_i$
$\beta$	Reliability index of Hasofer-Lind
$\epsilon$	Flow potential eccentricity in the CDP model
$\mathbf{X}$	Random vector of input variables
$\mu_X$	Mean of a random variable
$\psi$	Dilation angle of concrete in the CDP model
$\rho_{X_1 X_2}$	Correlation coefficient of two random variables $X_1$ and $X_2$
$\sigma_c$	Concrete compressive stress
$\sigma_s$	Steel stress
$\sigma_t$	Concrete tensile stress
$\sigma_X$	Standard deviation of a random variable
$\epsilon_{c1}$	Compressive strain of concrete at the compressive strength $f_c$
$\epsilon_{ce}$	Compressive elastic strain of concrete corresponding to the end of linear elastic phase
$\epsilon_{cr}$	Tensile strain of concrete at the tensile strength $f_t$
$\epsilon_{cu}$	Ultimate strain of concrete in compression
$\epsilon_c$	Concrete compressive strain corresponding to the stress $\sigma_c$
$\epsilon_c^{in}$	Crushing (inelastic) strain of concrete
$\epsilon_c^{pl}$	Plastic strain of concrete in compression
$\epsilon_{sh}$	Strain of steel at which strain hardening initiates
$\epsilon_s$	Steel strain corresponding to the stress $\sigma_s$

$\varepsilon_{te}$	Tensile elastic strain of concrete corresponding to the end of linear elastic phase
$\varepsilon_t$	Concrete tensile strain corresponding to the stress $\sigma_t$
$\varepsilon_t^{ck}$	Cracking strain of concrete
$\varepsilon_t^{pl}$	Plastic strain of concrete in tension
$\varepsilon_u$	Ultimate strain of steel
$\varepsilon_y$	Yield strain of steel at the yield strength $f_y$
$\zeta_i$	Omission factor of variable $X_i$
$c_c$	Impedance that accounts for the contact viscosity in mass-spring models
$c_s$	Impedance that accounts for the slab viscosity in mass-spring models
$COV(X), COV$	Coefficient of variation of a random variable
$COV(X_1, X_2)$	Covariance of two random variables $X_1$ and $X_2$
$d_c$	Damage of concrete in compression
$d_{impact}$	Dimension of impact zone square
$d_t$	Damage of concrete in tension
$e$	RC slab thickness
$E_c$	Young's modulus of concrete
$E_{s1}$	Deformation modulus of steel at the hardening phase
$E_s$	Elastic modulus of steel
$F_X(x)$	Cumulative distribution function of a random variable
$f_X(x)$	Probability density function of a random variable
$f_{\mathbf{X}}(x)$	Joint probability density function of random variables
$f_b$	Biaxial compressive strength of concrete
$f_{ck}$	Characteristic value of concrete
$f_{cu}$	Compressive stress of concrete corresponding to the ultimate strain
$f_c$	Uniaxial compressive strength of concrete
$f_t$	Uniaxial tensile strength of concrete
$f_u$	Ultimate stress of steel corresponding to the ultimate strain
$f_y$	Yield strength of steel
$g(\mathbf{X})$	Limit state function
$G_f$	Fracture energy of concrete

$K_c$	Ratio of the second invariant on the tensile meridian to that on the compressive meridian at any given value of the pressure invariant (parameter of CDP model)
$k_c$	Contact stiffness in mass-spring models
$k_s$	Slab stiffness in mass-spring models
$m_i$	Impactor mass in mass-spring models
$m_s$	Slab mass in mass-spring models
$N$	Number of generated samples or simulations of the random vector $\mathbf{X}$
$ne$	Number of elements in slab thickness direction
$P_f$	Failure probability
$SizeElImpactZoneMax$	Maximum finite element size of slab in the impact zone
$SizeElImpactZoneMin$	Minimum finite element size of slab in the impact zone
$SizeElReinf$	Finite elements size of reinforcement
$SizeElSlab$	Finite elements size of slab edges
$Var_X$	Variance of a random variable
$X$	A random variable
$x$	Particular realization of a random variable or a random vector
$x_{impact}$	Coordinate of impact point in x-direction
$Y$	Variable of interest
$y_{impact}$	Coordinate of impact point in y-direction

# List of Figures

2.1	Some accidental impact loading cases in civil engineering field: a) Rockfall on protection galleries, b) Aircraft impact on nuclear containments, c) Dropped objects impact during handling operations . . . . .	9
2.2	Accidental dropped object impact during handling operations within nuclear plant buildings	10
2.3	Response types during impact on plates according to [149] . . . . .	11
2.4	Structure and impactor deformations according to the impact type [45] : a) Initial conditions ( $t=0$ ), b) Hard impact ( $t>0$ ), c) Soft impact ( $t>0$ ) . . . . .	13
2.5	Mass-spring model proposed by Eibl [55] to simulate an impact [45] . . . . .	14
2.6	Classification of low velocity impacts according to Koechlin and Potapov [95] . . . . .	15
2.7	Overall response failure modes of impacted RC slabs [119] : a) Flexural failure, b) Punching shear failure . . . . .	17
2.8	Local damage failure modes of impacted RC slabs [119] : a) Surface failure, b) spalling, c) scabbing, d) perforation . . . . .	18
2.9	Energy transformation process during an impact event [130] . . . . .	19
2.10	Impact test system used by Zineddin and Krauthammer [189] . . . . .	21
2.11	Load-time history for slabs impacted with a drop height of 152 mm [189] . . . . .	22
2.12	Failure mode of slabs impacted with a drop height of 610 mm and reinforced with reinforcement type: (a) Reinf. 3, (b) Reinf. 1, (c) Reinf. 1-Failure of one steel bar [189] . . .	22
2.13	Cracks patterns on top surface of slabs reinforced with reinforcement type Reinf. 3 and impacted with a drop height of : (a) 305 mm, (b) 610 mm[189] . . . . .	23
2.14	Details of slabs (dimensions in mm): a) 760 mm square slabs, b) 2320 mm square slabs, c) Boundary conditions [34] . . . . .	24
2.15	Details of impactors (dimensions in mm): a) Hemispherical impactor, b) Cylindrical impactor [34] . . . . .	24
2.16	Transient impact load of slabs 2-6 [34] . . . . .	25
2.17	Local damage of slabs bottom faces after impact: (a) Slab 2, (b) Slab 3, (c) Slab 4, (d) Slab 5, (e) Slab 6 [34] . . . . .	26
2.18	Details of slabs (dimensions in mm): a) Slab with additional links at the impact region, b) Boundary conditions [84] . . . . .	27
2.19	Cracking patterns on the bottom surface of a slab with a longitudinal reinforcement ratio of 0.42%: a) Impact #1, b) Impact #2, c) Impact #3 [84] . . . . .	27
2.20	Final cracking patterns on the bottom surface of slabs with a longitudinal reinforcement ratio of: a) 0.273%, b) 0.42%, c) 0.592% [84] . . . . .	28
2.21	One degree of freedom mass-spring model used in Tonello IC design office [174] . . . . .	29
2.22	Simplified model of CEB for a hard impact [29] . . . . .	30
2.23	Nonlinear force-displacement relationship for spring: (a) $R_1$ , (b) $R_2$ [29] . . . . .	30
2.24	Mass-spring models of impact on composite structures according to [10] . . . . .	31
2.25	The two “mass-spring-damper” models used by [47] to analyze SDR response: (a) “contact: model, (b) “post-impact” model . . . . .	32

2.26	Models for low velocity impact response in structures according to [184]	32
2.27	3D FE model of SDR protection galleries proposed by Berthet-Rambaud <i>et al.</i> [19]	33
2.28	Damage distribution in and around the repaired zone [19]	34
2.29	Comparison of numerical and experimental results: (a) Calibration on friction parameter, (b) Vertical displacement at a point near the impact zone [19]	34
2.30	Details of finite element model of Mokhatar and Abdullah [137]	35
2.31	Comparison of numerical and experimental transient impact force with different: (a) Mesh densities, (b) Constitutive concrete models [137]	36
2.32	Final crack pattern of Slab3 bottom face: (a) Experimental result, (b) Numerical result [137]	36
2.33	Details of Trivedi and Singh FE model: (a) One fourth of a slab with 2 meshes of longitudinal and transversal steel bars, (b) Time-amplitude curve in case of a hammer dropped with a height of 610 mm [175]	37
2.34	Identification of slabs failure mode by inflection point criterion: (a) Transition from flexure to punching shear, (b) Flexural mode [175]	38
2.35	Identification of a slab flexural failure mode by strain based failure criterion: (a) Top elements, (b) Bottom elements [175]	38
2.36	Uniaxial compressive stress-strain curve for concrete [4]	40
2.37	Uniaxial tensile stress-strain curve for concrete [156]	44
2.38	Concrete stress-crack opening curve with: (a) Linear softening branch [7], (b) Bi-linear softening branch [78], (c) Tri-linear softening branch [170]	46
2.39	Experimental tensile stress-strain curve for reinforcing steel [112]	49
2.40	Average tensile stress-strain curve for reinforcing steel embedded in concrete [16]	51
3.1	Unloading response of: (a) elastic plastic, (b) elastic damage, (c) elastic plastic damage models [88]	59
3.2	Drucker-Prager hyperbolic function of CDP flow potential and its asymptote in the meridional plane [94]	61
3.3	Yield surface for the CDP model in: (a) plane stress, (b) the deviatoric plane corresponding to different values of $K_c$ [6]	62
3.4	Response of concrete to uniaxial loading in compression for CDP model [6]	63
3.5	Response of concrete to uniaxial loading in tension for CDP model [6]	64
3.6	Finite elements used for the problem involving contact-impact of reinforced concrete [5]	66
3.7	Constraints with the contact pair algorithm: a) Kinematic contact, b) Penalty contact [5]	67
3.8	Contact interaction properties: a) Hard contact model, b) Coulomb friction model [5]	68
3.9	Approaches to represent steel in RC numerical analysis: a) smeared approach, b) embedded approach, c) discrete approach [138]	69
3.10	Tie constraint to tie two surfaces together in Abaqus [5]	69
4.1	Limit state function [59]	75
4.2	PDF of Gauss, Lognormal, Uniform and Weibull distributions with same mean and standard deviation [107]	76
4.3	CDF of Gauss, Lognormal, Uniform and Weibull distributions with same mean and standard deviation [107]	77
4.4	Correlation of two random variables	78
4.5	Representation of a sample of an output variable by a histogram [107]	80
4.6	Reliability index in standard space [44]	82
4.7	Approximation of limit state surface by FORM [75]	83
4.8	Approximation of limit state surface by SORM [75]	84
4.9	Principle of Monte Carlo method, illustration in the standard space [46]	85

4.10	Principle of importance sampling method, illustration in the standard space [46]	86
4.11	Principle of directional simulation method, illustration in the standard space [46]	87
4.12	Principle of Latin hypercube sampling method, illustration in the standard space [46]	88
4.13	Linear stepped model for tension stiffening [35]	94
5.1	Part of slab	102
5.2	Part of reinforcement	103
5.3	Part of impactor	103
5.4	Part of support	104
5.5	Reinforcement in the model assembly	109
5.6	Assembly of the model after creating instances	110
5.7	Mesh of cylindrical support instances	110
5.8	Partitions used to create Mesh1 and Mesh2	111
5.9	Mesh1 and Mesh2 of slab in xy-plane and in the direction of thickness	111
5.10	Partitions used to create Mesh3	112
5.11	Mesh3 of slab in xy-plane and in the direction of thickness	112
5.12	Partitions used to create Mesh4	113
5.13	Mesh4 of slab in xy-plane and in the direction of thickness	113
5.14	Mesh4 with different sizes of impact region	114
5.15	Mesh4 for different impact positions	114
5.16	The impactor mesh used with Mesh1, Mesh2 and Mesh3 of slab	115
5.17	The impactor mesh used with Mesh4 of slab	115
5.18	Comparison of different mesh types proposed for Slab2	119
5.19	Comparison of contact algorithms available in Abaqus for Slab2 meshed with Mesh4	120
5.20	Sensitivity of mesh in term of the number of elements in the thickness direction and the size of elements in the impact zone for Slab2 meshed with Mesh4	121
5.21	Sensitivity of mesh in term of the size of elements in the slab and the size of elements in the reinforcement for Slab2 meshed with Mesh4	121
5.22	Comparison of concrete compressive stress-strain curves for Slab2	123
5.23	Comparison of concrete compressive stress-strain curves for Slab2	124
5.24	Comparison of concrete compressive stress-strain curves for Slab2	125
5.25	Comparison of concrete tensile stress-strain curves for Slab2	126
5.26	Comparison of concrete tensile stress-strain curves for Slab2	127
5.27	Comparison of concrete tensile stress-cracking displacement curves for Slab2	128
5.28	Comparison of fracture energy values for Slab2	129
5.29	Comparison of steel stress-strain curves for Slab2	130
5.30	Comparison of steel stress-strain curves for Slab2	131
5.31	Comparison of C6T1S1 and C6D3S1 simulations for Slab3 and Slab4	132
5.32	Comparison of C6T1S1 and C6D3S1 simulations for Slab5 and Slab6	132
5.33	Finite element model of slab: a) meshing, b) reinforcement	134
5.34	Mass-spring model without damping	135
5.35	Mass-spring model with damping	135
5.36	Slab stiffness decrease in term of displacement for several values of thickness and the variation of the stiffness initial value in term of the thickness	137
5.37	Comparison of mass-spring models with and without damping	139
5.38	Comparison of FEM and MSM for the same kinetic energy	141
6.1	RC beam tested experimentally in the framework of the LESSLOSS project [108]	144
6.2	Discretization of multifiber beam into elements, nodes and degrees of freedom [76]	144
6.3	Geometrical properties of the multifiber beam	145

6.4	Beam displacement distribution estimated with Kernel Smoothing method . . . . .	150
6.5	Comparison of the beam displacement sample to several parametric distributions . . . . .	150
6.6	QQ-plot test to graphically compare the beam displacement sample to several parametric distributions . . . . .	151
6.7	Number of calls of beam FEM in term of failure probability magnitude for different probabilistic methods . . . . .	155
6.8	Effect of the number of random variables on the accuracy and precision of different probabilistic methods in comparison to MC . . . . .	156
6.9	Variation of failure probability in terms of the force applied at the free end of the beam and the number of random variables considered . . . . .	157
6.10	Effect of the distribution type of random variables on the accuracy and precision of different probabilistic methods in comparison to MC . . . . .	158
6.11	Effect of the type of random variables distribution on the estimation of failure probability for different probabilistic methods . . . . .	159
6.12	Effect of the COV of random variables on the accuracy and precision of different probabilistic methods in comparison to MC . . . . .	160
6.13	Variation of failure probability in term of the mean of the force for different values of COV	161
6.14	Variation of failure probability in term of the COV for different values of the mean of the force . . . . .	161
6.15	Comparison of the beam displacement distributions estimated with the initial model and Taylor expansion . . . . .	162
6.16	Comparison of the beam displacement distributions estimated with the initial model and Least Square method . . . . .	163
6.17	Comparison of the beam displacement distributions estimated with the initial model and polynomial chaos . . . . .	163
6.18	Comparison of failure probability estimated with the initial model and several response surface types . . . . .	164
6.19	Finite element model of slab: a) meshing, b) reinforcement . . . . .	166
6.20	Failure probability with different deterministic models and displacement criterion . . . . .	170
6.21	Comparison of different failure criteria in term of impact velocity mean . . . . .	172
6.22	Effect of the mean of slab length for the displacement criterion . . . . .	172
6.23	Effect of the mean of slab length for the displacement criterion . . . . .	173
6.24	Effect of the mean of concrete density for the displacement criterion . . . . .	174
6.25	Effect of the mean of steel bars diameter for the displacement criterion . . . . .	174
6.26	Effect of the mean of impactor mass for the displacement criterion . . . . .	175
6.27	Effect of the mean of slab stiffness for the displacement criterion . . . . .	175
6.28	Effect of the mean of impactor velocity for the displacement criterion (m=3600 kg) . . . . .	180
6.29	Effect of the mean of impactor mass for the displacement criterion . . . . .	181
6.30	Effect of the mean of slab thickness for the displacement criterion . . . . .	182
6.31	Effect of the mean of concrete compressive strength for the displacement criterion . . . . .	183
6.32	Effect of the mean of steel yield strength for the displacement criterion . . . . .	184
6.33	Effect of the mean of steel diameter for the displacement criterion . . . . .	185
6.34	Effect of numbers of transversal and longitudinal bars for the displacement criterion . . . . .	185
6.35	Effect of stirrups for the displacement criterion . . . . .	186
6.36	Effect of boundary conditions for the displacement criterion . . . . .	187
6.37	Effect of impact position for the displacement criterion . . . . .	188
6.38	Containment building [161] . . . . .	189
6.39	Geometry of the containment building of the Flamanville nuclear power plant . . . . .	190
6.40	The selected zone of the containment building to be modeled . . . . .	190
6.41	Mesh of the selected zone of study of the containment building . . . . .	192

6.42	Horizontal and vertical cables considered in the reliability analysis of containment building . . . . .	194
6.43	Variation of the average tensile stress in term of height . . . . .	196
6.44	Mean and COV of height in term of the number of simulations . . . . .	197
6.45	Histogram of tension zone height samples obtained with initial model and meta-model for 1000 simulations . . . . .	197
6.46	CDF of tension zone height samples obtained with initial model and meta-model for 1000 simulations . . . . .	198
6.47	PDF of tension zone height samples obtained with initial model and meta-model for 1000 simulations . . . . .	199
6.48	Comparison of initial model and meta-model output samples using QQ-plot . . . . .	199
6.49	Failure probability and reliability index estimated with different probabilistic methods depending on the number of points of the design of experiments . . . . .	200
6.50	Convergence at level 0.95 of the estimate of failure probability for different probabilistic simulation methods . . . . .	201
6.51	Importance factors of containment random variables using quadratic combination method and FORM . . . . .	202
6.52	Importance factor of concrete shrinkage coefficient in term of number of points in the design of experiments . . . . .	202
6.53	Comparison of initial model and meta-model for different number of points in the design of experiments . . . . .	204
B.1	Displacement and velocity of slab and impactor: $v = 2.5\text{ m/s}$ , $m = 34151\text{ kg}$ . . . . .	223
B.2	Displacement and velocity of slab and impactor: $v = 5\text{ m/s}$ , $m = 8537\text{ kg}$ . . . . .	224
B.3	Displacement and velocity of slab and impactor: $v = 7.7\text{ m/s}$ , $m = 3600\text{ kg}$ . . . . .	225
B.4	Displacement and velocity of slab and impactor: $v = 10.5\text{ m/s}$ , $m = 1936\text{ kg}$ . . . . .	226
B.5	Displacement and velocity of slab and impactor: $v = 13.2\text{ m/s}$ , $m = 1225\text{ kg}$ . . . . .	227
B.6	Displacement and velocity of slab and impactor: $v = 15.5\text{ m/s}$ , $m = 888\text{ kg}$ . . . . .	228
B.7	Displacement and velocity of slab and impactor: $v = 19.7\text{ m/s}$ , $m = 550\text{ kg}$ . . . . .	229
B.8	Displacement and velocity of slab and impactor: $v = 2.5\text{ m/s}$ . . . . .	230
B.9	Displacement and velocity of slab and impactor: $v = 5\text{ m/s}$ . . . . .	231
B.10	Displacement and velocity of slab and impactor: $v = 7.7\text{ m/s}$ . . . . .	232
B.11	Displacement and velocity of slab and impactor: $v = 10.5\text{ m/s}$ . . . . .	233
B.12	Displacement and velocity of slab and impactor: $v = 13.2\text{ m/s}$ . . . . .	234
B.13	Displacement and velocity of slab and impactor: $v = 15.5\text{ m/s}$ . . . . .	235
B.14	Displacement and velocity of slab and impactor: $v = 19.7\text{ m/s}$ . . . . .	236
B.15	Displacement and velocity of slab and impactor: $m = 750\text{ kg}$ . . . . .	237
B.16	Displacement and velocity of slab and impactor: $m = 1000\text{ kg}$ . . . . .	238
B.17	Displacement and velocity of slab and impactor: $m = 2000\text{ kg}$ . . . . .	239
B.18	Displacement and velocity of slab and impactor: $m = 3000\text{ kg}$ . . . . .	240
B.19	Displacement and velocity of slab and impactor: $m = 3600\text{ kg}$ . . . . .	241
B.20	Displacement and velocity of slab and impactor: $m = 5000\text{ kg}$ . . . . .	242
B.21	Displacement and velocity of slab and impactor: $m = 6000\text{ kg}$ . . . . .	243
B.22	Displacement and velocity of slab and impactor: $d_A = 0.006\text{ m}$ . . . . .	244
B.23	Displacement and velocity of slab and impactor: $d_A = 0.008\text{ m}$ . . . . .	245
B.24	Displacement and velocity of slab and impactor: $d_A = 0.01\text{ m}$ . . . . .	246
B.25	Displacement and velocity of slab and impactor: $d_A = 0.012\text{ m}$ . . . . .	247
B.26	Displacement and velocity of slab and impactor: $d_A = 0.014\text{ m}$ . . . . .	248
B.27	Displacement and velocity of slab and impactor: $d_A = 0.016\text{ m}$ . . . . .	249
B.28	Displacement and velocity of slab and impactor: $d_A = 0.02\text{ m}$ . . . . .	250

B.29 Displacement and velocity of slab and impactor: $d_A = 0.03\text{ m}$ . . . . .	251
B.30 Displacement and velocity of slab and impactor: $\rho_c = 1200\text{ kg/m}^3$ . . . . .	252
B.31 Displacement and velocity of slab and impactor: $\rho_c = 1600\text{ kg/m}^3$ . . . . .	253
B.32 Displacement and velocity of slab and impactor: $\rho_c = 2000\text{ kg/m}^3$ . . . . .	254
B.33 Displacement and velocity of slab and impactor: $\rho_c = 2300\text{ kg/m}^3$ . . . . .	255
B.34 Displacement and velocity of slab and impactor: $\rho_c = 2500\text{ kg/m}^3$ . . . . .	256
B.35 Displacement and velocity of slab and impactor: $\rho_c = 3000\text{ kg/m}^3$ . . . . .	257
B.36 Displacement and velocity of slab and impactor: $\rho_c = 3500\text{ kg/m}^3$ . . . . .	258
B.37 Displacement and velocity of slab and impactor: $\rho_c = 4000\text{ kg/m}^3$ . . . . .	259
B.38 Displacement and velocity of slab and impactor: $\rho_c = 4500\text{ kg/m}^3$ . . . . .	260
B.39 Displacement and velocity of slab and impactor: $e = 0.3\text{ m}$ . . . . .	261
B.40 Displacement and velocity of slab and impactor: $e = 0.4\text{ m}$ . . . . .	262
B.41 Displacement and velocity of slab and impactor: $e = 0.5\text{ m}$ . . . . .	263
B.42 Displacement and velocity of slab and impactor: $e = 0.6\text{ m}$ . . . . .	264
B.43 Displacement and velocity of slab and impactor: $e = 0.7\text{ m}$ . . . . .	265

# List of Tables

2.1	Details of impact tests . . . . .	23
2.2	Impact loading protocol [84] . . . . .	26
2.3	Values of $\varepsilon_{c0}$ parameter for high strength concrete [54] . . . . .	41
4.1	Typical limit states for structures [121] . . . . .	82
4.2	Summary on compressive strength of concrete according to various references . . . . .	93
4.3	Summary on tensile strength of concrete according to various references . . . . .	95
4.4	Summary on Young's modulus of concrete according to various references . . . . .	96
4.5	Summary on yield and ultimate strengths of steel according to various references . . . . .	97
4.6	Summary on elasticity modulus of steel according to various references . . . . .	98
4.7	Summary on dimensions of RC members according to various references . . . . .	99
5.1	Linear mechanical properties of concrete and steel materials for Chen and May slabs . . . . .	104
5.2	Nonlinear mechanical properties of concrete and steel materials for Chen and May slabs . . . . .	105
5.3	Parameters of the damaged plasticity model . . . . .	106
5.4	Compressive concrete behaviors for CDP model . . . . .	106
5.5	Tensile concrete behaviors for CDP model . . . . .	107
5.6	Idealized stress-strain curves for reinforcing steel . . . . .	108
5.7	Linear mechanical properties of concrete and steel materials for the slab in nuclear plant . . . . .	132
5.8	Nonlinear mechanical properties of concrete and steel materials for the slab in nuclear plant . . . . .	133
6.1	Random variables of the multifiber beam and their descriptions . . . . .	145
6.2	Importance factors of beam random variables . . . . .	146
6.3	Stress and resistance variables of the cantilever beam and their variability influence . . . . .	147
6.4	Omission factors of the cantilever beam variables and their influence on $P_f$ . . . . .	147
6.5	Variability of the cantilever beam variables according to their mean and standard deviation values . . . . .	148
6.6	Summary of sensitivity studies for the cantilever beam . . . . .	148
6.7	Results of Kolmogorov-Smirnov test to verify beam displacement distribution . . . . .	149
6.8	Failure probability estimated with different methods for all the cases studied of the cantilever beam (number of random variables=2) . . . . .	152
6.9	Failure probability estimated with different methods for all the cases studied of the cantilever beam (number of random variables=3) . . . . .	152
6.10	Failure probability estimated with different methods for all the cases studied of the cantilever beam (number of random variables=7) . . . . .	153
6.11	Failure probability estimated with different methods for different types of probability distribution (number of random variables=2) . . . . .	159
6.12	Random variables of the RC slab and their statistical descriptions (elastic behavior) . . . . .	168

6.13 Comparison of displacement of slab at the impact point for different deterministic models and different values of velocity (elastic behavior) . . . . . 170

6.14 Comparison of probabilistic methods combined with the MSM for the displacement criterion 171

6.15 Deterministic variables, random variables and their statistical descriptions . . . . . 178

6.16 Factorial experiment factors and mass-spring model parameters . . . . . 179

6.17 Failure probability with FE and mass-spring models and displacement criterion . . . . . 179

6.18 Random variables of the containment building and their descriptions . . . . . 194

# Chapter 1

## Introduction

### 1.1 Background

In civil engineering field, the main problem consists in finding an optimal design that ensures to maximum the continuous safety of structures throughout its service life. The design should also ensure a satisfactory structural performance with an economical cost. Reinforced concrete structures are subjected to several sources of uncertainties that highly affect their response. These uncertainties are related to the structure geometry, material properties and the loads applied. Engineers have always used traditional and deterministic approaches to simplify the problem and account for these uncertainties through the application of safety factors according to limit states. However, these factors are based on engineering judgment, they are calibrated to a certain level of security and presented as fixed values. In addition, they do not provide sufficient information on the effect of different uncertain variables on the structural safety. Consequently, for an optimal and robust design that guarantees a real prediction of the behavior of structures, uncertainties should be taken into account and propagated in the structural deterministic analysis. To address this issue, probabilistic approaches were developed to correctly model the variation of input variables and to ensure a higher reliability of representative mechanical models used for the design of new structures or the monitoring of performance of existing structures. These approaches allow assessing failure probability of structures according to one or several criteria, but also studying the influence of uncertain variables on the structure response. Sensitivity analysis can be performed to analyze the variation of structure resistance during the design phase or the surveillance testing phase with respect to conventional parameters, such as loads and material properties, but also with respect to nonlinear inaccurately known parameters such as the creep in concrete or its damage due to cracking. Thus, structural reliability analysis based on the principle of combining a stochastic model with a deterministic model enables to deduce a more realistic estimate of the safety margin in terms of the variation of different variables. Stochastic models should include the probabilistic characteristics of random input variables including a suitable probability distribution and appropriate values of their mean and coefficient of variation. Deterministic models allow predicting structural response and evaluating the variables of interest, they can be based on analytical, empirical or numerical deterministic approaches.

Therefore, the physical problem and mechanical phenomena applied should be evaluated before performing reliability analysis. Among structures considered in this study, only the physical problem of reinforced concrete (RC) slabs subjected to impact is investigated in detail. Such types of problem is classified as low velocity impact event and considered as one of the most difficult nonlinear dynamic problems in civil engineering because it involves several factors, including the nonlinear behavior of concrete, the interaction effects between the concrete and reinforcement, and contact mechanics between the slab and the impactor. The complexity of impact problems also lies in the dynamic response of RC slabs and the time-dependent evolution of impact velocity. Design

of RC slabs to resist impact loads represents an area of research that is increasingly gaining importance. Their design is generally based on static method which is often not sufficiently accurate to describe an impact phenomenon. An optimal design requires taking into account the main physical processes involved and the potential development of nonlinearities due to material damage. Numerous studies were carried out on the transient behavior of RC slabs under low velocity impact and three approaches were usually used. Many researchers studied the actual response of impacted slab with the development of crack patterns and resulting failure modes through full-scale impact tests [34, 189]. Advanced numerical approaches, which take into account materials constitutive models and contact algorithms, have proven to be reliable to analyze the failure modes of RC slabs subjected to impact [19, 119, 137]. Simplified analytical methods were also developed and used as an initial approximation of the impact behavior of slabs [10, 29, 47], they are generally based on simplifying assumptions and account for the complexity of the studied phenomenon. However, these approaches are deterministic and do not consider the randomness of the basic variables of an impact problem. These variables affect the response of the slab which has also a random character, thus reliability analysis seems to be the more appropriate to study the behavior of slabs under impact. Based on this approach, a number of studies were carried out to estimate the reliability of different types of RC structures. Low and Hao [111] performed a reliability analysis of RC slabs subjected to blast loading using two loosely coupled single degree of freedom system and Val *et al.* [177] evaluated the reliability of plane frame structures with ultimate limit state functions. However, reliability analyses that consider the effect of uncertainties in a low velocity impact phenomenon are scarce.

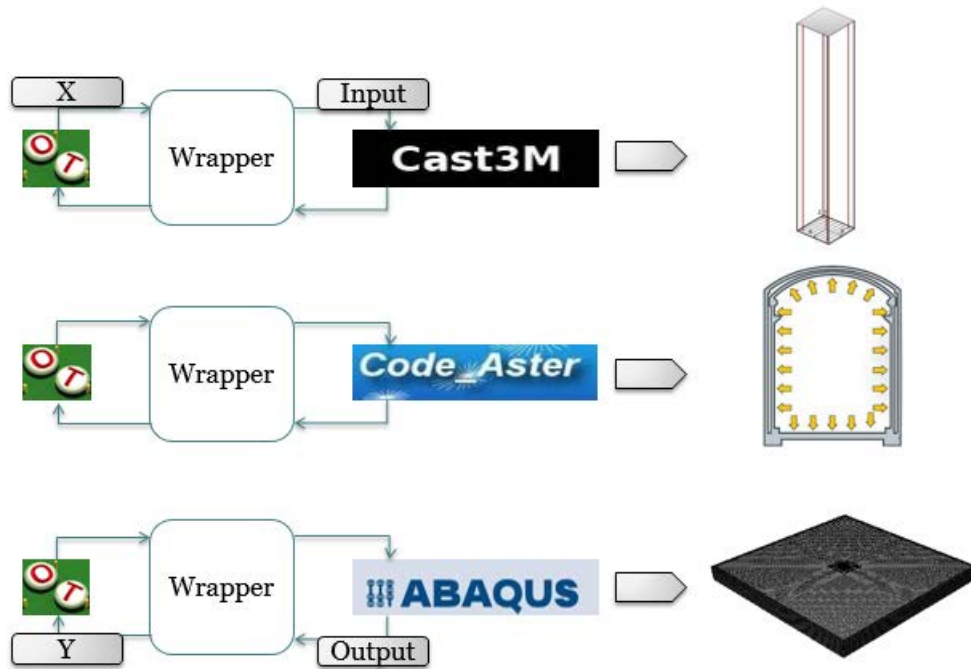
## 1.2 Research motivation

The lack of knowledge on the potential load applied to a RC structure, as well as the uncertainties related to its features (geometry, mechanical properties) shows that the design of RC structures could be made in a reliability framework. Structural reliability provides the tools necessary to account for these uncertainties and evaluate an appropriate degree of safety. This research discusses the use of reliability analysis for three different civil engineering applications of different degrees of complexity. The platform OpenTURNS is used to perform the reliability analysis of the RC structures considered in the present study and propagate uncertainties in their physical models. OpenTURNS is used because it offers a large set of methods that enable the quantification of the uncertainty sources, the uncertainty propagation and the ranking of the sources of uncertainty. However, OpenTURNS should be linked to the software used to perform deterministic analysis. The link of any external software to OpenTURNS can be made using the generic wrapper and is called “wrapping”. Wrapping allows an easy connection to the deterministic simulation as well as an easy evaluation of its response due to several features provided in OpenTURNS. A wrapper is a Python based programming and necessitates the description of input and output variables using regular expressions that enable the substitution of the values of these variables with random values in the initial deterministic model. Thus, the input file of the deterministic code and the output file corresponding to output variable values should be specified, since the first will be modified according to the random values generated and the second will be read by OpenTURNS. The command to submit the deterministic model should be also provided in the wrapper, it allows running the external software using the specific random values generated for each call of the wrapper. A wrapper works as follows:

- Values of random variables are generated in OpenTURNS.
- The wrapper uses the input file of the deterministic code in order to create a new file corresponding to the random values generated. The new file will be placed in a temporary directory.

- Once the submission command of the deterministic model is accomplished, the wrapper reads the results file and send the mechanical response obtained to OpenTURNS in order to perform a reliability analysis for the structure considered.

The capacity of OpenTURNS to be linked to different finite element software is tested through the three applications considered in this study. Therefore, OpenTURNS is linked to CASTEM to study the reliability of a RC multifiber cantilever beam subjected to a concentrated load at the free end. It is also coupled to Abaqus in order to study the reliability of RC slabs which are subjected to accidental dropped object impact during handling operations within nuclear plant buildings. Furthermore, a combination of ASTER and OpenTURNS is considered in the aim of studying the reliability of a prestressed concrete containment building. In the case where a structure is presented with an analytical model, OpenTURNS is combined with Matlab.



The combination of mechanical and stochastic models is necessary in reliability analysis in order to compute failure probability for one or several failure modes, which can be very time consuming and in some cases impossible. Indeed, either the complexity of the deterministic model considered implies important computing time (from minutes to hours) or reliability methods evaluating failure probability require a too large number of simulations of the deterministic model.

### 1.3 Study scope and objectives

There are many objectives behind this research. One of these objectives is to discuss the principles of structural reliability analysis, as well as the types of uncertainty related to the structure and the deterministic model used. This study describes the basic statistical concepts required to perform a reliability analysis in structural engineering, as well as the probabilistic methods available in OpenTURNS to assess failure probability of existing or new structures according to a specific limit state function.

Another main objective of the current research is to address the issue of computational effort of reliability analysis. Thus, two strategies are proposed to accurately assess failure probability with the minimum computational cost:

- The first strategy consists in using deterministic analytical models that are as simple as possible, but that are able to predict the structural response appropriately. In general, the constraining assumptions of analytical models allow studying only a few configurations of the structure. Thus, the objective is to reduce the computational cost of the deterministic analysis to the minimum, while also explore as far as possible how to use this type of simplified models. Due to their low computational time, these models can be coupled with simulation probabilistic methods that need to carry out several deterministic analyses.
- The second strategy is used when the structure is simulated with a finite element model. It consists in choosing an appropriate probabilistic method where failure probability can be assessed from a small number of simulations of the numerical model, or substituting the finite element model by a meta-model less expensive in computational time.

The reliability of three different structures is examined in this study:

- A simple application to a RC beam is firstly used as a preliminary example in the aim of mastering the basics of OpenTURNS and examining the efficiency of several probabilistic methods available in OpenTURNS. This application enables to compare probabilistic methods with an example necessitating low computational effort in order to initially select an appropriate method to use in the case of more complex structures depending on the deterministic model considered and the computational effort constraints required.
- The second application focuses on RC slabs which are subjected to accidental dropped object impact during handling operations within nuclear plant buildings. In this case, dropped objects are characterized by small impact velocities and damage can arise at the impact zone depending on the impact energy and the relative masses of the colliding bodies. The following example is used to compare the strategies proposed to reduce the computational effort of reliability analysis, as well as to perform parametric studies in order to locate the most critical impact points for the slab design and illustrate how to optimize the design of reinforced concrete slabs under impact in terms of dimensions, material properties and reinforcement ratio. The reliability of slabs subjected to impact assuming an elastic linear behavior of materials is examined first followed by the reliability of slabs when nonlinear behaviors of concrete and steel are considered in deterministic models.
- The third application consists of a prestressed containment building in order to study the stress evolution with time in the containment during periodic surveillance testing carried out 20 years after its implementation. The problem is examined under aging phenomena, including relaxation of reinforcement, creep and shrinkage of concrete. The aim of this application is to investigate the efficiency of meta-modeling strategy in reliability analysis of very complicated structures. In this case, the deterministic model is approximated by a polynomial function and the reliability analysis is performed for this approximation. The computational effort of this strategy depends on the number of simulations needed to obtain an accurate approximated model.

As previously mentioned, only the physical problem of reinforced concrete (RC) slabs subjected to unplanned impact events due to dropped objects is investigated in detail. The aim of this application is to provide an efficient procedure to predict RC slabs response under low velocity impact. Numerical and analytical approaches are used and models are validated using physical experimental tests from the literature which provide high quality input data and a wide range of output results. As a part of the fundamental objectives of this research, the following investigations are carried out in order to be able to examine the structure performance and carry out designs:

- Study the complex phenomenon of impact and the structural behavior associated to impact by:
  - classifying the impact response types of RC slabs according to the impactor mass and velocity,
  - defining the impact event types according to the impactor deformability, material properties and impact velocity,
  - describing the failure modes of RC slabs under impact according to their characteristics and impact conditions,
  - presenting the energy transformation process of the impact energy to slabs as different forms of energy.
- Characterize concrete and steel materials properties by:
  - describing their mechanical behaviors according to several stress-strain relationships proposed in the literature,
  - choosing suitable material constitutive models to use in finite element analysis and identifying properly their parameters,
  - providing an accurate statistical description of material variables intervening in the reliability analysis of impacted RC slabs.
- Choose an appropriate finite element software for impact problems by:
  - presenting the different steps necessary to create a finite element model using the software selected,
  - describing the principles of finite element components implemented in the software and adopted for the model.
- Develop a three-dimensional finite element model of an impacted slab in Abaqus using an explicit configuration, which allows taking into account the nonlinear behavior of concrete and modeling the contact between the impactor and the slab. The model should also allow a better representation of the actual structure geometry and boundary conditions. The model is validated with experiments carried out on several RC slabs under drop-weight loads at Heriot-Watt University by Chen and May [34]. Then, the model adopted is used to model RC slabs which are subjected to accidental dropped object impact during handling operations within nuclear plant buildings.
- Develop a simplified analytical model that consists of two degrees of freedom mass-spring system which accounts for potential viscous damping, and describes the degradation of slab stiffness using a frequency decrease approach

The modeling procedure adopted in this study simulates the impacted slabs as close as possible to the actual structure without any geometrical or material simplifications. The full geometry of slabs is considered in the model and no symmetry boundary conditions are modeled in order to be able to study several configurations of impact position. The model is parametrized through a code developed using a Python script in Abaqus Python edition. It should be noted that strain rate effect is not taken into account in this research as only low velocity impacts are studied.

## 1.4 Thesis contents

**Chapter 2** This chapter provides a classification of impact response types of RC slabs according to the impactor mass and velocity. Then a definition of impact event types is introduced and the behavior of RC slabs subjected to a transient dynamic load is described by determining their failure modes according to their characteristics and impact conditions. An overview of approaches used to determine slabs response is also given and several studies from the literature performed on their transient behavior under low velocity impact are detailed. Next, the nonlinear static and dynamic mechanical material behaviors are presented and many uniaxial stress-strain relationships for steel and concrete in compression and tension proposed in the literature are provided.

**Chapter 3** This chapter discusses the choice of deterministic software used in the present study to simulate the problem of RC slabs which are subjected to accidental dropped object impact during handling operations within nuclear plant buildings. First, the basic phases of finite element analysis are described and the different steps which are necessary to create a finite element model in Abaqus are presented. Furthermore, plasticity constitutive models used to represent concrete and steel in numerical simulations are discussed by describing and identifying their fundamental parameters, and contact algorithms used for modeling the interaction between two bodies are presented. Other numerical features which are necessary for simulating impact analysis are also discussed.

**Chapter 4** In this chapter, the principles of structural reliability analysis, as well as the types of uncertainty related to the structure and the deterministic model used, are presented. Next, the steps of a reliability analysis are detailed and the methods used in OpenTURNS for uncertainty quantification, uncertainty propagation and sensitivity analysis are described. Finally, statistical descriptions of random variables intervening in RC structures are examined according to several studies in the literature.

**Chapter 5** In this chapter, two deterministic models are used and evaluated for the problem of impacted slabs. The first model consists of a 3D finite element model simulated with Abaqus/Explicit. The steel is modeled as an elasto-plastic material with hardening and, the behavior of concrete is described by the damage plasticity model. A detailed step-by-step procedure for creating FE models of impacted slabs with Abaqus is described. This model is used for Chen and May RC slabs [34] and validated with experimental results. The model adopted is used to simulate RC slabs which are subjected to accidental dropped object impact during handling operations within nuclear plant buildings. Then, a simplified analytical model is also used for these slabs. It consists of a two degrees of freedom mass-spring system which accounts for potential viscous damping. A frequency decrease approach is used to describe the degradation of the slab.

**Chapter 6** In this chapter, 3 case studies are used in order to address the issue of solving reliability problems in the domain of civil engineering. The first application consists of a RC multifiber cantilever beam and is used in the aim of mastering the basics of OpenTURNS and examining the probabilistic methods proposed in OpenTURNS to estimate failure probability in structural reliability analysis in terms of their accuracy, precision and computational effort. The second application is the problem of RC slabs subjected to impact in the aim of addressing the issue of computational cost of reliability analysis and proposing computational strategies allowing the accurate assessment of the failure probability for minimum computational time. Firstly, the problem of impacted slab is studied assuming a flexural mode of failure and an elastic behavior for steel and concrete. Following this, the problem of impacted slabs is studied using deterministic models that take into account the nonlinear material properties. In both cases, elastic and nonlinear behaviors, a parametric study is performed to identify the influence of deterministic model parameters on the reliability of RC slabs

under low velocity impact. The third application consists of the prestressed concrete containment building of the Flamanville nuclear power plant and is considered in the aim of presenting a procedure to be followed to study the response of very complicated structures in a reliability framework. Polynomial chaos expansion is used to simplify the physical model and study the reliability of the containment.

## Chapter 2

# Reinforced concrete slabs behavior under impact: Dynamic response and literature review

### 2.1 Introduction

In civil engineering field, reinforced concrete (RC) structures are often subjected to some extreme dynamic loadings due to accidental impacts of rigid bodies that may occur during their service life with a very low probability of occurrence. The failure resulting consequences of structures subjected to such extremely severe loadings might be extremely high, which makes their analysis and design very complex especially when working with nonelastic materials. Impact loadings are characterized by a force of considerable magnitude applied within a short duration, they may be caused by falling rock impact on protection galleries, missile and aircraft impact on nuclear containments, vehicles collision with buildings or bridges, ships or ice crash impact with marine and offshore structures, flying objects due to natural forces such as tornados and volcanos, fragments generated due to military or accidental explosions on civil structures, or by dropped objects impact on industrial or nuclear plant floors as a consequence of handling operations. Figure 2.1 shows some examples of impact loading cases in civil engineering field. For all these applications, the problem of impact has to be studied with convenient considerations since structures undergo, depending on their stiffness, different failure modes such as flexure and punching shear failure, in addition to different types of local damage such as crushing, cracking, scabbing, spalling and perforation. Furthermore, the velocity, angle and position of impact, as well as the shape, mass and rigidity of impactors vary broadly from one application to another.

Design of RC slabs to resist impact loads represents an area of research that is increasingly gaining importance and numerous studies were carried out by many researchers on the behavior of RC slabs subjected to dynamic impact loading, especially under high velocity regimes [17, 52, 80, 86, 92]. However, when slabs are exposed to unplanned impact events such as accidental collisions with dropped objects, the problem is classified as low velocity impact event. Several studies that will be detailed in section 2.3 were carried out on the transient behavior of RC slabs under low velocity impact, but there is a growing need to more investigate the behavior of slabs for low velocity situations.

In the available design codes of civil engineering, the design of reinforced concrete (RC) structures subjected to impact is generally based on approximate static method. The dynamic forces during impact are usually considered by applying an equivalent dynamic impact factor and converted into a static force of equal magnitude. Such static design is often not sufficiently accurate to describe an impact phenomenon, as not only the maximum value of the impact force is crucial to predict the

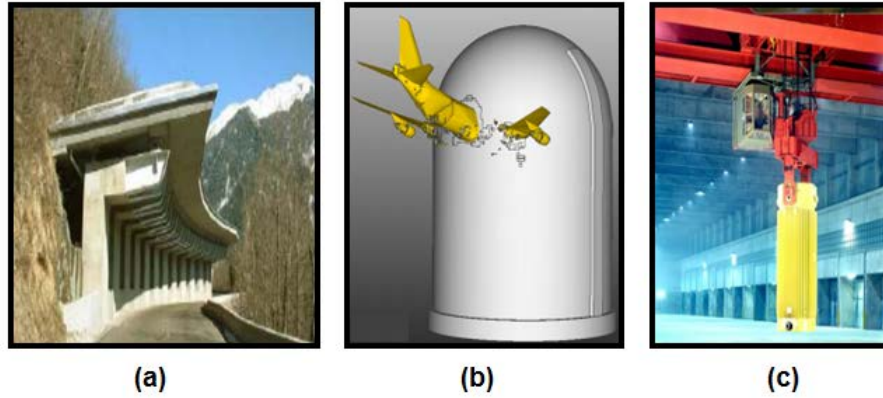


Figure 2.1: Some accidental impact loading cases in civil engineering field: a) Rockfall on protection galleries, b) Aircraft impact on nuclear containments, c) Dropped objects impact during handling operations

structural dynamic behavior, but also the loading duration and rate must be taken into account. The use of approximate static methods results in either an under- or over-dimensioned design for structures and, in some particular cases, the dynamic response of structures cannot be simplified to a quasi-static response. Moreover, an equivalent dynamic force can be just used in the case when structures withstand flexural mode. Nevertheless, during impacts, structures do not only fail under flexural mode but they may fail under punching shear or local damage, and higher modes of vibration can be expected. Thus the transient dynamic analysis has to be performed accounting for the main physical processes involved and accurate models are needed to describe and predict the structural behavior of RC members when subjected to impact loading. An optimal design that guarantees the structure resistance with an economical cost requires taking into account the potential development of nonlinearities due to the material damage (concrete cracking, steel yielding, etc.). Abrate [9] indicated that the study of impact on composite structures such as RC slabs involves many different topics (contact mechanics, structural dynamics, strength, stability, fatigue, damage mechanics, micromechanics) and that the prediction of dynamic response of composite structures to impact can be made by using analytical or finite element models which must appropriately account for the motion of the impactor, the overall motion of the structure, and the local deformation in the contact zone and in the area surrounding the impact point. Abrate also indicated that the parameters which affect the impact resistance of composite structures are the properties of the matrix, the reinforcing fibers, the fiber-matrix interfaces, the size, the boundary conditions, and the shape, mass, and velocity of the impactor.

The present study focuses on RC slabs which are subjected to accidental dropped object impact during handling operations within nuclear plant buildings (Figure 2.2). In this case, dropped objects are characterized by small impact velocities and damage can arise at the impact zone depending on the impact energy and the relative masses of the colliding bodies. The current chapter first provides a classification of impact response types of RC slabs according to the impactor mass and velocity. Then a definition of impact event types is introduced and the behavior of RC slabs subjected to a transient dynamic load is described by determining their failure modes according to their characteristics and impact conditions. Afterwards, an overview of approaches used to determine slabs response is given and several studies from the literature performed on their transient behavior under low velocity impact are detailed. Next, the nonlinear static and dynamic mechanical material behaviors are presented and many uniaxial stress-strain relationships for steel and concrete in compression and tension proposed in the literature are provided.

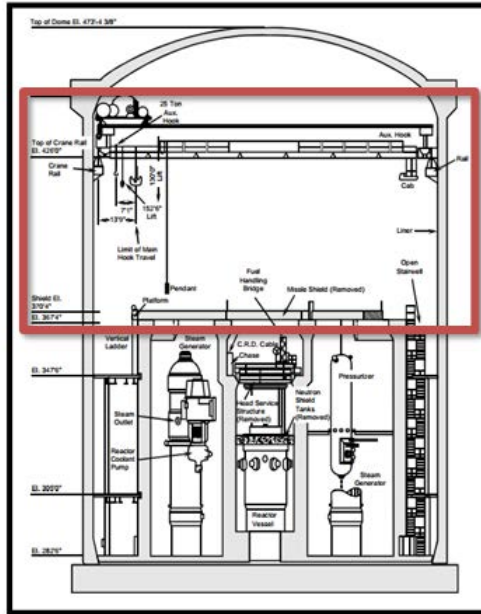


Figure 2.2: Accidental dropped object impact during handling operations within nuclear plant buildings

## 2.2 Reinforced concrete slabs behavior under impact

### 2.2.1 Impact dynamics

During handling and maintenance operations within nuclear plant buildings, impacts on RC slabs by foreign objects as tools and nuclear material packages can be expected to occur. Impacts create internal damage that depends on the load (velocity and mass of the impactor) and may cause severe reductions in strength [9]. The internal damage is often undetectable by visual inspection, hence the effects of dropped object impacts on RC slabs must be understood and taken into account in the design process. According to Abrate [10], composite structures subjected to impact have different types of behavior which must be properly evaluated in order to interpret experimental results and select convenient analytical or numerical models. Abrate studied and classified the currently available models used to predict the dynamic of impacts between a foreign object and a composite structure in the aim of presenting an approach to select an appropriate model for each particular case study. He showed that developing a model to analyze the overall response of the structure and the contact phenomenon requires understanding the different types of structural behavior, as well as the effects of several parameters on the impact dynamics.

According to [9], when the impactor enters in contact with the structure, shear and flexural waves propagate away from the impact point and reflect back when they reach the back face. These waves propagate at different speeds and decline progressively in response to materials damping, energy diffusion and several geometrical effects [151]. Thus, the impact response can be controlled by wave propagation and strongly influenced by impact duration [149]. The impact duration influence is illustrated in Figure 2.3, which shows three different types of response for very short, short and long impact times.

The response defined for very short impact times is dominated by three-dimensional wave propagation through the thickness direction and the impact time is in the order of waves transition time. This response is unaffected of structure size and boundary conditions and is generally associated with ballistic impacts (Figure 2.3.a). A definition of ballistic impacts was given by [9] as impacts

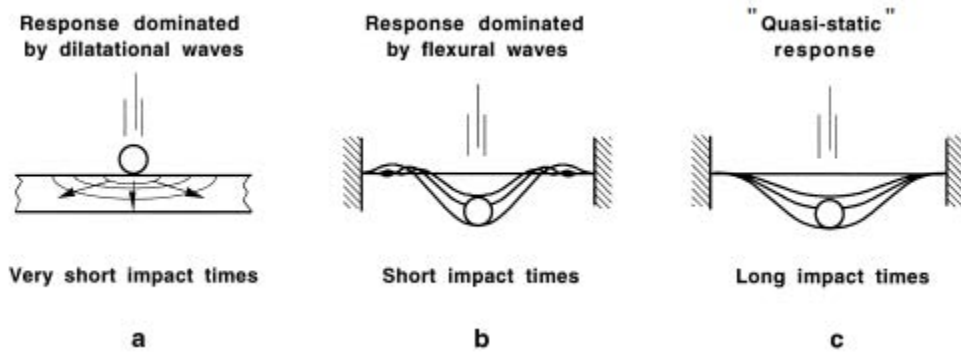


Figure 2.3: Response types during impact on plates according to [149]

resulting in complete perforation of the structure with a ballistic limit equal to the lowest initial velocity of the impactor causing this perforation. The ballistic limit increases with the structure thickness and is affected by material densities and mechanical properties. For short impact times, the response is governed by flexural waves and shear waves and is typical for impact by hail and runway debris (Figure 2.3.b). In this case, the response remains independent of boundary conditions as long as main waves have not reached a boundary. For long impact times, the response is “quasi-static” influenced by structure dimensions and boundary conditions. A typical example of long impact times is dropping of heavy tools. In this case, the time needed by waves to reach structure boundaries is much less than impact duration and the “quasi-static” response is in the sense that deflection and load have the same relation as in a static case (Figure 2.3.c). The two latter response types can be associated with the case of RC slabs subjected to foreign object impact.

A criterion related to the three-dimensional stress distribution under the impactor was proposed by Abrate [9] to classify impact dynamics by distinguishing between high-velocity and low-velocity impacts. His criterion consisted of defining low-velocity impacts in cases where stress wave propagation through the thickness has no significant role. In this case, damage is not introduced in the early stages of impact, but it is initiated after the overall structure bending behavior is established. For low-velocity impacts, stress levels remain low due to several wave reflections through the thickness and the structure dynamic properties are usually not affected by the presence of damage. Conversely, Abrate indicated that damage for high-velocity impacts is introduced during the first few compressive wave reflections through the thickness, while overall structure behavior is not yet initiated. Abrate’s criterion defined high-velocity impacts as cases related to the ratio of impact velocity versus the speed of propagation of compressive waves through the thickness direction, so that this ratio must be larger than the maximum failure strain. During high velocity impacts, failure near the structure back face may occur due to tensile stresses generated by the compressive wave after reflection. A velocity of 20 m/s was suggested by Olsson [151] as the upper limit of low velocity impacts, while the suggested limit of medium velocity ranges from 20 to 100 m/s. Very high velocities were considered to be greater than 2 km/s [9]. Classifying impact events by using velocity is the most common, however this classification is highly relative. For example in the case of impactors dropped at low velocity (a few m/s) on large plates, the response was demonstrated to be associated with “high-velocity impact” since it is governed by wave propagation [148].

Further, the initial kinetic energy of the impactor is an important parameter that affects the structure response [9, 149]. In consequence, although the kinetic energy is the same, a structure subjected to an impact of a large mass with a low initial velocity behaves differently than in case of a smaller mass with higher velocity. For the first problem, the indentation effect is negligible and the impact may involve an overall response of the structure. In the other case, damage initiates at earlier stages and the response can be introduced by deformations in a small zone surrounding the

impact point. Impactors with small mass cause more localized deflection and higher impact loads with a significant effect of the indentation on absorbing the impact energy that can be restituted to the impactor or transferred to the structure. The influence of impactor mass on the response behavior can be associated to Figure 2.3 as mentioned in [150]. A ballistic response occurs for very small masses, moderately small masses cause a response dominated by shear and flexural waves and large masses cause a “quasi-static” response.

However, Olsson [149] showed that response and damage are not influenced only by impact velocity, duration or initial kinetic energy, but also by the impactor vs. structure mass ratio. Olsson derived a simple criterion for impact plates response controlled by flexural waves and distinguished between small-mass, intermediate-mass and large-mass impacts. A sufficient condition for small-mass impact response is that dominating flexural waves does not reach the boundaries during the impact duration. For central impact on a quasi-isotropic plate, small-mass criterion corresponds to impactor masses less than one fifth of the mass of the plate area affected by the impact:

$$M/M_p \leq 1/5 \quad (2.1)$$

The response with intermediate-mass impactors is more complex and the mass criterion becomes:

$$1/5 < M/M_p < 2 \quad (2.2)$$

For large-mass impactors, the flexural wave reaches boundary conditions and a “quasi-static” impact response occurs for:

$$M/M_p > 2 \quad (2.3)$$

where  $M$  is the impactor mass and  $M_p$  is the mass of the impacted plate. For non-central impacts,  $M_p$  is calculated as the mass of a square zone centered at the impact with a side that coincides with the closest plate edge [151]. For square plates, the condition of small-mass impact response corresponds to a mass ratio less than 1/4 ( $M/M_p \leq 1/4$ ). It should be noted that this mass criterion becomes irrelevant for impact velocity resulting in penetration [151].

## 2.2.2 Types of impact

An existing definition allows normally classifying impact events into either hard or soft according to the impactor deformability. For hard impact, impactor is generally considered as rigid and its deformation is negligible compared to the structure deformation (Figure 2.4.b). In this case, the impact kinetic energy is to a great extent absorbed by the structure deformation and the impactor remains undamaged or barely deformed during impact. Hard impact results in both local and overall dynamic response of the structure and failure may occur due to complicated stress waves. According to [132], the shape and dimensions of impactor, as well as impact velocity are the essential parameters that may affect the classification of an impact as hard.

However, in the case of soft impact, the structure deformation is very small compared to the impactor. In other words, the structure that resists to impact is assumed to remain undeformed, while the impactor is strongly damaged and the impact kinetic energy is fully transferred into deformation energy of the impactor (Figure 2.4.c). The propagation of stress waves is considered as negligible and the structure failure response can be compared to that under static loading with no rebound of the impactor. An impact can be considered as soft owing to the failure region and the ratio between the impacted structure and the impactor masses [132]. The case of soft impact can be illustrated by a crash of a vehicle against a rigid wall or a crash of an airplane against a thick concrete containment wall of a nuclear power plant [29].

This basic and well-known definition of soft and hard impacts was proposed by Eibl [55] in order to consider the dissymmetry of an impact event along with the difference between structure and

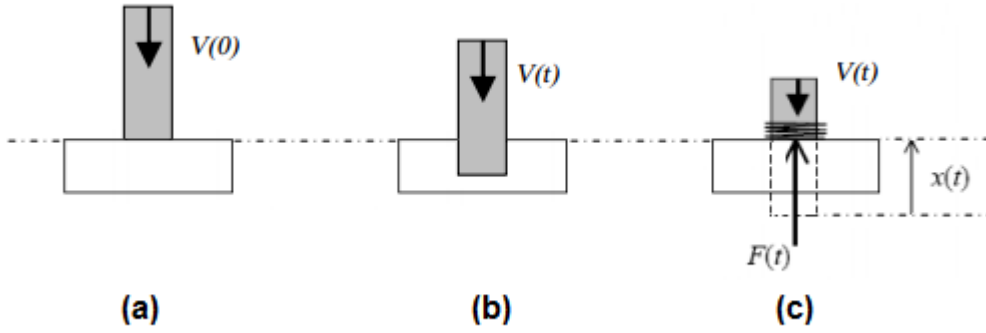


Figure 2.4: Structure and impactor deformations according to the impact type [45] : a) Initial conditions ( $t=0$ ), b) Hard impact ( $t>0$ ), c) Soft impact ( $t>0$ )

impactor responses. The dissymmetry of an impact event is due to the fact that the structure is stationary before impact, while the impactor moves with an initial velocity  $V(0)$ . As mentioned earlier, one of the two bodies in collision shows small deformations compared to the other one during soft and hard impact, which involves a dissymmetry in the behaviors of the structure and the impactor.

The classification of Eibl is based on a mass-spring model (Figure 2.5) that consists of the structure ( $m_2$ ) and the impactor ( $m_1$ ) masses, a contact spring associated with a stiffness  $k_1$  and a second spring with a stiffness  $k_2$ . The contact spring simulates the force that arises when the two bodies are in contact, while the second represents the structure behavior and its resisting force to impact. The mass-spring model is governed by two differential equations that describe the motion of the two bodies and can be expressed as follows:

$$\begin{cases} m_1 \ddot{x}_1(t) + k_1[x_1(t) - x_2(t)] & = 0 \\ m_2 \ddot{x}_2(t) - k_1[x_1(t) - x_2(t)] + k_2 x_2(t) & = 0 \end{cases} \quad (2.4)$$

In the case of a soft impact ( $x_1(t) \gg x_2(t)$ ), the contact force  $F(t)$  can always be deduced only from the impactor deformation by solving the first independent equation of the following system:

$$\begin{cases} m_1 \ddot{x}_1(t) + k_1 x_1(t) & = 0 \\ m_2 \ddot{x}_2(t) + k_2 x_2(t) & = F(t) \end{cases} \quad (2.5)$$

with  $F(t) = k_1 x_1(t)$ . The second equation allows determining the structure response under an independently acting force  $F(t)$ .

Hard impacts require to consider the local as well as the overall deformations of the structure, thus the two equations of system (2.4) cannot be independent and spring stiffnesses must be determined. Section 2.3.2.2 shows how to calculate  $k_1$  and  $k_2$  for hard impacts as indicated by the Euro-International Concrete Comity (CEB) [29] that assumes the same characterization of soft and hard impact as Eibl.

Nevertheless, Koechlin and Potapov [95] found that the definition of Eibl is qualitative and not precise enough to make a distinction between soft and hard impacts for low velocity impact events. Alternatively, they proposed a more precise quantitative classification which is based on the material properties and the impactor velocity, and permits to predict the type of impact that is expected even before the observation of the structural response during impact. They indicated that

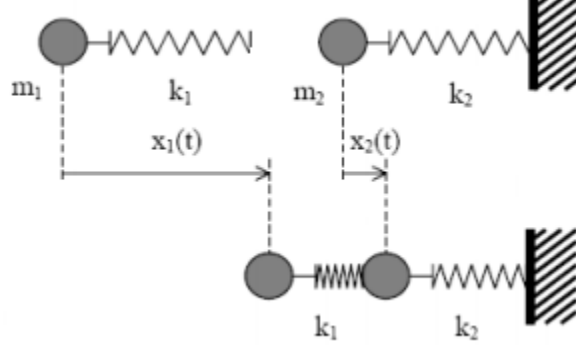


Figure 2.5: Mass-spring model proposed by Eibl [55] to simulate an impact [45]

considering the impactor deformation as described previously as the essential property of the impact type specification is not completely true since the terms “hardness” and “softness” are relative and the designation of a rigid impactor or a rigid structure is not identical for all studies that examine the effect of impact on RC structures. Consequently, they showed that the characterization of soft and hard impacts is related to the structure failure mode and to the fact that the impactor penetrates or not the structure. They indicated that in the case of soft impacts, failure occurs due to a shear cone failure mode, the structure is not damaged and the impactor is crushed. On the contrary, perforation is a consequence of a local failure and the impactor penetrates the structure for hard impacts.

In order to define an impact type, the new criterion of Koechlin and Potapov consists in comparing the structure compressive strength  $\sigma_s$  with the stress applied by the impactor during impact. This latter stress represents the sum of the impactor limit strength  $\sigma_i$  and a second component that depends on the impactor density  $\rho_i$  and velocity  $v_i$ . This criterion allows verifying if the structure withstands the impact and is expressed by:

$$\sigma_s = \sigma_i + \rho_i v_i^2 \quad (2.6)$$

Equation (2.6) can be written in terms of non-dimensional parameters, which permits to compare impacts at different scales and gives the boundary between hard and soft impacts (Figure 2.6):

$$\frac{\sigma_i}{\sigma_s} + \frac{\rho_i v_i^2}{\sigma_s} = 1 \quad (2.7)$$

This boundary provides the type of failure that could occur during impact and specifies whether the structure fails due to a direct perforation or a punching shear. In other words, it represents the boundary between the potential global and local failure modes.

Numerous experimental studies were carried out to assess the effect of soft and hard impact on the concrete behavior and the response of RC structures. Koechlin and Potapov presented and classified these tests using their new criterion that is based on an explicit graphic representation as shown above. Few experimental tests that were considered by their authors as soft impact are available in the literature, namely EDF tests [51] and Meppen tests [90, 140, 141, 162]. The classification of these experiments as soft impact is in accordance with Koechling and Potapov new classification. The EDF tests constituted a part of a research program that was initiated by EDF (Eléctricité de France/ French Electric Power Company) in order to analyze the nonlinear response of RC slabs subjected to short time accidental loads due to soft missiles impact. The main purpose of EDF tests was to deduce some practical rules for plastic design and reduce the reinforcement

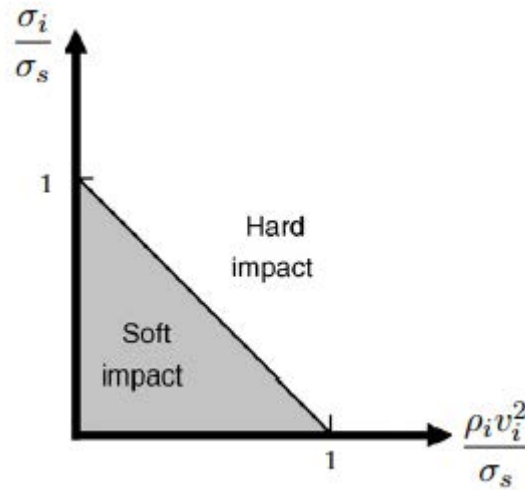


Figure 2.6: Classification of low velocity impacts according to Koechlin and Potapov [95]

ratio with ensuring that no failure or even large deflection would occur during impact. The full scaled Meppen tests consisted in a series of 21 RC slabs impacted by highly deformable missiles and aimed to assess the safety of containment buildings of German nuclear power plants against potential aircraft impacts. Meppen tests examined the effect of some parameters such as bending and shear reinforcement ratios, the impactor velocity and deformation, and the slab thickness on the bending and shear bearing capacities of slabs. They proposed a validation of methods that are usually applied to analyze aircraft impact loads with regard to the structural design.

Other experiments with soft missiles [97, 147, 166, 167] were incorrectly referred as soft impact due to the reason that the impactor is deformable. However, Koechlin and Potapov found that, according to their criterion, these tests must be classified as hard impact since the failure mode of slabs is similar to the hard impact one. Kojima tests [97] were performed in the aim of investigating the local behavior of RC slabs subjected to missile impact with varying the missile and slabs properties. Soft-nosed and hard-nosed missiles were used to study the degree of slab damages in both cases, while critical reinforcement ratio and slab thickness were evaluated in order to analyze slabs resistance to impact and prevent perforation. Ohno *et al.* [147] investigated experimentally the effect of missile nose shape on the local damage of RC slabs when impacted by deformable missiles. Five shapes of missiles were used for the impact tests and empirical formulas for perforation and scabbing were developed. The investigations carried out by Sugano *et al.* [166, 167] are among other experimental studies that examined local damage caused by deformable missiles impact on RC structures. Sugano *et al.* tests showed that reduced and full scale tests give similar results and that reinforcement ratio has no effect on local damage.

Moreover, it should be noted that tests performed by Kojima [97] and Sugano *et al.* [166, 167] with rigid missiles were also classified as hard impact by Koechlin and Potapov, which is in accordance with Eibl classification. CEA-EDF experiments [61, 71, 77] were also considered as hard impact for both criteria. They were performed by CEA (Commissariat à l'énergie atomique et aux énergies alternatives/ French Alternative Energies and Atomic Energy Commission ) and EDF to predict the perforation limit of RC slabs subjected to rigid missile impacts with varying slabs thickness, concrete strength, reinforcement ratio and impact velocity. Likewise, Koechlin and Potapov described impacts with high velocity as hard impacts, which is in agreement with the usual observations of Bischoff and Perry [22].

### 2.2.3 Failure modes

Structures subjected to impact loading show different behavior compared to that under static load, as a result of the transient and localized properties of impact loading. Furthermore, dynamic properties of materials are different than those under static loading and may be affected by the strain rate or load rate. Therefore, a solid understanding of this type of structures behavior under an impact event is essential to develop a satisfactory design and prevent their collapse. The prediction of the behavior of RC slabs when they are subjected to impact loading is of considerable complexity since impact event involves several phenomena and slabs have been observed to react both locally and globally. Failure modes of slabs during impact change with time and are influenced by stress waves and inertial forces. The impact behavior of concrete is also considered as quite complicated due to heterogeneity of material. Several parameters may significantly influence the impact response of RC slabs:

- Type of impact plays a role in dissipating energy.
- Slab dimensions and boundary conditions control the stiffness of the slab.
- Material properties have a significant influence on the slab transient response by affecting the contact and overall slab stiffnesses.
- Impactor characteristics including impact velocity, shape, position, mass and rigidity influence the impact dynamics.

Changes in slab stiffness arise from cracking or crushing of concrete, yielding of reinforcement, or other mechanisms such as local unloading behaviors and post-cracking dilation [84].

A RC slab subjected to a dropped object will be exposed to a transient dynamic load. As a result, both local and global dynamic response of the slab can be induced. The identification of the various modes of failure that occur during impact is important to correctly evaluate the dynamic response. The elastic-plastic response of RC slabs may cause two main overall response failure modes: flexural failure or punching shear failure [119] (Figure 2.7). At flexural failure mode, the slab bends strongly and fails due to excessive tension stresses which lead to the formation of cracks through the RC slab thickness and yielding in tension reinforcement. At the punching shear failure mode, a shear cone that engenders tensile stresses within the transverse steel is created and the slab fails due to excessive shear stresses. The kinematic mechanism of punching was described by [173] for a static load: the application of an increasing load to a RC slab presents a roughly circular crack that appears around the loading zone on the slab tension surface and propagates subsequently into the compressed zone of concrete. Then new flexural cracks arise and inclined shear cracks are observed. The further increase in load develops curved shear cracks which affect steel in tension and compression zone. Punching shear mode is characterized by brittle response with minimal tension cracking damage and little or no yielding of reinforcement [130]. However, an intermediate failure mode between flexural and punching shear failure modes can also be expected [8]. A combined flexure-shear failure mode is characterized by a flexural failure at the early stages of loading followed by a transition into the punching shear failure mode.

The local damage of impacted slabs can be divided into four local failure modes: surface crushing, spalling of concrete and formation of a crater on the impacted surface, scabbing of the rear face and perforation [138] (Figure 2.8). The severity of the local damage is primarily dependent upon the velocity of the impactor [93]. According to [92, 138] when the impactor strikes the slab for low impact velocities, a failure surface mode occurs. At failure surface, concrete is fallen off the impacted face of the slab at and around the impact zone. The impactor penetrates the slab to low depth and then bounces back. The further increase in velocity causes ejection of concrete from the upper surface and spalling occurs producing a spall crater in the surrounding zone of impact. The impactor penetrates

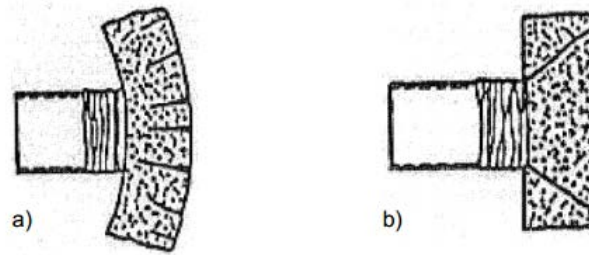


Figure 2.7: Overall response failure modes of impacted RC slabs [119] : a) Flexural failure, b) Punching shear failure

deeper into the RC slab without causing any effect on rear face [93] and sticks to the slab rather than rebounding. Spall crater surface is generally greater than the impactor cross-sectional surface and depends upon the mass, velocity and shape of the impactor. Normally, impactors with low velocity cause more spalling with a bigger spall crater than for high velocity cases [109]. As the impactor velocity increases further, scabbing arises on the rear face and pieces of concrete will be spalled off the back surface of the slab. Since concrete is very weak in tension, scabbing takes place when the tensile stresses generated by the tensile reflected wave produced during impact become equal or higher than the concrete tensile strength. Generally, scabbing shows a wider zone and higher depth than spalling and indicates that concrete has no further strength remained to resist more local impact effects [109]. If the impactor velocity is high enough the impactor will perforate the slab and exit from its rear face with residual velocity. Perforation is the last process of damage due to impact event and is caused by extending penetration hole through scabbing crater. The local damage failure modes are caused by stress wave response and usually occur in conjunction with the two overall response failure modes.

The evaluation of each of the above failure modes is completely difficult either experimentally or numerically. For example, complete perforation usually takes place under high-velocity impact when slab deformations are localized in the impact zone, but it can also be achieved under low-velocity impacts after the slab reaches its overall deflections [9]. Spalling and scabbing generally occur during bending failure, while they cannot be observed during a full penetration [189]. These failure modes must be taken into account when designing RC slabs under impact: it is obvious that flexural failure mode represents the critical parameter to design longitudinal reinforcement, punching shear is important to determine shear reinforcement, while spalling and scabbing helps to evaluate the appropriate concrete properties [19].

The onset and growth of damage in slabs represent another aspect that should be treated as well to a better understanding of slabs dynamic behavior under impact, since the main orientation of major cracks can be helpful to distinguish the corresponding failure mode during impact event. According to Abrate [9] that studied the impact on composite structures, during a low-velocity impact event, two types of cracks are observed, namely tensile cracks and shear cracks. Tensile cracks are created by tensile flexural stresses and appear when in plane normal stresses exceed the concrete tensile strength. Shear cracks are inclined relative to the normal to the midplane and indicate a significant role of shear stresses. Cracks initiate the damage process and follow a complicated and irregular path in concrete. For thick slabs, cracks are first induced on the upper surface subjected to impact as a result of high and localized contact stresses, then they progress from the top downwards. For thin slabs, cracks are induced on the bottom surface due to bending stresses, which leads to a reversed shear cracks pattern. Therefore, a detailed prediction of final cracks pattern is very difficult, but it is not necessary since its shape has no important contribution on the reduction in slab residual properties.

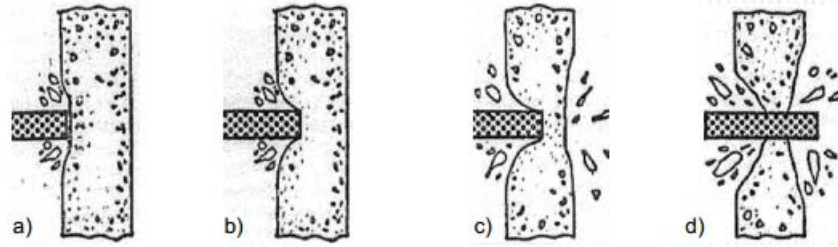


Figure 2.8: Local damage failure modes of impacted RC slabs [119] : a) Surface failure, b) spalling, c) scabbing, d) perforation

Zineddin and krauthammer [189] performed an experimental study in the aim of understanding the dynamic behavior of structural concrete slabs under impact loading. It was shown that the failure modes of slabs are dependent on the rate of the applied load, i.e. static or quasi-static loading favors a global bending mode while for harder and shorter impact the local response could dominate the slab behavior with a likelihood of punching mode. In case of soft impact, a direct shear failure could take place at the boundary conditions due to high stresses. These results are in agreement with Miyamoto and King [130] study that also considered the effect of loading rate on slab failure mode. Miyamoto and King proposed a dynamic design procedure for RC slabs subjected to soft impact loads and found that failure modes are affected by loading rates, slabs fail under flexural mode for low loading rates while the punching shear failure is dominant for higher loading rates. The experiments of Zineddin and Krauthammer showed also that the response of a slab is affected by the amount of steel reinforcement and the drop height (i.e. the impact velocity), RC slabs may change their failure mode from a flexural failure at low drops to punching one under higher drops. As well, Martin [119] indicated that the overall response failure of a RC slab depends upon the impactor velocity and reinforcement strength: for lower impact velocities flexural failure is more likely while for high impact velocities punching shear failure occurs; for a strong reinforcement flexural failure is more likely and for a weaker one punching shear failure takes place. However, reinforcement ratio shows an adverse effect on RC slabs behavior under impact, as indicated by Abbasi *et al.* [8]. Abbasi *et al.* mentioned that for weakly reinforced slabs failure is identified by a global and pure flexural mode with a measure of ductility due to reinforcement plasticity, whereas increasing reinforcement ratio enhances the punching capacity and slabs may fail under combined flexural-shear mode for medium levels of reinforcement and under punching shear mode for high reinforcement ratio.

## 2.2.4 Energy considerations

An impact event can be defined as an interaction of two bodies where mechanical energies are transformed. Miyamoto and King [130] mentioned that the energy criterion would be the most efficient method of designing concrete structures under impact loads, especially for a flexural failure mode. They show that structural failure of a concrete structure subjected to impact likely occurs if the structure is not capable of absorbing all of the energy transmitted during impact. Therefore it is necessary to examine the energy balance, especially in case of evaluating the results of numerical impact analyses. As illustrated in Figure 2.9, before the impact there is only the impactor kinetic energy of which the main part is then transmitted to the RC slab when the impactor hits the slab. After impact a small part of the impactor kinetic energy is transferred to slab as kinetic energy due to slab vibrations that occur as a result of impact, while a considerable part of this energy is converted into the energy absorbed by the structure. The energy not transmitted into the structure is progressively converted into elastic and plastic strain energy in the impactor as a result of its elastic and plastic deformation. The energy absorbed by the RC slab involves irrecoverable (plastic) energy

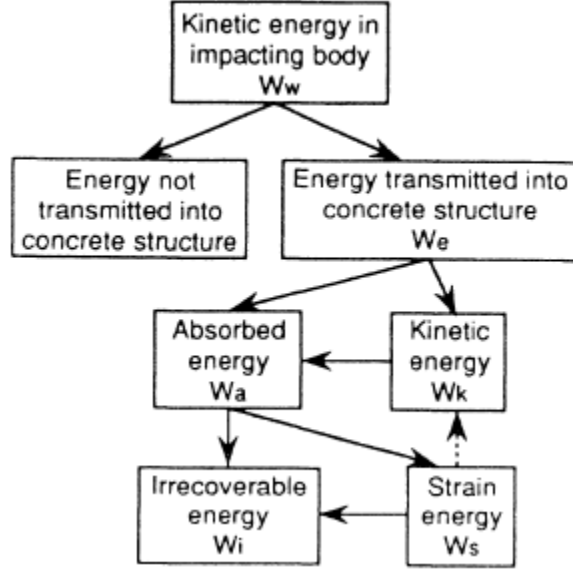


Figure 2.9: Energy transformation process during an impact event [130]

and recoverable strain (elastic) energy. These energies are absorbed by the mechanisms of concrete and reinforcement [92], as well as elastic and plastic parts of strain energy in slab are associated with its deformation after impact [119]. A part of the recoverable strain energy is subsequently re-transmitted to slab as kinetic energy in response to slab vibrations, as indicated in Figure 2.9 by a dashed line. In addition to plastic deformation, the irrecoverable energy in RC slabs results from the formation of cracks, friction and damping. Thus, a part of the initial kinetic energy of the impactor is dissipated as damage energy due to concrete damage and as viscous energy due to viscous damping inside the RC slab.

Martin [119] indicated that an energy balance of an impact on a RC slab can be written as follows:

$$E_{kin0}^I = E_{kin1}^I + E_{str1}^I + E_{kin1}^S + E_{str1}^S + E_{dam}^S + E_{vis} \quad (2.8)$$

with

$E_{kin0}^I$  = kinetic energy of impactor before impact

$E_{kin1}^I$  = kinetic energy of impactor after impact

$E_{str1}^I$  = strain energy of impactor after impact

$E_{kin1}^S$  = kinetic energy of concrete slab after impact

$E_{str1}^S$  = strain energy of concrete slab after impact

$E_{dam}^S$  = damage energy due to damage of concrete

$E_{vis}$  = viscous energy due to viscous damping

Miyamoto *et al.* [133] found that the kinetic energy transmitted to a RC slab structure by an impacting body as well as the energy absorbed by the structure are affected by the final structural failure mode and RC slabs may respond in several ways as indicated by [84]. For overall response failure modes the energy absorbed is due to global structural bending or shear deformations of the slab, while the main part of impact energy is dissipated through local damage mechanisms for local response failure modes. In case where both local and global dynamic response of the slab are involved, the initial kinetic energy of impactor is dissipated through a combination of structure deformations and local damage mechanisms. Moreover, Miyamoto *et al.* indicated that the energy absorbed by slabs under flexural failure mode is higher than in case of punching shear failure mode

which results in less energy being dissipated. The process of dissipating energy is also affected by mechanical properties of the RC structure and the impactor, it can vary significantly depending upon the type of impact event (hard or soft) [84, 119]. Therefore, the energy transformation process of the impactor kinetic energy to different forms of energy mentioned in equation 2.8 is influenced by the impactor velocity, the slab rigidity and the reinforcement of the concrete slab; e.g. in case of a strongly reinforced slab subjected to a soft impact with a high initial velocity, the majority of the impact energy is converted into strain energy of the impactor [119]. The impactor shape and size have also a considerable effect on the energy absorption mechanism since failure modes can be quite different, consequently impactors with nose shape dissipate more energy during penetration than flat impactors and the energy absorbed during a perforation failure mode increases with impactor diameter [9].

## 2.3 Methods to determine the response of RC slabs under impact

This section presents the three approaches that are usually used to determine the global and local dynamic responses of RC slabs subjected to impact loading. Several studies from the literature that are considered as important investigations in the context of impact phenomenon effect on RC slabs are also presented for each approach. These three approaches can be classified as follows:

- Experimental methods based on either laboratory or field studies and leading to empirical formula;
- Simplified analytical solutions such as spring-mass system;
- Advanced numerical approaches such as finite element method.

### 2.3.1 Experimental approaches

This approach, based on either laboratory or field studies, is considered to be fundamental for extending the understanding of the dynamic behavior of RC slabs under the action of impact loading. The main aim of this approach is to study the actual response of the slab including the development of crack patterns and the resulting failure modes. Various data can be gathered from tests such as the variation of the impact load with respect to the slab deflection, the impactor acceleration, the reactions at supports and the reinforcing steel strains. Experimental data are important for validating analytical and numerical models. The accuracy of the measurement of physical parameters depends on observations and the equipment used to store data from the test. Empirical expressions which are derived from experimental data are especially important due to their simplicity to represent the complex impact phenomena and can be useful to get a first order approximation of impact effects.

However, experimental approach is not a cost-effective practicable solution since it requires a series of full-scale tests in order to perform a reliable estimation of RC structures response. This approach can be an excessively time-consuming and costly procedure, especially in terms of providing the necessary test materials and equipment.

#### 2.3.1.1 Zineddin and Krauthammer tests

Zineddin and Krauthammer [189] performed an experimental study in the aim of understanding the dynamic behavior of structural concrete slabs under impact loading, and investigating the effect of reinforcement type and the applied load on the dynamic response of RC slabs.

9 slabs of 3.353x1.524 m span and 90 mm thickness were tested and reinforced with three different types of reinforcement placed along the slabs width and length at spacing of 152 mm, as follows:

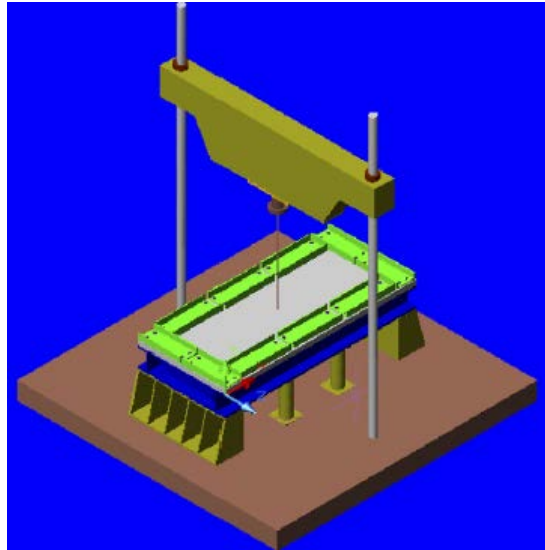


Figure 2.10: Impact test system used by Zineddin and Krauthammer [189]

- 1 single mesh of longitudinal and transversal steel bars of 9.5 mm diameter, located at slabs center with a cover of 45 mm (Reinf. 1).
- 2 meshes of welded-wire fabric with a 5 mm wire diameter, placed at a cover distance of 25 mm from the top and bottom of slab faces (Reinf. 2).
- 2 meshes of longitudinal and transversal steel bars of 9.5 mm diameter, placed at a cover distance of 25 mm from the top and bottom of slab faces (Reinf. 3).

Slabs were impacted with a cylindrical drop hammer with a 2608 kg mass and 250 mm diameter. The impact mass was dropped from different heights of 152 mm, 305 mm or 610 mm at the center of slabs in order to examine the variation of slab failure modes under low and high drop heights. Slabs were supported on a stiff steel frame of 305 mm width and bolted on all four sides of the top face with steel channels of the same width (Figure 2.10). Zineddin and Krauthammer mentioned that boundary conditions could be described as somewhere between simply supported and fixed.

Output that were gathered from these impact tests included impact force-time history, slab deflection, reinforcement strains, as well as accelerations that were measured for the slab, the steel frame and the impact mass. Cracks propagation was also examined by means of high-speed videos.

Zineddin and Krauthammer studied the transition of slab behavior modes in term of force-time history curves and indicated that, according to these curves, four stages could be distinguished:

1. Slab resistance to the impact load as an elastic plate, followed by concrete failure at the impact zone.
2. Reinforcement resistance with severe cracking of concrete around the perimeter of the impacted zone.
3. Steel yielding that started in bars under the impact mass and propagated radially in the non-impacted zone.
4. Increase in the slab deflection at the center, which may lead to a concrete ejection or slab perforation.

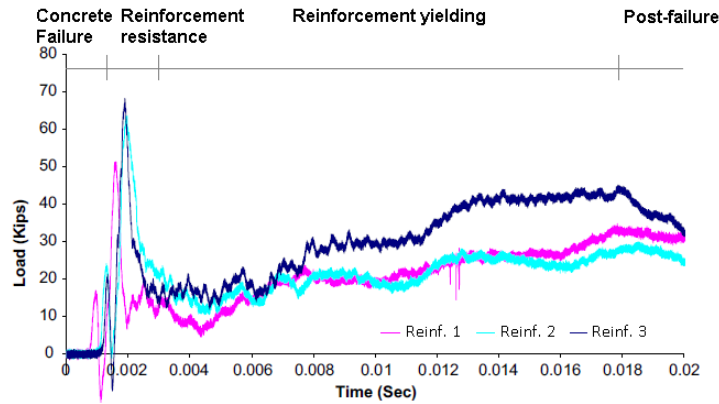


Figure 2.11: Load-time history for slabs impacted with a drop height of 152 mm [189]

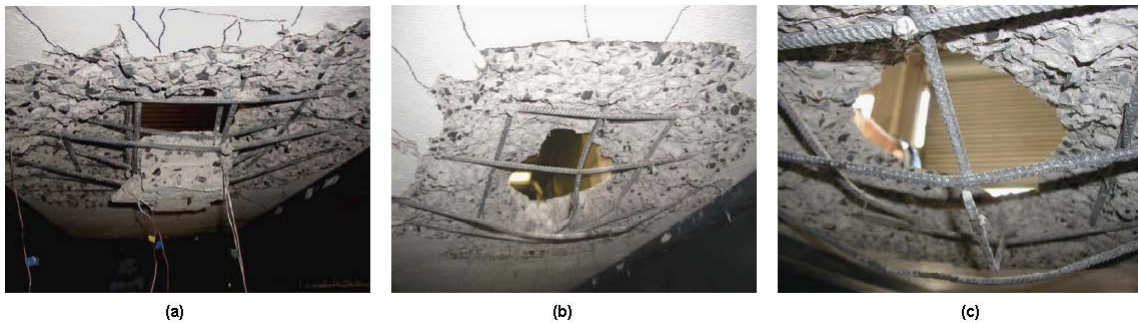


Figure 2.12: Failure mode of slabs impacted with a drop height of 610 mm and reinforced with reinforcement type: (a) Reinf. 3, (b) Reinf. 1, (c) Reinf. 1-Failure of one steel bar [189]

Figure 2.11 shows these four stages for 3 slabs with 3 different types of reinforcement and impacted with a drop height of 152 mm. These curves indicate that slab response is affected by reinforcement type and, particularly by reinforcement ratio. Although all curves had a similar shape, the peak load for slab with lower reinforcement ratio (Reinf. 1) was not significant as the peak for other slabs and was reached at earlier time. Reinforcement ratio had also an important influence on slab failure modes, as can be seen in Figure 2.12 which presents the failure modes of two slabs impacted with a drop height of 610 mm but with different reinforcement ratio. In fact, slabs with more steel reinforcement showed a localized punching shear failure (Figure 2.12.a), whereas slabs with less steel reinforcement failed by brittle failure of concrete with a considerable amount of debris ejected from the bottom surface (Figure 2.12.b). Reinforcement bars were yielded for both slabs, but one longitudinal steel bar was cut in the case of slab with lower reinforcement ratio (Reinf. 1) due to the excessive shear failure that occurs at the impact zone and to its location at the mid-thickness of the slab (Figure 2.12.c).

Zineddin and Krauthammer found that slabs response was also affected by drop height of the impact mass, hence RC slabs may change their failure mode from a flexural at low drops to punching one under higher drops. Slabs impacted with the lower drop height of 152 mm were designed in the objective to fail by flexural failure mode regardless of their reinforcements. Nevertheless, only slab reinforced with Reinf. 3 type underwent flexural failure with large cracks on the bottom surface, and the two slabs reinforced with Reinf. 1 and Reinf. 2 types failed in a brittle manner since the change in the failure mode was compensated by the strength increase due to the loading rate. For

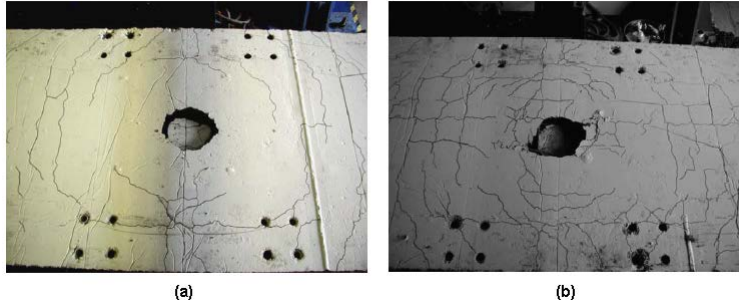


Figure 2.13: Cracks patterns on top surface of slabs reinforced with reinforcement type Reinf. 3 and impacted with a drop height of : (a) 305 mm, (b) 610 mm[189]

Slab no.	Striker mass ( <i>kg</i> )	Impactor	Impact velocity ( <i>m/s</i> )
1	98.7	Hemispherical	6.5
2	98.7	Hemispherical	6.5
3	98.7	Flat	6.5
4	98.7	Hemispherical	8.0
5	196.7	Hemispherical	8.7
6	382.0	Hemispherical	8.3

Table 2.1: Details of impact tests

higher drops, a local failure mode dominated the behavior of slabs. Consequently, tests performed with 305 mm and 610 mm drops showed a punching shear failure with a smaller punching shear hole and more cracks at the top slab surface for higher drops (Figure 2.13)

### 2.3.1.2 Chen and May tests

A series of experiments were carried out on several RC slabs under drop-weight loads at Heriot-Watt University by Chen and May [34]. The aim of these impact tests was to investigate the behavior of RC slabs subjected to high-mass, low-velocity impact and to provide sufficient input data with high quality for the validation of numerical procedures.

Six square slabs were tested under impact loads using a drop-weight impact system. Four 760 mm square slabs with a depth of 76 mm (Slabs 1-4) were reinforced with 6 or 8 mm diameter high yield steel bars at the bottom and the top with a concrete cover of 12 mm. Slab 5 and Slab 6 were 2320 mm square and 150 mm thick and reinforced with 12 mm diameter high yield steel bars at the bottom and the top with a concrete cover of 15 mm. The slabs, shown in Figure 2.14, consisted of two parts: a reinforced concrete region surrounded by a steel support of 17.5 mm width, where the support was clamped at the four corners to restrain horizontal and vertical displacements (Figure 2.14.c).

The striker that struck the slabs was released with a velocity of up to 8.7 m/s and consisted of a mass, a load cell and an impactor. The tests were performed with a striker mass of up to 380 kg and a stainless steel hemispherical impactor of a 90 mm diameter dropped at the center of slabs (Figure 2.15a), except for Slab 3 which was impacted by a mild steel cylindrical impactor of a 100 mm diameter (Figure 2.15b). Although the vertical movement of the impactor was not restrained and a second impact might occur after a rebound, only the first impact of duration of 20-30 ms was considered to study the slabs behavior. Table 2.1 summarizes the details of impact test for each slab.

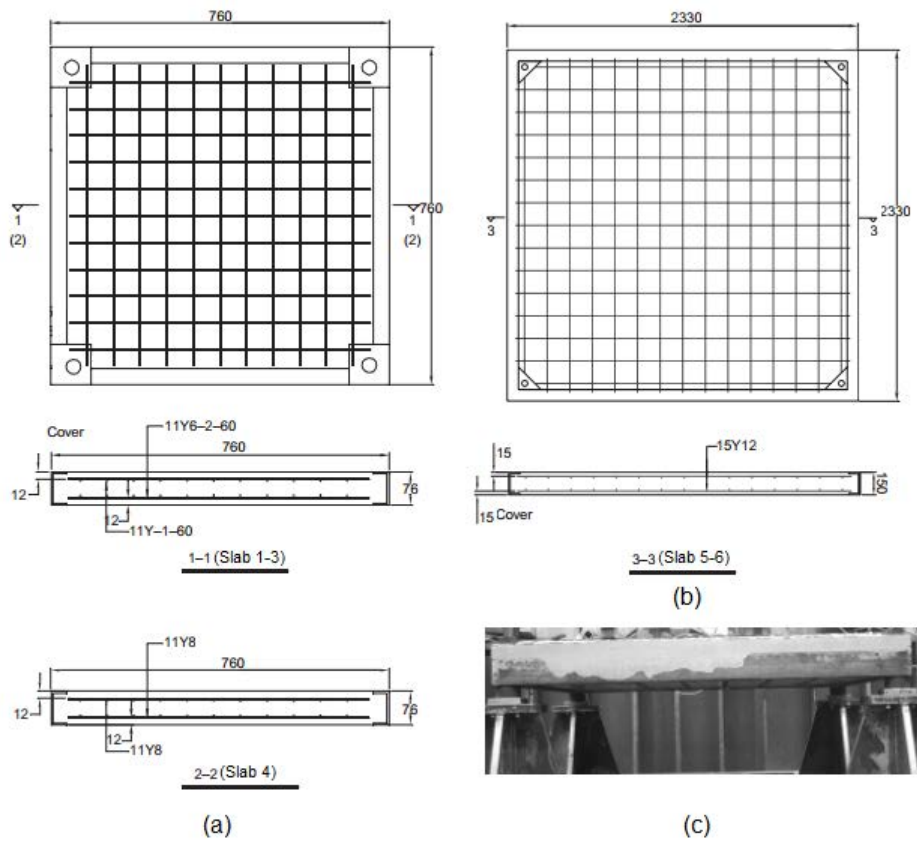


Figure 2.14: Details of slabs (dimensions in mm): a) 760 mm square slabs, b) 2320 mm square slabs, c) Boundary conditions [34]

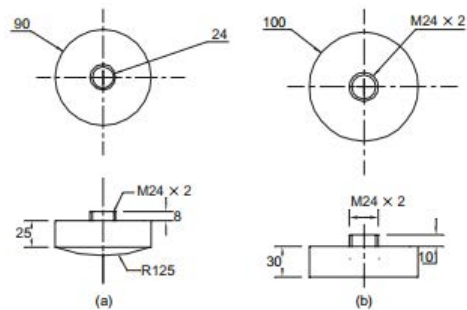


Figure 2.15: Details of impactors (dimensions in mm): a) Hemispherical impactor, b) Cylindrical impactor [34]

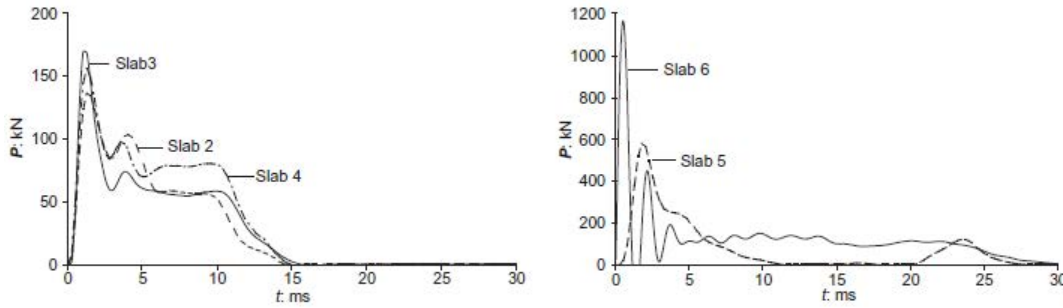


Figure 2.16: Transient impact load of slabs 2-6 [34]

These experimental studies, considered as well monitored, allowed gaining a better understanding of the impact behavior of RC slabs. The transient impact force-time histories were determined using a load cell placed between the mass and the impactor. Strain gauges placed inside bars and accelerometers were used to measure transient reinforcement strains and accelerations, respectively. Experimental output were sampled at a rate of 500 kHz and filtered with a Butterworth filter using a cutoff frequency of 2 kHz. The local impact response of slabs was recorded with a high-speed camera to show the development of failure modes in terms of cracking, scabbing and spalling.

Impact force-time histories show a plateau for slabs 2, 3, 4 and 6 after reaching the peak load (Figure 2.16). The presence of this plateau is related to the fact that local failures due to penetration and scabbing, accompanied by reinforcement yielding, were observed. As can be seen in Figures 2.17.d and 2.17.e, scabbing was not fully developed for slab 5 while more scabbing was observed on slab 6 which have the same geometric and material properties as slab 5, but impacted by a higher mass. Moreover, these two slabs of 150 mm thick show a less amount of concrete debris ejected due to scabbing than the 76 mm thick slabs. For slab 4 which is similar to slab 2 but impacted with a higher velocity, a significant amount of penetration of the impactor in the slab occurred, indicating that the thickness used was not sufficient to prevent penetration for velocities higher than 6.5 m/s (Figure 2.17.c). As illustrated in Figures 2.17.a and 2.17.b, the size and shape of scabbing zone could be affected by the impactor shape since the stress wave caused by the progressive contact between the impactor and the slab could propagate more uniformly in the case of a hemispherical impactor. Thus, the scabbing zone on slab 2 bottom face caused by the hemispherical impactor had a more circular shape than that created on slab 3 with a flat impactor.

From these experimental investigation results, it can be seen that several parameters such as the slab thickness, the impactor mass, velocity and shape have a significant effect on RC slabs behavior under impact.

### 2.3.1.3 Hrynyk tests

The research program of Hrynyk [84] consisted of several tests of RC and steel fiber reinforced concrete (SFRC) slabs subjected to dynamic drop-weight impact, in the aim of verifying the accuracy of his finite element software program (VecTor4) developed on the basis of capturing shear-critical behavior for the analysis of RC structures under impact. The experimental program consisted of a series of tests of eight intermediate-scale simply supported slabs subjected to high-mass low-velocity impact. The experiments, considered as well-instrumented, investigated the behavior of RC and SFRC slabs under impact and addressed the lack of high quality data issue in the research field of RC structures under dynamic loading where limited data are available in the literature. Thus, these experiments allow obtaining a well-documented data set that might be useful to develop and evaluate any further numerical analysis of slabs under impact.

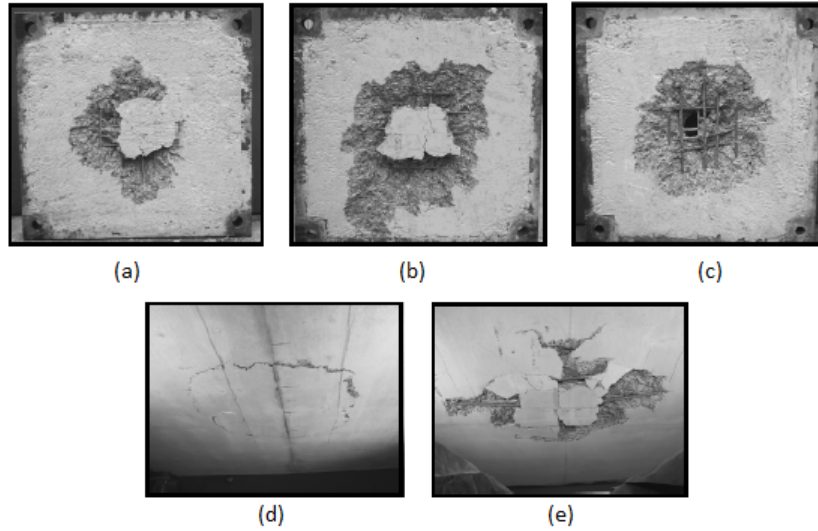


Figure 2.17: Local damage of slabs bottom faces after impact: (a) Slab 2, (b) Slab 3, (c) Slab 4, (d) Slab 5, (e) Slab 6 [34]

Table 2.2: Impact loading protocol [84]

Impact #	1	2	3	4	5	6	7	8	9	10
Drop-weight mass (kg)	150	180	210	240	240	270	270	300	300	300

Amongst the eight slabs, only impact tests of the four RC square slabs of 1.80 m width and 130 mm thickness are presented in the following section. The slabs were reinforced with top and bottom layers with equal amount of reinforcement in x and y directions ( $\rho_x = \rho_y$ ). Upper and lower reinforcing layers were joined with steel links in the corners and the center regions of slabs to prevent reinforcement movement during casting. Figure 2.18.a presents the geometry and reinforcement layers of a slab with additional links at the center that were used in the aim of stiffening the impact region. In order to reduce axial confinement effects with ensuring an overall stability boundary conditions during tests, the four corner supports were restrained to translate vertically and free to rotate in all directions, while lateral restraint conditions varied with a simple pinned support, two supports restrained to translate laterally in only one direction, and a support free to translate laterally in all directions (Figure 2.18.a). Slabs were impacted sequentially with a drop-weight of a constant velocity of 8.0 m/s but an increasing mass ranging from 120 kg to 300 kg. The contact surface of the impactor with slabs had a flat square shape of 300x300 mm and the impact was defined as hard. For all except one of the experiments, slabs were impacted with an initial mass of 150 kg which was increased for the subsequent impacts as indicated in Table 2.2. Hrynyk considered that the impact testing of slabs could be terminated in case of a completion of the impact loading protocol presented in Table 2.2, a significant decrease of the measured support reaction forces between two successive impacts, or a potential damage of the instrumentation under an additional impact.

Experimental results were obtained using detailed instrumentation and data measurement techniques such as load cells to measure reaction forces at the four corner supports, accelerometers to estimate the transverse acceleration behavior of slabs and the applied impact force, potentiometers to determine transverse and lateral slab displacements, and strain gauges to evaluate the magnitude and rate of strain in reinforcing bars. Furthermore, a high-speed video camera was used to observe cracking patterns, mass penetration and concrete scabbing.

Figure 2.19 illustrates the typical damage behavior and cracking patterns of RC slabs that were

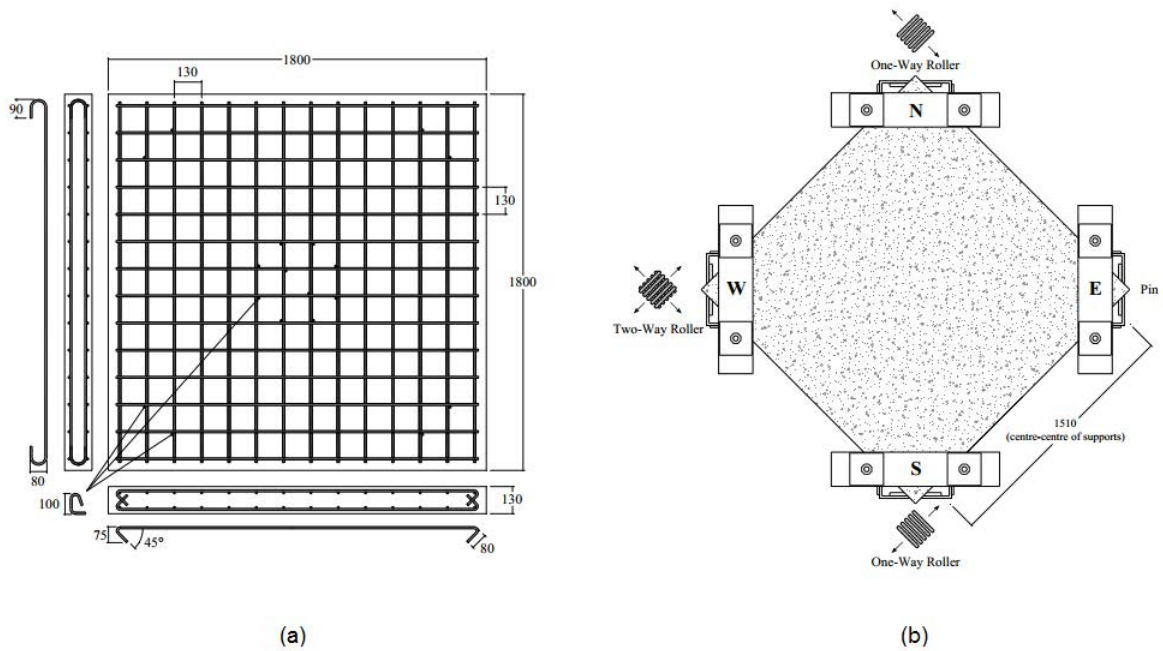


Figure 2.18: Details of slabs (dimensions in mm): a) Slab with additional links at the impact region, b) Boundary conditions [84]

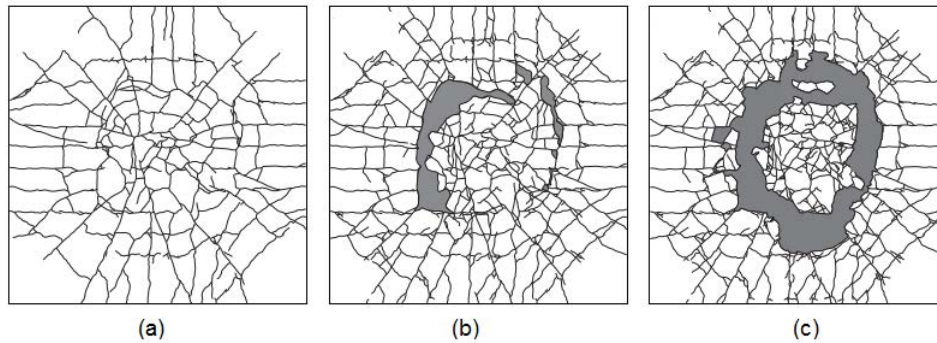


Figure 2.19: Cracking patterns on the bottom surface of a slab with a longitudinal reinforcement ratio of 0.42%: a) Impact #1, b) Impact #2, c) Impact #3 [84]

observed during three consecutive impacts with masses ranging from 150 kg to 210 kg. Cracking patterns were marked after each impact event. As can be seen, under the first impact, cracks developed circumferentially along the reinforcing bars configuration and more densely in the impact region, while no scabbing or penetration was apparent. Then a punching shear failure occurred at the location of circumferential cracks as a result of subsequent impacts, associated with extensive concrete scabbing and mass penetration.

Hrynyk varied the reinforcement ratio parameter in order to study its influence on the response of slabs. It was found that slabs stiffness increased with the reinforcement ratio while it had a limited influence on slabs capacity to absorb impact energy. The final cracking patterns of three RC slabs with different reinforcement ratio presented, for all cases, an extensive damage at the impact region with a concrete scabbing occurring on the bottom surface (Figure 2.20). The bottom reinforcement layer bars were more exposed in the case where the slab was less reinforced.

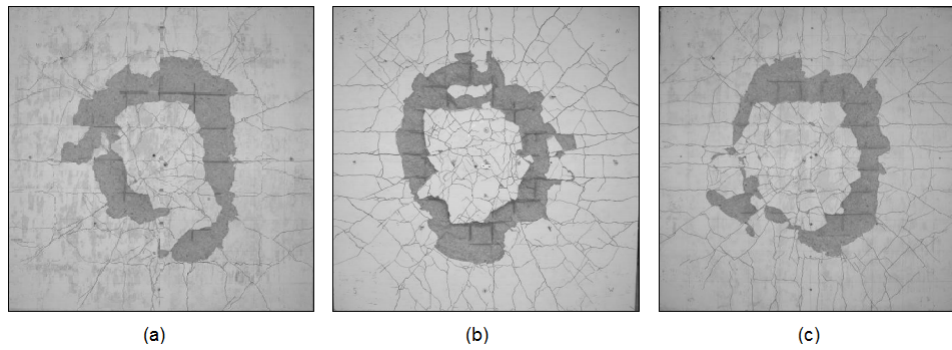


Figure 2.20: Final cracking patterns on the bottom surface of slabs with a longitudinal reinforcement ratio of: a) 0.273%, b) 0.42%, c) 0.592% [84]

It should be noted that the experimental program of Hrynyk provided all data necessary for a numerical analysis since it also included a series of tensile coupon tests to evaluate the stress-strain curve of reinforcing steel, as well as a series of concrete cylinder and bending prism tests which were performed to characterize the properties of concrete and investigate its compressive and tensile behaviors. Furthermore, in comparison to the RC slabs response, SFRC slabs showed a different behavior as the addition of steel fibers resulted in an important increase in slabs strength and post-cracking stiffness. Slabs with higher fiber volume fraction led to reduce the development of the localized punching behavior and prevented a fully scabbing of concrete from the bottom surfaces of slabs. The fiber volume fraction had a significant influence on the midpoint displacement responses, the support reaction magnitudes and the increasing of impact energy capacities of slabs that tended to fail more toward flexural mode.

### 2.3.2 Analytical approaches

In order to be able to choose an appropriate and accurate simplified model, the effect of impact on composites has been extensively studied by several researchers [10, 39, 40, 42, 41, 149]. They indicated that understanding the different types of response and the knowledge of parameters governing the response type are necessary for the selection of an appropriate analytical model. Abrate [9] specified that several analytical models may be used to predict the impact dynamics, namely spring-mass models, energy-balance models, infinite plate models and models based on plate theory. In this section, analytical mass-spring models developed in various research studies to predict the dynamic response of RC slabs subjected to low impact velocity are presented.

The analytical approach, which is commonly regarded to be the most representative simplified method to simulate an impact event between a slab and an impactor, consists in a one or more degrees of freedom mass-spring system. The slab and the impactor are modeled as two colliding masses and springs are used to represent the local and global behaviors of the slab. In the case of hard impact (the impactor is considered to be rigid), the analytical model is based on the assumption that the deformation and failure of the impactor are negligible. The local slab response is normally neglected and the approach focuses on the global response which plays an important role for low impact velocities. Analytical approaches have limited applicability since they are based on assumptions which separate the local and global response of the slab, therefore they can only be used as an initial approximation of the slab impact behavior.

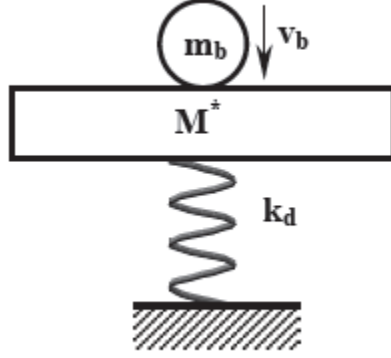


Figure 2.21: One degree of freedom mass-spring model used in Tonello IC design office [174]

### 2.3.2.1 Tonello model

Tonello IC design office used a mass-spring model with one degree of freedom to represent impact on RC slabs [174]. Their approach consisted in estimating the maximum dynamic load reached during an impact on the structure and took into account the elasto-plastic behavior of materials. Several assumptions were adopted for this model: the impact is considered as soft, the impactor stays in contact with the slab after impact (no rebound or penetration are allowed), and the slab equivalent mass is calculated based on a static bending deformation (Figure 2.21).

### 2.3.2.2 CEB model

The Bulletin of Information initiated by CEB [29] provides simplified models in the aim of helping and guiding civil engineers in designing RC structures subjected to impact. This bulletin shows that, in the case of a hard impact where the kinetic energy of the impactor is absorbed by the structure deformation, an impact problem on RC slabs can be reduced to a mass-spring model with two degrees of freedom as shown in Figure 2.22. In this case, the slab local behavior must be considered as well as its overall deformation and the two differential equations of equilibrium for the two masses can be written as:

$$\begin{cases} m_2 \ddot{u}_2 + R_2(u_2 - u_1) & = 0 \\ m_1 \ddot{u}_1 + R_1 u_1 - R_2(u_2 - u_1) & = 0 \end{cases} \quad (2.9)$$

$m_1$  and  $m_2$  represent the two colliding masses. The spring  $R_1$  represents the overall behavior of the slab and has a nonlinear force-displacement relationship which can be considered similar to a static behavior (Figure 2.23.a), while  $R_2$  represents the local behavior and simulates the contact force between the impactor and the structure. The nonlinear relationship of  $R_2$  is more difficult to determine, but can be obtained by using a nonlinear finite element code. CEB indicated that the general force-displacement relationship of  $R_2$  in the contact zone of a solid, e.g. concrete, shows an elastic compression phase in the range  $0 < \Delta u < \Delta u^1$ , followed by an elastic-plastic phase for  $\Delta u^1 < \Delta u < \Delta u^2$  where irreversible internal damage occurs (Figure 2.23.b).

### 2.3.2.3 Abrate model

Abrate [10] has presented an approach for selecting an appropriate model for analyzing the impact dynamics for each particular case. He classified models according to how the structure is modeled:

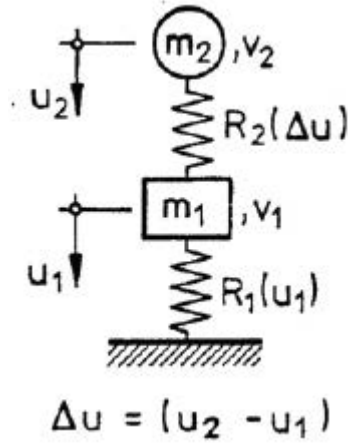


Figure 2.22: Simplified model of CEB for a hard impact [29]

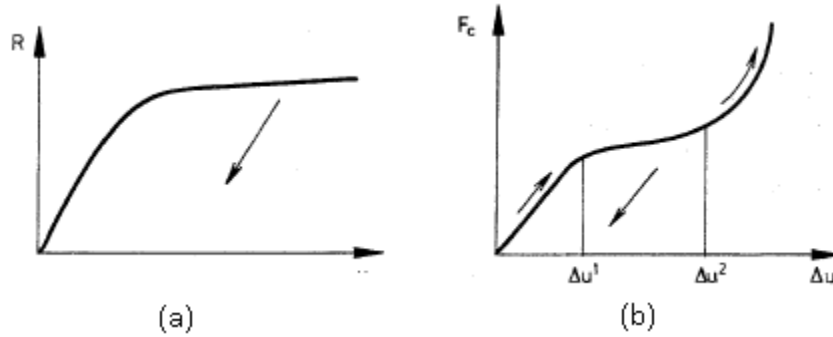


Figure 2.23: Nonlinear force-displacement relationship for spring: (a)  $R_1$ , (b)  $R_2$  [29]

spring-mass models, energy balance models, complete models, and a model for impact on infinite plates.

The complete model consists of the impactor mass  $M_1$ , the effective mass of the structure  $M_2$ , the nonlinear contact stiffness  $K$ , the shear stiffness  $K_s$ , the bending stiffness  $K_b$  and the nonlinear membrane stiffness  $K_m$  (Figure 2.24.a). This model presents two situations for which a nonlinear SDOF can provide accurate predictions of the contact force history. The first situation is when the overall deflection of the structure is negligible compared to the local indentation. In this case, the response of the structure can be modeled by the spring in Figure 2.24.b and the equation of motion is:

$$M_1 \ddot{x}_1 + kx_1^{3/2} = 0 \quad (2.10)$$

The second situation is when the membrane stiffening is significant and the deflections of the structure are large. In this case, the local indentation is negligible and the equation of motion of the nonlinear SDOF model is:

$$M \ddot{x} + k_b x + k_m x^3 = 0 \quad (2.11)$$

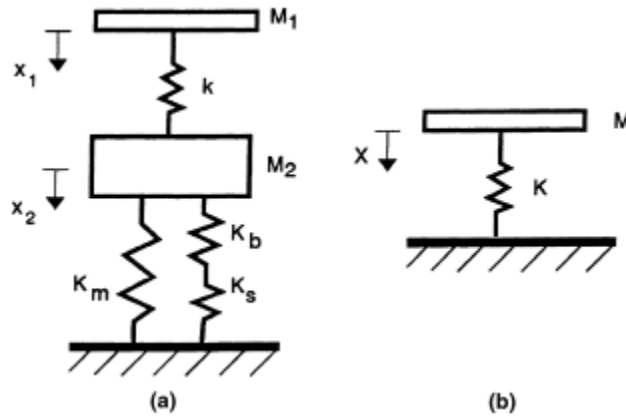


Figure 2.24: Mass-spring models of impact on composite structures according to [10]

### 2.3.2.4 Delhomme *et al.* model

Delhomme *et al.* [47] performed their study in the aim of analyzing the structural response of Structurally Dissipating Rock-shed (SDR) protective system against rockfalls by a mass-spring model. The principle of the model consisted in separating the contact phase between the block and the slab from the slab free vibration phase after impact. Thus, two “mass-spring-damper” models were generated: the “contact” model with two degrees of freedom that simulates the contact phase during the first milliseconds (Figure 2.25.a) and the “post-impact” model with one degree of freedom that simulates the free vibration phase for several seconds (Figure 2.25.b).

Delhomme *et al.* [47] indicated that  $M^*$  and  $k_s$  which represent the equivalent mass and the static stiffness of the slab, respectively, are not constant during the impact phenomenon since they depend on the slab surface in bending. Thus,  $M_1^*$  is lower than  $M_2^*$  and  $k_{s1}$  is higher than  $k_{s2}$ , since in the contact phase only a reduced surface is considered in bending, while the equivalent mass and the stiffness are calculated for the total slab surface for the “post-impact” model.

The contact was considered as an elasto-plastic in order to take into account the cracking of concrete and the Hertz contact law was used to estimate the contact force. Therefore, the equations of the “contact” model can be written as:

$$\begin{cases} m_b(\ddot{u}_b + g) + k_c(u_b - u_s)^{3/2} & = 0 \\ M_1^*\ddot{u}_s - k_c(u_b - u_s)^{3/2} + k_{s1}(u_s) + c_1\dot{u}_s & = 0 \end{cases} \quad (2.12)$$

where  $m_b$ ,  $u_b$  are respectively the mass and the displacement of the block,  $u_s$  is the slab displacement at the impact point. The contact stiffness  $k_c$  and the impedances  $c$  were derived from experimental results.

### 2.3.2.5 Yigit and Christoforou model

The model shown in Figure 2.26.a was proposed by [184] to model low velocity impact response of composite plates. In this model,  $m_s$  represents the modal mass and the impactor has a mass of  $m_i$  and an initial velocity of  $v_0$ . The plate stiffness  $K_{st}$  and the linear contact stiffness  $K_y$  account for the structural contribution and the local contact behavior, respectively. The amount of energy transferred to the structure during impact is presented by the impedance  $c$ . This full model is used for impacts that do not correspond to small or large mass impacts.

According to [42], if the size of the structure is very large and the impactor mass is very small, the impact is defined as an infinite structure impact which can be modeled as a SDOF (Single Degree Of Freedom) system, where the mass of the impactor is supported by the local contact stiffness and

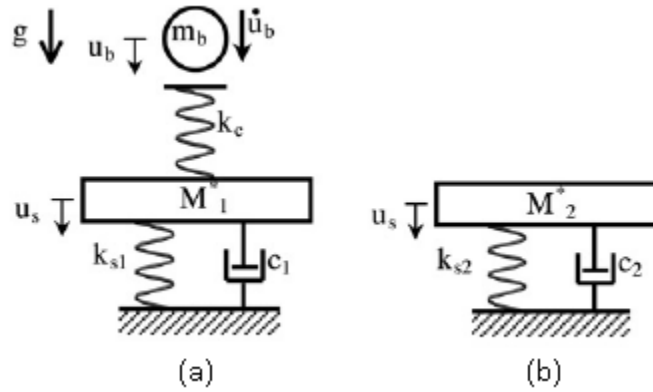


Figure 2.25: The two “mass-spring-damper” models used by [47] to analyze SDR response: (a) “contact” model, (b) “post-impact” model

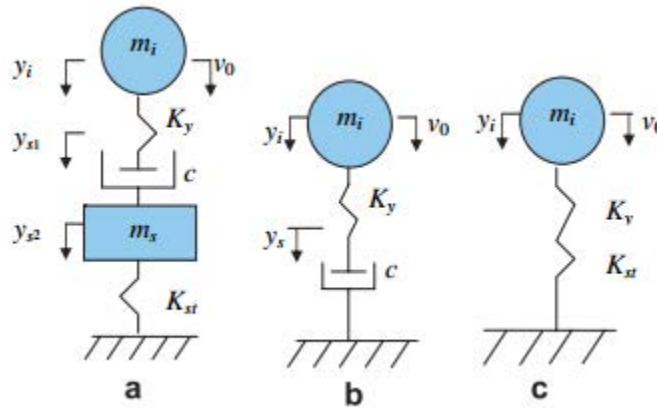


Figure 2.26: Models for low velocity impact response in structures according to [184]

the structure acts as a damping mechanism (Figure 2.26.b). During this kind of impacts, the waves are not reflected back from the boundaries.

On the other hand, if the impactor mass is very large, the mass of the structure can be neglected and the impact response can be modeled with a SDOF system, where the mass of the impactor is supported by the local contact stiffness and the static stiffness of the structure in series (Figure 2.26.c). This type of impact is defined as a quasi-static impact and its duration is relatively long.

### 2.3.3 Finite element approaches

In order to solve a complete impact problem and to gain knowledge of the physical behavior of slabs, numerical approaches such as finite element (FE) method can be considered to be more appropriate to determine the behavior of RC slabs subjected to impact loading. A three-dimensional finite element model allows modeling, as close as possible to the real case, the various aspects of any complex problem including the boundary conditions and the loads applied to the structure. In the case of impacted slabs, the RC slab and the impactor can be fully modeled and nonlinearities due to material behaviors can be taken into account. The numerical simulation of RC slabs subjected to impact loads is a complex phenomenon. Therefore an accurate simulation requires using an appropriate model for concrete and a contact algorithm which can be used in nonlinear explicit finite element

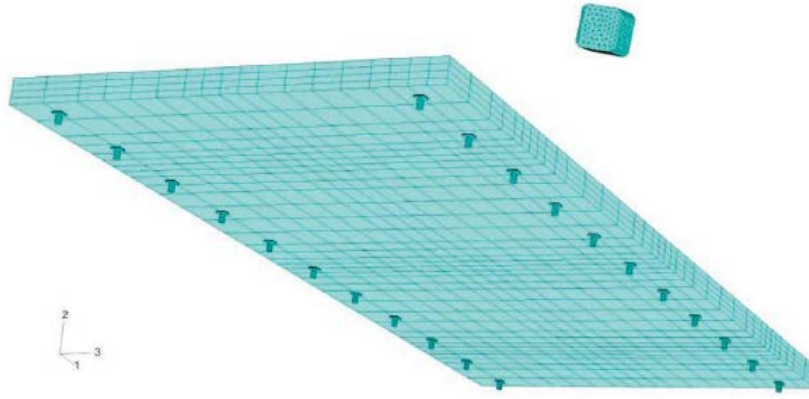


Figure 2.27: 3D FE model of SDR protection galleries proposed by Berthet-Rambaud *et al.* [19]

analysis. Once the FE model effectiveness is verified with precision, numerical simulations can replace costly full-scale tests by providing more details of the dynamic response and an expansion of experimental measurements which would be inaccessible during tests. They also provide a large output data including the stress and deformation fields and make possible to perform sensitivity analyses and parametric studies to determine the influence of one parameter or another. Despite all these advantages that can offer FE approaches, the main difficulty consists in choosing appropriately the set of numerical tools in order to accurately simulate the impact phenomenon and to identify the induced failure modes due to transient dynamic loading.

### 2.3.3.1 Berthet-Rambaud *et al.* model

Berthet-Rambaud *et al.* [19] investigated numerically the response of SDR protection galleries in order to improve their design and reduce costs in response to the increasing request of using such type of structures to provide protection in mountainous regions against rockfalls risk. These galleries are composed of a RC slab which is directly subjected to falling rock impacts, and steel fuse supports that allow transmitting slab reactions to the sub-structures and dissipating energy. Berthet-Rambaud *et al.* used ABAQUS to propose a 3D model of the slab and supports (Figure 2.27) and compared their numerical results to experimental tests that were conducted by Delhomme *et al.* [47] on a 1/3 reduced scale system model. The slab of 4.8 m wide and 12 m length was modeled and meshed with C3D8R solid elements with four layers in the thickness of 0.28 m. The slab was impacted, at various positions, by a cubic RC block of 450 kg mass and a velocity varying from 17.2 to 24.2 m/s. The block was introduced in the FE model respecting the actual block geometry of the experiments and meshed with C3D4 tetrahedral elements. The slab is supported by two lines, each with 11 steel fuse supports spaced at a distance of 1.14 m. The supports were considered with all their components in the model, but their simulation will not be detailed in the present study (for more details about supports simulation, see [19]). The slab and block reinforcements were represented by bar elements which were embedded within the concrete mesh in order to create a perfect bond between steel and concrete. Steel was modeled as an elasto-plastic material with hardening, while the PRM (Pontiroli-Rouquand-Mazars) damage model that uses one scalar damage variable [157] was used to represent concrete in the numerical simulation and was implemented in the FE code using a Fortran subroutine. The kinematic contact algorithm was adapted to model the contact between the slab and the block using “hard” contact for the normal interaction and a Coulomb-type friction law for the tangential reaction. The explicit time integration method was used to solve the problem and the Hillerborg regularization method [81] was integrated to reduce mesh dependence effects.

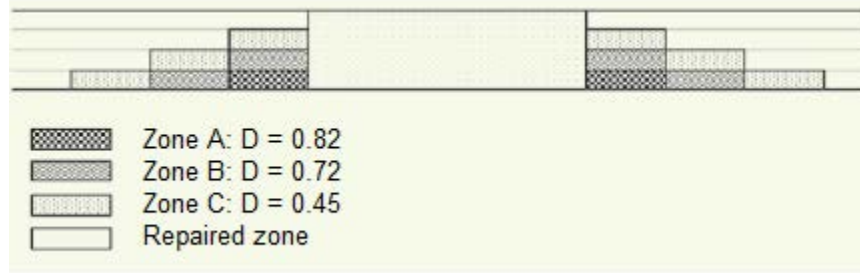


Figure 2.28: Damage distribution in and around the repaired zone [19]

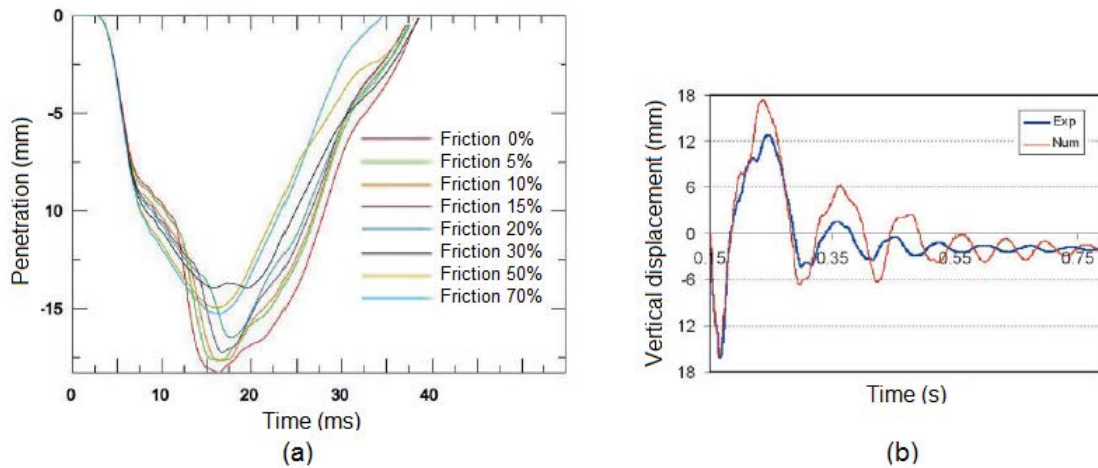


Figure 2.29: Comparison of numerical and experimental results: (a) Calibration on friction parameter, (b) Vertical displacement at a point near the impact zone [19]

An analysis of two successive impacts at the same point and under the same conditions was performed. After the first impact, the damaged zone was repaired and the damage of elements corresponding to this zone was reduced to zero. However, the potential damage on the remaining part of the slab around the repaired part is taken into account by introducing three damaged zones in the model. The damage distribution was supposed to have a cone shape that starts at the impact point and goes through the slab thickness (Figure 2.28). The effect of gravity was included in the model through a step of duration of 0.15 sec that allows a numerical gravity application before the impact step.

A parametric study on the tangential friction at the slab and the impactor interface was carried out since this parameter has a considerable influence on the sliding of the impactor corner in contact with the slab. An optimal value of 0.15 was found to be in agreement with experimental results and permitted to correctly identify the experimental impact phase (Figure 2.29.a). Following the calibration on the friction parameter, a comparison between experimental and numerical results of the vertical displacement evolution at several points of the slab proves the accuracy of Berthet-Rambaud *et al.* model in predicting the overall structure behavior. Figure 2.29.b depicts the vertical displacement of a point close to the impact zone and shows that slab oscillations were very well simulated. However, numerical amplitude values were found to be high after the first oscillation, which may be related to a general damping problem or to the complexity of boundary conditions.

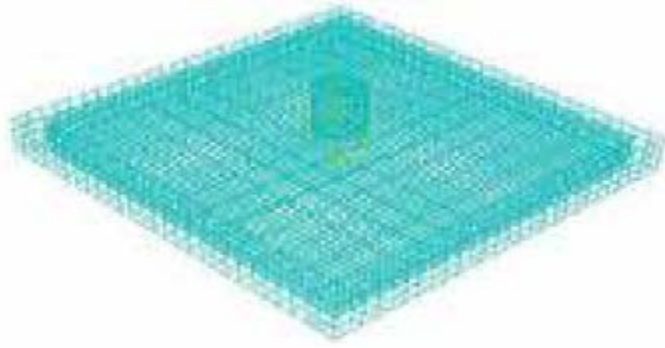


Figure 2.30: Details of finite element model of Mokhatar and Abdullah [137]

### 2.3.3.2 Mokhatar and Abdullah model

The aim of the study performed by Mokhatar and Abdullah [137] was to verify the accuracy of numerical modeling technique in assessing the response of RC slabs and the steel reinforcement failure mechanism when subjected to impact loading. A FE model was carried out using ABAQUS in order to gain a better understanding of impacted slabs behavior and was validated with Slab 3 experimental results of Chen and May tests [34] described in section 2.3.1.2. The model was divided into four main parts: the concrete region of slab, the steel reinforcement, the steel support and the steel projectile (Figure 2.30). The concrete region was modeled using eight-node continuum solid elements (C3D8R) while the steel support was considered as rigid and modeled with undeformable discrete rigid elements (R3D4). These two parts were connected to each other using the tie contact technique after assembling all elements. A proper bond action using the embedded technique was created between the solid elements of the concrete region and the two-node beam elements of steel reinforcement. The interaction between the steel impactor and the concrete region was defined as surface-to-surface contact with the kinematic contact method for mechanical constraint formulation and a friction coefficient of 0.2. Material properties, as well as stress-strain and damage curves were chosen based on several experimental works [34, 87, 169]. The increasing of concrete compressive and tensile strengths due to impact load was considered with a rate of 1.5.

The FE model was validated with experimental results using impact force-time history and the final crack pattern. First, a mesh sensitivity was performed in order to find the sufficiently refined mesh which provides a reasonably accurate result (Figure 2.31.a). Then, the transient impact load was estimated for three constitutive models of concrete, the Concrete Damage Plasticity (CDP) considered having a brittle-cracking behavior, and the Drucker-Prager and the Cap-Plasticity models characterized by their ductile behaviors. The results show that ductile models can evaluate the RC slabs behavior under dynamic impact loading and provide a good agreement with experimental results rather than brittle-cracking model (Figure 2.31.b). However, it can be seen from (Figure 2.32) that the final crack pattern obtained using the CDP model shows a good correlation with experimental results, but no effect of spallation could be observed which does not correspond to the actual slab failure mode.

### 2.3.3.3 Trivedi and Singh model

The numerical analysis performed by Trivedi and Singh [175] is among other numerical studies that focus on identifying the global and local failure modes of RC slabs subjected to impact using ABAQUS. Due to symmetry, Trivedi and Singh simulated one fourth of RC slabs of Zineddin and Krauthammer experimental tests [189] using a 3D inelastic finite element model (Figure 2.33.a).

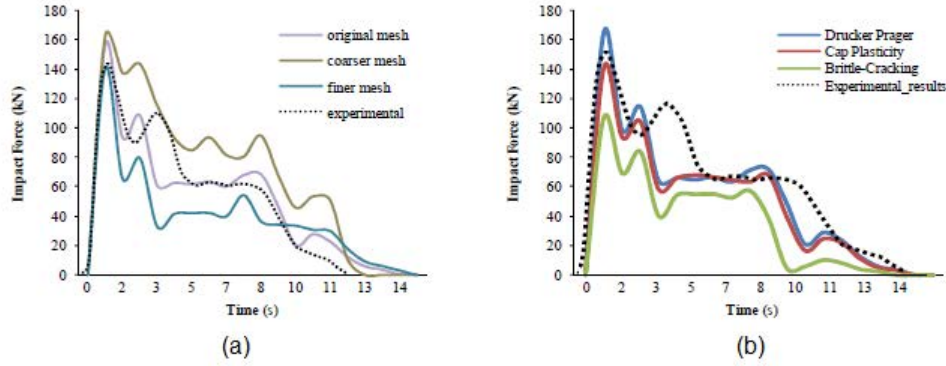


Figure 2.31: Comparison of numerical and experimental transient impact force with different: (a) Mesh densities, (b) Constitutive concrete models [137]

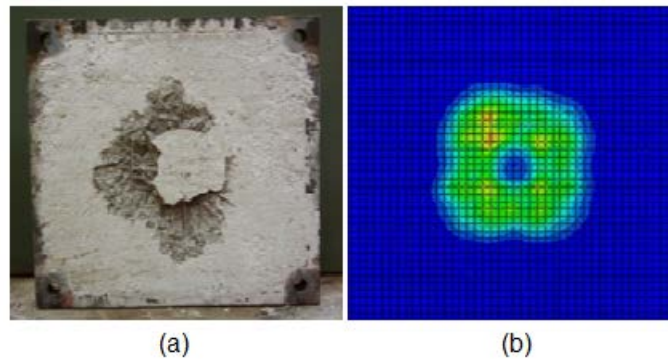


Figure 2.32: Final crack pattern of Slab3 bottom face: (a) Experimental result, (b) Numerical result [137]

As mentioned in section 2.3.1.1, slabs were impacted by a cylindrical drop hammer which was not introduced in Trivedi and Singh study, hence no contact modeling was presented. Alternatively, a time dependent pressure loading applied at the slab center was considered to model the impact loading and was distributed over a circular area with the same diameter as the hammer. The pressure loading values were calculated by distributing the peak load over the impacted zone area, while their amplitude curves in term of time were obtained using load-time histories available in Zineddin and Krauthammer study (Figure 2.33.b). The amplitude values represent the ratio of the load value at a certain time to the peak load.

Slabs were supposed to be fully constrained at the edges (no displacement is allowed in the three directions), while displacement was restrained vertically on the x-plane of symmetry and horizontally on the y-plane of symmetry. The concrete region of slabs was modeled as a 3D deformable part and meshed with 3D continuum elements, whereas reinforcement was considered as a deformable wire part and meshed with linear truss elements. No slip between concrete and steel was assumed, hence reinforcement was embedded in the concrete part defined as the host component. Material behaviors were incorporated in the FE model using the CDP model for concrete and a plasticity model for steel.

Two approaches for post-cracking softening model were used to define tension stiffening for CDP model, namely the limiting strain and fracture energy based approaches. Results showed that the fracture energy cracking criterion gave mesh independent results which were in agreement with

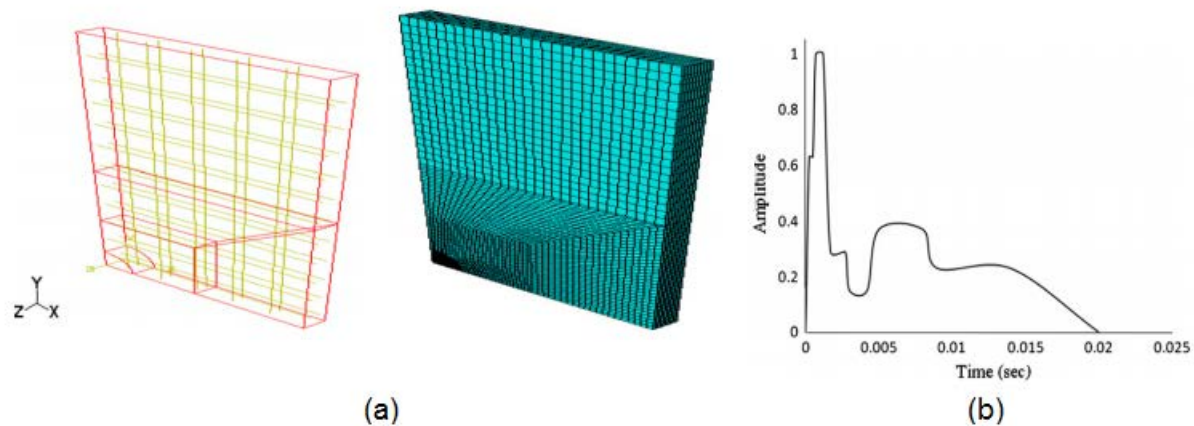


Figure 2.33: Details of Trivedi and Singh FE model: (a) One fourth of a slab with 2 meshes of longitudinal and transversal steel bars, (b) Time-amplitude curve in case of a hammer dropped with a height of 610 mm [175]

those obtained in experiments, but results using the strain criteria were inconsistent due to a mesh sensitivity problem. Therefore, Trivedi and Singh limited their discussions to the fracture energy approach and recommended its use as a robust method to study the behavior of RC structures under impact. Besides the tension stiffening, the effect of strain rate was investigated in the aim of developing an adequate nonlinear dynamic FE model. Based on Tedesco *et al.* study [172], Trivedi and Singh used a rate of 1.5 for concrete in compression and a rate in range of 1.7 to 1.75 for concrete in tension. These rates are functions of the strain rate and allow taking into account the increase in compressive and tensile strengths due to a dynamic loading. However, no significant change was observed in numerical results due to the use of strain rate, since the problem was associated with low strain rates of the order of  $10^{-4}$  to  $10^{-2}s^{-1}$ .

Trivedi and Singh studied several criteria in order to predict the failure modes of slabs, such as inflection point, limiting strain based failure, bi-axial failure, shear failure, strain in steel and tensile damage. Only some results using the first two criteria are presented here:

- Miyamoto *et al.* identification by inflection point using the slab deformed shape [131]. As can be seen in figure 2.34.a, for a RC slab with one mesh of longitudinal and transversal steel bars impacted with a height of 610 mm, the formation of an inflection point in the deflected profile indicates the transition from flexure to punching shear failure which occurs at the slab center under the impact region. A flexural mode can be identified by a smooth deflection curve with parabolic shape (Figure 2.34.b).
- Limiting strain based failure criterion by evaluating strain variations in XZ and YZ planes at various elements of concrete selected at the top and the bottom of slabs, and localized at and distant from the impact zone. Based on this criterion, a slab has a mixed mode failure of flexure and shear when strain in top elements localized at the impact zone exceeds the compressive limiting strain and the top distant elements show tensile behavior. In addition, bottom elements near the impact zone and distant elements have tensile and compressive strain, respectively. When a slab fails in flexure, elements at the impact zone show a crushing failure at the top surface and cracking failure at the bottom surface (Figure 2.35).

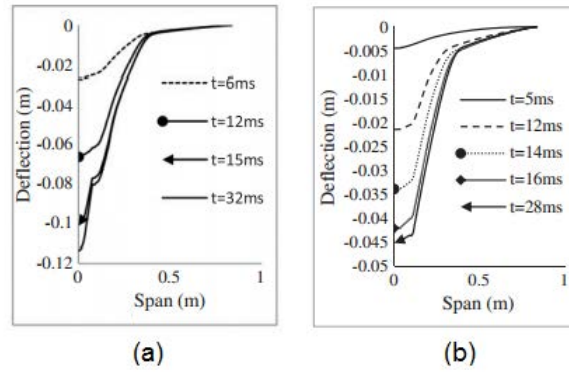
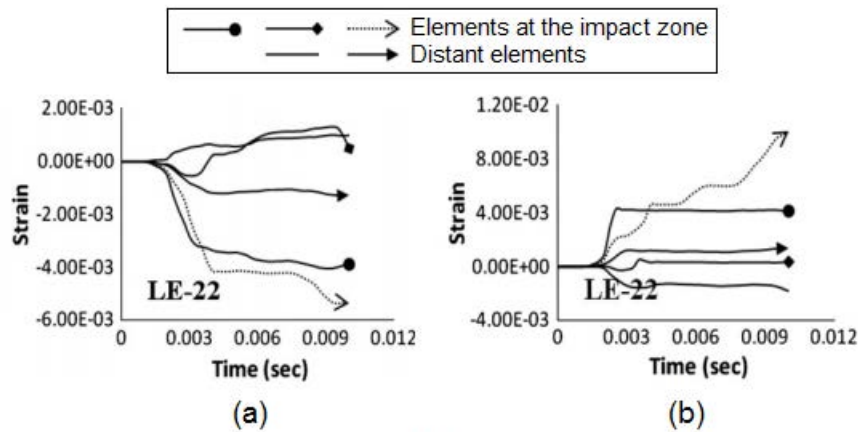


Figure 2.34: Identification of slabs failure mode by inflection point criterion: (a) Transition from flexure to punching shear, (b) Flexural mode [175]



\* Limiting strain value for concrete is 0.0035 in compression and 0.002 in tension  
 \* LE-22 is the strain in YZ plane

Figure 2.35: Identification of a slab flexural failure mode by strain based failure criterion: (a) Top elements, (b) Bottom elements [175]

## 2.4 Mechanical behavior of concrete

As a strongly heterogeneous material, concrete shows a complex nonlinear mechanical behavior characterized by softening response in tension and low confined compression. Softening is defined as decreasing stress with increasing deformation beyond the concrete compressive strength, and results in a reduction of the unloading stiffness of concrete and irrecoverable deformations localized at cracks. However, the confinement of concrete with reinforcement results in a significant increase in the strength of compressed concrete and in a ductile hardening response described by increasing stress with increasing deformations. In the current study, uniaxial compressive and tensile stress-strain curves based on experimental observations are adopted and defined in terms of concrete properties in compression and tension, respectively, as follows:

$$\sigma_c = f(E_c, f_c, f_{cu}, \varepsilon_c, \varepsilon_{c1}, \varepsilon_{cu1}) \quad (2.13)$$

Where  $\sigma_c$  represents the concrete compressive stress values calculated,  $E_c$  is the Young's modulus of concrete,  $f_c$  is the maximum compressive strength of concrete,  $f_{cu}$  is the compressive stress of

concrete corresponding to the ultimate strain,  $\varepsilon_c$  represents the concrete compressive strain value corresponding to the stress  $\sigma_c$ ,  $\varepsilon_{c1}$  is the compressive strain of concrete at the compressive strength  $f_c$ , and  $\varepsilon_{cu}$  is the ultimate strain of concrete in compression.

$$\sigma_t = f(E_c, f_t, \varepsilon_t, \varepsilon_{cr}) \quad (2.14)$$

Where  $\sigma_t$  represents the concrete tensile stress values calculated,  $f_t$  is the tensile strength of concrete,  $\varepsilon_t$  represents the concrete compressive strain value corresponding to the stress  $\sigma_t$ , and  $\varepsilon_{cr}$  is the tensile strain at concrete cracking at the tensile strength  $f_t$ .

### 2.4.1 Uniaxial compression

The properties of concrete in uniaxial compression are obtained from cylinder tests or cube tests. The nonlinear stress-strain behavior under uniaxial compressive stress, shown in Figure 2.36, is divided into three regions: linear elastic, non-linear plastic (hardening region) and post-peak stress (softening region). The first region, in which the concrete behaves almost linearly, is observed during 30-60% of the maximum uniaxial compressive strength  $f_c$ . At this level of strain, the specimen deformation is recoverable and localized cracks are initiated but they do not propagate. This could be linked to the balance of energy present in the concrete specimen which is in this case less than the energy required to create new cracks.

In the plastic regime the response is typically characterized by stress hardening followed by strain softening beyond the peak stress. Beyond the limit of elasticity, the deformation is no longer recoverable and the stress-strain curve begins to deviate from a straight line. The concrete behaves in a non-linear manner up to the peak stress and the crack system continues to grow slowly with the increasing of the applied load. During this phase, cracks cause an increase in volume and a small lateral expansion associated with Poisson's ratio effect is observed.

Immediately after the peak stress, the concrete undergoes strain softening and the lateral expansion increases dramatically with the cracks propagation. The energy released by the propagation of a crack is greater than the energy needed for propagation. The load carrying capacity of the test specimen decreases and the stress-strain curve starts to decrease until a crushing failure occurs at the ultimate strain. The shape of the stress-strain curve depends on the concrete strength which continues to behave in a linear manner up to a higher stress level than that for normal strength concrete. Also higher strength concrete must have a steeper descending curve and exhibits a brittle failure mode due to the fact that the specific fracture energy of concrete in compression does not increase much with the concrete strength.

When the concrete specimen is unloaded from any point of the strain softening branch of the stress-strain curve, the nonlinear behavior can be easily noted from the residual deformation present in the stress-strain curve. The concrete stiffness is reduced because of the increase of the internal damage which causes irrecoverable deformation in loading.

**Compression stress-strain curve without detailed laboratory test results** The way in which the concrete behaves can be accurately determined on the basis of uniaxial compression test results. However, problems arise when no such test results are available and when the only available quantities for the analysis are the compressive strength and the modulus of elasticity of concrete. Many uniaxial stress-strain relationships for concrete in compression were proposed in the literature, such as the expressions developed by [3, 4, 31, 49, 99, 116, 154, 178, 180].

**Desayi & Kirshnan formula [49]** Among many formulas proposed in the literature to represent nonlinear stress-strain characteristics of concrete, Desayi and Krishnan suggested a simplified equation that describes the ascending and descending parts of concrete compressive stress-strain curve in a single expression as follows:

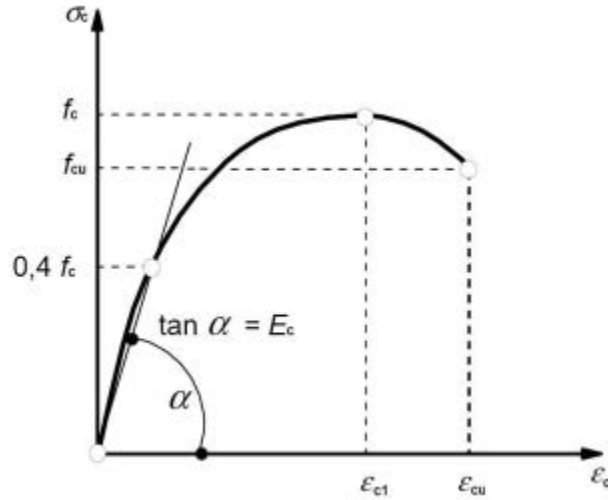


Figure 2.36: Uniaxial compressive stress-strain curve for concrete [4]

$$\sigma_c = \frac{E_c \varepsilon_c}{1 + \left(\frac{\varepsilon_c}{\varepsilon_{c1}}\right)^2} \quad (2.15)$$

**Madrid parabola [31, 32]** Considered as a good relation by CEB, the conventional “Madrid parabola” is a parabolic equation that allows defining the uniaxial stress-strain curve of concrete in compression as given below:

$$\sigma_c = E_c \varepsilon_c \left[1 - \frac{1}{2} \left(\frac{\varepsilon_c}{\varepsilon_{c1}}\right)\right] \quad (2.16)$$

However, Kmiecik and Kaminski [94] mentioned that this function is not accurate enough to correctly describe the behavior of concrete. They also suggested, in case of parabolic relations, using a lower value of initial modulus  $E_c$  so as to ensure that the parabola curve passes through the correct value of  $f_c$ .

**Eurocode 2 curve (EN 1992-1-1) [4, 54]** According to Eurocode 2 (EC2), concrete acts elastically up to  $0.4f_c$ . Then, the compressive stress  $\sigma_c$  for hardening and softening parts is defined as a function of uniaxial strain  $\varepsilon_c$  by using the concrete compressive strength  $f_c$  and expressed by:

$$\sigma_c = f_c \frac{k\eta - \eta^2}{1 + (k - 2)\eta} \quad (2.17)$$

with  $k = 1.1 E_c \varepsilon_{c1} / f_c$  and  $\eta = \varepsilon_c / \varepsilon_{c1}$ .

EC2 provides a formulation of the strain at peak stress in term of the compressive strength ( $f_c$  in MPa), which can be used for normal and high strength concrete:

$$\varepsilon_{c1} = 0.7 f_c^{0.31} \quad (2.18)$$

A constant value  $\varepsilon_{cu} = 0.0035$  can be used for concrete with a characteristic value  $f_{ck}$  less than 55 MPa, however for  $f_{ck} \geq 55$  MPa the ultimate strain value should be replaced by:

$$\varepsilon_{cu} = 2.8 + 27 [(98 - f_c) / 100]^4 \quad (2.19)$$

Table 2.3: Values of  $\varepsilon_{c0}$  parameter for high strength concrete [54]

$f_{ck}$ (MPa)	50	60	70	80	90
$\varepsilon_{c0}$ ( $10^{-3}$ )	0.807	0.579	0.338	0.221	0.070

and the descending branch of stress-strain curve for high strength concrete ( $f_{ck} \geq 50$  MPa) should be formulated by:

$$\sigma_c = f_c / \left[ 1 + \{(\eta_1 - 1) / (\eta_2 - 1)\}^2 \right] \quad (2.20)$$

where  $\eta_1 = \varepsilon_c / \varepsilon_{c1}$  and  $\eta_2 = (\varepsilon_{c1} + \varepsilon_{c0}) / \varepsilon_{c1}$ .  $\varepsilon_{c0}$  is the parameter for high strength concrete and its value can be taken from Table 2.3. Concrete compressive strength can be estimated from its characteristic value by  $f_c = f_{ck} + 8$ .

**Pavlovic et al. curve [154]** Pavlovic *et al.* found that the EC2 compressive stress-strain curve is not accurate to estimate the crushing strength of concrete when high crushing strains are expected, as in the case of slabs subjected to impact. Plasticity curve in EC2 considers concrete compression behavior only up to the ultimate strain  $\varepsilon_{cu1}$  limited to a maximum value of 0.0035, which may lead to unrealistic overestimation of concrete strength. Consequently, Pavlovic *et al.* suggested an extension of the compressive stress-strain curve beyond the EC2 ultimate strain and proposed a new value. The extension was performed with a sinusoidal descending curve between two points, the first point corresponds to EC2 ultimate strain ( $\varepsilon_{cu1}, f_{cu1}$ ) while the second is the end of the sinusoidal part at Pavlovic *et al.* ultimate strain ( $\varepsilon_{cu2}, f_{cu2}$ ). The sinusoidal part is defined by the following equation:

$$\sigma_c = f_c \left[ \frac{1}{\beta} - \frac{\sin(\mu^{\alpha_{t1}} \cdot \alpha_{t2} \pi / 2)}{\beta \cdot \sin(\alpha_{t2} \pi / 2)} + \frac{\mu}{\alpha} \right], \quad \varepsilon_{cu1} < \varepsilon_c < \varepsilon_{cu2} \quad (2.21)$$

where  $\mu = (\varepsilon_c - \varepsilon_{cu1}) / (\varepsilon_{cu2} - \varepsilon_{cu1})$  and  $\beta = f_c / f_{cu1}$ . At the end of the sinusoidal descending part at strain  $\varepsilon_{cu2}$ , concrete strength was reduced to  $f_{cu2}$  by a factor  $\alpha = f_c / f_{cu2}$ . Pavlovic *et al.* adopted a value of 20 to the reduction factor  $\alpha$  and 0.03 to the ultimate strain  $\varepsilon_{cu2}$ . Factors  $\alpha_{t1}$  and  $\alpha_{t2}$ , which represent the governing tangents angles at the starting and end points of the sinusoidal curve respectively, were chosen in order to obtain a stress-strain curve with a smooth overall shape, hence  $\alpha_{t1} = 0.5$  and  $\alpha_{t2} = 1.0$ .

**Chinese code curve (GB50010-2002) [3]** Chinese code for design of concrete structures is considered as the only code among many design codes that allows defining uniaxial concrete strength at high strains. The ascending and descending parts of stress-strain curve are described by two different softening parameters related to the material strength and their values generally range from 0.4 to 2.0. According to the design Chinese code, the uniaxial compressive stress-strain curve of concrete can be estimated using the following equations:

$$\begin{cases} \sigma_c = f_c [\alpha_a \eta + (3 - 2\alpha_a) \eta^2 + (\alpha_a - 2) \eta^3], & \eta \leq 1 \\ \sigma_c = f_c \eta / [\alpha_d (\eta - 1)^2 + \eta], & \eta > 1 \end{cases} \quad (2.22)$$

where  $\eta = \varepsilon_c / \varepsilon_{c1}$ , while  $\alpha_a$  and  $\alpha_d$  represent the ascending and descending softening parameters and they are expressed in term of the concrete strength ( $f_c$  in MPa) as follows:

$$\alpha_a = 0.0475 f_c \quad (2.23)$$

$$\alpha_d = 0.0485 f_c \quad (2.24)$$

**Wang and Hsu curve [180]** Wang and Hsu proposed two equations to describe the ascending and descending parts of concrete stress-strain curve in compression. These equations are expressed in terms of concrete compressive strength  $f_c$ , concrete strain at maximum compressive stress  $\varepsilon_{c1}$ , which is considered having a value of 0.002; and a softened coefficient  $\zeta$  that is a function of reinforcement ratios in x and y directions:

$$\begin{cases} \sigma_c = \zeta f_c \left[ 2 \left( \frac{\varepsilon_c}{\zeta \varepsilon_{c1}} \right) - \left( \frac{\varepsilon_c}{\zeta \varepsilon_{c1}} \right)^2 \right], & \text{if } \frac{\varepsilon_c}{\zeta \varepsilon_{c1}} \leq 1 \\ \sigma_c = \zeta f_c \left[ 1 - \left( \frac{\varepsilon_c / \zeta \varepsilon_{c1} - 1}{4/\zeta - 1} \right)^2 \right], & \text{if } \frac{\varepsilon_c}{\zeta \varepsilon_{c1}} > 1 \end{cases} \quad (2.25)$$

$\zeta$  represents the reduction in compressive stress resulting from locating reinforcing bars in the compressed zone, hence the value  $\zeta = 1.0$  is considered in case of plain concrete behavior when no reinforcement is taken into account. It should be noted that, in order to avoid any potential numerical problem when using the following concrete stress-strain curve in a FE analysis, Wang and Hsu suggested a minimal value of  $0.2\zeta f_c$  of the compressive stress in the descending part.

**Majewski curve [116]** Although Eurocode 2 assumes a limit of  $0.4f_c$  for the linear elastic part of concrete stress-strain curve, Majewski found that a linear elasticity limit should increase with the uniaxial concrete compressive strength. Elasticity limit  $e_{lim}$  is considered as a scale factor and calculated as a percentage of stress to concrete strength according to this formula ( $f_c$  in MPa):

$$e_{lim} = 1 - \exp(-f_c/80) \quad (2.26)$$

Consequently, Majewski adopted a linear stress-strain relation for the initial stresses ( $\sigma_c \leq e_{lim}f_c$ ). Beyond this limit, hardening and softening parts were described by a nonlinear relation that depends on several parameters, including the elasticity limit:

$$\begin{cases} \sigma_c = E_c \varepsilon_c, & \text{if } \sigma_c \leq e_{lim}f_c \\ \sigma_c = f_c \frac{(e_{lim}-2)^2}{4(e_{lim}-1)} \left( \frac{\varepsilon_c}{\varepsilon_{c1}} \right)^2 - f_c \frac{(e_{lim}-2)^2}{2(e_{lim}-1)} \left( \frac{\varepsilon_c}{\varepsilon_{c1}} \right) + f_c \frac{e_{lim}^2}{4(e_{lim}-1)}, & \text{if } \sigma_c > e_{lim}f_c \end{cases} \quad (2.27)$$

On the basis of experimental results, Majewski [116] proposed the following formulas to approximate the values of  $\varepsilon_{c1}$  and  $\varepsilon_{cu}$  :

$$\begin{cases} \varepsilon_{c1} = 0.0014[2 - \exp(-0.024f_c) - \exp(-0.140f_c)] \\ \varepsilon_{cu} = 0.004 - 0.0011[1 - \exp(-0.0215f_c)] \end{cases} \quad (2.28)$$

**Kratzig and Polling curve [99]** Based on the recommendations of the Model code 1990 [2], the concrete compressive stress-strain relation suggested by Kratzig and Polling was divided into three part to describe the phases of elasticity, hardening and softening of concrete behavior. Thus, three formulations were derived and expressed as follows:

$$\begin{cases} \sigma_c = E_c \varepsilon_c, & \text{if } \sigma_c \leq f_c/3 \\ \sigma_c = \frac{E_{ci} \frac{\varepsilon_c}{f_c} - (\varepsilon_c/\varepsilon_{c1})^2}{1 + (E_{ci} \frac{\varepsilon_{c1}}{f_c} - 2) \frac{\varepsilon_c}{\varepsilon_{c1}}} f_c, & \text{if } f_c/3 < \sigma_c \leq f_c \\ \sigma_c = \left( \frac{2 + \gamma_c f_c \varepsilon_{c1}}{2f_c} - \gamma_c \varepsilon_c + \frac{\gamma_c \varepsilon_c^2}{2\varepsilon_{c1}} \right)^{-1}, & \text{if } \sigma_c > f_c \end{cases} \quad (2.29)$$

The first two equations describe the ascending part up to the maximum compressive strength  $f_c$  at  $\varepsilon_{c1}$  by assuming an elasticity limit equal to one third of  $f_c$ . In the hardening equation, the modulus  $E_{ci}$  was used to guarantee the stress-strain curve to pass through the point  $(\varepsilon_{ce}, f_c/3)$  where  $\varepsilon_{ce}$  denotes the elastic strain of concrete corresponding to the end of linear elastic phase. The modulus  $E_{ci}$  can be defined in terms of initial Young's modulus  $E_c$  and compressive strength  $f_c$ :

$$E_{ci} = \frac{1}{2E_c} \left( \frac{f_c}{\varepsilon_{c1}} \right)^2 - \frac{f_c}{\varepsilon_{c1}} + \frac{3}{2}E_c \quad (2.30)$$

The third equation represents the descending part of concrete stress-strain curve and includes the descent function  $\gamma_c$  that permits to take account for the descending part dependency on the specimen geometry, which ensures mesh independent results in numerical analysis.  $\gamma_c$  controls the area under the stress-strain curve, it depends on the constant material parameter  $G_{cl}$  that represents the localized crushing energy and on the characteristic length  $l_c$  derived from the respective element mesh. Consequently, the descent function can be expressed by:

$$\gamma_c = \frac{\pi^2 f_c \varepsilon_{c1}}{2 \left[ \frac{G_{cl}}{l_c} - \frac{1}{2} f_c \left( \varepsilon_{c1} (1 - b_c) + b_c \frac{f_c}{E_c} \right) \right]} \quad (2.31)$$

where  $b_c$  is a constant factor assumed equal to the ratio of the plastic strain to the inelastic strain ( $\varepsilon_c^{pl} = b_c \varepsilon_c^{in}$ ) with  $0 < b_c \leq 1$ . Values  $b_c = 0.7$  and  $G_{cl} = 15KN/m$  were found by [21, 118] to fit well with experimental data from literature. For solid elements, the characteristic length is calculated by  $l_c = V_e^{1/3}$  where  $V_e$  represents the element volume.

**Wahalathantri curve [178]** Wahalathantri *et al.* developed a complete stress-strain curve for concrete under uniaxial compression by only using compressive strength, they also suggested slight modifications from the original version of Hsu and Hsu [85] in order to be used and comparable with the damaged plasticity model in Abaqus. Modifications were made only for concrete with maximum compressive strength up to 62 MPa. In the ascending part, concrete acts elastically up to  $0.5f_c$ . Beyond this limit, compressive stress values can be calculated in terms of the compressive strength  $f_c$ , the strain at peak stress  $\varepsilon_{c1}$  and a parameter  $\beta$  which depends on the stress-strain curve shape:

$$\sigma_c = \left( \frac{\beta (\varepsilon_c / \varepsilon_{c1})}{\beta - 1 + (\varepsilon_c / \varepsilon_{c1})^\beta} \right) f_c \quad (2.32)$$

with

$$\beta = \frac{1}{1 - [f_c / (\varepsilon_{c1} E_c)]} \quad (2.33)$$

$$\varepsilon_{c1} = 8.9 \times 10^{-5} f_c + 2.114 \times 10^{-3} \quad (2.34)$$

and the initial modulus  $E_c$  is given by:

$$E_c = 1.2431 \times 10^2 f_c + 3.28312 \times 10^3 \quad (2.35)$$

Wahalathantri *et al.* formula can be used only for stresses between  $0.5f_c$  at elastic strain  $\varepsilon_{ce}$  in the ascending part and  $0.3f_c$  at ultimate strain  $\varepsilon_{cu}$  in the descending part. Wahalathantri *et al.* suggested to iteratively calculate  $\varepsilon_{cu}$  through the equation 2.32 for  $\sigma_c = 0.8f_c$ . It should be noted that in the above equations,  $\sigma_c$  and  $E_c$  are expressed in  $kip/in^2$  ( $1MPa = 0.145037743kip/in^2$ ).

## 2.4.2 Uniaxial tension

### 2.4.2.1 Uniaxial tensile stress-strain curve

Indirect tensile tests as cylinder splitting and bending prisms are often preferred over direct tension test and are used as an indirect way to determine concrete properties in tension (Figure 2.37). The mechanical behaviors of concrete under the action of tensile and compressive loadings have many

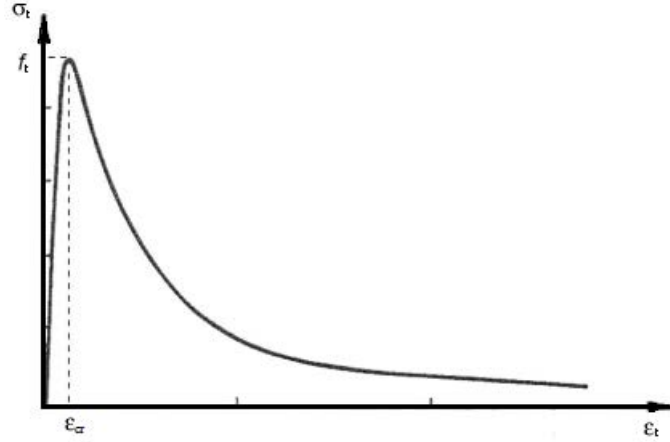


Figure 2.37: Uniaxial tensile stress-strain curve for concrete [156]

similarities. In general the limit of elasticity is observed to be about 60-80% of the uniaxial tensile strength which corresponds to the onset of micro-cracking in the concrete material. Above this level the response of concrete exhibits highly nonlinear behavior and the formation of microcracks is represented macroscopically with a softening stress-strain response. The tensile stress drops gradually with increasing deformations until a complete crack is formed. The reduction in strength of the test specimen resulting from the opening of initial cracks in concrete leads to increase the stress-strain curve nonlinearity. When the concrete specimen is unloaded from any point of the strain softening branch of the stress-strain curve, the unloading response is weakened and the material elastic stiffness appears to be damaged.

**Tensile stress-strain curve without detailed laboratory test results** In the present section, several uniaxial stress-strain relationships for concrete in tension proposed in the literature are detailed, such as the expressions developed by [3, 83, 99, 178, 180].

**Wang & Hsu curve [180]** Wang and Hsu divided concrete behavior in tension into two ascending and descending parts, the first describes the elastic phase while the second indicates the softening stress-strain response and is given in terms of cracking strength of concrete  $f_t$ , strain at concrete cracking  $\varepsilon_{cr}$  and the rate of weakening  $n$ :

$$\sigma_t = E_c \varepsilon_t, \text{ if } \varepsilon_t \leq \varepsilon_{cr} \quad (2.36)$$

$$\sigma_t = f_t \left( \frac{\varepsilon_{cr}}{\varepsilon_t} \right)^n, \text{ if } \varepsilon_t > \varepsilon_{cr} \quad (2.37)$$

Wang and Hsu adopted a value of  $n = 0.4$ . However, this parameter can be used to calibrate the relation for a given simulation since tension stiffening may considerably affect numerical results, hence Kmieciak and Kaminski[94] proposed a range of values from 0.4 to 1.5. This tensile stress-strain curve is characterized by a sharp change at the cracking strain, which may result in some numerical difficulties during a FE analysis. For similar cases, Wang and Hsu suggested to define a short plateau at the peak point.

**Chinese code curve (GB50010-2002) [3, 187]** According to the Chinese code for design of concrete structures, the uniaxial tensile stress-strain curve of concrete includes ascending stiffening

and descending softening parts. When concrete is subjected to tension, it is assumed to exhibit initially a linear elastic response up to the uniaxial tensile strength  $f_t$ . After the tensile stress reaches  $f_t$  and as stresses increase, concrete response becomes nonlinear and the softening stress-strain curve recommended by the Chinese code is given in term of the peak tension strain  $\varepsilon_{cr}$  corresponding to  $f_t$  :

$$\sigma_t = f_t \frac{(\varepsilon/\varepsilon_{cr})}{\alpha_t \left( \frac{\varepsilon}{\varepsilon_{cr}} - 1 \right)^{1.7} + \frac{\varepsilon}{\varepsilon_{cr}}} \quad (2.38)$$

$\alpha_t$  is the coefficient at the descent stage of the uniaxial tension stress-strain curve of concrete and determined by:

$$\alpha_t = 0.312 f_t \quad (2.39)$$

**Wahalathantri curve [178]** Wahalathantri *et al.* selected the experimentally validated tensile stiffening model of concrete proposed by Nayal and Rasheed [143] in order to define the stress-strain curve of concrete in tension. Nayal and Rasheed model consists of two linear descending parts and has the ability to accurately simulate the response during primary and secondary cracking stages. However, Wahalathantri *et al.* indicated that using Nayal and Rasheed curve for damaged plasticity model under tension in Abaqus leads to runtime errors due to a sudden vertical stress drop at the cracking tensile strain  $\varepsilon_{cr}$ . To avoid this problem, Wahalathantri *et al.* introduced a tensile stress-strain curve with three linear descending parts characterized by a gradual reduction in stress:

- The proposed modified part where stress is gradually reduced from maximum tensile stress  $f_t$  to  $0.77f_t$  between strain of values  $\varepsilon_{cr}$  and  $1.25\varepsilon_{cr}$ ,
- The primary cracking part where stress decreases steadily to  $0.45f_t$  between strain values  $1.25\varepsilon_{cr}$  and  $4\varepsilon_{cr}$ ,
- The secondary cracking part that ends at point  $(8.7\varepsilon_{cr}, 0.10f_t)$ .

**Kratzig and Polling curve [99]** Kratzig and Polling considered a linear and elastic response of concrete in tension until the maximum strength  $f_t$  is reached. They assumed that at strain  $\varepsilon_{cr}$  a crack is initiated and occurs as tensile stress in concrete exceeds  $f_t$ . Thereafter, a descending exponential curve was adopted to represent softening behavior of concrete in tension after crack initiation. Their tensile stress-strain relation after cracking can be expressed as:

$$\sigma_t = f_t e^{(\varepsilon_{cr} - \varepsilon_t)/\gamma_t} \quad (2.40)$$

In the above equation,  $\gamma_t$  is a shape parameter that controls the area under the stress-strain curve and depends on the fracture energy  $G_f$  and the characteristic length  $l_t$ :

$$\gamma_t = \varepsilon'_{cr} - \varepsilon_{cr}/2 \quad (2.41)$$

in which  $\varepsilon'_{cr}$  is the strain after which crack expands and is estimated by the following expression:

$$\varepsilon'_{cr} = \frac{G_f}{l_t f_t} \quad (2.42)$$

The estimation of fracture energy and characteristic length values is detailed in the next section.

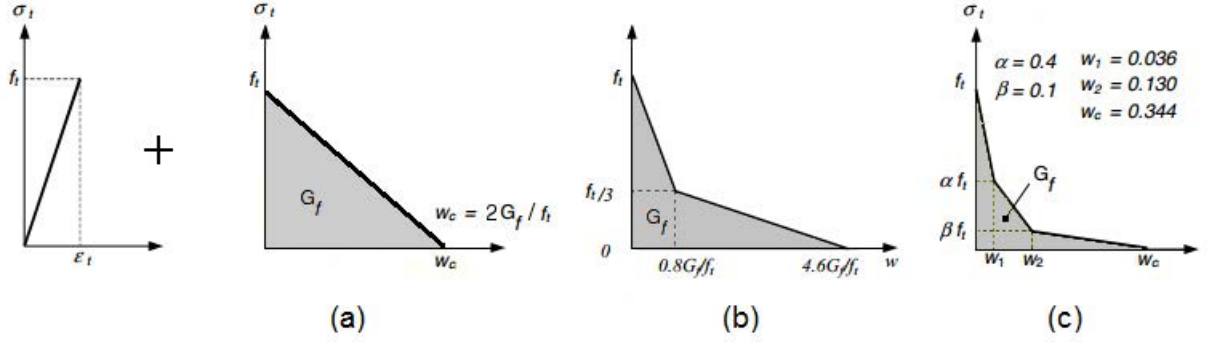


Figure 2.38: Concrete stress-crack opening curve with: (a) Linear softening branch [7], (b) Bi-linear softening branch [78], (c) Tri-linear softening branch [170]

### 2.4.2.2 Uniaxial stress-crack opening curve

Another approach could be also used to define concrete behavior in tension, namely the energy balance approach that showed a reasonable agreement with results from a tensile test according to Hillerborg *et al.* study [81]. Hillerborg *et al.* assumed that the response of concrete under tension is linear until the fracture surface is reached and a linear softening branch beyond cracking was adopted (Figure 2.38.a). Consequently, concrete post-cracking behavior is governed by the equivalent fracture energy criterion that is based on the amount of energy absorbed by the formation of a unit area of crack surface. Cracks arise in planes perpendicular to the direction of maximum principle tensile stress when the maximum tensile strength of concrete is reached, they present a highly irregular shape by following the weakest path in the material. In fracture mechanics experiments, the fracture energy is determined as the ratio of the total energy that is supplied to fracture a specimen (area under the load-deformation relation) to the fractured cross-sectional area [83]. In Hillerborg *et al.* “frictitious crack model”, the fracture energy  $G_f$  is assumed as a material property and presented by the area under the stress-crack opening relation:

$$G_f = \int \sigma dw \quad (2.43)$$

Nowadays, this model is presented in most finite element codes and used to ensure mesh independence of results since the amount of absorbed energy is not very sensitive to the mesh size [81]. This enables to perform finite element analysis with a rather coarse mesh and treat complicated problems with a limited computational cost.

Descending branch after cracking can be also presented by a bi-linear or tri-linear tension softening curve. Haidong [78] adopted in his analysis a bi-linear softening branch with a maximum crack width of  $4.6G_f/f_t$  at which no stress is transferred by the opened crack (Figure 2.38.b). Tajima *et al.* [170] used a tri-linear softening branch with fracture energy as depicted in Figure 2.38.c.

The simplified concrete equation for uniaxial tensile loading of Hordijk [83] is based on the principle of the “frictitious crack model” proposed by Hillerborg *et al.* [81] and depends on the specimen geometry. The corresponding tensile stress-strain relation consists of a loading linear part up to the strength  $f_t$  and a nonlinear descending part which is derived from the following stress-crack opening relation:

$$\sigma_t = f_t \left\{ \left[ 1 + \left( c_1 \frac{w}{w_c} \right)^3 \right] e^{-c_2 \frac{w}{w_c}} - \frac{w}{w_c} (1 + c_1^3) e^{-c_2} \right\} \quad (2.44)$$

The relation between crack opening and stress was found to be the most important input parameter for the nonlinear fracture mechanics analyses of concrete [156]. In the previous equation, the crack opening is expressed as a product of inelastic strain  $\varepsilon_t^{in}$  and characteristic length  $l_t$ :

$$w = l_t \varepsilon_t^{in} = l_t (\varepsilon_t - \sigma_t E_c^{-1}) \quad (2.45)$$

Tajima *et al.* [170] indicated that the definition of the characteristic length of concrete in compression and tension are similar, hence  $w$  is smeared over the average element length  $l_t$  which can be calculated for 3D problems in term of the element volume by  $l_t = V_e^{1/3}$  according to [118] or  $l_t = 2 \sqrt[3]{\frac{3V_e}{4\pi}}$  according to [170]. Hillerborg *et al.* [81] defined the characteristic length in terms of concrete Young's modulus, fracture energy and tensile strength with  $l_t = \frac{G_f E_c}{f_t^2}$ .

Hordijk used a test series on normal-weight concrete from the literature in order to determine the unknown variables in the stress-crack opening relation. The best fit was obtained for  $c_1 = 3$ ,  $c_2 = 6.93$  and  $w_c = 160 \mu m$  where  $w_c$  represents the critical crack opening.

**Fracture energy without detailed laboratory test results** Several relations were proposed in the literature to estimate the fracture energy in case of lack of experimental data [2, 15, 83, 146].

**Hordijk energy [83]** The fracture energy of Hordijk can be calculated in terms of the tensile strength  $f_t$  and the critical crack opening  $w_c$  by the integration of equation 2.44:

$$G_f = f_t w_c \left[ \frac{1}{c_2} \left\{ 1 + 6 \left( \frac{c_1}{c_2} \right)^3 \right\} - \left\{ \frac{1}{c_2} + c_1^3 \left( \frac{1}{c_2} + \frac{3}{c_2^2} + \frac{6}{c_2^3} + \frac{6}{c_2^4} \right) + \frac{1}{2} (1 + c_1^3) \right\} \exp(-c_2) \right] \quad (2.46)$$

By replacing  $c_1$  and  $c_2$  by their values as mentioned previously, the fracture energy can be estimated by:

$$G_f = 0.195 w_c f_t \quad (2.47)$$

**CEB-FIP energy [2, 158]** CEB-FIP model code proposed a relation between the fracture energy and compressive strength of concrete. Fracture energy  $G_f$  is calculated for mode I in  $N/mm$  in term of coefficient  $\alpha_f$  that depends on the maximum aggregate size in concrete  $d_{max}$ :

$$G_f = \alpha_f \left( \frac{f_c}{10} \right)^{0.7} \quad (2.48)$$

with  $f_c$  representing the compressive strength of concrete in MPa and  $\alpha_f = (1.25 d_{max} + 10) \cdot 10^{-3}$ , where  $d_{max}$  is introduced in  $mm$  and may vary between 2 and 32  $mm$ . As can be seen,  $G_f$  has generally a tendency to increase with  $f_c$  and  $d_{max}$ . In the present study, a value of 16  $mm$  is adopted for  $d_{max}$ .

**Oh-Oka *et al.* energy [146, 170]** Oh-Oka *et al.* also determined the fracture energy of concrete in  $N/mm$  in term of the compressive strength according to the following formula:

$$G_f = \frac{0.23 f_c + 136}{1000} \quad (2.49)$$

**Bazant and Oh energy [15, 134]** Based on numerous experimental results, Bazant and Oh proposed an equation of the fracture energy of concrete in terms of Young's modulus  $E_c$ , tensile strength  $f_t$  and the maximum size of coarse aggregate  $d_{max}$ :

$$G_f = \frac{(0.3044f_t + 2.72) f_t^2 d_{max}}{E_c} \quad (2.50)$$

$G_f$  is calculated in  $kgf/cm$ ,  $E_c$  and  $f_t$  are given in  $kgf/cm^2$  ( $kgf/cm^2 = 0.0980665 MPa$ ) and  $d_{max}$  is in cm.

## 2.5 Mechanical behavior of steel

Considered as a composite material, reinforced concrete consists of steel reinforcement embedded in plain concrete. Steel is used in RC structures to carry tensile forces and to recover the low tensile strength of concrete. Inclusion of steel reinforcement is very effective to control the development of cracks by distributing cracks uniformly over the cracked regions, but it does not prevent the cracking of concrete under tension. The behavior of reinforcing steel may control the response of RC structures subjected to impact, thus the prediction of fundamental characteristics and behavior of steel is necessary. In the current study, uniaxial steel stress-strain curves based on experimental observations are adopted and defined in terms of steel properties as follows:

$$\sigma_s = f(E_s, E_{s1}, f_y, f_u, \varepsilon_s, \varepsilon_y, \varepsilon_{sh}, \varepsilon_u) \quad (2.51)$$

Where  $\sigma_s$  represents the steel stress values calculated,  $E_s$  is the elastic modulus of steel,  $E_{s1}$  is the deformation modulus of steel at the hardening phase,  $f_y$  is the yield strength of steel,  $f_u$  is the ultimate stress of steel corresponding to the ultimate strain,  $\varepsilon_s$  represents the steel strain value corresponding to the stress  $\sigma_s$ ,  $\varepsilon_y$  is the yield strain of steel at the yield strength  $f_y$ ,  $\varepsilon_{sh}$  is the strain of steel at which strain hardening initiates, and  $\varepsilon_u$  is the ultimate strain of steel.

### 2.5.1 Uniaxial tension

Steel behavior can be determined from coupon tests of bars loaded monotonically in tension. These tests allow obtaining a typical stress-strain curve for reinforcing steel in tension to failure (Figure 2.39). Steel response exhibits an initial linear elastic region, a yield plateau, a strain hardening region and a post-ultimate stress region. The compression stress-strain curve of reinforcing steel is assumed to be equal and opposite of its curve in tension.

The linear elastic region is up to the steel yield strength  $f_y$  and steel stiffness is governed by the elastic modulus  $E_s$  at low strains. Stress in this region is expressed as:

$$\sigma_s = E_s \varepsilon_s \quad (2.52)$$

After the strain  $\varepsilon_y$  corresponding to the yield strength, steel response is referred as the yield plateau or Lüder's plateau. At the beginning of this region, steel behavior shows a slight drop in strength below the initial yield strength. Then, stress remains steady at this lower yield strength and steel behaves nonlinearly and plastically. Steel stress-strain curve is generally idealized and assumed to be horizontal in the yield plateau region with an average strength equal to the material yield strength. Thus, the idealized stress-strain relationship in this region is:

$$\sigma_s = f_y \quad (2.53)$$

The yield plateau size depends on the steel tensile strength, e.g. the yield plateau is considerably shorter for high-strength, high-carbon steels than for low-strength, low-carbon steels [179].

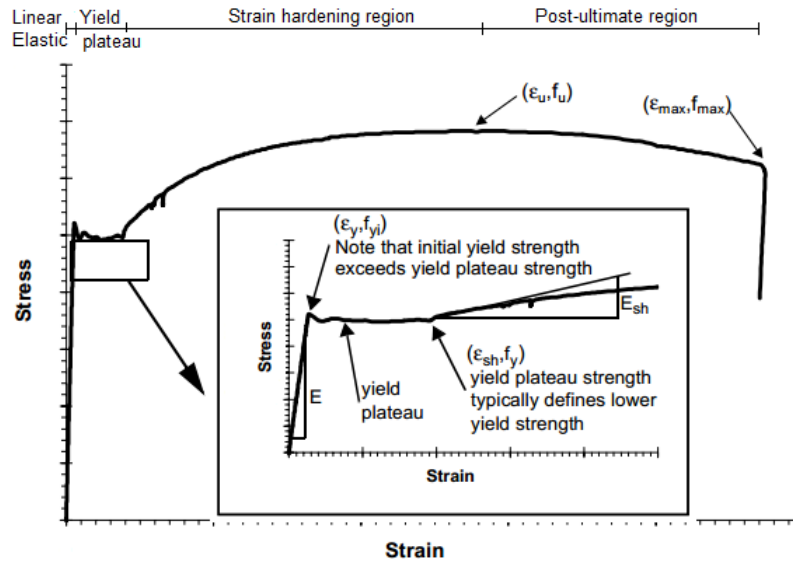


Figure 2.39: Experimental tensile stress-strain curve for reinforcing steel [112]

The strain-hardening region starts at the idealized point of coordinates  $(\varepsilon_{sh}, f_y)$  and ends at the ultimate point of coordinates  $(\varepsilon_u, f_u)$ . At this phase, stress increases again with strain and exceeds the yield strength by 30 to 60 % at the ultimate point, and stiffness decreases with permanent plastic deformation. The ratio of ultimate strength to yield strength depends on the steel specification and grade [112]. At the ultimate point, the maximum tensile load is resisted and the tensile stress-strain curve of steel has zero slope.

Finally, in the post-ultimate region, stress reduces with strain until steel reinforcement fracture occurs and load capacity is lost. However, steel stress-strain curve is assumed to end at the ultimate point since its shape at the post-ultimate region is related to the gauge location and the length over which the data are collected [185].

## 2.5.2 Idealizations

This section discusses idealized stress-strain curves proposed in the literature to describe steel behavior. For practical application, typical stress-strain curve of steel can be idealized in two different ways depending on the desired level of accuracy. For the first idealization, steel is considered as a linear elastic, perfectly plastic material with a bilinear stress-strain curve. The first branch is linear elastic up to yield strength  $f_y$  and the second branch represents the yield plateau with a stress equal to  $f_y$ . In this idealization, the stress increase due to strain hardening is neglected. This idealization was found to be sufficient to analyze RC structures under service load conditions [36] and very satisfactory in the case of low-strength, low-carbon steels characterized by a strain hardening much greater than the yield strain [171]. The design equations of the ACI code are based on this assumption [171]. However, this approximation underestimates steel stresses at high strains in cases where the onset of yielding is directly followed by steel hardening [171]. According to Kwak and Filippou [101], an elastic-perfectly plastic curve may lead to numerical convergence problems when used in a FE analysis in cases where a RC structure is highly affected by reinforcing steel hardening. On the contrary, this idealization was adopted by Kratzig and Polling [99] to derive an elasto-plastic damage model for reinforced concrete and was found to be successfully used to model RC structures.

The second idealization assumes a linear elastic, linear plastic steel behavior with hardening. The stress-strain curve consists of two linear branches, the elastic branch is up to yield strength  $f_y$  while stress varies in the plastic branch between  $f_y$  and  $f_u$  for strain varying between  $\varepsilon_y$  and  $\varepsilon_u$ ,

respectively. This approximation is generally more used to estimate steel stresses at strains higher than yield strain and considered as more accurate since it takes into account the strain hardening effect. According to [171], this approximation would be more appropriate than the first idealization to model the steel behavior and allows assessing the corresponding ductility of a structure investigated under high strains. Several researchers adopted the second idealization to represent steel behavior [21, 28, 101]. Kwak and Fillippou [101] indicated that assuming a gradually increasing plastic hardening branch immediately after yielding for the steel stress-strain curve does not affect the accuracy of results. Britel and Mark [21] used a value of  $E_{s1} = 1111 \text{ MPa}$  for the deformation modulus of plastic-hardening branch, while Cao *et al.* [28] estimated  $E_{s1}$  in term of steel Young's modulus  $E_s$  as:

$$E_{s1} = 0.01E_s \quad (2.54)$$

In order to predict the ultimate punching shear strength of slab-column connections, the second idealization was also used by Theodorakopoulos and Swamy [173] by assuming a value of  $E_{s1} = 5 \text{ GPa}$  to express the strain hardening effect up to a stress equal to  $1.2 f_y$ . However, the elastic part before yielding was divided into two linear branches, a branch up to  $0.8 f_y$  with a modulus of elasticity  $E_s = 200 \text{ GPa}$  and a branch between stresses of  $0.8 f_y$  and  $f_y$  with a modulus equal to:

$$E'_s = \frac{0.2f_y}{0.002 + 0.2f_y/E} \quad (2.55)$$

The yield strain can be calculated using the following expression:

$$\varepsilon_y = 0.002 + f_y/E \quad (2.56)$$

### 2.5.3 Steel-concrete bond

Stress-strain curve of reinforcing steel bars embedded in concrete is slightly different from that of a bare steel bar due to tension-stiffening effect caused by the surrounding concrete bonded to steel. During a tension-stiffening phenomenon, the bond action between concrete and reinforcement develops a number of cracks in the structure and results in the redistribution of tensile loads from concrete to steel. The response of a RC structure with tension-stiffening is more complicated and stiffer than the response with a brittle failure [171]. The development of bond between concrete and steel is represented by three stress transfer mechanisms, namely mechanical interaction, chemical adhesion and surface friction [36]. The mechanical interaction is the main mechanism that maintains the composite interaction between the two materials and for which load transfer can be idealized as a continuous stress field developed at the deformed surface of reinforcement and concrete [171]. Bond stresses located along the surface between reinforcement and the surrounding concrete effectively transfer tensile stresses between reinforcing bars and concrete. Steel and the surrounding concrete are considered as full bonded and behave as a unit as long as the loading applied to the RC structure does not exceed the bond stress capacity. Stresses at the interface of concrete and steel increase with increasing the load applied, which results in a localized bond stress exceeding the bond capacity and a localized damage that propagates gradually to the surrounding concrete. Consequently, steel starts to yield at cracked sections and a significant movement between the reinforcing steel and the surrounding concrete may occur. The quality of bond between reinforcing steel and concrete has a considerable influence on cracks distribution and affects their width and spacing. For this reason, the interface properties between concrete and steel are very important to analyze RC structures and hence steel can be included in numerical analyses with an equivalent stress-strain relation that considers bond effects by assuming a perfect bond between concrete and steel elements.

The main difference between a bare steel bar behavior and that of a steel bar embedded in concrete is related to the stress value at which steel yields. For an embedded steel bar, stresses

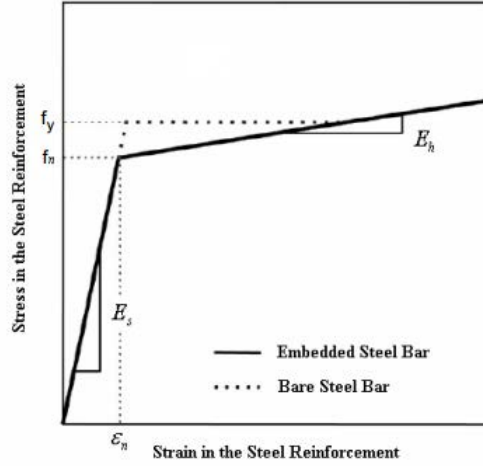


Figure 2.40: Average tensile stress-strain curve for reinforcing steel embedded in concrete [16]

in reinforcing steel between cracks is less than the yield stress at cracks since tensile forces can still partially be resisted by the concrete matrix located between cracks. Therefore, yielding of an embedded bar traversing several cracks starts at an average value  $f_n$  which is less than the yield strength of a bare steel bar  $f_y$  (Figure 2.40). In addition, stress-strain relationship of reinforcing steel bars embedded in concrete can be obtained by averaging stresses and strains between cracks. A bilinear average stress-strain relation was proposed by Belarbi and Hsu [16] based on experimental results:

$$\begin{cases} \sigma_s = E_s \varepsilon_s, & \text{if } |\varepsilon_s| \leq \varepsilon_n \\ \sigma_s = f_y \left( (0.91 - 2B) + \left( 0.02 + 0.25B \frac{\varepsilon_s}{\varepsilon_y} \right) \right), & \text{if } |\varepsilon_s| > \varepsilon_n \end{cases} \quad (2.57)$$

As illustrated in Figure 2.40, the average behavior of steel embedded in concrete still maintains an initial elastic phase up to a stress value  $f_n$  at which yielding of steel bars starts. The second branch is expressed in term of a parameter  $B$  that determines the difference between  $f_n$  and  $f_y$ . The parameter  $B$  is a function of the ratio  $f_t/f_y$  and the reinforcement steel ratio  $\rho_s$  limited to a minimum value of 0.25%:

$$B = (f_t/f_y)^{1.5} / \max\{\rho_s, 0.25\%\} \quad (2.58)$$

with  $f_t$  is the tensile strength of concrete. In Figure 2.40,  $\varepsilon_n$  is the limiting boundary strain defined as follows:

$$\varepsilon_n = \varepsilon_y (0.93 - 2B) \quad (2.59)$$

The average stress-strain curve proposed by Belarbi and Hsu that incorporates the effect of tension stiffening was adopted by several researchers [117, 158, 171] to define the behavior of reinforcing steel embedded in concrete.

## 2.6 Conclusion

In civil engineering field, RC structures are often subjected to some extreme dynamic loadings due to accidental impacts of rigid bodies that may occur during their service life with a very low probability of occurrence. In the available design codes of civil engineering, the design of RC structures subjected

to impact is generally based on approximate static method. However, the transient dynamic analysis has to be performed accounting for the main physical processes involved and accurate models are needed to describe and predict the structural behavior of RC members subjected to impact loading. This study focuses on RC slabs subjected to accidental dropped object impact during handling operations within nuclear plant buildings. The objective of this chapter is to provide a general overview of research programs which have been carried out in regards to analyzing structures under general loading conditions, evaluating global response of RC slabs under drop-weight impact loading conditions. A classification of impact response types of RC slabs according to the impactor mass and velocity was provided. Then types of impact event and the transient behavior of RC slabs subjected to impact are described and identified. In order to properly predict the behavior of RC slabs under impact, impact dynamics, type of impact, failure modes and energy consideration should be examined and identified. The impact response of RC slabs depends on several parameters, including slab dimensions, material properties and impact conditions. In this chapter, uniaxial compressive and tensile stress-strain curves of concrete and steel based on experimental observations in the literature are adopted.

## Chapter 3

# Deterministic analysis: Software and steps

### 3.1 Introduction

This chapter discusses the choice of deterministic software used in the present study to simulate the problem of RC slabs which are subjected to accidental dropped object impact during handling operations within nuclear plant buildings. First, the basic phases of finite element analysis are described and the different steps which are necessary to create a finite element model in Abaqus are presented. Furthermore, plasticity constitutive models used to represent concrete and steel in numerical simulations are discussed by describing and identifying their fundamental parameters, and contact algorithms used for modeling the interaction between two bodies are presented. Other numerical features which are necessary for simulating impact analysis are also discussed.

### 3.2 Finite element analysis

As an alternative of experimental approach, finite element analysis (FEA) represents an advanced engineering tool to design structural and civil engineering applications. Based on the finite element method, FEA is a numerical technique for obtaining approximate solutions of partial differential equations as well as of integral equations. These equations may be generated from complex structures with complicated features, for which it is difficult to find an analytical solution. Thus, the simulation procedure should be performed with an intensive attention in order to improve the quality of FEA studies and obtain models that comply with the physical properties of the actual structure as far as possible. Computational tools based on the finite element method are increasingly improved with the development of computer technology, thus FEA is widely used as a powerful and helpful technique to assess complex engineering problems. Once the numerical model is validated with experimental results, FEA enables an accurate calculation of stress distributions and an evaluation of the influence of model parameter variations.

A finite element model is based on dividing the complex structure into several small elements of finite dimensions that are connected to associated nodal points. Each element is assigned with a specific geometric shape and appropriate material properties and has its own functions of dependent variables. These functions can be interpolated using shape functions and describe the element response in terms of the value of dependent variables at a set of nodal points. These functions and the actual element geometry are used to determine the equilibrium equations that express the displacement occurring at each node in term of the external forces acting on the element. The unknown displacements are determined by solving a system of finite element equations that are

generated, with the element stiffness matrices, through the equilibrium equations and stress-strain relationships.

Generally, FEA procedure involves the following three basic phases:

- The pre-processing phase represents the most consuming in time among the three phases, it is the phase where the numerical model of the physical problem should be defined and ready to be submitted to the solution or analysis phase. It consists in dividing the model into a number of discrete interconnected elements with common discrete nodes and applying certain appropriate boundary conditions with reasonable assumptions. Suitable finite element types should be selected correctly and a sufficiently refined mesh should be created, especially in regions where high stresses are expected. The following process of creating the mesh, choosing suitable elements connected with their respective nodes, and defining boundary conditions is referred to as “discretization” of the physical problem.
- The solution/Analysis phase represents the phase of defining the analysis type and submitting the finite element model to finite element code solver. The analysis type can be either static or dynamic depending on the structure response to applied loads. A numerical output database will be generated by solving a series of linear or nonlinear equations. In this phase, numerical output can be controlled in the finite element code solver and quantities such as displacements, stresses, reactions, or other variables can be determined.
- Post-processing phase represents the final phase that provides a visualization environment of results by using a post-processing software. Results can be displayed in contour plots or other approaches which assist to get a better evaluation and interpretation of the simulation results. However, at this stage, the task of interpreting results should be performed carefully in order to verify the accuracy of FEA and assess whether the assumptions adopted during simulation are satisfied and accurate. These assumptions related to the structure geometry, boundary and loading conditions, material properties, and interaction between different parts of the model will potentially affect the results, as well as mesh sizes that may have important effects on predicted solutions.

The three basic phases of FEA procedure also can be used to describe the main framework of any available FE software. Hence, almost all FE software are based on the same fundamental principle of FE method and have the same general purpose that includes three components, namely, the pre-processor, the processor and the post-processor. A pre-processor establishes the FE model and the input data for the processor that solves the different equations generated during analysis. A post-processor helps in reviewing and interpreting results, as well as checking the validity of the solution.

### 3.3 Choice of commercial FE software

Several commercial software packages are developed to assist in reducing the complexities of FEA application. Due to advancement of computer technology, FE computer software have evolved to become so powerful to conduct sophisticated analyses and assist in design process stages. However, every commercial computer software is developed with its own capabilities, features and algorithms that are different from others. Most FE code are computer-aided design (CAD) software developed with a graphical user interface (GUI) that significantly reduces the actual application of FEA and provides a powerful tool for engineers to perform analyses with minimal effort and without knowing the governing equations or the limitations of the analysis process. Recent computer-aided engineering (CAE) software offer a robust and reliable technology to automate critical intensive tasks and integrate CAD. They permit to graphically generate complex 3D geometries and to automatically

create refined mesh by merely indicating the desired mesh density. Most FE code are written using programming languages such as Fortran, C and C++ that provide, with very less additional code, the advantage of writing subroutines for purposes of adding new elements to the element library and defining unique material models.

Choosing among the currently available commercial software is a very important task that is based on requirement of applications and involves several criteria such as analysis type, ease of use, efficiency, software limits, computational cost, technical support and training. Furthermore, the accuracy of numerical results is very dependent on the proficiency and the fundamental theoretical knowledge of the engineer in FEA. Most of the time, engineers will interact only with the pre- and post- processor components of the software, which may lead to the danger of using its tools as a “black box” in case of the engineer does not understand what happens in this essential part between the two processors. Mistakes like accepting results with an inappropriate mesh, not considering reasonable assumptions for an analysis and misrepresenting model properties can still be easily made despite all the modern and sophisticated improvements in FE software. For example, the automatic mesh generators that are provided in most commercial software offer a robust tool for meshing complex geometries, but if misused, they would result in a loss of accuracy and a dramatic increase in computational time that may even exceed available hardware and software resources. Therefore and before starting an analysis, a FE model must be extracted from the real problem in order to solve the problem using the most efficient modeling method with the less computational time and a high degree of reliability. Likewise, the selection of the right FE software is absolutely crucial, as well as understanding its limits and the computational resources.

The present study focuses on RC slabs subjected to low impact velocity, thus the FE software chosen should include the ability of creating 3D geometries, applying impact conditions and defining nonlinear material behaviors. In addition, it should be capable of simulating contact and interaction between different parts of the structure, which is highly required for an impact problem. Given the many available software, the well-known commercial FE software, Abaqus, is used to illustrate how to simulate the geometric and material properties of the slab and impactor, as well as to define contact, boundary and initial conditions. Data input for FEA with Abaqus can be done through:

- Abaqus interactive edition by using the graphical user interface Abaqus/CAE,
- Abaqus Keyword edition by using an input file written with a text editor (.inp), or
- Abaqus Python edition by using a script written with Python (.py)

### 3.4 Components of an Abaqus analysis model

Abaqus is a series of powerful engineering programs that are based on the FE method with a high quality of pre- and postprocessing capabilities. The user-friendly nature of Abaqus offers the possibility of modeling and solving even the most complicated engineering problems. Simulations ranging from relatively simple and linear to highly difficult and nonlinear can be performed easily with Abaqus by only providing the engineering data such as the structure geometry, material behaviors, loads, boundary and initial conditions. Abaqus provides complete numerical solutions and controls their efficiency by automatically choosing appropriate values for load increments and convergence tolerances and continually adjusting them during the analysis in order to obtain accurate results.

Abaqus is divided into modules that permit to build a FE model by performing a successive passage through modules. Each module defines a fundamental step in the modeling process. In the present section, the different steps which are necessary to create a FE model in Abaqus and the data that must be included are presented:

- Part module: The structure geometry can be divided into multiple parts, each part represents a main component of the model and is created out of a two-dimensional sketch.

- **Property module:** Mechanical behaviors and properties of materials can be specified by using the Abaqus material library that contains an extensive list of linear and nonlinear material models, or by creating new material models through several subroutines that are provided in Abaqus and programmed in Fortran language. The behavior of most typical engineering materials can be simulated with Abaqus, which includes metals, concrete, composites, polymers, and so on. Section properties of the physical structure are also defined in this module. Each section is associated with a material and assigned to a correspondent part of the geometry.
- **Assembly module:** Geometry of the model is defined by creating instances of each part which is independent of each other. Instances are positioned relative to one another in a global coordinate system in order to assemble the model.
- **Mesh module:** Generating finite element meshes can be actually done either on the part or the assembly module. Meshing involves choosing appropriate element types and mesh density. Various types of geometrical elements that can model virtually any geometry are available in Abaqus element library. All elements use numerical integration and must refer to a section property definition.
- **Configuring analysis module:** The analysis procedure type must be defined in order to solve the numerical problem. Abaqus can be used to solve general static and dynamic response problems and consists of two main analysis products, Abaqus/Standard and Abaqus/Explicit. Abaqus/Standard allows carrying out static analyses where the structure has a long-term response to the applied load and solves a coupled system of equations implicitly at each increment. Abaqus/Explicit is particularly used to simulate transient dynamic events and uses an explicit formulation to perform a large number of small time increments without the need of solving a system of equations at each increment. The whole analysis procedure may comprise one or multiple steps. Thus, as many steps as needed must be created for the case load by providing the required parameters and controlling the output data requested for each step.
- **Load module:** Specifying boundary and initial conditions and applying loads to the structure are step-dependent. Loads can be applied in Abaqus with many different ways which include concentrated or distributed loads, pressures and loads per unit volume such as due to gravity or acceleration. Zero-valued, including symmetry conditions, or non-zero boundary conditions can be imposed to model regions where the displacements and/or rotations are known. Most loads or boundary conditions can follow an amplitude curve varying with time. Non-zero initial conditions can be also specified as predefined fields, these include initial stresses, velocities or temperatures.
- **Interaction and constraints module:** Interaction and constraints between different parts or surfaces of the model can be defined. Abaqus provides two algorithms for simulating contact, general contact algorithm that allows defining contact between all model regions and contact pairs algorithm that describes contact between two surfaces. Interaction properties are used to enhance contact modeling, normal or tangential behavior can be defined with friction or contact damping. Abaqus includes also several constraint types such as rigid bodies, coupling constraints and surface-based ties. Constraints are used to couple a group of nodes motion to the motion of other nodes.
- **Output control module:** A large amount of output variables can be generated with an Abaqus simulation, they depend on the analysis and element types used. Output are specified with Field and History output managers that generate a default output request, but also enable to control and manage the analysis requested output in order to only produce results that are required to be interpreted and avoid excessive disk space.

- Job module: A job is associated with the model and submitted to the solver for analysis. Submission of input files can be performed through Abaqus/CAE or manually from the command prompt. Abaqus offers the possibility of checking incorrect or missing data through a data check analysis that can be used before running a simulation and helps in minimizing the probability of errors in the model.
- Visualization module: This module is only available in Abaqus/CAE which writes the analysis results to an output database file with the extension (.odb). The evaluation of results are performed interactively using the program Abaqus/viewer that allows viewing and displaying results related to the model through a variety of options including color contour, X-Y and deformed shape plots. Note that three other types of output are available in Abaqus and results can be written to the Abaqus data file (.data) in tabular form, to the Abaqus restart file (.res) that uses restart data to continue the analysis, and to Abaqus results file (.fil) that can be used with third-party software for subsequent postprocessing. Moreover, a Python script can be used to read data from a (.odb) file and gather numerical results as tables, plots or animations.

### 3.5 Configuring analysis

Selecting an appropriate approach to solve the equation governing the response of the finite element analysis of a specific problem is very important since an incorrect solution and a highly computational analysis may result from choosing the wrong simulation method. Two methods are available in Abaqus to solve a finite element problem, namely the implicit and explicit methods. Both methods consist of a numerical direct time integration scheme to evaluate the unknown displacement at the end of the time step. Implicit method is generally used for static, harmonic or modal analyses in which the time dependency of the solution is not a significant factor, while explicit method is used for blast and impact problems involving high deformation and time dependent solution. However, Abaqus allows using the implicit method to perform dynamic analysis of problems in which inertia effects are considered, and using the explicit method quasi-static problems that experience convergence difficulties in implicit analysis methods. Implicit direct integration is provided in Abaqus/Standard, while explicit direct integration is provided in Abaqus/Explicit [5].

The direct-integration dynamic procedure provided in Abaqus/Standard offers a choice of implicit operators using the implicit Hilber-Hughes-Taylor operator for integration of the equations of motion, while Abaqus/Explicit uses the central-difference operator. In an implicit dynamic analysis the integration operator matrix must be inverted and a set of nonlinear equilibrium equations must be solved at each time increment. In an explicit dynamic analysis displacements and velocities are calculated in terms of quantities that are known at the beginning of an increment. Therefore, the global mass and stiffness matrices need not be formed and inverted, which means that each increment is relatively inexpensive compared to the increments in an implicit integration scheme. However, the size of the time increment in an explicit dynamic analysis is limited because the central-difference operator is only conditionally stable, whereas the implicit operator options available in Abaqus/Standard are unconditionally stable. Thus, there is no such limit on the size of the time increment that can be used for most analyses in Abaqus/Standard (accuracy governs the time increment in Abaqus/Standard).

The explicit scheme is only stable if the size of the time step is smaller than the critical time step size for the structure being simulated. This very small time step size requirement for stability thereby makes explicit solutions recommendable for short transient situations. But, even though the number of time steps in an explicit solution may be orders of magnitude greater than that of an implicit solution, it may be more efficient than an implicit solution since no matrix inversion is required. Very Large deformation problems such as impact analysis can result in millions of

degrees of freedom effectively increasing the size of stiffness matrix. The implicit scheme requires considerable computation time, disk space, and memory because of the iterative procedure involving the inversion of a large global stiffness matrix (determined by the number of degrees of freedom). The computational cost for problems based on the implicit scheme is roughly proportional to the square of the number of degrees of freedom, while the analysis cost for problems based on the explicit scheme rises only linearly with problem size. Hence there is a need for an explicit method which would prevent the inversion of stiffness matrix. It is possible to solve complicated, very general, three-dimensional contact problems with deformable bodies in Abaqus/Explicit. Problems involving stress wave propagation can be more efficient computationally in Abaqus/Explicit than in Abaqus/Standard.

## 3.6 Material properties

### 3.6.1 Concrete constitutive model

Modeling concrete within finite element packages is a very complicated task due to the complexity of its behavior. For an accurate simulation of RC structures, both elastic and plastic behavior of concrete in compression and tension should be taken into account using a proper material model in finite element analysis. Simulation of compressive behavior should include elastic behavior of concrete, as well as strain hardening and softening regimes. Simulation of concrete under tension should include tension softening, tension stiffening and interaction between concrete and steel elements.

There are different theories available in the literature to model the constitutive behavior of concrete, namely elasticity theory, viscoelasticity theory, viscoplasticity theory, classical plasticity theory, endochronic theory, fracture mechanics, continuum damage mechanics and stochastic approach [2, 96]. Among these, the most commonly used frameworks are based on plasticity, continuum damage mechanics and combinations of plasticity and damage mechanics.

Plasticity theory was widely used to describe concrete behavior [72, 122]. Stress-based plasticity models obviously have advantages over elastic theory since they allow modelling concrete behavior when subjected to triaxial stress states, as well as representing hardening and softening regimes. The main characteristic of these models is a plastic yield surface that corresponds at a certain stage of hardening to the strength envelope of concrete and includes a nonassociative flow rule [72, 122]. The expression of the yield surface includes a hardening-softening function and inelastic strains are considered in order to represent realistically the deformations in concrete [73, 96, 122]. Nevertheless, such models do not incorporate a damage process to capture the variations of the elastic unloading stiffness upon mechanical loading accurately. As a result, they are not able to describe unilateral effects and the reduction of material stiffness due to microcracks [88, 96] (Figure 3.1.a).

Conversely, continuum damage mechanics models are based on the concept of a decrease of the elastic stiffness [73, 88]. The continuum damage theory was also widely used to model the nonlinear behavior of concrete [33, 120]. For these models, phenomena such as strain softening, stiffness decrease and unilateral effects due to progressive microcrackings and microvoids are taken into account [88, 96]. The mechanical effect of these phenomena is represented by a set of internal state variables that describes the decrease of the elastic stiffness at the macroscopic level [88, 120]. Nevertheless, such models do not consider the plastic strain (Figure 3.1.b), hence they are unable to describe irreversible deformations nor predict dilatancy behavior under multiaxial loadings [73, 88].

On the other hand, several models were proposed in literature as a combination of isotropic damage and plasticity in order to model both tensile and compressive behaviors of concrete [88, 104] since neither pure elastic damage models nor pure elastoplastic constitutive models can satisfactorily describe the concrete behavior. Both models fail in capturing the evolution of unloading stiffnesses accurately [88, 152]. Thus, damage-plastic models are used to overcome this problem since both irreversible deformations and microcrackings contribute to the nonlinear behavior of concrete (Figure

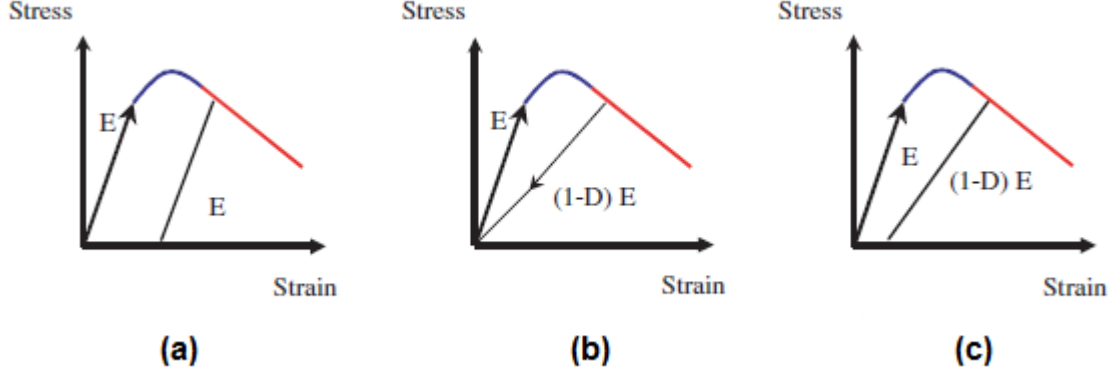


Figure 3.1: Unloading response of: (a) elastic plastic, (b) elastic damage, (c) elastic plastic damage models [88]

3.1.c). Damage plasticity models are formulated in the effective (undamaged) stress space combined with a strain based damage model, which is numerically more stable and more appropriate to represent tension and compression behaviors of concrete [73, 152]. Plastic yield function is no longer expressed in term of the applied stress, but it is written in term of the effective stress that represents the stress in undamaged material in between the microcracks [88].

Several plasticity models which have been implemented in ABAQUS were widely used to represent concrete in numerical simulations, namely the Drucker-Prager/Cap model, the brittle cracking model and the concrete damage plasticity model. These models require multiple and complex parameters, which are generally obtained from material tests.

Plasticity models available in ABAQUS are decomposed into an elastic part and a plastic part. They are usually formulated in terms of a yield surface, a flow rule and evolution laws that define the hardening. The yield function represents a surface in effective stress space, for which a failure or damage state can be determined. For a plastic-damage model the yield function arrives at:

$$F(\bar{\sigma}, \tilde{\varepsilon}^{pl}) \leq 0 \quad (3.1)$$

The states of stress corresponding to material failure are on this surface while the states of safe behavior are inside.

The plastic flow is governed by a flow potential function  $G(\bar{\sigma})$  which is also defined in the effective stress space according to nonassociative flow rule:

$$\dot{\varepsilon}^{pl} = \dot{\lambda} \frac{\partial G(\bar{\sigma})}{\partial \bar{\sigma}} \quad (3.2)$$

### 3.6.2 Concrete damage plasticity model (CDP)

For an accurate simulation of the response of RC slabs under impact, a realistic representation of concrete behavior under dynamic loads is necessary. The concrete model adopted for numerical analysis should include the hardening behavior that occurs under compressive loading, the softening behavior that results from the formation of microcracks, the damage that describes the decrease in material stiffness, stiffness recovery related to crack opening and closing under cycling loading, and rate dependence. Among different models available in Abaqus, CDP model represents a convenient model to simulate concrete behavior due to its capabilities to represent irreversible deformations but also stiffness degradation [6]. A comparison to experimental results has proved the accuracy of this

model to capture the complete behavior of concrete up to failure, and to be the most stable regime for modeling concrete nonlinear behavior [135]. Therefore, the CDP model is used for concrete to study the response of RC slabs under impact in the present study

CDP model is a continuum, plasticity-based, damage model for concrete that uses concepts of isotropic damaged elasticity in combination with isotropic tensile and compressive plasticity to represent the inelastic behavior of concrete. It is based on the models proposed by Lubliner *et al.* [113] and Lee and Fenves [104], and designed for applications in which the concrete is subjected to arbitrary loading conditions, including cyclic loading. The model assumes that the main two failure mechanisms are tensile cracking and compressive crushing of the concrete material. Two hardening variable related to concrete failure mechanisms under tension and compression, respectively, are used in the CDP model in the aim of controlling the evolution of the yield surface. The model takes into account the degradation of the elastic stiffness induced by plastic straining both in tension and compression by introducing two independent scalar damage variables for tension and compression, respectively. The elastic behavior of concrete in CDP model is assumed to be isotropic and linear.

### 3.6.2.1 Plastic flow and yield surface

The plastic flow potential function and the yield surface in CDP model make use of two stress invariants of the effective stress tensor, namely the hydrostatic pressure stress (or the effective hydrostatic stress),  $\bar{p} = -\frac{1}{3}\text{trace}(\bar{\boldsymbol{\sigma}})$  and the Mises equivalent effective stress,  $\bar{q} = \sqrt{\frac{3}{2}(\bar{\mathbf{S}} : \bar{\mathbf{S}})}$  where  $\bar{\mathbf{S}}$  is the effective stress deviator (or deviatoric part of the effective stress tensor), defined as  $\bar{\mathbf{S}} = \bar{\boldsymbol{\sigma}} + \bar{p}\mathbf{I}$ .

The CDP model assumes a nonassociated potential plastic flow that allows a realistic modeling of the volumetric expansion under compression for concrete [152]. The flow potential  $G$  used for this model is the Drucker-Prager hyperbolic function:

$$G = \sqrt{(\epsilon f_t \tan \psi)^2 + \bar{q}^2} - \bar{p} \tan \psi \quad (3.3)$$

where  $f_t$  is the uniaxial tensile strength of concrete. The parameters  $\psi$  and  $\epsilon$  determine the shape of the flow potential surface:  $\psi$  is the dilation angle measured in the  $p - q$  plane at high confining pressure, while  $\epsilon$  is referred to as the eccentricity of the plastic flow potential surface. The dilation angle represents the angle of inclination of the failure surface towards the hydrostatic axis in the meridian plan [94]. The flow potential eccentricity affects the exponential deviation of  $G$  from the linear Drucker-Prager flow potential [118] (Figure 3.2) and defines the rate at which the function approaches the asymptote (the flow potential tends to a straight line as the eccentricity tends to zero)[187].

The nonassociative flow rule, which is used in the CDP model requires a yield surface that determines states of failure or damage. The model uses a yield condition based on the loading function proposed by Lubliner *et al.* [113], with the modifications proposed by Lee and Fenves [103] to account for different evolutions of strength under tension and compression. The yield function used in CDP model is expressed in the effective stress space and depends on two hardening variables  $\epsilon_t^{pl}$  and  $\epsilon_c^{pl}$ :

$$F = \frac{1}{1 - \alpha} (\bar{q} - 3\alpha\bar{p} + \beta(\epsilon^{pl}) \langle \bar{\sigma}_{max} \rangle - \gamma \langle -\bar{\sigma}_{max} \rangle) - \bar{\sigma}_c(\epsilon_c^{pl}) = 0 \quad (3.4)$$

with  $\epsilon_t^{pl}$  and  $\epsilon_c^{pl}$  are the plastic strain of concrete in tension and compression, respectively. In this expression,  $\bar{\sigma}_{max}$  represents the maximum principal effective stress and  $\langle . \rangle$  is the symbol of the Macaulay bracket which is defined by  $\langle x \rangle = \frac{1}{2}(|x| + x)$ .

Moreover,  $\alpha$  is a dimensionless material constant and depends on the ratio of concrete strengths under biaxial and uniaxial compression as follows:

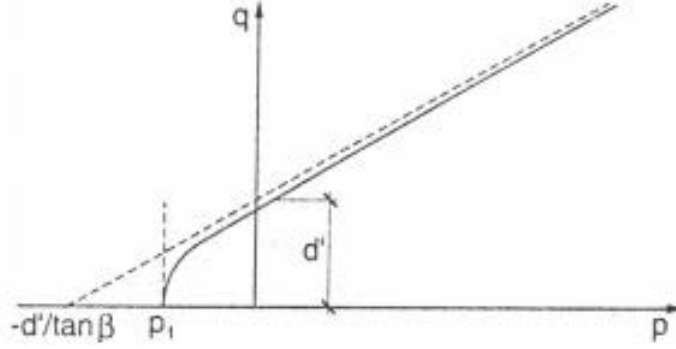


Figure 3.2: Drucker-Prager hyperbolic function of CDP flow potential and its asymptote in the meridian plane [94]

$$\alpha = \frac{(f_b/f_c) - 1}{2(f_b/f_c) - 1}, \quad 0 \leq \alpha \leq 0.5 \quad (3.5)$$

A biaxial laboratory test is necessary to define the value of  $\alpha$  [100] (Figure 3.3.a). Typical experimental values of  $\alpha$  are within 0.08 and 0.12 [113], while Abaqus allows a range of values between 0 and 0.5 [6].  $f_b$  represents the biaxial compressive strength of concrete and  $f_c$  is its uniaxial compressive strength.

$\beta$  is a material function of the two hardening variables  $\varepsilon_t^{pl}$  and  $\varepsilon_c^{pl}$  and includes the ratio of the biaxial to uniaxial compressive strength. It is expressed in terms of the effective tensile stress  $\bar{\sigma}_t$  and effective compressive stress  $\bar{\sigma}_c$  as follows:

$$\beta = \frac{\bar{\sigma}_c(\varepsilon_c^{pl})}{\bar{\sigma}_t(\varepsilon_t^{pl})}(1 - \alpha) - (1 + \alpha) \quad (3.6)$$

The coefficient  $\gamma$  represents a dimensionless material constant included in the CDP model only for the stress states of triaxial compression when  $\bar{\sigma}_{max} < 0$  [187] to better predict the concrete behavior in compression under confinement [152].  $\gamma$  is calculated in terms of the coefficient  $K_c$  that controls the failure surface in the deviatoric cross section:

$$\gamma = \frac{3(1 - K_c)}{2K_c - 1} \quad (3.7)$$

$K_c$  is the ratio of the second invariant on the tensile meridian to that on the compressive meridian at any given value of the pressure invariant  $p$  [6]. Physically, it represents the ratio of the distances between the hydrostatic axis and respectively the compression meridian and the tension meridian in the deviatoric cross section [94] (Figure 3.3.b). In Abaqus,  $K_c$  must satisfy the condition  $0.5 \leq K_c \leq 1.0$ . For  $K_c = 1$ , the deviatoric cross section of the failure surface becomes a circle.

### 3.6.2.2 Stress-strain curve for uniaxial compression

The constitutive equation under uniaxial compression for the CDP model takes the following form [6, 113]:

$$\sigma_c = (1 - d_c)E_c(\varepsilon_c - \varepsilon_c^{pl}) = E(\varepsilon_c - \varepsilon_c^{pl}) \quad (3.8)$$

where  $d_c$  is the damage variable in the compression zone, it can take value from zero, representing the undamaged material, to one, representing the total loss of strength.  $E_c$  is the initial (undamaged) elastic stiffness of the material, while  $E = (1 - d_c)E_c$  is the degraded elastic stiffness in compression.

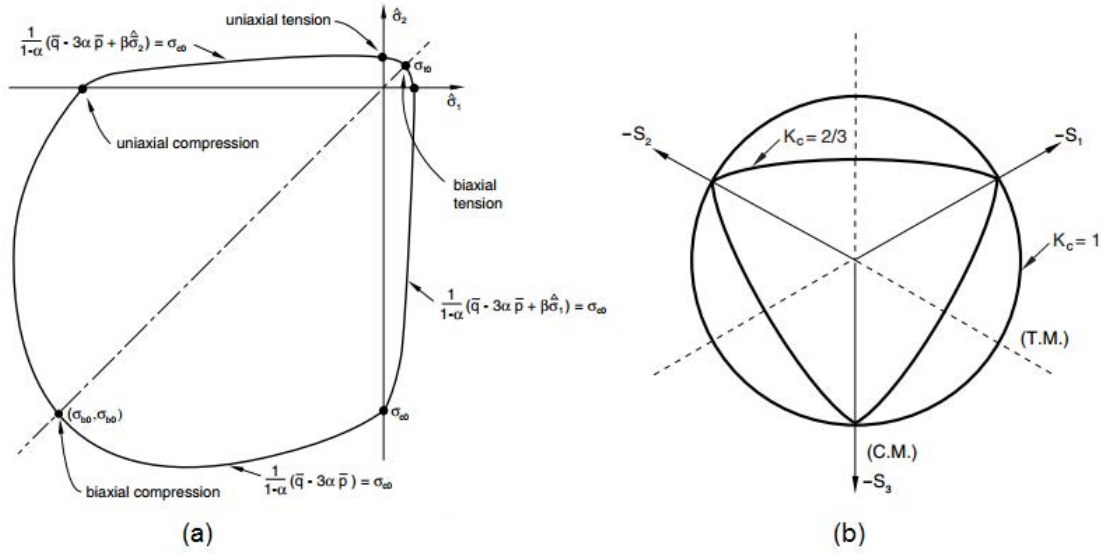


Figure 3.3: Yield surface for the CDP model in: (a) plane stress, (b) the deviatoric plane corresponding to different values of  $K_c$  [6]

The effective compressive stress is defined as:

$$\bar{\sigma}_c = \frac{\sigma_c}{(1 - d_c)} = E_c(\varepsilon_c - \varepsilon_c^{pl}) \quad (3.9)$$

where  $\varepsilon_c^{pl}$  is the equivalent plastic strain in compression.

Inelastic strains  $\varepsilon_c^{in}$  are used in the CDP model to describe the hardening rule. As illustrated in Figure 3.4, the compressive inelastic strain is defined as the total strain minus the elastic strain  $\varepsilon_{ce}$  corresponding to the undamaged material,

$$\varepsilon_c^{in} = \varepsilon_c - \varepsilon_{ce} \quad (3.10)$$

where

$$\varepsilon_{ce} = \frac{\sigma_c}{E_0} \quad (3.11)$$

### 3.6.2.3 Stress-strain curve for uniaxial tension

The stress-strain relation under uniaxial tension is similar to that in compression and takes the following form [6, 113]:

$$\sigma_t = (1 - d_t)E_t(\varepsilon_t - \varepsilon_t^{pl}) = E(\varepsilon_t - \varepsilon_t^{pl}) \quad (3.12)$$

where  $d_t$  is the damage variable in the tension zone and  $E = (1 - d_t)E_c$  is the degraded elastic stiffness in tension.

The effective tensile stress is defined as:

$$\bar{\sigma}_t = \frac{\sigma_t}{(1 - d_t)} = E_c(\varepsilon_t - \varepsilon_t^{pl}) \quad (3.13)$$

where  $\varepsilon_t^{pl}$  is the equivalent plastic strain in tension. The values of  $d_t$  range from 0 to 1 representing the undamaged material and the total loss of strength, respectively.

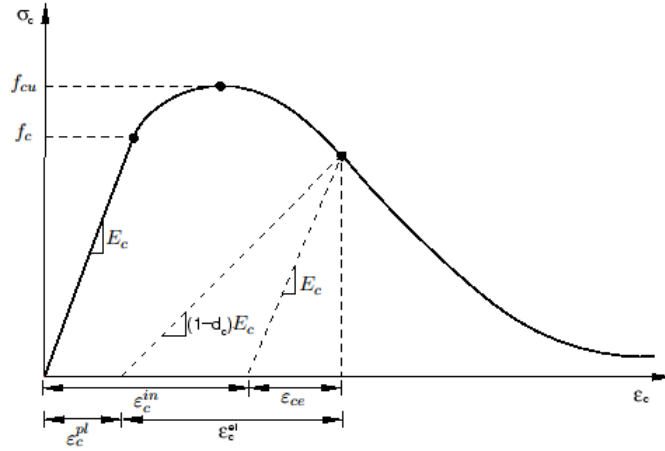


Figure 3.4: Response of concrete to uniaxial loading in compression for CDP model [6]

The strain-softening behavior for cracked concrete is defined by the phenomenon called tension stiffening which is required in the CDP model. The tension stiffening effect depends on several factors such as the density of reinforcement, the quality of the bond between the rebar and the concrete, the relative size of the concrete aggregate compared to the rebar diameter, and the mesh ([7]).

The tension stiffening can be specified in two ways:

- A postfailure stress-strain relation in term of the cracking strain  $\varepsilon_t^{ck}$  which is used in the CDP model for numerical analyses. The strain after cracking is defined as the difference between the total tensile strain and the elastic strain  $\varepsilon_{te}$  for the undamaged material (Figure 3.5):

$$\varepsilon_t^{ck} = \varepsilon_t - \varepsilon_{te} \quad (3.14)$$

where

$$\varepsilon_{te} = \frac{\sigma_t}{E_c} \quad (3.15)$$

The specification of a postfailure stress-strain relation introduces mesh sensitivity in the results, especially in cases with little or no reinforcement.

- A fracture energy cracking criterion which is adequate to reduce the concern of the mesh sensitivity. Hillerborg [81] defines the energy required to open a unit area of crack ( $G_f$ ) as a material parameter, using brittle fracture concepts. CDP model assumes a linear loss of strength after cracking (Figure 2.38.a). The cracking displacement at which complete loss of strength takes place is, therefore,  $w_c = 2G_f/f_t$ . Descending branch after cracking can be also presented by a bi-linear or tri-linear tension softening curve. In Abaqus, the fracture energy cracking model is introduced by specifying the postfailure stress as a tabular function of cracking displacement.

### 3.6.2.4 Damages

The variation of the elastic modulus of concrete can be due to two damage mechanisms of concrete in tension and compression, respectively [27]. In uniaxial tension, plastic strains are very small compared to those in compression, and concrete nonlinear response induces a lot of damage due to microcracking. Positive strains controls the tension damage by producing microcrack opening and

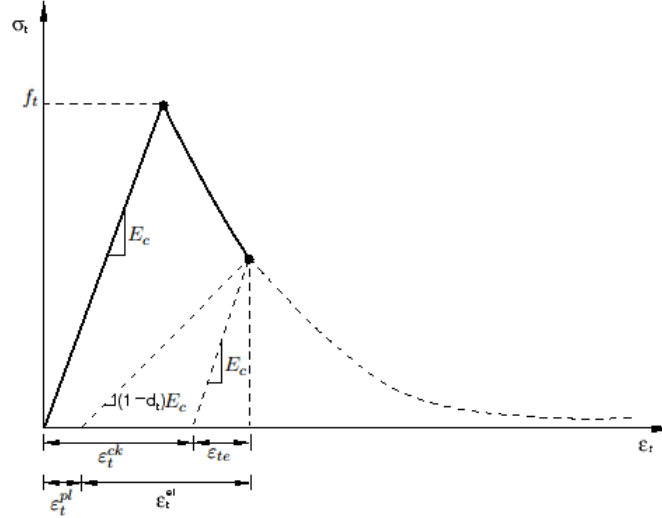


Figure 3.5: Response of concrete to uniaxial loading in tension for CDP model [6]

growth. In uniaxial compression, important plastic strains are observed with little damage. The compression damage mechanism is the crushing in material which induces the volume fraction of voids due to irreversible plastic strains. Thus, tensile damage and compressive damage of concrete provide quite different responses, as indicated in some experimental observations [104].

To account for this difference, the CDP model considers two independent damage variables, namely the tensile damage  $d_t$  and compressive damage  $d_c$ . As previously mentioned, these damages can take values ranging from zero, for the undamaged concrete, to one, for the fully damaged concrete. Experiments to determine the damage variable in terms of the equivalent plastic strains are very difficult to perform, thus many researchers studied the decrease of elastic stiffness and proposed expressions to tensile and compressive damages [27, 48, 73, 96, 104, 113, 118, 120]. Damage evolution of concrete in tension and compression can be derived from uniaxial stress strain curves and formulated as increasing functions of the inelastic strains. Pavlovic *et al.* [154] as well as Jankowiak and Lodygowski [87] compared undamaged and damaged concrete responses in order to determine the expressions of tensile and compressive damages, respectively, as follows:

$$d_t = 1 - \frac{\sigma_t}{f_t} \quad (3.16)$$

$$d_c = 1 - \frac{\sigma_c}{f_c} \quad (3.17)$$

However, Korotkov *et al.* [98] and Wahalathantri *et al.* [178] assumed the tensile damage variable to be equal to the ratio of the cracking strain to the total tensile strain, and similarly defined the compressive damage variable as the ratio of the crushing strain to the total compressive strain.

In Abaqus, the accuracy of damage evolution should be evaluated by ensuring that no negative and/or decreasing plastic strain are produced with the increase of stress [7]. Tensile and compressive plastic strains can be expressed in Abaqus for the CDP model in terms of the cracking and crushing strains, respectively, as follows:

$$\varepsilon_t^{pl} = \varepsilon_t^{ck} - \frac{d_t}{(1-d_t)} \frac{\sigma_t}{E_c} \quad (3.18)$$

$$\varepsilon_c^{pl} = \varepsilon_c^{in} - \frac{d_c}{(1 - d_c)} \frac{\sigma_c}{E_c} \quad (3.19)$$

Negative and/or decreasing plastic strains are indicative of incorrect damage evolutions, which leads to generate error message in Abaqus before the analysis is performed [7].

### 3.6.3 Constitutive model of reinforcing steel

The uniaxial behavior of steel shows that steel can be modeled as an elasto-plastic material with isotropic strain hardening characterized by an increase in stress with the increase of inelastic strain. Thus, plasticity models are found to be the simplest and most computationally efficient models for predicting steel behavior.

In Abaqus, the von Mises yield criterion, associative flow rule and isotropic hardening are typically used for modeling structural steel. The von Mises yield criterion can be written as:

$$F(\sigma, R) = \bar{q} - f_y - R(p) \leq 0 \quad (3.20)$$

where  $f_y$  is the yield stress,  $R(p)$  is the isotropic hardening stress and  $\bar{q}$  is the von Mises equivalent stress (see 3.6.2.1).

The evolution of the plastic strain is governed by the following plastic flow rule:

$$\dot{\varepsilon}_{ij}^p = \dot{\lambda} \frac{\partial f}{\partial \sigma_{ij}} \quad (3.21)$$

with  $\dot{\varepsilon}_{ij}^p$  is the plastic strain rate and  $\dot{\lambda}$  is the plastic multiplier.

## 3.7 Finite elements

Abaqus provide a wide variety of element types available, it is important to select the correct element for a particular application. Choosing an element for a particular analysis can be simplified by considering specific element characteristics: first- or second-order, full or reduced integration, hexahedra/quadrilaterals or tetrahedra/triangles. By considering each of these aspects carefully, the best element for a given analysis can be selected.

In this study, hexahedral solid elements with 8 nodes with reduced integration (C3D8R) are used during the simulations of the problem involving contact-impact of reinforced concrete (Figure 3.6). These solid (or continuum) elements in Abaqus can be used for complex nonlinear analyses involving contact, plasticity, and large deformations. These elements use linear interpolation in each direction and are often called linear elements or first order elements. These elements have only three displacement degrees of freedom and are stress/displacement elements. Hourglassing can be a problem with first-order, reduced-integration elements (such as C3D8R) in stress/displacement analyses. Since the elements have only one integration point, it is possible for them to distort in such a way that the strains calculated at the integration point are all zero, which, in turn, leads to uncontrolled distortion of the mesh. First-order, reduced-integration elements in Abaqus include hourglass control, but they should be used with reasonably fine meshes. There are advantages involved with the use of the hexahedral elements since they provide solution of equivalent accuracy at less computational cost and allow a better convergence rate and a more uniform mesh compared to tetrahedral elements. The computational efficiency of reduced-integration element is very high compared to the fully integrated element, especially in the problems involving contact-impacts.

Three dimensional truss elements having two degrees of freedom (T3D2) are used to represent the reinforcement in FEM (Figure 3.6). Truss elements are used in two and three dimensions to model slender structures that support loading only along the axis or the centerline of the element. No

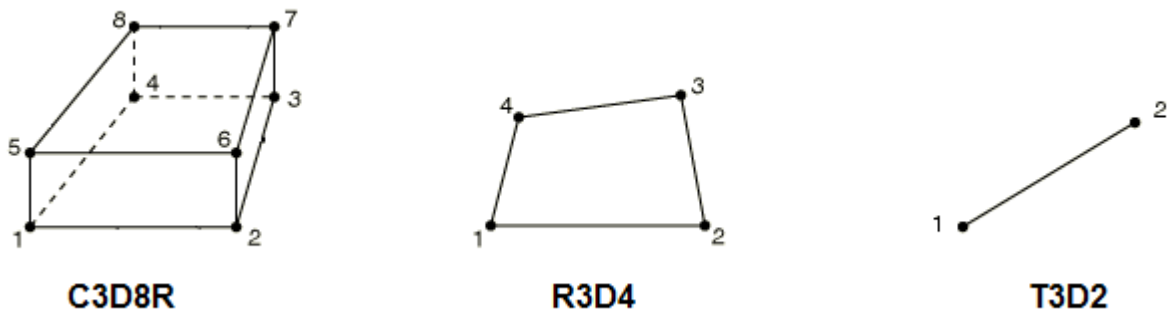


Figure 3.6: Finite elements used for the problem involving contact-impact of reinforced concrete [5]

moments or forces perpendicular to the centerline are supported. A 2-node straight truss element, which uses linear interpolation for position and displacement, has a constant stress. The cross-sectional area associated with the truss element as part of the section definition. When truss elements are used in large-displacement analysis, the updated cross-sectional area is calculated by assuming that the truss is made of an incompressible material, regardless of the actual material definition. Truss elements have no initial stiffness to resist loading perpendicular to their axis. The most common applications of trusses at large strains involve yielding metal behavior in which cases the material is effectively incompressible.

4-node R3D4 rigid elements are used to define the surfaces of rigid bodies presented in the FEM (Figure 3.6). R3D4 elements can be used in three-dimensional analysis to define master surfaces for contact applications. Rigid elements must always be part of a rigid body. By default in Abaqus/Explicit, rigid elements do not contribute mass to the rigid body to which they are assigned. To define the mass distribution, you can specify the density of all rigid elements in a rigid body. When a nonzero density and thickness are specified, mass and rotary inertia contributions to the rigid body from rigid elements will be computed in an analogous manner to structural elements.

### 3.8 Contact modeling between slab and impactor

Abaqus/Explicit provides two algorithms for modeling contact and interaction problems: the general contact algorithm and the contact pair algorithm. Both algorithms can be used with three-dimensional surfaces. The general contact algorithm allows very simple definitions of contact with very few restrictions on the types of surfaces involved. The contact pair algorithm has more restrictions on the types of surfaces involved and often requires more careful definition of contact. The general contact and contact pairs algorithms in Abaqus/Explicit differ by more than the user interface; in general they use completely separate implementations with many key differences in the designs of the numerical algorithms. Contact definitions are greatly simplified with the general contact algorithm which allows generating contact forces to resist node-into-face. To define a contact pair, pairs of surfaces that will interact with each other must be indicated.

Abaqus/Explicit uses two different methods to enforce contact constraints with the contact pair algorithm, namely the kinematic contact algorithm that uses a kinematic predictor/corrector contact algorithm to strictly enforce contact constraints and the penalty contact algorithm that has a weaker enforcement of contact constraints but allows for treatment of more general types of contact. There are differences in the way in which the kinematic and penalty contact algorithms enforce contact constraints (Figure 3.7). Using Abaqus analysis guide [5], the differences can be described as follows:

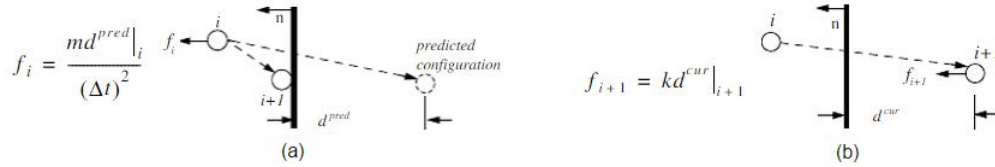


Figure 3.7: Constraints with the contact pair algorithm: a) Kinematic contact, b) Penalty contact [5]

- The kinematic algorithm is a predictor/corrector method. When kinematic contact is considered in the analysis, Abaqus/explicit carries out a predictor phase and a corrector phase in each time increment. In the predictor phase the kinematic state of the model is advanced by ignoring any contact conditions. This can result in overclosure or penetration. In the corrector phase of the time increment, an acceleration correction is applied to the slave and master nodes to correct for this predicted penetration, while conserving momentum. This correction results in a final configuration for increment in which the slave node is exactly in compliance with the master surface.
- The penalty algorithm uses an explicit approach to enforce contact constraints. In contrast to the kinematic algorithm, a corrector phase is not processed for an increment. Rather, an interface “spring” is inserted automatically between the slave node and the master face in increment to minimize the contact penetration. The force associated with the interface spring is equal to the spring stiffness multiplied by the penetration distance. Therefore, a small residual penetration will exist since contact forces are not generated unless there is some amount of penetration at the beginning of the increment.

In a mechanical contact simulation the interaction between contacting bodies is defined by assigning a contact property model to a contact interaction, including a constitutive model for the contact pressure-overclosure relationship that governs the motion of the surfaces and a friction model that defines the force resisting the relative tangential motion of the surfaces. The contact pressure-overclosure relationship used in this study is referred to as the “hard” contact model (Figure 3.8.a). Hard contact implies that the surfaces transmit no contact pressure unless the nodes of the slave surface contact the master surface. No penetration is allowed at each constraint location and no limit to the magnitude of contact pressure can be transmitted when the surfaces are in contact. The classical isotropic Coulomb friction model is used to model the friction between the contacting bodies in terms of the stresses at the interface of the bodies (Figure 3.8.b). The basic concept of the Coulomb friction model is to relate the maximum allowable frictional (shear) stress across an interface to the contact pressure between the contacting bodies. In the basic form of the Coulomb friction model, two contacting surfaces can carry shear stresses up to a certain magnitude across their interface before they start sliding relative to one another. The friction coefficient needs to be defined for the mechanical tangential interaction.

## 3.9 Constraints

### 3.9.1 Approaches to represent steel in RC numerical analysis

Typically, three distinct approaches are available in finite element analysis to represent steel reinforcement in a 3D finite element model of a RC structure, namely smeared approach, embedded

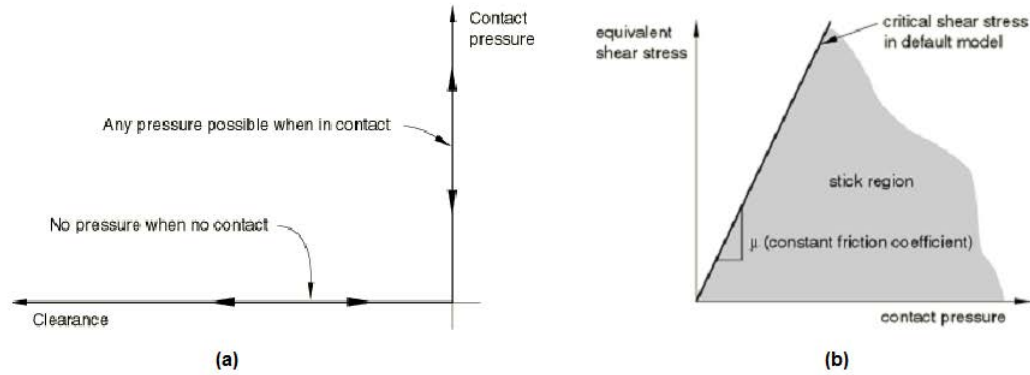


Figure 3.8: Contact interaction properties: a) Hard contact model, b) Coulomb friction model [5]

approach and discrete approach. These approaches allow the interactions between the concrete elements and the reinforcement elements by specifying the constraints on the degrees of freedom of the relevant nodes.

In the smeared or distributed approach (Figure 3.9.a), the distribution of reinforcing steel is assumed to be uniform over the concrete elements in the appropriate direction. As a result, the total stiffness of a smeared RC finite element depends on the stiffness of concrete and that assigned to steel reinforcement. In addition, the material properties in a smeared finite element are estimated according to composite theory based on individual properties of concrete and reinforcement. In this approach, reinforcing bars are considered in the model using a ratio that depends on the size of the concrete structure and the amount of steel used. Therefore, it is not necessary to discretely simulate the bars as they are distributed in the finite model assuming a complete compatibility between steel and concrete. Abaqus allows modeling this approach using the rebar option to define layers of uniaxial reinforcement in concrete elements as smeared layers with a constant thickness. The thickness of layers is equal to the ratio of each reinforcing bar area to the spacing between bars [5]. This approach is usually applied for large structural models when modeling details of the reinforcement is not essential to evaluate the overall response of the structure [138, 169], or when the structure is heavily reinforced with a huge number of reinforcing bars and an exact definition of every single reinforcing bar is difficult [36].

The embedded approach allows an independent choice of concrete mesh, it is generally used to create a bond and arbitrarily define the reinforcing steel regardless of the mesh shape and size of the concrete element (Figure 3.9.b). Each reinforcing bar is considered as an axial member and its stiffness is evaluated independently from the concrete elements. The displacements of the reinforcement elements are compatible with those of the surrounding concrete elements. In this approach, the identification of the intersection points of concrete elements with reinforcement bars leads to additional nodes created in the model and located at the intersection points. This results in increasing the number of degrees of freedom in the analysis, and hence the computational time becomes more important. Abaqus allows the embedded element technique to model reinforcing bars as a group of elements embedded in 'host' solid elements that represent the concrete elements in a RC structure. Abaqus searches for the intersection nodes of the host and embedded elements and constrains their translational degrees of freedom to the interpolated values of the corresponding degrees of freedom of the host element [5]. This approach is generally found to be very advantageous in cases where modeling the reinforcement of a structure is complex [138], and to be more efficient than the discrete approach in term of the computational effort and improving the simulated interaction [169, 183].

The discrete approach is based on the use of separate elements to represent the reinforcing steel. Reinforcement can be modeled using truss or beam elements connected to the concrete mesh nodes in

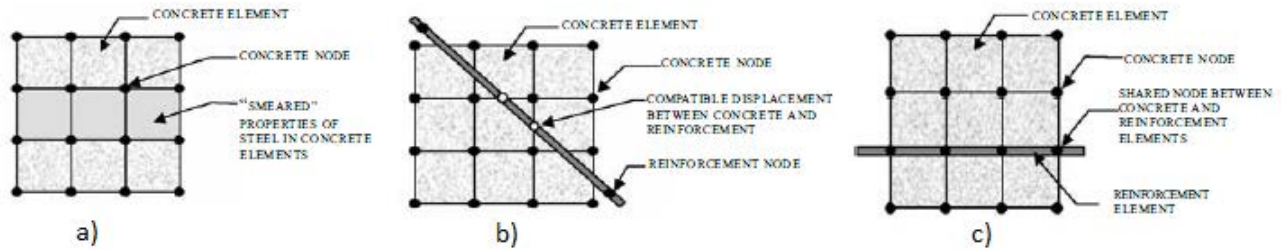


Figure 3.9: Approaches to represent steel in RC numerical analysis: a) smeared approach, b) embedded approach, c) discrete approach [138]

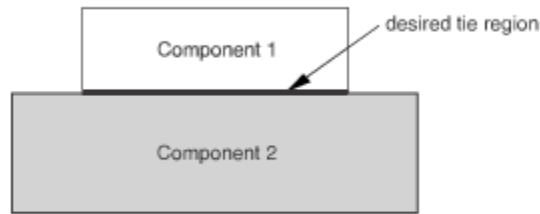


Figure 3.10: Tie constraint to tie two surfaces together in Abaqus [5]

the way that the mesh discretization boundary of concrete elements must overlap the direction and location of the steel reinforcement elements (Figure 3.9.c). As a result, concrete and reinforcement elements share common nodes and they are superimposed at some specified same regions. Perfect bond is usually assumed between concrete and steel. However, in cases where slip of reinforcing bars with respect to the surrounding concrete is of concern, fictitious spring elements of no physical dimension can be used to model the bond-slip between reinforcing steel and concrete. These elements are defined as linkage elements to connect concrete nodes with reinforcement nodes having the same coordinates, and are determined by their mechanical properties and a specific bond-slip relationship [36, 138].

### 3.9.2 Tie constraint

A surface-based tie constraint in Abaqus is used to define a fully constrained contact behavior by providing a simple way to tie two surfaces together for the duration of a simulation. It uses a master-slave formulation to prevent slave nodes from separating or sliding relative to the master surface. As a result, an assignment of slave and master surfaces should be carried out to define the contacting surfaces. Typically, a rigid surface is always considered as master surface, and slave surface mesh must be sufficiently refined to interact with the master surface. In case where two deformable surfaces need to be tied, master surface should be that of the material with higher Young's modulus or larger cross-sectional area [7]. This type of constraints enables to tie translational and rotational motions between two surfaces, hence each of the nodes of the slave surface is constrained to have the same motion as the node of the master surface to which it is closest. Abaqus eliminates the degrees of freedom of the slave surfaces nodes that are constrained and allows the tie constraints only in cases where the two surfaces to tie are close to one another (Figure 3.10) [5].

### 3.10 Output

For the analysis of RC slabs subjected to impact, a large amount of output can be requested and evaluated in Abaqus:

- Energies: kinetic energies for whole model and slab (ALLKE), internal energy (ALLIE), energy dissipated by plastic deformation (ALLPD), recoverable strain energy (ALLSE), artificial strain energy (ALLAE) and energy dissipated by viscous effects (ALLVD). When concrete damage is taken into account in simulations, the damage dissipation energy (ALLDMD) is also evaluated.
- Distributions of stresses (S11, S22, S33) on the upper and bottom surfaces of the RC slab at different given times of the simulation.
- Distributions of accelerations (A11, A22, A33) on the upper and bottom surfaces of the RC slab at different given times of the simulation.
- Distributions of velocities (V11, V22, V33) on the upper and bottom surfaces of the RC slab at different given times of the simulation.
- Distributions of displacements (U11, U22, U33) on the upper and bottom surfaces of the RC slab at different given times of the simulation.
- Distributions of stresses (S11) in the upper and lower reinforcement layers at different given times of the simulation.
- Graphical visualization of the cracking patterns in the slab obtained by assuming that cracking initiates at points where the tensile equivalent plastic strain is greater than zero and the maximum principal plastic strain is positive.
- Displacements, velocities and accelerations for the impactor, as well as for different nodes of the slab.
- Evolution of contact load (CFN3) between the impactor and the slab in terms of time and slab displacement at the point of impact.
- Compressive damage variable (DAMAGEC), tensile damage variable (DAMAGET) and the equivalent plastic strain (PEEQ) at different elements positioned at the center and the corner of the impacted face of the slab.

# Chapter 4

## Reliability analysis: principles and methods

### 4.1 Introduction to reliability

The concept of security is very old and inseparable from the state of knowledge of nature's laws and the concept of lifetime. It is simultaneous to construction practices and related to uncertain events as well as to the notion of codes and regulations. The early builders built for their personal use and were therefore interested in what the structure fulfills the functions that had been assigned. By referring to the history of constructions, many structures are no longer in use because of a lack of knowledge about nature's laws, in particular materials and loadings, but mostly because of the time elapsed since their application. It was only in the 18th century that numerical approaches have replaced by empirical approaches. Numerical approaches allowed reducing the concept of security to a deterministic notion since they are based on the analysis of stresses: stress is obtained by a "safety factor" that comprises a certain number of unknowns and limits them to a single factor.

In the fifties, Freudenthal became the head of the safety probabilistic approach that has made a significant progress in the domain of structures [63, 64, 65, 66]. This approach is based on the uncertain aspect of loadings on structures, material properties and mechanical models used for design. Thus, any probabilistic approach requires the acquaintance of a risk that is not identified and does not exist in deterministic approaches. The control of risk would first result from expert knowledge and algorithmic knowledge (rules and techniques). Both knowledge increase exponentially with human development. The reliability theory and its tools were initiated in the modern era based on probability theory. Recently, probabilistic approaches were introduced in the domain of civil engineering to control risks related to design choices. This control can be included in design process by combining a stochastic data model to a mechanical data model for a mechanical behavior [106] (couplage mécano-fiabiliste).

Reliability is defined as the probability so that an *“equipment could be used without failure for a given period of time, under specified operational conditions”* (*Grand Larousse*). Considered as the ability of a structure to achieve a required function under certain given conditions and within a given timeframe, reliability can be applied to any system that is expected to correctly carry out its functions, e.g. a civil engineering structure. Reliability theory is based on methods using probabilities to assess failure probability that is mathematically considered as the complement of the reliability of the unit. A reliability approach of a mechanical system allows examining the statistical dispersion of quantities, rejecting values out of tolerance and verifying their variability. Many methods based on probability theory were developed, they permit to calculate the probability of failure of structures on the one hand, and to study the influence of variability of design parameters on the structural behavior on the other hand. Uncertainties are modeled in terms of the mean, the

variance and the probability density of input variables. Reliability approach was widely used in order to ameliorate the design of RC structures. Arafah [12] studied the reliability of RC beam sections by considering a limit state in flexion and using Monte Carlo method. Araujo [13] presented a reliability analysis of RC columns by combining a FEM with MC in order to calculate the mean and standard deviation of the ultimate load applied to column. Val *et al.* [177] proposed a probabilistic method to evaluate the reliability of RC frames with respect to an ultimate limit state. The method consisted in coupling a nonlinear FEM with FORM by considering all the possible sources of uncertainty. Low *et al.* [110] performed a reliability study on RC slabs subjected to explosion. Two deterministic models were considered: a FEM and an analytical model of one degree of freedom. The comparison of these two models was performed in a probabilistic framework by estimating the failure probability with MC in the case of FEM, and with FORM/SORM in the other case. Two failure criteria related to the slab displacement and the deformation in reinforcement were considered. The simplified model was used in a parametric study to evaluate the effect of various parameters on the slab reliability.

In the current study, the platform OpenTURNS (version 13.2) is used under Linux environment to perform reliability approach for several types of RC structures. The name OpenTURNS is for open source Treatment of Uncertainty, Risk 'N Statistics. OpenTURNS was developed as a C++ library and a Python TUI by EDF R&D, Airbus Group and Phimeca Engineering at the beginning of 2005, with the collaboration of EMACS in 2014 [14]. OpenTURNS is an open source software dedicated to uncertainty propagation by probabilistic methods, it includes a set of efficient mathematical methods for reliability analysis and can be easily connected to any external computational code. These features allow using OpenTURNS for different engineering and industrial problems. In addition, a complete documentation is provided for OpenTURNS and can be found on its dedicated website [www.openturns.org](http://www.openturns.org).

In this chapter, the principles of structural reliability analysis, as well as the types of uncertainty related to the structure and the deterministic model used, are presented. Next, the steps of a reliability analysis are detailed and the methods used in OpenTURNS for uncertainty quantification, uncertainty propagation and sensitivity analysis are described. Finally, statistical descriptions of random variables intervening in RC structures are examined according to several studies in the literature.

## 4.2 Principles of structural reliability analysis

A civil engineering structure is a complex system composed of more or less simple elements behaving in series or in parallel. This structure should provide a number of functions (mechanical strength, durability, ...) with a certain level of reliability. In general, structural analysis and design are based on deterministic methods and attempt to assure reliability by the application of safety factors. However, due to many sources of uncertainties associated with loads, material properties, geometry and modeling approach of structures, probabilistic concepts have to be used. Thus, structural reliability analysis should be considered and functions are performed by not exceeding a certain threshold level.

The aim of structural reliability analysis is to determine the probability that the structure does not perform its functional requirements. Structural reliability theory is based on the probabilistic modeling of the uncertainties and provides methods to estimate the probability of failure. The failure of the structure is defined through the concept of limit state which represents a boundary between satisfactory and unsatisfactory performance of the structure.

Sorensen [165] has provided the main steps in a reliability analysis:

1. Selection of an accepted or specified target reliability level.
2. Defining failure modes of the structure, i.e. flexure, shear, torsion, fatigue, local damage.

3. Decomposition of failure modes into series systems or parallel systems of single components, in the case where failure modes consist of more than one component. A series system leads to the failure of the entire system if one of the system components fails, while for a parallel system no failure is induced as long as not all the system components fail.
4. Modeling the uncertainty of deterministic parameters (loads, dimensions, materials properties) by random variables and specifying the probability distribution types and statistical parameters for these variables and the correlation between them.
5. Definition of limit state functions corresponding to each component in failure modes (ultimate and serviceability limit states). Limit states are formulated in terms of the basic random variables.
6. Estimating the probability of failure for each failure mode (simulation methods, approximations methods, response surface methods).
7. Performing sensitivity analyses in order to evaluate the sensitivity of the probability of failure with respect to stochastic variables.

According to [153], the acceptable probabilities for structural failure are in order of  $10^{-3}$  for serviceability limit states and  $10^{-6}$  for ultimate limit states.

Sorensen [165] showed that the estimated probability of failure should be considered as a nominal measure of reliability since the information used in reliability analyses are generally not complete.

### 4.3 Uncertainty sources

Reliability analysis requires the knowledge of uncertainties related to the structure or system studied. Nevertheless, before proceeding to reliability analysis and collecting information about uncertainties, an engineer needs to know that engineering systems are exposed to several types of uncertainty and each type requires a different process to be used in the evaluation of reliability. The uncertainties in structures or systems can be classified into five groups [165, 59], namely physical uncertainties, measurement uncertainties, statistical uncertainties, model uncertainties and others.

#### 4.3.1 Physical uncertainties

Physical uncertainties are typically associated with loads, geometry of the structure and mechanical properties of materials. A perfect knowledge of geometric dimensions is impossible since their variability highly depends on errors in manufacturing and construction process. The uncertain aspect of material properties is due to heterogeneity that describes the variability of material characteristics from one point to another even in the same structural element. Loadings that can be classified as permanent, unstable or accidental actions represent also an uncertain aspect in time since their time history cannot be predicted in advance with certainty. Consequently, reliability analysis allows representing these uncertainties by random variables and/or stochastic processes and fields of which statistical parameters must be evaluated properly. In most cases, random variables defined by probability distributions are sufficient to model the uncertain quantities. A stochastic process can be defined as a random function of time in a way that the value of the stochastic process is considered as random variable for any given point in time. Stochastic fields are defined as a random function of space and the value of the stochastic field is a random variable for any given point in the structure.

### 4.3.2 Measurement uncertainties

Measurement uncertainties are caused by inaccurate measurements of variable values and are attributed to uncontrolled factors and imperfections in test conditions. Because of several fluctuations in the environment, test procedures, tools and so on, repeated measurements of the same physical variable do not give the same value. In addition, resistance of actual physical structures includes more uncertainties than structures tested under restrained laboratory conditions as they are subjected to more uncertain environments that may be sometimes very severe. Thus, an engineer should respond to this type of uncertainty by collecting a large number of observations, which may be limited to the availability of resources such as money and time, as well as to the scale of the structure considered. The procedure of collecting observations can provide sufficient information about the measured quantity variability and may lead to a certain level of confidence in the value used for design.

### 4.3.3 Statistical uncertainties

Uncertainties in reliability analysis can also result from statistical parameters that are significantly dependent on sampling methods, variance estimation and choice of probability distribution type for random variables. These parameters should be properly assessed and a confidence interval should be estimated and associated for each parameter. Statistical uncertainties are due to incomplete statistical information owing to limited sample sizes of observed quantities. Statistical parameters can be considered as random variables and are used to fit an input data sample to a mathematical function [163].

### 4.3.4 Model uncertainties

Model uncertainties are associated with structural idealizations of deterministic models used to predict the physical behavior of structures and their response. Mechanical models are based on several assumptions and can be performed using an empirical, analytical or numerical approach. However, these assumptions considered in deterministic models can lead to inaccuracy results and simple models do not take into account all possible factors that influence the structural behavior. Therefore, mechanical models introduce another type of uncertainty related to modeling error. They are considered as an approximate prediction of the structural behavior since they always show some difference compared to actual response. The difference between calculated and actual responses can be used to develop a statistical description of the modeling error that can be introduced as an additional random variable in reliability analysis.

### 4.3.5 Other uncertainties

Other sources of uncertainty that cannot be covered by reliability analysis can arise from the definition of certain parameters, the performance of structures, human factors, i.e. the competence and experience of builders and engineers.

## 4.4 Reliability approach

The aim of deterministic models is to analyze structural behavior and predict the physical phenomena observed by evaluating mechanical loads or stresses ( $S$ ) and resistances ( $R$ ). Nevertheless, a validation of these models is necessary in order to reduce the difference between the response of the actual structure and that of the model. Input data of a calculation model are generally known with only some significant digits in spite of their uncertain aspect. By neglecting uncertainties the calculated results may deviate significantly from reality, hence they should be taken into account

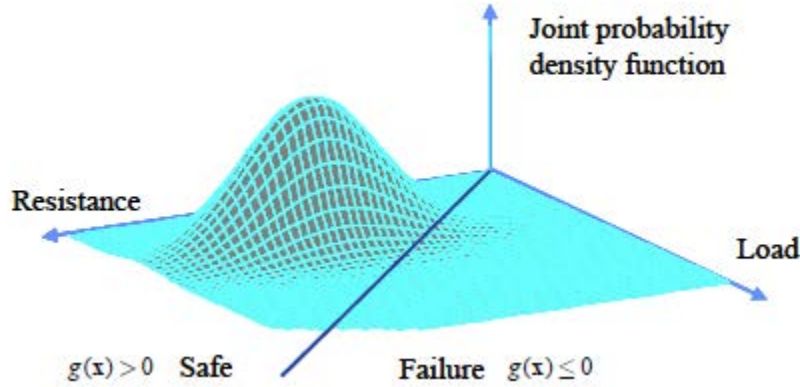


Figure 4.1: Limit state function [59]

during analysis. This can be accomplished by coupling the deterministic model with a probabilistic model that allows modeling uncertainties and performing structural reliability analysis. Design requirements become more complex by introducing uncertainties as the structure need to satisfy different criteria of failure, security and durability. The design should involve all relevant components so that the structure does not reach its limit state. For example, a structure must be designed in such a manner that its resistance is greater than the applied loads. In this case, the structure limit state can be expressed with a single random variable as  $Z = R - S$ . Figure 4.1 illustrates a volume integral of a two dimensional joint probability density function, where the two random variables are the load and the resistance, and failure is defined as the event when the load exceeds the resistance.

Reliability approaches have the advantage of providing a realistic examination of uncertainties and controlling their effect on structures response. However, their application shows some limitations as they replace the reassuring notion of “safety factor” and confirm the acceptance of risks. In addition, limitations also arise as a result of lack of probabilistic knowledge and reasoning in engineering, lack of sufficient data, the difficulty of considering human errors and the novelty of development of tools and software to analyze reliability problems. A reliability approach is based on a statistical knowledge of basic random variables such as geometric properties, material characteristics and actions. Each variable requires a coefficient of variation (COV) and a probability distribution defined by statistical parameters such as mean and standard deviation. Then by using probabilistic methods, such as simulation or approximation methods, failure probability can be assessed by studying all possible failure modes in order to make better decisions for an economical design. For each mode, the equilibrium between loads and resistances is defined by a specific failure criterion represented by a limit state function ( $g(\mathbf{X})$ ) which is expressed in term of input random variables, but also depends on the deterministic model and the threshold of the output variable considered. A limit state function represents the state beyond which a structure can no longer perform the function for which it was designed and separates safe domain  $\mathbf{D}_s$  from failure domain  $\mathbf{D}_f$ , the latter corresponds to the domain for which the limit state function is negative ( $g(\mathbf{X}) \leq 0$ ) (Figure 4.1). Let’s first consider the simplest case of  $Z = R - S$ , safe domain corresponds to values that are reasonable and physically possible and acceptable, while failure domain corresponds to inadmissible values of the variable  $Z$ .

#### 4.4.1 Modeling of uncertainty

In practice, probabilities are rarely known and need to be estimated, which represent the most difficult part of reliability analysis. But before addressing this issue, uncertainties in structures

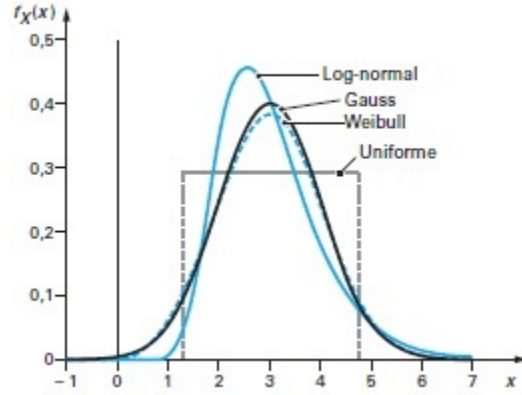


Figure 4.2: PDF of Gauss, Lognormal, Uniform and Weibull distributions with same mean and standard deviation [107]

or systems need to be quantified. This section describes how to model and quantify uncertainties in OpenTURNS, as well as the essential parameters and characteristics to include in a reliability analysis. Uncertainties are generally introduced in a probabilistic model as input variables assigned with a random aspect. Thus, the mathematical modeling of random variables is an essential task in any probabilistic formulation. A random variable and a particular realization of this variable are denoted in this dissertation with an uppercase letter  $X$  and a lowercase letter  $x$ , respectively. Only continuous random variables are considered in this study.

The probability density function (PDF),  $f_X(x)$ , allows modeling the uncertainty of a random variable. The cumulative distribution function (CDF),  $F_X(x)$ , allow estimating directly the probability that a random variable is found to have a value less or equal to a specific value. For continuous distributions, CDF represents the area under the PDF from minus infinity to the value desired and is given by:

$$P(X \leq x) = F_X(x) = \int_{-\infty}^x f_X(x)dx \quad (4.1)$$

PDF is hence expressed as:

$$f_X(x) = \frac{dF_X(x)}{dx} \quad (4.2)$$

Figures 4.2 and 4.3, respectively, show the probability density and cumulative distribution functions for four types of probability distributions of a random variable (Gaussian, Lognormal, Uniform and Weibull).

To define PDF, some parameters are needed to be identified, such as mean, variance, coefficient of variation, etc. The number of parameters depends upon the nature of uncertainty and the type of distribution. Therefore, the mean  $\mu_X$  of a continuous random variable  $X$  with PDF  $f_X(x)$ , also known as the first central moment, can be calculated as:

$$\mu_X = \int_{-\infty}^{+\infty} x f_X(x)dx \quad (4.3)$$

The corresponding variance of  $X$ , also known as the second central moment and denoted as  $Var(x)$ , indicates how data are distributed about the mean and can be estimated as:

$$Var(X) = \int_{-\infty}^{+\infty} (x - \mu_X)^2 f_X(x)dx \quad (4.4)$$

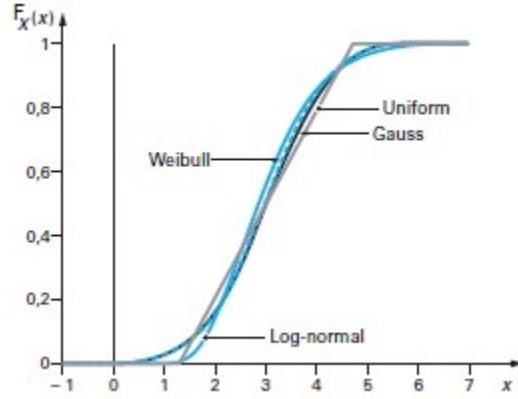


Figure 4.3: CDF of Gauss, Lognormal, Uniform and Weibull distributions with same mean and standard deviation [107]

The standard deviation, denoted as  $\sigma_X$ , is expressed in the same units as the mean value and is calculated as the square root of the variance:

$$\sigma_X = \sqrt{Var(X)} \quad (4.5)$$

The coefficient of variation of a random variable, denoted as  $COV(X)$  or  $COV$  is introduced as the ratio of the standard deviation to the mean. It is a nondimensional parameter that allows indicating the degree of dispersion in the random variable. A high  $COV$  indicates a significant uncertainty and an important aspect of randomness in the variable. For a deterministic variable,  $COV(X)$  is equal to zero.

$$COV(X) = \frac{\sigma_X}{\mu_X} \quad (4.6)$$

#### 4.4.1.1 Joint probability density function

From a practical point of view and in order to correctly formulate a reliability problem, it is necessary to model uncertainties jointly and to not limit the analysis to random variables modeled separately. Therefore, a reliability analysis should involve the modeling of multiple random variables. This can be accomplished by considering the joint probability density function  $f_{\mathbf{X}}(x)$ , which allows more information to be provided. In case of multiple random variable,  $\mathbf{X}$  represents the random vector of input variables and  $x$  is a particular observation of this vector. Each variable in  $\mathbf{X}$  is a random variable that can be related to structure parameters such as geometry, material properties or loads.  $f_{\mathbf{X}}(x)$  permits to calculate the probability that each of random variables exists in any particular range of specific values of that variable and satisfies the following condition:

$$\int_{R^n} f_{\mathbf{X}}(x_1, x_2, \dots, x_n) dx_1 dx_2 \dots dx_n = 1 \quad (4.7)$$

In case of independent variables, the joint density is the product of the probability distributions of variables. For two random variables, the joint probability density function can be described by a three-dimensional plot as show in Figure 4.1.

#### 4.4.1.2 Covariance and correlation

Covariance and correlation analyses are generally used to study the dependence or independence between two random variables in the aim of extracting as much information as possible for a reliability

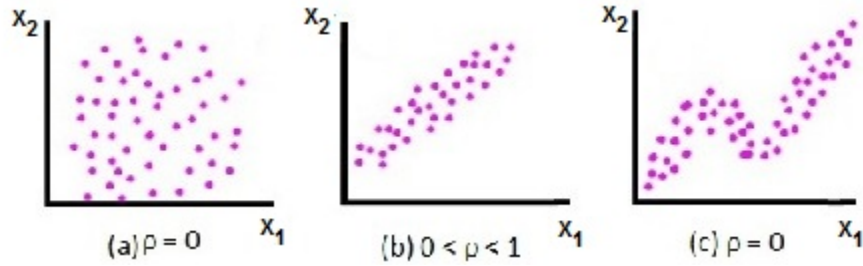


Figure 4.4: Correlation of two random variables

analysis. The covariance of two random variables  $X_1$  and  $X_2$ ,  $COV(X_1, X_2)$ , represents the second moment about their respective means  $\mu_{X_1}$  and  $\mu_{X_2}$ , and indicates the degree of linear relationship between  $X_1$  and  $X_2$ .  $COV(X_1, X_2)$  can be calculated as:

$$Cov(X_1, X_2) = \mu_{X_1 X_2} - \mu_{X_1} \mu_{X_2} \quad (4.8)$$

with  $\mu_{X_1 X_2} = \int_{-\infty}^{+\infty} \int_{-\infty}^{+\infty} x_1 x_2 f_{X_1 X_2}(x_1, x_2) dx_1 dx_2$ . Statistically independent variables have a covariance equal to zero.

The correlation coefficient,  $\rho_{X_1 X_2}$ , also represents the degree of linear dependence between two random variables and its values range between -1 and +1.  $\rho_{X_1 X_2}$  can be expressed as a nondimensional parameter by:

$$\rho_{X_1 X_2} = \frac{Cov(X_1, X_2)}{\sigma_{X_1} \sigma_{X_2}} \quad (4.9)$$

Figure 4.4 depicts the physical properties of the correlation coefficient. In Figure 4.4.a, the two random variables are uncorrelated, the correlation coefficient is expected to be zero and no linear relationship exists between them. Figure 4.4.b indicates a non perfect linear relationship between the two variables, with a correlation coefficient value that is expected to range between 0 and 1. In this case, the relationship between  $X_1$  and  $X_2$  is positive since  $X_2$  increases as  $X_1$ . However, in the case of a nonlinear relationship between two random variables (Figure 4.4.c),  $\rho_{X_1 X_2}$  is equal to zero.

In the present study, the correlation between random variables is not taken into consideration due to the lack of information provided on the relationship between the different parameters of the structures considered.

#### 4.4.2 Variable of interest

The aim of a reliability analysis is to assess the probability of a variable of interest exceeding a certain threshold. Variables of interest represent the output variables of the deterministic model considered in the study. The propagation of uncertainties of input variables is performed through the deterministic model towards output variables, hence these variables are affected by the randomness of the basic input variables and have also a random character. Therefore, a description of the randomness of a variable of interest is essential to provide the necessary information on its uncertainty. OpenTURNS allows evaluating the statistical characteristics of an output variable through a dispersion analysis and a distribution analysis. In engineering applications concerning structural reliability, a variable of interest can be related to forces (resistance of structure), deflections, stresses, strains, energies, etc. An output random variable is denoted in this dissertation as  $Y$ .

#### 4.4.2.1 Dispersion analysis

The purpose of a dispersion analysis is to characterize statistical parameters of one or more quantities of interest. This involves determining the statistical moments (e.g. mean and standard deviation) of the output variable, which depends on the accuracy desired and the method used. The quality of this estimation depends on the output sample size, the amount of uncertainty present in the corresponding variable and the confidence of level required for the prediction. A confidence interval corresponds to a range of values in which the mean of a variable are located. Two different methods can be used in OpenTURNS in order to estimate statistical moments of a variable of interest:

- Monte Carlo method which is a numerical integration method using sampling. This method consists in performing a sufficient number of random simulations of the input vector  $\mathbf{X}$  and evaluating the value of  $Y$  for each simulation. Then, the mean and standard deviation of the output sample can be estimated as:

$$\mu_Y = \frac{1}{N} \sum_{i=1}^N y_i \quad (4.10)$$

$$\sigma_Y = \left[ \frac{1}{N} \sum_{i=1}^N (y_i - \mu_Y)^2 \right]^{1/2} \quad (4.11)$$

The confidence interval that represents the mean estimation uncertainty permits to control the difference between the estimated and exact values. Its size decreases with the increase of the number of simulations and the convergence of the estimators to exact values can be assured if the sample size tends to infinity. However, the only limitation of this method resides in cases where the number of simulations is not sufficiently high, for example in case of a deterministic model with a significant computational effort. This can result in an important uncertainty for the estimations of  $\mu_Y$  and  $\sigma_Y$ , hence it is necessary to choose another propagation method, such as the quadratic combination method, to estimate the central uncertainty of  $Y$ .

- Quadratic combination method which enables to assess the central dispersion of an output variable by using a Taylor decomposition of  $Y$  in the vicinity of the mean point  $(\mu_{X_1}, \mu_{X_2}, \dots, \mu_{X_n})$  of random vector  $\mathbf{X}$ . This method depends on the order of the Taylor decomposition. OpenTURNS allows obtaining the estimations of  $\mu_Y$  and  $\sigma_Y$  with a Taylor approximation at first or second order, which may lead to inaccurate results in highly nonlinear deterministic models. However, quadratic combination method does not require any assumptions on the PDF type of input variables, it only depends on their mean value and their dispersion.

#### 4.4.2.2 Distribution analysis

The aim of a distribution analysis is to determine the PDF of output variables. The distribution of a variable of interest can be determined using its values calculated by the physical model through a sufficient number of simulations. The determination of the distribution that fits an output sample can be established graphically by plotting a histogram (Figure 4.5). A histogram can be developed by arranging the values of  $Y$  in increasing order and subdividing them into several equal intervals in each of which the number of observations is drawn. Then a distribution that fits the histogram needs to be selected to model the behavior of the randomness. OpenTURNS proposes 17 parametric distribution types to represent the uncertainty of a continuous variable, including normal, lognormal, Gamma, Weibull, etc. The values of the distribution parameters are estimated in terms of the output sample statistical moments. The probability density functions available in OpenTURNS are listed in Appendix A with their formulas and their statistical parameters. Once the type of distribution is selected and its parameters are evaluated, a statistical test of goodness-of-fit must

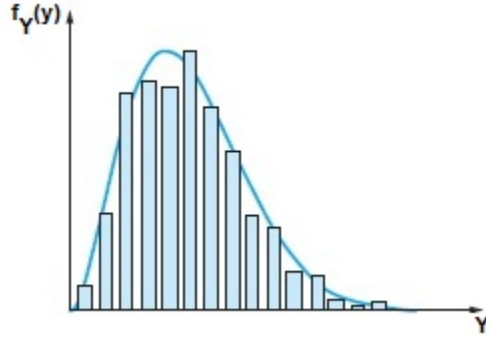


Figure 4.5: Representation of a sample of an output variable by a histogram [107]

be conducted to verify if the output sample and the probability distribution chosen are in good agreement. OpenTURNS provides Chi-squared goodness-of-fit test for discrete distributions and Kolmogorov-Smirnov test for continuous distributions. Graphical statistical tests such as QQ-plot can be also used to verify graphically if the assumed probability distribution is appropriate to describe the output variable  $Y$ .

Kolmogorov-Smirnov test compares the observed CDF of the sample and that of an assumed parametric distribution by estimating the maximum difference between the two CDF as follows:

$$D_n = \max |F_Y(y) - F_Y^S(y)| \quad (4.12)$$

where  $F_Y(y)$  is the theoretical CDF of the assumed distribution and  $F_Y^S(y)$  is the sample CDF.  $D_n$  is a random variable and its CDF is related to a risk of error  $\alpha$  as:

$$P(D_n \leq D_n^\alpha) = 1 - \alpha \quad (4.13)$$

$D_n^\alpha$  is the critical value of Kolmogorov-Smirnov test which is identified by default in OpenTURNS. The assumed distribution is considered as accepted if the maximum difference  $D_n$  is less or equal to  $D_n^\alpha$ . OpenTURNS introduces the notion of “p-value” which is equal to the limit error probability under which the assumed distribution is rejected (p-value =  $P(D_n \leq D_n^\alpha)$ ) and compares it to the p-value threshold  $\alpha$ . Thus, the assumed distribution is accepted only if p-value is greater than the value  $\alpha$  (a value of 0.05 is used in this study).

QQ-plot is based on estimates of the quantiles. The principle is to estimate the  $\alpha$ -quantiles that correspond to the output sample  $q_Y^S(\alpha)$  and the probability distribution chosen  $q_Y(\alpha)$ . Then, the points  $(q_Y^S(\alpha), q_Y(\alpha))$  are plotted and their positions according to the diagonal are verified. Consequently, the assumed distribution is considered as acceptable if these points are close to the diagonal.

In case where no parametric distribution fit the output sample, OpenTURNS provides a non-parametric statistical technique that allows representing the probability distribution of a random variable graphically and without referring to any statistical model, namely the Kernel Smoothing method. This method depends on the size of the sample.

### 4.4.3 Probability of failure

The aim of structural reliability is to determine the probability that the structure does not perform its functional requirements. This probability or failure probability  $P_f$  may be determined by the integral (4.14) in term of the limit state function:

$$P_f = P[g(\mathbf{X}) < 0] = \int_{g(x) \leq 0} f_{\mathbf{X}}(x) dx \quad (4.14)$$

In this equation  $f_{\mathbf{X}}(x)$  is the joint probability density function of the random variables  $\mathbf{X}$  which represent the uncertainties included in the reliability analysis and  $g(\mathbf{X})$  is the limit state function which is related to a specific failure mode. The integration is performed over the failure domain, for which  $g(\mathbf{X})$  is smaller or equal to zero. Integral 4.14 is considered as the fundamental equation for reliability analysis, however it is not easy to calculate because of the complexity of the failure domain  $D_f$  and the joint probability density function  $f_{\mathbf{X}}(x)$ , which may involve a large number of variables. In addition, the estimation of failure probability becomes even more difficult when complex deterministic models such as finite element models are considered. In order to assess failure probability, first, the limit state function should be defined for a special failure mode in term of input random variables, then several probabilistic methods can be used to solve the integral 4.14:

- Direct integration method allows estimating failure probability only in some particular cases where joint density functions have simple shapes.
- Numerical integration method may lead to significant errors for very low probabilities and the integration domain is not always bounded as well.
- Probabilistic simulation methods, such as Monte Carlo (MC), Latin Hypercube Sampling (LHS), Directional Simulation (DS) and Importance Sampling (IS), are based on a number of samples of random variables corresponding to failure
- Approximation methods are based on an approximation of the limit state function and an identification of the most probable point that permits to estimate failure probability. The limit state function is linearized in the First Order Reliability Method (FORM), while it is approximated by a quadratic surface for the Second Order Reliability Method (SORM)
- Response surface methods replace the initial deterministic model by an approximation response surface expressed by a function whose values can be computed more easily.

#### 4.4.3.1 Limit states

The response and failure modes of an engineering structure depend on the type and the magnitude of the applied load, as well as on the strength and stiffness of the structure. Melchers [121] indicates that limit states which describe the structural failure modes are generally divided in (Table 4.1):

1. Ultimate limit states which are mostly related to the loss of load-carrying capacity, e.g. excessive plasticity, rupture due to fatigue, deterioration, etc.
2. Damage limit states which are related to loss of strength under repeated loads and can be caused by excessive cracking or permanent inelastic deformation.
3. Serviceability limit states which are related to normal use of the structure and can be expressed in terms of deflections or vibrations.

#### 4.4.3.2 Approximation methods

The application of FORM and SORM first requires the application of an isoprobabilistic transformation that aims to simplify the joint probability density function while failure probability retains its estimated value. This transformation associates random variables in the physical space with standardized and independent random variables that define the basic vectors of the standard normal space.

The limit state function should also be expressed in the standard space and turns into  $H(\mathbf{U})$ . Then the integral of failure probability in equation 4.14 becomes:

Table 4.1: Typical limit states for structures [121]

Limit state type	Description	Examples
Ultimate (safety)	Collapse of all or part of structure	Tipping or sliding, rupture, progressive collapse, plastic mechanism, instability, corrosion, deterioration, fire, fatigue
Damage (often included in above)		Excessive or premature cracking, deformation or permanent inelastic deformation
Serviceability	Disruption of normal use	Excessive deflections, vibrations, local damage, etc.

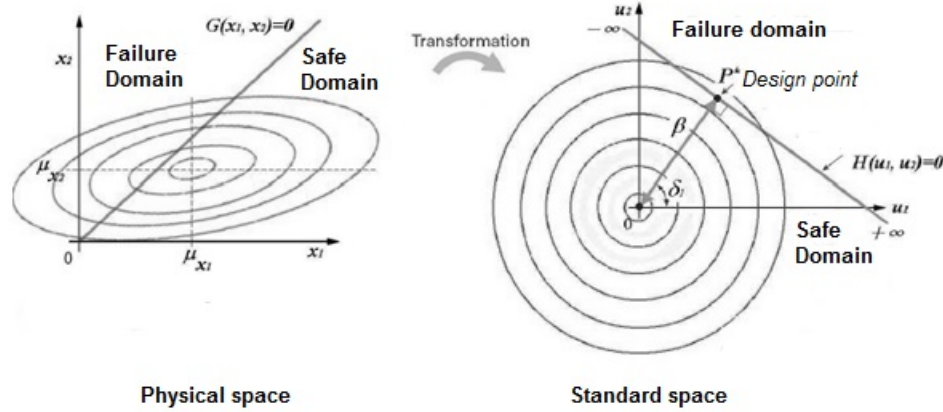


Figure 4.6: Reliability index in standard space [44]

$$P_f = \int_{g(x) \leq 0} f_{\mathbf{X}}(x) dx = \int_{H(u) \leq 0} f_{\mathbf{U}}(u) du \quad (4.15)$$

where  $f_{\mathbf{U}}(u)$  is the density function of the distribution in the standard space, this distribution is spherical and invariant by rotation. The Rosenblatt transformation [102] is the isoprobabilistic transformation used by default by OpenTURNS when random variables are independent and can only be used if the density function  $f_{\mathbf{X}}(x)$  of all random variables is well known.

The second step consists calculating the reliability index of Hasofer-Lind  $\beta$  [106] by solving the following constrained optimization problem:

$$\beta = \min \left( \sqrt{\sum_{i=1}^n u_i^2} \right)_{H(u_i) \leq 0} \quad (4.16)$$

Geometrically,  $\beta$  is the distance of the design point from the origin of the standard space (Figure 4.6).

OpenTURNS uses the algorithm of Rackwitz-Fiessler [159] to solve this type of problem. This algorithm is the most widely used in structural reliability as it can be simply formulated and gives satisfactory results in practice. Resolving this problem allows assessing the value of  $\beta$ , as well as the coordinates of the design point  $P^*$  in the standard space. This point represents the most likely point of failure, or in other words the point on the limit state surface nearest to the origin. Afterwards, the limit state function is approximated by a Taylor expansion of first order for FORM and of second order for SORM around the design point.

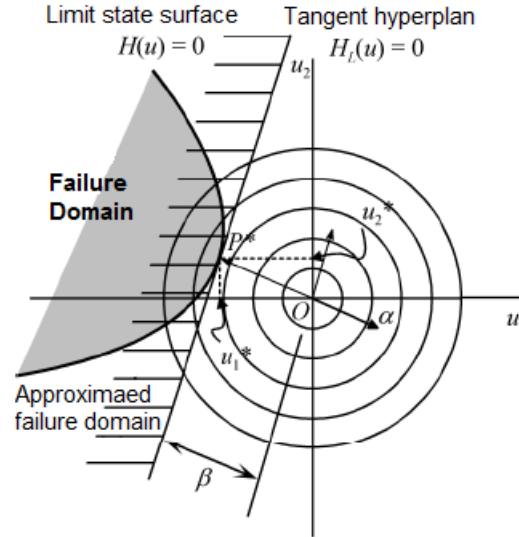


Figure 4.7: Approximation of limit state surface by FORM [75]

FORM and SORM require a reduced number of calls of the deterministic code and their computational effort is independent of the magnitude of failure probability. They ensure a reasonable accurate estimate of failure probability [50], while SORM improves the accuracy of result and gives a very good estimate for large values of  $\beta$  [164]. FORM and SORM lose their accuracy when the limit state surface is highly nonlinear in the vicinity of the design point (main curvatures at the failure surface at the design point are large) [164], or when there may exist other important local optimum points (the contribution of the global optimum point  $P^*$  is not taken into account) [1]. In this case, failure probability is only a function of the geometric properties of the limit state surface (the design point position and the main curvatures). It is recommended not to use FORM and SORM in the case of several failure criteria.

**FORM** FORM approximates the failure domain to the half-space defined by means of the hyperplane which is tangent to the limit state surface at the design point (Figure 4.7). This approximation of first order permits to calculate failure probability using equation (4.17), where  $\Phi$  is the standard normal cumulative distribution function (CDF).

$$P_f \approx \Phi(-\beta) \quad (4.17)$$

**SORM** SORM consists in approximating the failure surface to a quadratic surface at the design point, with the same main curvatures as the true failure surface at the design point (Figure 4.8). To calculate the main curvature  $\kappa_i$ , the Hessian matrix ( $H_{ij}(f) = \frac{\partial^2 f}{\partial x_i \partial x_j}$ ) should be determined since the terms of second orders are considered. Failure probability can be calculated by the Breitung formula (Equation 4.18) [26] which estimates the probability with an asymptotic analysis, in the sense  $\beta \rightarrow \infty$  with  $\beta\kappa_i$  fixed.

$$P_f \approx \Phi(-\beta) \prod_{i=1}^{n-1} (1 + \beta\kappa_i)^{-1/2} \quad (4.18)$$

This expression seems as the product of the approximation of FORM by a correction factor expressed in terms of the principal curvatures at the most likely point of failure.

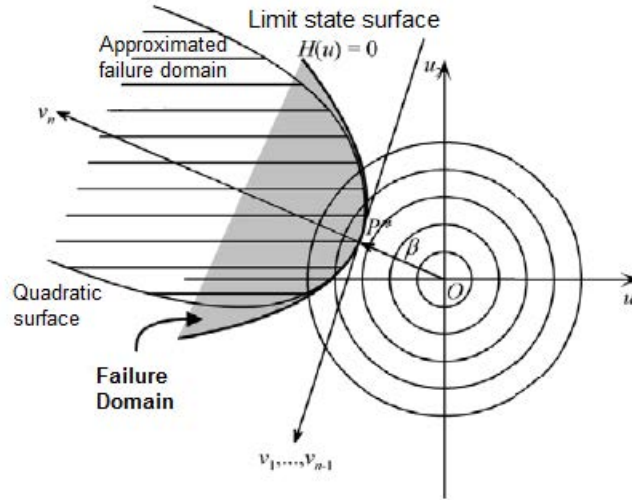


Figure 4.8: Approximation of limit state surface by SORM [75]

#### 4.4.3.3 Simulation methods

Simulation methods are the most basic and simple methods to apply in order to assess failure probability, they enable to evaluate that takes a limit state function for a representative sample of input variables. A large number of samples are generated according to the probability density of each random variable and the correlation coefficients that link them. Simulation methods require calculating the simulation coefficient of variation in order to ensure their convergence. Results are always expressed with a confidence interval which allows examining if the number of simulations or samples is sufficient to obtain an accurate estimation of failure probability. Therefore, they necessitate a significant computational effort as they need a huge number of calls of the deterministic model. Furthermore, they show a very slow convergence since the number of simulations should be greater to the inverse of failure probability and the accuracy of results is proportional to samples size. No particular assumptions are needed for the limit state function, hence simulation methods remain valid in all cases even in cases where limit state function is very complicated and represents high nonlinearities and curvatures.

**Monte Carlo (MC)** Despite its computational effort, Monte Carlo is the most effective and widely known method to determine failure probability. This method represents a very powerful tool, but also the most reliable technique for engineers for evaluating reliability of complicated structures with only a basic knowledge of probability and statistics. It consists in estimating failure probability in term of the number of simulation cases, among the total number of generated simulations, which indicate failure (Figure 4.9). An estimate of failure probability by MC can be provided by the expression:

$$P_f \approx \frac{1}{N} \sum_{i=1}^N I(x_i) \quad (4.19)$$

In this equation,  $N$  is the number of generated samples of the random vector  $\mathbf{X}$ ,  $I(x_i)$  describes the indicator function so that  $I(x_i) = 1$  if  $g(x_i) \leq 0$  and  $I(x_i) = 0$  otherwise. The accuracy of the estimate certainly depends on the number of simulations and the magnitude of failure probability. For a small value of  $N$  the estimation of  $P_f$  may be subjected to a considerable uncertainty, thus a large number of simulations may be required to reduce this uncertainty to an acceptable level. A large number of samples is also required in case of low probabilities. Therefore the efficiency of Monte

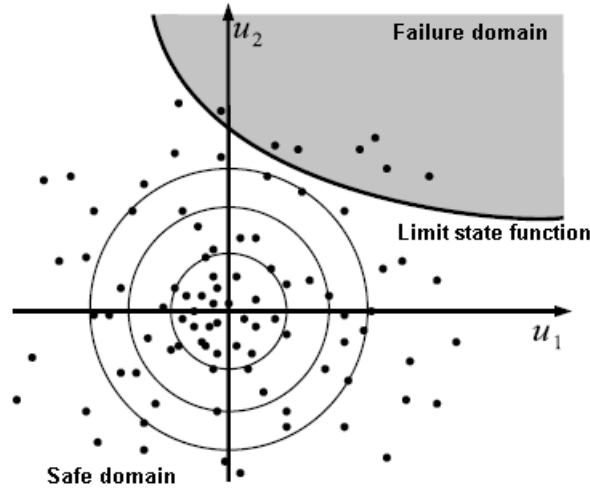


Figure 4.9: Principle of Monte Carlo method, illustration in the standard space [46]

Carlo should be evaluated to study the error associated with the number  $N$ . OpenTURNS uses the Central Limit Theorem in order to calculate the percentage error by means of a 95% confidence interval. Results provided by Monte Carlo indicate that the estimated value of  $P_f$  is very likely (with a probability of at least 0.95) in the confidence interval  $[P_{f,inf}, P_{f,sup}]$ .

The concept of Monte Carlo appears to be simple, however, its application in structural reliability analysis where very low probabilities usually appear may be impossible for complex structures that necessitate a huge computational effort during deterministic analyses. Therefore, and in order to achieve efficiency of simulation methods, the number of simulations needs to be greatly reduced [79]. For this purpose, several variance-reduction techniques were developed to increase efficiency by reducing the variance or the error of the estimate of probability of exceeding a threshold. The expected or mean value are not influenced by these alternative techniques and the number of simulations required to assess failure probability decreases significantly. The most commonly used variance-reduction methods are importance sampling, directional simulation and Latin hypercube sampling.

**Importance sampling (IS)** Importance sampling consists in generating samples that lead more frequently to failure instead of extending them uniformly over all possible values of random variables. The distribution of sampling points is concentrated in the region of most importance that mainly contributes to failure probability (Figure 4.10). In order to obtain results in the desired region, samples are simulated from a new probability density function  $h_{\mathbf{U}}(u)$  instead of the original joint probability density function  $f_{\mathbf{X}}(x)$  and the probability of failure is given by:

$$P_f \approx \frac{1}{N} \sum_{i=1}^N I(u_i) \frac{f_{\mathbf{X}}(u_i)}{h_{\mathbf{U}}(u_i)} \quad (4.20)$$

In this expression,  $h_{\mathbf{U}}(u)$  is known as the importance sampling density function used to generate samples and centered at the design point,  $\mathbf{U}$  is the random vector of samples based on the new density function such that  $h_{\mathbf{U}}(u) > 0$  in the failure domain [1].

Although the efficiency of this method depends on the selection of the density  $h_{\mathbf{U}}(u)$  (the optimum importance sampling density function gives the minimum variance, i.e. the variance of  $P_f$  is equal to zero), importance sampling is generally recognized as the most efficient variance reduction technique. It is very effective for estimating low failure probabilities and allows obtaining more

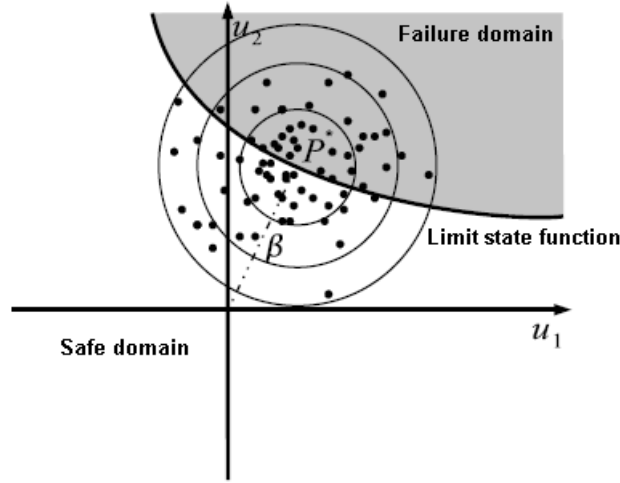


Figure 4.10: Principle of importance sampling method, illustration in the standard space [46]

information on failure domain since samples are concentrated in the region of high density of failure probability around the design point. Importance sampling produces accurate and satisfactory results if the design point is correctly identified and reduces significantly the number of simulations for an appropriate choice of  $h_{\mathbf{U}}(u)$  (OpenTURNS uses a normal importance distribution, centered on the standard design point). In addition, the number of samples affects the efficiency of the sampling method and sufficient simulations in the failure region are needed. Indeed, the number of simulations required to assess an accurate estimation of failure probability increases with the dimension of input random vector. As the estimation of failure probability by importance sampling method depends on the identification of the design point, this method shows the same disadvantages of FORM and SORM related the nonlinearity of the limit state surface and the number of optimum points.

**Directional simulation (DS)** Directional simulation is also frequently used for the structural reliability assessment. This method is more economical than Monte Carlo in term of computational effort and requires no additional information. Directional simulation is based on the concept of conditional probability and implicates the rotational symmetry of multi-normal probability density in the standard space. The simulations are performed radially, hence random directions are generated in the space instead of generating random simulation points and determining whether these simulations are in failure or safe domain (Figure 4.11). Random directional vectors are generated according to a uniform density distributed on the unit hypersphere and are expressed in polar coordinates. For each random direction, the intersection of the direction and the limit state surface is determined iteratively and the distance  $\rho_i$  from the origin to the limit state surface is searched. Failure probability is evaluated in the conditional directional by a Chi-Square probability function with  $n$  degrees of freedom ( $\chi_n^2$ ) as follows:

$$P_f \approx \frac{1}{N} \sum_{i=1}^N [1 - \chi_n^2(\rho_i)^2] \quad (4.21)$$

OpenTURNS requires the use of a numerical solver at every step of directional simulation method, this solver necessitates a certain number of calls of the external deterministic code in addition to the number of simulations required by directional simulation to assess failure probability. As a simulation probabilistic method, directional simulation has the characteristic that failure probability converges to an accurate value if the number of simulations increases. However, in the case of large number of

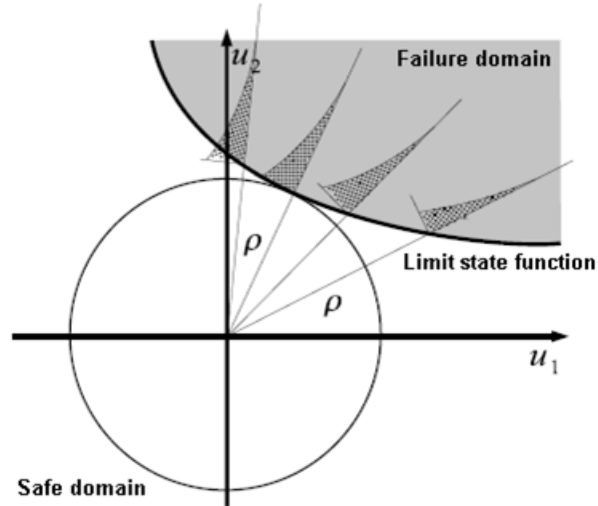


Figure 4.11: Principle of directional simulation method, illustration in the standard space [46]

random variables, Monte Carlo requires less simulations than directional simulation to converge to a solution of similar accuracy [74].

**Latin hypercube sampling (LHS)** Latin hypercube sampling is also another simulation based technique to evaluate reliability. This method is based on a stratified sampling strategy, hence it allows a better cover of the domain of input variables variation. The sampling procedure consists in dividing the domain of each random variable into several intervals and assigning the same probability to all intervals. The number of intervals depends on the sample size generated for each variable. From each interval, a value is selected randomly with respect to the probability density in the interval. A combination of random variable intervals permit to form the hypercube. In this method, all the areas of the space are represented by input values, which results in a smoother sampling of the probability distributions. The estimator of failure probability with Latin hypercube sampling method is similar to that followed in Monte Carlo method and the governing is given in Eq.(4.19).

Latin hypercube sampling can also be combined with importance sampling method in the aim of reducing the failure probability variance. In this case, simulations are generated uniformly in an hypercube centered at the design point (Figure 4.12) and failure probability can be estimated by the following equation:

$$P_f \approx \frac{V(p)}{N} \sum_{i=1}^N I(x_i) f_{\mathbf{X}}(u_i) \quad (4.22)$$

where  $V(p)$  is the volume of the hypercube.

OpenTURNS does not allow assessing failure probability by combining Latin hypercube sampling with importance sampling, but also it requires input variables to be independent so that this method could be applicable. Latin hypercube sampling methods can give comparable results to Monte Carlo, but with a reduced number of calls of the deterministic model. It also improves the manner of generating samples and enables a better exploration of the domain variations of input variables [1]. As all simulation probabilistic methods, a small number of simulations may not give accurate results, while large sample size may not be convenient for deterministic models that are time consuming.

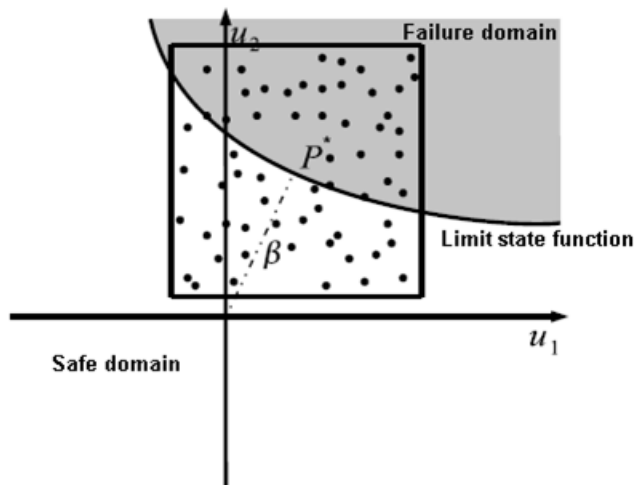


Figure 4.12: Principle of Latin hypercube sampling method, illustration in the standard space [46]

#### 4.4.3.4 Response surface methods

Response surface methods are generally used in cases where the physical model requires a huge computational effort in order to perform the reliability analysis. The principle of response surface methods consists in replacing the deterministic model with an approximate polynomial model, called response surface or meta-model. The approximate model is characterized and parametrized by a certain number of coefficients and its output values can be estimated more easily. Several techniques are provided in OpenTURNS to choose the response surface type, namely the Taylor expansion, the Least Square method and the polynomial chaos expansion. Once the type of response surface is selected, its coefficients are estimated through a finite number of simulations of the deterministic model.

The Taylor expansion method allows replacing the initial model by an approximate model in a restricted domain of the input variables. Its concept consists in performing a 1st or 2nd order polynomial expansion of the deterministic model around a certain point. The approximation by Taylor response surface is very useful to study central tendencies and determine the PDF of the variable of interest. In this case, the expansion should be performed around the point of mean values of input variables. However, if the aim is to assess the probability of exceedance of a threshold, the Taylor expansion should be performed around the design point and its accuracy must be justified.

The Least Square method enables to replace the initial model limit state function by a linear response surface of type:

$$\tilde{g}(\mathbf{X}) = A\mathbf{X} + B \quad (4.23)$$

where  $A$  is the matrix of the coefficients to be determined, and  $B$  is the constant term. The coefficients can be determined from a sample of output values obtained with the initial model and calculated for different values of the input variables. The Least Square method allows determining these coefficients by minimizing the quadratic error between the output values of the initial model and the approximate output values obtained by the response surface for the same input values.

The polynomial chaos expansion allows approximating the initial deterministic model by a response surface considered as a projection of the physical model in a truncated Hilbertian orthonormal basis:

$$\tilde{g}(\mathbf{X}) = \sum_{i=0}^{P-1} \alpha_i \psi_i \circ T(\mathbf{X}) \quad (4.24)$$

where  $T$  is an isoprobabilistic transformation which transforms the input random vector into a reduced vector of independent components. In OpenTURNS, the Nataf transformation is used if the input random vector has a Normal copula, while the Rosenblatt transformation is used for all other cases [1].  $\psi_i$  represents a multivariate polynomial basis in the Hilbertian space associated with a particular polynomial family. OpenTURNS provides 4 polynomial family types, namely Hermite, Legendre, Jacobi and Generalized Laguerre orthogonal polynomials. The polynomial chaos is described by a degree  $P$  and a finite number of coefficients  $\alpha_i$  that represent the unknown quantities of the problem. These coefficients are evaluated in OpenTURNS using least squares strategy through a finite number of realizations of the input physical vector. The principle consists in selecting the realizations according to a convenient experimental design and minimizing the square residual between the initial model and meta-model responses.

In order to construct a basis of the meta-model with polynomial chaos expansion, three strategies are implemented in OpenTURNS:

- The Fixed strategy corresponds to a polynomial chaos basis with a specific number of terms and depends on the degree of the polynomial chaos and the number of input random variables.
- The Sequential strategy does not take into consideration the number of terms nor the degree of the polynomial chaos. First, an initial basis is proposed and then updated iteratively depending on a convergence criterion based on the difference between the physical model response and the polynomial chaos prediction.
- The Cleaning strategy consists in generating an initial basis with a finite number of terms and eliminating the non-efficient terms (i.e. the terms associated to coefficients less than a given value). Then, a new term is generated and the polynomial basis is updated according to the new coefficient. The procedure is repeated iteratively until only the most significant terms are considered.

#### 4.4.3.5 Comparison of methods according to some reviews in the literature

Reliability results are sensitive to the used reliability analysis method [68, 70, 69]. Thus, probabilistic method should be properly chosen for a particular problem. Two methodologies were proposed by [68, 70, 69] in order to compare approximation and simulation probabilistic methods in term of their efficiency in assessing the same results of failure probability. The first consisted in coupling the probabilistic methods directly to the finite element model, while response surface method was used to simplify the model. The approximated model was also coupled to the same probabilistic methods. The influence of random variables PDF was also investigated.

The physical problem examined in [68, 70, 69] is performed within the context of performance based seismic engineering design. The finite element model is based on a nonlinear static pushover analysis in [68, 70], while the problem is studied assuming a linear elastic behavior in [69]. Ghoulbzouri *et al.* [68] studied the reliability of two-story RC building structure taking the uncertainties of three input variables into account. OpenSees was used to estimate failure probability using three different types of probability distribution for random variables (lognormal, normal and gamma). Ghoulbzouri *et al.* [70] developed their reliability analysis to the case of four-story RC building structure. OpenSees was also used to assess failure probability and the same random variables were considered and modeled using a lognormal distribution. Another reliability analysis four-story RC building structure was also performed by Ghoulbzouri *et al.* [69] using FERUM and considering 15 random lognormal variables related to the structure geometry, material properties and loading

conditions. The limit state function examined in the three references was related to the horizontal displacement at the roof of the structure in order to fulfill the requirements of the Moroccan seismic code RPS 2000.

Goulbzouri *et al.* found that the direct coupling of probabilistic methods with the finite element model does not predict the same results as the approximated response surface coupled to the same probabilistic methods. This latter underestimates in general failure probability, but it allows performing the reliability analysis with less computational effort compared to the direct coupling with the finite element model. The computational effort of response surface method depends only on the time needed to identify the approximated function. In addition, FORM does not give the same results with respect to IS for both methodologies proposed. In general, FORM overestimates failure probability when coupled with the finite element model, but shows good accuracy when coupled to the approximated model. Goulbzouri *et al.* recommended the use of IS in the case of finite element model, although it is hugely time consuming in comparison to FORM. Goulbzouri *et al.* indicated also the importance of specifying appropriate probability density functions to model uncertainties and that is not sufficient to describe random variables only by mean values and COV. However, the choice of PDF has a reduced effect when surface response based reliability analysis is performed. It should be noted that these conclusions could not be generalized and should be used with attention for other problems when assessing failure probability.

## 4.5 Sensitivity analysis

The objective of reliability sensitivity analysis is to identify input variables that mostly contribute to the variability of the variable of interest and that of failure probability. Sensitivity analysis is important to gain more information about the deterministic model and its probabilistic behavior, especially for models with large number of input variables and those that represent a high nonlinear response and several failure modes. Results from sensitivity analysis can be used to ameliorate structural design in engineering, for examples the dimension of a design problem can be reduced by determining the variables that have a negligible probabilistic effect, the probabilistic response can be also improved by reducing the uncertainty in random variables. Several methods permit to estimate the sensitivity of input random variables:

- Quadratic combination method that is based on a Taylor expansion of the output variable and evaluates the importance factors (IF) of input variables on the estimator of the output variable mean:

$$IF_{x_i} = \frac{\partial g}{\partial x_i}(\mu_X) \quad (4.25)$$

- FORM permit to calculate direction cosines that describes the sensitivity of each standard variable  $U_i$  on the reliability index around the design point.

$$IF_{x_i} = \frac{\partial \beta}{\partial u_i}(u^*) \quad (4.26)$$

However, it is impossible to compare one factor to another since variables have different physical units. Therefore, importance factors are multiplied by normalized factors in OpenTURN, which enables the comparison of these factors independently of the original units of the deterministic model variables.

## 4.6 Statistical descriptions of random variables

In order to study the reliability of RC structures, a statistical description of intervening random variables must be provided. The basic information required is the probability distribution (PDF) of each random variable and its statistical parameters, such as the mean and the coefficient of variation (COV). According to [91], the mean and COV of variables should be representative of values that would be expected in actual structures in-situ. A sufficient data are required in order to obtain a reasonable estimate of the probability distribution. However, in other cases where the data do not exist it is difficult to develop statistical description for variables. Hence, a literature review is conducted in this section in order to examine statistical descriptions of random variables intervening in RC structures according to several studies in the literature.

### 4.6.1 Concrete properties

In practice, the strength of concrete in a structure may differ from its specified design strength [123] and may not be uniform throughout the structure [91]. According to [91], the major sources of variations in concrete strength are due to variations in material properties and proportions of concrete mix, variations in mixing, transporting, placing and curing methods, variations in testing procedures and the rate of loading, and finally the size effects.

#### 4.6.1.1 Compressive strength of concrete

Mirza *et al.* [123] have derived a relationship for the COV in-situ compressive strength as:

$$V_c = (V_{ccyl}^2 + 0.0084)^{1/2} \quad (4.27)$$

where  $V_{ccyl}$  is the COV of the cylinder tests. For average control  $V_{ccyl}$  is about 0.15 and 0.12 for 20.68 MPa and 34.47 MPa concretes, respectively, and  $V_c$  can be taken as 0.18 and 0.15. The concrete strength  $f_c$  is assumed to follow a normal distribution and the COV of the concrete in-situ compressive strength can be considered to vary between 0.15 and 0.18. These values were also suggested by [57, 114, 115]

A reliability analysis was performed by Jonsson [91] on RC beams in bending and concrete offshore structures which are exposed to extreme environmental load such as icebergs and waves. The mean value of the compression strength considered in this study and presented in table 4.2 is adjusted for the rate of loading.

In the paper of Val *et al.* [177], a probabilistic method for reliability evaluation of plane frame structures with respect to ultimate limit states was proposed. The mean value of the compressive strength was estimated by:

$$f_{cm} = f_c + 8 \quad (4.28)$$

Val *et al.* assumed that the compressive strength has a normal distribution, thus the COV may be obtained by:

$$COV_{f_c} = \frac{8}{1.645 f_{cm}} \quad (4.29)$$

Sun [168] has studied the effect of corrosion on the reliability of bridge girders. In this study and according to [115], the concrete strength  $f_c$  is assumed to follow a normal distribution with COV of 0.16.

Choi and Kwon [35] have used Monte Carlo simulation in order to assess the variability of deflections of RC beams and one-way slabs with known statistical data and probability. Their results showed that the variability of deflections can be high due to the random nature of the parameters

related to the concrete and steel strength, as well as the structural dimensions. The parameters were considered to be independent except for the modulus of elasticity and the tensile strength of concrete which were considered correlated with the compressive strength of concrete. The values of variables in this study were given in 'psi' for strengths and in 'in' for dimensions. The mean of the concrete compressive strength was given by:

$$0.675f_{ck} + 1100 \leq 1.15f_{ck} \quad (4.30)$$

with a COV equal to 0.176.

Braverman *et al.* [25] have performed a study to evaluate, in probabilistic terms, the effects of age-related degradation on the structural performance of reinforced concrete members at nuclear power plants. The paper focuses on degradation of reinforced concrete flexural members (beams and slabs) and shear walls due to the loss of steel reinforcing area and loss of concrete area (cracking/spalling). As shown in Table 4.2, the mean value of the in-situ concrete strength and its COV considered in this paper for RC slabs were based on [58, 115].

In order to combine the dynamic analysis of the structural slab subjected to blast loading with its various aspects of uncertainties, a reliability study has been performed via the setting up of displacement and strain performance functions [110]. This paper presents also results from a parametric investigation of the reliability of RC slabs under blast loading. The results showed that the variation of Young's modulus of concrete has a largest influence on the failure probability of the slab, followed by the yield strength of steel bar and the crushing strength of concrete. The mean values of random variables adopted in this study present the dynamically enhanced values with an enhancement factor of 1.4 for the concrete compressive strength.

Low and Hao [111] have used two loosely coupled SDOF systems to model the flexural and direct shear responses of one-way RC slabs subjected to explosive loading. Incorporating the effects of random variables of the structural and blast loading properties, as well as the strain rate effect caused by rapid load application, failure probabilities of the two failure modes were analyzed. Failure probabilities of the two failure modes were evaluated by considering statistical variations of material strengths, structural dimensions, and blast loading properties. Strain rate effect on material strengths were also taken into account in the analysis. Therefore, the mean values of random variables considered in this study present the dynamically enhanced values with an enhancement factor of 2.3 for the concrete compressive strength.

The aim of the study of Firat and Yucemen [62] was to analyze the different sources of uncertainties involved in the mechanical properties of materials and geometrical quantities of RC beams, columns and shear walls in Turkey. They have showed that the in-situ compressive strength of concrete ( $f_{ck}$ ) can be expressed in term of the compressive strength of the cylindrical specimens ( $f'_c$ ) (Eq. 4.31):

$$f_{ck} = N_{f_c} \cdot f'_c \quad (4.31)$$

where  $N_{f_c}$  is the overall bias in  $f_c$  and is equal to 0.72. In this study, the COV of concrete strength is found to be equal to 0.18.

Wisniewski *et al.* [182] have presented probabilistic models of ultimate shear and bending resistance of RC and prestressed concrete bridge cross-sections. Statistical material and geometrical parameters were defined according to [144, 145, 181]. All random variables were considered normally distributed. Remaining parameters were considered as deterministic and their representative values were taken from [4]. Wisniewski *et al.* have indicated that the value of COV of concrete compressive strength for plant cast concrete (COV = 0.09) is smaller than the one for concrete cast in-situ (COV = 0.12). In addition, they showed that the concrete compressive strength is correlated with the concrete elasticity modulus and its tensile strength, with coefficients of correlation  $C = 0.9$  and  $C = 0.7$ , respectively.

Table 4.2: Summary on compressive strength of concrete according to various references

Ref.	Nominal of $f_c$ (MPa)	Mean of $f_c$ (MPa)	COV	PDF	Main Ref.
Mirza <i>et al.</i> (1979) [123]	20.68	19.03	0.18	Normal	-
	27.58	23.37	0.18	Normal	-
	34.47	27.77	0.15	Normal	-
Jonsson (1992) [91]	-	27.77	0.18	Normal	[123]
Val <i>et al.</i> (1997) [177]	30	38	0.13	Normal	-
	-	$f_c + 8$	$\frac{8}{1.645f_{cm}}$	-	[30]
Sun (1999) [168]	40	-	0.16	Normal	[115]
Braverman <i>et al.</i> (2001) [25]	27.58	24.49	0.16	Normal	[58, 115]
Low and Hao (2001) [110]	-	51.2	0.11	Normal	[123]
Low and Hao (2002) [111]	-	84.08	0.11	Normal	[123]
Firat and Yucement (2008) [62]	C14 to C30*	29.87	0.105	-	-
Wisnieski <i>et al.</i> (2009) [182]	30	30	0.12	Normal	[144, 145, 181]
Ref.	Nominal of $f_c$ (psi)	Mean of $f_c$ (psi)	COV	PDF	Main Ref.
Choi and Kwon (2000) [35]	-	$0.675f_{ck} + 1100$	0.176	Normal	[123, 126, 139]

\* *TS Turkish standards: Requirements for design and construction of RC structures*

#### 4.6.1.2 Tensile strength of concrete

According to [123], the COV of the in-situ tensile strength of concrete can be taken equal to 0.18 which is the value assumed for the compressive strength, and it was assumed that the tensile strength follow a normal distribution.

Several equations exist in literature in order to calculate the tensile strength of concrete in term of its compressive strength (Table 4.3).

According to [30], the concrete tensile strength may be estimated on the basis of the concrete compressive strength using the following relationship:

$$0.95\left(\frac{f_c}{f_{co}}\right)^{2/3} \leq f_t \leq 1.85\left(\frac{f_c}{f_{co}}\right)^{2/3} \quad (4.32)$$

where  $f_t$  is the concrete tensile strength in MPa,  $f_c$  is the concrete compressive strength in MPa and  $f_{co}$  is 10 MPa.

According to [177], the value of the tensile strength may be estimated from its relationship with  $f_c$ :

$$f_t = \alpha_{f_t} f_c^{2/3} \quad (4.33)$$

where  $\alpha_{f_t}$  was taken as an independent normal random variable and the COV of  $f_t$  was obtained from:

$$COV_{f_t}^2 = COV_{\alpha_f}^2 + (2COV_{f_c}/3)^2 \quad (4.34)$$

Choi and Kwon [35] have provided an equation of the tensile strength and the in-situ compressive strength of concrete (the strengths are given in psi):

$$f_t = 8.3\sqrt{f_{ck}} \quad (4.35)$$

In addition, they have considered the tension stiffening effect of concrete in their study in order to include the effect of cracking in the analysis. The tension stiffening effect of concrete can be

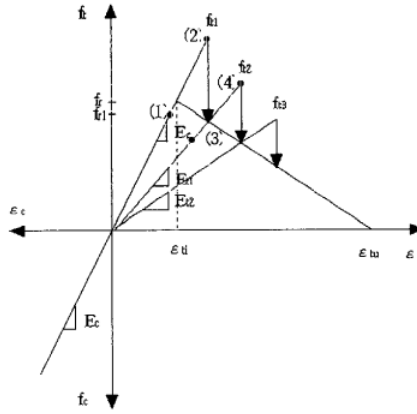


Figure 4.13: Linear stepped model for tension stiffening [35]

estimated by a tension stiffening parameter,  $\beta_t$  defined as  $\beta_t = \varepsilon_{tu}/\varepsilon_{ti}$ . This parameter was used to characterize the post-peak of the tensile stress-strain relationship and was also considered as a random variable in order to model the variability of post-tensile response of concrete, which was represented as a linear reduction in the tensile stress as shown in Figure 4.13. This parameter was also considered as a random variable in the study of [177] and it was assumed that it follows a normal distribution with a mean equal to its nominal value and a COV equal to 0.15 since no available data are available for this parameter.

A study on the cover failure in concrete structure following concrete deterioration has been carried out by Choo *et al.* [37]. The purpose of this study was to analyze the relationship between the range of the steel expansion and the crack creation and propagation. The tensile strength was directly calculated from the compressive strength of concrete using the following equation:

$$f_t = 0.18f_c^{0.7} \quad (4.36)$$

$f_t$  and  $f_c$  are given in MPa.

Pandher [153] has studied the reliability-based Partial safety factors for compressive strength of concrete with partial replacement of cement by Fly ash having fibers. Pandher has assumed that the tensile strength of concrete is approximately one tenth of its compressive strength.

#### 4.6.1.3 Young's Modulus

Although several equations are available in the literature to estimate the static modulus of elasticity of concrete (Table 4.4).

In [11], the concrete elastic modulus was also estimated on the basis of the compression strength:

$$E_c = 33\rho_c^{1.5}f_c^{0.5} \quad (4.37)$$

where  $f_c$  is the compressive strength (psi),  $E_c$  is the elastic modulus (psi),  $\rho_c$  is the weight density of the concrete ( $lb/ft^3$ ).

Jonsson [91] has proposed to use the following approximate expression of the Young's modulus in the cases where only the compressive strength of the concrete is known:

$$E_c = 5500\sqrt{f_c} \quad (4.38)$$

In the paper of Val *et al.* [177], the statistical variation of the modulus of elasticity of concrete was expressed through the variability of the compressive strength of concrete and a coefficient  $\alpha_E$ :

Table 4.3: Summary on tensile strength of concrete according to various references

Ref.	Nominal of $f_c$ (MPa)	Mean of $f_t$ (MPa)	COV	PDF	Main Ref.
Mirza <i>et al.</i> (1979) [123]	20.68	2.11	0.18	Normal	-
	27.58	2.34	0.18	Normal	-
	34.47	2.52	0.18	Normal	-
Val <i>et al.</i> (1997) [177]	-	$\alpha_{f_t} f_c^{2/3}$	Eq.(4.34)	Normal	[4]
	30	$\alpha_{f_t} = 0.3$	$COV_{\alpha_f} = 0.15$	Normal	-
Braverman <i>et al.</i> (2001) [25]	27.58	2.46	0.18	Normal	[58, 115]
Choo <i>et al.</i> (2008) [37]	-	$0.18 f_c^{0.7}$	-	-	-
Pandher (2008) [153]	-	$f_c/10$	-	-	-
Wisnieski <i>et al.</i> (2009) [182]	30 ( $C = 0.7$ )	2.0	0.2	Normal	[144, 145, 181]
	50 ( $C = 0.7$ )	2.85	0.2	Normal	
Ref.	Nominal of $f_c$ (psi)	Mean of $f_t$ (psi)	COV	PDF	Main Ref.
Choi and Kwon (2000) [35]	-	$8.3\sqrt{f_{ck}}$	0.218	Normal	[123, 139]
Ref.	Tension stiffening	Mean of $\beta_t$	COV	PDF	Main Ref.
Choi and Kwon (2000) [35]		3.0	0.11	Normal	[139]
Val <i>et al.</i> (1997) [177]		0.6	0.15	Normal	[30]

$$E_c = \alpha_E (0.1 f_c)^{1/3} \quad (4.39)$$

$f_c$  and  $\alpha_E$  were considered to be independent random variables and the COV of  $E_c$  was obtained through the following relation:

$$COV_{E_c}^2 \approx COV_{\alpha_E}^2 + (COV_{f_c}/3)^2 \quad (4.40)$$

In [37], the Young's modulus of concrete was calculated as follows:

$$E_c = 4.73\sqrt{f_c} \quad (4.41)$$

where  $E_c$  is estimated in GPa.

## 4.6.2 Steel properties

In order to understand the effects of their variability on the reliability of RC slabs subjected to impact, the variability of the mechanical properties of reinforcing steel needs to be studied. According to [126], the variations of yield strength and modulus of elasticity of steel may be caused by varying rolling practices and quality control measures used by different manufacturers, as well as possible variations in cross-sectional area, steel strength, and rate of loading.

### 4.6.2.1 Yield strength of steel

Different researches have been carried out to evaluate the statistical parameters for yield strength of reinforcement (Table 4.5). In [114], the probability distribution for the yield strength of steel bars and stirrups was assumed to be lognormal. The study of Mirza and MacGregor [126] was based on a sample that included 3947 bars taken from 13 sources. They have found that the probability

Table 4.4: Summary on Young's modulus of concrete according to various references

Ref.	Nominal of $f_c$ (MPa)	Mean of $E_c$ (MPa)	COV	PDF	Main Ref.
Jonsson (1992) [91]	27.77	24530	0.1	Normal	[123]
	-	$5500\sqrt{f_c}$	-	-	[43]
Val <i>et al.</i> (1997) [177]	30	-	0.08-0.1	Normal	[123]
	-	$\alpha_E(0.1f_c)^{1/3}$	Eq.(4.40)	-	[30]
	30	$\alpha_E = 2.15 \times 10^4$	$COV_{\alpha_E} = 0.05$	Normal	-
Braverman <i>et al.</i> (2001) [25]	27.58	26200	0.18	-	[58, 115]
Low and Hao (2001) [110]	51.2	31200	0.1	Normal	[123]
Low and Hao (2002) [111]	84.08	38500	0.1	Normal	[123]
Choo <i>et al.</i> (2008) [37]	-	$4.73\sqrt{f_c}$ (GPa)	-	-	-
Wisniewski <i>et al.</i> (2009) [182]	30	33000	0.08	Normal	[144, 145, 181]
	50	37000	0.08	Normal	
Ref.	Nominal of $f_c$ (psi)	Mean of $E_c$ (psi)	COV	PDF	Main Ref.
ACI (1992) [11]	-	$33\rho_c^{1.5} f_c^{0.5}$	-	-	-
Choi and Kwon (2000) [35]	-	$60400\sqrt{f_{ck}}$	0.119	Normal	[123, 139]

distribution of yield strength of steel could be represented by either a beta distribution or normal distribution.

In [125], the stress-strain curve for reinforcing bars was assumed to be composed of three regions:

1. Region I, for which  $0 < \varepsilon \leq f_y/E_s$ , consists of a straight line from zero stress to the yield stress

$$f = E_s \varepsilon \quad (4.42)$$

2. Region II, for which  $f_y/E_s < \varepsilon \leq 0.01$ , consists of a straight horizontal line and a stress equal to the yield stress

$$f = f_y \quad (4.43)$$

3. Region III, for which  $0.01 < \varepsilon \leq \varepsilon_u$ , consists of a parabola in term of the ultimate stress

$$f = f_y + (f_u - f_y) \left\{ \frac{\varepsilon - 0.01}{\varepsilon_u - 0.01} \right\}^{1/2} \quad (4.44)$$

where  $f_u$ ,  $\varepsilon_u$ ,  $E_s$  and  $f_y$  are the ultimate strength, ultimate strain, modulus of elasticity, and yield strength of reinforcement.

The ultimate strain of reinforcing bars was assumed to be a deterministic variable and the ultimate strength was assumed to be 1.55 times the yield strength of reinforcing bars. The probability distribution of the yield strength reinforcing bars was assumed to follow a beta distribution with a mean value of 460 MPa and a COV of 0.09.

The aim of the study of Bournonville *et al.* [23] was to evaluate the variability of the physical and mechanical properties of reinforcing steel produced throughout the United States and Canada and to develop expressions to represent the probability distribution functions for yield strength of reinforcing bars. The representation of the statistical distribution of the yield strength was expressed using a beta distribution which was found to provide a reasonably accurate description of the yield strength distribution. The general form of the beta probability density function is:

Table 4.5: Summary on yield and ultimate strengths of steel according to various references

Ref.	Nominal of $f_y$ (MPa)	Mean of $f_y$ (MPa)	COV	PDF	Main Ref.
Mirza and MacGregor (1979) [125]	415	460	0.09	Beta	[126]
	27.58	23.37	0.18	Normal	-
	34.47	27.77	0.15	Normal	-
Jonsson (1992) [91]	-	445.34	0.093	LogNormal	[129]
Braverman <i>et al.</i> (2001) [25]	415	455	0.1	LogNormal	-
Bournonville <i>et al.</i> (2001) [23]	-	-	-	Beta	-
Low and Hao (2001) [110]	-	556	0.08	Normal	[126]
Low and Hao (2002) [111]	415	-	-	Normal	[126]
Nowak and Szeszen (2003) [145]	-	595	0.08	Normal	-
Firat and Yucement (2008) [62]	-	$0.9f_y$	0.09	-	-
Wisnieski <i>et al.</i> (2009) [182]	500	500	0.05	Normal	[144, 145, 181]
Ref.	Nominal of $f_y$ (MPa)	Mean of $f_u$ (MPa)	COV	PDF	Main Ref.
Mirza and MacGregor (1979) [125]	-	$1.55f_y$	-	-	[126]
Wisnieski <i>et al.</i> (2009) [182]	500	$575$ ( $C = 0.85$ )	0.05	Normal	[144, 145, 181]

$$PDF = Cx\left(\frac{f - LB}{D}\right)^{\alpha}x\left(\frac{UB - f}{D}\right)^{\beta} \quad (4.45)$$

The variable  $f$  represents the yield strength value, and the variable  $D$  represents the difference between the values for the upper bound  $UB$  and the lower bound  $LB$ . The values of the parameters presented in equation 4.45 were evaluated for different grades and sizes of reinforcement bars. For A 615 Grade 75 reinforcement, the average of the probability distribution of yield strength was estimated for all bar sizes, with:

$$C = 37335, \alpha = 2.59, \beta = 1882.86, LB = 75000, UB = 4000000, D = 3925000.$$

Nowak and Szeszen [145] have focused on the yield strength distribution of steel reinforcing bars through 416 samples of Grade 60 reinforcement. It was found that, regardless of the bar size, a normal distribution provides a good representation for the yield strength of steel.

Wisnieski *et al.* [182] showed that the yield strength of steel is correlated with its ultimate strength, with a coefficient of correlation  $C = 0.85$ .

#### 4.6.2.2 Modulus of elasticity

The modulus of elasticity of steel has been found to have a small dispersion and to be more or less insensitive to the rate of loading or the bar size. But it was assumed to be a random variables in some researches (Table 4.6). According to [124], the probabilistic distribution of the modulus of elasticity for reinforcing bars can be considered as normal with a mean value equal to the specified value and a coefficient of variation of 0.033. In [125], the modulus of elasticity of reinforcing bars was taken to be normally distributed with a mean value of 200000 MPa and a standard deviation of 6600 MPa.

#### 4.6.3 Dimensions

The variability of geometrical properties of RC slabs is generally a consequence of inaccuracies in the construction process and the curing operation of concrete [62, 91]. Therefore, the dimensional characteristics of RC members constructed at site are different from the values specified in the

Table 4.6: Summary on elasticity modulus of steel according to various references

Ref.	Nominal of $f_y$ (MPa)	Mean of $E_s$ (MPa)	COV	PDF	Main Ref.
Mirza and MacGregor (1979) [125]	-	200000	0.033	Normal	[126]
Mirza et al. (1980) [124]	-	specified value	0.033	Normal	-
Jonsson (1992) [91]	445.34	200000	0.033	Normal	[129]
Ref.	Nominal of $f_y$ (psi)	Mean of $E_s$ (ksi)	COV	PDF	Main Ref.
Choi and Kwon (2000) [35]	-	29200	0.024	Normal	[126, 139]

design of the structure. Mirza and MacGregor [127] demonstrated that variations in dimensions can significantly affect the size and the strength of concrete members, and thus dimensions must be considered as random variables. They also indicated that all suggestions for geometric properties should be considered as preliminary since they are based on interpretation of available data. Most researchers have indicated that the probability distributions for the geometric properties should be taken as normal [124, 115] (Table 4.7). According to Hong *et al.* [82] and Sun [168], the COV of dimensions decreases as the RC member size increases and for massive elements the effect of uncertainty in dimensions is negligible. The paper of Udoeyo and Ugbem [176] focuses on a study of dimensional variations of structural members measurements which were carried out on beams, columns and slabs. Based on this study, normal distributions are recommended to represent the probability distributions of all dimensions and slab thickness presents nominal values ranging from 150 to 180 mm and a coefficient of variation between 0.0183 and 0.0689.

According to [91], the diameter of reinforcement can be considered one of the dimensional random variables involved in evaluating reliability of RC structures and it was modeled with a lognormal distribution with a mean equal to 1.0048 times the nominal diameter and a COV of 0.02. Mirza and MacGregor [128] also considered a lognormal distribution for the diameter of bars with a mean equal to 1.01 times the nominal diameter and a COV of 0.04.

Another dimensional variable which may be considered as a random variable is the cover of concrete. In [25], the mean of the cover was taken equal to 4.45 cm with a COV of 0.36.

## 4.7 Conclusion

The aim of structural reliability analysis is to determine the probability that the structure do not perform its functional requirements. A reliability approach is based on a statistical knowledge of basic random variables such as geometric properties, material characteristics and actions. Failure probability can be assessed using probabilistic methods such as simulation and approximation methods, or response surface methods allowing the approximation of the deterministic model with a polynomial function. The first order (FORM) and second order (SORM) approximation of limit state function methods consist first in transforming random variables of the physical space into standardized and independent random variables that define the basic vectors of the standard normal space. Next, the most likely point of failure is identified which represents the point on the limit state surface nearest to the origin in the standard space and also called the design point. Afterwards, the limit state function is approximated by a Taylor expansion of first order for FORM and of second order for SORM around the design point. FORM approximates the failure domain to the half-space defined by means of the tangent hyperplane to the limit state surface at the design point, and provides accurate results in case of linear limit state functions in the standard space. SORM approximates the failure surface to a quadratic surface at the design point and gives a very good estimate for large values of  $\beta$ . Probabilistic simulation methods are commonly used to estimate failure probability. Random

Table 4.7: Summary on dimensions of RC members according to various references

Ref.	Mean of	COV	PDF	Main Ref.
Mirza <i>et al.</i> (1980) [124]	nominal	-	Normal	-
MacGregor <i>et al.</i> (1983) [115]	nominal	-	Normal	-
Jonsson (1992) [91]	beam width = 50 cm	0.013	Normal	[129]
	beam width = 13 cm	0.005	Normal	
Udoeyo and Ugbem (1995) [176]	150 to 180 mm	0.0183 to 0.0689	-	-
Low and Hao (2001) [110]	1x3x0.2 m	0.05	Normal	[127]
Low and Hao (2002) [111]	as designed	0.03	Normal	[127]
Wisnieski <i>et al.</i> (2009) [182]	Slab thickness = 25 cm	0.04	Normal	[144, 145, 181]

Ref.	Mean of	COV	PDF	Main Ref.
	$d_A$			
Mirza and MacGregor (1982) [128]	$1.01d_A$	0.04	LogNormal	-
Jonsson (1992) [91]	$1.0048d_A$	0.02	LogNormal	-
	35.34 mm	0.024	Normal	[126]

Ref.	Mean of	COV	PDF	Main Ref.
	$c$			
Braverman <i>et al.</i> (2001) [25]	4.45 cm	0.36	-	-
Jonsson (1992) [91]	4.85	0.087	Normal	[129]

simulations are generated and the structure response is evaluated for each simulation. Monte Carlo is the most simple simulation technique. Special methods, such as importance sampling, directional simulation and Latin hypercube sampling are developed to optimize the strategies of sampling in the aim of reducing the computational effort related to the number of calls of the external deterministic model.

# Chapter 5

## Deterministic models of RC slab

### 5.1 Introduction

A detailed step-by-step procedure for creating FE models of impacted slabs with Abaqus is described in this chapter. Abaqus/CAE is used to visualize the FE model geometry and properties, as well as to view results. However, Abaqus Python edition is used to create the model since a parameter-based model is definitely required to perform reliability analyses that necessitate a written code of the deterministic model to be coupled with probabilistic methods. The model Python script includes variation of geometric and mesh sizes, material properties, number of steel bars and initial conditions. Python script permit to easily take into consideration variations of the model geometric parameters and to generate mesh in term of these variations which is not possible with an input file (.inp).

A 3D nonlinear explicit finite element (FE) analysis was proven to be effective for transient and dynamic impact analysis [138]. 3D models allow simulating the behavior of 3D structures more realistically than 2D models, especially that nowadays, computational resources are not an issue anymore. However, an engineer should keep in mind that complicated models are not necessarily more trustworthy than simpler models since they may contain large numbers of errors. The aim should not be to develop a model with an exact representation of the physical problem or the most accurate model possible, but rather to develop the simplest model that provides an idealized representation of the problem and though enables to represent the structural components and behaviors with accuracy. The assumptions adopted during a FE model construction should be addressed correctly in order to verify and evaluate FE results quality. For this reason, valid answers should be provided to this type of questions: Is the analysis static or dynamic? Do the material behaviors include nonlinearities and plasticity? What are the main physical loadings applied? How to define boundary conditions? Which are the suitable FE elements to use? How to create a regular mesh?, etc.

In general, the analysis of the response of a RC slab subjected to impact loading is complex due to the many non-linearities involved. Different factors contribute to the nonlinear behavior of the reinforced concrete such as the nonlinear stress-strain response, the damage due to crushing and tensile failure, the effect of the loading rate, the interaction between the concrete and the reinforcement. In order to accurately simulate the structure and obtain detailed information from finite element approach, all these factors and contact algorithms must be correctly incorporated into the finite element model. Section 5.2 is included as an illustrative example to show how to develop a FEM of an impacted slab in Abaqus by performing a successive passage through its modules. This section describes in detail the 3D FE model of Chen and May RC slabs [34] subjected to impact using Abaqus v6.11. The analysis is performed with an explicit configuration that allows a better representation of impact problems. In order to improve the modeling process and optimizing the postprocessing of results, the model is parametrized through a code developed using the Python

programming language. This code can easily be read using Abaqus/CAE and allows obtaining a better consistency between the geometry and the quality of mesh. Python script enables to systematically prioritize the accuracy of results in the regions of interest. The model developed is then validated with the experimental results of Chen and May tests. The model adopted is used to model RC slabs which are subjected to accidental dropped object impact during handling operations within nuclear plant buildings. Then, a simplified analytical model is also used for these slabs. It consists of two degrees of freedom mass-spring system which accounts for potential viscous damping. A frequency decrease approach is used to describe the degradation of slab stiffness.

## 5.2 FEM of Chen and May slabs

### 5.2.1 Creating model

All input data should be specified in consistent units in Abaqus. In addition, selecting a coordinate system to use during the FE analysis is of high importance in order to create the FE model and interpret results. In this study, all variables used to simulate the FEM of impacted slabs are given in the SI system of units and results are automatically displayed with SI units. Model assembly and results are displayed according to the default global coordinate system in Abaqus. This coordinate system consists in a right-handed Cartesian system with z-axis perpendicular to xy-plane. Positive values of z-axis are oriented upward in the vertical direction. In this dissertation, the 1-axis, 2-axis and 3-axis denote the x-axis, y-axis and z-axis, respectively. The origin  $(x_1, x_2, x_3)$  of the global coordinate system is located at the center of the lower surface of slabs.

### 5.2.2 Creating parts

Numerical simulations of RC structures require an accurate representation of the geometry of all the structural components that constitute the feature of the structure. Every component may affect the structural response and excessive simplifications in geometry will obviously lead to inaccurate results. Therefore, experience and engineering judgement are necessary to develop an appropriate model for a specific type of problem. FE analysis allows considering complex geometries and a physical representation of the FEM close to the actual structure. The complex mechanical behavior of RC slabs under impact necessitates an adequate 3D simulation in terms of slab and impactor characteristics.

In Abaqus, Part module is used to divide the structure geometry into multiple parts. Each part defines a main component of the model and needed to be meshed separately. The Part module permits to create deformable, discrete rigid, analytical rigid, or Eulerian parts. The simulation of Chen and May slabs has 4 main components, namely the slab, the reinforcement, the impactor and the supports (for more details about these components geometry, see section 2.3.1.2). Slab part represents the slab concrete region surrounded by a steel frame and reinforcement part includes longitudinal and transversal bars of one layer of reinforcement. Impactor part describes the striker geometry used in experiments and support part represents the shape of cylinder components on which the slab is supported.

#### 5.2.2.1 Part of slab

The first part created for Chen and May impacted slabs problem represents the slabs concrete region surrounded by a steel frame. A three-dimensional, deformable solid part is created by sketching the 2D square geometry of dimension equal to the total width of slab and frame. The sketch is placed on a square sheet of size equal to the approximate size specified to create the part. The sketcher is defined by a certain number of units square depending on the approximate size. The sketch created for slab is then extruded in the z-axis direction with a depth equal to the slab thickness.

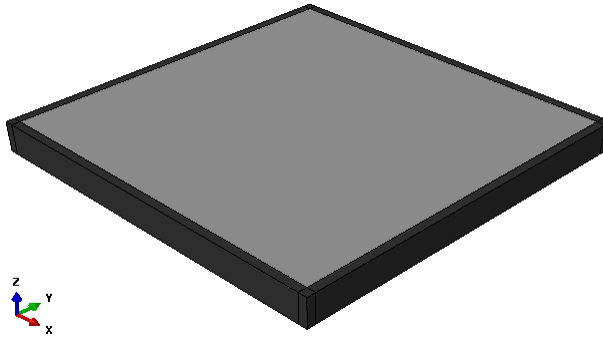


Figure 5.1: Part of slab

The geometries of slab concrete region and steel frame are continuous, hence they are merged in the same part and not separated in two different parts in order to reduce the problem. The merging process permits to facilitate the desired meshing technique and to avoid creating constraints to tie the two parts together, which would result in reducing the computational cost of numerical analysis. Therefore, the full geometry of slab is partitioned with many partitions to create the steel frame around the concrete region, which allows the simplification of the meshing process leading to an easier discretization and a higher quality of structured mesh.

The full geometry of slab represents a solid single cell. Partitions are performed by cutting the cell with a plane that passes completely through the cell. The method used to define the cutting plane in the aim of creating the frame geometry is the `PartitionCellByPlanePointNormal` method. In this method, partition is created by selecting a point on the cutting plane then selecting an edge or datum axis that defines the normal to this plane. Figure 5.1 shows a three-dimensional view of the part which is used to develop the typical geometry of Chen and May slabs and highlighted the partition scheme adopted. The section in dark gray represents the steel frame, while the light gray represents the concrete part of slabs. Details of the geometry and dimensions of Chen and May slabs are illustrated in Figure 2.14. Slabs have two different geometries: 760 mm square slabs with a thickness of 76 mm and 2320 mm square with a thickness of 150 mm. Steel frame that surrounds the concrete region is considered with a width of 17.5 mm.

### 5.2.2.2 Part of reinforcement

The geometry of reinforcement is considered identical to that of the experiments of Chen and May (Figure 2.14). Reinforcement part includes longitudinal and transversal bars of one layer of reinforcement. It consists of 11 longitudinal and 11 transversal bars in the case of 760 mm square slabs, and of 15 longitudinal and 15 transversal bars in the case of 2320 mm square slabs. The reinforcement is modeled as a 3D deformable wire part using the wire option in Abaqus. The 2D sketch is created by modeling a single transversal bar and a single longitudinal bar, then using the linear pattern option available in Abaqus. The spacing of reinforcement bars is equal to 60 mm for 760 mm slabs and 142 for 2320 mm slabs.

Figure 5.2 shows a three-dimensional view of the modeling of longitudinal and transversal reinforcement in 760 mm square slabs. It should be noted that no shear reinforcement is present in Chen and May slabs, otherwise an additional part should be considered to incorporate stirrups in the FEM.

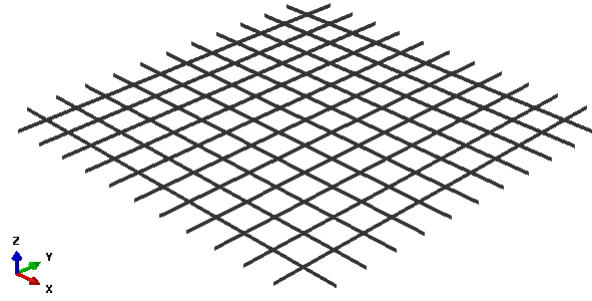


Figure 5.2: Part of reinforcement

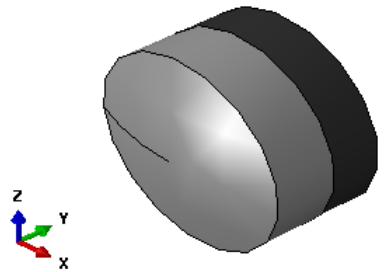


Figure 5.3: Part of impactor

### 5.2.2.3 Part of impactor

Impactors used in Chen and May experiments have a complex shape. They are composed of two sections, the first consists of the mass with which slabs are impacted while the second represents the section of impactor that enters in interaction with RC slabs. Slabs were tested with two different shapes of the interaction impactor section, a steel hemispherical section of 90 mm diameter was used to test Slabs 1,2,4,5 and 6, while a steel cylindrical section of 100 mm diameter was used to test Slab 3. Details of this section shape are presented in Figure 2.15.

In the FEM, impactors geometry is considered identical to that of the experiments of Chen and May. A three-dimensional, deformable solid part is created by sketching the 2D impactor profile and then revolving it by an angle of  $360^\circ$  about the y-axis of the impactor part coordinate system. The mass and interaction sections of the impactor are considered in one part in order to avoid creating constraints to tie the two sections together. However, the impactor is partitioned with a cutting plane in order to distinguish both sections and facilitate the generation of mesh. The cutting plane is defined with a point and a normal vector, and the partition scheme adopted for hemispherical impactors is illustrated in Figure 5.3. The upper part represents the mass section is highlighted in dark gray, while the bottom part represents the interaction section highlighted in light gray.

### 5.2.2.4 Part of support

In Chen and May experiments, slabs were supported on 4 cylindrical supports (Figure 2.14.c). Thus, in order to have a better representation of the actual structure and develop realistic structural supports, these latter are developed in the FEM as rigid bodies having a cylindrical shape with a diameter equal to the steel frame width and a thickness of 10 mm. The shape of rigid body does not

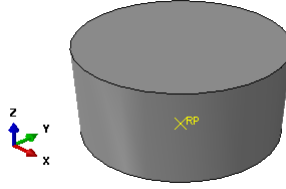


Figure 5.4: Part of support

Table 5.1: Linear mechanical properties of concrete and steel materials for Chen and May slabs

Material	Density $kg/m^3$	Young's modulus (MPa)	Poisson's ratio
Concrete	2500	35000	0.2
Steel	7850	200000	0.3

change during simulation. The following part models the geometry of a single cylindrical support as a 3D deformable, discrete rigid part (Figure 5.4). A circle of 17.5 mm of diameter is created in the sketcher, and then extruded in the z-axis with a depth equal to 10 mm. In Abaqus, a rigid body must refer to a reference point that governs its motion.

### 5.2.3 Creating materials

Material properties greatly influence the structural response of RC slabs and play an essential role in dissipating impact energy. Thus, proper material models capable of representing both elastic and plastic behaviors of materials are required for the finite element analysis. In Abaqus, Property module is used to define materials and sections, as well as to assign sections to each element of mesh of the relevant part. Material properties can be modeled in Abaqus as isotropic, orthotropic, and anisotropic. In the current study, materials are assumed to be homogeneous and isotropic having the same properties in all directions. This results in only two independent quantities to identify for each material, namely the Young's modulus and Poisson's ratio. In addition, density must be defined for all materials used in any dynamic analysis where inertia effects are important.

Abaqus includes an extensively material library that can be used to model most engineering materials, including metals, polymers, concrete, fabrics and composites [7]. It also allows creating new material models through subroutines. For concrete, Abaqus provides three different constitutive models, namely the smeared crack concrete model, the brittle cracking model and the concrete damaged plasticity model. Among these crack models, the concrete damaged plasticity model is adopted in the present study as it is the only model that can be used in both Abaqus/Standard and Abaqus/Explicit, which make it very useful for the analysis of RC structures under both static and dynamic loadings. Furthermore, CDP model is the only model that allows representing the complete inelastic behavior of concrete in both tension and compression including damage characteristics. The classical metal plasticity model available in Abaqus is used to define the elastic-plastic behavior of steel, which permit to express the steel stress as a tabular function of plastic strain.

Table 5.1 shows the linear mechanical properties of concrete and steel materials used in the FE model for all Chen and May slabs, while Table 5.2 shows their nonlinear mechanical properties that are used to define the stress-strain curves for each slab materials.

Table 5.2: Nonlinear mechanical properties of concrete and steel materials for Chen and May slabs

Slab	Concrete		Steel
	$f_c$ (MPa)	$f_t$ (MPa)	$f_y$ (MPa)
2	50	4.06	560
3	50	4.06	560
4	50	4.06	560
5	37	2.93	1035
6	45	2.93	1035

### 5.2.3.1 Identification of constitutive parameters for CDP model

The fundamental constitutive parameters for CDP model consists of four parameters which identify the shape of the flow potential surface and the yield surface in the three-dimensional space of stresses, namely  $\psi$ ,  $\epsilon$ ,  $K_c$  and the ratio  $f_b/f_c$ . A biaxial failure in plane state of stress and a triaxial test of concrete are necessary to identify these four parameters, while a uniaxial compression and uniaxial tension tests are needed to be carried out to describe the evolution of the stress-strain curves of concrete (the hardening and the softening rule in tension and compression).

**Flow potential parameters** Physically,  $\psi$  is interpreted as a concrete internal friction angle, it represents the angle of inclination of the failure surface towards the hydrostatic axis, measured in the meridional plane (Figure 3.2). Jankowiak and Lodygowski [87] supposed that  $\psi$  ranges from  $34^\circ$  to  $42^\circ$ , while Kmiecik and Kaminski [94] indicated that a value of  $40^\circ$  is usually assumed in simulations.

In the CDP model the plastic potential surface in the meridional plane assumes the form of a hyperbola (Figure 3.2). The flow potential eccentricity  $\epsilon$  is a small positive value which expresses the rate of approach of the plastic potential hyperbola to its asymptote. In ABAQUS user's manual [7], it is recommended to assume  $\epsilon = 0.1$ , which implies that the material has almost the same dilation angle over a wide range of confining pressure stress values. Increasing the value of  $\epsilon$  provides more curvature to the flow potential, implying that the dilation angle increases more rapidly as the confining pressure decreases. For  $\epsilon = 0$ , the surface in the meridional plane becomes a straight line.

**Yield surface parameters** Experimental results for biaxial loading on concrete reported by Kupfer *et al.* [100] are the most reliable to determine the ratio of biaxial strength to compression strength ( $f_b/f_c$ ) which represents the point in which the concrete undergoes failure under biaxial compression. Kupfer *et al.* [100] found that this ratio ranges from 1.10 to 1.20, while Lubliner *et al.* [113] reported a range of 1.10 to 1.16. Jankowiak and Lodygowski [87] indicated that  $f_b/f_c$  ratio is sensitive to the change of parameters  $\psi$  and  $\epsilon$ . ABAQUS user's manual [7] specifies a default value of 1.16.

Physically,  $K_c$  is interpreted as a ratio of the distances between the hydrostatic axis and respectively the compression meridian and the tension meridian in the deviatoric cross section (Figure 3.3). Typical values range for  $K_c$  is between 0.64 and 0.8 [113]. According to experimental results, Majewski [116] indicates that the value of  $K_c$  increases slowly with the decrease of mean stress and that it is equal to 0.6 for mean normal stress equal to zero. ABAQUS user's manual [7] recommends to assume  $K_c = 2/3$ . This ratio must always higher than 0.5 and when the value of 1 is adopted, the deviatoric cross section of the failure surface becomes a circle (as in the classic Drucker–Prager strength hypothesis).

Table 5.3 summarizes the parameters of yield surface and flow potential adopted in this study according to several research previously mentioned.

Table 5.3: Parameters of the damaged plasticity model

Parameter	Dilation angle $\psi$	Eccentricity $\epsilon$	$f_b/f_c$	$K_c$	Viscosity $\mu$
Value	38	0.1	1.12	0.0666	0.0

Table 5.4: Compressive concrete behaviors for CDP model

Symbol	Curve name	Ref.
C1	Desayi and Kirshnan curve	[49]
C2	Madrid parabola	[31]
C3	Eurocode 2 curve	[4]
C4	Pavlovic <i>et al.</i> curve	[154]
C5	Chinese code curve	[3]
C6	Wang and Hsu curve	[180]
C7	Majewski curve	[116]
C8	Kratzig and Polling curve	[99]
C9	Wahalathantri curve	[178]

**Compression behavior** The CDP model has the potential to develop complete stress-strain curves of concrete for compression and tension separately based on experiment results. In this study, no experimental results are available to perform an analysis of the stress-strain curve for the concrete. Therefore, the expressions considered to describe the stress-strain curve are based on several studies in literature (see section 2.4.1) with some modifications in order to fit the curve with the behavior of CDP model.

The stress-strain relations proposed by [3, 31, 49, 154, 178, 180] represent parabolic stress-strain relations for both the ascending and descending curve (see 2.4.1). They show that the nonlinear elastic behavior of concrete occurs almost from the beginning of the compression process. The CDP model requires that the elastic behavior of the material to be linear, therefore the nonlinear elastic behavior in the initial stage of these curves was neglected and replaced in this study by a linear branch. A linear elasticity limit can be assumed as  $0.4f_c$  according to Eurocode 2 [4]. Beyond this limit, the strain-hardening and strain-softening regimes keep their parabolic shapes according to the relations proposed by [3, 31, 49, 154, 178, 180]. The stress-strain relations proposed by [4, 99, 116] can directly be used in the CDP model since their elastic behavior is linear.

The evolution of the scalar damage variable for compression is determined using equation 3.17. Compressive stress and damage of concrete is included in Abaqus as tabular functions of the crushing strain. Table 5.4 summarizes the compressive concrete behaviors considered for the CDP model in this study. The first column contains the symbol attributed to each compressive stress-strain curve.

**Tensile behavior** The choice of tension stiffening parameters is important since too little tension will introduce unstable behavior in the overall response of the model and it will be difficult to obtain numerical solutions. In order to model the behavior of concrete in tension in the FEM, several expressions for stress-strain curve, stress-crack opening curve and fracture energy are adopted from the literature (see section 2.4.2.1). Expressions of tensile stress-strain curves developed by [3, 99, 180, 178] can be directly used in the CDP model since their initial elastic behavior is linear. Tensile stress is included in Abaqus as tabular functions of the cracking strain.

As previously discussed in section 3.6.2.3, the tension stiffening can be specified by a fracture energy cracking criterion by directly specifying the fracture energy  $G_f$  as a material property. Thus, tensile behavior of concrete is also modeled with stress-crack opening curves. Three types of concrete stress-crack opening curve are used with linear, bilinear and trilinear descending softening branches,

Table 5.5: Tensile concrete behaviors for CDP model

Symbol	Curve name	Ref.
<b>Stress-strain curve</b>		
T1	Wang and Hsu curve (n=1)	[180]
T2	Wang and Hsu curve (n=0.5)	[180]
T3	Wang and Hsu curve (n=1.5)	[180]
T4	Chinese code curve	[3]
T5	Wahalathantri curve	[178]
T6	Kratzig and Polling curve	[99]
<b>Stress-crack opening curve</b>		
D1	Hillerborg <i>et al.</i> curve	[81]
D2	Haidong curve	[78]
D3	Tajima curve	[170]
<b>Fracture energy</b>		
G1	Hordijk energy	[83]
G2	CEB-FIP energy	[2]
G3	Oh-Oka <i>et al.</i> energy	[146]
G4	Bazant and Oh energy	[15]

respectively (Figure 2.38). Finally, the tensile behavior of concrete is modeled by considering only the fracture energy as material property. According to ABAQUS user's manual [7], typical values of  $G_f$  range from 40 N/m for a typical construction concrete (with a compressive strength of approximately 20 MPa) to 120 N/m for a high-strength concrete (with a compressive strength of approximately 40 MPa). The relations proposed by [2, 15, 83, 146] are adopted in this study to estimate the fracture energy.

The evolution of the scalar damage variable for tension is determined using equation 3.16. Damage of concrete are included in Abaqus as tabular functions of the cracking strain. Table 5.5 summarizes the tensile concrete behaviors considered for the CDP model in this study. The first column contains the symbol attributed to each tensile description of concrete.

### 5.2.3.2 Identification of parameters for reinforcing steel stress-strain curve

Idealizations are usually used to model the reinforcing steel for a numerical analysis. In this study, five stress-strain curves are proposed. The first assumes a linear elastic, linear plastic steel behavior with hardening and is based on the idealization proposed [173]. The parameters of this curves related to ultimate strength, as well as yield and ultimate strains are presented in section 2.5.2. For other curves, the values of yield strain and ultimate strain of steel are considered from the literature with  $\varepsilon_y = 0.25$ [119] and  $\varepsilon_u = 0.4$  [171]. The idealization proposed by [171] models a linear elastic, perfectly plastic material with a yield plateau of stress equal to the yield strength of steel. The stress-strain curve proposed by [16] represents the average behavior of steel embedded in concrete with a bilinear stress-strain curve taking hardening of steel into considerations. For more details, see section 2.5.2.

In Abaqus, stress-strain curve of steel is included as tabular function of the plastic strain. Table 5.6 summarizes the stress-strain curves considered for the reinforcing steel in this study. The first column contains the symbol attributed to each stress-strain curve of steel.

Table 5.6: Idealized stress-strain curves for reinforcing steel

Symbol	Curve name	Ref.
S1	Theodorakopoulos and Swamy curve	[173]
S2	Taqieddin curve	[171]
S3	Kratzig and Polling curve	[28]
S4	Cao <i>et al.</i> curve	[99]
S5	Belarbi and Hsu curve	[16]

### 5.2.4 Defining and assigning section properties

Defining sections is an essential step to create finite element models in Abaqus. A definition of section requires information about properties of a part or a region of a part, such as the cross-sectional area and the material type to be assigned to this region. Each section is created independently and must refer to a material name. However, a single section can be assigned to several regions or parts as necessary and a single material can be referred to as many sections as necessary. Once sections are created, section properties can be then assigned to the homogeneous set that contains the region or part in question. As a result, the properties of the material referring to a particular section are also assigned to the region or part considered, as well as to all relevant instances in the assembly. Assigning sections to instances is automatically performed in Abaqus and elements related to those instances have the same section properties specified. Property module in Abaqus allows several types of sections, including homogeneous solid sections, shell sections, beam sections and truss sections.

A homogeneous solid section is the simplest section type that can be defined since the only information required in this case are a material reference and the section thickness for 2D regions. Truss sections are used to model slender 2D or 3D structures that provide axial strength but no bending stiffness. Thus, a truss section is specified and assigned to reinforcement part. It consists of steel material and a cross-sectional area equal to one steel bar area. Slabs 2 and 3 are reinforced with steel bars of 6 mm diameter, Slab 4 is reinforced with steel bars of 8 mm diameter, while Slabs 5 and 6 are reinforced with steel bars of 12 mm diameter.

3 other sections are created to model Chen and May slabs under impact. A homogeneous solid section that refers to concrete material is assigned to the concrete part of slabs highlighted with light gray in Figure 5.1. A second homogeneous solid section is also created and assigned to the steel frame surrounding the concrete region of slabs (section in dark gray in Figure 5.1). This section refers to steel material and is also used to describe properties of the bottom section of the impactor part (section in light gray in Figure 5.3). Due to a lack of information, impactor and frame materials are assumed to have the same mechanical properties and behavior as steel reinforcement. The third homogeneous solid section created refers also to steel material and is assigned to the upper section of the impactor part (section in dark gray in Figure 5.3), but the density used for steel material of this section is magnified for each slab case in order to obtain the value of mass with which the impactor hits the corresponding slab (Table 2.1).

In the case of rigid bodies, no section can be defined. They are simulated with point mass and rotary inertia property features available in Abaqus. A mass must be assigned to a discrete rigid part that refers to a reference point and whose motion is governed by the motion applied to this point.

### 5.2.5 Defining the assembly

Assembly module is used in order to create the final geometry of the FEM by defining instances of parts which are independent of each other. Each part created in Abaqus is oriented in its own local coordinate system independently of other parts of the model. When an instance of a part is created,

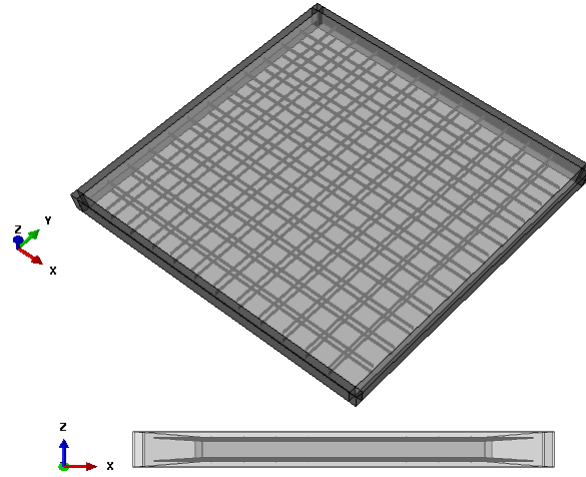


Figure 5.5: Reinforcement in the model assembly

Abaqus positions the instance in a way that the origin of the part sketch corresponds to the origin of the default coordinate system of the assembly. Thus, instances should be positioned relative to each other in the global coordinate system in order to properly assemble the model. Multiple instances can be created for a single part and the model contains only one assembly despite the fact that it may involve several parts.

For Chen and May slabs problem, 8 instances are defined. An instance refers to the part of slabs, the center of the lower surface of slabs corresponds to the origin of the global coordinate system. As the slabs are reinforced with an upper and bottom layers of reinforcement, 2 instances are created using the reinforcement part. The first describes the bottom layer of reinforcement and is translated with a distance equal to the concrete cover, while the second represents the upper layer and is translated with a distance equal to  $e - 2c$  ( $e$  is the slab thickness and  $c$  is the concrete cover) (Figure 5.5). Concrete cover is equal to 12 mm in the case of 760 mm square slabs, and 15 mm in the case of 2320 mm square slabs (Figure 2.14). Thereafter, 4 instances are defined in the assembly in order to create the cylindrical supports on which the slab part is supported. Each support instance is translated and positioned at a corner of intersection of the steel frame with the concrete region of slab part. Finally, a rotation of  $90^\circ$  around the x-axis then a translation of a distance equal to  $e + 0.001$  are performed in order to position the impactor instance in the assembly. The impactor instance is positioned in the way that the y-axis of the local coordinate system of the impactor part coincides with the z-axis of the global coordinate system of the assembly. This position corresponds to Chen and May experiments and allows applying the appropriate initial conditions.

The final model of Slab 2 is displayed in a three-dimensional view (Figure 5.6). The triad in the lower-left corner of the figure indicates the orientation of the global coordinate system, the origin of this system is located at the center of the lower surface of slabs.

### 5.2.6 Meshing the model

Generating meshes in Abaqus is performed in the Mesh module that provides a variety of tools and meshing techniques to simulate structures of different geometries. Meshing techniques are used to control mesh characteristics and automatically generate a mesh that meets the need of a particular structure analysis. Free, structured and swept techniques are available in Abaqus with the possibility of using the medial axis or advancing front meshing algorithm. The automated process of these techniques results in a mesh that exactly conforms to the original geometry of the structure. Partition toolset can be used in the Mesh module to create partition for structures of complex

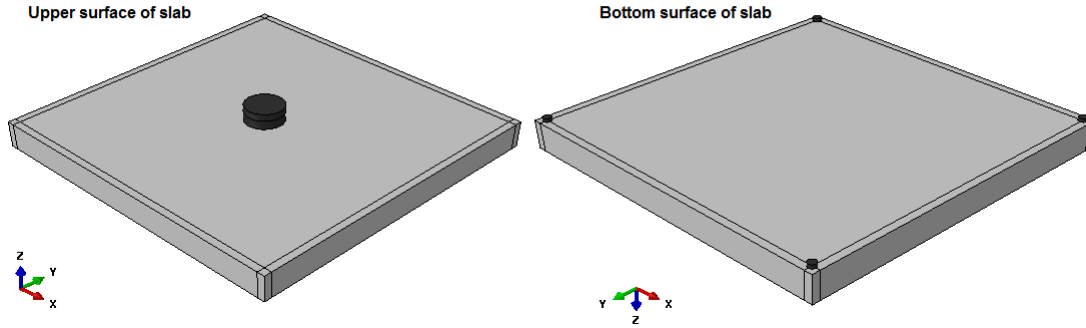


Figure 5.6: Assembly of the model after creating instances

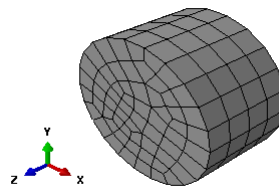


Figure 5.7: Mesh of cylindrical support instances

geometries in the aim of dividing the model into regions with simpler geometries. Seeding tools are used to specify the mesh density for a part or a selected region of a part by creating seeds along its edges. In Mesh module, the element type to be assigned to the mesh must be chosen by specifying the element family, geometric order and shape. It should be noted that if an instance part is created as independent, the mesh must be performed in the Assembly module. However, the mesh must be operated in Part module for any dependent instance part.

In the current study of impacted RC slabs, A 3D solid element, the eight-node continuum element (C3D8R) is used to develop the mesh of the concrete slab and the steel frame, as well as to create the mesh of the impactor. The reinforcement is modeled with two nodes linear 3D truss elements (T3D2), while the rigid parts of supports are meshed with four-node tetrahedral elements (R3D4) using free meshing technique with the medial axis algorithm (Figure 5.7). Finite elements size of reinforcement *SizeElReinf* is considered equal to 0.01 m, and cylindrical supports are modeled with a seed equal to 0.0025 m.

### 5.2.6.1 Slab

4 different types of mesh are used to model the slab part (Mesh1, Mesh2, Mesh3, Mesh4) and then compared in the aim of choosing the appropriate mesh that gives the most similar results to those of experiments. For all mesh types, the steel frame is modeled with 3 elements in width. Different partition schemes are considered in order to emphasize on the impact zone and allow a better transformation of energy and force from the impactor to the slab.

**Mesh1** Thus, the first mesh consists of several partitions that permit to mesh the concrete region of slab into three different densities of mesh (Figure 5.8). Partitions are performed in 3D by cutting the solid slab cell with a plane that passes completely through the cell. The sweep meshing technique with the medial axis algorithm are used to generate the mesh of the slab. The region at the center

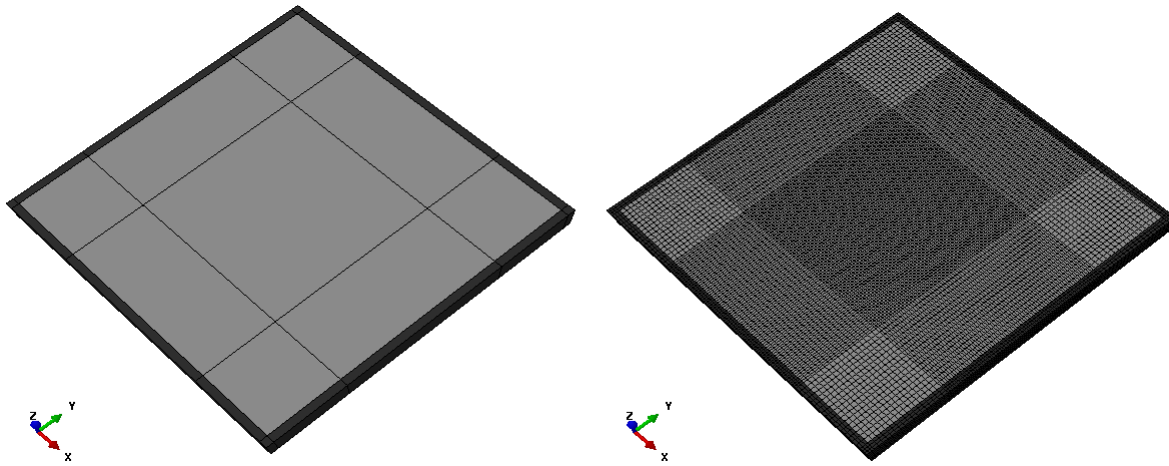


Figure 5.8: Partitions used to create Mesh1 and Mesh2

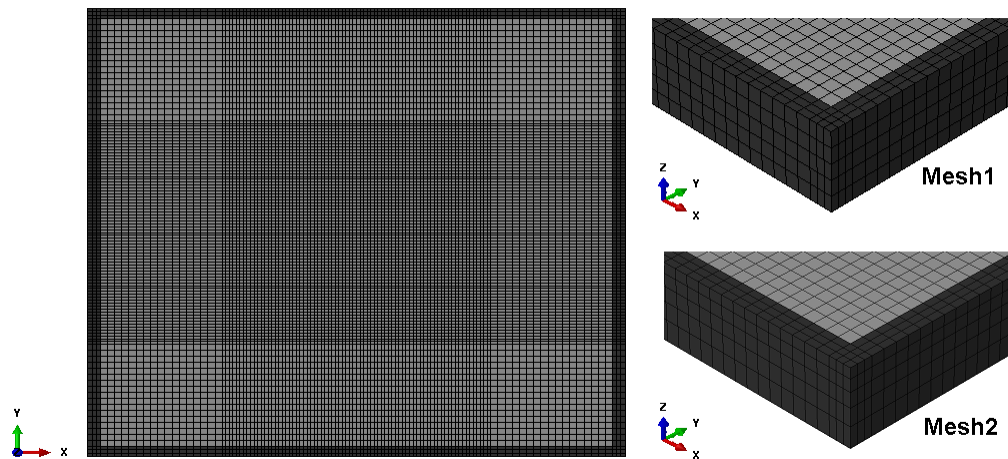


Figure 5.9: Mesh1 and Mesh2 of slab in xy-plane and in the direction of thickness

represents the zone where the impact loading is applied, it has a dimension equal to half of the slab width and is modeled with finer mesh in order to accurately capture the contact force. Dimensions in width and length of elements at this region are governed by the number of elements  $ne$  in the thickness direction, and they are equal to  $e/2ne$  ( $e$  is the slab thickness). For Mesh1, elements along the thickness of the slab are assumed to have the same size of  $e/ne$  (Figure 5.9). The corner regions of slab have a coarse density mesh with elements of an aspect ratio of 1 and a size of  $e/ne$ . For Slab 2 and  $ne = 5$ , elements at the impact region have dimensions of  $7.6 \times 7.6 \times 15.2$  mm, while those at corner regions have dimensions of  $15.2 \times 15.2 \times 15.2$  mm.

**Mesh2** Mesh2 is the same as Mesh1 with only one difference related to the size of elements in the thickness direction. For Mesh2, elements along the thickness of the slab have different size, but a bias command is used in order to have finer mesh at the upper surface of the slab. This surface is where the impact loading is applied, hence it is preferred to be modeled with fine mesh allowing a better representation of the impact zone in the FEM and more accurate results. Consequently, the thickness of the slab is modeled with  $ne$  elements and a bias ratio of 2 (Figure 5.9).

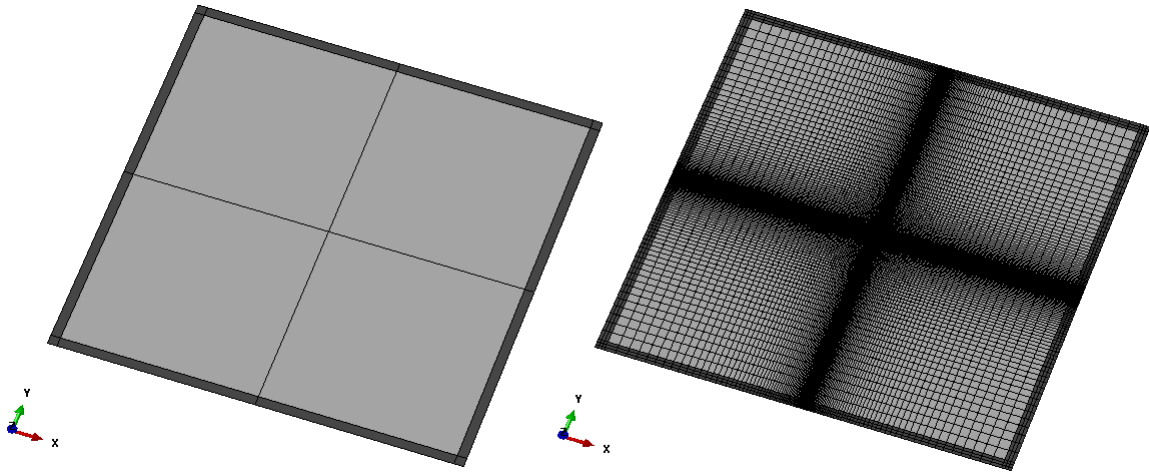


Figure 5.10: Partitions used to create Mesh3

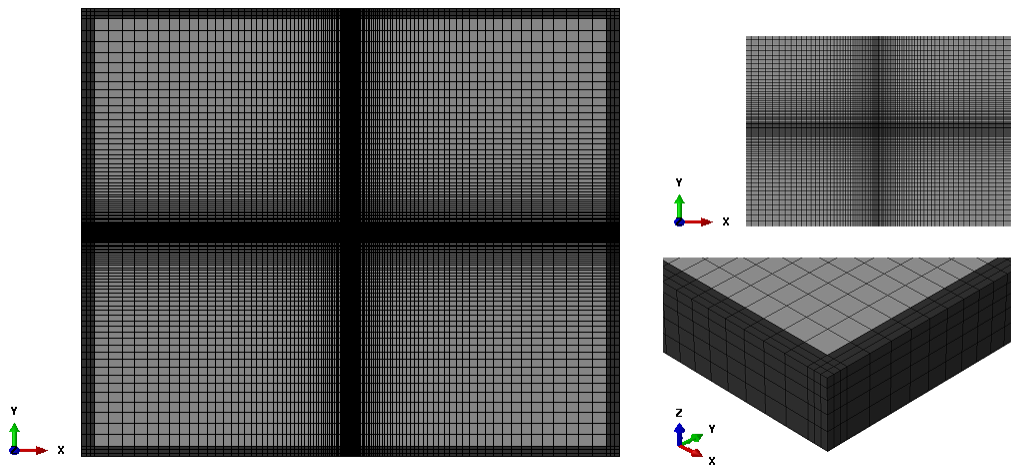


Figure 5.11: Mesh3 of slab in xy-plane and in the direction of thickness

**Mesh3** For Mesh3, the slab is partitioned with 2 cutting planes in x- and y- direction, respectively (Figure 5.10). Then, the edges of the concrete region of slab as well as those of the steel frame are meshed using the bias command with a maximum element size of 20 mm at the slab corner and a minimum element size of 1 mm at the center of the slab. The basic aim of this mesh type is to concentrate the fine mesh density at the impact point since the region that is highly affected during an impact analysis represents the contact zone of the impactor and the slab. For Mesh3, the thickness is also meshed with  $ne$  elements and a bias ratio of 2 (Figure 5.11) and the mesh is generated using the structured meshing.

**Mesh4** The concrete region of slab and the steel frame are partitioned in 3D with 2 cutting planes in x-direction and 2 cutting planes in y-direction in order to create an square that refers to the impact zone. Next, this square is partitioned in both diagonal directions to be able to create finer mesh at the impact point (Figure 5.12). The diagonals of the impact zone are meshed using the bias command with a maximum element size  $SizeElImpactZoneMax$  of 10 mm at the square corner and a minimum element size  $SizeElImpactZoneMin$  of 1 mm at the center of the slab. The concrete

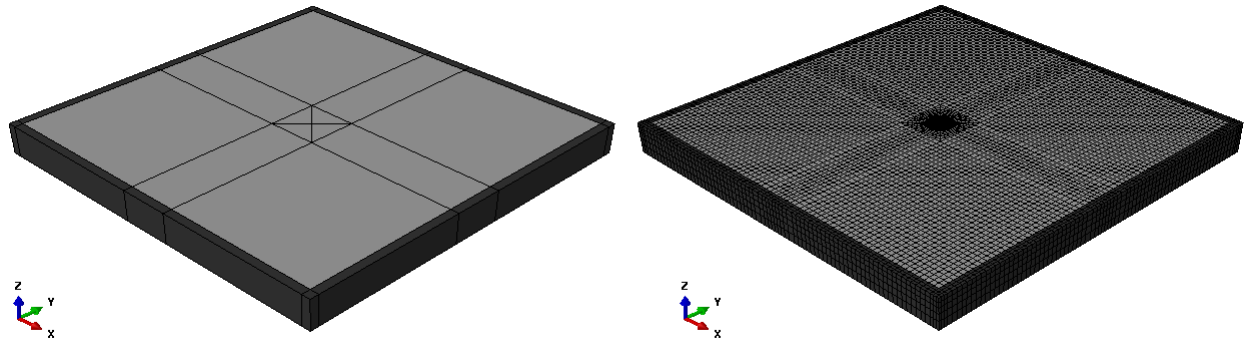


Figure 5.12: Partitions used to create Mesh4

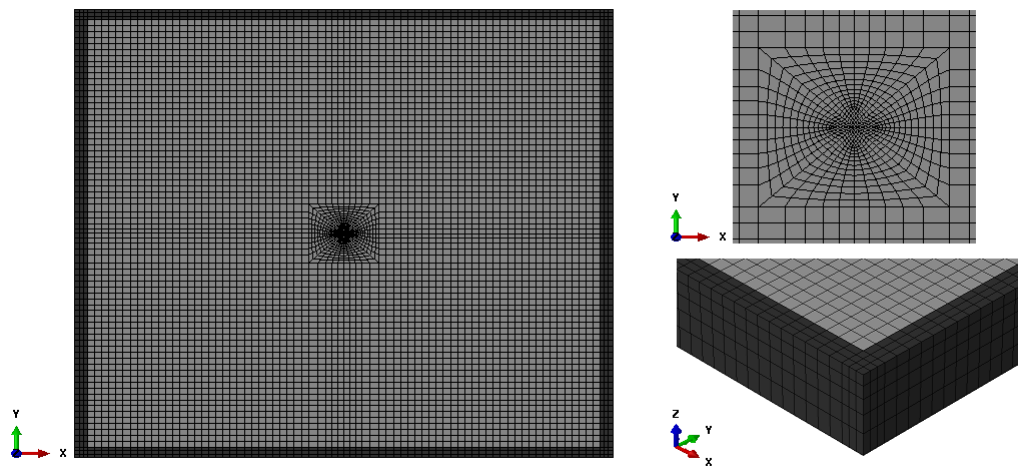


Figure 5.13: Mesh4 of slab in xy-plane and in the direction of thickness

region around the impact square, as well as the steel frame, are meshed with elements having the same size along all edges. The size of elements of slab edges  $SizeElSlab$  are taken equal to 10 mm, which permits to have an uniform mesh in xy-plane for all the slab except the impact zone. A zoom view of the impact square mesh with biased seeding along its diagonals is illustrated in Figure 5.13, this mesh allows having fine mesh density only in the impact zone where the loading is applied. For Mesh4, the thickness is also meshed with  $ne$  elements and a bias ratio of 2 (Figure 5.13) and the mesh is generated using the sweep meshing technique with the medial axis algorithm.

The Python script written for Mesh4 allows changing the size of the impact square by only specifying the desired dimension  $d_{impact}$ , then the mesh can be automatically generated according to the seeds provided for slab and impact square edges by running the script in Abaqus/CAE (Figure 5.14). Another important advantage of Python script written for Mesh4 is that it allows studying the effect of impact position by only specifying the coordinates of impact point in x-direction  $x_{impact}$  and in y-direction  $y_{impact}$ . The mesh can be then automatically generated according to the impact square by running the script in Abaqus/CAE, and the impactor will be always located above the center of the impact square. (Figure 5.15). The script enables to perform the impact analysis of RC slabs at any point on the slab.

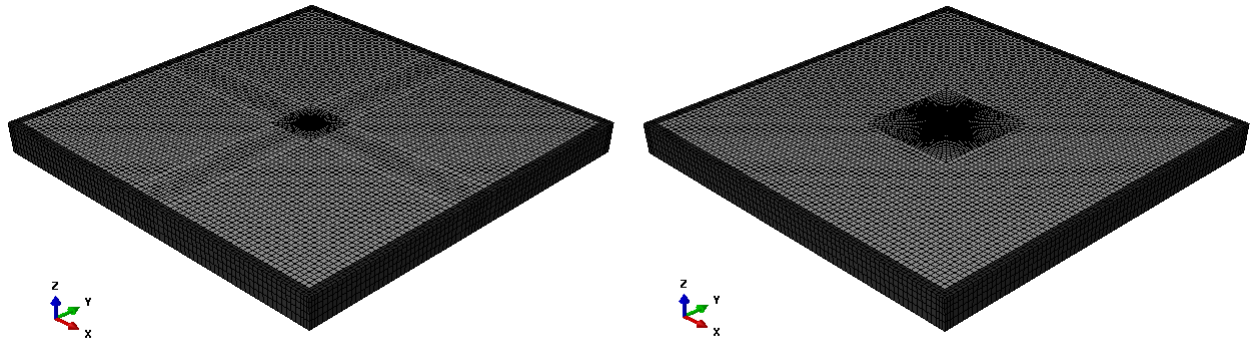


Figure 5.14: Mesh4 with different sizes of impact region

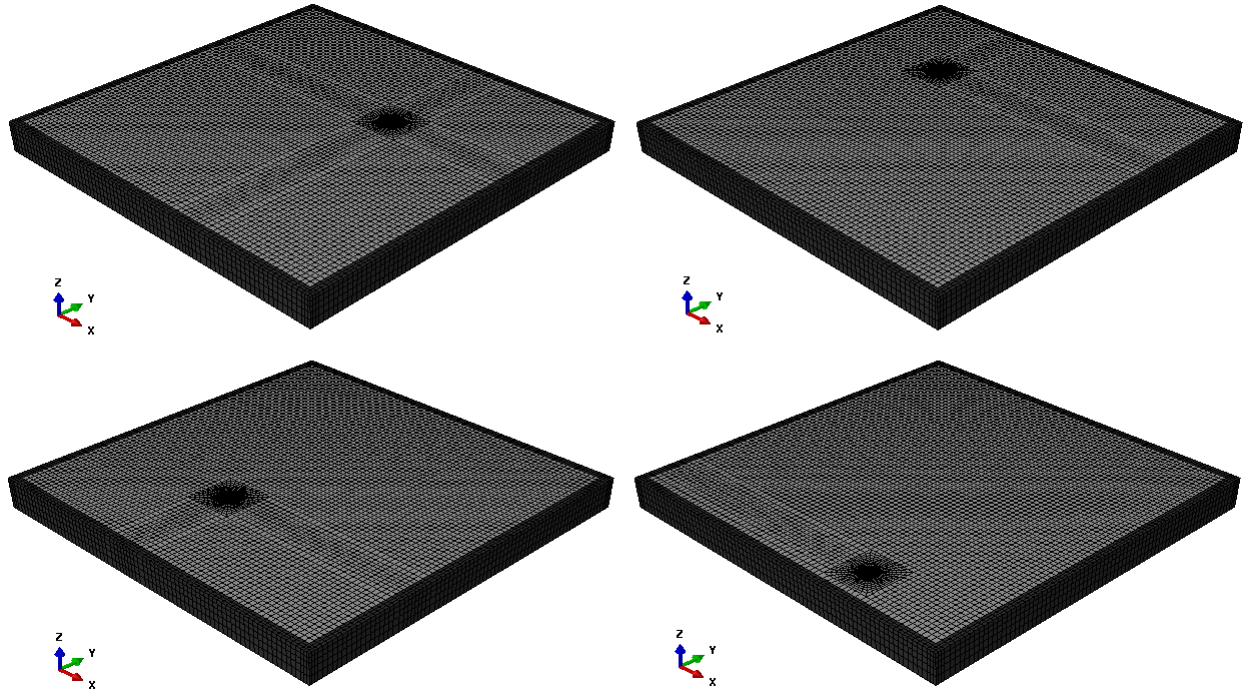


Figure 5.15: Mesh4 for different impact positions

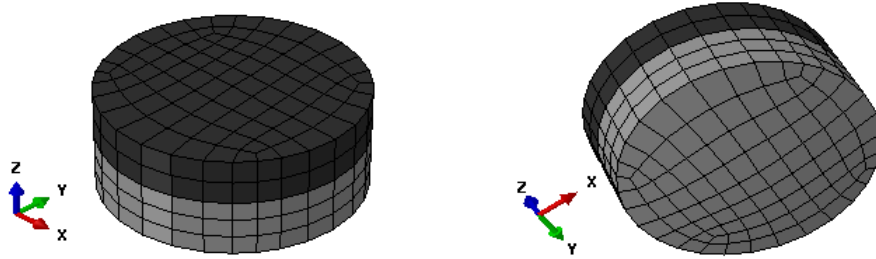


Figure 5.16: The impactor mesh used with Mesh1, Mesh2 and Mesh3 of slab

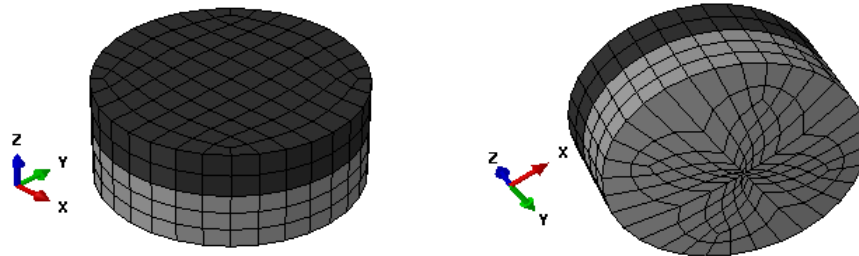


Figure 5.17: The impactor mesh used with Mesh4 of slab

### 5.2.6.2 Impactor

The mesh of impactor is generated using the sweep technique with the medial axis algorithm and a constant seed of 10 mm considered along all the impactor edges (Figure 5.16). The following mesh type is used for the impactor in cases where Mesh1, Mesh2 or Mesh3 are used to model the slab.

A second mesh type is considered for the impactor and used in the model with Mesh4 of the slab. In this case and in order to allow a better contact between the slab and the impactor, more partitions are needed. First, the impactor must be partitioned with a cutting plane passing through the region of intersection of its cylindrical and hemispherical parts. Next, the hemispherical part is partitioned to create a finer mesh at the center of the impactor surface that enters in contact with the slab. The mesh of the hemispherical part is generated using the structured meshing technique, while the cylindrical part is meshed using the sweep meshing technique with the medial axis algorithm. The size of elements in the cylindrical part is considered the same as that in the previous mesh, while the hemispherical part is meshed using the bias command with a maximum element size of 10 mm and a minimum element size of 1 mm.

### 5.2.7 Configuring analysis

Abaqus can be used to solve different types of problems such as static, dynamic, quasi-static, seismic, etc. Analyses are configured in Abaqus through one or multiple steps to describe the various loading conditions of the problem. Steps are created using the Step module and two types of analysis steps can be defined in Abaqus, namely general response analysis steps and linear perturbation steps. General analysis steps can be used to analyze the overall structural response that can be linear or nonlinear. Linear perturbation steps are used to calculate the linear perturbation response of the problem such as extraction of natural frequency, transient modal analysis and response spectrum analysis.

In order to determine the dynamic response of RC slabs under low velocity impact of dropped objects, only one dynamic/explicit step is created for the simulation as the problem consists of a single event. In this step, initial conditions are applied to the impactor and the time period is set to 0.03 s with a maximum time increment of 1e-6. The current analysis consists of two steps, the impact step and the initial step generated automatically in Abaqus and in which the boundary conditions are applied.

### 5.2.8 Applying loads, boundary and initial conditions to the model

As previously mentioned in section 3.4, Abaqus provides several ways to introduce loads, boundary conditions and initial conditions in finite element analysis. Specifying boundary and initial conditions and applying load conditions to the structure is step-dependent, which means that the step or steps at which these conditions become active should be specified in the FEM.

To simulate the motion of the dropped object, the impactor is dropped at the center of Slab 2 and Slab 3 with a velocity of 6.5 m/s, while the impactor hits Slab 4 with an initial velocity of 8.0 m/s. Slab 5 and Slab 6 are subjected to an impact velocity of 8.7 m/s and 8.3 m/s, respectively. Velocity values are considered as in experimental tests of Chen and May (Table 2.1). In the finite element model of each slab, the impactor hits the slab with a constant velocity that is applied to each of the nodes of the impactor in the direction perpendicular to the slabs and opposite to z-axis direction. In this study, the effect of impact loading of dropped objects on the behavior of RC slabs using a finite element analysis is examined in the presence of gravity load. Therefore, the analysis of Chen and May slabs is carried out by applying a gravity load of  $9.81 \text{ m/s}^2$  on the whole model. It should be noted that gravity load does not act on rigid bodies included in the FEM, namely the four cylindrical supports on which the slab is supported. Gravity load is not prescribed as a function of time nor defined according to an amplitude curve. In this case, Abaqus assumes that the loading is applied instantaneously at the beginning of the step. Gravity load is created at the impact step and acts in the negative z-axis direction.

The motion of a rigid body is governed by that of its reference point. Therefore, boundary conditions used to constrain the cylindrical support instances are applied to their reference points that are located at the center of the bottom circular surface of supports, respectively. The same boundary conditions are applied to each of the cylindrical supports on which the slab is supported, thus it is more convenient to group the reference points of these rigid bodies into a single set of geometry. The ENCASTRE boundary condition is used to fully constrain the movement of the relevant reference points and set their degrees of freedom to zero. Translational displacements of the reference points in the x-, y- and z-directions, as well as their rotations about the x-, y- and z-axes, remain restrained during the whole analysis. An additional boundary condition is applied to the model in order to ensure the motion of the impactor in the vertical direction only. Thus, a set of geometry that includes the upper circular surface of the impactor is created and the displacement/rotation boundary condition is used to prescribe its displacement and rotation degrees of freedom. A nonzero displacement in the z-axis direction is prescribed to the impactor upper surface set, while the remaining degrees of freedom are constrained to zero. Boundary conditions of supports and impactor are applied at the initial step.

### 5.2.9 Creating interaction and constraints

In the Assembly module, the various parts of the model are positioned relative to each other in order to create the final geometry of the model but they are still unconnected. Therefore, interaction and constraints between parts or surfaces need to be defined to connect instances properly to each other. As previously mentioned in section 3.4, Abaqus provides two algorithms to simulate contact between different regions in the model and several constraint types to couple the motion of a group of nodes

to that of other nodes. In the current study, the embedded and tie constraints are used to represent the reinforcing steel bars in the model and to tie the four cylindrical supports to the slab bottom surface, respectively. Both algorithms for simulating contact are used and compared, namely general contact algorithm and contact pairs algorithm.

The embedded approach is used to create bond between the two instances of steel reinforcement and the slab instance and overcome the mesh dependency of the discrete approach. In this case, it is not necessary to adapt the concrete mesh to overlap the common reinforcement nodes. Concrete elements of slabs are grouped in a set of geometry and considered as the host elements. The set of truss reinforcement elements are embedded in the set of three-solid elements of concrete that constrain the translational degrees of freedom of the embedded reinforcement nodes. The embedded constraint available in Abaqus couples the nodal degree of freedom automatically assuming a full bond action between the reinforcement and concrete elements with no relative slip.

Four surface-to-surface tie constraints are used to create proper interaction between the discrete rigid elements of cylindrical supports and the solid elements of the steel frame and the concrete region of slab. Each tie constraint connects the upper surface of a cylindrical support to the corresponding quarter of the slab bottom surface. The upper surfaces of supports are designated to be the master surface as they represent the rigid surfaces, while the bottom surfaces of slab are defined as slave surface. As cylindrical supports are positioned at the intersection points of the slab concrete region and the steel frame, the slave surfaces of slab must include the bottom surfaces related to the slab concrete region as well as those related to the steel frame. A tie constraint is mesh-independent, the master surfaces are modeled with a coarser mesh. No relative motion between master and slave surfaces is allowed throughout the whole analysis, thus shear interaction is avoided between the elements of the selected surfaces.

To analyze the impact problem of RC slabs, the contact algorithms available in Abaqus are used and compared in order to model the contact between the slab and the impactor. The first algorithm is the general contact algorithm which allows very simple definitions of contact with very few restrictions on the types of surfaces. The second algorithm is the contact pair algorithm that represents more restrictions on the types of surfaces involved. The contact pair algorithm necessitates the definition of the contact surfaces. Thus the surface-to-surface contact is used to describe the interaction between the upper surface of the slab and the impactor hemispherical surface. Both algorithm need to define the mechanical interaction property model in Abaqus/Explicit, while the contact pair algorithm requires more definition such as the sliding formulation and the contact constraint enforcement method.

Concerning the interaction properties, the hard contact pressure-overclosure relationship is used to define the mechanical normal interaction of the contact model. The hard contact implies that any contact pressure can be transmitted between surfaces when they are in contact, while no contact pressure is transmitted when surfaces separate. The frictional behavior between the slab and the impactor is defined using the penalty friction formulation to define the mechanical tangential interaction. These formulation allows some relative motion between the surfaces in contact. A uniform coefficient of friction of 0.45 is assumed for contact surfaces.

For contact pair algorithm, the finite sliding formulation which allows any arbitrary motion of surfaces is used to account for the relative motion of the upper surface of the slab and the impactor surface. The position of surfaces in contact changes during the analysis, then the element faces and nodes that are in contact change. In order to enforce contact constraints, both the pure master-slave kinematic and penalty contact methods are used and compared in the aim of finding the best method to model the contact in the FEM. The impactor surface is considered as the master surface since the surfaces attached to rigid bodies must always be designated as master surfaces in Abaqus/Explicit. The slave surface in this case must be the upper surface of the slab since this latter represents the deformable body and must be with the finer mesh in order to avoid significant penetration for hard contact.

### 5.2.10 Output requests

In order to compare numerical results to those obtained from the experiments of Chen and May, several Field and History output are defined in the Step module, but only the contact force versus time is presented in this study. The aim is to compare the force-time histories of different slabs with experimental results in order to find the finite element features that allow a good agreement with experiments. Therefore, the contact force on the master surface of the impactor in the global z-direction (CFN3) is evaluated. It should be noted that a Butterworth filter of order 6 is used in the model as Chen and May used a Butterworth filter with a cut-off frequency of 2000 Hz to filter results and reduce noise. In Abaqus, filtering of contact force-time history can be applied only in the case of general contact. For kinematic and penalty contact, results are presented with no filtering as it is not allowed for contact pairs in Abaqus/Explicit.

### 5.2.11 Creating an analysis job

The final step in a finite element analysis in Abaqus is to create a job that permits to analyze the model. Therefore, the Job module is used to create a job and submit it for analysis.

## 5.3 Discussion of results of Chen and May slabs FEM

First, the FEM of Chen and May slabs is validated for Slab2 using the C6T1S1 simulation. (C refers to the compression stress-strain curve, T refers to the tension stress-strain curve and S refers to the steel stress-strain curve).

### 5.3.1 Comparison of mesh types

The problem of impact is a very complex problem that involves several nonlinearities. Thus, it is important to create a mesh that allows an accurate transfer of impact energy to the slab. The region of concern in this type of problem lies at the impact where the impactor hits the slab and damage under compression caused by impact is concentrated in this zone. This region needs more attention and more refined mesh is necessary as the main physical mechanisms of RC slabs under impact occur at this region. 4 types of meshes are used in this study as indicated in section 5.2.6. Mesh1 allows a more refined mesh at the impact zone compared to the remaining regions of the slab. Mesh2 is the same as Mesh1 with the only difference that elements in thickness direction do not have the same size, more refined elements are used at the upper surface where the impact phenomenon occurs. Mesh3 is the mesh allowing the most refined mesh at the impact point among the meshes considered for Chen and May slabs, elements size varies linearly in the edges direction as well as in the thickness direction. However, an excessive refinement could lead to distortion problem due to the aspect ratio of very small elements at the impact point. For this reason, Mesh4 is developed in order to provide a refined mesh at the impact zone with an acceptable aspect ratio of elements. Mesh4 allows a refined mesh only at the selected zone of impact, while elements at the slab part surrounding the impact square have the same size.

For all mesh types, the three-dimensional model of Slab2 with 5 elements in the thickness consists of:

- 3168 truss elements of type T3D2 with 2970 nodes to represent reinforcement,
- 460 solid elements of type C3D8R with 648 nodes to represent the impactor (except for Mesh4),
- 828 rigid elements of type R3D4 with 836 nodes to represent the cylindrical supports.

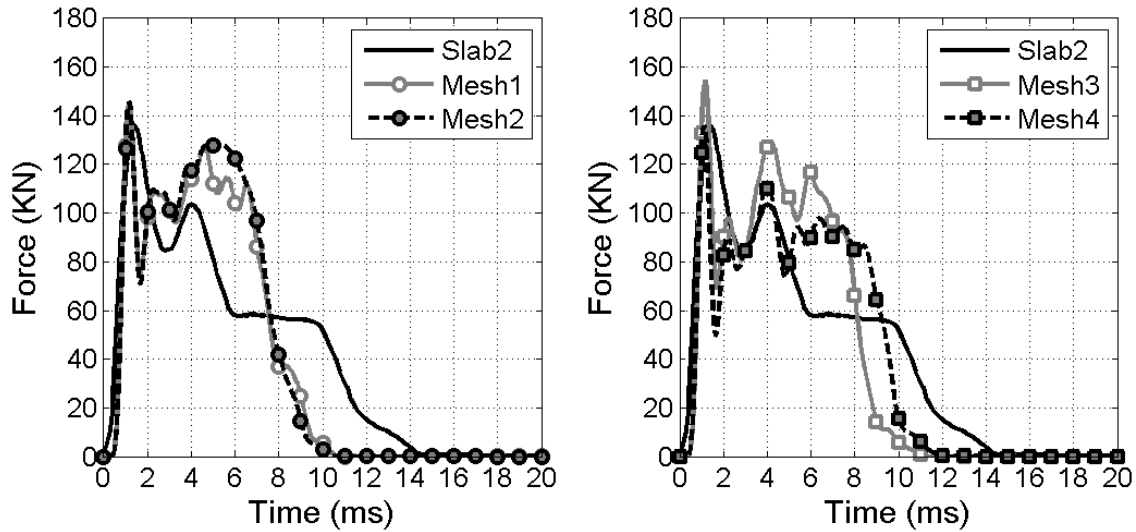


Figure 5.18: Comparison of different mesh types proposed for Slab2

The impactor is modeled with 736 solid elements with 953 nodes when Mesh4 is used, as a different mesh is considered for the impactor in this case. Although the mesh of impactor used with Mesh1, 2 and 3 presents a better aspect ratio for elements, the mesh used with Mesh4 is more convenient to represent the concentrated forces acting on hemispherical impactor geometry. The concrete region of Slab2 as well as the steel support consist of:

- 67280 solid elements of type C3D8R with 82134 nodes for Mesh1 and Mesh2,
- 69620 solid elements of type C3D8R with 84966 nodes for Mesh3,
- 33020 solid elements of type C3D8R with 40566 nodes for Mesh4.

As can be seen, Mesh4 allows reducing the number of elements and nodes, and hence the number of degrees of freedom in the numerical analysis, in comparison to other proposed meshes. Consequently, the computational effort is reduced. The comparison of experimental force-time curve of Slab2 with those obtained with the different mesh types in this study shows the efficiency and accuracy of developing Mesh4 in predicting the behavior of the slab (Figure 5.18). The peak impact force is accurately estimated and is obtained at the same time as experimental results, while the curve shape in the after peak phase shows some difference in comparison to experimental results. The accurate value of peak force obtained can be attributed to a good estimation of contact stiffness using general contact algorithm. Impact duration does match with the tests. In numerical analysis, the slab and the impactor remain in contact for about 12 ms, while the contact duration is estimated by 14 ms in experiments.

### 5.3.2 Comparison of contact algorithms

The influence of the contact algorithm used to model the contact phenomenon between the slab and the impactor is also studied. Figure 5.19 shows the contact force-time curve obtained using general contact algorithm and contact pair algorithm. The kinematic and penalty methods used to enforce constraints in contact pair algorithm are also compared. As can be seen, both algorithms provide good results which are in agreement with experimental results. The general contact slightly presents more accurate results, especially for the initial linear phase of the curve and the peak value

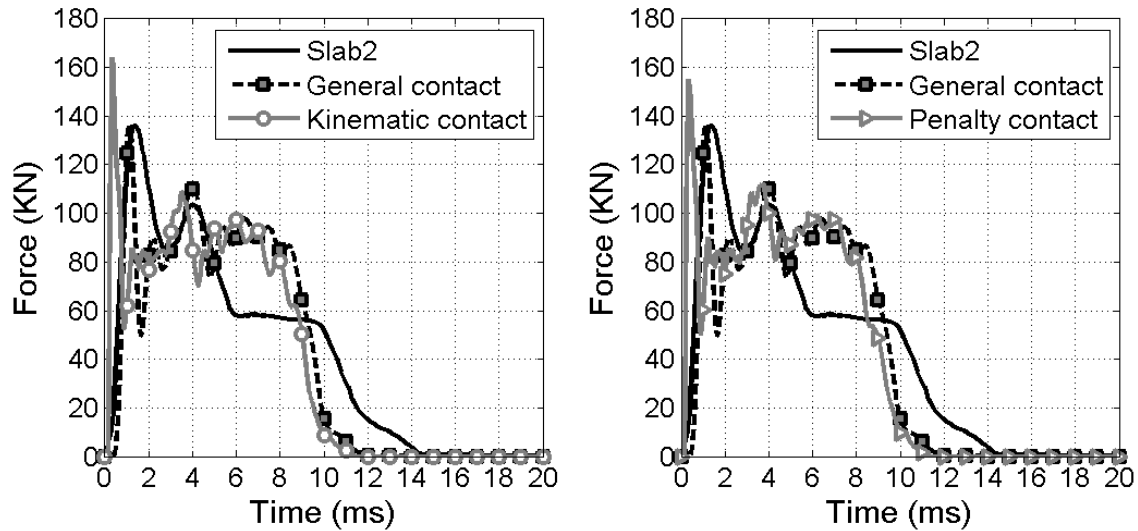


Figure 5.19: Comparison of contact algorithms available in Abaqus for Slab2 meshed with Mesh4

of contact force. The reason is that Abaqus allows using filters to filter the force-time output curve only when the contact is defined as general algorithm. For contact pair algorithm, force-time curves are presented with no filtering. The difference between general contact and contact pair algorithms is that the first permits to specify automatically the contact surfaces in the finite element model, which can be very useful for complex contact problems. The contact pair algorithm necessitates specifying each of the surfaces that are in interaction.

### 5.3.3 Mesh sensitivity

A mesh sensitivity analysis is conducted in order to choose a convenient mesh that is sufficiently refined to converge to an accurate solution with the minimum computational effort. Therefore, several sensitivity analyses are performed:

- The number of elements in the thickness direction is investigated, and it is found that 5 elements are sufficient to obtain numerical results that are in good agreement with experiments. Using 7 or 9 elements in the thickness direction does provide a more improvement in results (Figure 5.20).
- The maximum and minimum size of elements in the impact zone is studied. Elements are generated in this zone using the bias seeding option. It can be seen that there is no need to use very small elements at this region and that a maximum size of 0.01 m and a minimum size of 0.001 are sufficient to converge to a unique solution (Figure 5.20).
- The size of elements surrounding the impact region is varied using a finer, intermediate and coarser mesh. Numerical results obtained with elements of seed of 0.01m are in good agreement with experimental results, while smaller elements do not give more accurate results (Figure 5.21).
- The size of elements in reinforcement is studied. It can be seen that the size of these elements has no effect on results (Figure 5.21).

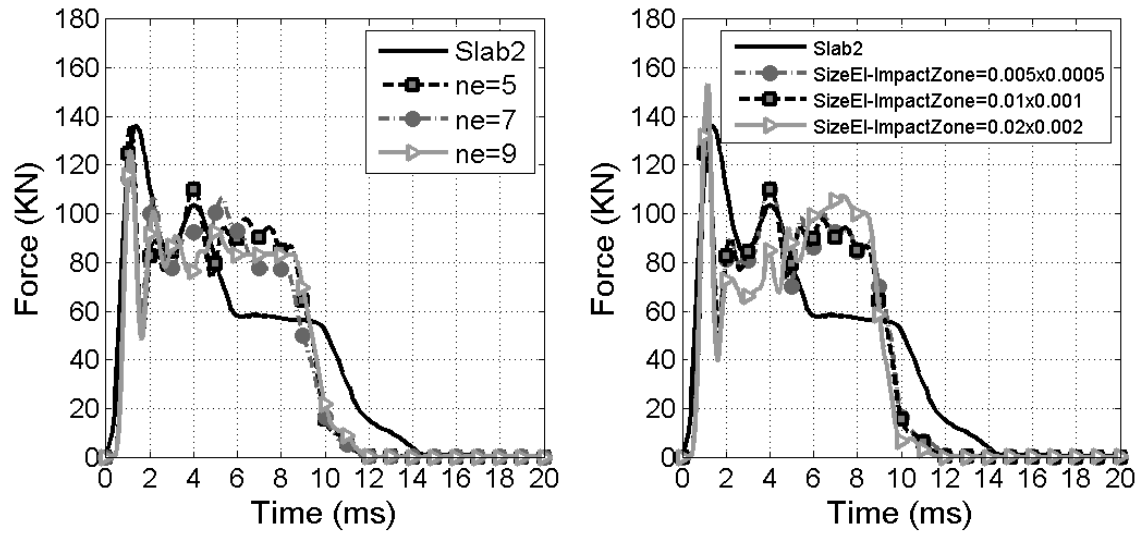


Figure 5.20: Sensitivity of mesh in term of the number of elements in the thickness direction and the size of elements in the impact zone for Slab2 meshed with Mesh4

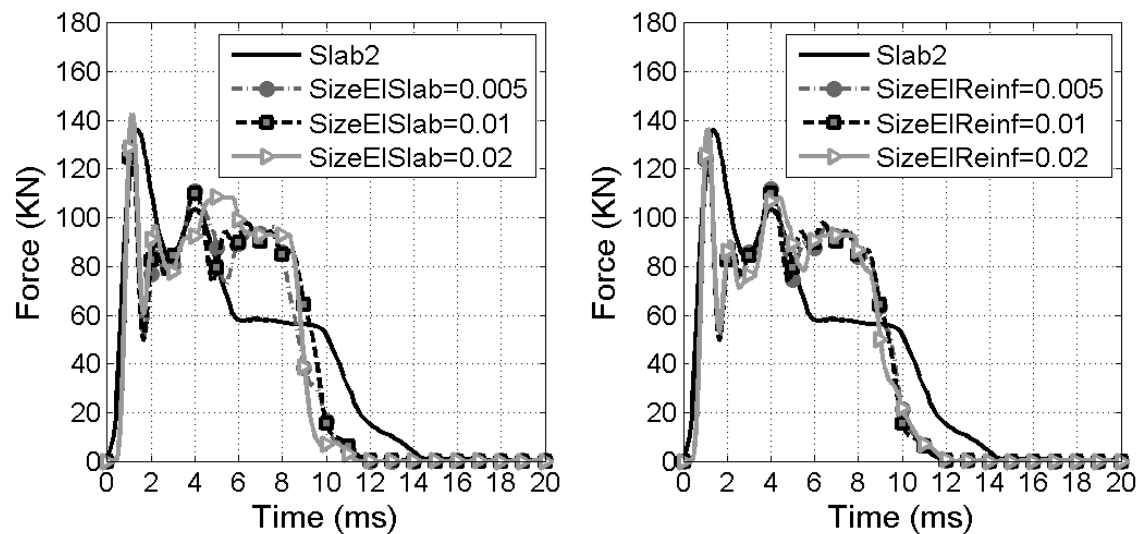


Figure 5.21: Sensitivity of mesh in term of the size of elements in the slab and the size of elements in the reinforcement for Slab2 meshed with Mesh4

### 5.3.4 Choice of materials behavior

In this study, the dynamic problem of impact is investigated in order to predict the structural behavior of RC slabs. Although the impactor is modeled as a deformable body in the FEM of Chen and May slabs, the response of impactor is not of concern. The reason for which the impactor is modeled as deformable body is related to the aim of allowing the best quality of transmission of impact energy between the impactor and the slab. The response of slab is more important in terms of deformations and damages. The upper surface of the slab is the first element that enters in collision with the impactor, this surface is under compression due the compressive wave generated by the impactor at the moment of impact. Then, the compressive wave progresses in the slab thickness and reflects from the bottom surface as a tensile wave. Thus, it is important to first specify the behavior of concrete in compression, as it is the first physical mechanism involved during an impact event. Thereafter, its behavior in tension can be studied.

The most difficult parameters to identify for the CDP model are those related to the behavior of concrete in tension and compression. In order to accurately define the concrete behavior in a numerical analysis of an impact problem, several relationships that describe the compressive stresses in concrete in term of compressive strain are considered. Those stress-strain curves are based on several experimental results from the literature (see Chapter 2). Force-time curves obtained using these curves in the model are depicted in Figures 5.22-5.24. It can be seen that compressive stress-strain curves with a higher resistance to crushing allow a better estimation of the peak impact force (C6 and C9), while compressive stress-strain curve with more softening allow a linear plateau as experiments and a better estimation of the shape of the force-time curve after the first peak. Consequently, the curve C6 is adopted since it provides the best fit with experimental results.

Subsequently, the behavior of concrete in tension is studied. CDP model permits to describe the tensile behavior of concrete using a stress-strain curve, a stress-cracking displacement curve and a fracture energy value. Several cases from the literature are considered and compared (Figures 5.25-5.28). It can be seen that for stress-strain curves T1 gives results which are in good agreement with experiments. However, the trilinear stress-cracking displacement curve D3 seems to be the most accurate way to describe concrete in tension in the CDP model. It provides a good estimation of the peak impact force, it also predicts correctly the plateau in the force-time curve. Curves based on the fracture energy cracking criterion seem to be more efficient as they permit a better assessing of deformation and cracks opening. These curves are more adequate to reduce the concern of the mesh sensitivity, however they results in more computational effort compared to tensile stress-strain curves.

Figures 5.29-5.30 show that the steel behavior has no significant effect on the prediction of force-time curves.

### 5.3.5 Validation of model for other slabs

C6T1S1 and C6D3S1 simulations with the relevant constitutive behaviors of materials are found to give the most accurate in the case of Slab2. Thus, both simulations are used to validate the model for the other slabs of Chen and May experiments (Figures 5.31-5.32). As can be seen, using stress-cracking displacement curve to describe the tensile behavior of concrete in numerical analysis provides more accurate results for all slabs then using tensile stress-strain curve.

In the case of Slab3, a flat impactor is used in experiments as well as in the FEM. The peak impact force is overestimated in this case indicating the difficulty of general contact algorithm in accurately modeling the interaction between the slab and the impactor when a flat surface is considered for the impactor. In the case of hemispherical impactor, the general contact algorithm allows a better interaction between the two bodies in collision (Slab2, Slab4, Slab5). Slab4 is impacted with higher velocity than in the case of Slab2 and Slab3, the FEM allows a good prediction of the peak value for higher velocity values. For Slab3, 4 and 5 the times at which the impact force reaches its peak are in

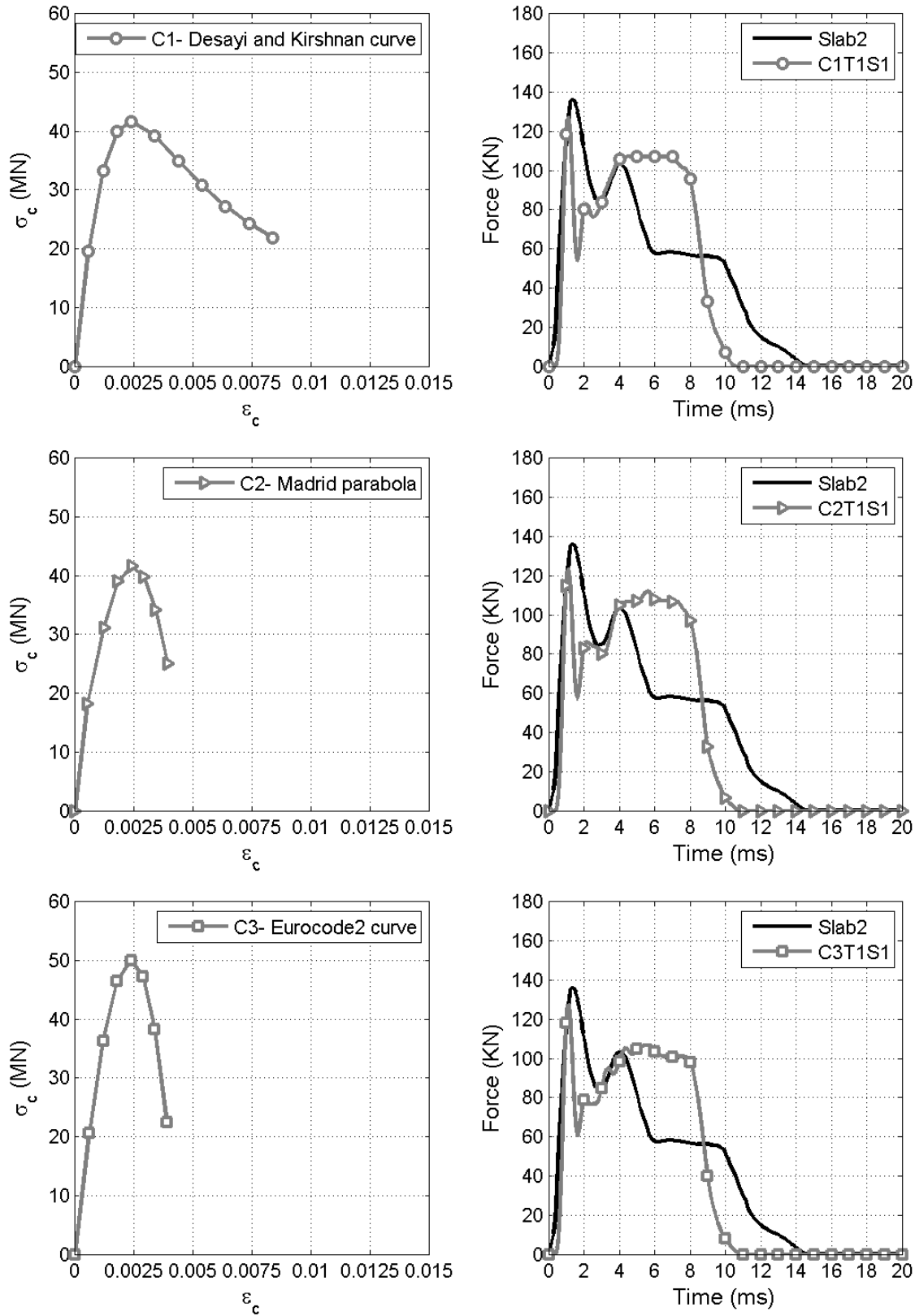


Figure 5.22: Comparison of concrete compressive stress-strain curves for Slab2

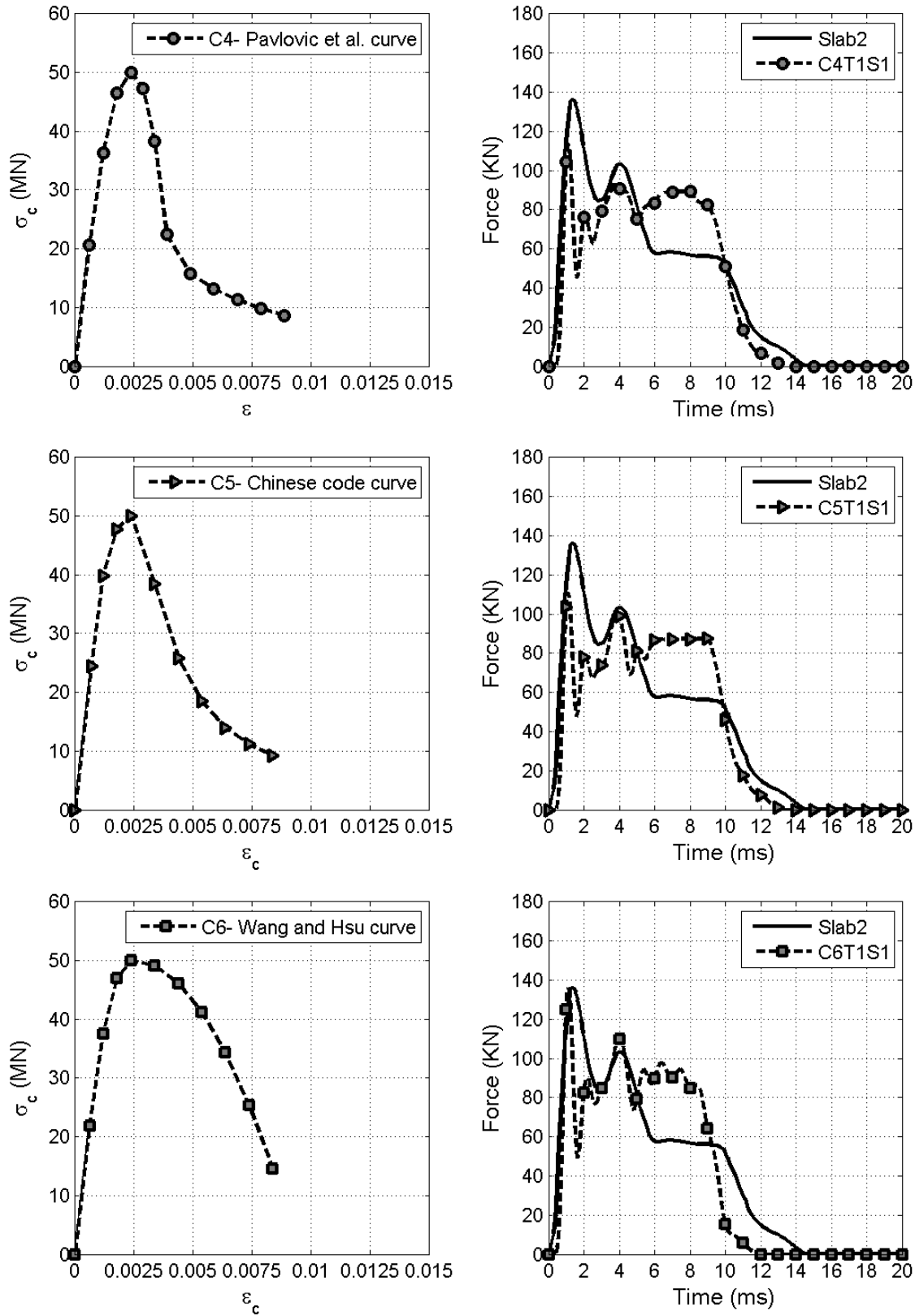


Figure 5.23: Comparison of concrete compressive stress-strain curves for Slab2

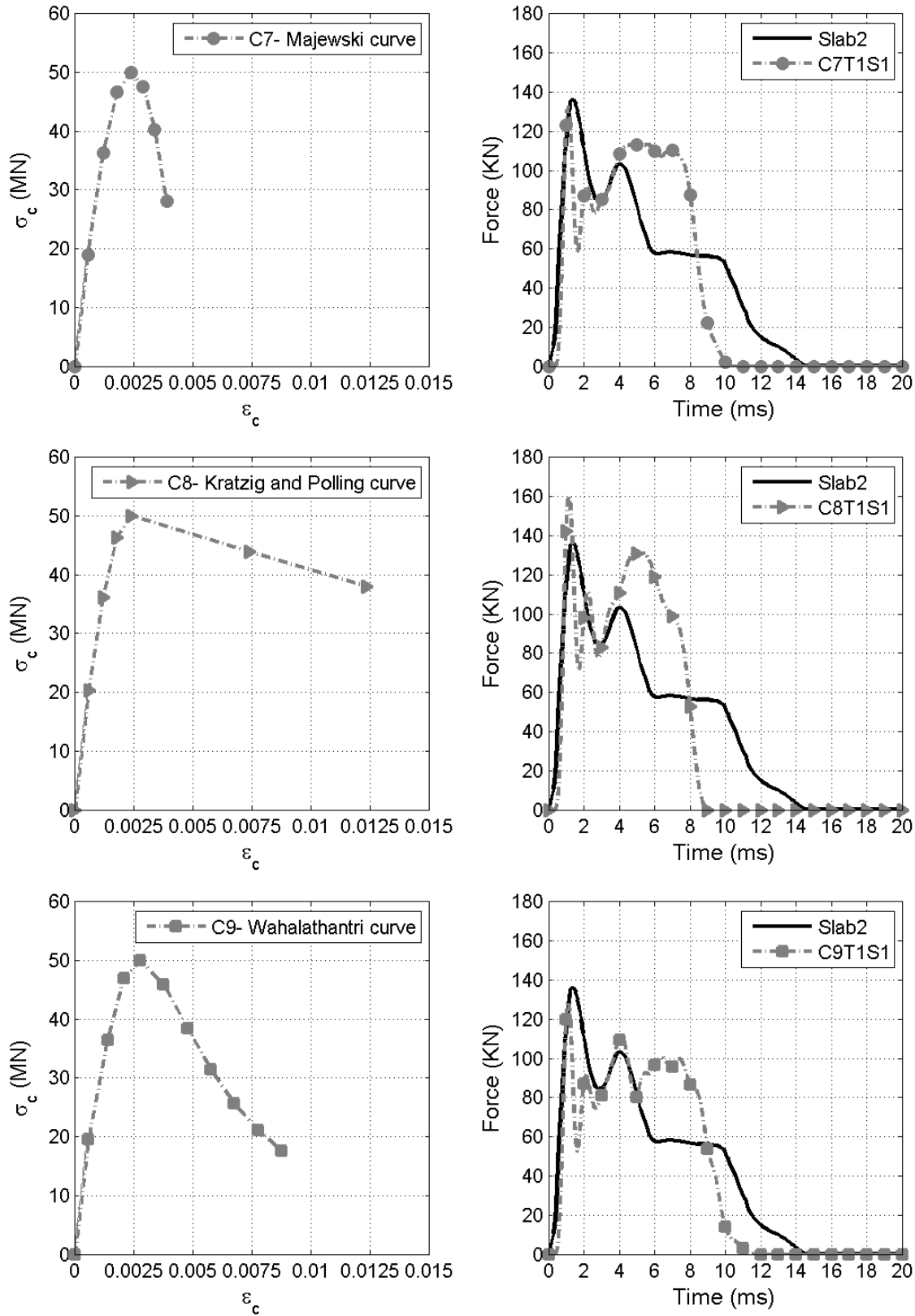


Figure 5.24: Comparison of concrete compressive stress-strain curves for Slab2

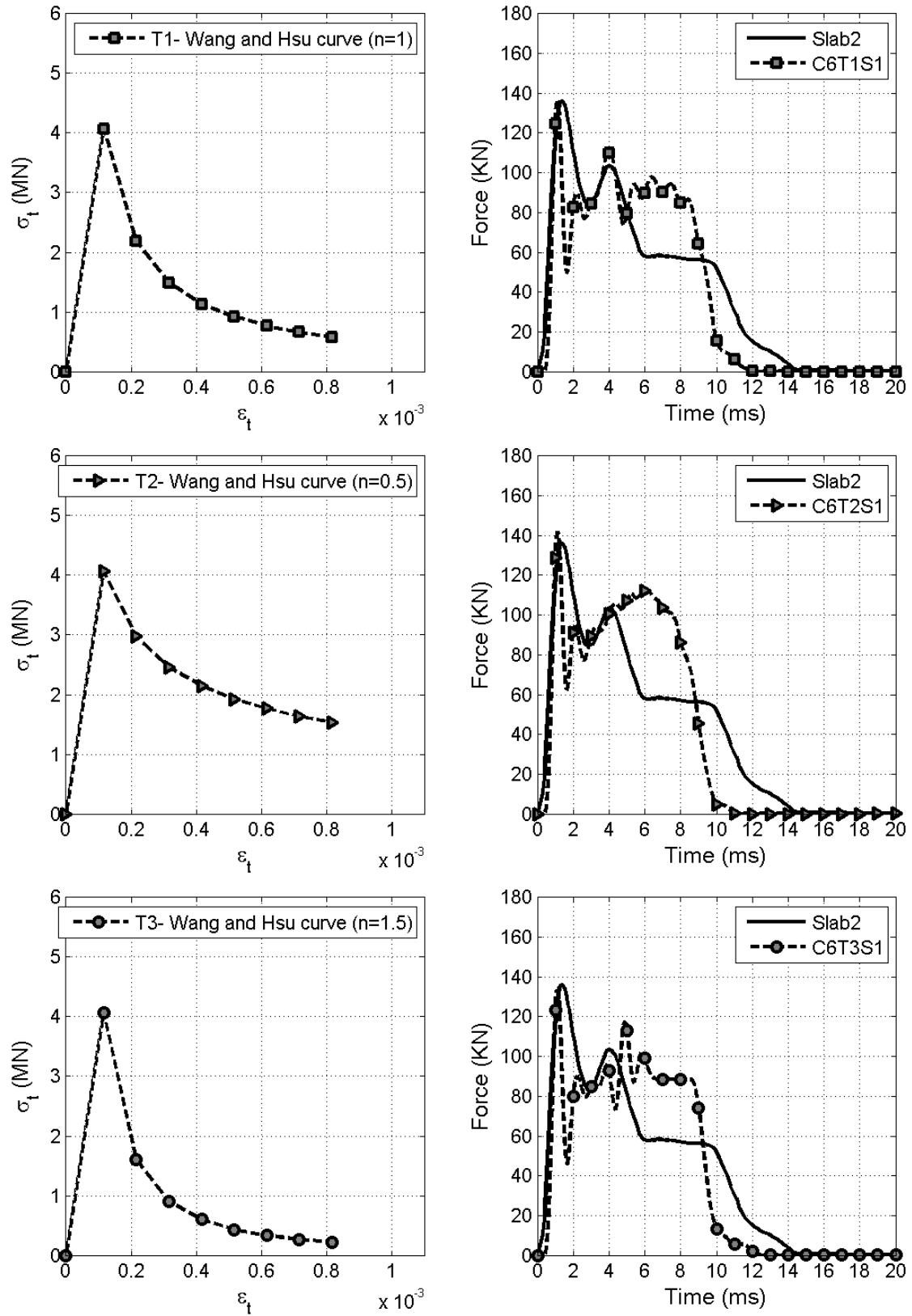


Figure 5.25: Comparison of concrete tensile stress-strain curves for Slab2

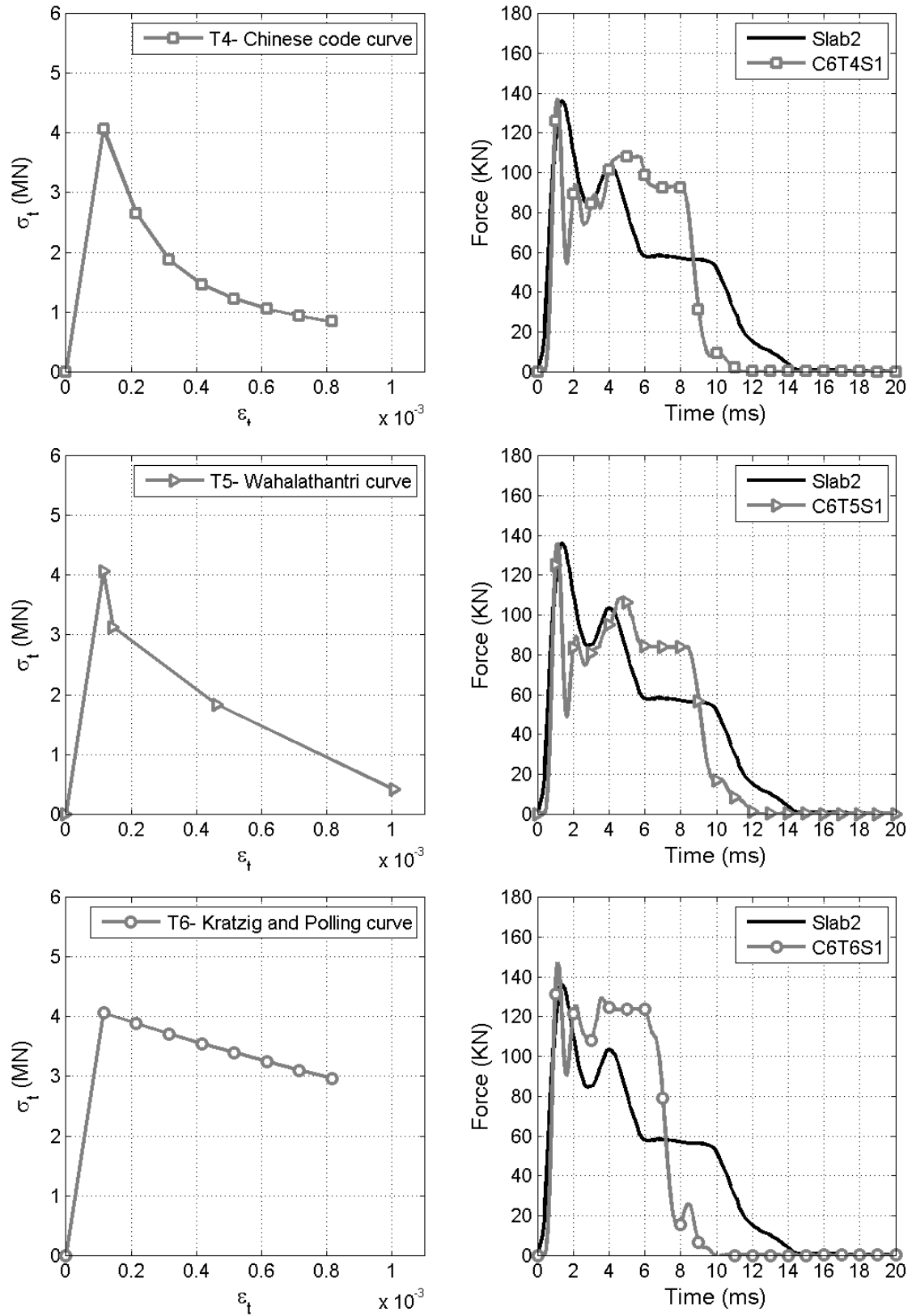


Figure 5.26: Comparison of concrete tensile stress-strain curves for Slab2

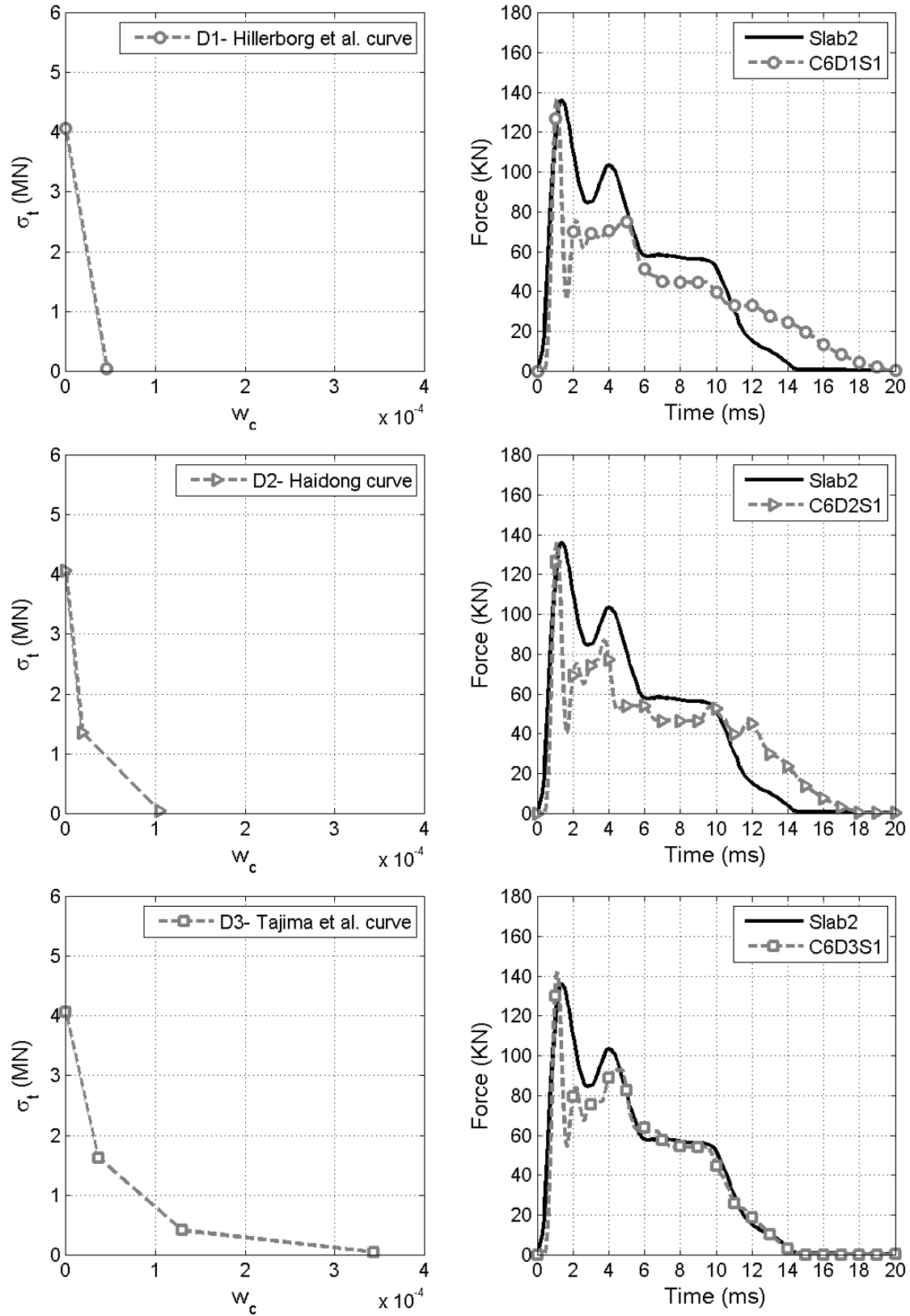


Figure 5.27: Comparison of concrete tensile stress-cracking displacement curves for Slab2

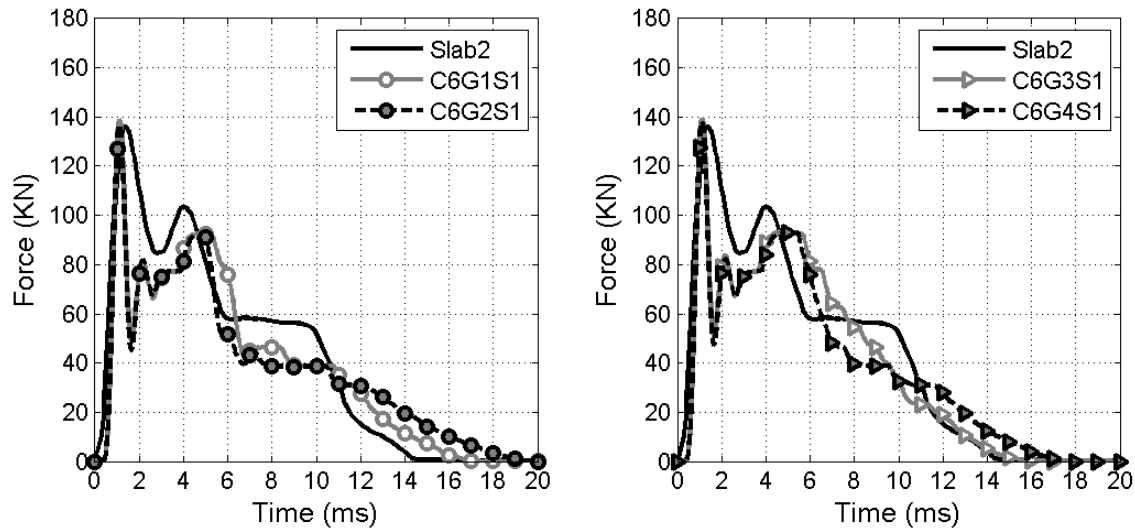


Figure 5.28: Comparison of fracture energy values for Slab2

good agreement with experiments. However, in the case of Slab6, the peak force is underestimated. It should be mentioned that only for Slab6 the load was determined from the accelerations measured by an accelerometer attached to the dropping mass in experiments, while a load cell is used to measure the loads for other slabs. This indicates the importance of using the appropriate output variable in the finite element analysis.

## 5.4 Deterministic models of the slab in nuclear plant

### 5.4.1 Finite element model (FEM)

The following section discusses the FEM of a RC slab which is subjected to accidental dropped object impact during handling operations within nuclear plant buildings. From the previous section where the FEM proposed for impact problems is validated with experiments from the literature, an accurate FEM of impacted slabs should introduce different factors that involve several nonlinearities in the response of impacted RC slabs. The factors that should be correctly incorporated into the model and that contribute to the nonlinear behavior of the reinforced concrete are the nonlinear stress-strain response, the damage due to crushing and tensile failure, the interaction between the concrete and the reinforcement, and the contact algorithm. In order to accurately simulate the structure and obtain detailed information from finite element approach, all these factors and contact algorithms must be correctly incorporated into the finite element model. However, since the FEM of slab in nuclear plant is used for reliability analysis, the aim is to choose finite element features that allow the minimum computational cost, but also provide an accurate representation of the impact phenomenon. The slab is studied in a reliability framework for 2 cases:

- Assuming an elastic behavior of steel and concrete materials.
- Assuming a nonlinear behavior of steel and concrete materials. The choice of stress-strain curves adopted is based on those used in the FEM of Chen and May slabs by considering the relations that give a good agreement with experimental results with the minimum computational effort.

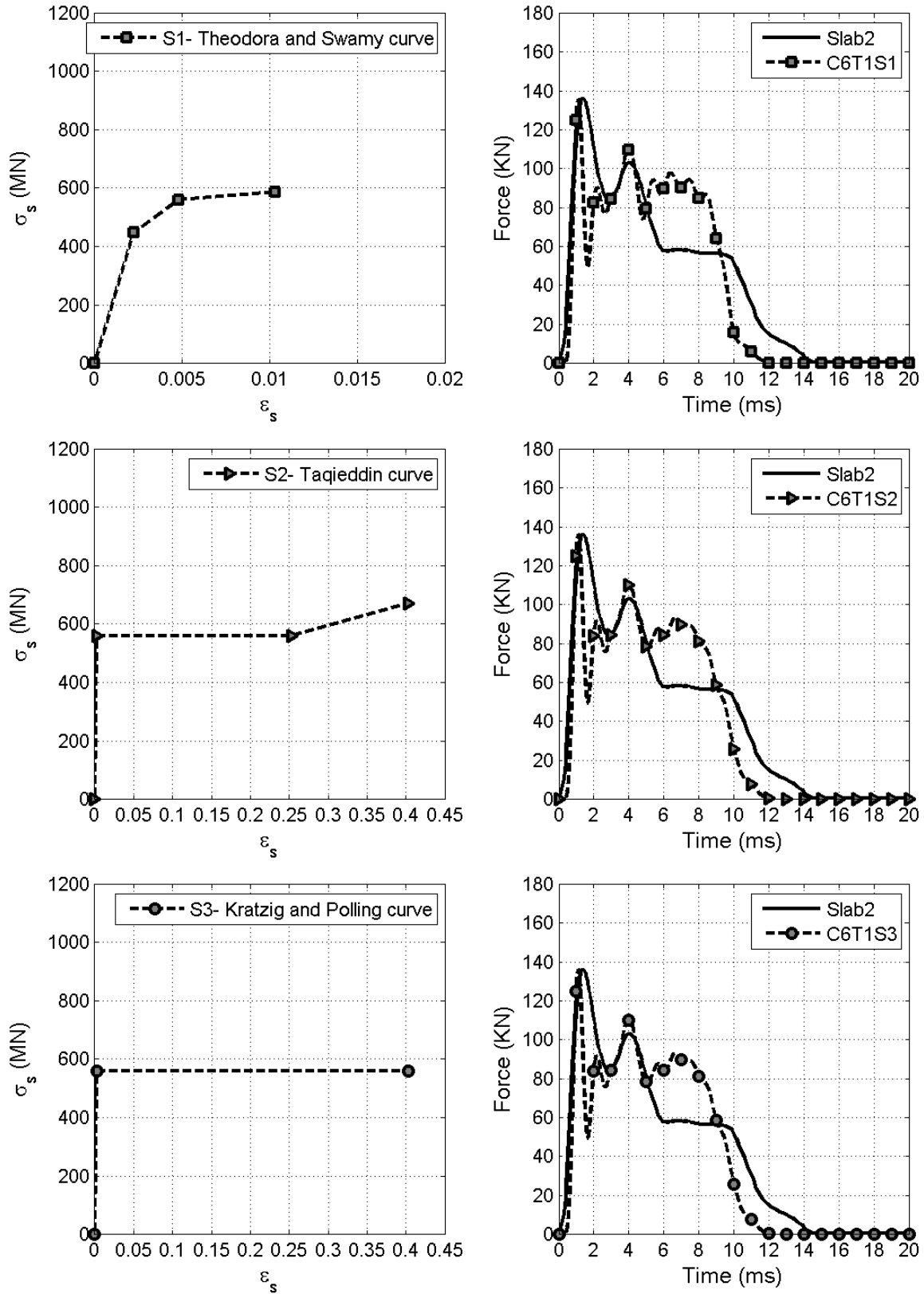


Figure 5.29: Comparison of steel stress-strain curves for Slab2

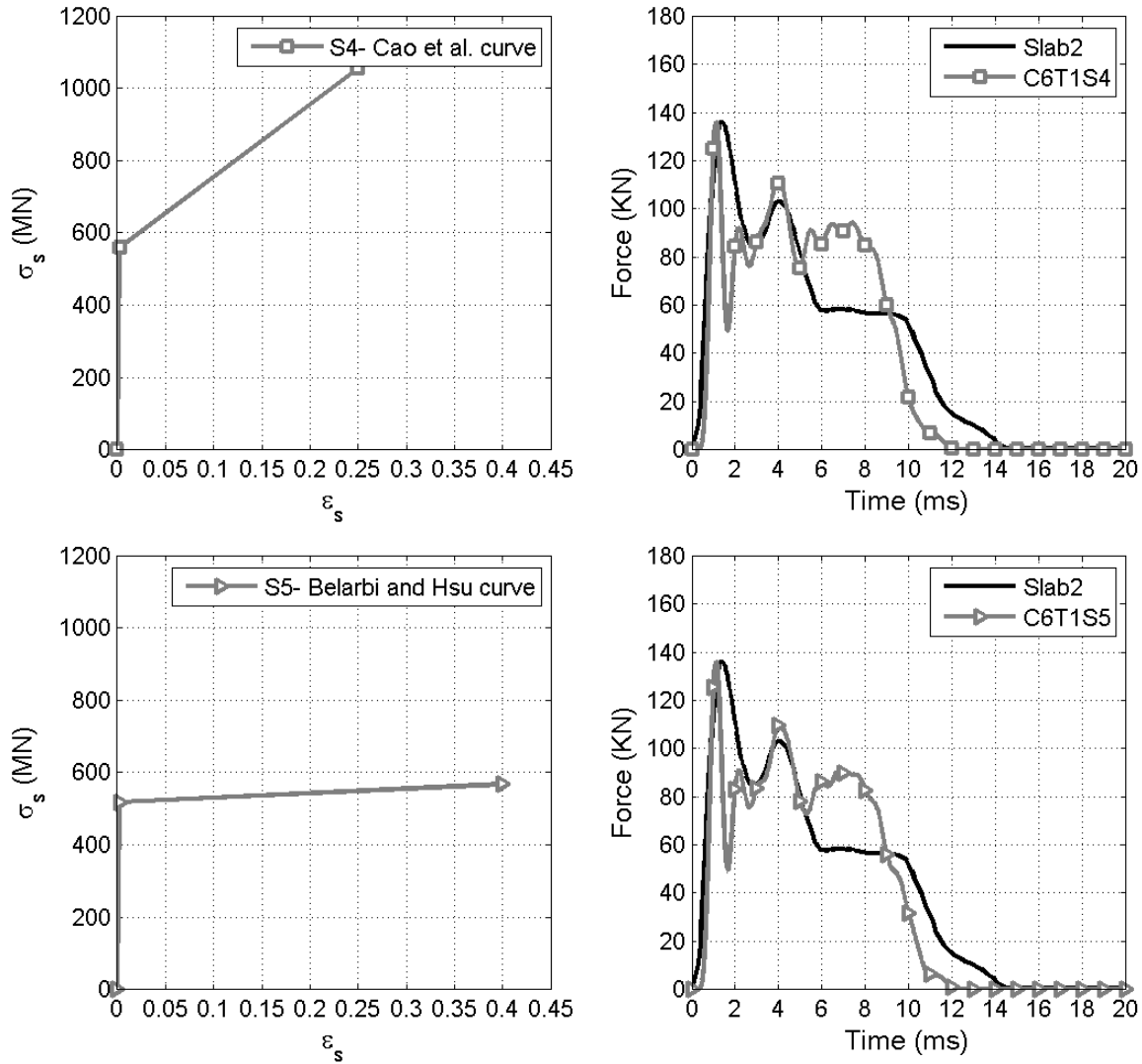


Figure 5.30: Comparison of steel stress-strain curves for Slab2

The slab is considered as simply supported on all the four sides and consists of a 4.85 m wide with a length of 8.1 m and a thickness of 0.5 m. Each of the upper and lower slab steel layers consists of 20 longitudinal and 12 transversal reinforcement bars of 20 mm diameter. In order to evaluate the transmission of impact energy to the slab during an impact phenomenon and consider the interaction between the slab and the impactor, the impactor is incorporated into the model as a sphere rigid body with 3600 kg mass and 30 cm diameter, dropped at the center of the slab with a velocity of 7.7 m/s. Table 5.7 shows the linear mechanical properties of concrete and steel materials used in the FE model for the slab in nuclear plant, while Table 5.8 shows its nonlinear mechanical properties that are used to define the stress-strain curves for each slab materials.

Finite element features used for elastic case are detailed in Chapter 6. Only the FEM of nonlinear case is detailed in this section. Mesh 4 is adopted from the study of Chen and May slabs as it is the most suitable to use in the case of an impact problem. This mesh allows a better simulation of the contact between the slab and the impactor and hence a better estimation of impact force. A 3D solid element, the eight-node continuum element (C3D8R) is used to develop the mesh of the concrete slab. Abaqus/Explicit provides three alternative kinematic formulations for the C3D8R solid

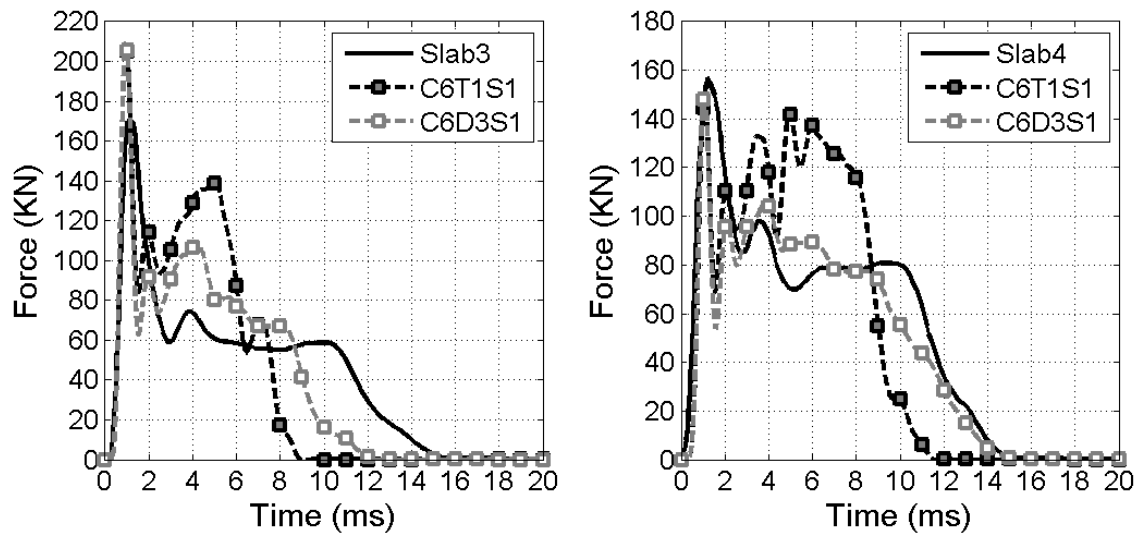


Figure 5.31: Comparison of C6T1S1 and C6D3S1 simulations for Slab3 and Slab4

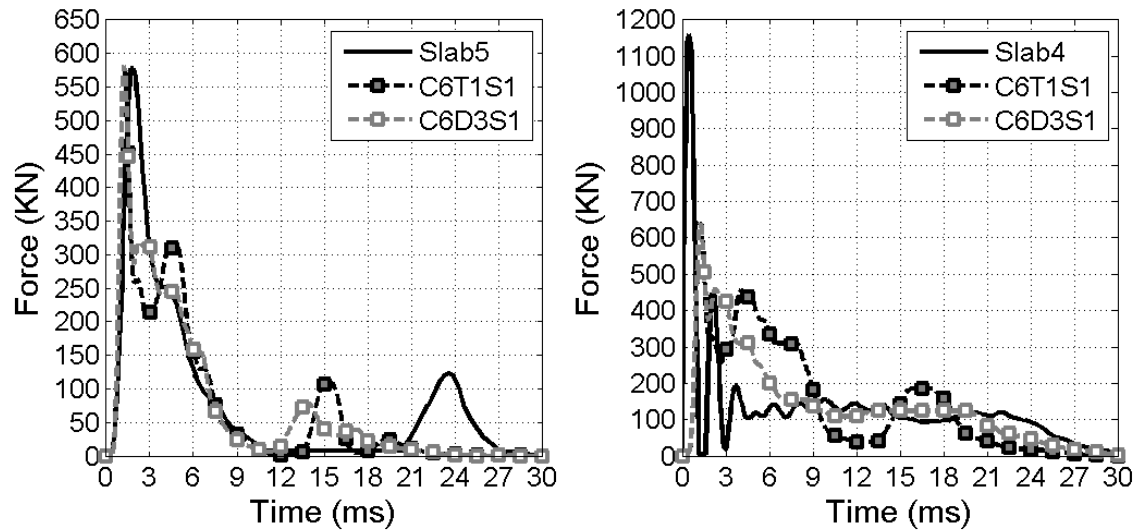


Figure 5.32: Comparison of C6T1S1 and C6D3S1 simulations for Slab5 and Slab6

Table 5.7: Linear mechanical properties of concrete and steel materials for the slab in nuclear plant

Material	Density $kg/m^3$	Young's modulus (MPa)	Poisson's ratio
Concrete	2500	35000	0.2
Steel	7850	200000	0.3

Table 5.8: Nonlinear mechanical properties of concrete and steel materials for the slab in nuclear plant

Slab	Concrete		Steel
	$f_c$ (MPa)	$f_t$ (MPa)	$f_y$ (MPa)
in nuclear plant	40	3.5	500

element, namely the average strain formulation, the orthogonal formulation and centroid formulation. This latter is selected for the nonlinear case in the aim of reducing the finite element analysis computational effort since it is the most economical among the three formulations. As illustrated in Figure 5.33.a, elements along the slab thickness have different size with finer elements located at the upper surface of the slab. The thickness is modeled with five elements in the thickness direction and a bias ratio of 2. The slab is modeled with two different densities of mesh. The impact zone is modeled with finer mesh, it consists of a square of 1.0 m with a maximum element size of 10 cm and a minimum element size of 1 cm. The mesh around the impact zone is considered uniform in the xy-plane with a size of 10 cm. The reinforcement is modeled with truss elements (T3D2) of 10 cm of size and the embedded approach is used to create the bond between the steel reinforcement and concrete. This approach allows independent choice of concrete mesh and arbitrarily defines the reinforcing steel regardless of the mesh shape and size of the concrete element. The impactor is meshed with four-node tetrahedral elements (R3D4) having a constant seed of 2 cm.

The contact pair algorithm is selected in order to model the contact and interaction problems between the slab and the impactor since the model involves only two contact surfaces, namely the upper surface of the slab and the impactor surface. In addition, it is more efficient in term of computational cost when used with kinematic contact constraints. The finite sliding formulation which allows any arbitrary motion of surfaces is used to account for the relative motion of the upper surface of the slab and the impactor surface. The contact constraints are enforced with a pure master-slave kinematic contact algorithm which does not allow the penetration of slave nodes into the master surface (surfaces attached to rigid bodies must always be defined as master surface in Abaqus/Explicit). Two interaction properties are presented in the model, a hard contact normal interaction defined as hard contact and a penalty tangential interaction with a friction coefficient of 0.45.

Stress-strain curves of concrete in tension and compression considered are those proposed by Wang and Hsu [180], while steel is modeled according to Theodorakopoulos and Swamy curve [173]. The FEM of the slab consists of 32072 nodes and more than 27400 elements (21800 elements of type C3D8R, 4448 elements of type T3D2, 1152 elements of type R3D4), and a simulation takes a total time of 43 minutes for an impact step of 0.1 s. The Python script written for this enables to easily change the impact position, as well as add stirrups (Figure 5.33.b), in the FEM (the main FEM of this slab does not include shear reinforcement).

#### 5.4.2 Mass-spring models (MSM)

In order to simulate the impact of a dropped object on RC slab, two simplified analytical models of the slab are used. The two models consist in a two degrees of freedom mass-spring system which accounts for nonlinearity of RC by a stiffness degradation approach. The second model also accounts for potential viscous damping. The input parameters that involve in these models are slab geometry, reinforcement ratio, concrete and steel densities, impactor mass and velocity. Outputs of these models are the time-history curves of slab displacement at impact point, slab velocity at impact point, impactor displacement and impactor velocity.

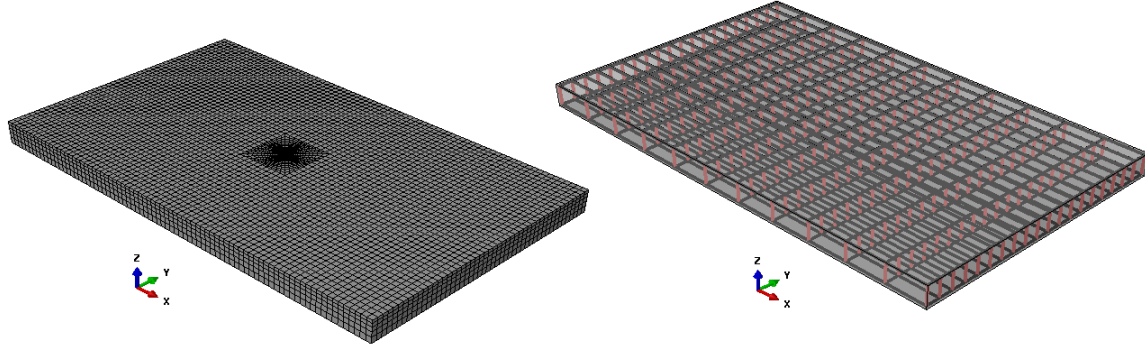


Figure 5.33: Finite element model of slab: a) meshing, b) reinforcement

#### 5.4.2.1 Mass-spring model without damping

This model describes the interaction between the slab and the impactor via two springs (Figure 5.34). The parameters which represent the dynamic of the system are:

1. The impactor mass :  $m_i$
2. The slab mass :  $m_s$
3. The contact stiffness :  $k_c$
4. The slab stiffness :  $k_s$

From the mechanical equilibrium of the two masses, two coupled ordinary differential equations of second-order are derived and solved in time by an approximated method, namely the Runge-Kutta fourth order method:

$$\begin{cases} \frac{d^2 x_i}{dt^2} + \frac{k_c}{m_i} x_i - \frac{k_c}{m_i} x_s = 0 \\ \frac{d^2 x_s}{dt^2} - \frac{k_c}{m_s} x_i + \frac{k_c + k_s}{m_s} x_s = 0 \end{cases} \quad (5.1)$$

with the initial conditions

$$\dot{x}_i(0) = v, \quad \dot{x}_s(0) = 0, \quad x_i(0) = x_s(0) = 0 \quad (5.2)$$

Assuming that  $\mathbb{X} = \begin{pmatrix} x_i \\ x_s \end{pmatrix}$  and  $\mathbb{M} = \begin{pmatrix} \frac{k_c}{m_i} & -\frac{k_c}{m_i} \\ -\frac{k_c}{m_s} & \frac{k_c + k_s}{m_s} \end{pmatrix}$ , the system of equations for the mass-spring model without damping can be written in a matrix form as:

$$\frac{d^2 \mathbb{X}}{dt^2} + \mathbb{M} \mathbb{X} = 0 \quad (5.3)$$

#### 5.4.2.2 Mass-spring model with damping

In this model, viscous damping is taken into consideration in addition to the slab and impactor stiffnesses and masses (Figure 5.35). It is assumed that the structural damping is to be of the viscous type according to [20], i.e., the damping force is opposite but proportional to the velocity.

The impedance  $c_c$  accounts for the viscosity of the contact, while  $c_s$  accounts for the viscosity of the slab.

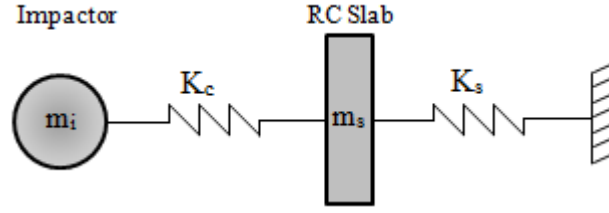


Figure 5.34: Mass-spring model without damping

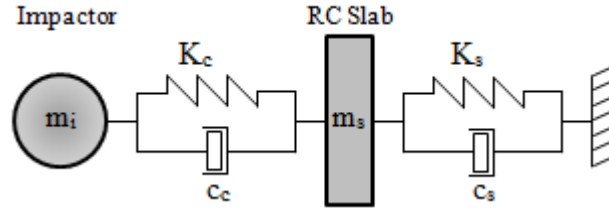


Figure 5.35: Mass-spring model with damping

In this case, the two differential equations can be expressed by:

$$\begin{cases} \frac{d^2 x_i}{dt^2} + \frac{k_c}{m_i} x_i - \frac{k_c}{m_i} x_s + \frac{c_c}{m_i} \dot{x}_s - \frac{c_c}{m_i} \dot{x}_i = 0 \\ \frac{d^2 x_s}{dt^2} - \frac{k_c}{m_s} x_i + \frac{k_c+k_s}{m_s} x_s + -\frac{c_c}{m_s} \dot{x}_i + \frac{(c_s+c_c)}{m_s} \dot{x}_s = 0 \end{cases} \quad (5.4)$$

with the same initial conditions considered for the previous model and the equations are also solved in time by the Runge-Kutta fourth order method.

Assuming that  $\mathbb{X} = \begin{pmatrix} x_i \\ x_s \end{pmatrix}$ ,  $\mathbb{C} = \begin{pmatrix} \frac{c_c}{m_i} & -\frac{c_c}{m_i} \\ -\frac{c_c}{m_s} & \frac{(c_s+c_c)}{m_s} \end{pmatrix}$ , and  $\mathbb{M} = \begin{pmatrix} \frac{k_c}{m_i} & -\frac{k_c}{m_i} \\ -\frac{k_c}{m_s} & \frac{(k_c+k_s)}{m_s} \end{pmatrix}$ , the system of equations for the mass-spring model with damping can be written in a matrix form as:

$$\frac{d^2 \mathbb{X}}{dt^2} + \mathbb{C} \frac{d\mathbb{X}}{dt} + \mathbb{M} \mathbb{X} = 0 \quad (5.5)$$

### 5.4.2.3 Identification of MSM parameters

In order to define the equivalent two-degrees of freedom systems presented in the previous section, it is necessary to evaluate the parameters of these models. The equivalent system is selected so that the deflection of the concentrated mass is equal to the deflection of the slab at the impact point.

**Effective mass of slab** In order to obtain the slab mass of the equivalent system, the mass of the real slab is multiplied by a transformation factor  $\alpha_M$  [20].

$$m_{s_{equi}} = \alpha_M \times m_s \quad (5.6)$$

According to [42, 56], the equivalent mass of the slab can be obtained by equating the kinetic energy for the equivalent and real system:

$$\frac{1}{2} \left( \iint \alpha_M \rho dA \right) \times \left( \frac{du_{imp}}{dt} \right)^2 = \frac{1}{2} \iint_A \rho \left[ \frac{du(x,y)}{dt} \right]^2 dA \quad (5.7)$$

$$\alpha_M = \frac{\iint_A \rho \phi^2(x, y) dA}{\iint \rho dA} \quad (5.8)$$

In the above equations,  $u_{imp}(t)$  is the deflection of the slab at the impact point and  $u(x, y, t)$  represents the deflection at any point on the slab of  $x$ - and  $y$ -coordinates;  $\phi(x, y, t) = \frac{u(x, y, t)}{u_{imp}(t)}$  is the deflected shape function;  $A$  is the slab area and  $\rho$  represents the mass per unit area of the slab.

According to [20], the mass transformation factor, for two-way slabs with simple and fixed supports, is evaluated on the basis of an assumed deflected shape of the actual structure which is taken to be the same as that resulting from the static application of the dynamic loads. The approximation of the deflected shape is based on the classical plate theory and is considered to satisfy the boundary conditions of simply supported slabs:

$$u(x, y, t) = \sum_{m=1}^{\infty} \sum_{n=1}^{\infty} W_{mn}(t) \sin \frac{m\pi x}{a} \sin \frac{n\pi y}{b} \quad (5.9)$$

In the following, only the first mode will be considered, that is,  $m = n = 1$ . Thus, the deflected shape will be:

$$u(x, y, t) = W_1(t) \sin \frac{\pi x}{a} \sin \frac{\pi y}{b} \quad (5.10)$$

The maximum deflection at the impact point of the slab ( $x = a/2$ ,  $y = b/2$ ) is therefore  $u_{imp} = W_1(t)$ .

After substituting the  $u_{imp}(t)$  and  $u(x, y, t)$  in Equation 5.7, the equivalent mass of the slab is found to be equal the fourth of its real mass.

**Slab stiffness** A frequency decrease approach is used to describe the RC's degradation which is due to cracks in concrete and yielding in steel. This approach allows considering the nonlinearities presented in RC. The slab stiffness decrease is identified by quasi-static "pushover" tests in term of the displacement of the slab at the center. The initial value of slab stiffness is estimated to be equal to  $1.8e8 \text{ N/m}$  for the main case of study with a thickness of 0.5 m. Figure 5.36 shows the variation of the initial value of slab stiffness in term of the slab thickness, as well as the stiffness decrease in term of displacement for several values of thickness.

**Contact stiffness** In impact dynamics analysis, a detailed description of the contact between the impactor and the structure during impact is not required and statically determined contact laws can be used [9]. Thus, a contact law relating the contact force to the indentation is needed to define the contact between slab and impactor. The indentation is defined as the difference between the displacement of the impactor and the displacement of the slab at the impact point.

The local indentation  $\alpha = x_b - x_d$  is represented by the spring ( $k_c$ ) which can be linear or nonlinear. Thus during the loading phase of the impact, the impact force can be obtained by using a linearized contact law ( $q = 1$ ) or an Hertzian contact law ( $q = 3/2$ ).

$$F_c = k_c \alpha^q \quad (5.11)$$

For Hertzian contact between a plate and a hemispherical indenter, the contact stiffness is given by [10]:

$$k_c = \frac{4}{3} E R^{1/2} \quad (5.12)$$

where  $R$  represents the impactor radius [149] and  $E$  is given by

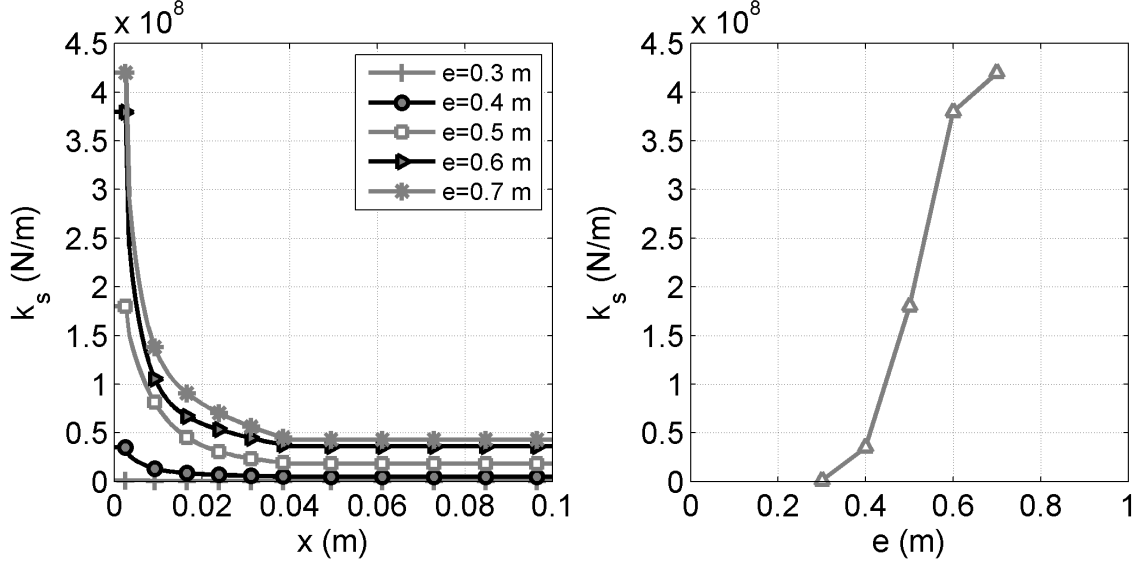


Figure 5.36: Slab stiffness decrease in term of displacement for several values of thickness and the variation of the stiffness initial value in term of the thickness

$$\frac{1}{E} = \frac{1 - \nu_s^2}{E_s} + \frac{1 - \nu_i^2}{E_i} \quad (5.13)$$

In the present study, we assumed that the impactor is rigid so  $E$  is in this case equal to:

$$\frac{1}{E} = \frac{1 - \nu_s^2}{E_s} \quad (5.14)$$

By substituting the parameters by their values in the above equations, the contact stiffness is found to be equal to  $7.29e^9$  N/m for a linearized contact law and  $1.88e^{10}$  N/m<sup>3/2</sup> for a Hertzian contact law.

**Impedances** Biggs [20] indicated that the inclusion of damping in multidegree analysis involves some rather troublesome problems since there is little theoretical means for determining the nature of the damping. The damping was assumed to be viscous, thus the damping force applied to a mass is directly proportional to the velocity of the structure at the impact point and may be expressed by:

$$F_v = -c\dot{x} \quad (5.15)$$

where  $c$  is the impedance and  $\dot{x}$  is the velocity of the mass.

Biggs also indicated that the magnitude of  $c$  is extremely difficult to determine. Thus, in order to be sure that the damping coefficients are reasonable, it is convenient to introduce the concept of critical damping which represents the amount of damping that would completely eliminate vibration. For a SDOF, the critical damping is given by:

$$c_{cr} = 2\sqrt{km} \quad (5.16)$$

while for multiple degree of freedom, the critical damping matrix is defined by [186]:

$$\mathbb{C}_{cr} = 2\mathbb{M}^{-1/2} \mathbb{K} \mathbb{M}^{-1/2} = 0 \quad (5.17)$$

According to [184], the contact impedance  $c_c$  is only valid during contact and damping mechanism is due to the energy transfer from the impactor to the structure. Definitions of the impedances of impactor and plates were given by [149] for small-mass impact models for composite plates. The impedance of the plate is expressed by:

$$c_s = 8\sqrt{\rho D^*} \quad (5.18)$$

where  $\rho$  is the mass per unit area of the slab and  $D^*$  the equivalent bending rigidity which is defined as:

$$D^* \approx \sqrt{D_{11}D_{22}(A+1)/2} \text{ where } A = (D_{12} + 2D_{66})/\sqrt{D_{11}D_{22}} \quad (5.19)$$

By substituting the parameters by their values in the above equations, the slab impedance is found to be equal to  $5.52e^6 N/(m/s)$ .

The impactor impedance is defined for an Hertzian contact ( $q=3/2$ ) by:

$$c_c = k_c^{2/5} \left(\frac{5}{4}m_i\right)v_0^{1/5} \quad (5.20)$$

and for a linear contact ( $q=1$ ) by:

$$c_c = \sqrt{k_c m_i} \quad (5.21)$$

By substituting the parameters by their values in the above equations, the contact impedance is found to be equal to  $1.26e^7 N/(m/s)$  for a linearized contact law and  $3.01e^6 N/(m/s)$  for a Hertzian contact law.

## 5.5 Discussion of results of deterministic models of the slab in nuclear plant

### 5.5.1 Comparison of FEM and MSM results

The aim of using a mass-spring model is to develop a simplified model economical in computational cost, but also allows an accurate and precise estimation of the structural response. Thus, both MSM models proposed for the slab in nuclear plant assuming a nonlinear behavior of material are compared with its FEM. The values of MSM parameters identified previously are used as preliminary values to initially present the model, then they are calibrated in order to find the best fit with FEM results. As a result, the values adopted for the MSM are as follows:

- The equivalent mass of the slab:  $m_{s_{equi}} = 0.015 \times m_s$ .
- The initial value of slab stiffness varies according to the case studied in terms of the input variable values.
- The contact stiffness:  $k_c = 2e9 N/m$ .
- The impedance of contact:  $c_c = 1e5 N/(m/s)$ .
- The impedance of slab:  $c_s = 1.7e5 N/(m/s)$ .

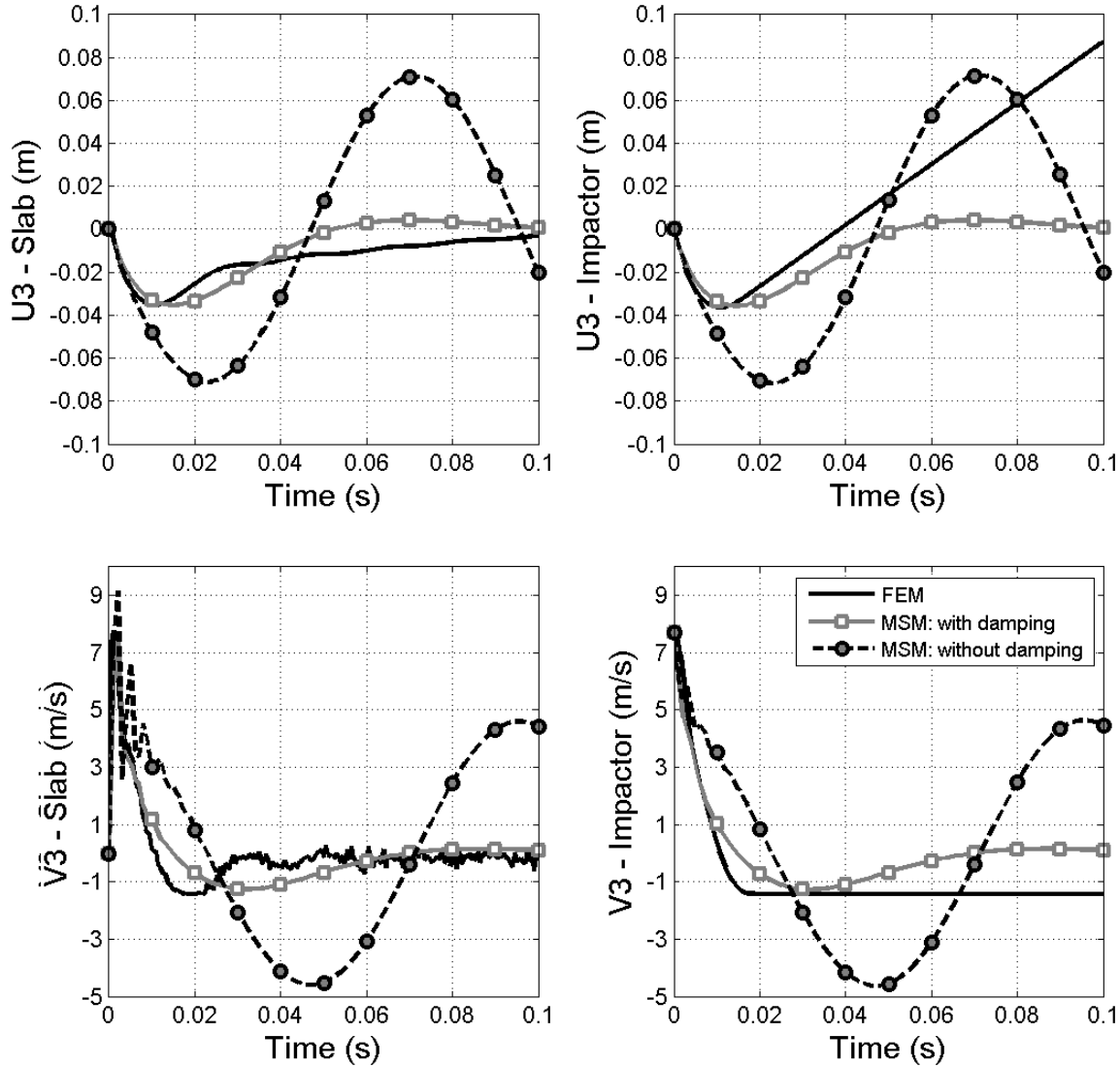


Figure 5.37: Comparison of mass-spring models with and without damping

First, a comparison of the two mass-spring models used in this study is proposed (Figure 5.37). The following comparison permits to show the importance of taking the potential viscous damping in the analytical analysis of an impact problem. As can be seen, the mass-spring model without damping overestimates the slab and impactor displacements, as well as their velocities. The reason is that this type of models does not accurately model the dissipation of energy related to the plastic deformation of materials, formation of cracks, friction and damping. Considering only the stiffness degradation approach to describe the reinforced concrete degradation due to cracks in concrete and yielding in steel seems then insufficient, hence viscous dampers with a constant impedance should be used to provide a better dissipation of energy in the system. Thus, the mass-spring model with damping gives more accurate results.

Accordingly, several cases are studied to compare the MSM accounting for viscous damping and the FEM by varying several input variables involved in the MSM, including the impactor mass and velocity for the same kinetic energy, the impactor velocity, the impactor mass, the slab thickness,

the steel diameter and the concrete density. 38 cases are investigated and detailed in Annex B. The cases studied enable to determine the limitations of the MSM proposed, as well as the range of values of its variables for which the simplified model is verified. As a result, the two degrees of freedom mass-spring model which accounts for potential viscous damping and for nonlinearity of RC by a stiffness degradation approach can be used for the following conditions:

- Low-velocity high-mass impacts when the same impact energy is considered ( $v = 2.5 \text{ m/s}$ ,  $m = 34151 \text{ kg}$ ,  $v = 5.0 \text{ m/s}$ ,  $m = 8537 \text{ kg}$ ,  $v = 7.7 \text{ m/s}$ ,  $m = 3600 \text{ kg}$ ,  $v = 10.5 \text{ m/s}$ ,  $m = 1936 \text{ kg}$ ). For these cases, the maximum values of slab displacement, impactor displacement and slab velocity, as well as the shape of the corresponding curves, are in good agreement with numerical results. The simplified model shows less efficiency in predicting the shape of the impactor velocity in term of time for low-velocity high-mass impacts, although it allows a good estimation of the impactor velocity maximum value. In the cases of high-velocity low-mass impacts, the MSM allowed assessing the maximum values of slab and impactor displacements. However, the shape of their curves in term of time shows a great difference with respect to those obtained with the FEM for the after contact phase. For these cases, the MSM estimates accurately the maximum value and the curve shape of the impactor velocity. The maximum values of slab velocity is not properly assessed with the MSM for high-velocity low-mass impacts, but the shape of slab velocity-time curve is predicted with precision for the after contact phase.
- Low-velocity impacts when the same mass is considered ( $v = 2.5 \text{ m/s}$ ,  $v = 5.0 \text{ m/s}$ ,  $v = 7.7 \text{ m/s}$ ,  $v = 10.5 \text{ m/s}$ ). In these cases, the maximum values and the curves shape of the slab and impactor displacements show a good agreement with numerical results, respectively. The MSM is very efficient in estimating the slab and impactor velocities (maximum values and curves shape) for all cases studied by varying the initial velocity value, including high-velocity impacts.
- High-mass impacts when the same velocity is considered ( $m = 2000 \text{ kg}$ ,  $m = 3000 \text{ kg}$ ,  $m = 3600 \text{ kg}$ ,  $m = 5000 \text{ kg}$ ,  $m = 6000 \text{ kg}$ ). For these cases, the MSM results are in good agreement with numerical results for all the output variables examined. The maximum values and the curves shape are properly assessed. However, for low-mass impacts ( $m \leq 1000 \text{ kg}$ ) the MSM loses its accuracy and cannot be used to estimate impacted RC slab response as it is governed by more localized deflection.
- Thick slabs ( $e \geq 0.4 \text{ m}$ ). For these cases, the MSM results are in good agreement with numerical results for all the output variables examined. This may be related to the fact that thin slabs are more subjected to penetration and perforation failure modes than thick slabs for the same impact conditions, and the MSM does not allow predicting these types of failure modes.
- All values of steel reinforcing bars considered. In these cases, the maximum values and the curves shape of all output variables show a good agreement with numerical results.
- All values of concrete density considered. In these cases, the maximum values and the curves shape of all output variables show a good agreement with numerical results. It should be noted that the MSM presents a higher precision and accuracy for high concrete density ( $\rho_c \geq 3500 \text{ kg/m}^3$ ).

In the present section, only two cases are presented. Figure 5.38 represents the slab displacement at the impact point, slab velocity at the impact point, impactor displacement and impactor velocity in term of time for different values of masses and velocities with the same impact energy. The figure shows that the response of the slab varies with the mass and the velocity of the impactor. As can be seen, the MSM provides results which are in good agreement with numerical results, especially for

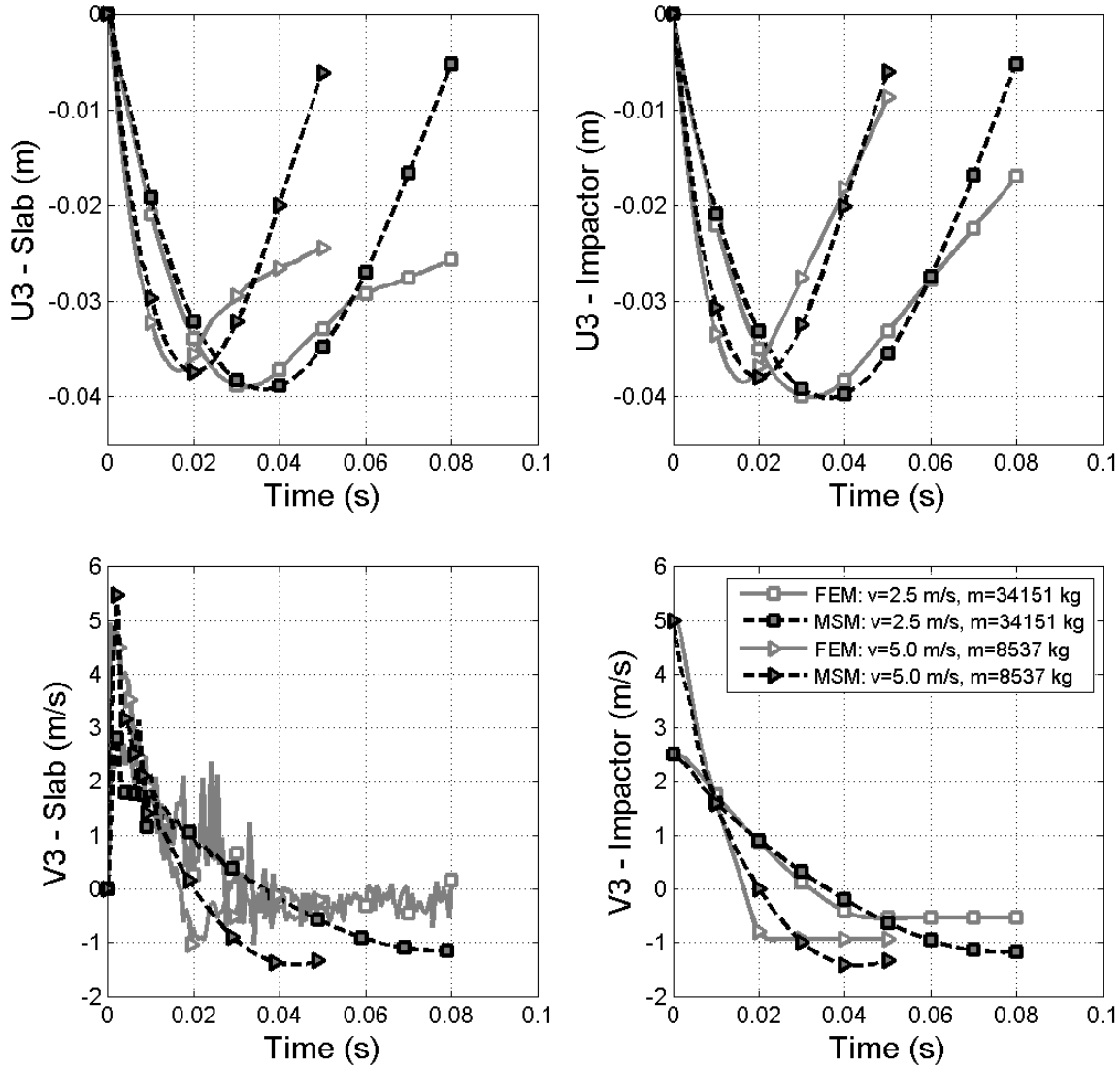


Figure 5.38: Comparison of FEM and MSM for the same kinetic energy

the phase where the slab and the impactor are in contact. When the impactor is separated from the slab, the MSM does not permit to accurately predict the numerical results. For large masses and low velocities the time of contact between the slab and the impactor, as well as the displacement at the impact point, is higher than the cases of small masses and higher velocities. For these latter cases, when the impactor strikes the slab the damage initiates and the impactor rebound earlier. These results, which agree with [149], demonstrate that the slab response to impact is influenced by impactor mass and impact duration and not only by impact velocity.

## Chapter 6

# Structural reliability: application to RC structures

### 6.1 Introduction

The determination of limit state functions is necessary to perform structural reliability analysis. But it is typically impossible to define an explicit expression of a limit state function, and to assess the probability of failure with analytical integration, especially in cases of complex structures modeled with the finite element method. To address this problem, numerous probabilistic methods can be used to estimate failure probability as previously mentioned in Chapter 4. Selection of the most suitable method for a particular type of problem is not apparent since the accuracy and computational effort of probabilistic methods depend on several factors, such as degree of nonlinearity of the limit state function, type of random variable distributions, number of random variables and their variance [53].

First, a simple application to a RC beam is performed in the aim of mastering the basics of OpenTURNS and examining the probabilistic methods proposed in OpenTURNS to estimate failure probability in structural reliability analysis in terms of their accuracy, precision and computational effort. This application is used to address the issue of solving reliability problems in the domain of civil engineering and to propose solutions based on the case studied.

Next, the problem of RC slabs subjected to low velocity impact is addressed. The aim is to address the issue of computational cost of reliability analysis and to propose computational strategies allowing the accurate assessment of the failure probability for minimum computational time. The first strategy consists in using deterministic analytical models involving low computational time. The second one consists in choosing an appropriate probabilistic method where the failure probability is assessed from a small number of simulations. Probabilistic methods, such as Monte Carlo, FORM, SORM and importance sampling, are adopted from the beam application and used to calculate the probability of failure. The choice of random variables and their distributions, as well as failure criteria are discussed according to several studies in the literature. Firstly, the problem of impacted slab is studied assuming a flexural mode of failure and an elastic behavior for steel and concrete. Several deterministic models are used and combined with a suitable probabilistic method. Studying slabs under elastic behavior is important to examine the limitations of deterministic models and to adopt the most convenient procedure to use in case of nonlinear behavior. Following this, the problem of impacted slab is studied using deterministic models that take into account the nonlinear material properties. In both case, elastic and nonlinear behaviors, a parametric study is performed to identify the influence of deterministic model parameters on the reliability of RC slabs under low velocity impact.

Finally, a third application is also considered in the aim of presenting a procedure to be followed

to study the response of very complicated structures in a reliability framework. For this purpose, the prestressed concrete containment building of the Flamanville nuclear power plant is used. The deterministic model of the containment building consists of a numerical model in which the full process of aging is taken into account, including relaxation of the reinforcement, creep and shrinkage of concrete. This application allows examining stress evolution with time in the containment building during periodic surveillance testing carried out 20 years after its implementation. Polynomial chaos expansion is used to simplify the physical model and study the height at which the containment is under tension.

## 6.2 Application to RC beams

In order to illustrate the principle of each step of a structural reliability analysis presented in Chapter 4 and compare the available probabilistic methods in terms of their accuracy and computational effort, the case of a RC beam modeled with CASTEM is studied. Combining CASTEM with OpenTURNS is possible using the wrapper interface that allows linking any external code to the OpenTURNS library and using it through the library functionalities.

### 6.2.1 Deterministic model

The first step in reliability analysis consists in providing a deterministic model (analytical or numerical) that correctly represents the structure studied in order to predict the structural response. The case of a RC cantilever beam is proposed from experiments in the framework of the LESSLOSS project [108] (Figure 6.1). The beam under investigation is fixed at only one end and subjected to a concentrated load at the free end. A numerical model based on a multifiber FE approach is proposed to examine the response of the cantilever beam. Multifiber finite elements are used to develop the mesh of the beam (Figure 6.2), they permit to describe the behaviors of concrete and reinforcement with a one-dimensional way and are assumed to follow the kinematics of the Timoshenko beam theory which allows taking into account shear deformation effects in the cross section. Materials are supposed to have an elastic behavior.

### 6.2.2 Probabilistic model

The variables which may be subjected to statistical variations in RC cantilever beams under an end load condition can be classified into five categories:

1. Dimensional variables related to the geometric properties of the beam: length and section width
2. Dimensional variables related to the position of reinforcement and its size: reinforcement section width and its eccentricity
3. Variables related to the concrete properties: Young's modulus and Poisson's ratio of concrete.
4. Variables related to the steel properties: modulus of elasticity and Poisson's ratio of steel.
5. Variables related to loading: concentrated force at the free end.

For this application, the probabilistic characterization of random variables is not based on the literature review detailed in Chapter 4. The aim of this example is to study the effect of type of random variable distributions, number of random variables and their variance on the estimation of failure probability. Thus, first, all random variables are assumed to have a lognormal distribution with a mean value equal to the nominal value and a COV of 0.1. Table 6.1 represents the random

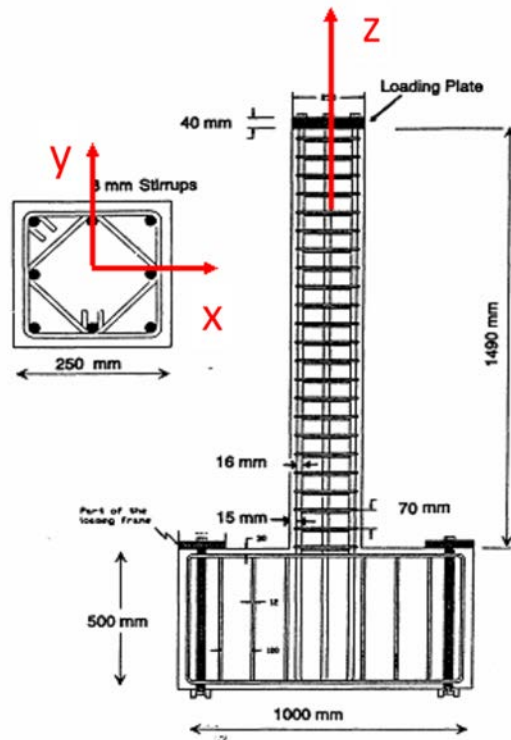


Figure 6.1: RC beam tested experimentally in the framework of the LESSLOSS project [108]

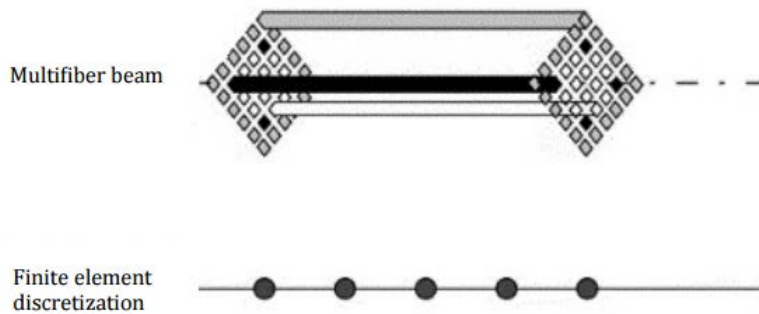


Figure 6.2: Discretization of multifiber beam into elements, nodes and degrees of freedom [76]

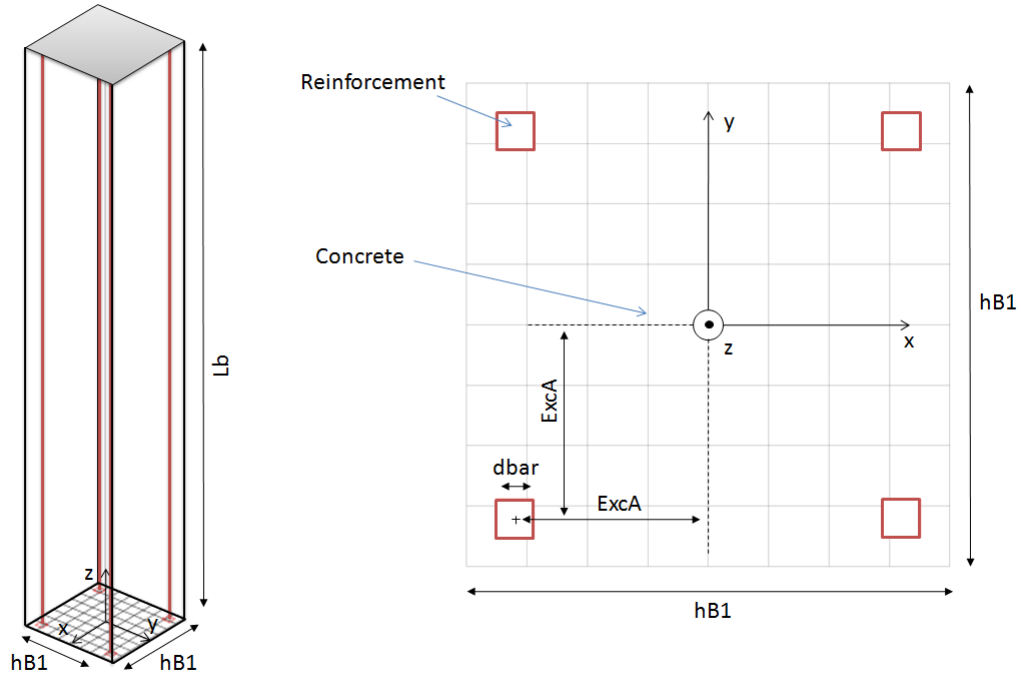


Figure 6.3: Geometrical properties of the multifiber beam

Table 6.1: Random variables of the multifiber beam and their descriptions

Variables	Description	Mean	COV	PDF
<b>Geometric properties of the beam</b>				
$Lb$	Beam length in z-direction	2.75 m	0.1	Lognormal
$hB1$	Width of beam section	0.25 m	0.1	Lognormal
<b>Position and size of reinforcement</b>				
$dbar$	Width of reinforcement section	0.02 m	0.1	Lognormal
$ExcA$	Eccentricity of reinforcement	0.1 m	0.1	Lognormal
<b>Concrete properties</b>				
$E_c$	Young's modulus of concrete	25 GPa	0.1	Lognormal
$\nu_c$	Poisson's ratio of concrete	0.2	0.1	Lognormal
<b>Reinforcement properties</b>				
$E_s$	Modulus of elasticity of steel	200 GPa	0.1	Lognormal
$\nu_s$	Poisson's ratio of steel	0.3	0.1	Lognormal
<b>Loading variables</b>				
$Force1$	Maximum force applied	1000 N	0.1	Lognormal

variables adopted in the present study in the case of multifiber beam, their probability distribution, their mean and COV.

### 6.2.3 Failure criteria

Failure of structure is investigated according to a displacement failure criterion. Failure probability is estimated for the following limit state function:

Table 6.2: Importance factors of beam random variables

<i>Lb</i>	<i>hB1</i>	<i>dbar</i>	<i>ExcA</i>	$E_c$	$\nu_c$	$E_s$	$\nu_s$	<i>Force1</i>	$f_{max}$		
Quadratic combination	0.3529	0.3228	0.0128	0.0124	0.0203	0.0	0.0032	0.0	0.0396	0.2358	
FORM	0.3753	0.4015	0.0243	0.0236	0.0223	0.0	0.0061	0.0	0.047	0.0997	

$$g = f_{max} - f \quad (6.1)$$

where  $f_{max}$  is the threshold of the displacement of beam at the free end and  $f$  is the displacement at the free end calculated by CASTEM.  $f_{max}$  is considered as an additional random variable to the variables presented in Table 6.1 and also modeled with a lognormal distribution and a COV of 0.1.

## 6.2.4 Discussion of results of beam reliability

### 6.2.4.1 Sensitivity analysis

A detailed sensitivity analysis is performed in this section in order to identify the random variables that mostly contribute to the variability of the displacement of cantilever beams. 10 random variables are considered, including the threshold of displacement. The aim is to select the most significant variables which control the beam response. Importance factors are calculated using Quadratic combination method and FORM and detailed in Table 6.2.

In order to verify the accuracy of these estimations, several sensitivity studies are performed. First, a study of mechanical sensitivity that enables to estimate the variation of the limit state function when variable change is conducted. This study is purely deterministic and measures the sensitivities with respect to the design variables [107]. In order to be able to make comparisons, a non-dimensional quantity, namely the mechanical elasticity  $\bar{S}_i$ , is calculated as:

$$\bar{S}_i = \frac{\partial g(\mathbf{X})}{\partial x_i}(x = x_r) \frac{x_r}{g(x_r)} \quad (6.2)$$

where  $x_r$  are particular representative values of different input variables, such as the mean. Mechanical sensitivity allows distinguishing stress variables from resistance variables and is very useful to select the random variables to take into consideration. The sign of  $\bar{S}_i$  values that are calculated with CASTEM determines the type of variables. If  $\bar{S}_i$  is a positive value then the variable is a resistance variable, while a negative value indicates a stress variable. The mechanical elasticity multiplied by the COV of the variable permit to study the variability of the corresponding variable. This can be achieved by comparing the product  $\bar{S}_i \times COV_i$  to the variable mean. The variability of a variable is considered high in the case where  $|\bar{S}_i \times COV_i|$  is higher than its mean (mean of this product is equal to 0.0746). Table 6.3 presents the stress and resistance variables for the cantilever beam and shows if their variability affects highly the beam response.

Then a statistical sensitivity analysis is performed by calculating omission factors  $\zeta_i$  that express the relative error of the reliability index when a random variable is replaced by a deterministic value [107]:

$$\zeta_i = \frac{\beta_{X_i}}{\beta} \quad (6.3)$$

$\beta_{X_i}$  is the reliability index calculated for the case where all variables are considered as random, except  $X_i$  which is considered as deterministic.  $\beta$  is the reliability index in case where all variables are random. An omission factor value close to unity indicates that the corresponding variable has

Table 6.3: Stress and resistance variables of the cantilvever beam and their variability influence

Random Variable	$\mu_i$	Unit	$\bar{S}_i$	Type	$ \bar{S}_i \times COV_i $	Influence
<i>Lb</i>	2.75	m	-2.07	Stress	0.207	high
<i>hB1</i>	0.25	m	2.01	Resistance	0.201	high
<i>dbar</i>	0.02	m	0.0069	Resistance	0.0007	low
<i>ExcA</i>	0.1	m	0.293	Resistance	0.0293	low
<i>E<sub>c</sub></i>	25	GPa	0.499	Resistance	0.0499	low
<i>ν<sub>c</sub></i>	0.2	-	-0.0006	Stress	0.0000	low
<i>E<sub>s</sub></i>	200	GPa	0.195	Resistance	0.0195	low
<i>ν<sub>s</sub></i>	0.3	-	-0.0001	Stress	0.0000	low
<i>Force1</i>	1000	N	-0.693	Stress	0.0693	low
<i>f<sub>max</sub></i>	0.0015	m	1.69	Resistance	0.169	high

Table 6.4: Omission factors of the cantilvever beam variables and their influence on  $P_f$ 

Random Variable	$\beta_{X_i}$	$\gamma_i$	Influence
<i>Lb</i>	2.7785	1.309	high
<i>hB1</i>	2.8962	1.365	high
<i>dbar</i>	2.1564	1.016	medium
<i>ExcA</i>	2.1559	1.016	medium
<i>E<sub>c</sub></i>	2.1467	1.012	medium
<i>ν<sub>c</sub></i>	2.1221	1.000	low
<i>E<sub>s</sub></i>	2.8735	1.354	high
<i>ν<sub>s</sub></i>	2.1221	1.000	low
<i>Force1</i>	2.1811	1.028	medium
<i>f<sub>max</sub></i>	2.1220	1.000	low

no effect on the failure probability estimation. Table 6.4 shows omission factors of random variables of the cantilever beam, as well as their influence on the estimation of failure probability for a displacement criterion.

Next, the variability of variables in terms of their mean and standard deviation are evaluated. The reliability index is calculated for the case where all random variables, except for one variable, have the same mean and standard deviation as mentioned in Table 6.1. The variation of this variable is assessed for four cases by multiplying its mean or standard deviation by 2 or by 4. The variable sensitivity is considered high if the calculated reliability index varies by more than 50% compared to  $\beta$  [44] ( $\beta = 2.1221$ ). Table 6.5 shows the variability of each random variable of the cantilever beam according to their mean and standard deviation values.

As mentioned earlier, the mechanical and statistical sensitivity studies are performed in order to verify the accuracy of results provided by Quadratic combination and FORM with respect to importance factors. Table 6.6 summarizes the results of these studies and shows the influence of each variable on the estimation of failure probability for a displacement criterion in case of a cantilever beam. As can be seen, the most influential variables are related to the beam dimensions (*hB1* and *Lb*), which is in good agreement with results found by Quadratic combination and FORM (Table 6.2). In addition, these results show that mean and standard deviation values have an important effect on the estimation of failure probability. Thus, they must be properly identified in structural reliability analysis in order to assess accurate estimation.

Table 6.5: Variability of the cantilever beam variables according to their mean and standard deviation values

Random Variable	Influence of the mean value			Influence of the standard deviation value		
	$\mu_{1i} = 2 \times \mu_i$	$\mu_{2i} = 4 \times \mu_i$	Influence	$\sigma_{1i} = 2 \times \sigma_i$	$\sigma_{2i} = 4 \times \sigma_i$	Influence
<i>Lb</i>	5.7891	9.9750	high	1.4167	1.1869	high
<i>hB1</i>	1.5688	4.0158	high	1.9994	1.1435	high
<i>dbar</i>	4.0489	6.2843	high	2.0344	1.0806	medium
<i>ExcA</i>	4.0182	6.3017	high	2.0358	1.7097	medium
<i>E<sub>c</sub></i>	3.1490	4.3862	medium	2.0475	1.7433	medium
<i>ν<sub>c</sub></i>	2.1204	2.1182	low	2.1221	2.1221	low
<i>E<sub>s</sub></i>	2.8766	4.0282	low	2.0987	2.0092	low
<i>ν<sub>s</sub></i>	2.1219	2.1211	low	2.1221	2.1221	low
<i>Force1</i>	0.4860	0.8769	high	1.9885	1.6975	medium
<i>f<sub>max</sub></i>	3.8401	5.4505	high	1.9531	1.3468	high

Table 6.6: Summary of sensitivity studies for the cantilever beam

Random Variable	Mechanical sensitivity		Statistical sensitivity			Total influence
	Variable type	Influence	$\zeta_i$ influence	$\mu_i$ influence	$\sigma_i$ influence	
<i>Lb</i>	Stress	high	high	high	high	high
<i>hB1</i>	Resistance	high	high	high	high	high
<i>dbar</i>	Resistance	low	medium	high	medium	medium
<i>ExcA</i>	Resistance	low	medium	high	medium	medium
<i>E<sub>c</sub></i>	Resistance	low	medium	medium	medium	medium
<i>ν<sub>c</sub></i>	Stress	low	low	low	low	low
<i>E<sub>s</sub></i>	Resistance	low	high	low	low	low
<i>ν<sub>s</sub></i>	Stress	low	low	low	low	low
<i>Force1</i>	Stress	low	medium	high	medium	medium
<i>f<sub>max</sub></i>	Resistance	low	low	high	high	medium

#### 6.2.4.2 Distribution analysis

After examining the most influential input variables, the sensitivity analysis performed in the previous section allowed reducing the number of random variables to two (beam width and length). The next step is to analyze the dispersion and the distribution of the output variable, which is in this case the displacement at the free end of the beam. For this purpose, 100000 random simulations of the input vector are generated using the numerical integration Monte Carlo method (see section 4.4.2.1). Displacement values are determined for each simulation, they are then arranged in increasing order and subdivided into several equal intervals. Their percentage frequency values are calculated for each interval of displacement in order to plot the histogram that enables to determine the distribution of the variable of interest (Figure 6.4). The displacement probability distribution is first represented graphically using the Kernel Smoothing method. As can be seen, the number of simulations used is sufficient to obtain a very smooth Kernel density estimate and displacement values are distributed around a mean value of 0.614 mm with a standard deviation of 0.254 mm. Note that the estimated density captures the peak that characterizes the mode, and represents a nonparametric alternative to the fitting of a parametric probability density function.

Another parametric way to determine the distribution that fits the output sample of the beam displacement can be also used. It consists in selecting a parametric distribution to model the randomness behavior of the variable of interest and verify if it is in good agreement with the output

Table 6.7: Results of Kolmogorov-Smirnov test to verify beam displacement distribution

Distribution type	Parameters	p-value threshold	p-value	Success
Beta	$r = 3.2035$ $t = 17.467$ $a = 9.74208e^{-5}$ $b = 0.00314393$	0.05	$4.48e^{-60}$	False
Normal	$\mu = 0.00065616$ $\sigma = 0.000274354$	0.05	0.0	False
Lognormal	$\mu_{log} = -7.6105$ $\sigma_{log} = 0.509836$ $\gamma = 9.74208e^{-5}$	0.05	$8.96e^{-64}$	False
Logistic	$\alpha = 0.00065616$ $\beta = 0.000151259$	0.05	0.0	False
Gamma	$k = 4.14759$ $\lambda = 7423.12$ $\gamma = 9.74208e^{-5}$	0.05	$2.98e^{-12}$	False
Gumbel	$\alpha = 4674.8$ $\beta = 0.000532686$	0.05	$1.05e^{-05}$	False

sample. Among parametric distribution types proposed in OpenTURNs to represent the uncertainty of a continuous variable, 6 types are assumed and verified using statistical tests of goodness-of-fit. The output sample distribution is compared with Beta, Normal, Lognormal, Logistic, Gamma, and Gumbel distributions. The parameters of these distributions are estimated in terms of the output sample statistical moments and verified using Kolmogorov-Smirnov test (see section 4.4.2.2). A p-value threshold of 0.05 is used and compared to the p-value calculated. The assumed distribution is considered as accepted, and thus the Kolmogorov-Smirnov test succeeds to find a distribution that fits the output sample, only if the p-value calculated is greater than the threshold. Table 6.7 shows the distributions selected to verify if they fit the beam displacement sample, as well as their statistical parameters estimated in terms of the mean and standard deviation of the displacement. As shown, Kolmogorov-Smirnov test fails for all the distribution types selected, hence none of them is appropriate to describe the beam displacement density. Figure 6.5 provides a graphical comparison of the output sample distribution with the parametric distributions selected and shows that the Gumbel distribution gives the best fit. These results are also found using the QQ-plot with quantiles estimated at 95%. The quantile points estimated with Gumbel distribution of parameters  $\alpha = 4674.8$  and  $\beta = 0.000532686$  are the closest to the diagonal (Figure 6.6).

### 6.2.4.3 Comparison of probabilistic methods

The aim of this section is to discuss and compare probabilistic methods proposed in OpenTURNs (see section 4.4.3) in order to examine their accuracy, precision and computational effort. These methods are used to evaluate failure probability of the beam displacement criterion under the influence of several parameters, such as the number of random variables, their coefficient of variation and the type of their probability distribution. Parametric cases considered are detailed in Tables 6.8-6.10 with the corresponding values of failure probability estimated with different methods (FORM, SORM, MC, IS, DS and LHS). All cases studied are divided into several subset as following:

- 3 subset of cases with the same random variables number: 2 random variables ( $hB1, Lb$ ), 3 random variables ( $hB1, Lb, f_{max}$ ), and 7 random variables ( $hB1, Lb, E_c, dbar, ExcA, E_s, Force1$ ).

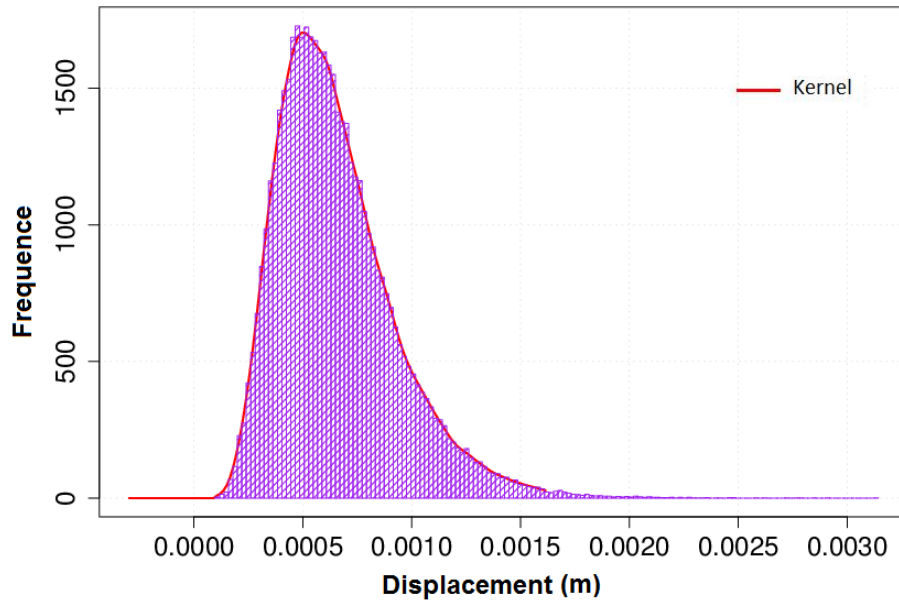


Figure 6.4: Beam displacement distribution estimated with Kernel Smoothing method

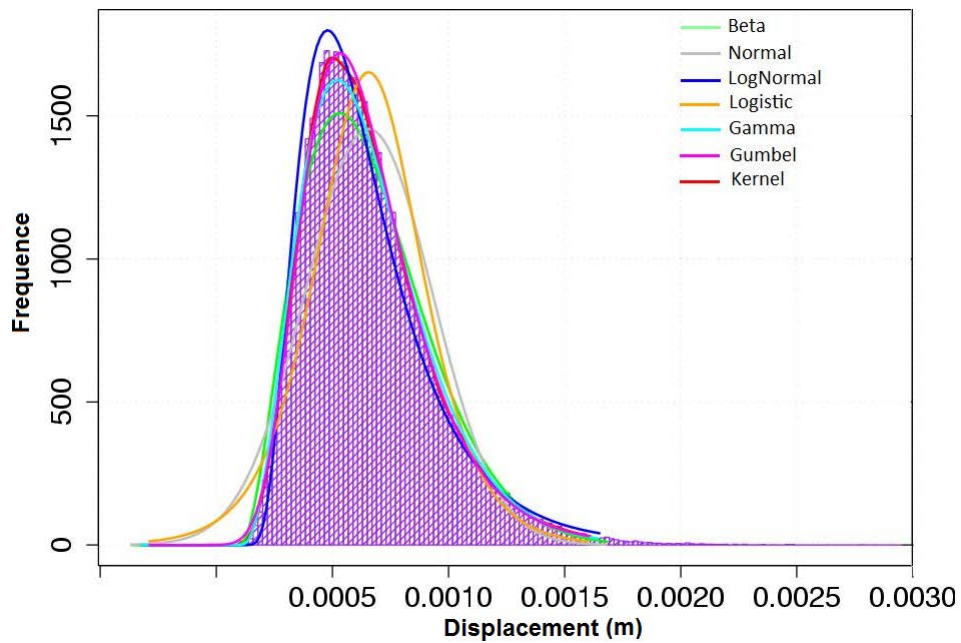


Figure 6.5: Comparison of the beam displacement sample to several parametric distributions

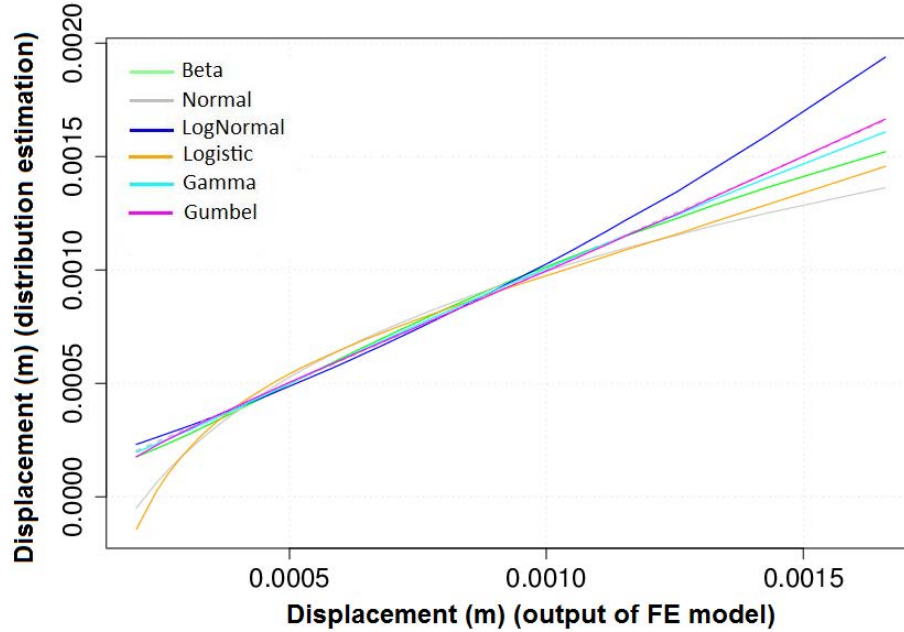


Figure 6.6: QQ-plot test to graphically compare the beam displacement sample to several parametric distributions

Random variables are selected according to the sensitivity analysis results by considering the most influential parameters.

- 2 subset of cases where random variables taken into consideration are presented with identical distribution type (normal, lognormal), and 1 subset that contains all cases with mixed distributions (i.e. cases where random variables are modeled with different distribution types).
- 5 subset of cases where random variables taken into consideration are presented with the same COV (0.05, 0.1, 0.2, 0.3, 0.5), and 1 subset that contains all cases with mixed COV (i.e. cases where random variables have different COV values).

For each subset, the mean value and COV of  $\frac{P_f(\text{method})}{P_f(\text{MC})}$  ratio are calculated for all methods. MC is assumed to be the method that gives the most accurate results, hence other methods are compared to MC and examined in terms of their accuracy and precision. Accuracy is estimated in term of the mean value of  $\frac{P_f(\text{method})}{P_f(\text{MC})}$  ratio and refers to closeness to MC results. Precision is estimated in term of the COV of  $\frac{P_f(\text{method})}{P_f(\text{MC})}$  ratio and refers to the degree of variation of results. A particular method is supposed to give the same results as MC in the case where the corresponding failure probabilities ratio has a mean value of 1.0 and a COV of 0.

It should be noted that, although a sufficient number of cases is necessary to make better conclusions on probabilistic methods effectiveness, the number of cases studied is limited to 27 and not all possible cases are considered because of the computational effort needed by different probabilistic methods to estimate failure probability for each case. However, this procedure can be useful to have a general understanding of each method limitations and how to select an appropriate method for a specific type of problem.

Table 6.8: Failure probability estimated with different methods for all the cases studied of the cantilever beam (number of random variables=2)

Case	Random variables	Distribution	COV	FORM	SORM	MC	IS	DS	LHS
1	$hB1, Lb$	Lognormal	0.05	3.26E-06	3.03E-06	6.00E-06	2.86E-06	3.29E-06	2.00E-06
2	$hB1, Lb$	Lognormal	0.1	0.01176	0.01098	0.01004	0.00967	0.01237	0.011486
3	$hB1, Lb$	Lognormal	0.2	0.12427	0.11593	0.12273	0.12656	0.24328	0.11294
4	$hB1, Lb$	Lognormal	0.3	0.21348	0.19846	0.18263	0.18459	0.21168	0.19014
5	$hB1, Lb$	Lognormal	0.5	0.29791	0.27239	0.24675	0.25535	0.21762	0.21467
6	$hB1$	Lognormal	0.1	0.13678	0.13414	0.12865	0.13254	0.15701	0.13162
	$Lb$	Lognormal	0.3						
7	$hB1, Lb$	Normal	0.1	0.01147	0.01072	0.00974	0.01036	0.00982	0.01115
8	$hB1$	Normal	0.1	0.01308	0.01265	0.01199	0.01274	0.01249	0.01334
	$Lb$	Lognormal	0.1						
9	$hB1$	Lognormal	0.1	0.00975	0.00885	0.00828	0.00809	0.01081	0.00852
	$Lb$	Normal	0.1						

Table 6.9: Failure probability estimated with different methods for all the cases studied of the cantilever beam (number of random variables=3)

Case	Random variables	Distribution	COV	FORM	SORM	MC	IS	DS	LHS
10	$hB1, Lb$	Lognormal	0.05	3.45E-06	3.26E-06	6.00E-06	3.28E-06	3.72E-06	2.32E-06
	$f_{max}$	Lognormal	0.05						
11	$hB1, Lb$	Lognormal	0.1	0.01470	0.01378	0.01291	0.01717	0.01316	0.01318
	$f_{max}$	Lognormal	0.1						
12	$hB1, Lb$	Lognormal	0.2	0.13781	0.12905	0.11029	0.10655	0.11422	0.13766
	$f_{max}$	Lognormal	0.2						
13	$hB1, Lb$	Lognormal	0.3	0.23292	0.21762	0.22649	0.21090	0.18678	0.18043
	$f_{max}$	Lognormal	0.3						
14	$hB1, Lb$	Lognormal	0.5	0.32725	0.30371	0.28458	0.27807	0.38822	0.34040
	$f_{max}$	Lognormal	0.5						
15	$hB1$	Lognormal	0.1	0.13937	0.13684	0.11772	0.25863	0.14539	0.20151
	$Lb$	Lognormal	0.3						
	$f_{max}$	Lognormal	0.1						
16	$hB1, Lb$	Normal	0.1	0.01421	0.01369	0.01446	0.01466	0.01322	0.01313
	$f_{max}$	Normal	0.1						
17	$hB1$	Normal	0.1	0.01561	0.01554	0.01519	0.01637	0.01997	0.01704
	$Lb$	Lognormal	0.1						
	$f_{max}$	Normal	0.1						
18	$hB1, Lb$	Normal	0.1	0.01449	0.01356	0.01298	0.01349	0.01311	0.01328
	$f_{max}$	Lognormal	0.1						

Table 6.10: Failure probability estimated with different methods for all the cases studied of the cantilever beam (number of random variables=7)

Case	Random variables	Distribution	COV	FORM	SORM	MC	IS	DS	LHS
19	$hB1, E_c$	Lognormal	0.05	3.76E-06	3.61E-06	6.00E-06	3.58E-06	3.94E-06	2.59E-06
	$dbar, ExcA, E_s$	Lognormal	0.05						
	$Lb$	Lognormal	0.05						
	$Force1$	Lognormal	0.05						
20	$hB1, E_c$	Lognormal	0.1	0.01798	0.01557	0.01648	0.01899	0.01643	0.01632
	$dbar, ExcA, E_s$	Lognormal	0.1						
	$Lb$	Lognormal	0.1						
	$Force1$	Lognormal	0.1						
21	$hB1, E_c$	Lognormal	0.2	0.14949	0.13680	0.11741	0.11175	0.13177	0.14121
	$dbar, ExcA, E_s$	Lognormal	0.2						
	$Lb$	Lognormal	0.2						
	$Force1$	Lognormal	0.2						
22	$hB1, E_c$	Lognormal	0.3	0.24779	0.22652	0.18385	0.21789	0.19206	0.21644
	$dbar, ExcA, E_s$	Lognormal	0.3						
	$Lb$	Lognormal	0.3						
	$Force1$	Lognormal	0.3						
23	$hB1, E_c$	Lognormal	0.5	0.34869	0.33052	0.26618	0.71120	0.24515	0.28015
	$dbar, ExcA, E_s$	Lognormal	0.5						
	$Lb$	Lognormal	0.5						
	$Force1$	Lognormal	0.5						
24	$hB1, E_c$	Lognormal	0.1	0.04633	0.04056	0.03791	0.03459	0.04606	0.03702
	$dbar, ExcA, E_s$	Lognormal	0.3						
	$Lb$	Lognormal	0.1						
	$Force1$	Lognormal	0.2						
25	$hB1, E_c$	Normal	0.1	0.01798	0.01634	0.01640	0.01867	0.01755	0.01659
	$dbar, ExcA, E_s$	Normal	0.1						
	$Lb$	Normal	0.1						
	$Force1$	Normal	0.1						
26	$hB1, E_c$	Lognormal	0.1	0.01716	0.01692	0.01648	0.01567	0.01796	0.01745
	$dbar, ExcA, E_s$	Lognormal	0.1						
	$Lb$	Normal	0.1						
	$Force1$	Normal	0.1						
27	$hB1, E_c$	Normal	0.1	0.01836	0.01709	0.01651	0.01766	0.01727	0.01621
	$dbar, ExcA, E_s$	Normal	0.1						
	$Lb, Force1$	Lognormal	0.1						

**Computational effort** The computational effort required for a reliability analysis depends on the computational time needed by the physical model to evaluate the response of the structure considered, as well as on the number of calls of the deterministic model needed to assess failure probability. In the current study, minimizing the computational effort of a reliability analysis is of a great concern, especially for deterministic models, such as finite element models, that are very time consuming to evaluate the output variable values. Therefore, the computational effort of each probabilistic method is examined in term of the number of calls of the deterministic model in order to analyze their efficiency and help to initially select an appropriate method that provides accurate results and reduces considerably the reliability analysis computational cost for a specific type of problem. The number of calls of the deterministic model is highly dependent on the magnitude of failure probability in the case of simulation methods, and on the convergence criterion of AbdoRackwitz algorithm to find the design point in the case of approximation methods.

By comparing the number of calls of the deterministic model required by the various methods for the beam problem, it is clear that approximation methods can reduce this number tremendously and independently of the failure probability magnitude and ensures a reasonable accurate estimate of failure probability for all cases studied in comparison with MC (Tables 6.8-6.10). However, a degree of verification for a specific type of problem is necessary to ensure that FORM and SORM provides convenient results, notably in case of highly nonlinear limit state functions. In the computations performed by means of simulation probabilistic methods for cantilever beam, the COV that represents the desired degree of precision on failure probability estimate is fixed at 10% with a confidence level of 95% and the number of simulations required to assess failure probability is limited to a maximum allowed value of 100000 simulations. It should be noted that the number of calls of deterministic method for simulation methods depends on the convergence criterion in term of this COV and a more significant number of simulations is needed for less values of this COV. MC is well-known to be the most effective and robust tool to estimate failure probability, but this method becomes very time consuming when computing small failure probabilities due to the large number of calls of the deterministic model required in such a case. As can be seen in Tables 6.8-6.10, for cases 1, 10 and 19, failure probability is of the order of  $1E-6$  and values provided by MC are not accurate since the maximum allowed value of 100000 simulations is not sufficient to reduce the uncertainty on the estimate of failure probability to an accepted level. Thus, the efficiency of MC is not verified for these cases and a larger number of simulations is necessary to assess an accurate estimate. Alternatively, simulation methods based on a variance-reduction principle are more efficient in term of accuracy and provide similar results as FORM and SORM for cases with low failure probabilities. In addition, the number of simulations is significantly reduced by 97.5% for IS (number of simulations  $< 2500$ ) and 69% for DS (number of simulations  $< 31000$ ). LHS is as much time consuming as MC (number of simulations  $> 100000$ ) but leads to an accurate estimate of probability exceeding a displacement threshold.

For other cases studied, the number of calls of deterministic model is presented in term of failure probability magnitude for different probabilistic methods (Figure 6.7). As can be seen, FORM and SORM are the less time consuming methods and the corresponding number of calls does not depend on the failure probability magnitude. For DS, the number of calls of the deterministic model varies according to the random radial directions generated. For failure probabilities higher than 0.01 and in the cases of large number of random variables, MC requires less simulations than DS to converge to results of similar accuracy. LHS gives comparable results to MC for all cases studied, but no reduction in computational effort is observed, as expected, for any magnitude of failure probability. Considering the duration of computations associated to IS, it is clear that, among simulation probabilistic methods, IS is the less time consuming since it requires only a limited number of evaluations of the deterministic model, and the number of simulations decreases with the increase of failure probability. But, for low failure probabilities, IS is more time consuming in comparison with approximation methods. IS loses its accuracy in the cases of random variables with

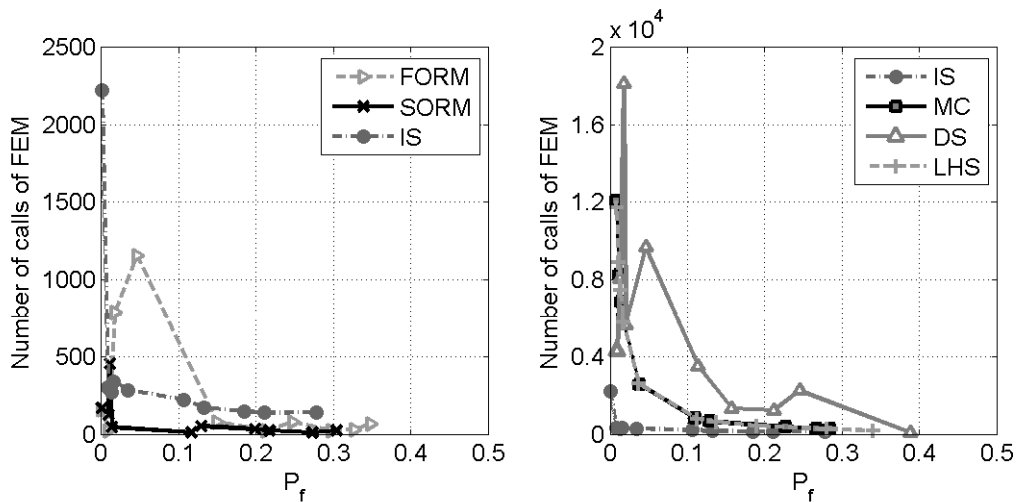


Figure 6.7: Number of calls of beam FEM in term of failure probability magnitude for different probabilistic methods

high COV of 0.5.

**Effect of random variables number** In order to compare the accuracy and precision of probabilistic methods in assessing similar results to MC and examine the effect of the number of random variables considered, all cases studied are divided into 3 subset of 2, 3 and 7 random variables. Cases 1, 10 and 19 are not considered for the following steps of the reliability analysis of the cantilever beam since MC failed to provide an accurate estimate of failure probability due to an insufficient number of simulations. As previously mentioned, the mean value and COV of the ratio  $\frac{P_f(\text{method})}{P_f(\text{MC})}$  estimate the accuracy and the precision of probabilistic methods in comparison to MC, respectively. A mean value close to 1.0 indicates that the relevant method provides similar results to MC and a COV close to 0 indicates an estimation of failure probability with high precision.

As can be seen in Figure 6.8, simulation and approximation methods give good results for most cases and failure probabilities are estimated with high accuracy in comparison to MC, the mean of probabilities ratio for each subset of random variables number is identical. For approximation methods, accuracy decreases as the number of random variables increases. This may be due to the fact that, as the number of random variables increases, the limit state surface becomes more complex with potentially other local optimum points and AbdoRackwitz algorithm may converge to a local but not a global optimum point. For both methods (FORM and SORM) there is a significant difference in precision for the subset of 2 and 7 random variables. For a higher number of random variables, overall precision of SORM is observed to be low with a high degree of variation ( $COV\left(\frac{P_f(\text{SORM})}{P_f(\text{MC})}\right) = 0.175$ ). For IS, precision decreases with the number of random variables. Low precision as well as low accuracy results are particularly found for random variables with high and mixed COV (cases 14, 15, 23 and 24). It should be noted that the case 23 with 7 random variables of a COV of 0.5 is not considered for IS to represent the mean and COV of probabilities ratio. Otherwise, the ratio  $\frac{P_f(\text{IS})}{P_f(\text{MC})}$  is found to have a COV of 0.439. When LHS and DS are considered, precision increases significantly with the number of random variables and a the estimate of failure probability is achieved with a COV less than the desired degree of variation of 0.1.

According to the sensitivity analysis performed to identify the random variables that mostly contribute to the variability of the displacement of cantilever beams, the variation of failure probability in terms of the force applied at the free end of the beam and the number of random variables

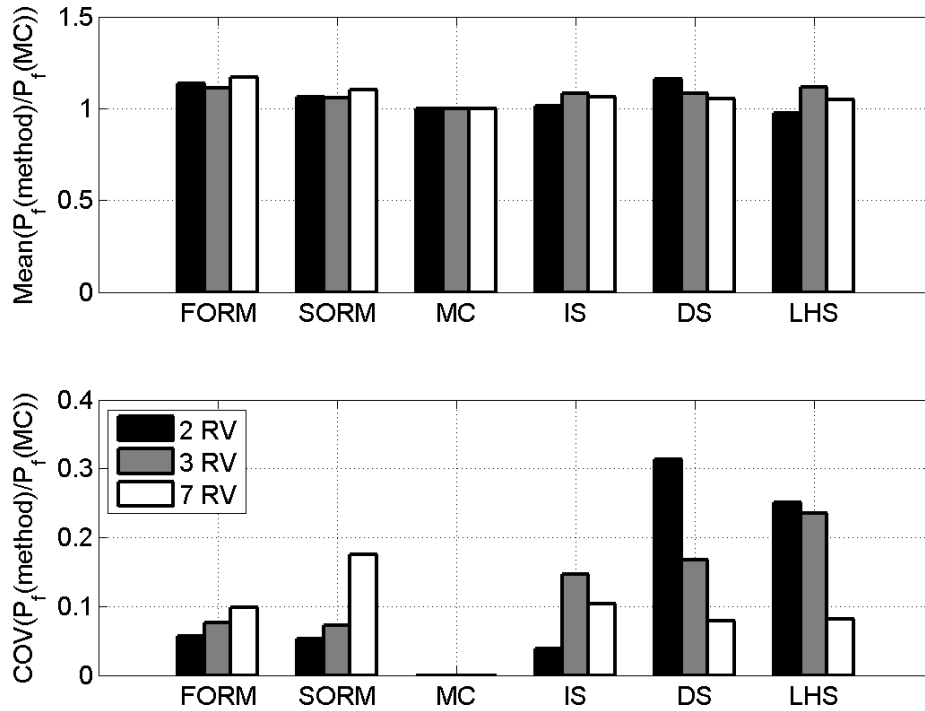


Figure 6.8: Effect of the number of random variables on the accuracy and precision of different probabilistic methods in comparison to MC

considered in the reliability analysis is also examined. 4 cases are considered:

- The first corresponds to the case where all variables are considered as random variables (10 variables).
- The second corresponds to the case of the 7 variables that affect the most the estimate of failure probability with respect to their omission factor (Table 6.4).
- The third represents the case of the most significant variables identified by Quadratic combination method (3 variables, Table 6.2).
- The fourth represents the case with the 2 most influential variables related to the beam dimensions (Table 6.6).

Statistical description of these variables is detailed in Table 6.1. As can be seen in Figure 6.9, a good agreement is found between the estimated values of failure probabilities in the case where all random variables are taken into account and the case where the number of random variables is reduced to two after performing a sensitivity analysis. The variation of failure probability is presented in term of the force applied at the free end of the beam, which indicates that the difference between failure probabilities estimated for each case is not significant. To emphasize the importance of considering all the most influential parameters in a reliability analysis, the case of one random variables is studied. In this case, only the beam width  $hB1$  is represented as a random variable and its length  $Lb$  is considered as a deterministic variable. Results with one random variable shows a substantial difference in comparison to cases where the 2 most influential variables are modeled as random variables. Figure 6.9 illustrates the importance of performing a sensitivity analysis since a bad choice of random variables may lead to erroneous values of  $P_f$ . In addition, sensitivity analysis helps

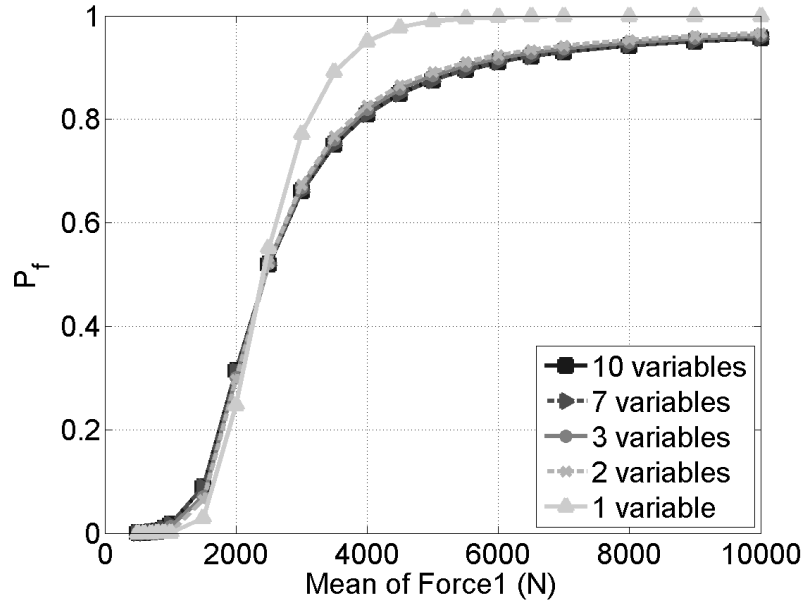


Figure 6.9: Variation of failure probability in terms of the force applied at the free end of the beam and the number of random variables considered

reducing the number of random variables, which subsequently reduces the computational effort of a reliability analysis.

**Effect of the type of random variables distribution** In order to compare the accuracy and precision of probabilistic methods in assessing similar results to MC and examine the effect of the type of random variables distribution, all cases studied are divided into 3 subset of normal, lognormal and mixed distributions (mixed term refers to cases where random variables are not modeled with the same probability distribution type). For this step, cases 1, 10 and 19 are also not considered as MC provides inaccurate results. The mean values and COV of probabilities ratio are also compared to MC results in order to estimate the accuracy and the precision of probabilistic methods with respect to the type of distribution.

As can be seen in Figure 6.10, simulation and approximation methods give good results for most cases and failure probabilities are estimated with high accuracy in comparison to MC, except for DS that shows low accuracy in cases containing distributions other than normal. FORM and SORM show lower accuracy and lower precision in the case of random variables modeled with Lognormal distribution, this is due to the isoprobabilistic transformation required by approximation methods to simplify the joint probability function. This transformation associates random variables in the physical space with standardized and independent random variables in the standard space. Thus, the transformation of random variables with normal probability distribution is more precise and accurate. Considering simulation probabilistic methods, IS gives best results for accuracy as well as for precision. Case 23 with 7 random variables of a COV of 0.5 is also not considered for IS to represent the mean and COV of probabilities ratio. Precision of LHS and DS is significantly affected by the type of random variables distribution with a high degree of variation in case of Lognormal distribution ( $COV \left( \frac{P_f(DS, LHS)}{P_f(MC)} \right) \simeq 0.25$ ).

Another study of the effect of the type of random variable distributions is performed. For this purpose, the main case of study is considered with two random variables, namely  $hB1$  and  $Lb$ . Both random variables are modeled with the same type of distribution by considering all parametric

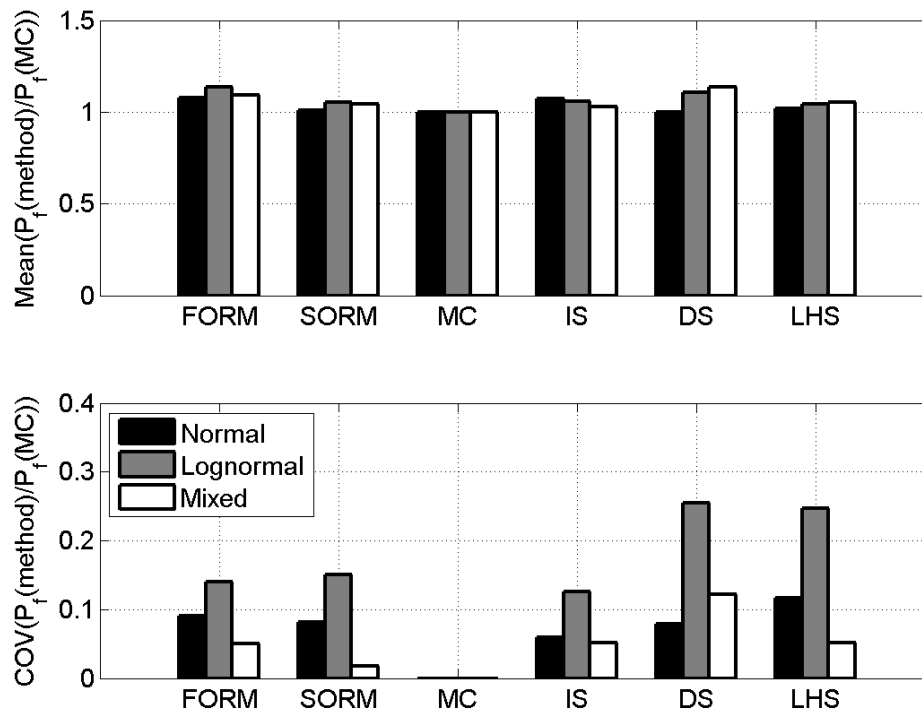


Figure 6.10: Effect of the distribution type of random variables on the accuracy and precision of different probabilistic methods in comparison to MC

distribution types proposed in OpenTURNS to represent the uncertainty of continuous variables. The values of distribution statistical parameters are estimated in terms of the statistical moments for each random variable. First, the mean and COV values of the beam displacement are evaluated in order to examine which distributions provide the same results for the variable of interest. Table 6.11 shows that the displacement mean value is not affected by the type of probability distribution, but its variance is highly dependent on the distribution type and the displacement COV may reach a value of 12.22 in the case where random variables are modeled with Logistic distribution. Among the probability distributions considered, only 8 distributions allow the same statistical characterization of the beam displacement that represents the output variable of the problem. Afterwards, the influence of these 8 probability distributions on the beam reliability is studied. Figure 6.11 indicates that reliability depends significantly on the probability distribution type used for random variables. Results obtained in the cases of Beta, Gamma, Lognormal and Normal distributions show a good agreement regardless of the probabilistic method used and the differences between the estimated values of failure probability are inconsiderable. The results obtained in the present section illustrate the necessity of selecting the appropriate probability distribution type to model variable uncertainties. Thus, it is not sufficient to provide the mean and COV of random variables, but an appropriate PDF must also be specified for each variable.

**Effect of COV** In order to compare the accuracy and precision of probabilistic methods in assessing similar results to MC and examine the effect of the COV of random variables, all cases studied are divided into 6 subset of 0.05, 0.1, 0.2, 0.3, 0.5 and mixed distributions (mixed term refers to cases where random variables are modeled with different COV values). The mean values and COV of probabilities ratio are also compared to MC results in order to estimate the accuracy and the precision of probabilistic methods with respect to the COV of random variables.

Cases 1, 10 and 19 are considered in this step, they represents the cases of a COV equal to

Table 6.11: Failure probability estimated with different methods for different types of probability distribution (number of random variables=2)

Type	Displacement			$P_f$					
	$\mu$ (mm)	$\sigma$ (mm)	COV	FORM	SORM	MC	IS	DS	LHS
Beta	0.614	0.254	0.42	0.01154	0.01060	0.01069	0.01133	0.01187	0.00968
ChiSquare	0.614	5.206	8.48	0.44222	0.44215	0.39102	0.35001	0.49413	0.34021
Exponential	0.614	0.254	0.42	0.02135	0.01763	0.01594	0.01842	0.01702	0.02245
Gamma	0.614	0.254	0.42	0.01157	0.01079	0.00941	0.00955	0.01061	0.01185
Gumbel	0.614	0.254	0.42	0.01533	0.01408	0.01192	0.01502	0.03935	0.01499
Histogram	0.614	0.415	0.72	0.04571	-	0.02605	0.03206	-	0.027282
Laplace	0.614	0.254	0.42	0.01054	0.01438	0.01551	0.01286	0.01585	0.01249
Logistic	0.614	12.79	20.84	0.47817	0.47311	0.07802	0.06679	0.04044	0.08630
Lognormal	0.614	0.254	0.42	0.01176	0.01098	0.01004	0.01001	0.01237	0.00892
NonCentral Student	0.614	7.92	12.89	0.46761	0.46361	0.12517	0.10236	-	0.10101
Normal	0.614	0.254	0.42	0.01147	0.01071	0.00974	0.01216	0.00982	0.00838
Rayleigh	0.614	1.33	2.16	0.26306	0.22506	0.25424	0.29613	0.26058	0.27137
Student	0.614	12.22	19.91	0.46794	0.46302	0.11042	0.09995	0.06498	0.09391
Triangular	0.614	0.809	1.32	0.24727	0.23364	0.21294	0.19674	0.21188	0.21763
Truncated normal	0.614	0.254	0.42	0.011471	0.10691	0.00974	0.01215	0.00982	0.00838
Uniform	0.614	1.14	1.86	0.35463	0.32210	0.26335	0.22915	0.24028	0.24516
Weibull	0.614	0.254	0.42	0.01621	0.01694	0.01567	0.01494	0.01888	0.01735

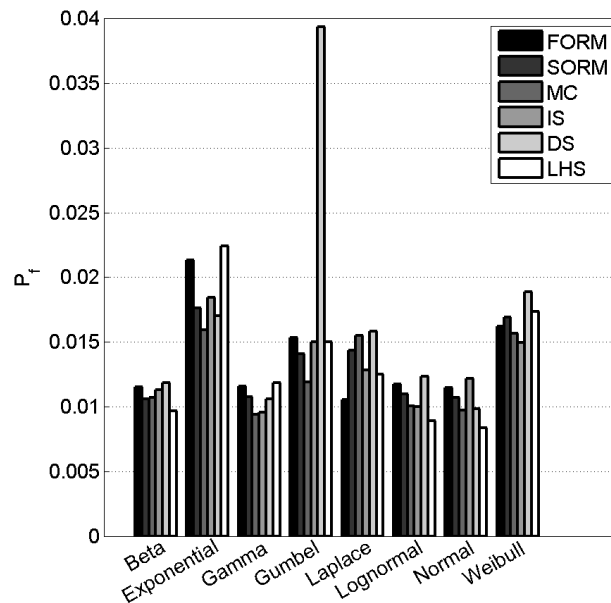


Figure 6.11: Effect of the type of random variables distribution on the estimation of failure probability for different probabilistic methods

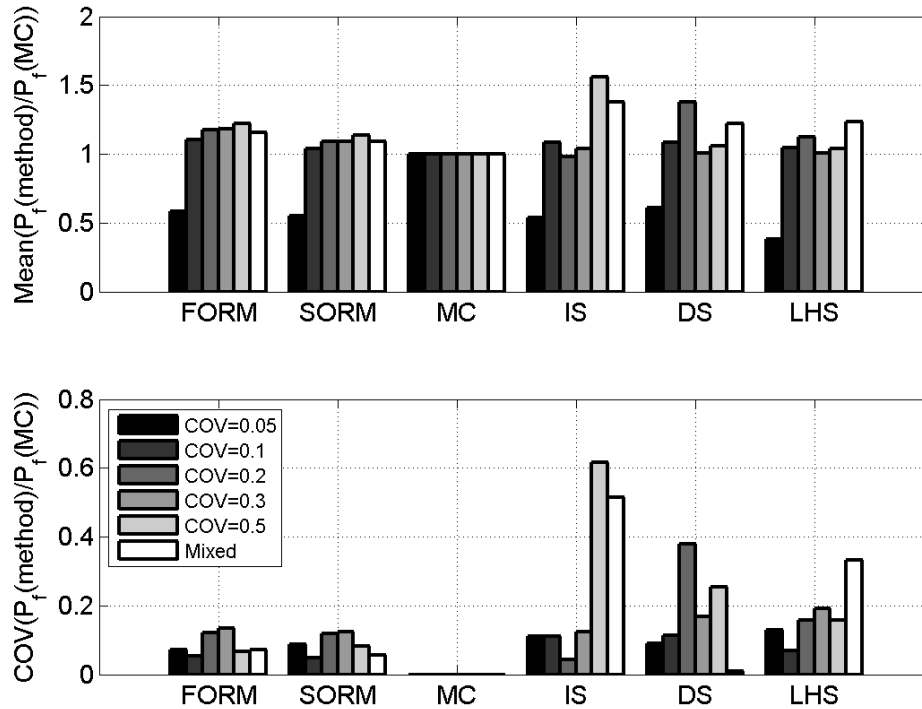


Figure 6.12: Effect of the COV of random variables on the accuracy and precision of different probabilistic methods in comparison to MC

0.05 and low failure probability values. As can be seen in Figure 6.12, the difference between MC and other probabilistic methods considered is huge due to the inaccurate results obtained by MC. For this subset failure probabilities are estimated with low accuracy for MC due to an insufficient number of simulations. However, IS and DS are more efficient in term of accuracy and provide similar results as FORM and SORM for cases with low failure probabilities. For other subset, it can be seen that the accuracy and precision of simulation and approximation methods degrades with the increase of the random variables COV. The most inaccurate and imprecise results are obtained with IS for  $COV \geq 0.3$  and DS for  $COV \geq 0.2$ . IS for  $COV \leq 0.2$ , FORM and SORM give best results for accuracy and precision in term of the COV of random variables.

In order to have a better understanding on the effect of COV of random variables, the case of 7 random variables modeled with Lognormal distribution is considered assuming that all random variables have the same COV value. The variation of failure probability is first presented in term of the mean of the force applied at the free end of the beam for different values of COV (Figure 6.13), then presented in term of the COV for different values of the mean of the force (Figure 6.14). MC is used to assess failure probability with a maximum allowed value of  $1E6$  simulations.

Figure 6.13 shows that the inflection point of curves corresponds to the case where the limit state function is equal to zero ( $G = f_{max} - f = 0$ ). At this point, the value of the displacement threshold is equal to the mean value of the calculated displacement and failure probability is equal to 0.5. The corresponding force value is approximately of the order of 2800 N. Figure 6.14 shows failure probability values as a function of the COV. The linear equation of  $P_f = 0.5$  describes the limit state function that corresponds to the point of intersection of the curves presented in the previous figure. This figure permits to evaluate the range of low failure probabilities in term of the mean value of the force applied at the free end of the beam. It can be seen that, for a force less than 200 N and a COV less than 0.4, failure probability represents values less than 0.005.

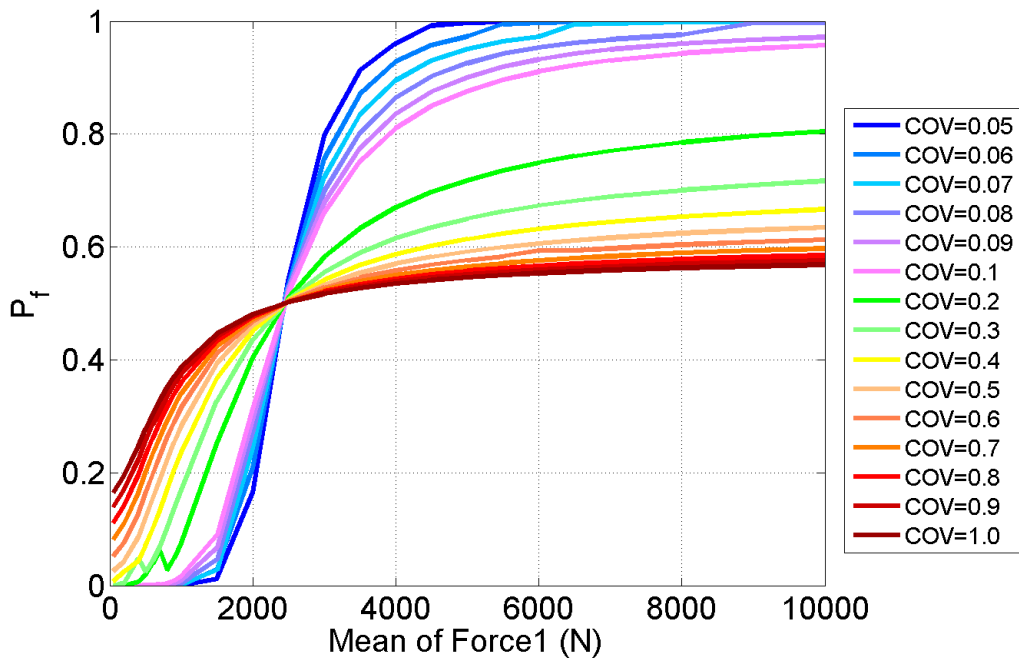


Figure 6.13: Variation of failure probability in term of the mean of the force for different values of COV

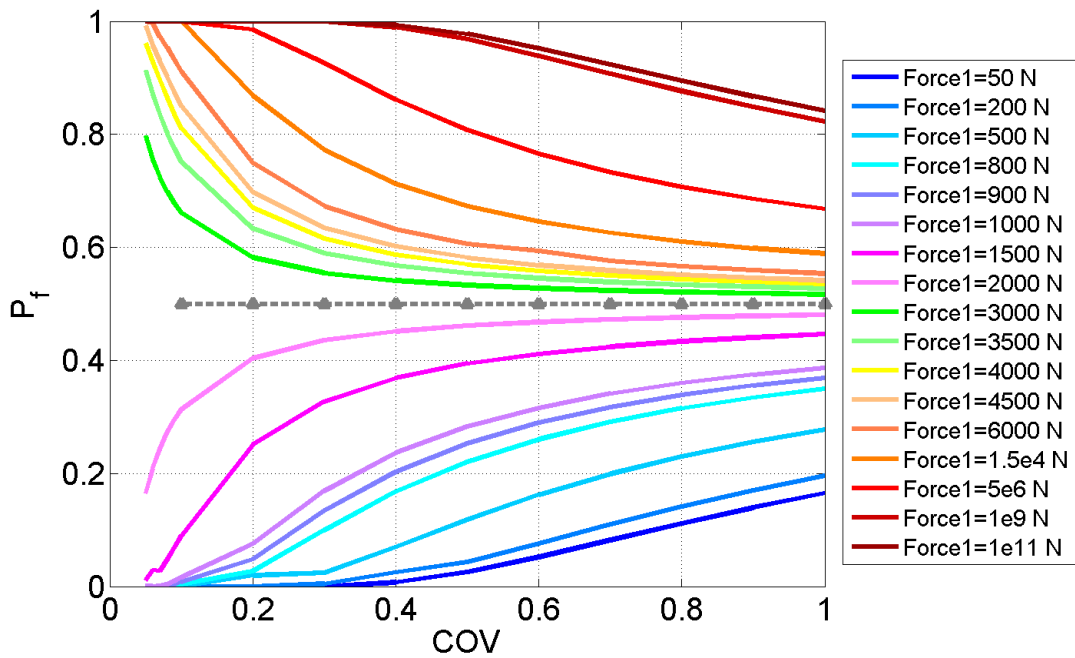


Figure 6.14: Variation of failure probability in term of the COV for different values of the mean of the force

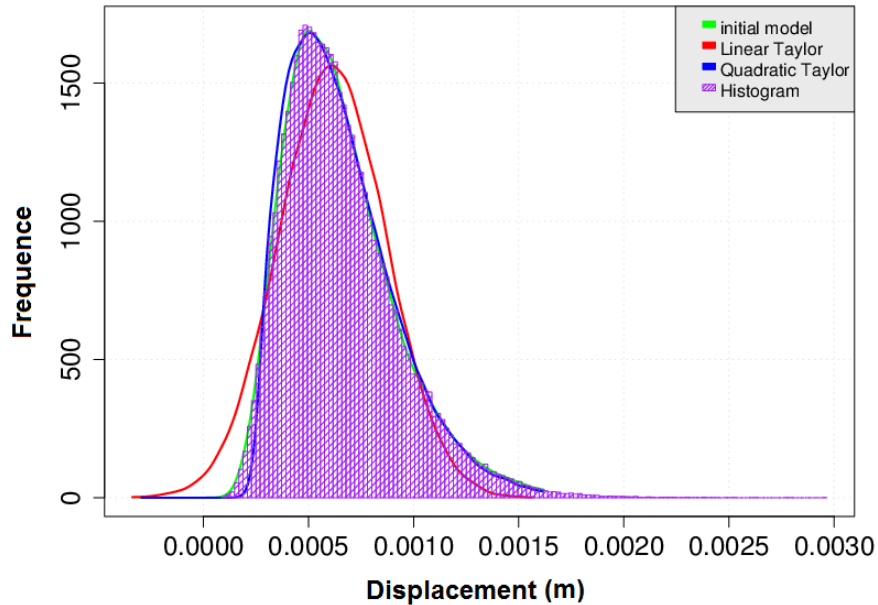


Figure 6.15: Comparison of the beam displacement distributions estimated with the initial model and Taylor expansion

#### 6.2.4.4 Metamodeling

After examining the most influential input variables, the number of random variables is reduced to two in this section (beam width and length). The next step consists in evaluating the validity and efficiency of response surface methods provided in OpenTURNS, namely the Taylor expansion, the Least Square method and the polynomial chaos expansion. The principal of such methods consists in replacing the initial model with an approximate polynomial model in the aim of simplifying reliability analysis of complex structures and reducing the computational effort to assess failure probability of exceeding a threshold. In this section, 2 random variables are considered and modeled with Lognormal probability distribution and a COV of 0.1. First, the distribution of the output variable, which is in this case the displacement at the free end of the beam, obtained with the initial model is analyzed and compared to that obtained with the available response surface types (Figures 6.15-6.17). For each type, 100000 random simulations of the input vector are generated with the initial model of the beam and using the numerical integration Monte Carlo method. Displacement values are determined for each simulation, then polynomial coefficients of the approximate model are estimated through the finite number of simulations of the deterministic model. The displacement probability distribution is first represented graphically using the Kernel Smoothing method. The number of simulations used is sufficient to obtain a smooth Kernel density estimate in the case of the initial model and displacement values are distributed around a mean value of 0.614 mm with a standard deviation of 0.254 mm. As can be seen, Least Square method and Taylor expansion of 1st order fails in describing the beam displacement density, while the best fit is obtained with polynomial chaos expansion for cleaning and fixed strategies.

Furthermore, approximate models obtained from several response surface types are combined with different probabilistic methods in order to study the efficiency of response surface methods in assessing failure probability. For each type, failure probability is compared with that obtained in the case of the beam FEM combined with the different probabilistic methods (Figure 6.18). Least Square method, Taylor expansion and polynomial chaos expansion with sequential strategy are found to significantly underestimate failure probability, while results provided by polynomial chaos

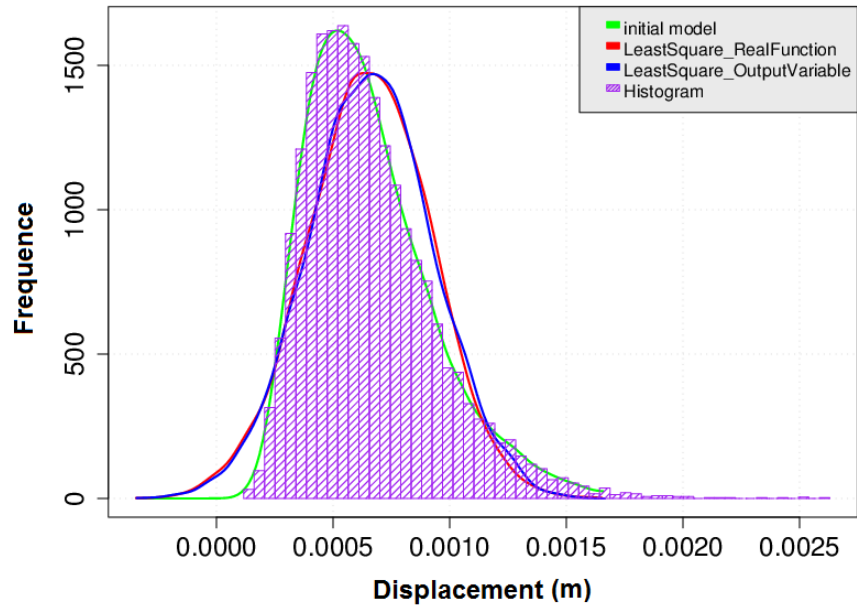


Figure 6.16: Comparison of the beam displacement distributions estimated with the initial model and Least Square method

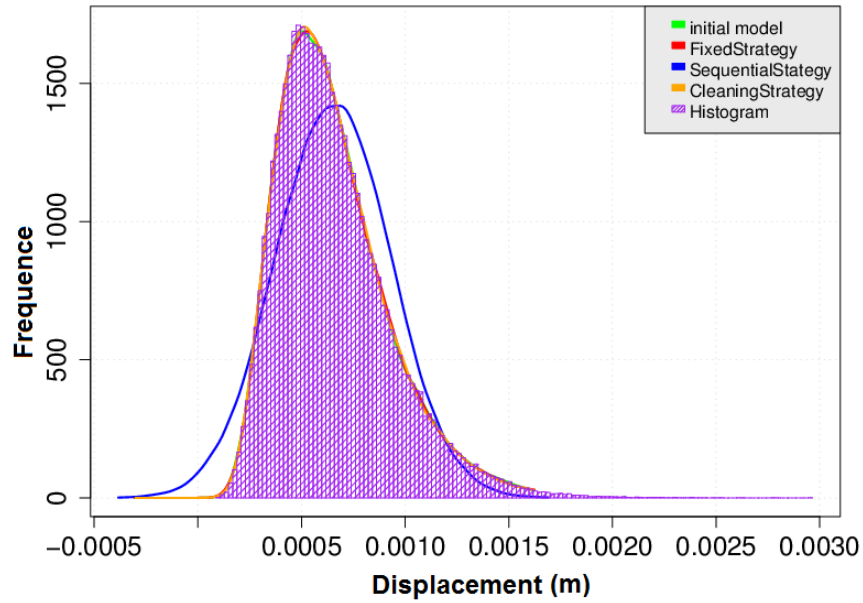


Figure 6.17: Comparison of the beam displacement distributions estimated with the initial model and polynomial chaos

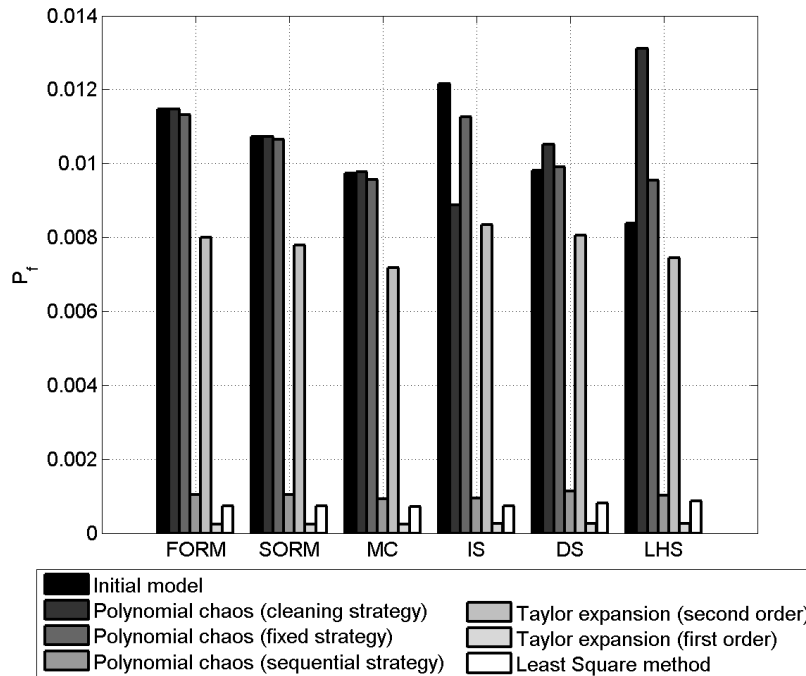


Figure 6.18: Comparison of failure probability estimated with the initial model and several response surface types

with fixed or cleaning strategy show good agreement with those obtained in the case of the beam FEM combined with a particular probabilistic method. It should be noted that the computational effort needed to assess failure probability in the case of approximate models combined with any probabilistic method is negligible (time of order of several seconds).

#### 6.2.4.5 Conclusion remarks

The problem of the cantilever beam is used as a simple example in the aim of mastering the basics of OpenTURNS and examining the probabilistic methods proposed in OpenTURNS to estimate failure probability in structural reliability analysis. The principle of each step of a reliability analysis is illustrated and the available probabilistic methods are compared in terms of their accuracy, precision and computational effort. The FEM of the RC beam is modeled with CASTEM and combined with OpenTURNS using the wrapper interface.

This application allows drawing some preliminary conclusions which highly served the purposes of other types of applications in order to initially select an appropriate probabilistic methods, given computational effort constraints. Although Monte Carlo method is a robust method for several structural reliability analysis, it is often impractical to use due to the large number of simulations required to reach the desired level of accuracy. Comparing other probabilistic methods to MC, IS is the method that gives best results in terms of accuracy and precision for different subset examined, except for the subset of random variables with high COV ( $COV=0.5$ ). For this subset, IS loses its accuracy in estimating MC failure probabilities. DS is significantly affected by the number of random variables and is less precise for high random variables cases (7 random variables). DS is the method that gives the highest values of the COV of probabilities ratio leading to less confidence in failure probabilities estimated with this method. LHS gives comparable results to MC, but no reduction in computational effort is observed. For FORM and SORM, failure probabilities are estimated with

high accuracy in comparison to MC, except in cases of high COV ( $COV > 0.2$ ). In term of reliability analysis computational effort, FORM and IS are the less consuming methods in comparison to other methods. However, these conclusions could not be generalized for every problem in reliability analysis and some degree of verification should be conducted to ensure the efficiency of methods used.

## 6.3 Application to RC slab subjected to impact - Elastic behavior

In this section, a reliability analysis of RC slabs under low velocity impact is presented assuming a flexural mode of failure and an elastic behavior for steel and concrete. The behavior of RC slabs in bending has two major phases before the failure, the first is related to the increase of deflection, the second is related to steel yielding [60]. Probabilistic methods used in this section to study the reliability of impacted slabs are the most known methods in the reliability domain, namely FORM, SORM, MC and IS. Several criteria of failure are considered, they are related to the displacement of slab at the impact point, the peak force of impact, stresses in reinforcement, and the impact energy absorbed by the slab. To study the dynamic effect of impact applied to RC slabs, 3 deterministic models are used and evaluated: a 3D FEM simulated with Abaqus/Explicit, a simplified model based on the plate theory [160] and a two degrees of freedom mass-spring system [29]. The aim is to select the most appropriate model to use in RC slabs reliability analysis, while accurately representing the mechanical behavior of the slab studied and reducing the computational cost to the minimum. The model chosen is then used in a parametric study in order to investigate the effect of several input parameters of the deterministic model on the calculation of failure probability.

### 6.3.1 Deterministic models

#### 6.3.1.1 Finite element model

This section describes the 3D FE model of the RC slab subjected to impact within nuclear plant buildings using ABAQUS/Explicit. Geometry of slab and impactor, reinforcement and material properties, as well as initial and boundary conditions are present in section 5.4. A 3D solid element, the eight-node continuum element (C3D8R) is used to develop the mesh of the concrete slab. As illustrated in Figure 6.19.a, the mesh of the concrete slab contains five elements in the thickness direction with three different densities of mesh. The elements at the center of the slab have dimensions of  $5 \times 5 \times 10$  cm, while the elements at the corners have dimensions of 5 cm in three directions. Thus, the elements of regions between the center and corner regions are of  $5 \times 10 \times 107$  cm dimensions. The reinforcement is modeled with truss elements (T3D2) (Figure 6.19.b) and the embedded approach is used to create the bond between the steel reinforcement and concrete. This approach allows independent choice of concrete mesh and arbitrarily defines the reinforcing steel regardless of the mesh shape and size of the concrete element.

The impactor is meshed with four-node tetrahedral elements (R3D4). The definition of contact properties and interaction types is very important for impact problems, but in this case of study this definition is limited to a normal interaction and a hard contact with finite sliding. The contact pair algorithm is used in order to model contact between the upper surface of the slab and the impactor surface. The contact constraints are enforced with a pure master-slave kinematic contact algorithm which does not allow the penetration of slave nodes into the master surface (surfaces attached to rigid bodies must always be defined as master surface in Abaqus/Explicit).

At first, nonlinearities due to concrete and steel behaviors are not considered, both materials are assumed to have an elastic behavior. The only nonlinearity present in the FEM is due to the contact algorithm between the impactor and the slab. The FEM of the slab consists of 53000 nodes

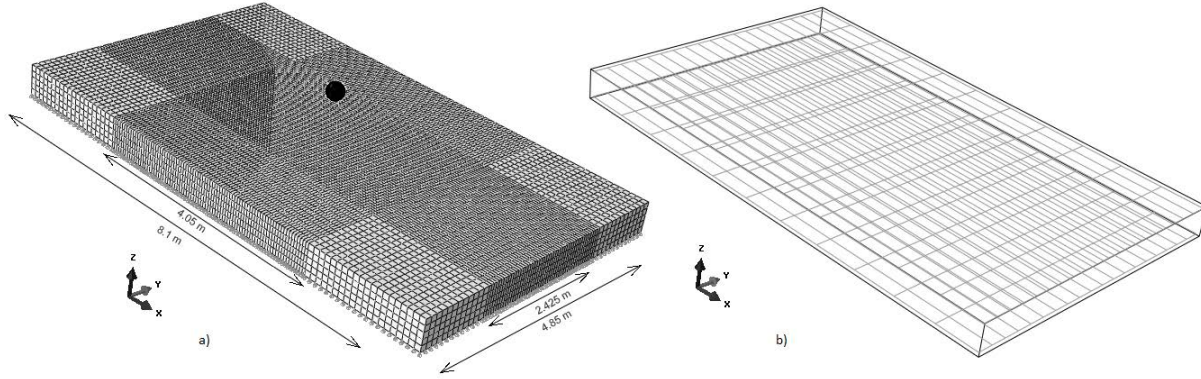


Figure 6.19: Finite element model of slab: a) meshing, b) reinforcement

and more than 44900 elements, and a simulation takes a total time of 25 minutes for an impact step of 0.1 s.

### 6.3.1.2 Model based on plate theory (PT)

The Classical Laminated Plate Theory is used to develop an analytical solution for RC slabs. This theory is based on the kinematic assumptions of Kirchhoff-Love for thin plates with small deflections. The approximate Navier solution is used to estimate the deflection of the mid-surface of the slab ( $w_0$ ). Thus, the deflection of slab can be expressed as:

$$w_0(x, y, t) = \sum_{m=1}^{\infty} \sum_{n=1}^{\infty} W_{mn}(t) \sin(\alpha x) \sin(\beta y) \quad (6.4)$$

The impactor in this model is replaced by a concentrated force  $q(x, y, t)$  applied at the impact point and expressed as following:

$$q(x, y, t) = \sum_{m=1}^{\infty} \sum_{n=1}^{\infty} Q_{mn}(t) \sin(\alpha x) \sin(\beta y) \quad (6.5)$$

where  $Q_{mn}(t) = \frac{4Q_0(t)}{ab} \sin(\alpha x_0) \sin(\beta y_0)$  for impacted slab cases ( $x_0, y_0$ ) are the coordinates of the impact point.

The aim is to determine the coefficients  $W_{mn}(t)$ . This can be achieved by integrating the following constitutive relation over the slab surface:

$$-\left( D_{11} \frac{\partial^4 w_0}{\partial x^4} + 2(D_{12} + 2D_{66}) \frac{\partial^4 w_0}{\partial x^2 \partial y^2} + D_{22} \frac{\partial^4 w_0}{\partial y^4} \right) + q(x, y, t) = I_0 \ddot{w}_0 - I_2 \left( \frac{\partial^2 \ddot{w}_0}{\partial x^2} + \frac{\partial^2 \ddot{w}_0}{\partial y^2} \right) \quad (6.6)$$

For this case of study, the coefficients  $W_{mn}(t)$  can be estimated as:

$$W_{mn}(t) = \frac{4 \sin(\alpha x_0) \sin(\beta y_0)}{ab w_{mn} I_0} \int_0^t Q_0(\tau) \sin(w_{mn}(t - \tau)) d\tau \quad (6.7)$$

where  $a$  and  $b$  are the slab length and width, respectively. Values of  $W_{mn}(t)$  are determined analytically assuming a sinusoidal evolution in time of impact loading [105].

This model is developed using Matlab, it consists of the same input variables as the FEM except those related to the impactor. Impactor velocity, mass and radius are replaced in this model by an

impact force which is estimated by means of the FEM. The impact time is taken equal to that of the FEM impact step.

### 6.3.1.3 Mass-spring model

A simplified model of two degrees of freedom mass-spring system is developed using Matlab. This model was proposed by CEB [29] to study the behavior of slabs subjected to hard impact. In this case, the kinetic energy of the impactor is absorbed by the structure deformation, and the slab local behavior as well as its overall deformation must be considered. The model consists of two masses, that represent the impactor and slab masses, respectively, and of two springs that describe the stiffness of slab and the contact force, respectively. The differential equations of equilibrium of the two masses are previously detailed in Section 1.3.2.2. The rigidity of slab and the contact force-time are determined by means of the FEM. The equivalent mass of slab in the MSM is obtained by multiplying the mass of the real slab with a transformation factor. The slab mass, as well as the transformation factor, highly depend on slab dimensions, material densities, bars diameter, and number of longitudinal and transversal reinforcement bars. Impactor velocity, mass and radius are the same as those used for the FEM. It should be noted that the transformation factor is the only parameter calibrated for the MSM in order to find the best fit with the FEM.

### 6.3.2 Probabilistic model

Assuming an elastic behavior for steel and concrete, the variables which may be subjected to statistical variations in RC slabs under impact can be classified into four categories:

1. Dimensional variables related to geometric properties of the slab: length, width and thickness of the slab.
2. Variables related to the impactor and its kinetic energy: radius, mass and velocity of the impactor.
3. Variables related to concrete properties: Young's modulus and density of concrete.
4. Variables related to steel properties: diameter of bars.

It should be noted that the length and width of slab are not introduced into deterministic models to model their relevant uncertainties, but they are considered to cover a wide range of slab geometries. The probabilistic characterization of random variables is based on some literature reviews. Table 6.12 represents the random variables adopted for this application, their probability distribution, their mean and COV. Mean values of random variables are taken equal to their nominal values, and their COV is determined according to references cited in the fourth column. Probability distributions are chosen according to the reliability based code calibration of JCSS (Joint Committee on Structural Safety) [89]. JCSS code contains several rules and basics that are essential for the design of new structures or evaluating the response evolution with time of already existing structures in a reliability framework. The modulus of elasticity of steel is considered as deterministic variable due to its small dispersion [126]. It should be noted that the following probabilistic characterization was adopted before performing the literature review detailed in section 4.6.

### 6.3.3 Failure criteria

Gay and Gambelin [67] described the problem that an engineer could expect during the analysis and design of RC structures under certain loading conditions. This problem involves two fundamental components:

Table 6.12: Random variables of the RC slab and their statistical descriptions (elastic behavior)

Variables	PDF	Mean	COV	Ref.
<b>Geometric properties of the slab</b>				
Length, $a$	Normal	8.1 m	0.05	[127]
Width, $b$	Normal	4.85 m	0.05	[127]
Thickness, $e$	Normal	0.5 m	0.05	[127]
<b>Impactor variables</b>				
Radius, $r$	Normal	15 cm	0.05	[38]
Mass, $m$	Lognormal	3600 kg	0.05	[38]
Velocity, $v$	Lognormal	7.7 m/s	0.1	[38]
<b>Concrete properties</b>				
Young's modulus, $E_c$	Lognormal	35 GPa	0.1	[123]
Density, $\rho_c$	Lognormal	2500 $kg/m^3$	0.1	lack of information
<b>Reinforcement properties</b>				
Bars diameter, $d_A$	Lognormal	20 mm	0.1	lack of information

- Stiffness design for which the structure must not endure displacements higher than a particular threshold defined in design specifications (serviceability limit states in Eurocode).
- Load-carrying capacity design for which the structure must continue to perform its functional requirements under the applied loadings (ultimate limit states in Eurocode).

The first aspect to consider for the application of impacted RC slabs assuming an elastic behavior of materials is the displacement of slab at the impact point. Thus, the first criterion is defined in term of this displacement:

$$g_1 = u_{max} - u \quad (6.8)$$

In this equation,  $u_{max}$  is the displacement threshold and  $u$  represents the maximum displacement of slab at the impact point.  $u_{max}$  is considered according to Eurocode specifications [142] equal to  $\frac{a}{250}$ , with  $a$  is the length of slab. The values of  $u$  are calculated according to the deterministic model used and the values of input random variables generated in OpenTURNS. The RC slab is modeled assuming an elastic behavior of materials, however this assumption does is not representative of the actual response and the maximum displacement of slab is underestimated of approximately 60% in this case [18]. Therefore, a coefficient of 1.5 is introduced in the expression of the displacement failure criterion in order to take into account plastic deformations related to actual materials behavior. The displacement criterion is then expressed as:

$$g_1 = u_{max} - 1.5u \quad (6.9)$$

A second aspect related to stresses in reinforcement can be also examined. Berthet-Rambaud [18] supposed that the failure of SDR protective slabs initiates when yielding of main reinforcement occurs. Thus, a second failure criterion can be expressed in term of steel stresses as following:

$$g_2 = f_y - \sigma_s \quad (6.10)$$

where  $f_y$  is the yield strength of reinforcement and  $\sigma_s$  is the stress in reinforcement. For this ultimate limit state function, failure probability can be assessed only through the combination of slab FEM with OpenTURNS, stresses in reinforcement cannot be evaluated using the mass-spring model nor that based on the plate theory. This criterion can be defined in such a way that stresses

in any finite element of reinforcement should not reach the yield strength of steel, but exceeding the threshold of stresses in one steel element does not necessarily lead to slab failure. Therefore the variable of interest of steel stress is replaced by the variable related to the number of reinforcement FE elements  $n_A$  in which yielding occurs, and a threshold  $n_{Amax}$  equal to the number of FE elements in 3 longitudinal bars and 3 transversal bars is assigned.

$$g_2 = n_{Amax} - n_A \quad (6.11)$$

An energy criterion for RC slabs subjected to impact was defined by Miyamoto and King [130]. They indicated that this criterion would be the most efficient method of designing RC structures under impact loads, especially for a flexural failure mode. The criterion consists of that structural failure is likely to occur if the slab is not capable of absorbing all of the energy transmitted during impact collision. A part of the impactor kinetic energy  $E_{kin0}^I$  is transferred to slab as kinetic energy and irrecoverable strain energy  $E_{plas1}^S$  that results from the formation of cracks, friction and damping. Therefore, a third ultimate limit state function corresponding to this criterion is considered assuming that the slab should absorb 80% of the impact energy:

$$g_3 = 0.8E_{kin0}^I - E_{plas1}^S \quad (6.12)$$

Another important criterion related to the impact force should also be examined. The evolution in time of impact force represents one of the main problems of impacts on RC structures. It depends on two colliding bodies geometry, their stiffnesses and the initial conditions of the impactor. Thus, a fourth ultimate limit state function is considered:

$$g_4 = F_{max} - F \quad (6.13)$$

where  $F_{max}$  represents the ultimate load-carrying capacity of slab and from is determined a limit load analysis,  $F$  is the peak of impact force calculated with the slab FEM.

### 6.3.4 Discussion of results of slab reliability (elastic behavior)

#### 6.3.4.1 Comparison of deterministic models

In order to be able to use simplified analytical model in reliability analysis, their effectiveness in predicting the response of slab should be first verified. Thus, mass-spring model and that based on plate theory are compared to the finite element model. Table 6.13 shows the displacement of slab at the impact point obtained with different models developed to evaluate the behavior of impacted RC slabs assuming an elastic behavior of materials. It can be seen that the mass-spring model allows a better estimation of displacement at the center of slab for different values of velocity with a maximum error of only 1.5%. However, the analytical model based on plate theory is less precise and estimate the displacement with a maximum error of 5%.

Next, deterministic models are compared in a reliability framework. Failure probability is assessed using FORM method by combining the different deterministic models to OpenTURNS for several values of velocity. Figure 6.20 shows that failure probability increases with the mean of velocity for the displacement criterion. Results obtained with MSM are in good agreement with failure probabilities estimated by coupling FORM with the FEM. In addition, the MSM is found to be more effective in term of computational cost. Thus, it is selected to study the effect of input variables on the estimate of failure probability in the case of impacted slabs with elastic behavior of materials.

Table 6.13: Comparison of displacement of slab at the impact point for different deterministic models and different values of velocity (elastic behavior)

Velocity (m/s)	FEM	TP	Error (%)	MSM	Error (%)
	$u_3$ (mm)	$u_3$ (mm)		$u_3$ (mm)	
7.7	14.85	14.11	4.95	14.62	1.54
10.5	18.29	17.97	1.74	18.24	0.27
13.2	21.51	21.23	1.32	21.57	0.27
15.5	24.26	24.09	0.67	24.23	0.14
19.7	29.24	28.88	1.24	29.19	0.17
24.4	34.32	33.36	1.94	34.13	0.55

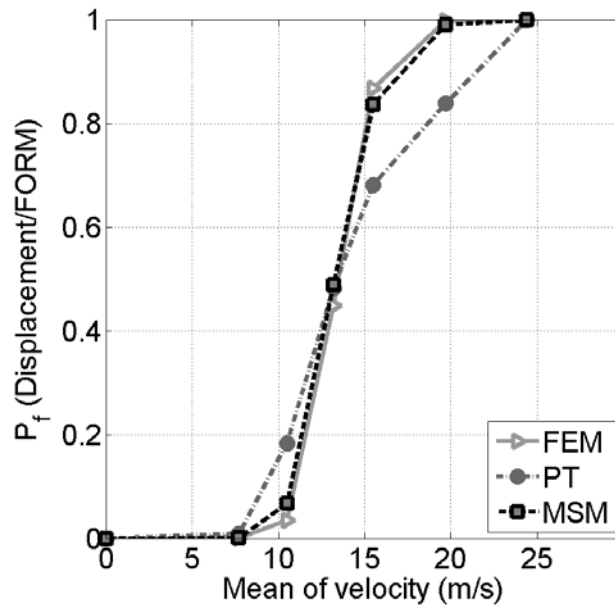


Figure 6.20: Failure probability with different deterministic models and displacement criterion

### 6.3.4.2 Comparison of probabilistic methods

For this application, two types of probabilistic methods are used and compared, namely approximation methods and simulation methods. As previously discussed in section 4.4.3, approximation methods such as FORM and SORM are based on an approximation of the limit state function, while simulation methods such as MC and IS are based on a number of samples of random variables to calculate failure probability. These methods are combined with the MSM and results are compared to failure probabilities obtained with the FEM combined with FORM in order to choose the most suitable probabilistic method to use in the parametric study. The MSM is used due to its reduced computational time which allows combining it with simulation probabilistic methods, and because it permits to accurately predict the physical response of slab as proven in the previous section. Table 6.14 shows that FORM coupled with the MSM gives the closest values of failure probabilities to those estimated with the numerical model. MC overestimates failure probabilities for velocities equal to 10.5 and 13.2 m/s, this may be related to the fact that MC necessitates a huge number of simulation for low probabilities range and that the transformation factor is considered as constant parameter for all samples generated by MC and is not calibrated in terms of slabs variables, such as slab dimensions, material densities and bars diameter.

Table 6.14: Comparison of probabilistic methods combined with the MSM for the displacement criterion

Velocity (m/s)	FEM	MSM			
	FORM	FORM	SORM	MC	IS
7.7	0.00016	0.00021	0.00001	-	0.00043
10.5	0.03469	0.06715	0.06542	0.023611	0.06924
13.2	0.44949	0.48965	0.49107	0.75781	0.47835
15.5	0.86815	0.83744	0.99508	0.84211	0.98103
19.7	0.99906	0.99149	0.99999	0.96552	-
24.4	1.0	1.0	1.0	1.0	1.0

### 6.3.4.3 Comparison of failure criteria

A comparison of different failure criteria defined in section 6.3.3 is important for a better understanding of the behavior of RC slabs subjected to impact with an elastic behavior of materials. Figure 6.21 shows failure probability in term of the mean of impact velocity for the different failure criteria considered for this application. It can be seen that the slab is more resistant to displacement and steel yielding, while it is less resistant to the contact force for the same values of impact velocity mean. In this case and for an optimal design, it is necessary to evaluate the maximum contact force value that the slab can sustain, as well as the impactor velocity for which this maximum value of force is reached. Once this velocity is determined, the performance of slab under displacement and steel yielding criteria is subsequently verified.

In this figure, the performance of slab regarding its capacity of dissipating impact energy is also examined. Unlike other criteria, failure probability decreases with the impact energy for this criterion as a result of the energy dissipated by steel and slab deformations that increase with velocity. The performance of slab in dissipating energy can be improved by considering the nonlinear behavior of concrete and steel, which allows modeling concrete damage and the onset of plastic deformations. It should be noted that this criterion does not indicate a failure mode of slab, it is used to study the energy transmitted to RC slabs during an impact phenomenon.

### 6.3.4.4 Parametric study

The following parametric study is performed in the aim of investigating the effect of different input variables on the estimation of failure probability for the application of impacted RC slabs. For this purpose, the MSM is selected because, among the deterministic models proposed for this problem, it is the most efficient in term of computational effort for a reliability analysis. In addition, the MSM model is verified to accurately predict the displacement of slab at the impact point. Thus, the parametric study is carried out by combining the MSM with FORM for the displacement criterion and the effect of several input variables on the reliability of impacted RC is examined. Variables such as slab dimensions, concrete density, steel bars diameter, impactor mass and rigidity of slab are considered and failure probability is estimated for different values of the mean of the variable studied.

**Slab length** Failure probabilities are calculated for several mean values of the slab length that varies between 2.35 and 12 m. Figure 6.22 shows that, for a simply supported slab, reducing the slab length leads to an increase in failure probability for the displacement criterion and that this probability depends on the impactor velocity. Thus, an optimal design of RC slabs requires to properly determine the structure dimensions and choose the appropriate values depending on impact velocity in order to improve the performance of slab. It can be seen that a low variation in length

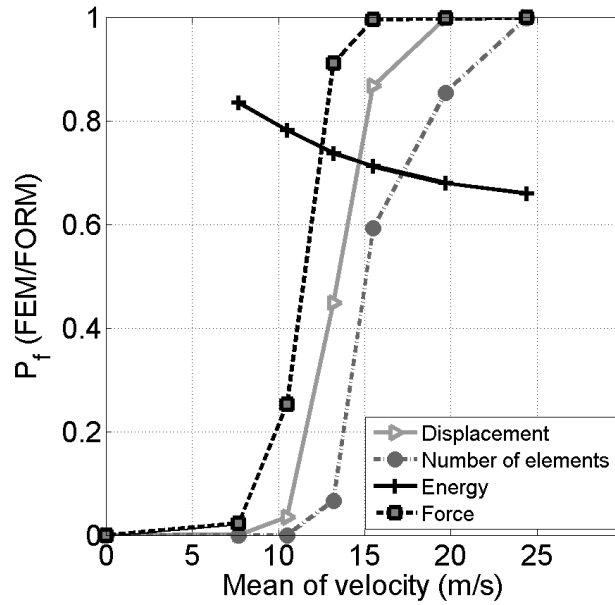


Figure 6.21: Comparison of different failure criteria in term of impact velocity mean

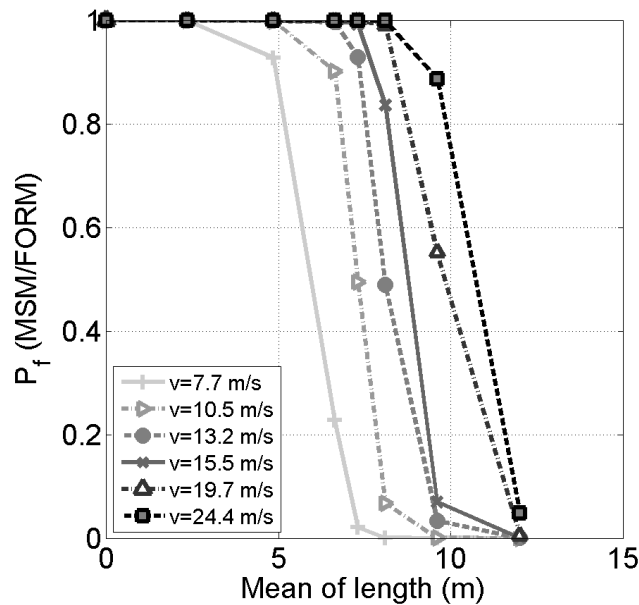


Figure 6.22: Effect of the mean of slab length for the displacement criterion

leads to an important variation in failure probability, this is due to the fact that the displacement threshold used to define the displacement failure criteria is directly related to the slab length and taken equal to  $L/250$ . This variation is less significant in the case of slabs with higher length value since the displacement threshold is higher.

**Slab thickness** Figure 6.23 shows failure probabilities of slabs having the same length of 8.1m and different mean values of thickness. It can be seen that the slab thickness directly affects the reliability of RC slabs, and that the nominal value of 0.5 initially chosen for slab thickness is sufficient to ensure

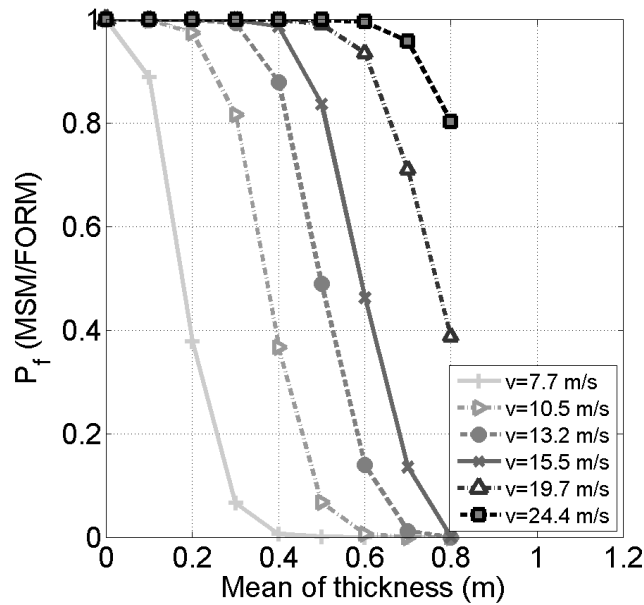


Figure 6.23: Effect of the mean of slab length for the displacement criterion

the reliability of slab only in the case of impact velocity less than 7.7 m/s ( $P_f = 10^{-3} - 10^{-4}$ ). For higher velocities, a higher value of thickness should be considered. The results observed indicate that for long and thin slabs, bending failure mode dominates. Thus, the displacement of slab at the impact point is more significant and failure probability of exceeding a constant displacement threshold increases with a reduction in thickness.

**Concrete density** The effect of the mean of concrete density is small in comparison to that of the slab length and thickness, especially in the cases where  $v=7.7$  m/s and  $v=24.4$  m/s (Figure 6.24). Therefore, this variable can be considered as deterministic variable in the case of low failure probabilities.

**Steel bars diameter** In order to study the effect of steel bars diameter on the reliability of impacted RC slabs, different diameters of reinforcement are considered while retaining the same number of longitudinal and transversal bars. Figure 6.25 shows that the diameter of bars has an inconsiderable influence on failure probability for all the impact velocity values considered. However, this influence should be examined in the case where the plastic behavior of steel is introduced in the analysis of RC slabs.

**Impactor mass** Figure 6.26 illustrates the variation of failure probability in term of the mean value of the impactor mass. It can be seen that the mass has the same influence as the impactor velocity and failure probability increases with the mean value of mass. For  $v=7.7$  m/s, failure probability remain in the domain of low probabilities for a mass less than 6000 kg. However, for velocities higher than 7.7 m/s, the effect of slab becomes more significant and failure probability varies greatly in term of the mean value of mass. Increasing the impactor mass and velocity lead to an increase in impact energy, so a slab with the same dimensions and material properties lose its performance to sustain the impact force applied.

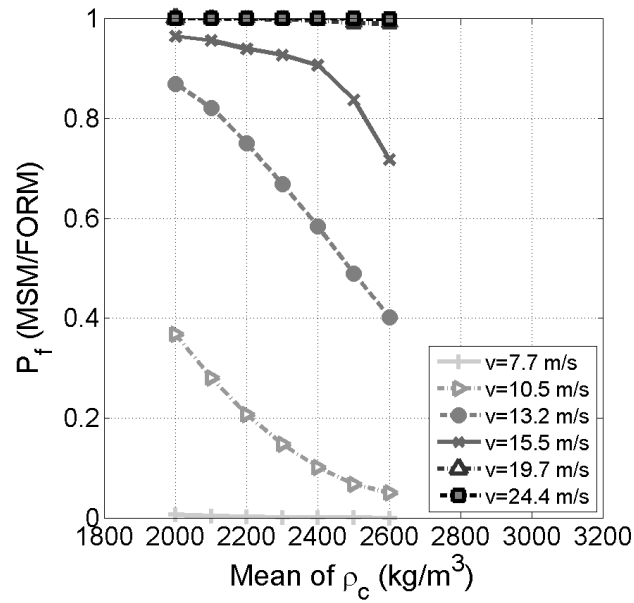


Figure 6.24: Effect of the mean of concrete density for the displacement criterion

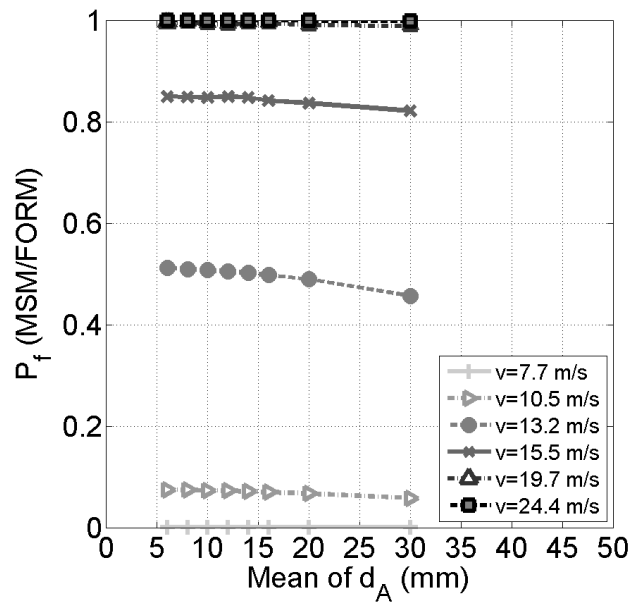


Figure 6.25: Effect of the mean of steel bars diameter for the displacement criterion

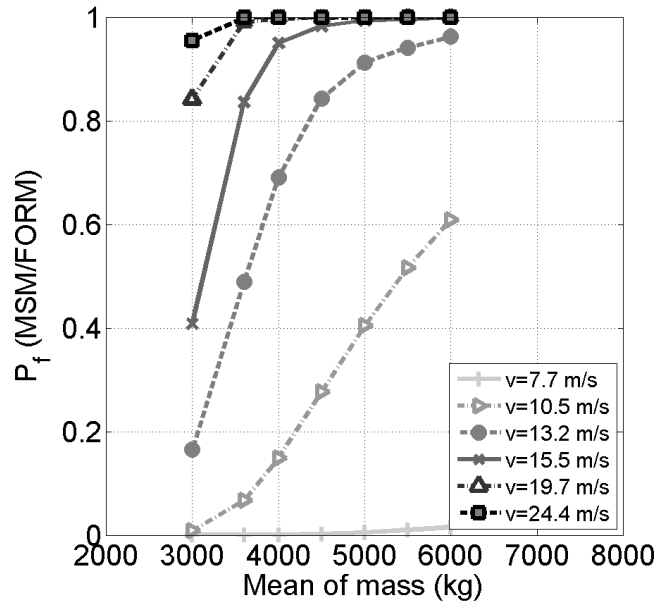


Figure 6.26: Effect of the mean of impactor mass for the displacement criterion

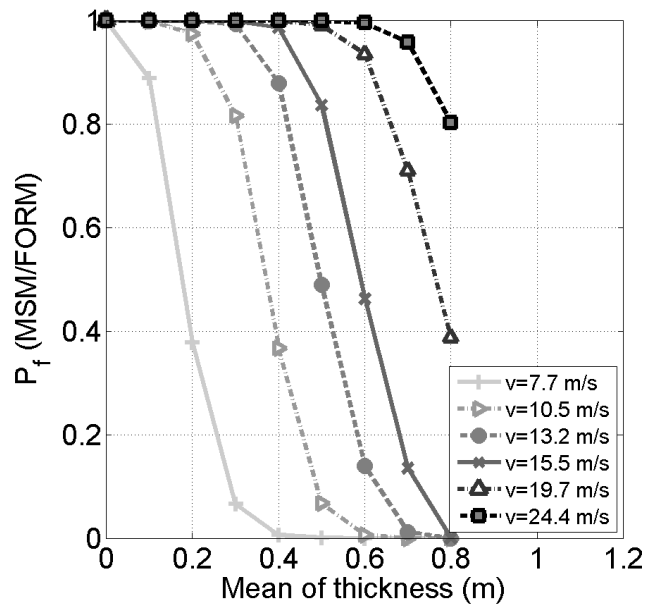


Figure 6.27: Effect of the mean of slab stiffness for the displacement criterion

**Slab rigidity** One of the most important parameters in a mass-spring model is the rigidity of the spring that represents the stiffness of slab. Figure 6.27 shows that increasing the slab stiffness results in a decrease of failure probability and improve the slab performance for a displacement criterion. This can be due to the fact that a more rigid slab is subjected to smaller displacement, hence its failure probability for a displacement criterion is lower. RC slabs stiffness can be increased depending on the slab dimensions and material properties.

### 6.3.5 Conclusion remarks

In this section, an application of reliability analysis to RC slabs under low velocity impact assuming a flexural mode of failure and an elastic behavior for steel and concrete is presented. Several criteria of failure related to the displacement of slab at the impact point, the peak force of impact, stresses in reinforcement, and the impact energy absorbed by the slab are considered. Probabilistic methods such as FORM, SORM, MC and IS are used to assess failure probability. In order to study the dynamic effect of impact applied to RC slabs, 3 deterministic models are used: a 3D FEM simulated with Abaqus/Explicit, a simplified model based on the plate theory and a two degrees of freedom mass-spring system. The aim is to select the most appropriate model to use in RC slabs reliability analysis, while accurately representing the mechanical behavior of the slab studied and reducing the computational cost to the minimum. The analytical MSM is seen to be very effective in predicting the same values of slab displacement at the impact point as the numerical model, as well as in estimating failure probabilities very similar to those obtained with the FEM for a displacement criterion. The MSM is more convenient than numerical models to use in reliability analysis in term of computational effort. Thus, it is used in a parametric study in order to investigate the effect of several input parameters of the deterministic model on the estimation of failure probability of RC slabs. The impact velocity is the most influential variable, followed by the slab length, thickness and stiffness. Results obtained for this type of problem can be useful for the design of RC slabs subjected to impact since they permit to identify the values of input variables for which failure probability is not in the range of low probabilities.

Studying the response of impacted slabs assuming an elastic behavior of materials represents a preliminary step in the procedure of evaluating the reliability of RC slabs under low velocity impact. This application is initially considered to simplify the problem and to avoid complicating structural reliability analysis of slabs as a first step. However, it is clear that nonlinearities due to materials behavior have a significant effect on RC slabs response, in particular that cracking in concrete under tension and plastic deformations in concrete at the impact zone and in reinforcement reduce significantly the peak of contact force obtained with an elastic model. The effect on nonlinearity due to material properties is discussed in the next section.

## 6.4 Application to RC slab subjected to impact - Nonlinear behavior

### 6.4.1 Deterministic models

Deterministic FEM model used for the slab subjected to accidental dropped object impact within nuclear plant building assuming a nonlinear behavior of materials is detailed in section 5.4, while the simplified model used consists of a two degrees mass-spring model which is detailed in section 5.4.2.

### 6.4.2 Probabilistic model

In the case when the nonlinear behavior of materials is considered in the FEM, the variables which may be subjected to statistical variations in RC slabs under impact can be classified into five categories:

1. Dimensional variables related to the geometric properties of the slab: length, width and thickness of the slab.
2. Dimensional variables related to the position of reinforcement and its size: concrete cover and diameter of bars.

3. Variables related to the concrete properties: Young's modulus, density, compressive strength and tensile strength of concrete.
4. Variables related to the steel properties: modulus of elasticity and yield strength of steel.
5. Variables related to the impactor and its kinetic energy: radius, mass and velocity of the impactor.

In this study, the probabilistic characterization of random variables is based on some literature reviews mentioned in previous section 4.6 and in which the statistical descriptions of material properties and geometry variables for reinforced concrete structures are relatively well documented. For variables related to the impactor, statistical descriptions that represent the variation of accidental dropped objects impact during handling operations within nuclear plant buildings are not available in the literature. Table 6.15 represents the random variables adopted in the present study, their probability distribution, their mean and COV, as well as the variables to be considered as deterministic.

#### 6.4.2.1 Concrete properties

As previously mentioned, stress-strain curves of concrete in tension and compression considered to study the reliability of RC slabs under impact assuming a nonlinear behavior of materials are described as stress-strain relations. These relations vary in terms of the tensile strength,  $f_t$ , and the compressive strength,  $f_c$ , respectively. Thus, the variation of these curves depends on the statistical description of  $f_t$  and  $f_c$ .

**Compressive strength of concrete** Mirza *et al.* [123] estimated the mean value of the compressive strength to be equal to  $0.8f_c$  assuming that  $f_c$  follows a normal distribution and the COV can be considered to vary between 0.15 and 0.18.

**Tensile strength of concrete** Tensile strength mean value is chosen according to Pandher [153] assuming that it is approximately one tenth of the concrete compressive strength. The COV is taken equal to 0.18 according to Mirza *et al.* [123] that studied the variation of concrete tensile strength in-situ. Mirza *et al.* found that  $f_t$  follows a normal distribution.

**Young's modulus** The elastic modulus of concrete is generally considered as a normally distributed variable with a COV of 0.1 [123]. Collins and Mitchell [43] approximated the Young's modulus in MPa by  $E_c = 5500\sqrt{f_c}$ .

#### 6.4.2.2 Steel properties

As previously mentioned, stress-strain curve of steel considered to study the reliability of RC slabs under impact assuming a nonlinear behavior of materials are described as stress-strain relations. These relations vary in term of the yield strength,  $f_y$ . Thus, the variation of this curve depends on the statistical description of  $f_y$ .

**Yield strength of steel** The distribution of steel yield strength is chosen according to Mirza and MacGregor [125] assuming that it follows a normal distribution. The mean of yield strength is generally considered equal to the nominal value with a COV of 0.08-0.1.

**Modulus of elasticity** The modulus of elasticity of steel is considered as deterministic variable due to its small dispersion with respect to other variables.

Table 6.15: Deterministic variables, random variables and their statistical descriptions

Variables	Nominal	Mean	COV	PDF	Ref.
<b>Geometric properties of the slab</b>					
Length, $a$	8.1 m	Deterministic			[82, 168]
Width, $b$	4.85 m	Deterministic			[82, 168]
Thickness, $e$	0.5 m	0.5	0.05	Normal	[127]
<b>Position and size of reinforcement</b>					
Concrete cover, $c$	3.5 cm	Deterministic			-
Bars diameter, $d_A$	20 mm	20	0.024	Normal	[126]
<b>Concrete properties</b>					
Compressive strength, $f_c$	40 MPa	$0.8f_c$	0.15	Normal	[123]
Density, $\rho_c$	2500 $kg/m^3$	Deterministic			-
Tensile strength, $f_t$	3.5 MPa	$f_c/10$	0.2	Normal	[153]
Young's modulus, $E_c$	35 GPa	$5500\sqrt{f_c}$	0.08	Normal	[91, 123]
<b>Reinforcement properties</b>					
Yield strength, $f_y$	500 MPa	500	0.05	Normal	[126]
Modulus of elasticity, $E_s$	200 GPa	Deterministic			[110]
<b>Impactor variables</b>					
Radius, $r$	15 cm	Deterministic			lack of information
Mass, $m$	3600 kg	3600	0.1	Lognormal	lack of information
Velocity, $v$	7.7 m/s	7.7	0.1	Lognormal	lack of information

#### 6.4.2.3 Dimensions

Only the thickness of slab is taken as random variable in the case of impacted slabs assuming a nonlinear behavior of materials. It is considered as normally distributed with a mean value equal to its nominal value and a COV of 0.05 [127]. The length and width are described as deterministic variables since slab dimensions are important, thus the effect of their uncertainty is negligible [82]. Steel bars diameter is also considered as a dimensional random variable and is modeled as a normal distribution with a mean equal to the nominal diameter and a COV of 0.024. The variation of concrete cover is not taken into account in this study.

#### 6.4.3 Failure criterion

Several output variables may be obtained as result from a finite element model. These variables allow defining limit state functions corresponding to the failure criteria studied. However, the only variable of interest considered for impacted slabs assuming a nonlinear behavior of materials is the displacement of the impact point on the front face of the RC slab,  $u$ . Thus, a serviceability limit state function can be written as:

$$g = u_{max} - u \quad (6.14)$$

where  $u_{max}$  is the displacement threshold and  $u$  represents the maximum displacement of the slab at the impact point. Since no information available in the literature to choose the value of  $u_{max}$ , a deterministic parametric study is performed in order to estimate the displacement for which yielding in tensile steel occurs. The displacement of steel yielding is evaluated for different impact energies, and it is found that the stresses in reinforcement exceed the yield strength for a displacement of 50 mm as mean value.

Table 6.16: Factorial experiment factors and mass-spring model parameters

Factors	$e$	$d_A$	$v$	$m$
Low level	0.3 m	6 mm	2.5 m/s	2000 kg
High level	0.7 m	30 mm	13.2 m/s	6000 kg
$m_s$	$k_s$	$c_s$	$k_c$	$c_c$
kg	N/m	N.s/m	N/m	N.s/m
$0.015M_{slab}$	$f(e, d_A, v, m)$	$1.7e^5$	$2e^9$	$1e^5$

Table 6.17: Failure probability with FE and mass-spring models and displacement criterion

$v$ (m/s)	$m$ (kg)	FE model	Mass-spring model	
		FORM	IS	MC
<b>Constant impact energy</b>				
7.7	3600	0.6824	0.6731	0.6557
10.5	1936	0.5475	0.5167	0.5311
13.2	1225	0.4150	0.7539	0.3895
<b>Constant mass</b>				
5.0	3600	0.1861	0.2152	0.1853
10.5	3600	0.7073	0.7288	0.7226
<b>Constant velocity</b>				
7.7	2000	0.2992	0.2976	0.2646
7.7	5000	0.7247	0.6883	0.6927

## 6.4.4 Discussion of results of slab reliability (Nonlinear behavior)

### 6.4.4.1 Comparison of strategies

In order to find the best fit with the FEM and estimate the effect of the slab and impactor properties on the mass-spring model parameters, a  $2^k$  factorial experiment is designed in the aim of expressing the slab stiffness in terms of slab thickness, steel diameter, mass and velocity of the impactor. Table 6.16 represents the low and high level for the specified factors, but also the values of the mass-spring model parameters which are found to give similar results to the FEM.

As discussed earlier, the two strategies proposed in this study to reduce the computational effort of reliability analyses consist in using simulation probabilistic methods with the mass-spring model and FORM with the finite element model. A comparison of these two strategies leads roughly to the same value of failure probability, except in the case of an impact velocity of 13.2 m/s and a mass of 1225 kg (Table 6.17). This may be related to the samples generated by IS and MC and which do not correspond to the mass and velocity selected range for the design of experiments. However, the second strategy is more time consuming since at least 36 simulations of the FEM are needed in order to assess the failure probability with an average time of 45 minutes per simulation. As a result, the first strategy is more effective in term of computational cost but cannot be used if the simplified model is not proven to be able to predict the behavior of the RC slab and give the same results as the FEM.

### 6.4.4.2 Parametric study

**Impactor velocity** Figure 6.28 shows failure probabilities for different values of velocity mean for the displacement criterion. As can be seen, failure probability increases with the impact velocity for

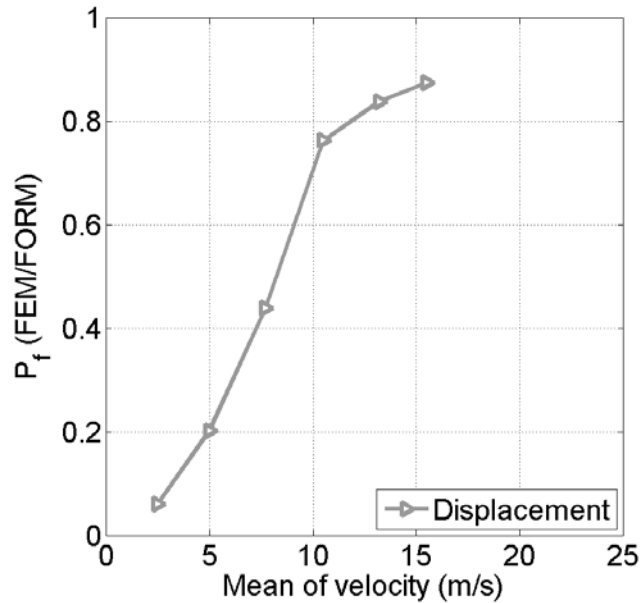


Figure 6.28: Effect of the mean of impactor velocity for the displacement criterion ( $m=3600$  kg)

the displacement criterion and impact duration increases with the impact energy. The displacement at impact point can be related to the overall deflection of slab, to the motion of shear cone during impact, or to spalling that occurs at the upper surface of slab. RC slabs are observed to undergo flexural failure under low impact velocities [119] along with scabbing. The local response of scabbing can dominate the slab behavior for impacts with low velocity as they are classified as short impact time according to [149, 150]. Furthermore, shorter impact duration leads to less critical yielding in steel [188], hence less displacement values are observed. However, under high impact velocities shear type failure occurs, but the impactor could perforate the slab if its velocity is sufficiently high. Therefore, higher displacements are observed at the impact point leading to an increase in failure probability with impact velocity. According to [149] (see Figure 2.3), high-velocity impacts can be associated with short impact times or long impact times depending on the slab stiffness and material properties. Consequently, for long impact times the displacement at impact point can be involved due to an overall structural response that is affected by the boundary conditions and slab size, and governed by several waves reflection through the thickness reaching slab boundaries. For short impact times, the local damage failure modes that govern the slab response are caused by flexural and shear waves with no significant propagation through the thickness. As can be seen, it is very difficult to predict the slab behavior in term of the mean of impactor velocity as the response of RC slabs under impact is significantly influenced by several parameters, including slab and impactor characteristics. Displacement at the impact point in case of perforation are more important than in case of flexural failure, thus it is important to design RC slabs to withstand smaller displacement values under impact to prevent perforation and scabbing.

**Impactor mass** As previously discussed, slabs subjected to large-mass low-velocity impacts have different behavior than slabs subjected to small-mass high-velocity impacts. This can be seen in Figure 6.29 that shows how the reliability of RC slabs subjected to impact is influenced by the mean value of the impactor mass. The mass has the same influence as the impactor velocity and failure probability increases with the mean value of mass. Values of maximum displacement and impact duration are more significant for higher masses and yielding in steel occurs leading to more

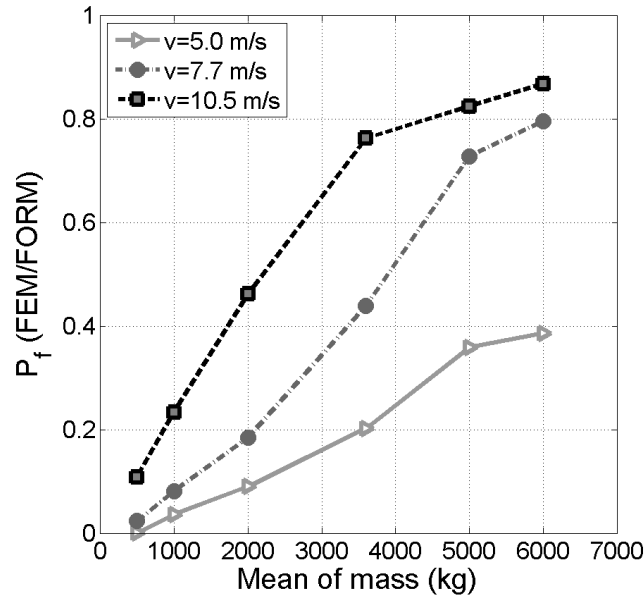


Figure 6.29: Effect of the mean of impactor mass for the displacement criterion

damage in the slab for higher impact energy. Impacts of large mass and low initial velocity involve an overall response of the RC slab as the dominating flexural waves reach the boundaries during the impact duration. This type of impact is classified as long impact times according to Olsson [149] and local damage has small effect on slab response. Conversely, impacts of small mass and high velocity cause deformation at a small zone surrounding the impact point leading to more localized deflection. Thus, the slab undergoes smaller displacements for smaller mass and failure probabilities for the displacement criterion increases with the mean of the impactor mass. Accordingly, impacts with  $v=5$  m/s and  $m > 3600$  kg can be classified as large-mass low velocity impacts using Abrate classification [9]. However, this classification does not satisfy the criterion of Olsson [149] that indicated that small-mass impacts correspond to impactor masses less than one fifth of the mass of the slab. The ratio of the mean of the impactor mass to the mean of the slab mass is always less than  $1/5$  for all the mean values of the impactor mass considered. According to Olsson criterion all cases studied must be classified as small-mass impacts. This is in contrast with Abrate classification, hence it is necessary to take into account all parameters present in an impact problem in order to be able to properly estimate the behavior of impacted RC slabs. It should be noted that small masses are more critical for a given impact energy because they result in higher impact loads and less energy absorbed by the slab.

**Slab thickness** Figure 6.30 shows how the reliability of RC slabs subjected to impact is influenced by the mean value of the slab thickness. Other values of random variables remain the same as defined in Table 6.15, including the length and width of the slab and the reinforcement ratio. As illustrated in this figure, increasing the thickness leads to lower failure probabilities for the different mean values of impact velocity considered as the slab deflection becomes less significant for larger thicknesses. Increasing the thickness results in increasing the slab stiffness as well as the compression concrete area, which leads to higher impact force and shorter impact times. In this case, a few compressive wave reflections through the thickness are observed and the damage is initiated at the early stages of impact. According to Abrate's criterion [9] that classify impact events according to the ratio of impact velocity versus the speed of propagation of compressive waves through the thickness direction, the impact problem with higher thickness can be classified as high-velocity impact depending on the

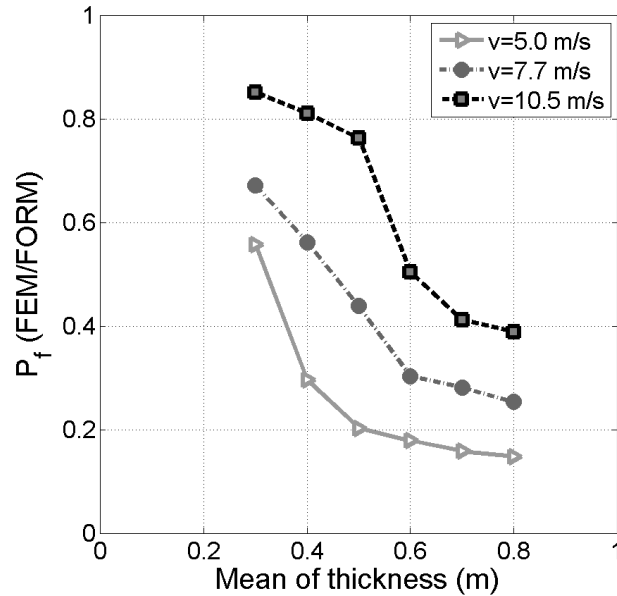


Figure 6.30: Effect of the mean of slab thickness for the displacement criterion

impact velocity. For  $v=5.0$  m/s, the problem can be classified as low-velocity impact for thickness value less than 0.5 m as the stress wave propagation through the thickness has no significant role and the slab would likely fail due to its overall bending behavior. For these thickness values and a velocity equal to 5.0 m/s, the response of slab is influenced by its dimensions and boundary conditions and the impact duration is described as long impact times according to Olsson [149] (see Figure 2.3). The reinforcement has more influence on the slab resistance during flexural failure mode, and the slab may undergo higher displacements at the impact point. For  $v=5.0$  m/s and thickness values higher than 0.5 m, the impact can be classified as high-velocity impact according to Abrate's criterion [9] and the impact duration can be described as short to very short impact times according to Olsson [149] (see Figure 2.3). For  $v=7.7$  m/s, the problem can be considered as high-velocity and short impact time for thickness value higher than 0.6 m. For  $v=10.5$  m/s, the problem can be considered as high-velocity and short impact time for thickness value higher than 0.8 m. It should be noted that increasing the slab thickness improves the slab performance to perforation and results in increasing the ballistic limit defined as the lowest initial velocity of the impactor causing complete perforation [9].

**Compressive strength of concrete** In a reliability analysis, it is important to investigate the effect of material parameters on failure probability estimation and how they contribute to the strength of RC structures. Only the mean value of the compressive strength is considered since those of the tensile strength and the modulus of elasticity are estimated in term of the compressive strength. Thus, an increase in the mean value of the compressive strength leads directly an increase in tensile strength and modulus of elasticity mean values. As can be seen in Figure 6.31, failure probability falls off with the mean value of the compressive strength. The compressive strength contributes significantly to the slab rigidity, so that increasing the compressive strength allows lower displacement at the impact point of the slab and yielding in steel is reduced. Nevertheless, increasing slab rigidity leads to higher peak value for the impact force and punching shear failure mode could occur. A high strength concrete improves the slab performance in term of perforation compared to normal strength concrete since higher impactor velocities are needed to perforate the slab in this case. The slab resistance to penetration can be enhanced by increasing the compressive strength of concrete.

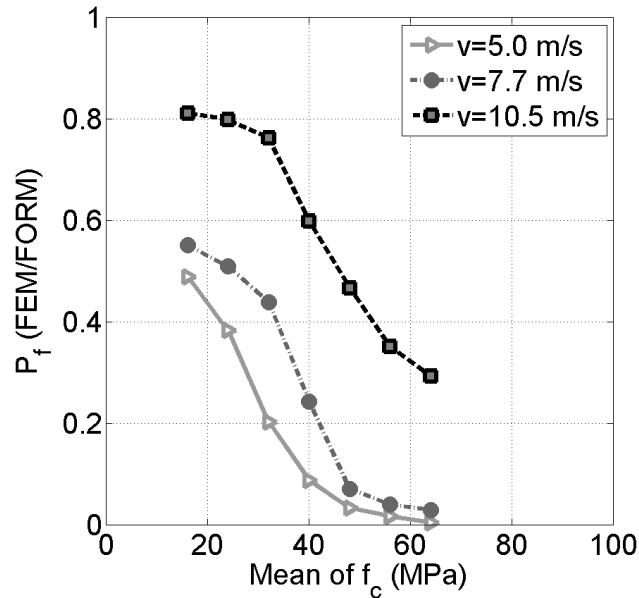


Figure 6.31: Effect of the mean of concrete compressive strength for the displacement criterion

Therefore, lower displacement values are observed for higher compressive strength mean values leading to lower failure probabilities. However, it can be seen that for  $v=5.0$  m/s and  $v=7.7$  m/s, using concrete with compressive strength greater than 50 MPa does not seem to give a significant improvement in slab reliability for the displacement criterion. Thus, using the appropriate concrete properties is important for an optimal design of impacted RC slabs to resist local failure modes, including spalling, scabbing, penetration and perforation. As in this reliability analysis increasing the concrete compressive strength means an increase in its tensile strength, scabbing takes place in a later phase of impact for the same impact conditions. This is due to the fact that scabbing occurs when the tensile stresses generated by the tensile reflected wave produced during impact become equal or higher than the concrete tensile strength, and higher value of tensile strength delays the scabbing local failure mode.

**Yield strength of steel** The influence of yield strength of steel on failure probability is investigated for the displacement criterion proposed for this application. As can be seen in figure 6.32, the yield strength of steel has no influence for  $v=5.0$  m/s and  $v=7.7$  m/s because the displacement criterion proposed in this study is chosen in order to not allow yielding in steel. The displacement threshold is estimated for slabs with reinforcement of yield strength of 500 MPa. Thus, for higher yield strength mean value, failure probability decreases for  $v=10.5$  m/s since the problem is classified in this case as long impact times and the overall response of slab dominates.

**Reinforcement ratio** In order to study the effect of reinforcement ratio on the impacted RC slabs reliability, failure probability is calculated by considering several mean values of the steel bars diameter (Figure 6.33). Other values of random variables remain the same as defined in Table 6.15, including the slab geometry and impact conditions input variables. In addition, the effect of numbers of transversal and longitudinal bars on failure probability for the displacement criterion is studied (Figure 6.34). Those numbers are presented in the study as deterministic variables. Reinforcement ratio depends on the steel bars diameter value as well as on the number of reinforcing bars in the slab, thus increasing the steel diameter or the number of reinforcing bars leads to an increase in

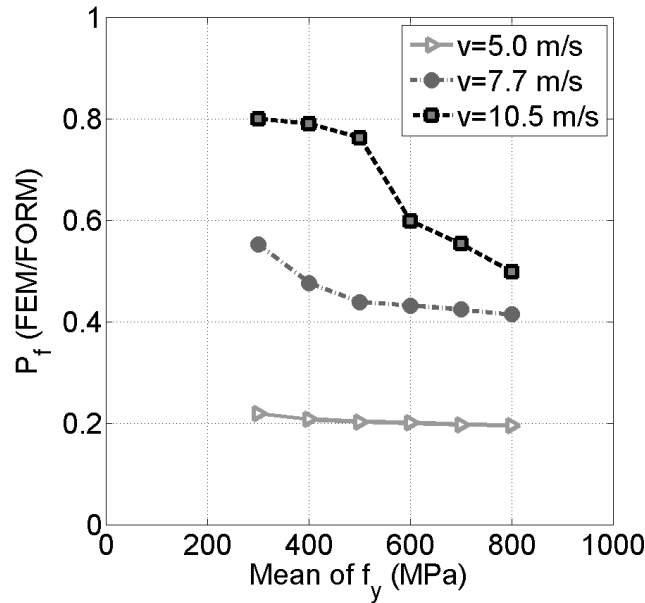


Figure 6.32: Effect of the mean of steel yield strength for the displacement criterion

reinforcement ratio. It can be seen that the number of transversal bars has no considerable effect for  $v=5.0$  m/s and  $v=7.7$  m/s, but it influences the magnitude of failure probability for  $v=10.5$  m/s up to 20 transversal reinforcing bars per layer. However, longitudinal reinforcing bars have more influence on the slab deflection, hence a higher number of longitudinal bars reduces the displacement at the impact point and results in lower failure probabilities. The slab stiffness increases with the reinforcement ratio and the flexural failure mode represents the most critical parameter to design longitudinal reinforcement, especially under high impact velocities. Thus, it can be concluded that the 20 longitudinal bars initially chosen for each of the upper and bottom reinforcement layers are not sufficient to ensure its reliability for the displacement criterion nor to have an optimal design under bending mode. This may be also the reason why steel bars diameter has no significant effect on the slab reliability, hence it will be interesting to examine its effect in case where the slab is reinforced with more than 20 longitudinal bars per layer. Although reinforcement ameliorates the ductility of RC slabs due to its plasticity, the steel ratio should be chosen with attention since a strongly reinforced slab may fail under punching shear failure mode when subjected to high velocity impacts. Consequently, it is important to design RC slabs under impact in a way which reduces the reinforcement ratio, but also ensures that no failure or large deflection would occur during impact.

**Stirrups** As previously indicated, the Python script written for the slab subjected to dropped object within nuclear power plant enables to add stirrups to the FEM. Therefore, the effect of reinforcing the slab with shear reinforcement on failure probability is also examined (Figure 6.35). It is found that for low impact velocities, stirrups do not improve the performance of slab for the displacement criterion proposed in the case where nonlinearities due to material behaviors are considered in the FEM. This may be due to the thickness of slab that can be described as thick slab. In the case of thick slabs subjected to low velocity impacts, cracks are first induced at the impact zone and then progress through the thickness without leading to a reversed shear cracks pattern. However, higher velocities result in shear type failure mode for thick and stiffer slabs. This can be illustrated in Figure 6.35 and, as a consequence, failure probability decreases for values of mean velocity greater or equal to 10.5 m/s if shear reinforcement is considered in the FEM. It can be also expected that stirrups have more influence on the slab displacement in case of thin slabs

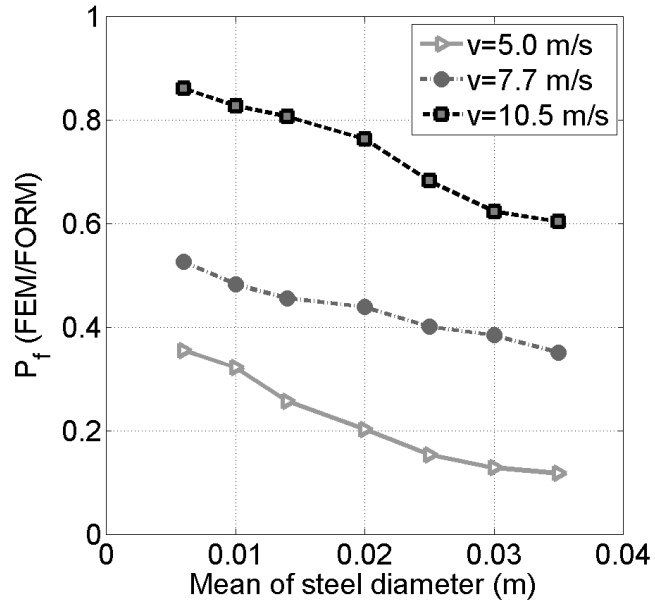


Figure 6.33: Effect of the mean of steel diameter for the displacement criterion

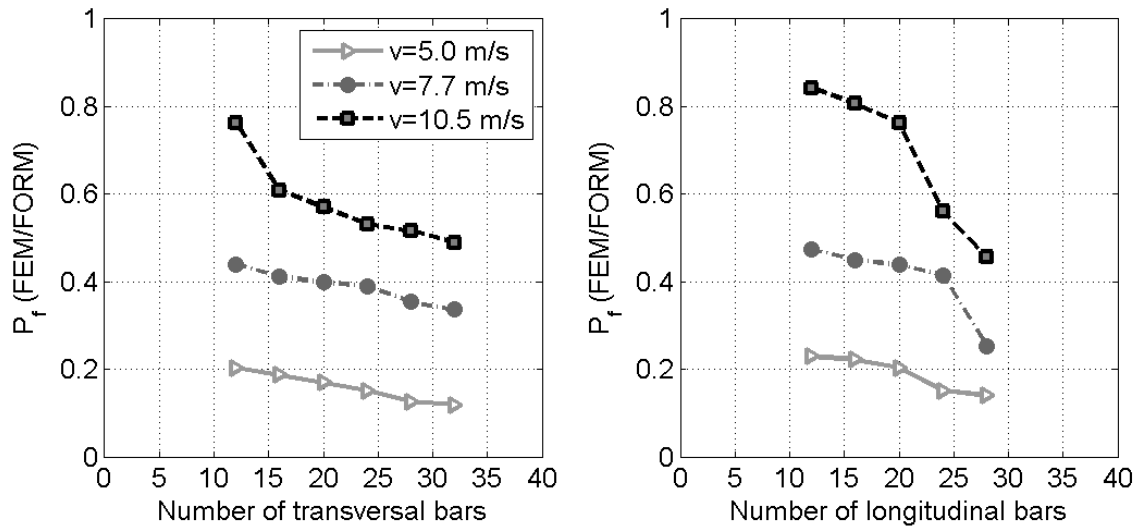


Figure 6.34: Effect of numbers of transversal and longitudinal bars for the displacement criterion

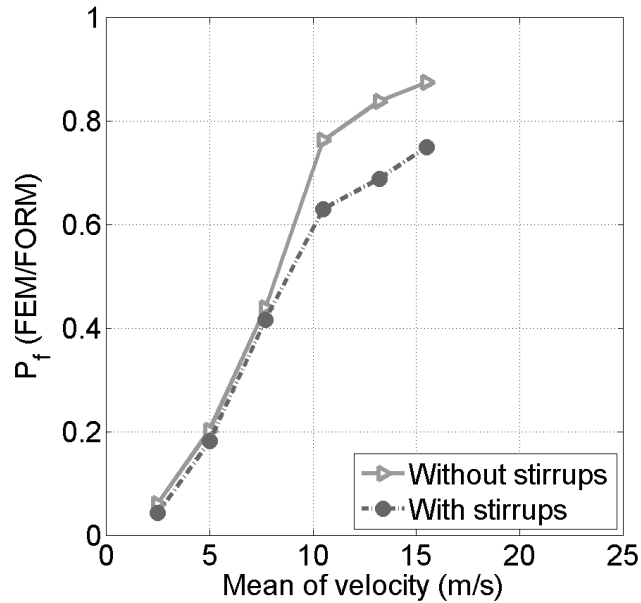


Figure 6.35: Effect of stirrups for the displacement criterion

under low velocity impact since they reduce shear cracks reversed from the slab bottom surface due to bending stresses. If a RC slab is designed to resist punching shear failure mode under impact, it is necessary to properly determine shear reinforcement which can improve the slab resistance by varying the failure mode from punching shear mode into an overall flexural failure mode

**Boundary conditions** To investigate the effect of varying boundary conditions of the slab on its reliability under an impact loading, four boundary conditions are examined as follows:

- The bottom four edges of the slab are considered as simply supported (pinned edges).
- The four faces of the slab in the  $xz$  and  $yz$  planes are considered as simply supported (pinned faces).
- The bottom four edges of the slab are considered as clamped (fixed edges).
- The four faces of the slab in the  $xz$  and  $yz$  planes are considered as clamped (fixed faces).

As can be seen in Figure 6.36, boundary conditions has a negligible effect on slab response for low velocities ( $v=5.0$  m/s and  $v=7.7$  m/s). This is due to the fact that in the case of impactors dropped at low velocity of a few m/s on large slabs, main flexural and shear waves do not reach the boundary, which can be associated with high-velocity impacts according to [148] and very short impact time according to [149]. As a result, failure probability increases with the mean of velocity as the slab undergoes higher displacements and tends to fail under flexural failure mode. For  $v=10.5$  m/s, the displacement of slab at the impact point is more important for the pinned edges boundary condition as the slab shows considerable rise in its rigidity for pinned faces and fixed boundary conditions. In this case, the problem is found to be dependent of boundary conditions and the time that main waves need to reach structure boundaries is less than the impact duration. Thus, it can be classified as low-velocity impact according to Abrate's criterion [9] and long impact time according to [149].

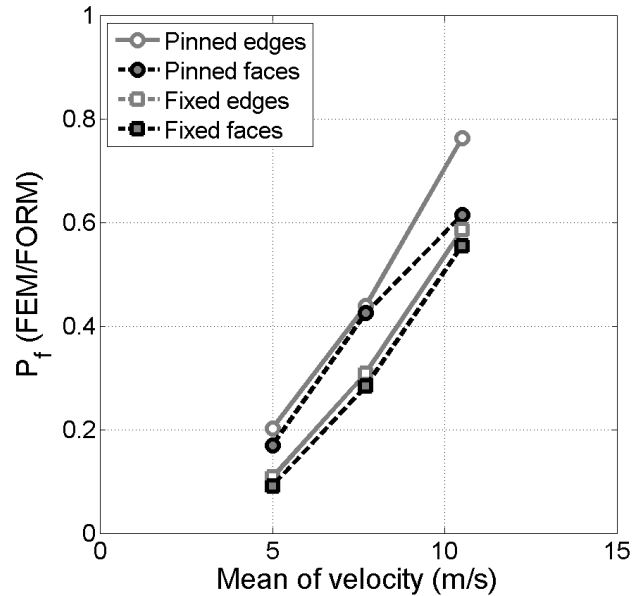


Figure 6.36: Effect of boundary conditions for the displacement criterion

**Impact position** As previously indicated, the Python script written for the slab subjected to dropped object within nuclear power plant enables to easily change the impact position in the FEM. Therefore, failure probability corresponding to displacement criterion is estimated for ten different impact point positions in the directions of the width, the length and the diagonal (Figure 6.37). The results show that the most critical point for the response of slabs subjected to impact loading is at the center of the slab. The more the impact point is close to supports, the more the slab is rigid and consequently, the displacement is lower.

#### 6.4.5 Conclusion remarks

The present case of study proposes strategies in order to reduce the computational time of reliability analyses. The first strategy consists in using analytical models instead of finite element models. Due to the low computational time of the simplified model proposed, probabilistic methods like Monte Carlo and importance sampling which require too large number of simulations of the deterministic model are coupled with this model. However, this strategy does not allow taking into account all random variables that affect the slab response to impact loading and can be only used when the simplified model is verified with the finite element model. Alternatively, the second strategy consists in assessing failure probability from a small number of simulations using FORM with the finite element model. Despite its computational cost, this strategy allows a better understanding of the slab behavior when subjected to low velocity impact. The results of failure probability show high values which are not acceptable for structural failure, this confirms that this type of loading must be considered in the design of RC slabs. Therefore the slab dimensions, material parameters and reinforcement ratio must be modified and evaluated in order to get better reliability of RC slabs.

## 6.5 Application to containment building of nuclear power plant

The long term behavior of a prestressed concrete structure like nuclear power plants, is affected by the delayed deformations that could initiate cracks, induce prestressing losses and result in a redistribution of stresses in the structure. They could also be the cause that the structure does

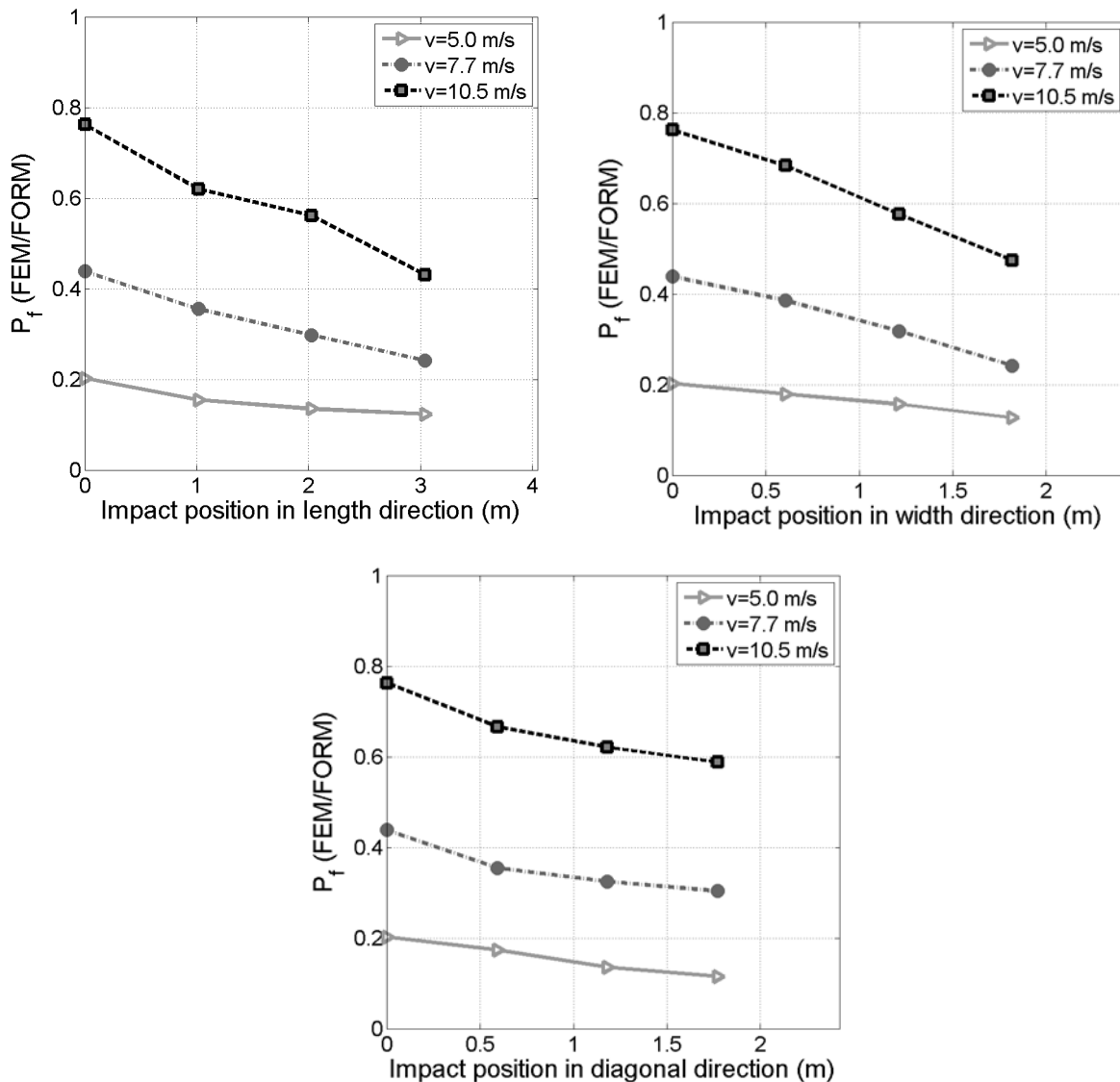


Figure 6.37: Effect of impact position for the displacement criterion

not perform its functional requirements. The evolution of creep and shrinkage deformations is the main cause of the loss in prestress in cables due to the reduction in the prestressing force and, consequently, the crack resistance of the interior wall of the nuclear power plant reduces. Thus, studying the behavior of a nuclear power plant is important to evaluate the safety of the nuclear facilities, i.e. maintaining the stability of the containment under different types of internal or external aggressions during service or accidental loadings. A nuclear power plant consists of a RC internal containment building and a prestressed external containment building (Figure 6.38). The external containment building in which the nuclear reactor is enclosed from natural or accidental aggressions, while the internal containment building protects the surrounding environment in case of a nuclear accident. The internal containment building could be covered with a waterproof coating in order to control the rate of leakage.

A prestressed containment building is designed to resist the increase of internal pressure in case of accidental situations. It is tested at least once every 10 years in order to experimentally verify the rate of leakage. These periodic surveillance tests are performed in the aim of examining the

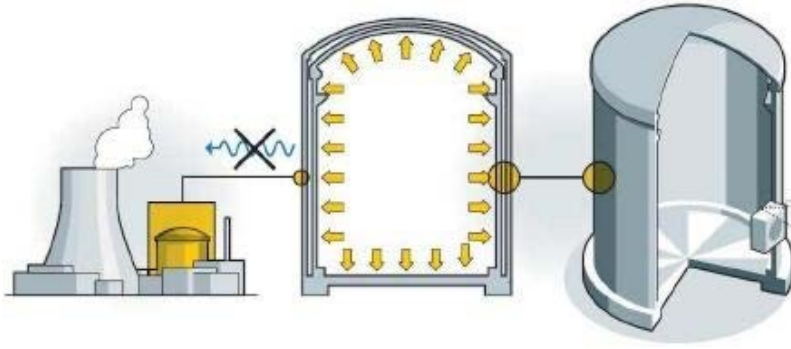


Figure 6.38: Containment building [161]

containment behavior in case of an accident and measuring the rate of leakage that increases when the loss in prestress in cables becomes more significant. During these tests and over the very long term, in cases where delayed deformation are underestimated during the design of structure, tensile stresses may appear in a common zone of the containment under accidental loadings. Thus, it is necessary to examine and predict the delayed behavior of the containment building in order to control the tension zone. For this purpose, numerical tools are very helpful since real scale experiments are impossible for such type of structures.

A FEM is performed by IOSIS [24] to model the containment behavior of the Flamanville nuclear power plant during a periodic surveillance testing carried out 20 years after its implementation using the FE software ASTER. The model takes into account the full process of aging, including relaxation of the reinforcement, creep and shrinkage of concrete. The aim is to estimate the evolution with of orthoradial stress in term of the structure height and determine at which height tensile stresses occur. The aim of this section is to conduct a reliability study based on IOSIS FEM by combining ASTER used to describe the physical model with OpenTURNS. Polynomial chaos expansion is used to simplify the physical model and to perform several analyses including dispersion, distribution and sensitivity analyses.

### 6.5.1 Deterministic model

The evolution of containment building is modeled for  $t \in ]t_c; t_{VD1}[$ , where  $t_c$  is the date at which the internal containment is prestressed and  $t_{VD1}$  is the date of the first periodic surveillance testing (20 years after its implementation). Time increment is estimated in term of years, which makes a total of 15 time increments between  $t_c$  and  $t_{VD1}$ . The confinement building of Flamanville nuclear power plant consists of a prestressed cylindrical concrete vessel of 45 m of diameter and 65.05 m of height (Figure 6.39). The vessel is capped with a dome and is supported on a flat foundation slab. The plate (gousset) linking the bottom of the internal containment to the foundation slab has height of 3.6 m and an extra thickness of 1.10 m.

In order to reduce the computational cost of the deterministic analysis, the geometry considered in the model is simplified as illustrated in Figure 6.40. The model is limited to an angle of 22.22 gr (symmetry with respect to vertical plans) and the containment building is modeled up to the height  $h = +30.0m$  which is approximately equal to half of its total height. Thus, the selected zone is located between the levels of  $-0.6m$  and  $+30.0m$ , and the azimuth of 377.778 and 400.0 gr. In this case, the length of sector at the neutral fiber is equal to 8 m. The origin O is located at the center of the containment, at  $z = 0$  corresponding to the level 0.0 m.

Two types of prestressed cables are used, namely the vertical cables of the vessel that are vertical straight lines in the common zone and the horizontal cable of the vessel. Taking into account the above simplification of geometry of the selected zone, ten vertical cables are modeled and located

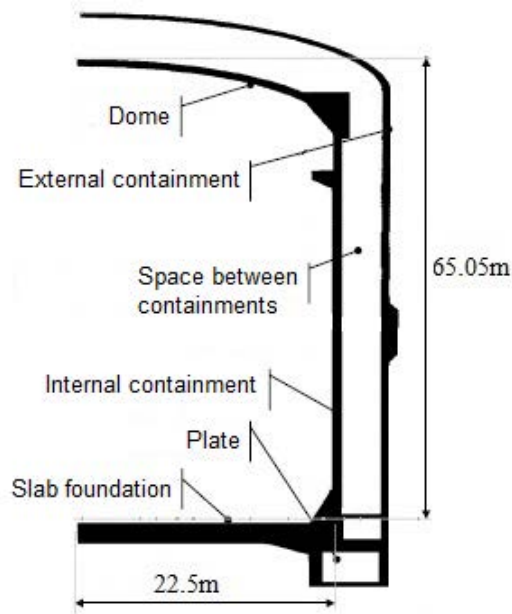


Figure 6.39: Geometry of the containment building of the Flamanville nuclear power plant

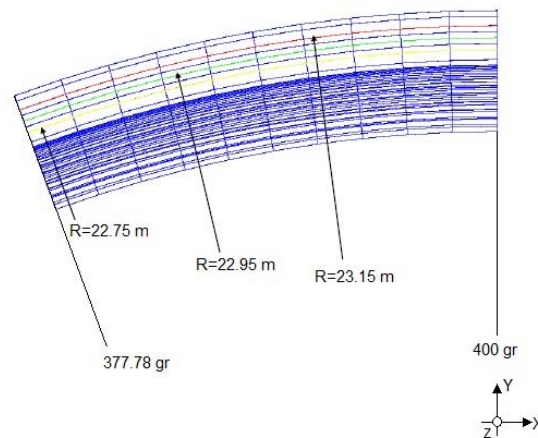


Figure 6.40: The selected zone of the containment building to be modeled

at the radius  $R_{moy} = 22.95 \text{ m}$ , while horizontal cables are located either at  $R_{int} = 22.75 \text{ m}$ ,  $R_{ext} = 23.15 \text{ m}$  or  $R_{moy} = 22.95 \text{ m}$ . They are modeled independently in the plate zone, and as groups of 2, 3 or 4 cables in the common zone. Overall, 34 horizontal cables are considered in the model, 15 independent cables, 8 groups of 2 cables, 1 group of 3 cables and 10 groups of 4 cables.

### 6.5.1.1 FE software

ASTER (Analyse des Structures et Thermomécanique pour des Etudes et des Recherches) is a numerical software developed by EDF and R&D. It is based on the theory of continuum mechanics and uses the finite element method to solve different types of problems, including mechanical, thermal, acoustics, seismic, etc. Prestress can be simulated in ASTER using the `DEFI_CABLE_BP` command that calculates the initial profiles of tension along the prestressed cables of a concrete structure. It uses specific data for prestress, such as the tension applied to tendon ends, the initial force applied at the active anchors of cables and other parameters that characterize the materials

and anchors. Furthermore, the basic creep of concrete can be modeled in ASTER using the model of Granger based on GRANGER\_FP\_INDT relation. This relation does not take into account the effect of temperature nor that of aging on the mechanical properties of concrete. The various parameters of Granger model are:

- The (2x8) constant variables of the creep function:
  - $J_i$  are the coefficients related to materials of the creep function (in  $m^2/N$ )
  - $\tau_i$  are the coefficients related to the 'delay' of the basic creep function
- The curve of sorption-desorption that gives the humidity in term of the drying of concrete
- The activation energy obtained from the time-temperature superposition.

### 6.5.1.2 Material properties and behaviors

Concrete is modeled as a visco-elastic material with a Young's modulus of 37000 MPa, a density of 2500  $kg/m^3$  and a Poisson's ratio of 0.2. The prestress is adopted in such type of structures in order to avoid tension zones and thereby reduce cracking in concrete. Therefore, it is designed so that concrete in the containment building can be fully compressed when fulfilling its functional requirements. For this case of study, the prestress is achieved with vertical and horizontal cables of 37T15 and a cross-section of 5143  $mm^2$ . Cross-sections of horizontal cables modeled as groups of 2, 3 or 4 cables are multiplied by 2, 3 or 4 respectively. The failure tensile stress is equal to 1814 MPa while the initial tensile stress at the anchorage is taken equal to 1429 MPa. Steel material of cables is modeled as a linear elastic material with a Young's modulus of 190000 MPa and a Poisson's ratio of 0.3. The prestress is evaluated taking into account the loss in tension along cables due to rectilinear and curvilinear friction, as well as to the relaxation in prestressing steel (2.5 % at 1000 hours, 3.0% at 3000 hours). Losses due to the creep and the shrinking of the concrete, as well as that resulting from the retreat of anchorage are also considered in the FEM. The relaxation of cables is estimated to be equal to 2.5 % at 1000 hours and 3.0% at 3000 hours, while the retreat of anchorage is supposed to be equal to zero for horizontal cables and 0.008 m for vertical cables. The model of Granger is used to represent the basic creep of concrete in the FEM.

### 6.5.1.3 Boundary conditions and loading

The selected zone of study necessitates choosing appropriate boundary conditions in order to take into account the symmetry (Figure 6.41):

- For the surface Surf1 located at the azimuth of 400 gr, displacement in x-direction is restrained so that  $d_x = 0$ .
- For the surface Surf2 located at the azimuth of 377.78 gr, displacement in x-direction is restrained so that  $d_x = -d_y \tan \alpha$ .
- For the upper surface Surf3 located at the level  $z = +30.0 m$ , rotations about x-,y- and z-axes are zero and displacement  $d_z$  in z-direction is constrained to an identical value for all the surface nodes. The effect of the weight of the upper part of the containment as well as the dome part is considered in the model by applying a compression stress upon this surface equal to  $\sigma_{zz} = 1.51$  MPa.
- For the surface Surf4 located at the level  $z = -0.6 m$ , the selected zone is clamped at the bottom. In addition, the foundation slab shrinkage is defined as a boundary condition of displacement in the plate base.

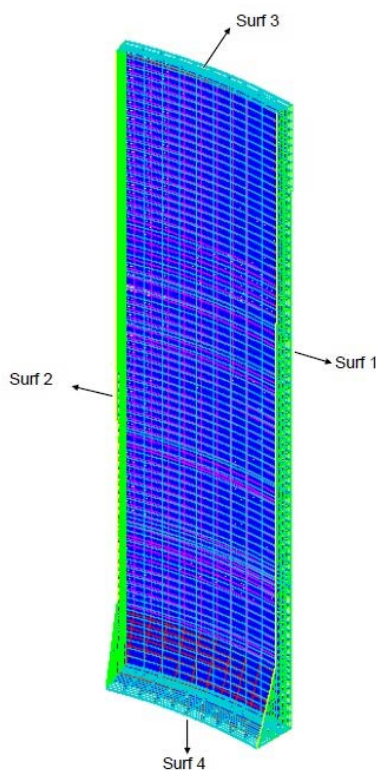


Figure 6.41: Mesh of the selected zone of study of the containment building

#### 6.5.1.4 Mesh

The FE mesh of the internal containment includes the concrete part of the structure, as well as the prestressed cables that significantly contribute to rigidity and the nonlinear behavior of the containment. The concrete part is modeled using solid FE with 8 nodes and linear integration, while prestressed cables are modeled with two nodes linear truss elements. Passive reinforcement are not taken into account in the FEM since their influence on the structural rigidity is relatively small. As previously mentioned, the dome and the foundation slab are replaced in the model by equivalent boundary conditions.

The mesh is performed in the way that concrete nodes overlap with those of horizontal cables, but vertical cables are meshed independently. Therefore, the discretization in space of horizontal cables and the concrete part is the same and a node is located every 0.8 m. Vertical cables, as well as the concrete part in the z-direction, are discretized in space with a node every 0.4 m. Consequently, the FEM of the selected zone of the internal containment consists of 9200 nodes and 7900 elements, including 6800 solid elements assigned to concrete and 1100 truss elements assigned to steel cables. Figure 6.41 shows the mesh adopted for the selected zone study.

#### 6.5.1.5 Delayed strains in concrete

The internal containment structure shows three different thicknesses related to the slab foundation, the plate and the common part of the containment. The difference of thickness along the structure necessitates the prediction of drying shrinkage and creep of concrete in terms of the geometry and boundary conditions of each zone of different thickness. Delayed strains in concrete may affect the sustainability of concrete structures for several reasons. Shrinkage strains  $\varepsilon_r$  may induce cracking in concrete until causing steel reinforcement corrosion, while creep strains  $\varepsilon_{rf}$  may result in a significant reduction in the prestressing force.

Concrete may be subjected to several types of delayed strains during its lifetime. In the case where there is no water exchange between the concrete structure and its surrounding environment, 3 types of delayed strains are observed:

- Early-age autogenous shrinkage  $\varepsilon_{re}$  is an important phenomenon in young concrete and is evaluated in term of water/cement ratio. Autogenous strains develops during hardening of concrete in the early days of casting.
- Early-age thermal shrinkage  $\varepsilon_{th}$  occurs due to excessive differences within a concrete structure or its surroundings.
- Basic creep  $\varepsilon_{fp}$  is defined as the creep that occurs under loading conditions and increases with the increase of stress and duration of loading.

In the case where water exchange occurs, 2 other types of delayed strains of concrete are observed:

- Drying shrinkage strain  $\varepsilon_{rd}$  is a function of the migration of the water through the hardened concrete and develops slowly.
- Drying creep strain  $\varepsilon_{fd}$  represents the extra creep component at drying over the sum of shrinkage and basic creep.

Consequently, the total strain that describes the time dependent behavior of concrete can be expressed as follows:

$$\varepsilon_{tot} = \varepsilon_{el} + \varepsilon_r + \varepsilon_f = \varepsilon_{el} + \varepsilon_{re} + \varepsilon_{th} + \varepsilon_{rd} + \varepsilon_{fp} + \varepsilon_{fd} \quad (6.15)$$

with  $\varepsilon_{el}$  is the instantaneous strain component.

## 6.5.2 Probabilistic model

The variables which may be subjected to statistical variations in containment building can be classified into four categories:

1. Variables related to the concrete properties: Young's modulus and Poisson's ratio of concrete.
2. Variables related to shrinkage in concrete: shrinkage coefficient.
3. Variables related to creep in concrete: creep coefficients.
4. Variables related to the steel properties: multiplying factors for horizontal and vertical cables.

23 random input variables are considered, they correspond to the physical phenomena observed in such type of structures, including relaxation of prestressing reinforcement, creep and shrinkage of concrete. Random variables are considered as independent since no experimental data are available to determine the correlation between them. All random variables are assumed to have a Lognormal probability distribution with a mean value equal to the nominal value of the relevant variable and a COV equal to 0.1. This choice is based on the fact that all input variables taken into account in the probabilistic model should have positive random values. In addition, the COV is chosen the same for all variables in order to study the influence of each variable mean on the estimation of the height corresponding to the tension zone without considering their effect of variation. It has be shown in the reliability analysis of RC cantilever beam that the COV value highly affects the probabilistic response and a variable with a higher COV has a significant effect on the dispersion of output variables as well as on the estimate of failure probability. Table 6.18 represents the random variables adopted

Table 6.18: Random variables of the containment building and their descriptions

Variables	Description	Mean	COV	PDF
<b>Concrete properties</b>				
$E_c$	Young's modulus of concrete	37 GPa	0.1	Lognormal
$\nu_c$	Poisson's ratio of concrete	0.2	0.1	Lognormal
<b>Reinforcement properties</b>				
$\alpha_h$	Multiplying factor for horizontal cables	10615000	0.1	Lognormal
$\alpha_v$	Multiplying factor for vertical cables	7210500	0.1	Lognormal
<b>Shrinkage in concrete</b>				
$ret_b$	Shrinkage coefficient	1e-5	0.1	Lognormal
<b>Creep in concrete</b>				
$J_1-J_5$	Creep coefficients	0.57048258e-12	0.1	Lognormal
$J_6-J_8$	Creep coefficients	33.8049253e-12	0.1	Lognormal

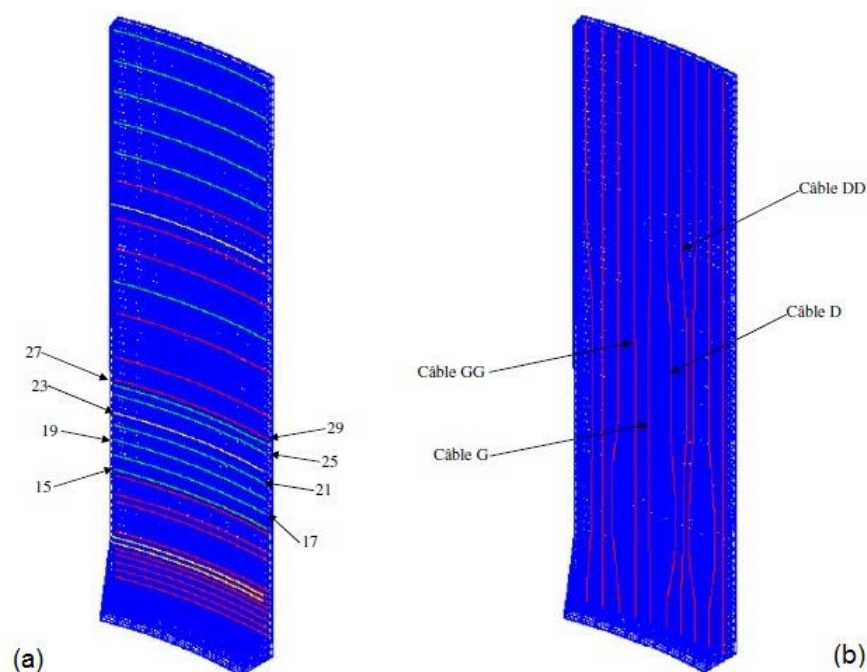


Figure 6.42: Horizontal and vertical cables considered in the reliability analysis of containment building

in the present study in the case of containment building, their probability distribution, their mean and COV.

The horizontal cables presented in the reliability analysis of containment by their multiplying factors are shown in Figure 6.42(a). Figure illustrate the vertical cables considered, they are located on both sides of the line over which the post-processing of stress is performed (2 cables on the left side and 2 cables on the right side).

### 6.5.3 Failure criteria

The aim of periodic surveillance testing is to measure the global leakage rate in the internal containment, which represents the percentage of decrease in dry air masses in the containment per day. A

containment should ensure a leakage rate less than 1.5% of the total mass of dry air per day. During periodic surveillance testing, tensile stresses may appear in some particular zone of the containment. Furthermore, in very long term, beyond the expected period of time for which the containment is designed, such tensile stresses may also occur in the common zone of the containment in cases where delayed strains were underestimated during the design process.

The effect of differential shrinkage is observed in the internal containment for height less than 5.8 m, which leads to tensile orthoradial stresses that reduce the compressive stress in concrete generated from prestressing forces. For this application, the limit state function is defined using the criterion of maximum height, that is failure occurs when the height of zone under tension is greater than the threshold  $h_{max}$  ( $h_{max} = 5.8\text{ m}$ ).

$$g = h_{max} - h \quad (6.16)$$

#### 6.5.4 Discussion of results of containment building reliability

Polynomial chaos method with cleaning strategy is used to study the reliability of the containment building of Flamanville nuclear power plant. As previously demonstrated in the reliability study of cantilever beam, the cleaning strategy is found to be the most efficient strategy, among those available in OpenTURNS for polynomial chaos, to estimate failure probability and analyze the dispersion of variables of interest. Two steps are necessary to perform the study:

- The first consists in coupling OpenTURNS and the initial deterministic code directly. The initial deterministic code is an ASTER FEM which is called by OpenTURNS for each assessment of the limit state function denoted in this case  $g_{model}$ .
- The second is based on an approximation of the function  $g_{model}$  using the polynomial chaos expansion which enables to substitute the containment initial deterministic model with an analytical expression. The approximated limit state function is denoted in this case  $g_{MetaModel}$ .

The aim is to analyze the efficiency of using polynomial chaos expansion for problems with an important number of random variables and a limit state which is not easy to evaluate. Thereafter, x-axis corresponds to the number of calls to the initial deterministic model in the case a direct combination between OpenTURNS and ASTER, while it indicates the number of sample points in the design of experiments in the case of an approximate limit state function.

##### 6.5.4.1 Deterministic output variable

This case of study presents a deterministic FE model for the selected zone of the containment that allows estimating the height at which the structure is under tension. Figure 6.43 shows the variation of the average tensile stress induced in concrete in term of the height. The average stress is estimated over the containment thickness for a given value of height. It can be seen that tensile stresses occur in the zone of height 4.906 m, which corresponds to a case belonging to the safe domain according to the failure criterion expressed in equation 6.16. This criterion is related to the height of zone under tension with a height threshold of 5.8 m.

##### 6.5.4.2 Dispersion analysis

Figure 6.44 shows the variation of the mean of the tension zone height in term of the number of simulations of the initial deterministic model that represents also the number of sample points used to evaluate the approximate limit state function. The height mean is calculated with the initial limit state function ( $g_{model}$ ) using the numerical integration method Monte Carlo, and with the approximate limit state function ( $g_{MetaModel}$ ) using Monte Carlo and the quadratic combination

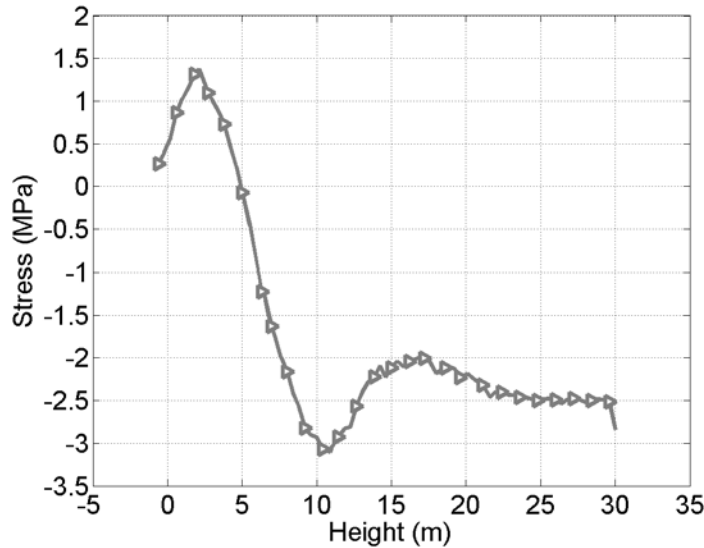


Figure 6.43: Variation of the average tensile stress in term of height

methods. It is assumed that convergence is achieved when the difference between the height mean values obtained with  $g_{model}$  and  $g_{MetaModel}$ , respectively, is of the order of  $10^{-2}$ . As can be seen, 1000 simulations are sufficient to obtain the desired convergence and a good agreement between calculated and approximated mean values of the tension zone height.

The COV of variation of the tension zone height is calculated as the ratio of the height standard deviation to its mean value. The higher the COV is, the more the dispersion about the mean is important. In other words, the estimation of mean value is more precise for lower values of COV. Thus, the number of simulations used should be sufficiently high to reach the precision desired. COV is expressed in percentage so the dispersion of variables of different units can be comparable. However, this does not represent a problem in this case of study since the same variable is compared using different methods to assess the output of models. Figure 6.44 shows that the most accurate estimation of the mean of tension zone height is obtained using the quadratic combination method with the meta-model as it allows reducing the COV to minimum. This is due to the fact the quadratic combination method depends only on the limit state function, but does not depend on the number of simulations or calls of the model as in the case of Monte Carlo numerical integration method. This latter necessitates a sufficient number of simulations in order to converge to the exact value of mean.

### 6.5.4.3 Distribution analysis

In order to verify the efficiency of polynomial chaos expansion in approximating accurately the limit state function of the initial deterministic model, the sample of height obtained with the initial model function  $g_{model}$  and that obtained with the approximated function  $g_{MetaModel}$  for the same realizations of the input physical vector are compared. The aim is to compare two statistical samples having the same population and the same size of 1000.

A histogram is considered as a graphical tool with which the identification of the distribution of a variable can be established. It can be used to verify if the meta-model provides a good estimation of the height output sample obtained with the initial FEM. In order to facilitate the comparison, both histograms obtained through the initial model and the approximate model, respectively, are plotted on the same graph (Figure 6.45). x-axis corresponds to the height values in m, while y-axis indicates the frequency values in %. Examining the histograms of the output samples allows some preliminary

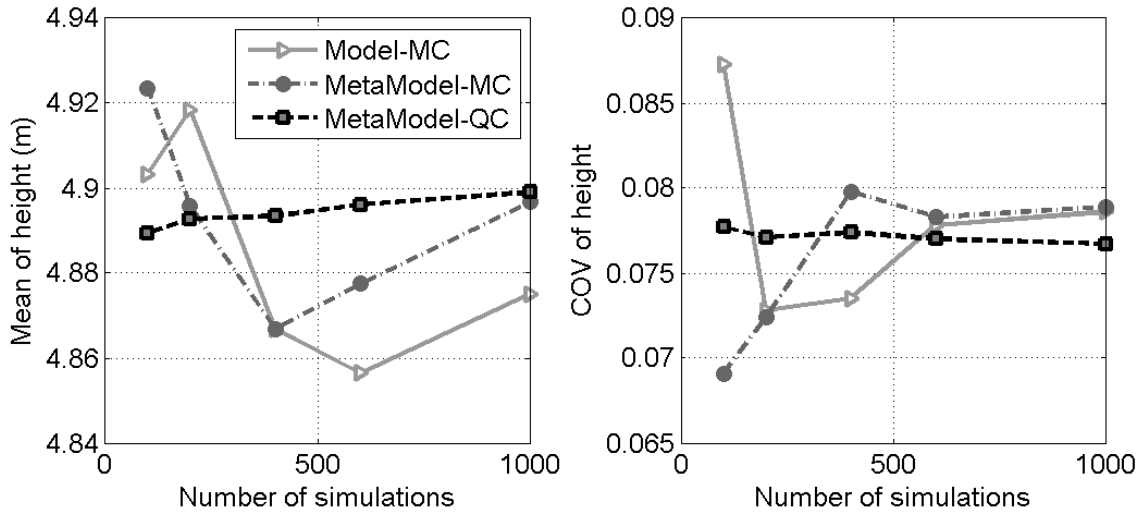


Figure 6.44: Mean and COV of height in term of the number of simulations

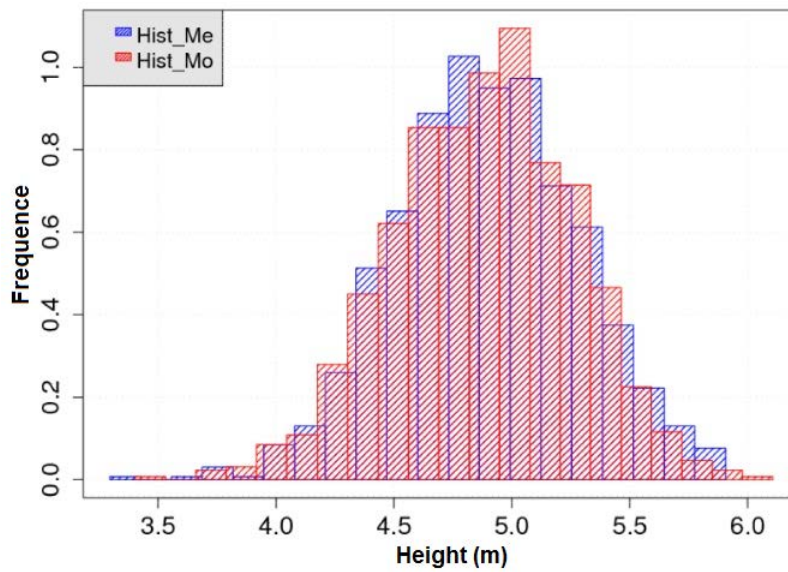


Figure 6.45: Histogram of tension zone height samples obtained with initial model and meta-model for 1000 simulations

conclusions to be drawn. First, it can be concluded that both samples have approximately the same mean and that height values are distributed around this mean of 4.906 m. The number of intervals as well as their width depend on the sample size which is equal in this case to 1000. They are calculated automatically in OpenTURNs in order to have the best display of the output variable and to accurately evaluate the real distribution of any sample, whilst it is not possible to adjust the properties of a histogram in OpenTURNs. For this reason, frequencies of each output sample are represented in different class intervals. However, the number of intervals as well as their width remain the same for both samples since they have the same size.

Furthermore, cumulative distribution functions are plotted on the same graph for both samples

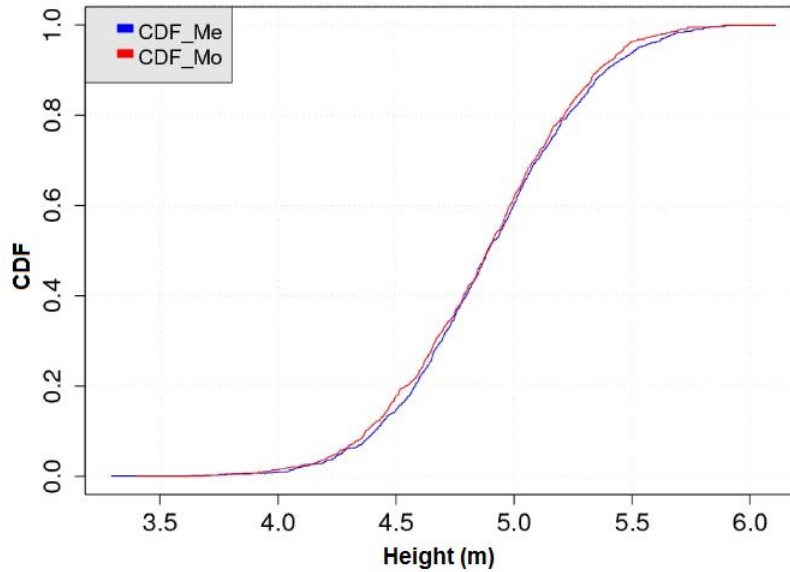


Figure 6.46: CDF of tension zone height samples obtained with initial model and meta-model for 1000 simulations

(Figure 6.46). As can be seen, the CDF of height sample obtained with the approximate model is below that obtained with the initial model for all values of height. Both distributions are in good agreement and are similar between height values of 4.75 m and 5.25 m, i.e. around the mean value of 4.906 m.

The probability distribution functions of output samples are estimated using Kernel Smoothing method that enables to represent those distributions graphically. As can be seen in Figure 6.47, the distribution function resulting from the meta-model is smoother than that resulting from the initial model, especially around the mean value of the height, or in other words, in the zones of high probability density. This problem can be solved by increasing the number of sample points in the design of experiments or by using a higher order for the polynomial chaos expansion [155]. A higher order of polynomial chaos permits a better representation of the third and fourth-order statistical moments that measure the skewness and the kurtosis of a distribution, respectively.

The graphical statistical test QQ-plot is used with quantiles estimated at 95% to compare the distributions of the height sample obtained with the initial model and that obtained with the approximated model. Figure 6.48 shows that quantile points are very close to the diagonal, which means that the distributions of the two samples are almost identical. It should be noted that the probability distribution obtained with the initial FEM model is not properly estimated since only 1000 random simulations are used to create the output sample. Thus, a higher number of random simulations is needed for a better estimation.

#### 6.5.4.4 Failure probability

The aim of this application is to study the likelihood of failure of the containment under tension stresses at a certain height. Subsequently, only the limit state function approximated by the polynomial chaos method is considered and failure probability is estimated by combining this function to different probabilistic simulation and approximation methods. The effect of the number of sample points in the design of experiments is examined in the aim of illustrating the importance of using a sufficient number of points to accurately estimate failure probability with a limit state function approximated by polynomial chaos expansion. Figure 6.49 shows failure probability and reliability index estimated with  $g_{MetaModel}$  that is coupled to different probabilistic methods for the failure

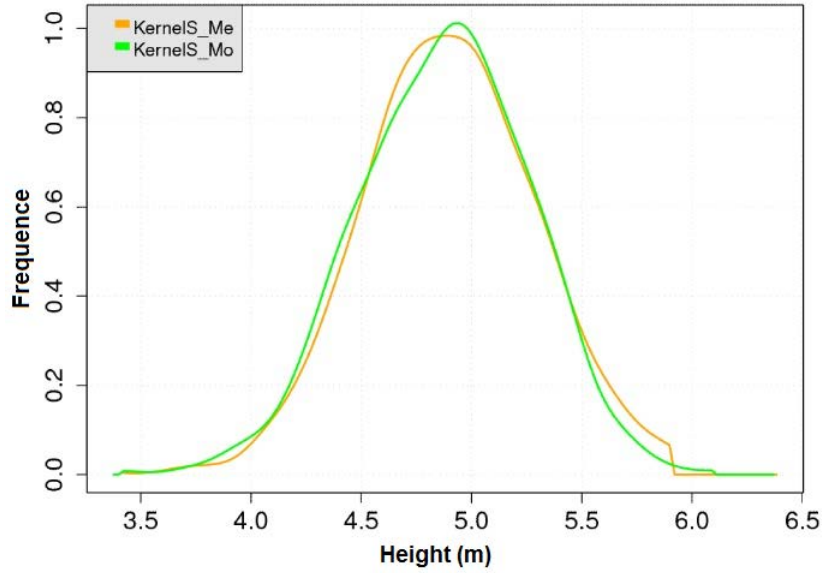


Figure 6.47: PDF of tension zone height samples obtained with initial model and meta-model for 1000 simulations

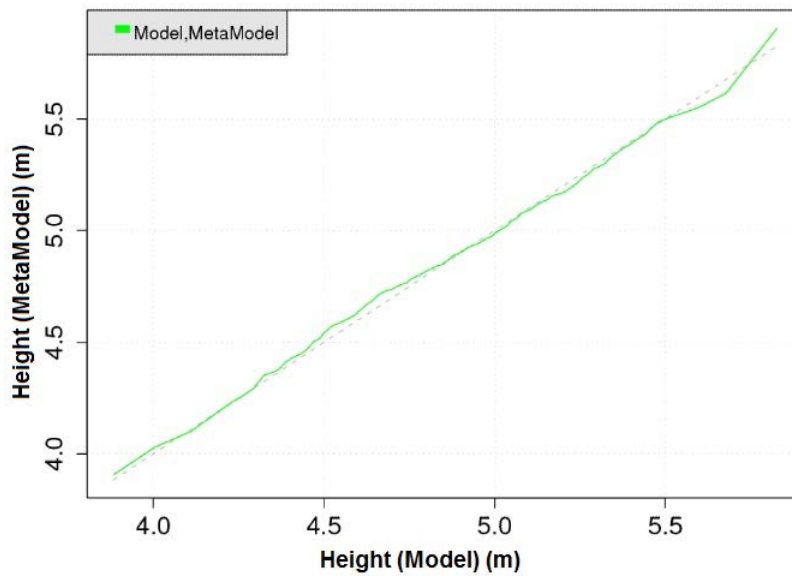


Figure 6.48: Comparison of initial model and meta-model output samples using QQ-plot

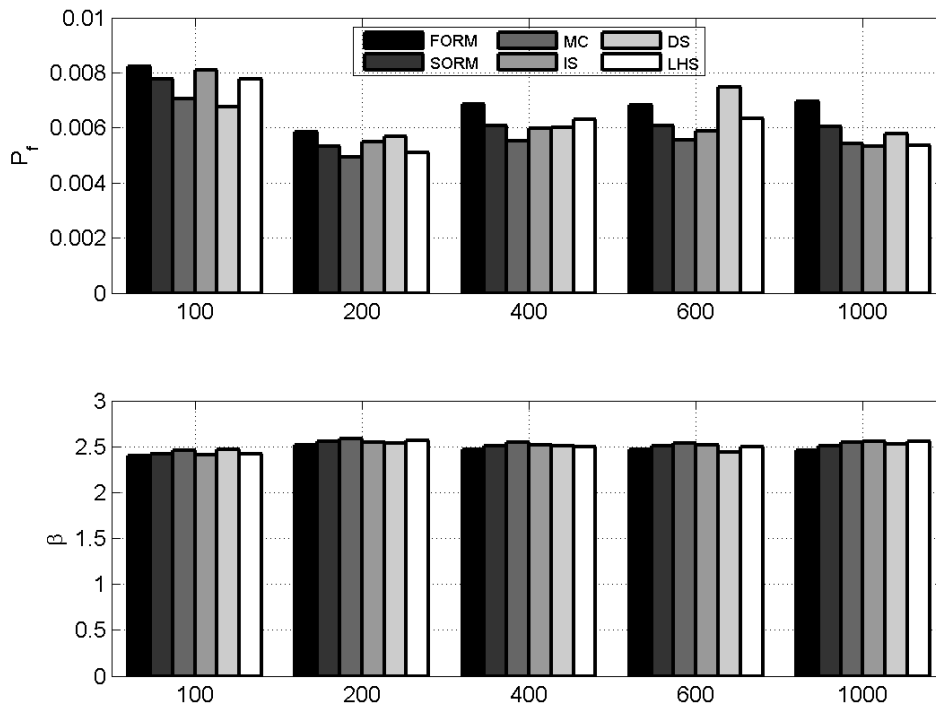


Figure 6.49: Failure probability and reliability index estimated with different probabilistic methods depending on the number of points of the design of experiments

criterion related to the height of tension zone. Number of points in the design of experiments varies from 100 to 1000 and 5 design of experiments are considered. As can be seen, results obtained using simulation probabilistic methods are more precise than those obtained using approximation probabilistic methods. The precision of methods increases with the number of points that allows verifying if failure probabilities, as well as reliability indices, are accurately evaluated and if the convergence to exact values is achieved. The convergence criterion of Mohammadkhani [136] is used in this study, it consists in calculating the difference of reliability indices of two successive iterations (2 different number of sample points). Mohammadkhani indicated that the convergence is reached when the difference of reliability indices is less than  $10^{-3}$  or  $10^{-6}$  depending on the probabilistic model and numerical model considered. According to this criterion, the convergence between 600 points and 1000 points is achieved. In the case of 1000 points, only IS provides the same failure probability compared to Monte Carlo. Approximation methods do not give satisfactory results, which may be due to the presence of large curvatures at the failure surface approximated with polynomial chaos expansion. As it is known, FORM and SORM do not allow a good estimate of failure probability in the case of highly nonlinear limit state functions.

Figure 6.50 illustrates the convergence of failure probability assessed using different simulation methods coupled the limit function approximated with 1000 points in the design of experiments. Convergence of simulation methods is evaluated for a confidence interval at level 0.95, which indicates that the true value of failure probability is, with a probability close to 1, within the range of confidence interval. x-axis in Figure 6.50 corresponds to the number of calls to the meta-model by a simulation method (number of simulations), while y-axis indicates the estimate of failure probability assessed using this method. Simulation methods can be classified according to their confidence interval and the number of simulations needed to assess failure probability. It can be seen that MC shows a high precision as it provides the tighter confidence bounds for failure probability, but it necessitate a significant number of simulations (more than 60000 simulations). However, IS is more

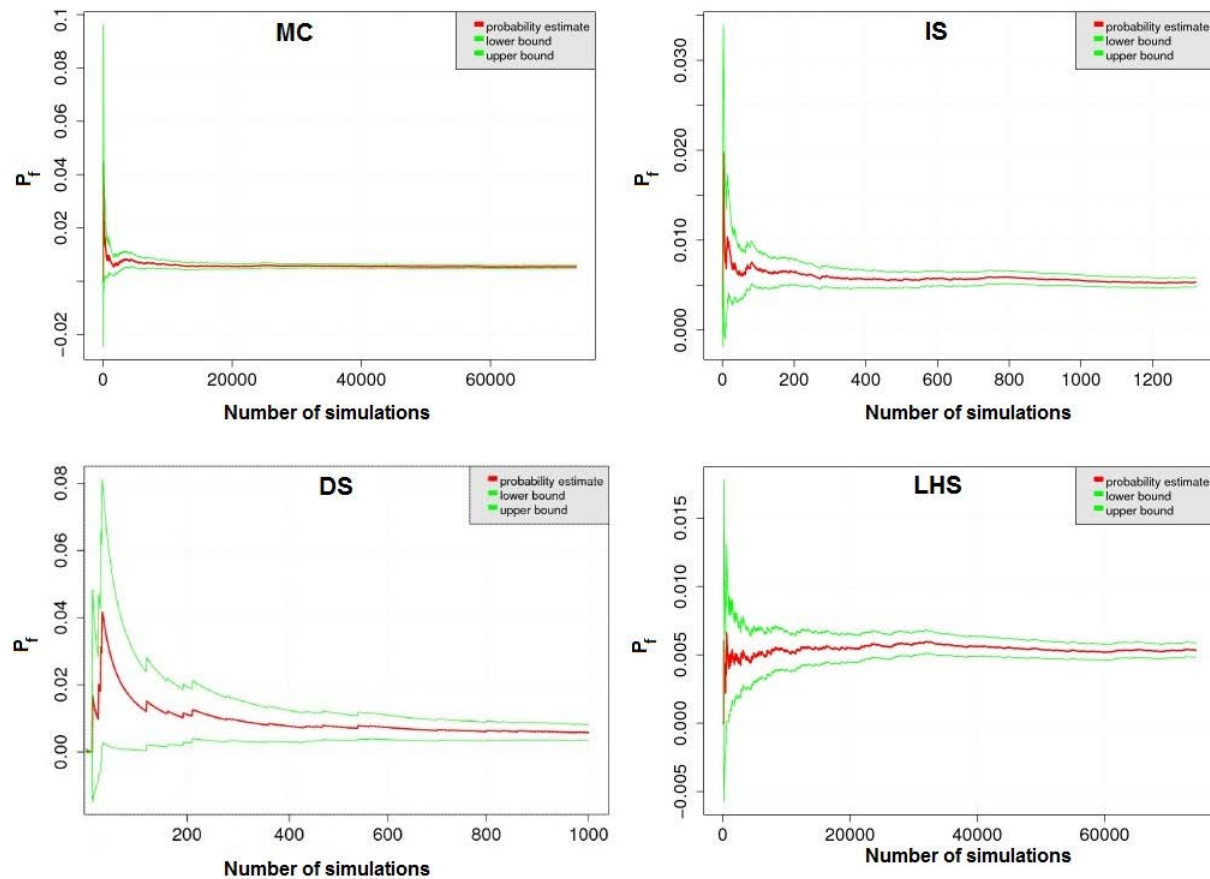


Figure 6.50: Convergence at level 0.95 of the estimate of failure probability for different probabilistic simulation methods

efficient in this case as it provides a tight confidence interval with less number of simulation (1200 simulations).

#### 6.5.4.5 Sensitivity analysis

Figure 6.51 shows the importance factors associated to the different random variables considered in the study of Flamanville internal containment. Importance factors are calculated using the quadratic combination method and FORM, respectively. The limit state function estimated with 1000 points using the polynomial chaos expansion is used for the sensitivity analysis. It can be seen that the shrinkage coefficient of concrete has the most important influence among other random variables in the containment probabilistic model for the considered failure criterion of tension zone height. On the contrary, the multiplying factors of horizontal cables (15, 17, 19 and 21), as well as Young's modulus and Poisson's ratio of concrete has less influence on the estimator of height mean and failure probability, respectively. Other random variables considered in the probabilistic model has no influence.

Figure 6.52 shows the effect of the number of points in the design of experiments on the shrinkage coefficient importance factor. It can be seen that, for higher number of points, the importance factor calculated with the quadratic combination method and which indicates the effect of shrinkage coefficient on the estimator of height mean, trends to converge towards a steady value. However, the importance factor calculated using FORM and which describes the sensitivity of shrinkage coefficient

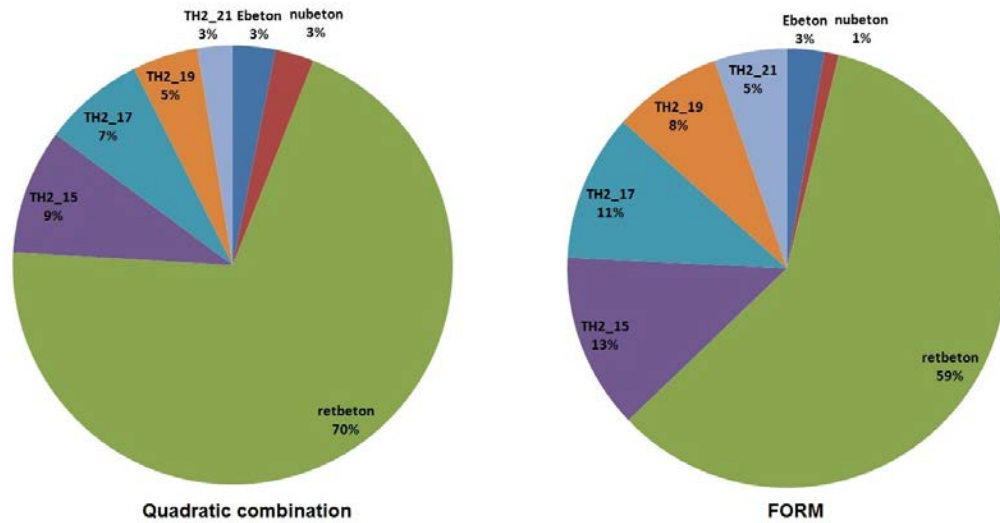


Figure 6.51: Importance factors of containment random variables using quadratic combination method and FORM

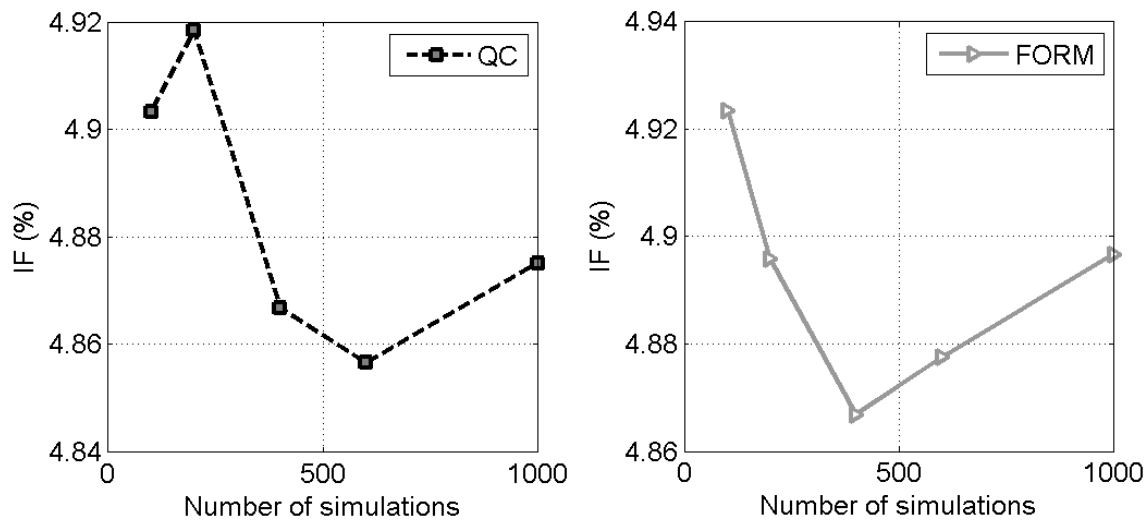


Figure 6.52: Importance factor of concrete shrinkage coefficient in term of number of points in the design of experiments

on the estimate of failure probability, trends to converge towards a steady value for a number of points equal to 600.

#### 6.5.4.6 Convergence?

In order to verify the efficiency of the meta-model approximated with polynomial chaos expansion, the output sample of height obtained with the approximated model is compared to that obtained with the initial FEM. The points  $(h_{model}, h_{MetaModel})$  are plotted on the same graph and their position with respect to the diagonal is examined. A point on the diagonal indicates that  $h_{model} = h_{MetaModel}$ . A good approximation of the initial model can be deduced in the case where the points are close

to the diagonal. In the other case, the number of points in the design of experiments should be increased. Figure 6.53 shows that the number of points ( $h_{model}, h_{MetaModel}$ ) that are close to the diagonal increases with the number of points in the design of experiments. However, widely spaced points from the diagonal indicate that the meta-model does not estimate accurately the height value obtained with the FEM for the relevant values of input variables. Therefore, a higher number of point in the design of experiments ( $>1000$ ) is needed in order to reach the desired convergence.

#### 6.5.4.7 Conclusion remarks

The application of reliability analysis to a containment building permits to investigate the effectiveness of the polynomial chaos method in estimating the initial physical model with an approximated model. The comparison is performed on the estimation of statistical moments of the output variable (dispersion analysis), as well as on the determination of its probability distribution (distribution analysis). The reliability analysis results are obtained by combining the meta-model with various approximation and simulation methods. Simulation methods are more accurate than approximation methods and allow more precise failure probability values. Monte Carlo and importance simulation provide the same value of failure probability and reliability index. However, the precision obtained should be verified since no reference results are available for comparison.

In conclusion, the efficiency of the polynomial chaos method is related to several factors, including the limit state function to be estimated, the degree of the polynomial chaos, the number of points in the design of experiments and the variation of random variables. Different methods are used to estimate the reliability of the containment. The efficiency of the response surface method used in this study necessitate the convergence of results towards a steady value for all types of conditions. These conditions can be related to the physical complexity and the precision of the mechanical model, geometric properties of limit state function, number of random variables considered, ...

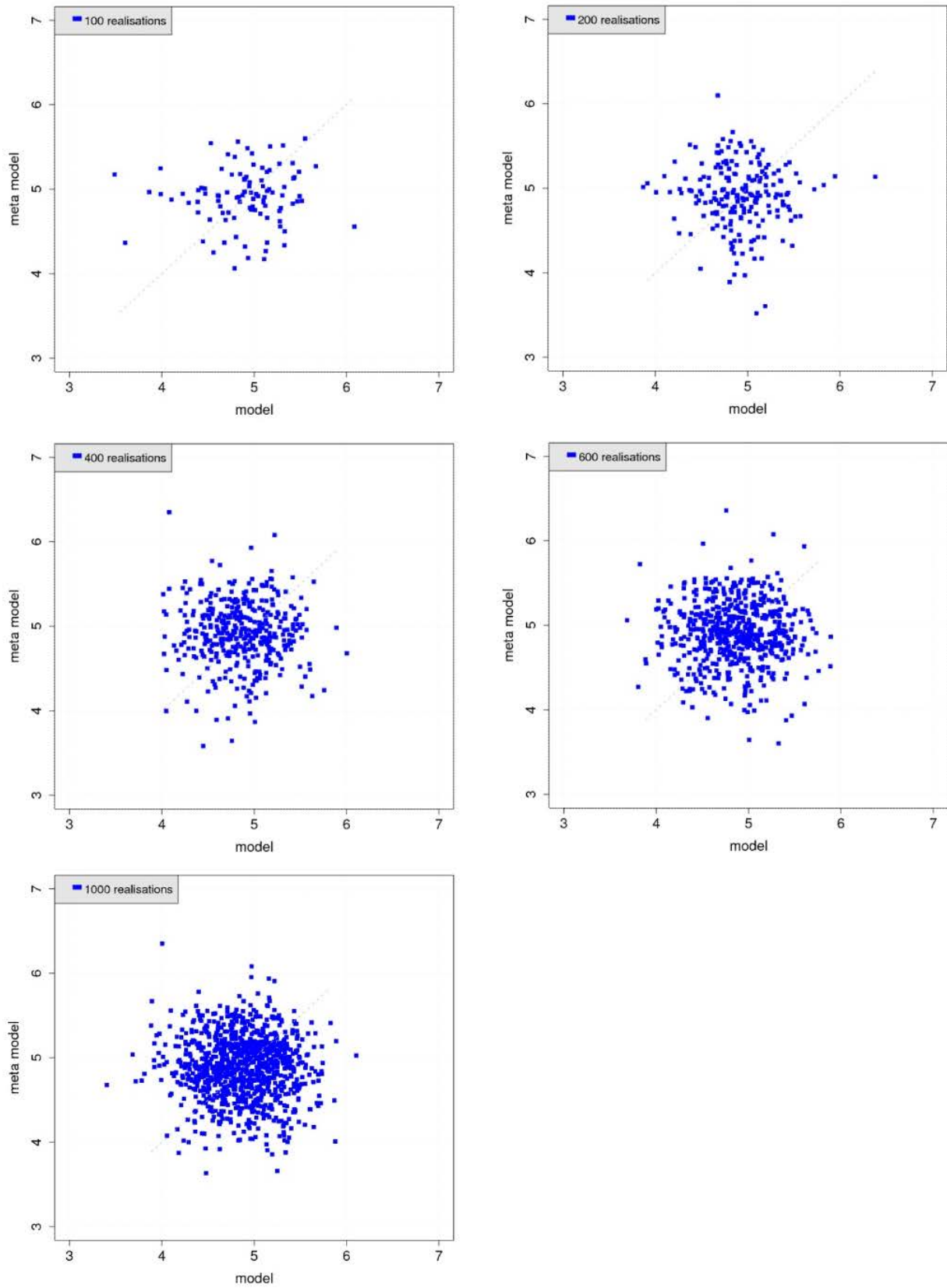


Figure 6.53: Comparison of initial model and meta-model for different number of points in the design of experiments

# Chapter 7

## Conclusions and perspectives

### 7.1 Conclusions

For an optimal and robust design that guarantees a real prediction of the behavior of structures, uncertainties should be taken into account and be propagated in the structural deterministic analysis. Probabilistic approaches were developed to correctly model the variation of input variables. The aim of these approaches is to assess failure probability of structures according to one or several criteria and to study the influence of uncertain variables on the structure response. Structural reliability analysis is based on the principle of combining a stochastic model with a deterministic model. Stochastic models should include the probabilistic characteristics of random input variables including a suitable probability distribution and appropriate values of their mean and coefficient of variation. Deterministic models allow predicting structural response and evaluating the variables of interest, they can be based on analytical, empirical or numerical deterministic approaches. The combination of mechanical and stochastic models can be very time consuming. Thus, the issue of computational effort of reliability analysis is addressed and strategies are proposed to accurately assess failure probability with the minimum computational cost.

This research discusses the use of reliability analysis for three different civil engineering applications of different degrees of complexity. The platform OpenTURN is used to perform the reliability analysis of the RC structures considered in the present study and propagate uncertainties in their physical models. Thus, the reliability of three applications are examined: a RC multifiber cantilever beam subjected to a concentrated load at the free end, RC slabs which are subjected to accidental dropped object impact during handling operations within nuclear plant buildings, a prestressed concrete containment building.

The physical problem of reinforced concrete (RC) slabs subjected to impact is classified as low velocity impact event and considered as one of the most difficult nonlinear dynamic problems in civil engineering because it involves several factors, including the nonlinear behavior of concrete, the interaction effects between the concrete and reinforcement, and contact mechanics between the slab and the impactor. The complexity of impact problems also lies in the dynamic response of RC slabs and the time-dependent evolution of impact velocity. Several parameters may significantly influence the impact response of RC slabs:

- Type of impact play role in dissipating energy.
- Slab dimensions and boundary conditions control the stiffness of the slab.
- Material properties have a significant influence on the slab transient response by affecting the contact and overall slab stiffnesses.

- Impactor characteristics including impact velocity, shape, position, mass and rigidity influence the impact dynamics.

A detailed step-by-step procedure for creating FE models of impacted slabs with Abaqus is described in this study. The FEM models correctly identify different factors that contribute to the nonlinear behavior of the reinforced concrete such as the nonlinear stress-strain response, the damage due to crushing and tensile failure, the effect of the loading rate, the interaction between the concrete and the reinforcement. The analysis is performed with an explicit configuration that allows a better representation of impact problems. The model developed is validated with the experimental results of Chen and May tests and used to model RC slabs which are subjected to accidental dropped object impact during handling operations within nuclear plant buildings. Numerical results obtained are in good agreement for several slabs tested.

The reliability analysis of beam allows concluding that selection of the most suitable method for a particular type of problem is not apparent since the accuracy and computational effort of probabilistic methods depend on several factors, such as degree of nonlinearity of the limit state function, type of random variable distributions, number of random variables and their variance. In addition, it is found that FORM and IS are the less consuming methods in comparison to other methods.

The reliability analysis of impacted RC slabs shows that analytical MSM can be very effective in predicting the same values of slab displacement at the impact point as the numerical model, as well as in estimating failure probabilities very similar to those obtained with the FEM for a displacement criterion. Studying the response of impacted slabs assuming an elastic behavior of materials represents a preliminary step in the procedure of evaluating the reliability of RC slabs under low velocity impact. This application is initially considered to simplify the problem and to avoid complicating structural reliability analysis of slabs as a first step. However, it is clear that nonlinearities due to materials behavior have a significant effect on RC slabs response, in particular that cracking in concrete under tension and plastic deformations in concrete at the impact zone and in reinforcement reduce significantly the peak of contact force obtained with an elastic model.

The application of reliability analysis to a containment building permits to investigate the effectiveness of the polynomial chaos method in estimating the initial physical model with an approximated model. It is found that the efficiency of the polynomial chaos method is related to several factors, including the limit state function to be estimated, the degree of the polynomial chaos, the number of points in the design of experiments and the variation of random variables.

## 7.2 Perspectives

For Chen and May experiments [34], only the transient impact force-time history obtained with numerical model is compared to experimental results. However, Chen and May provide more results such as accelerations, transient reinforcement strains, and damages on the upper and bottom surfaces of slabs. Thus, it is better to study also the efficiency of the FEM proposed for Chen and May slabs in predicting other experimental results.

Other studies exist in the literature that studied experimentally the behavior of RC slabs under impact. Zineddin and Krauthammer tests [189], as well as Hrynyk tests [84], are very important in terms of gaining a better understanding of the impact behavior of RC slabs. Therefore, validating the FEM for different slab geometries and reinforcement ratio under different impact conditions seems very important to study the limitation of the proposed FEM, especially that Hrynyk tests include successive impacts on the same slab. They also tested the impact behavior of steel fiber reinforced concrete, which represents an important problem to investigate numerically.

The behaviors of concrete and steel are considered in the FEM similar to their static behavior. However, an impact problem is a dynamic problem and concrete has different behavior under impact

than under static load. Thus, using subroutines in Abaqus to implement a new concrete model that takes into account its behavior under impact would provide more accurate prediction of the structural response.

In the current study, the evolution in time and in space of uncertainties related to loading and material properties, respectively, are not taken into account. These types of variation necessitate modeling the random functions as stochastic field if the evolution in space is studied, and as stochastic process if the evolution in time is considered. The latest version of OpenTURN allows more probabilistic methods such as kriging and subset methods, it also allows the definition of randomness as stochastic field or stochastic process. Thus, it would be interesting to compare the new available methods with those used in this study in order to examine their efficiency and precision in assessing failure probability. In addition, the description of the evolution in time of uncertainties related to loading and that in space related to material properties permits a better presentation of the physical problem in reliability analysis if data are available.

In this study, different failure criteria are examined, but independently. However a system analysis is necessary since output variables considered in structural reliability analysis does not reach their maximum values simultaneously. For example, the contact force reaches its maximum value at the first phases of contact while that of displacement occurs at the end of contact. Yielding of steel and energy dissipation may occur at any time during the impact phenomenon. Thus, it is necessary to study the reliability of slabs in the nonlinear case for several failure criteria, separately or using a system analysis.

Several relationships are presented in this study to describe the behavior of concrete in tension and compression based on research from the literature. It is found that these curves affect highly the response of the slab, thus a reliability analysis can be performed in order to investigate the effect of the tensile and compressive stress-strain curves of concrete on the probability of failure for one or several failure criteria.

# Bibliography

- [1] *Reference Guide - OpenTURNS version 0.13.2.*
- [2] *CEB-FIP: Model Code 1990.* Thomas Telford - London, 1993.
- [3] *GB50010-2002: Code for design of concrete structures.* Ministry of housing and urban-rural development of China, 2002.
- [4] *EN1992-1-1: Eurocode 2 - Design of concrete structures. Part 1-1: general rules and rules for building.* European Committee for Standardization (CEN) - Brussels, 2004.
- [5] *Abaqus Analysis User's Manual, version 6.11,* 2011.
- [6] *Abaqus Theory Manual, version 6.11,* 2011.
- [7] *Abaqus User's Manual, version 6.11,* 2011.
- [8] M. Abbasi, M. Baluch, A. Azad, and H. Abdel Rahman. Nonlinear finite element modelling of failure modes in rc slabs. *Computers and Structures*, 42(5):815–823, 1992.
- [9] S. Abrate. *Impact on composite structures.* Cambridge University Press, 1998.
- [10] S. Abrate. Modeling of impacts on composite structures. *Composite Structures*, 51:129–138, 2001.
- [11] ACI. Prediction of creep, shrinkage and temperature effects in concrete structures. Technical report, ACI Committee 209, Subcommittee II, 1992.
- [12] A. Arafah. Reliability of reinforced concrete beam section as affected by their reinforcement ratio. In *8th ASCE Speciality Conference on Probabilistic Mechanics and Structural Reliability*, 2000.
- [13] J. Araujo. Probabilistic analysis of reinforced concrete columns. *Advances in Engineering Software*, 32:157–178, 2001.
- [14] M. Baudin, A. Dutfoy, B. Iooss, and A. Popelin. An industrial software for uncertainty quantification in simulation. Technical Report hal-01107849v2, HAL, 2015.
- [15] Z. Bazant and B. Oh. Crack band theory for fracture of concrete. *Materiaux et Constructions*, 16(93):155–177, 1983.
- [16] A. Belarbi and T. Hsu. Constitutive laws of concrete in tension and reinforcing bars stiffened by concrete. *ACI Structural Journal*, 91(4):465–474, 1994.
- [17] N. N. Belov, N. T. Yugov, D. G. Kopanitsa, and A. A. Yugov. Stress analysis of concrete and reinforced concrete slab structures under a high velocity impact. *Journal of Applied Mechanics and Technical Physics*, 46(3):444–451, 2005.

- [18] P. BerthetRambaud. *Structures rigides soumises aux avalanches et chutes de blocs: modélisation du comportement mécanique et caractérisation de l'interaction "phénomène-ouvrage"*. PhD thesis, Université Grenoble I - Joseph Fourier, 2004.
- [19] P. BerthetRambaud, P. Perrotin, F. Delhomme, M. Mommessin, J. Mougin, J. Tonello, and J. Mazars. Analytical advantages and numerical modeling of impact testing on a structurally-dissipating rock-shed slab (sdr). *BLPC*, 263-264:19–42, 2006.
- [20] J. Biggs. *Introduction to structural dynamics*. McGraw-Hill, 1964.
- [21] V. Birtel and P. Mark. Parameterised finite element modelling of rc beam shear failure. In *ABAQUS Users' Conference*, 2006.
- [22] P. Bischoff and S. Perry. Compressive behaviour of concrete at high strain rates. *Materials and Structures*, 24:425–450, 1991.
- [23] M. Bournonville, J. Dahnke, and D. Darwin. Statistical analysis of the mechanical properties and weight of reinforcing bars. Master's thesis, University of Kansas - Structural Engineering and Engineering Materials, 2001.
- [24] E. BouSaid. Modèle physique de l'enceinte. Technical report, IOSIS, 2009.
- [25] J. Braverman, C. Miller, B. Ellingwood, D. Naus, C. Hofmayer, P. Bezler, and T. Chang. Structural performance of degraded reinforced concrete members. In *16th International Conference on Structural Mechanics in Reactor Technology*, 2001.
- [26] K. Breitung and M. Hoenbichler. Asymptotic approximations for multivariate integrals with an application to multinormal probabilities. *Journal of Multivariate Analysis*, 30(1):80–97, 1989.
- [27] N. Burlion, F. Gatuingt, G. Pijaudier-Cabot, and L. Daudeville. Compaction and tensile damage in concrete: constitutive modelling and application to dynamics. *Computer Methods in Applied Mechanics and Engineering*, 183:291–308, 2000.
- [28] W. Cao, Y. Zhang, H. Dong, Z. Zhou, and Q. Qiao. Experimental study on the seismic performance of recycled concrete brick walls embedded with vertical reinforcement. *Materials*, 7:5934–5958, 2014.
- [29] CEB. Concrete structures under impact and impulsive loading. Technical report, Comite Euro-International Du Beton, 1988.
- [30] CEB. Ceb-fip model code 1990 - ceb bulletin d'information no. 213/214. Technical report, Comite Euro-International du Beton, 1993.
- [31] M. Cervera and E. Hinton. Nonlinear analysis of reinforced concrete plates and shells using a three dimensional model. *Comp. Modeling of RC struct.*, 1:327–370, 1986.
- [32] M. Cervera, E. Hinton, and O. Hassan. Nonlinear analysis of reinforced concrete plate and shell structures using 20-noded isoparametric brick elements. *Computers and Structures*, 25(6):845–869, 1987.
- [33] M. Cervera, J. Olivier, and R. Faria. Seismic evaluation of concrete dams via continuum damage models. *Earthquake Engineering and Structural Dynamics*, 24(9):1225–1245, 1995.
- [34] Y. Chen and I.M. May. Reinforced concrete members under drop-weight impacts. *Proceedings of the Institution of Civil Engineers. Structures and buildings*, 162(1):45–56, 2009.

- [35] B. Choi and Y. Kwon. Probabilistic analysis of reinforced concrete beams and slab deflections using monte carlo simulation. *KCI Concrete Journal*, 12(2):11–21, 2000.
- [36] K.T. Chong. *Numerical modelling of time-dependent cracking and defromation of reinforced concrete structures*. PhD thesis, The University of New South Wales - School of Civil & Engineering - Sydney - Australia, 2004.
- [37] Y. Choo, Y. Lee, and K. Lee. A study on the cover failure in concrete structure following concrete deterioration - 8155. In *WM2008 Conference*, 2008.
- [38] M.A. Choudhury, N.A. Siddiqui, and H. Abbas. Reliability analysis of a buried concrete target under missile impact. *International Journal Of Impact Engineering*, 27:791–806, 2002.
- [39] A. Christoforou. Impact dynamics and damage in composite structures. *Composite Structures*, 52:181–188, 2001.
- [40] A. Christoforou and S. Swanson. Analysis of impact response in composite plates. *Inter. J. Solids Structures*, 27(2):161–170, 1991.
- [41] A. Christoforou and A. Yigit. Effect of flexibility on low velocity impact response. *Journal of Sound and Vibration*, 217(2):563–578, 1998.
- [42] A. Christoforou and A. Yigit. Scaling of low-velocity impact response in composite structures. *Composite Structures*, 91:15–24, 2009.
- [43] M. Collins and D. Mitchell. *Prestressed concrete basics*. CPCI, 1987.
- [44] T. Croston. *Etude expérimentale du comportement d'une poutre en béton armé en flexion 3 points réparée par matériaux composites (approche probabiliste)*. PhD thesis, L'école Nationale Supérieure d'Arts et Métiers - Centre de Bordeaux, 2006.
- [45] L. Daudeville and Y. Malecot. Concrete structures under impact. *European Journal of Environmental and Civil Engineering*, 15:101–140, 2011.
- [46] F. Deheeger. *Couplage mécano-fiabiliste: SMART - méthodologie d'apprentissage stochastique en fiabilité*. PhD thesis, Université Blaise Pascal - Clermont II, 2008.
- [47] F. Delhomme, M. Mommessin, J.P. Mougin, and P. Perrotin. Simulation of a block impacting a reinforced concrete slab with a finite element model and a mass-spring system. *Engineering Structures*, 29:2844–2852, 2007.
- [48] A. Deng and D. Xu. Experimental research on damage parameter of concrete in non-uniform stress field. *World Journal of Mechanics*, 1:155–157, 2011.
- [49] P. Desayi and S. Krishnan. Equation for the stress-strain curve for concrete. *ACI Journal*, 61(3):345–350, 1964.
- [50] K. Dolinski. First-order second-order moment approximation in reliability of structural systems: critical review and alternative approach. *Structural Safety*, 1:211–231, 1983.
- [51] J. Dulac and J.P. Giraud. Impact testing of reinforced concrete slabs. In *6th SMiRT Conference - Structural Mechanics in Reactor Technology*, 1981.
- [52] N. Duranovic and A.J. Watson. Impulsive loading on reinforced concrete slabs - local failur propagation -. Department of Civil and Structural Engineering, University of Sheffield, U.K.

- [53] C. Eamon, M. Thompson, and Z. Liu. Evaluation of accuracy and efficiency of some simulation and sampling methods in structural reliability analysis. *Structural Safety*, 27:356–392, 2005.
- [54] ECP. Commentary eurocode 2. Technical report, European Concrete Platform, 2008.
- [55] J. Eibl. Soft and hard impact. In *FIP Congress, The Concrete Society, Concrete for Hazard Protection*, 1987.
- [56] W. El-Dakhkhni, F. Meeky, and S. Rezaei. Validity of sdof models for analyzing two-way rc panels under blast loading. *Journal of Performance of Constructed Facilities, ASCE*, 24:311–325, 2010.
- [57] B. Ellingwood, T. Galambos, J. MacGregor, and C. Cornell. Development of a probability based load criterion for american standard a58. Technical Report 577, National Bureau of Standards Sepcial Publication, 1980.
- [58] B. Ellingwood and H. Hwang. Probabilistic descriptions of resistance of safety-related structures in nuclear plants. *Nuclear Engineering and Design*, 88(2):169–178, 1985.
- [59] M. Faber, O. Kubler, M. Fontana, and M. Knobloch. Failure consequences and reliability acceptance criteria for exceptional building structures. Technical report, Institute of Structural Engineering Swiss Federal Institute of Technology, Zurich, 2004.
- [60] F. Favre, J. Jaccoud, O. Burdet, and H. Charif. *Dimensionnement des structures en béton - Aptitude au service et éléments de structures*. Presse Polytechnique et Universitaires Romandes, 1997.
- [61] G. Fiquet and S. Dacquet. Study of the perforation of reinforced concrete slabs by rigid missiles - experimental study, part ii. *Nuclear Engineering and Design*, 41:103–120, 1977.
- [62] F. Firat and M. Yucemen. Uncertainty analysis for reinforced concrete members constructed in turkey. In *International Conference on Construction and Building Technology*, 2008.
- [63] A.M. Freudenthal. The statistical aspect of fatigue of materials. *Proceedings of the Royal Society of London*, A187(1011):416–429, 1946.
- [64] A.M. Freudenthal. The safety of structures. *Transactions of ASCE*, 112:125–180, 1947.
- [65] A.M. Freudenthal. Safety and the probability of structural failure. *Transactions of ASCE*, 121:1337–1397, 1956.
- [66] A.M. Freudenthal and E.J. Gumbel. On the statistical interpretation of fatigue tests. *Proceedings of the Royal Society of London*, A216:309–362, 1953.
- [67] D. Gay and J. Gambelin. *Dimensionnement des structures*. Hermès-Lavoisier, Paris, 1999.
- [68] A. Ghoulbzouri, A. Khamlichi, F. Almansa, M. Parron Vera, and M. Rubio Cintas. Evaluating some reliability analysis methodomethod in seismic design. *American Journal of Engineering and Applied Sciences*, 4(3):332–340, 2011.
- [69] A. Ghoulbzouri, B. Kissi, and A. Khamlichi. Reliability analysis in performance-based earthquake engineering. *Procedia Engineering*, 114:643–649, 2015.
- [70] A. Ghoulbzouri, B. Kissi, and A. Khamlichi. Reliability analysis of reinforced concrete buildings: comparison between form and ism. *Procedia Engineering*, 114:650–657, 2015.

- [71] S. Goldstein, C. Berriaud, and R. Labrot. Study of the perforation of reinforced concrete slabs by rigid missiles - experimental study, part iii. *Nuclear Engineering and Design*, 41:121–128, 1977.
- [72] P. Grassl, K. Lundgren, and K. Gylltoft. Concrete in compression: a plasticity theory with a novel hardening law. *International Journal of Solids and Structures*, 39:5205–5223, 2002.
- [73] P. Grassl, D. Xenos, U. Nystrom, R. Rempling, and K. Gylltoft. Cdpm2: A damage-plasticity approach to modelling the failure of concrete. *International Journal of Solids and Structures*, 50:3805–3816, 2013.
- [74] F.P. Grooteman. An adaptive directional importance sampling method for structural reliability. Technical report, National Aerospace Laboratory NLR, 2011.
- [75] Z. Guédé. *Approche probabiliste de la durée de vie des structures sollicitées en fatigue thermique*. PhD thesis, Université Blaise Pascal -Clermont II, 2005.
- [76] J. Guedes, P. Pegon, and A. Pinto. A fibre timoshenko beam element in castem 2000. Special publication nr. i.94.31, J.R.C, 1994.
- [77] R. Gueraud, A. Sokolovsky, M. Kavyrchine, and M. Astruc. Study of the perforation of reinforced concrete slabs by missiles - general introduction and experimental study, part i. *Nuclear Engineering and Design*, 41:91–102, 1977.
- [78] Z. Haidong. *Strengthening of RC slabs with openings using CFRP systems*. PhD thesis, Department of Civil Engineering - National University of Singapore, 2006.
- [79] A. Haldar and S. Mahadevan. *Probability, reliability and statistical methods in engineering design*. John Wiley & Sons, Inc., 2000.
- [80] G. Herve and F. Gatuingt. Simulation numérique de l’endommagement de dalles en béton armé impactées par un réacteur d’avion idéalisé. In *7e Colloque National en Calcul des Structures*, 2005.
- [81] A. Hillerborg, M. Modeer, and P. Petersson. Analysis of crack formation and crack growth in concrete by means of fracture mechanics and finite elements. *Cement and Concrete Research*, 6:773–782, 1976.
- [82] H. Hong, M. Nessim, T. Zimmerman, and D. Degeer. Calibration of material resistance factors in csa s474-m1989. C-FER Report 89-25, Centre for Frontier Engineering Research, 1990.
- [83] D.A. Hordijk. Tensile and tensile fatigue behaviour of concrete; experiments, modelling and analyses. *Heron*, 37(1):1–79, 1992.
- [84] T. Hrynyk. *Behaviour and modelling of reinforced concrete slabs and shells under static and dynamic loads*. PhD thesis, Graduate Department of Civil Engineering - University of Toronto, 2013.
- [85] L. Hsu and C. Hsu. Complete stress-strain behaviour of high-strength concrete under compression. *Magazine of Concrete Research*, 46(169):301–312, 1994.
- [86] M. Jahidulislam and Z. Liu and S. Swaddiwudhipong. Numerical study on concrete penetration/perforation under high velocity impact by ogive-nose steel projectile. *Computers and Concrete*, 8:111–123, 2011.

- [87] T. Jankowiak and T. Lodygowski. Identification of parameters of concrete damage plasticity constitutive model. *Foundations of Civil and Environmental Engineering*, 6:53–69, 2005.
- [88] L. Jason, A. Huerta, G. Pijaudier-Cabot, and S. Ghavamian. An elastic plastic damage formulation for concrete: Application to elementary tests and comparison with an isotropic damage model. *Computer Methods in Applied Mechanics and Engineering*, 195:7077–7092, 2006.
- [89] Joint Committee of Structural Safety. *Probabilistic model code*, 2001.
- [90] W. Jonas, R. Meschkat, H. Riech, and E. Rudiger. Experimental investigations to determine the kinetic ultimate bearing capacity of reinforced concrete slabs subjected to deformable missiles. In *5th SMiRT Conference - Structural Mechanics in Reactor Technology*, 1979.
- [91] G. Jonsson. *Reliability analysis of structural concrete elements*. PhD thesis, University of British Columbia, 1992.
- [92] O. Jovall. Airplane crash simulations: comparison of analyses results with test data. *SMIRT 19*, WJ2/2:8, 2007.
- [93] R.P. Kennedy. A review of procedures for the analysis and design of concrete structures to resist missile impact effects. *Nuclear Engineering and Design*, 37(2):183–203, 1976.
- [94] P. Kmiecik and M. Kaminski. Modelling of reinforced concrete structures and composite structures with concrete strength degradation taken into consideration. *Archives of Civil and Mechanical Engineering*, 11(3):623–636, 2011.
- [95] P. Koechlin and S. Potapov. Classification of soft and hard impacts - application to aircraft crash. *Nuclear Engineering and Design*, 239:613–618, 2009.
- [96] C. Koh, M. Teng, and T. Wee. A plastic-damage model for lightweight concrete and normal weight concrete. *International Journal of Concrete Structures and Materials*, 2(2):123–136, 2008.
- [97] I. Kojima. An experimental study on local behaviour of reinforced concrete slabs to missile impact. *Nuclear Engineering and Design*, 130:121–132, 1991.
- [98] V. Korotkov, D. Poprygin, K. Ilin, and S. Ryzhov. Determination of dynamic reaction in concrete floors of civil structures of nuclear power plant in accidental drops of heavy objects. In *ABAQUS Users Conference*, 2004.
- [99] W. Kratzig and R. Polling. An elasto-plastic damage model for reinforced concrete with minimum number of material parameters. *Computers and Structures*, 82:1201–1215, 2004.
- [100] H. Kupfer, H. Hilsdorf, and H. Rusch. Behavior of concrete under biaxial stresses. *ACI Journal*, 65(8):656–666, 1969.
- [101] H. Kwak and F. Filippou. Nonlinear fe analysis of rc structures under monotonic loads. *Computers and Structures*, 65(1):1–16, 1997.
- [102] R. Lebrun and A. Dutfoy. Do rosenblatt and nataf isoprobabilistic transformations really differ? *Probabilistic Engineering Mechanics*, 24:577–584, 2009.
- [103] J. Lee and G. Fenves. Numerical implementation of plastic damage model for concrete under cyclic loading : Application to concrete dam. Technical Report UCB/SEMM-94/03, Department of Civil Engineering, University of California, 1994.

- [104] J. Lee and G. Fenves. Plastic-damage model for cyclic loading of concrete structures. *ASCE*, 124:892–900, 1998.
- [105] Y. Lee and K. Lee. On the dynamic response of laminate circular cylindrical shells under impulse loads. *Composite and Structures*, 2(1):149–157, 1997.
- [106] M. Lemaire. *Fiabilité des structures: couplage mécano-fiabiliste statique*. Lavoisier, 2005.
- [107] M. Lemaire. *Structural reliability*. John Wiley & Sons, 2008.
- [108] LESSLOSS. Comparison of experimental results to those of nonlinear analyses with various model approach and degrees of sophistication. main model parameters affecting reliability of prediction of nonlinear analysis for member deformations. Technical report, 2006.
- [109] Q.M. Li, S.R. Reid, H.M. Wen, and A.R. Telford. Local impact effects of hard missiles on concrete targets. *International Journal of Impact Engineering*, 32(1-4):224–284, 2005.
- [110] H. Low and H. Hao. Reliability analysis of reinforced concrete slabs under explosive loading. *Structural Safety*, 23:157–178, 2001.
- [111] H. Low and H. Hao. Reliability analysis of direct shear and flexural failure modes of rc slabs under explosive loading. *Engineering Structures*, 24:189–198, 2002.
- [112] L.N. Lowes. *Finite element modeling of reinforced concrete beam-columns bridge connections*. PhD thesis, University of California, Berkeley, 1993.
- [113] J. Lubliner, S. Oliver, S. Oller, and E. Onare. A plastic-damage model for concrete. *International Journal of Solids and Structures*, 25(3):229–326, 1989.
- [114] J. MacGregor. Safety and limit states design for reinforced concrete. *CJCE*, 3(4):279–287, 1976.
- [115] J. MacGregor, S. Mirza, and B. Ellingwood. Statistical analysis of resistance of reinforced and prestressed concrete members. *ACI Journal*, 80(3):167–176, 1983.
- [116] S. Majewski. The mechanics of structural concrete in terms of elasto-plasticity. Technical report, Silesian Polytechnic Publishing House, Gliwice, 2003.
- [117] M. Mansour, J. Lee, and T. Hsu. Cyclic stress-strain curves of concrete and steel bars in membrane elements. *Journal of Structural Engineering*, 127(12):1402–1411, 2001.
- [118] P. Mark and M. Bender. Computational modelling of failure mechanisms in reinforced concrete structures. *Architecture and Civil Engineering*, 8(1):1–12, 2010.
- [119] O. Martin. Comparison of different constitutive models for concrete in abaqus/explicit for missile impact analyses. Technical report, European Commission - Joint Research Centre - Institute for Energy, 2010.
- [120] J. Mazars and G. Pijaudier-Gabot. Continuum damage theory: Application to concrete. *Journal of Engineering Mechanics*, 115:345–365, 1989.
- [121] R. Melchers. *Structural reliability analysis and prediction*. Wiley, 1999.
- [122] P. Menetrey and K. Willam. A triaxial failure criterion for concrete and its generalization. *ACI Structural Journal*, 92:311–318, 1995.

- [123] S. Mirza, M. Hatzinikolas, and J. MacGregor. Statistical description of the strength of concrete. *Journal of the Structural Division, ASCE*, 105:1021–1037, 1979.
- [124] S. Mirza, D. Kikuchi, and J. MacGregor. Flexural strength reduction factor for bonded prestressed concrete beams. *ACI Journal*, 77(4):237–246, 1980.
- [125] S. Mirza and J. MacGregor. Strength and ductility of concrete slabs reinforced with welded wire fabric. *ACI Journal*, 78(33):374–381, 1979.
- [126] S. Mirza and J. MacGregor. Variability of mechanical properties of reinforcing bars. *Journal of the Structural Division, ASCE*, 105:921–937, 1979.
- [127] S. Mirza and J. MacGregor. Variations in dimensions of reinforced concrete members. *Journal of the Structural Division, ASCE*, 105:751–765, 1979.
- [128] S. Mirza and J. MacGregor. Probabilistic study of strength of reinforced concrete members. *Canadian Journal of civil engineering*, 9:431–448, 1982.
- [129] S. Mirza and B. Skrabek. Reliability of short composite beam-column strength interaction. *Journal of the Structural Division, ASCE*, 117(8):2320–2339, 1991.
- [130] A. Miyamoto and M. King. Design concept for reinforced concrete slab structures under soft impact loads. *Transactions on the Built Environment*, 22:191–207, 1996.
- [131] A. Miyamoto, M. King, and M. Fuji. Analysis of failure modes for reinforced concrete slabs under impulsive loads. *ACI Structural Journal*, 88(5):538–545, 1991.
- [132] A. Miyamoto, M. King, and M. Fuji. Nonlinear dynamic analysis of reinforced concrete slabs under impulsive loads. *ACI Structural Journal*, 88(4):411–419, 1991.
- [133] A. Miyamoto, M. King, and M. Fujii. Integrated analytical procedure for concrete slabs under impact loads. *Journal of Structural Engineering*, 120(6):1685–1702, 1994.
- [134] A. Miyamoto, H. Nakamura, and A. Ramezani-pour. Impact-resistant design of rc slabs using immune algorithms. *Computer -Aided Civil and Infrastructure Engineering*, 15:391–408, 2000.
- [135] A. Mohamed, M. Shoukry, and J. Saeed. Prediction of the behavior of reinforced concrete deep beams with web openings using the finite element method. *Alexandria Engineering Journal*, 53:329–339, 2014.
- [136] S. Mohammadkhani. *Contribution à l'étude de la redondance dans les ponts: Analyses des mécanismes de défaillance par surfaces de réponse*. PhD thesis, Ecole Nationale des Ponts et Chaussées, 2007.
- [137] S.N. Mokhtar and R. Abdullah. Computational analysis of reinforced concrete slabs subjected to impact loads. *International Journal of Integrated Engineering*, 4(2):70–76, 2012.
- [138] A. Murthy, G. Palani, and N. Iyer. Impact analysis of concrete structural components. *Defence Science Journal*, 60(3):307–319, 2010.
- [139] A. Naaman and S. Amnuayporn. Reliability of partially prestressed beams at serviceability limit states. *PCI Journal*, 27:66–85, 1982.
- [140] W. Nachtsheim and F. Stangenberg. Impact of deformable missiles on reinforced concrete plates - comparative calculations of meppen tests. In *6th SMiRT Conference - Structural Mechanics in Reactor Technology*, 1981.

- [141] W. Nachtsheim and F. Stangenberg. Interpretation of results of meppen slab tests - comparison with parametric investigations. *Nuclear Engineering and Design*, 75:283–290, 1982.
- [142] R. Narayanan and O. Brooker. *How to design concrete structures using Eurocode 2: Introduction to Eurocodes*. The concrete center, 2005.
- [143] R. Nayal and H.A. Rasheed. Tension stiffening model for concrete beams reinforced with steel and frp bars. *Journal of Materials in Civil Engineering*, 18(6):831–841, 2006.
- [144] A. Nowak and K. Collins. *Reliability of structures*. MCGraw-Hill, 2000.
- [145] A. Nowak and M. Szeszen. Calibration of design code for buildings (aci 318): part 1 - statistical model for resistance. *ACI Structural Journal*, 100(3):377–382, 2003.
- [146] T. Oh-oka, Y. Kitsutaka, and K. Watanabe. Influence of short cut fiber mixing and curing time on the fracture parameter of concrete. *Journal of Structural and Construction Engineering*, 529:1–6, 2000.
- [147] T. Ohno, T. Uchida, N. Matsumoto, and Y. Takahashi. Local damage of reinforced concrete slabs by impact of deformable projectiles. *Nuclear Engineering and Design*, 138:45–52, 1992.
- [148] R. Olsson. Experimental verification of a theory for the impact response of composite plates. Technical report, Aeronautical Research Inst. of Sweden - Stockholm, 1991.
- [149] R. Olsson. Mass criterion for wave controlled impact response of composite plates. *Composites: Part A*, 31:879–887, 2000.
- [150] R. Olsson. Analytical prediction of large mass impact damage in composite laminates. *Composites - Part A: applied science and manufacturing*, 32:1207–1215, 2001.
- [151] R. Olsson. Experimental validation of delamination criterion for small mass impact. In *16th International Conference on Composite Materials*, 2007.
- [152] O. Omid and V. Lotfi. Finite element analysis of concrete structures using plastic-damage model in 3-d implementation. *International Journal of Civil Engineering*, 8(3):187–203, 2010.
- [153] A. Pandher. Reliability analysis of strength characteristics of fibre-reinforced fly ash concrete. Master’s thesis, Civil Engineering Departement - Thapar University, 2008.
- [154] M. Pavlovic, Z. Markovic, M. Veljkovic, and D. Budevaca. Bolted shear connectors vs. headed studs behaviour in push-out tests. *Journal of Constructional Steel Research*, 88:134–149, 2013.
- [155] F. Perrin. *Prise en compte des données expérimentales dans les modèles probabilistes pour la prévision de la durée de vie des structures*. PhD thesis, Université Blaise Pascal - Clermont II, 2008.
- [156] P. Peterson. Crack growth and development of fracture zones in plain concrete and similar materials. Technical Report TVBM-11-6, Division of Building Materials, University of Lund, 1981.
- [157] C. Pontiroli. *Comportement au soufflé des structures en béton armé, analyse expérimentale et modélisation*. PhD thesis, ENS Cachan, 1995.
- [158] G. Quaranta, S.K. Kunnath, and N. Sukumar. Maximum-entropy meshfree method for nonlinear static analysis of planar reinforced concrete structures. *Engineering Structures*, 42:179–189, 2012.

- [159] R. Rackwitz and B. Fiessler. Structural reliability under combined random load sequences. *Computers and Structures*, 9:489–494, 1978.
- [160] J. Reddy. *Mechanics of laminated composites plates and shells: theory and analysis*. CRC Press, 1997.
- [161] N. Reviron. *Etude du fluage des bétons en traction. Application aux enceintes de confinement des centrales nucléaires à eau sous pression*. PhD thesis, Ecole Normale Supérieure de Cachan, 2009.
- [162] E. Rudiger and H. Riech. Experimental and theoretical investigations on the impact of deformable missiles onto reinforced concrete slabs. In *7th SMiRT Conference - Structural Mechanics in Reactor Technology*, 1983.
- [163] G. Saporta. *Probabilités, analyse des données et statistiques*. Editions Technip, Paris, 1990.
- [164] N.K. Shetty. Probabilistic fatigue assessment of welded joints. *Probabilistic Methods for Structural Design - Solid Mechanics and its Applications*, 56:85–111, 1997.
- [165] J. Sorensen. Notes in structural reliability theory and risk analysis, 2004.
- [166] T. Sugano, H. Tsubota, Y. Kasai, N. Koshika, C. Itoh, K. Shirai, W.A. von Risemann, D.C. Bickel, and M.B. Parks. Local damage to reinforced concrete concrete structures caused by impact of aircraft engine missiles - part 2. evaluation of test results. *Nuclear Engineering and Design*, 140:407–423, 1993.
- [167] T. Sugano, H. Tsubota, Y. Kasai, N. Koshika, H. Ohnuma, W.A. von Risemann, D.C. Bickel, and M.B. Parks. Local damage to reinforced concrete concrete structures caused by impact of aircraft engine missiles - part 1. test program, method and results. *Nuclear Engineering and Design*, 140:387–405, 1993.
- [168] J. Sun. Probabilistic analysis of reinforced concrete bridge girders under corrosion. Master's thesis, University of Western Ontario, 1999.
- [169] F. Tahmasebinia. *Numerical modelling of reinforced concrete slabs subject to impact loading*. PhD thesis, University of Wollongong, 2008.
- [170] K. Tajima, T. Mishima, and N. Shirai. 3d finite element cyclic analysis of beam/column joint using special bond model. In *13th World Conference on Earthquake Engineering*, 2004.
- [171] Z. Taqieddin. *Elasto-plastic and damage modeling of reinforced concrete*. PhD thesis, Faculty of Louisiana State University, 2008.
- [172] J.W. Tedesco, J.C. Powell, C. Allen Ross, and M.L. Hughes. A strain-rate-dependent concrete material model for adina. *Computers and Structures*, 64(5-6):1053–1067, 1997.
- [173] D. Theodorakopoulos and R. Swamy. Ultimate punching shear strength analysis of slab-column connections. *Cement & Concrete Composites*, 24:500–521, 2002.
- [174] J. Tonello. Généralité et approche de modèles simples. Technical report, Cours Polytech'Grenoble "ouvrages paravalanches", 1988.
- [175] N. Trivedi and R.K. Singh. Prediction of impact induced failure modes in reinforced concrete slabs through nonlinear transient dynamic finite element simulation. *Annals of Nuclear Energy*, 56:109–121, 2013.

- [176] F. Udoeyo and P. Ugbem. Dimensional variations in reinforced concrete members. *Journal of Structural Engineering*, 121(12):1865–1867, 1995.
- [177] D. Val, F. Bljoger, and D. Yankelevsky. Reliability evaluation in nonlinear analysis of reinforced concrete structures. *Structural Safety*, 19(2):203–217, 1997.
- [178] B. Wahalathantri, D. Thambiratnam, T. Chan, and S. Fawzia. A material model for flexural crack simulation in reinforced concrete elements using abaqus. In *First International Conference on Engineering, Designing and Developing the Built Environment for Sustainable Wellbeing*, pages 260–264, 2011.
- [179] C. Wang and C. Salmon. *Reinforced concrete design*. Addison Wesley Education Publisher, 1998.
- [180] T. Wang and T. Hsu. Nonlinear finite element analysis of concrete structures using new constitutive models. *Computers and Structures*, 79:2781–2791, 2001.
- [181] D. Wisniewski. *Safety formats for all assessment of concrete bridges - with special focus on the precast concrete*. PhD thesis, University of Minho, Departement of Civil Engineering, 2007.
- [182] D. Wisniewski, J. Casas, A. Henriques, and P. Cruz. Probability-based assessment of existing concrete bridges - stochastic resistance models and applications. *Structural Engineering International*, 2:203–210, 2009.
- [183] E. Yamagushi and T. Ohta. Accurate and efficient method for analysis of reinforced concrete structures. *Journal of Structural Engineering*, 119(7):2017–2035, 1993.
- [184] A. Yigit and A. Christoforou. Limits of asymptotic solutions in low-velocity impact. *Composite Structures*, 81:568–574, 2007.
- [185] W. Yu. Inelastic modeling of reinforcing bars and blind analysis of the benchmark tests on beam-column joint under cyclic loading. Master’s thesis, European school for advanced studies in reduction of seismic risk, Rose School, 2006.
- [186] N. Zabaraz and T. Pervez. Viscous damping approximation of laminated anisotropic composite plates using the finite element method. *Computer methods in applied mechanics and engineering*, 81:291–316, 1990.
- [187] C. Zhang and Y. Zhang. Nonlinear dynamic analysis of the three gorge project powerhouse excited by pressure fluctuation. *Journal of Zhejiang University SCIENCE A*, 10(9):1231–1240, 2009.
- [188] Y. Zhang. *Analyse et dimensionnement d’ouvrages de protection contre les chutes de blocs*. PhD thesis, Ecole nationale des ponts et chassures, 2006.
- [189] M. Zineddin and T. Krauthammer. Dynamic response and behavior of reinforced concrete slabs under impact loading. *International Journal of Impact Engineering*, 34:1517–1534, 2007.

## Appendix A

# Probability distributions in OpenTRUNS 13.2

### Beta distribution

$$f_X(x) = \frac{2^{-\nu/2}}{\Gamma(\nu/2)} x^{(\nu/2-1)} e^{-x/2} \quad (\text{A.1})$$

with  $\nu$  is the shape parameters and  $\Gamma$  is the gamma function.

### ChiSquare distribution

$$f_X(x) = \frac{(x-a)^{r-1} (b-x)^{t-r-1}}{(b-a)^{t-1} B(r, t-r)} \quad (\text{A.2})$$

with  $r$  and  $t$  are the shape parameters,  $a$  and  $b$  are the lower and upper bounds, respectively, of the distribution, and  $B(r, t-r)$  is the beta function.

### Exponential distribution

$$f_X(x) = \lambda \exp(-\lambda(x-\gamma)) \quad (\text{A.3})$$

with  $\lambda$  is the scale parameter and  $\gamma$  is the location parameter.

### Gamma distribution

$$f_X(x) = \frac{\lambda}{\Gamma(k)} (\lambda(x-\gamma))^{k-1} \exp(-\lambda(x-\gamma)) \quad (\text{A.4})$$

with  $\lambda$  is the scale parameter,  $\gamma$  is the location parameter and  $k$  is the scale parameter.  $\Gamma$  is the gamma function.

### Gumbel distribution

$$f_X(x) = \alpha \exp\left(-\alpha(x-\beta) - e^{-\alpha(x-\beta)}\right) \quad (\text{A.5})$$

with  $\alpha$  is the scale parameter,  $\beta$  is the location parameter.

## Histogram distribution

$$f_X(x) = \sum_{i=1}^n H_i \quad (\text{A.6})$$

with  $H_i$  are the normalized heights of the histogram.

## Laplace distribution

$$f_X(x) = \frac{\lambda}{2} e^{-\lambda|x-\mu|} \quad (\text{A.7})$$

with  $\lambda$  is the scale parameter and  $\mu$  is the location parameter.

## Logistic distribution

$$f_X(x) = \frac{\exp\left(\frac{x-\alpha}{\beta}\right)}{\beta \left[1 + \exp\left(\frac{x-\alpha}{\beta}\right)\right]^2} \quad (\text{A.8})$$

with  $\beta$  is the scale parameter and  $\alpha$  is the location parameter.

## Lognormal distribution

$$f_X(x) = \frac{1}{\sigma_l (x - \gamma) \sqrt{2\pi}} \exp\left(-\frac{1}{2} \left(\frac{\ln(x - \gamma) - \mu_l}{\sigma_l}\right)^2\right) \quad (\text{A.9})$$

with  $\sigma_l$  is the shape parameter or the standard deviation of the log of the distribution,  $\gamma$  is the location parameter and  $\mu_l$  is the scale parameter or the median of the distribution.

## Normal distribution

$$f_X(x) = \frac{1}{\sigma\sqrt{2\pi}} \exp\left(-\frac{1}{2} \left(\frac{x - \mu}{\sigma}\right)^2\right) \quad (\text{A.10})$$

with  $\mu$  and  $\sigma$  are the mean and the standard deviation, respectively, of the variable  $X$ .

## Rayleigh distribution

$$f_X(x) = \frac{x - \gamma}{\sigma^2} e^{-\frac{(x-\gamma)^2}{2\sigma^2}} \quad (\text{A.11})$$

with  $\sigma$  is the scale parameter and  $\gamma$  is the location parameter.

## Student distribution

$$f_X(x) = \frac{1}{\sqrt{\nu} B\left(\frac{1}{2}, \frac{\nu}{2}\right)} \left(1 + \frac{(x - \mu)^2}{\nu}\right)^{-\frac{1}{2}(\nu+1)} \quad (\text{A.12})$$

with  $B$  is the beta function,  $\mu$  describes the most likely value and  $\nu$  is a measure of dispersion.

## Triangular distribution

$$\begin{cases} f_X(x) = \frac{2(x-a)}{(m-a)(b-a)}, & \text{if } a \leq x \leq m \\ f_X(x) = \frac{2(b-x)}{(b-m)(b-a)}, & \text{if } m \leq x \leq b \\ f_X(x) = 0, & \text{otherwise} \end{cases} \quad (\text{A.13})$$

with  $a$  and  $b$  are the lower and upper bounds, respectively, of the distribution, and  $m$  is the mode of the distribution.

## Truncated Normal distribution

$$f_X(x) = \frac{\varphi\left(\frac{x-\mu_n}{\sigma_n}\right)/\sigma_n}{\Phi\left(\frac{b-\mu_n}{\sigma_n}\right) - \Phi\left(\frac{a-\mu_n}{\sigma_n}\right)} \quad (\text{A.14})$$

with  $a$  and  $b$  are the lower and upper bounds, respectively, of the distribution.  $\mu_n$  is the location parameter and  $\sigma_n$  is the scale parameter.  $\varphi$  and  $\Phi$  represent the probability density and the cumulative distribution function, respectively, of the reduced centred Normal distribution.

## Uniform distribution

$$f_X(x) = \frac{1}{b-a} \quad (\text{A.15})$$

with  $a$  is the location parameter and  $b-a$  is the scale parameter.

## Weibull distribution

$$f_X(x) = \frac{\beta}{\alpha} \left(\frac{x-\gamma}{\alpha}\right)^{\beta-1} \exp\left(-\left(\frac{x-\gamma}{\alpha}\right)^\beta\right) \quad (\text{A.16})$$

with  $\beta$  is the shape parameter,  $\alpha$  is the scale parameter and  $\gamma$  is the location parameter.



## Appendix B

# MSM results - comparison with FEM results

### B.1 Impact kinetic energy

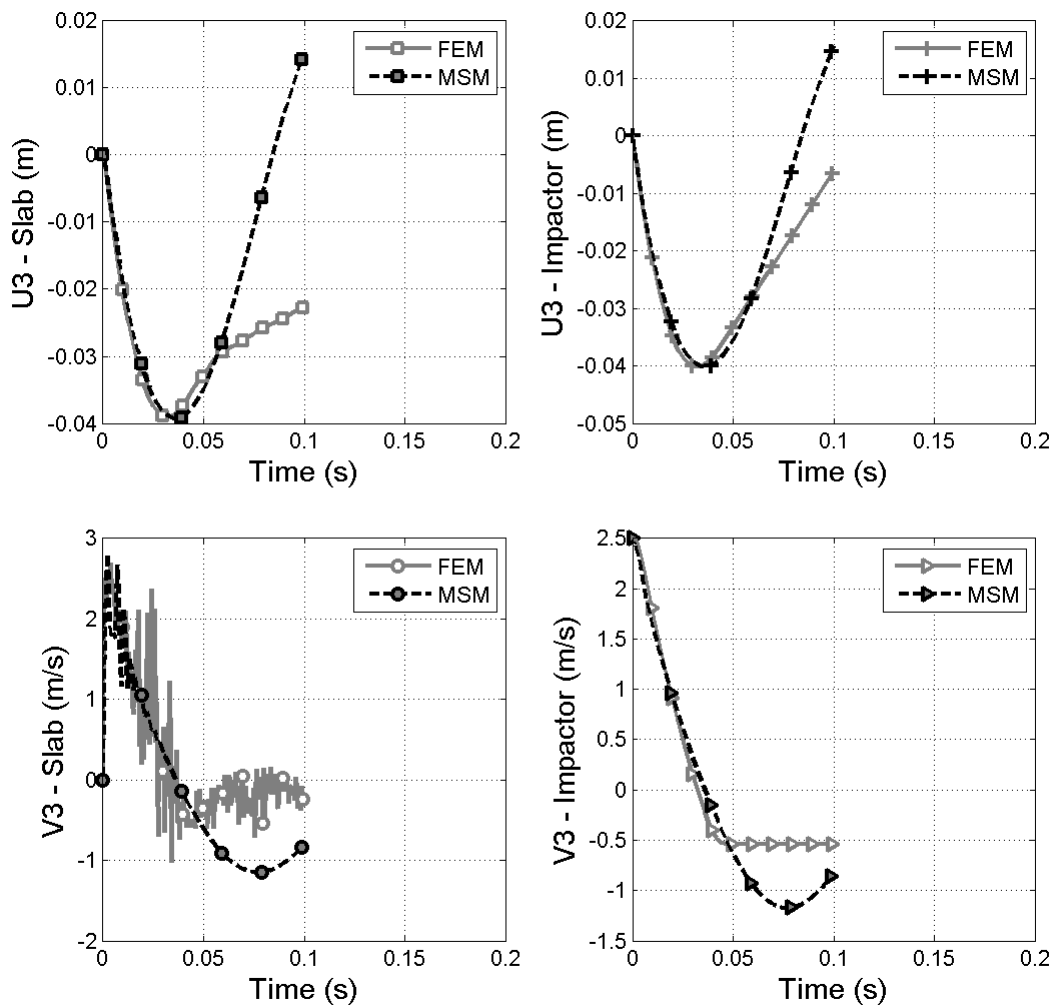


Figure B.1: Displacement and velocity of slab and impactor:  $v = 2.5 \text{ m/s}$ ,  $m = 34151 \text{ kg}$

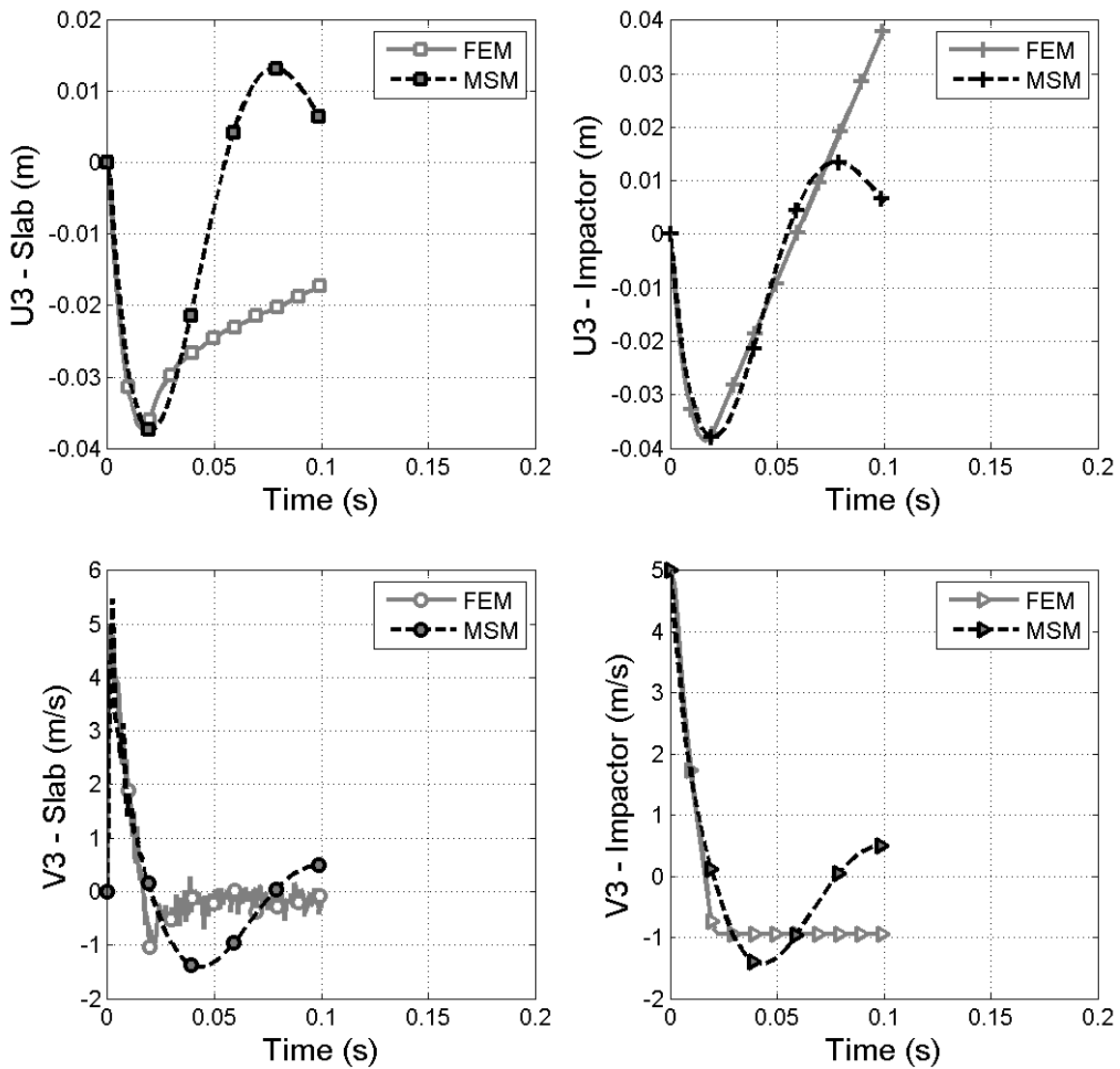


Figure B.2: Displacement and velocity of slab and impactor:  $v = 5 \text{ m/s}$ ,  $m = 8537 \text{ kg}$

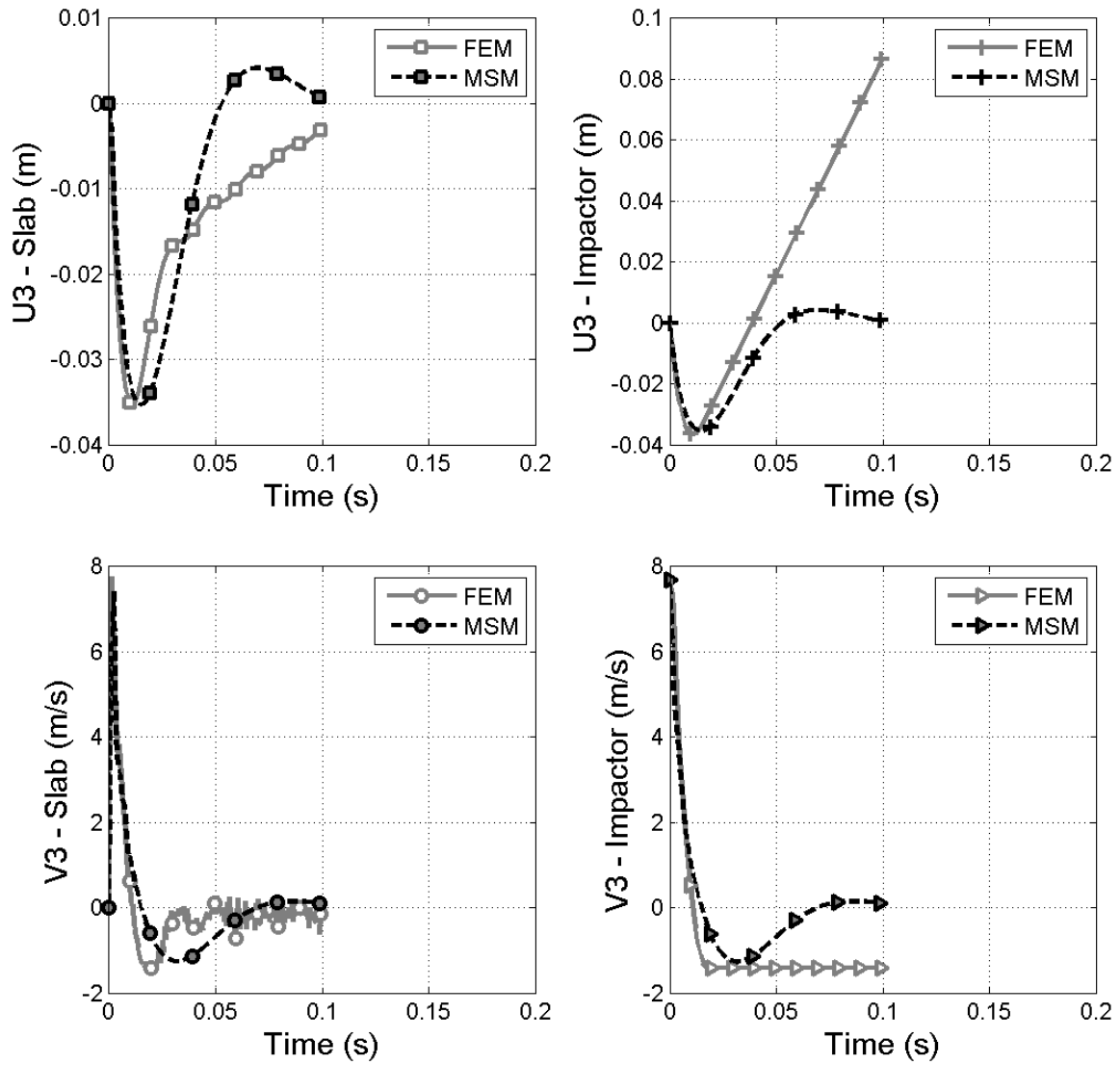


Figure B.3: Displacement and velocity of slab and impactor:  $v = 7.7 \text{ m/s}$ ,  $m = 3600 \text{ kg}$

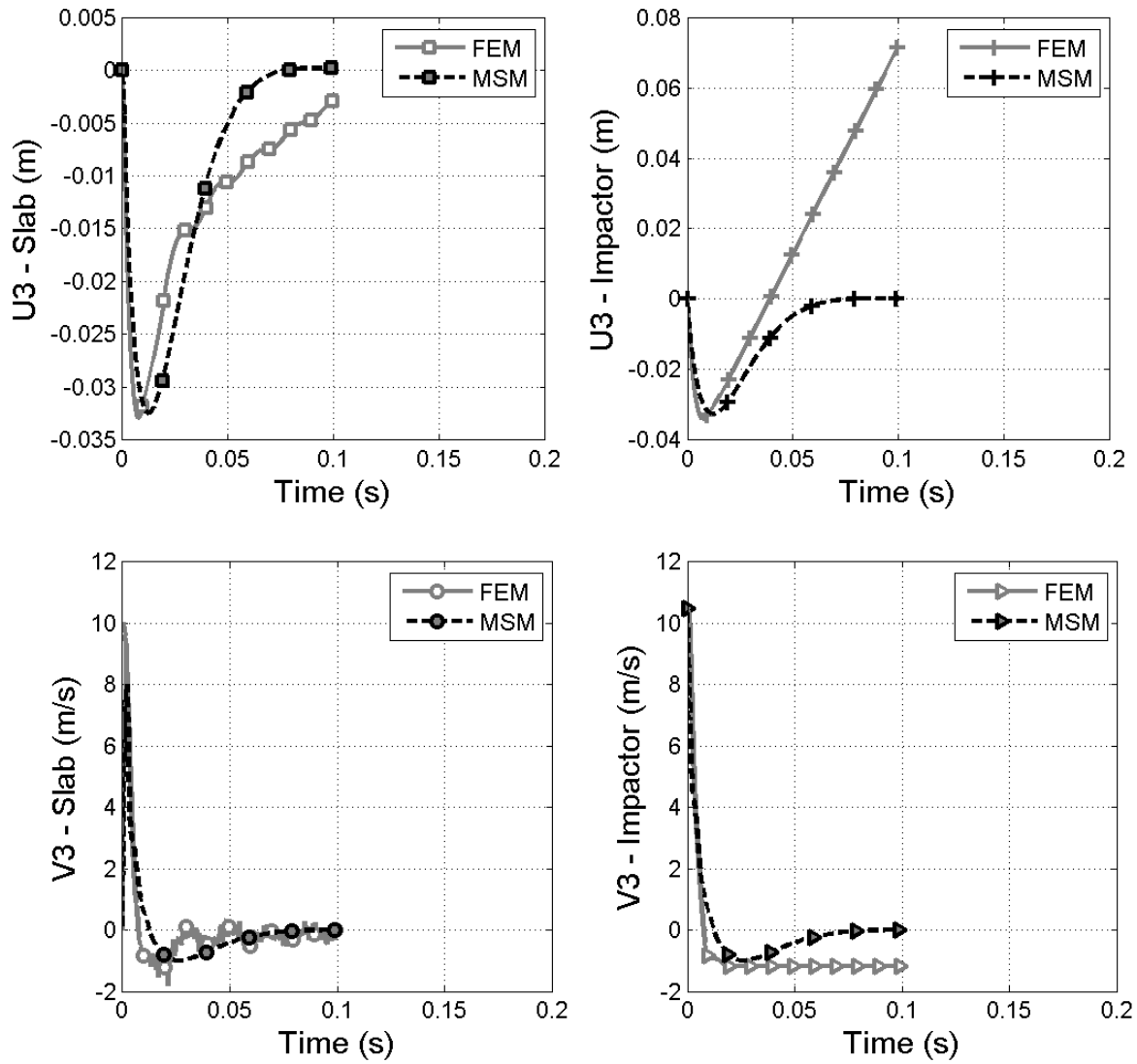


Figure B.4: Displacement and velocity of slab and impactor:  $v = 10.5 \text{ m/s}$ ,  $m = 1936 \text{ kg}$

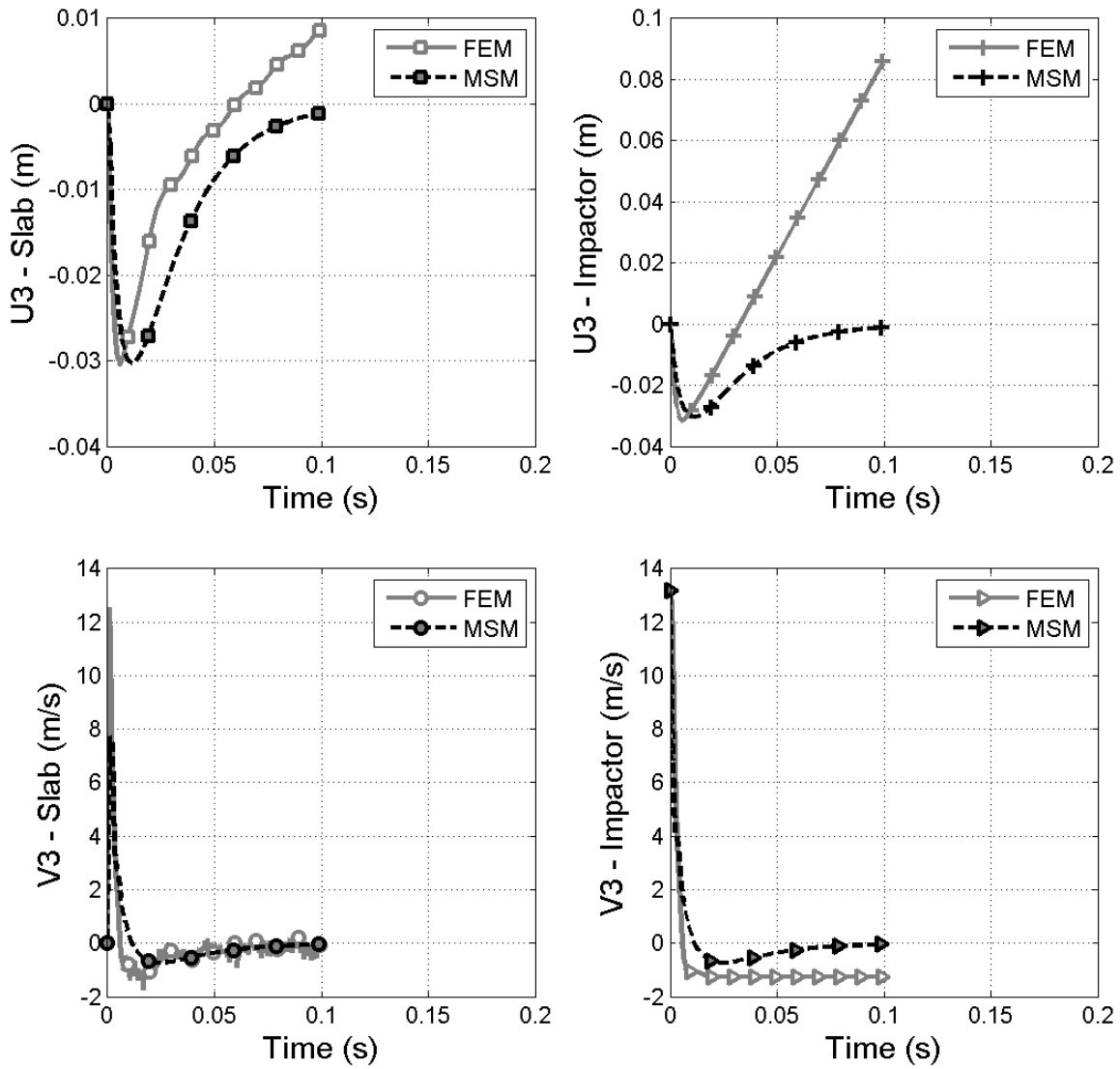


Figure B.5: Displacement and velocity of slab and impactor:  $v = 13.2 \text{ m/s}$ ,  $m = 1225 \text{ kg}$

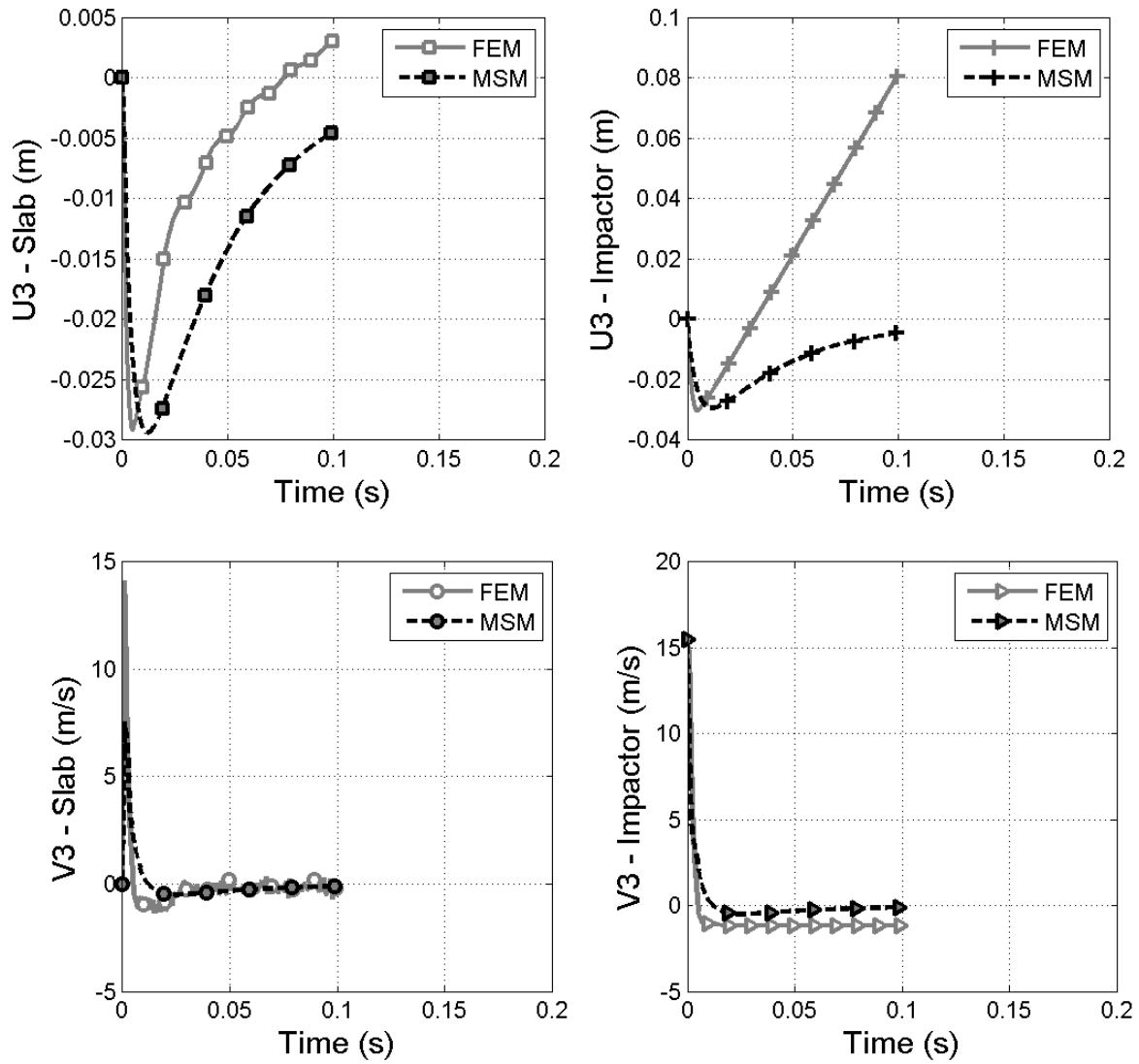


Figure B.6: Displacement and velocity of slab and impactor:  $v = 15.5 \text{ m/s}$ ,  $m = 888 \text{ kg}$

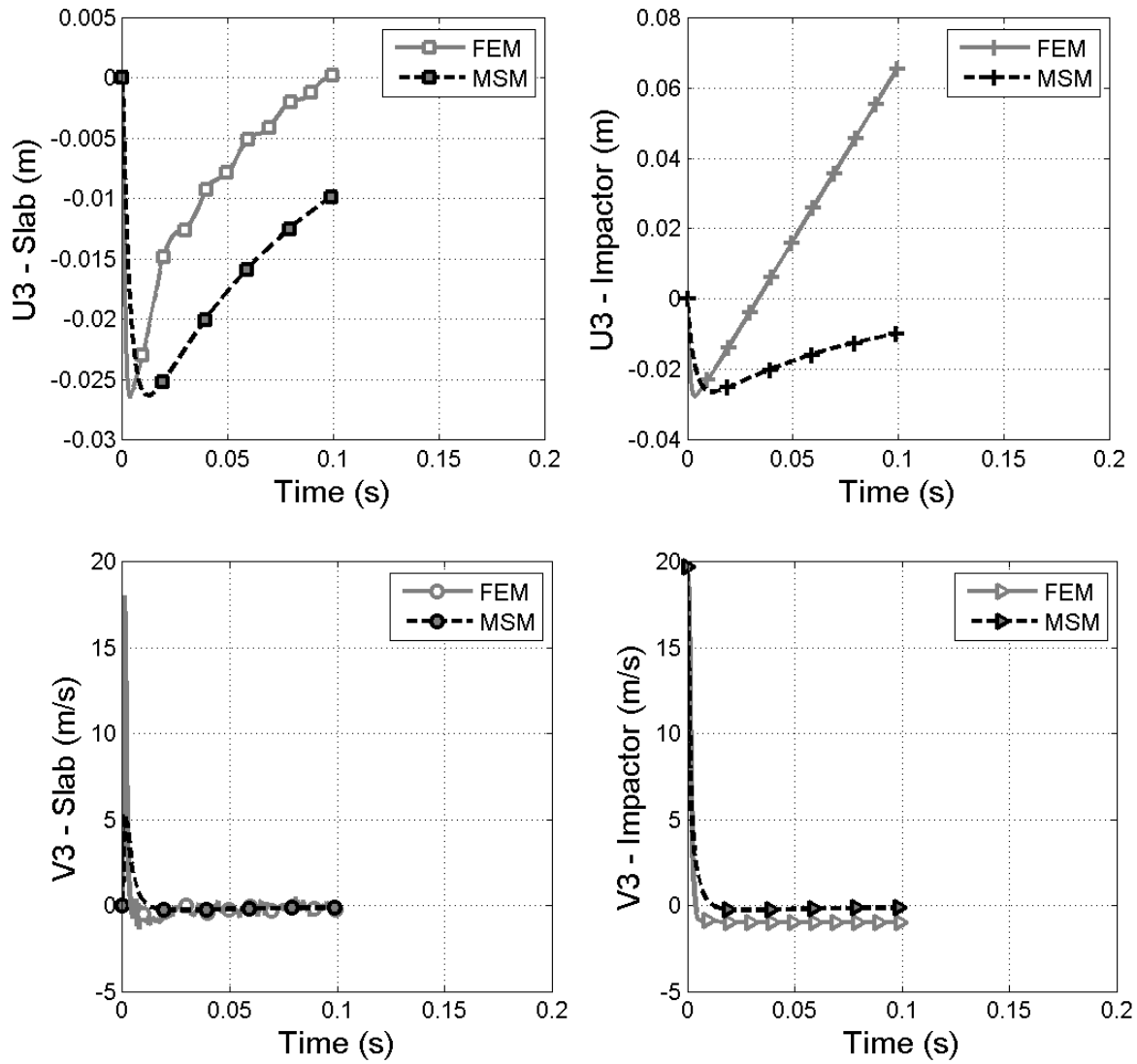


Figure B.7: Displacement and velocity of slab and impactor:  $v = 19.7 \text{ m/s}$ ,  $m = 550 \text{ kg}$

## B.2 Impactor velocity

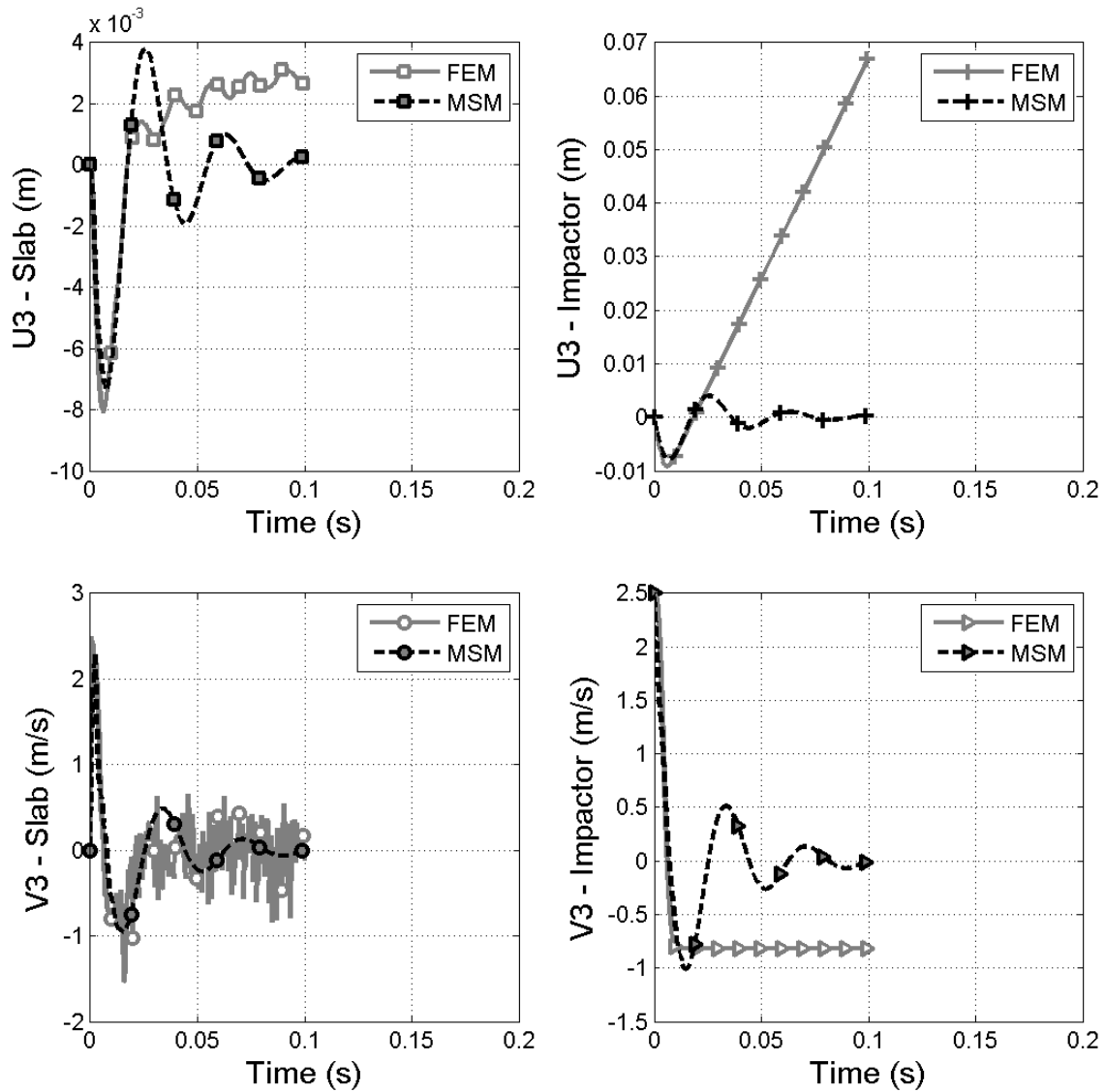


Figure B.8: Displacement and velocity of slab and impactor:  $v = 2.5 \text{ m/s}$

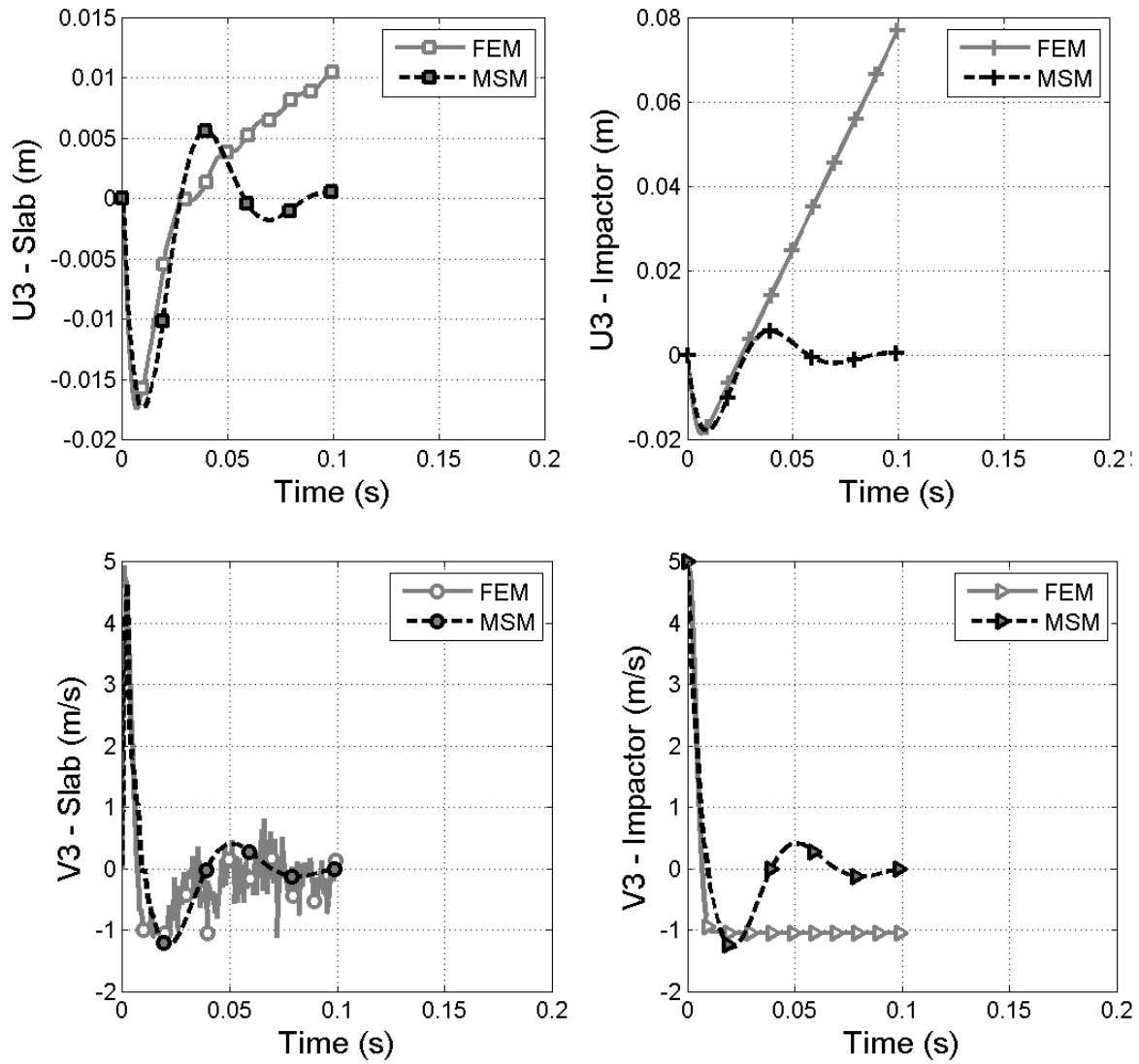


Figure B.9: Displacement and velocity of slab and impactor:  $v = 5 \text{ m/s}$

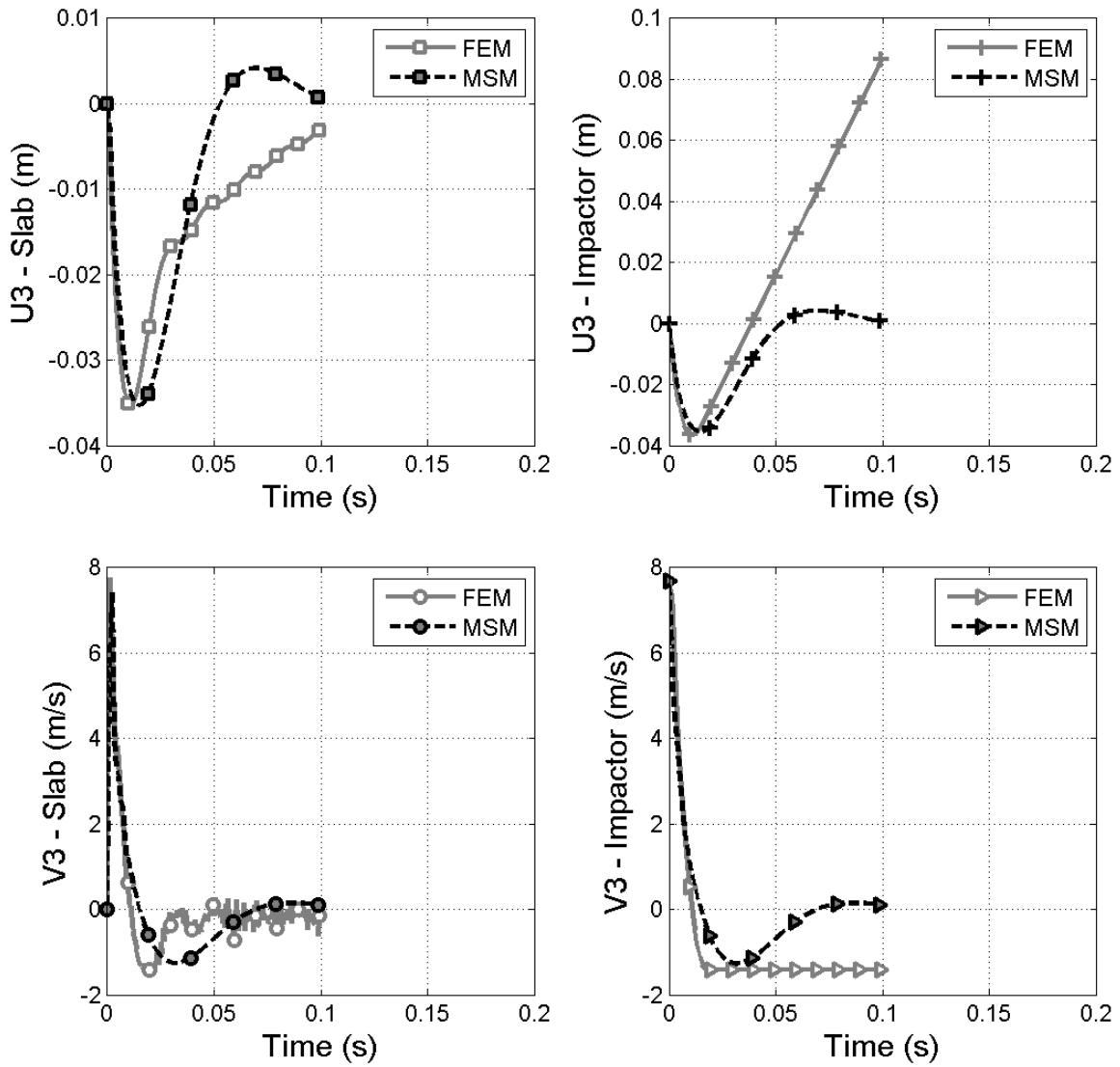


Figure B.10: Displacement and velocity of slab and impactor:  $v = 7.7 \text{ m/s}$

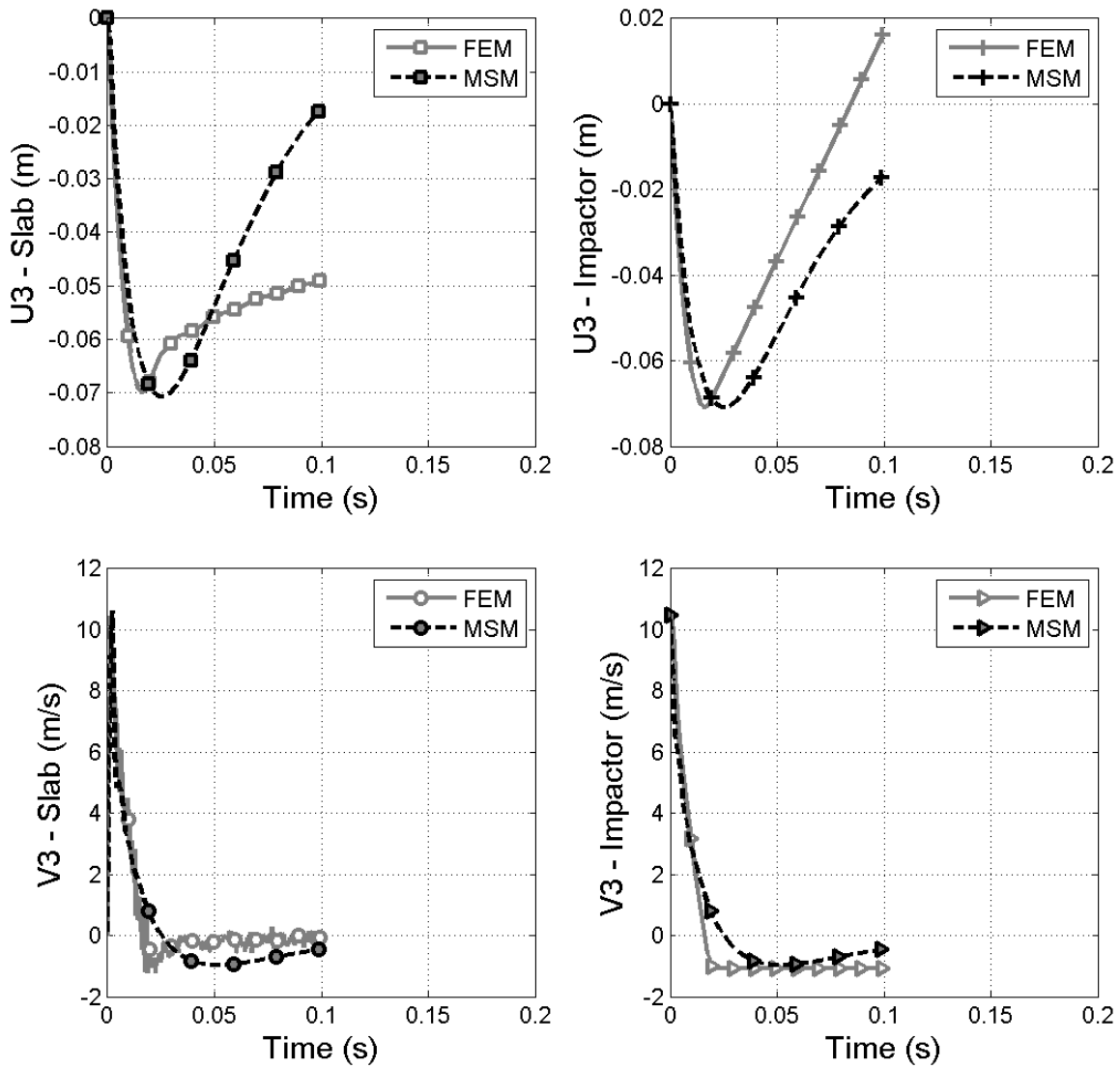


Figure B.11: Displacement and velocity of slab and impactor:  $v = 10.5 \text{ m/s}$

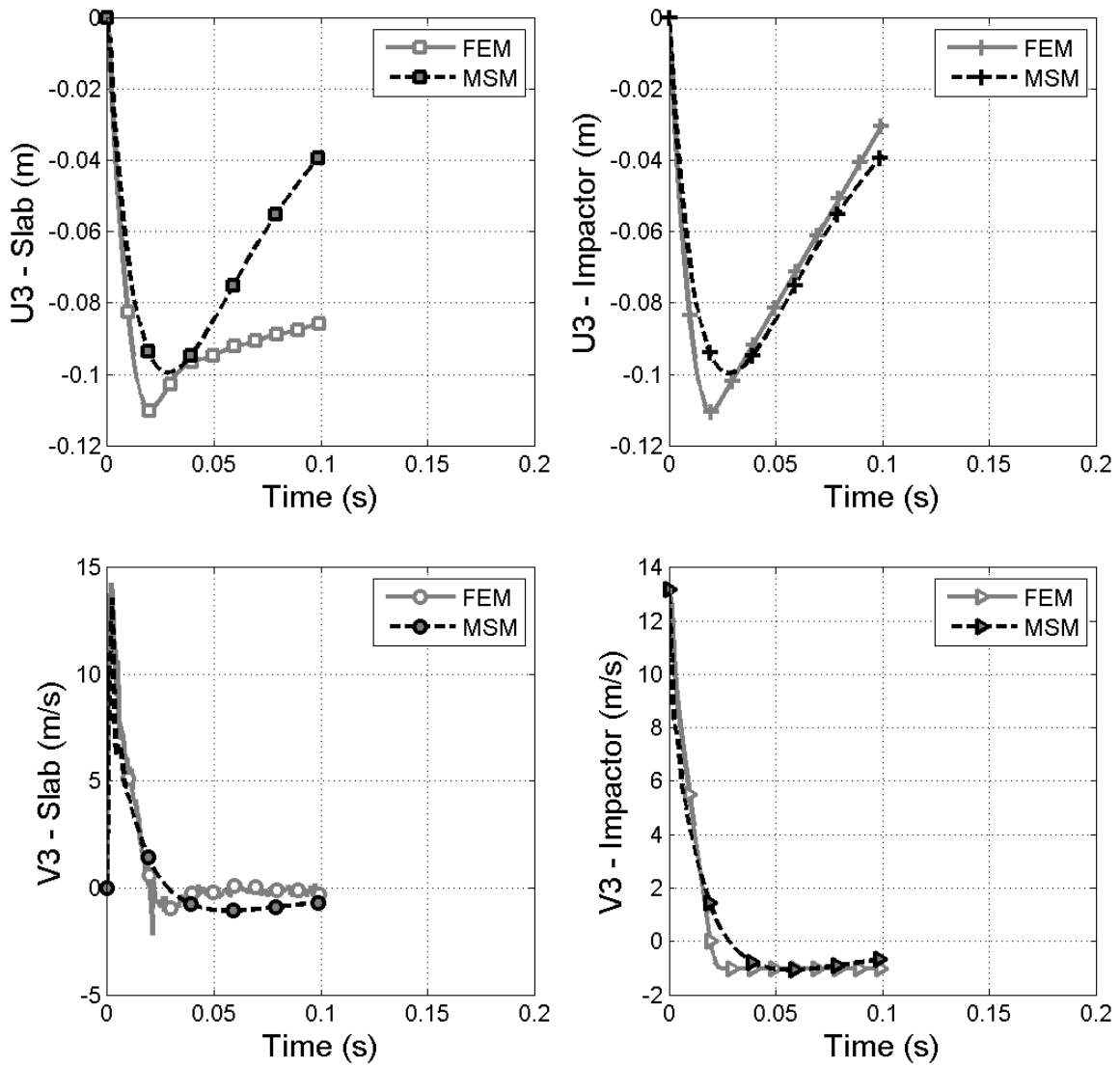


Figure B.12: Displacement and velocity of slab and impactor:  $v = 13.2 \text{ m/s}$

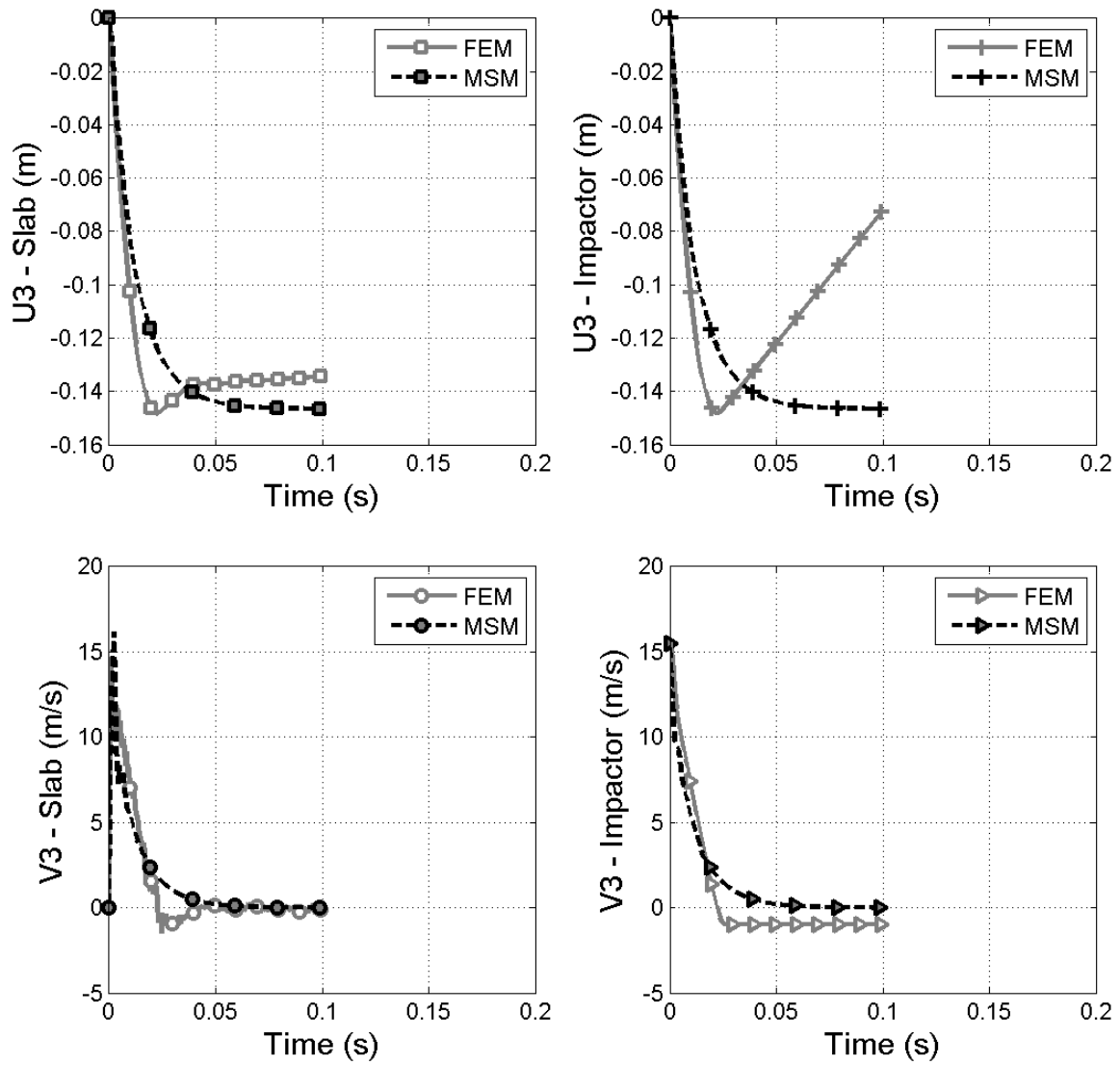


Figure B.13: Displacement and velocity of slab and impactor:  $v = 15.5 \text{ m/s}$

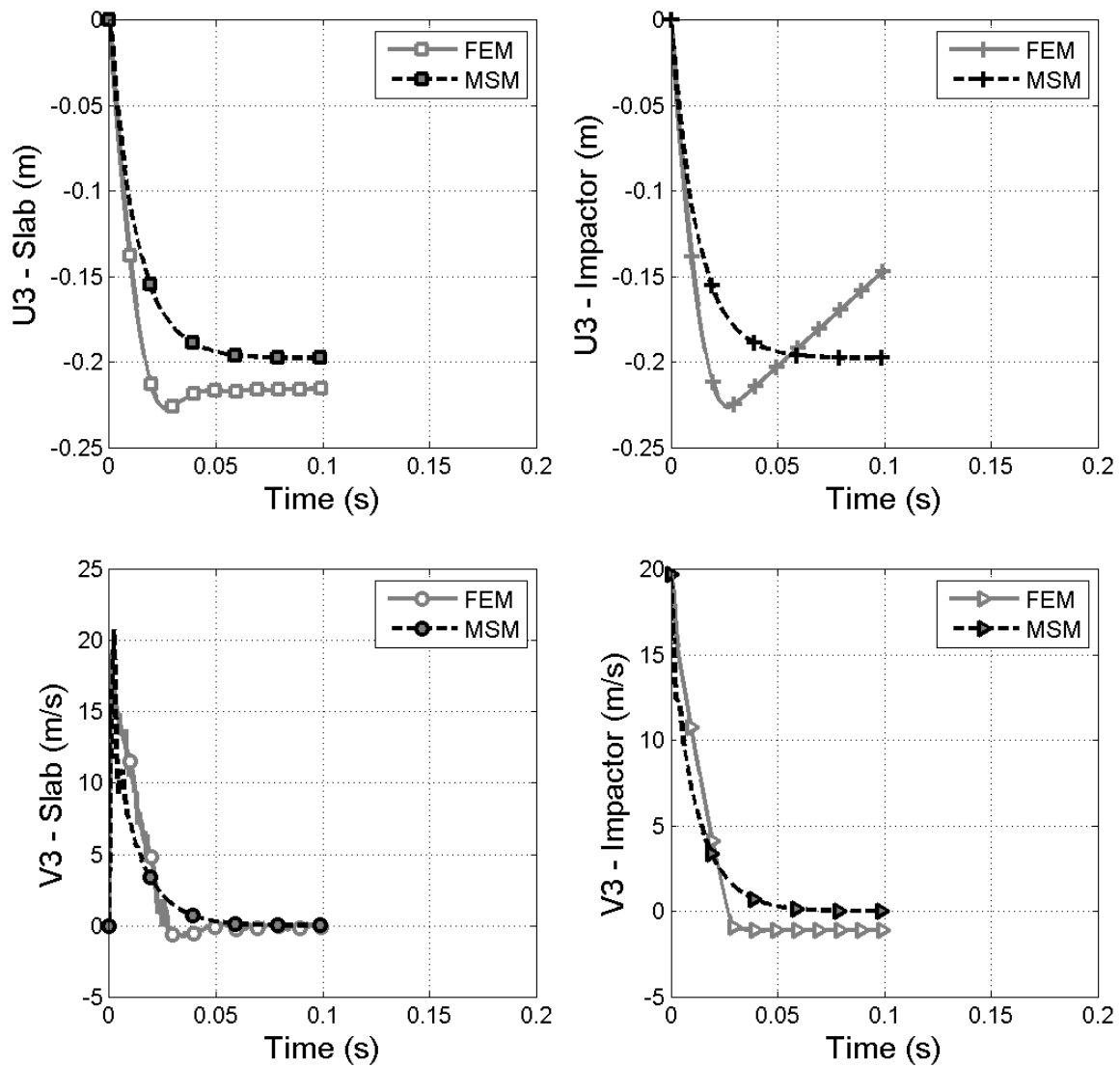


Figure B.14: Displacement and velocity of slab and impactor:  $v = 19.7 \text{ m/s}$

### B.3 Impactor mass

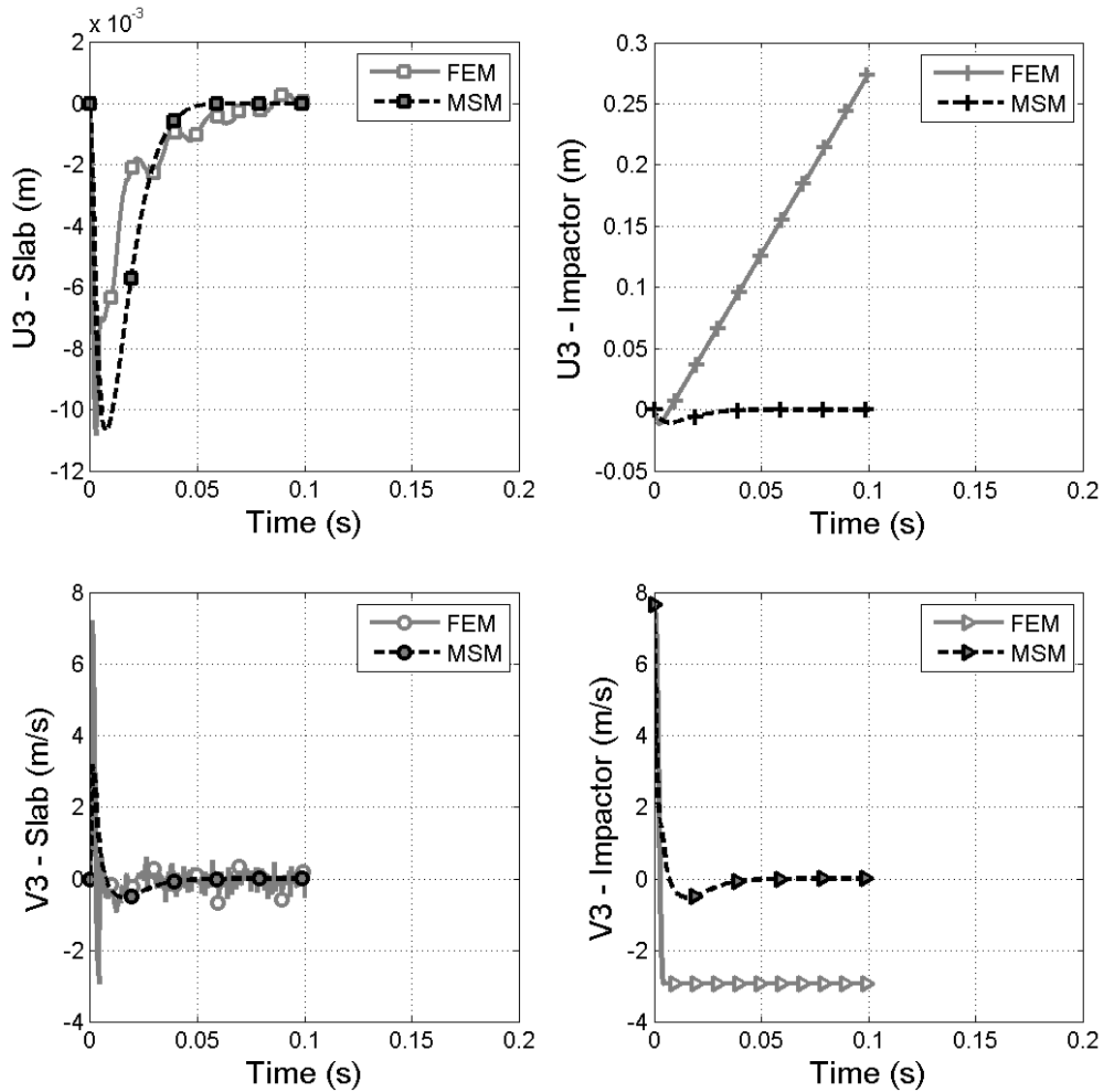


Figure B.15: Displacement and velocity of slab and impactor:  $m = 750 \text{ kg}$

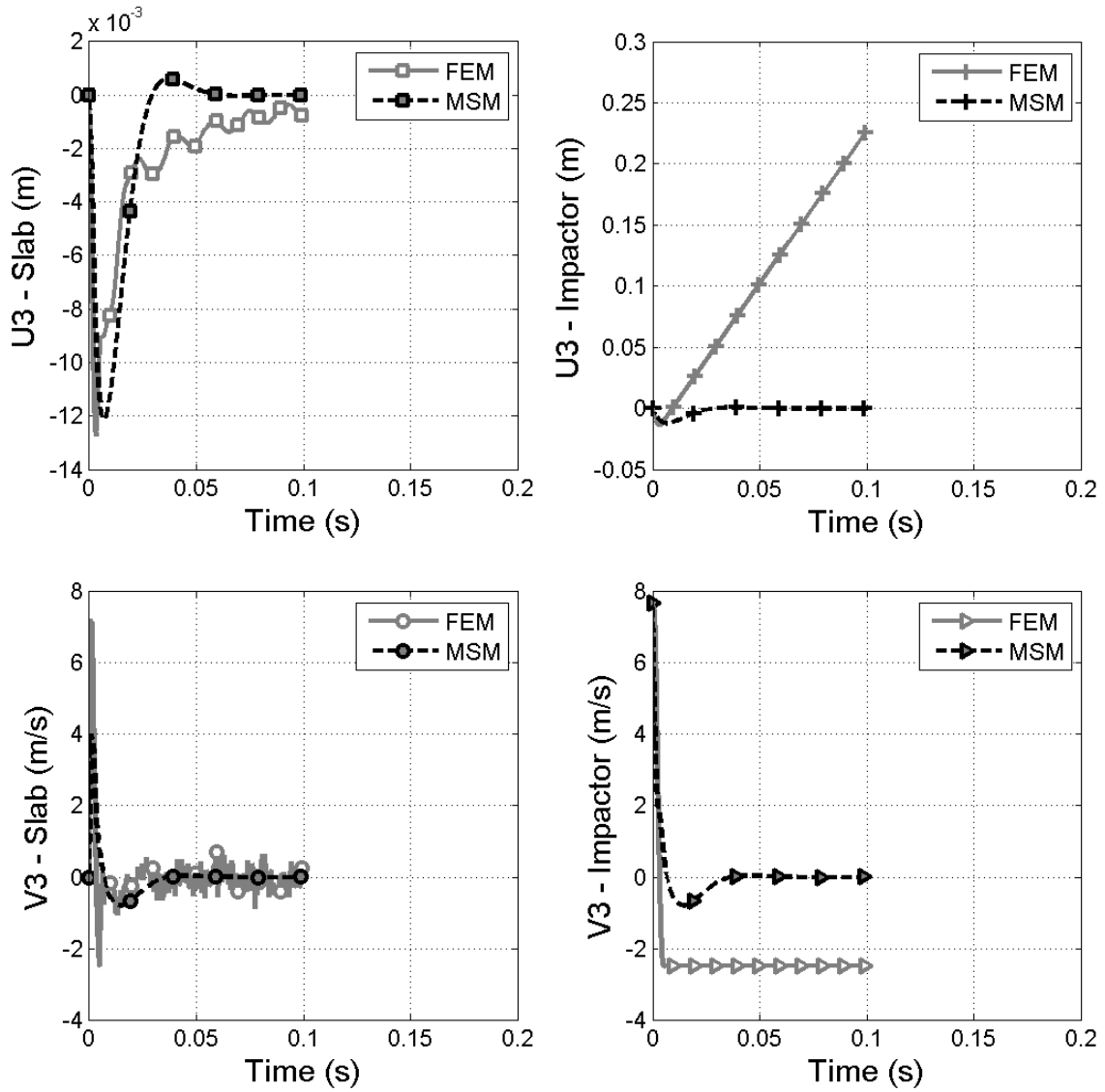


Figure B.16: Displacement and velocity of slab and impactor:  $m = 1000 \text{ kg}$

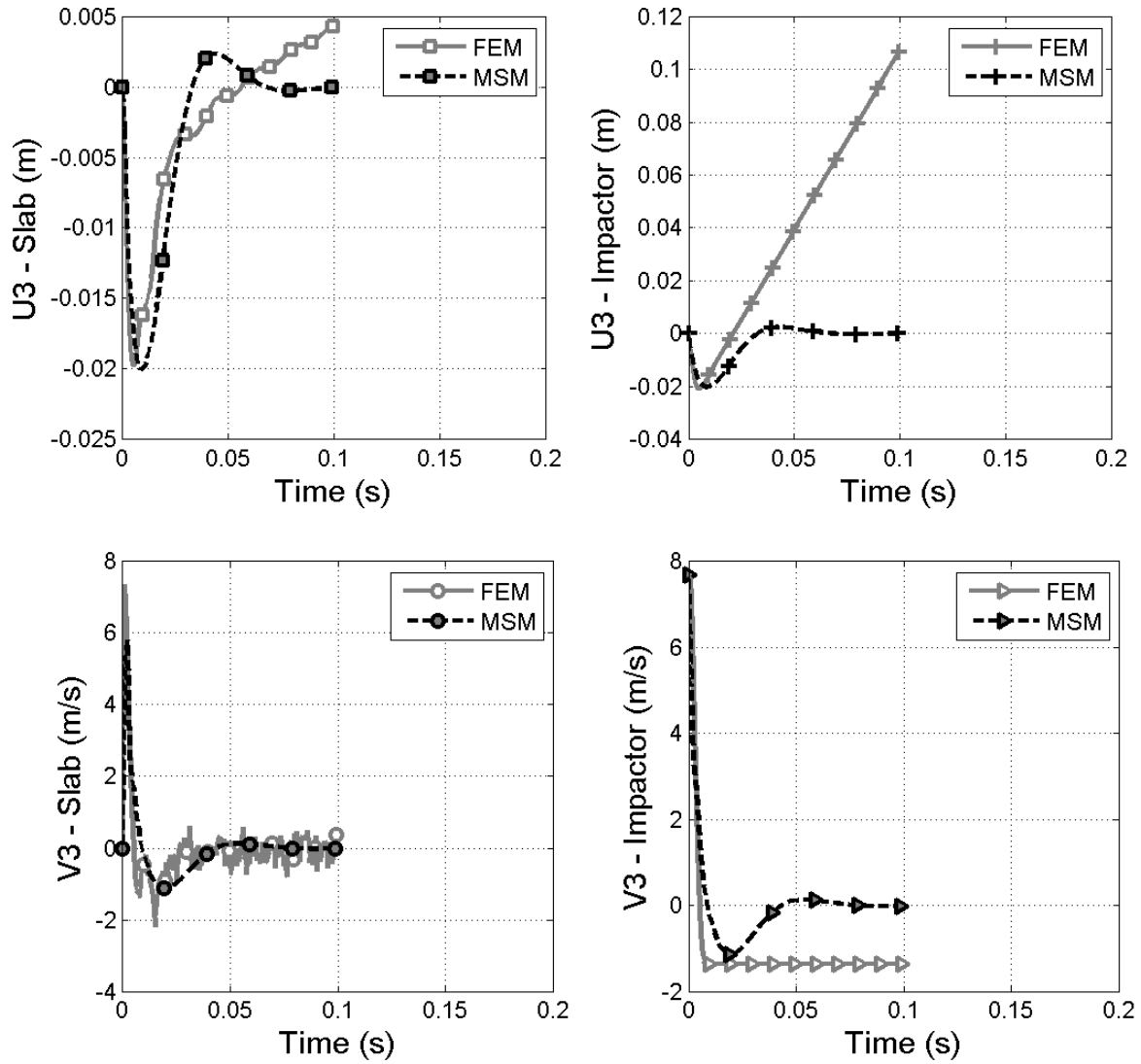


Figure B.17: Displacement and velocity of slab and impactor:  $m = 2000 \text{ kg}$

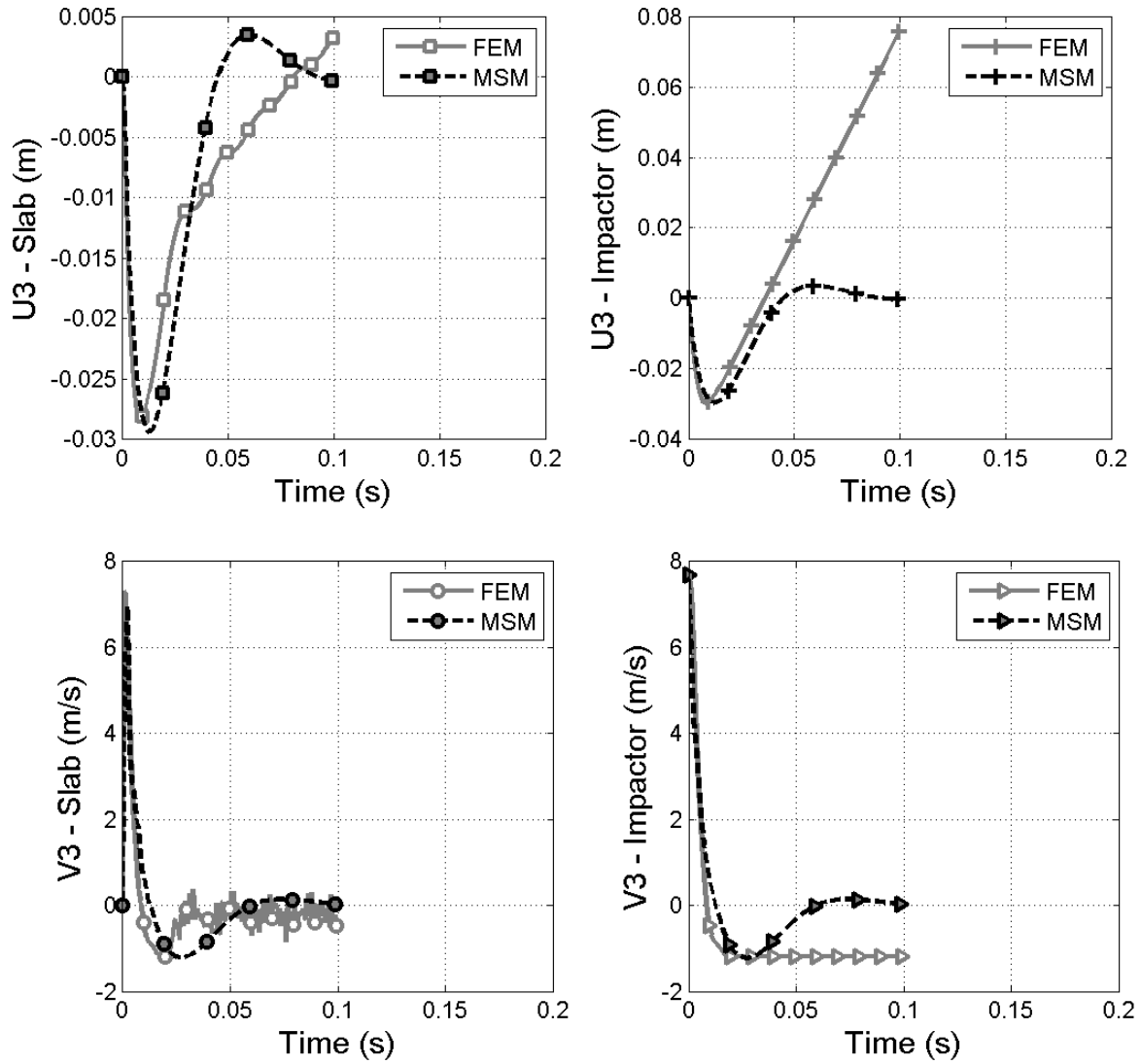


Figure B.18: Displacement and velocity of slab and impactor:  $m = 3000 \text{ kg}$

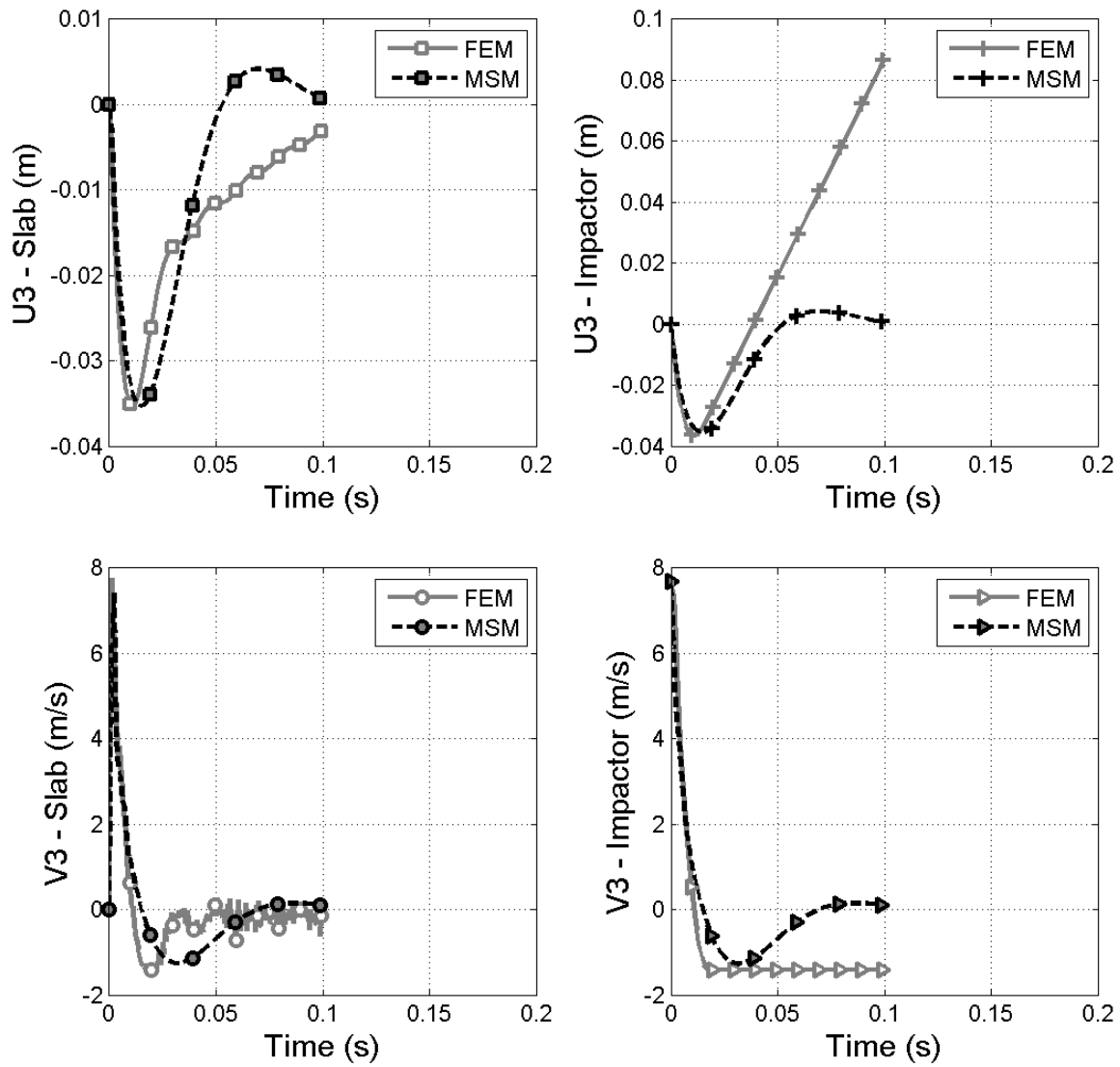


Figure B.19: Displacement and velocity of slab and impactor:  $m = 3600 \text{ kg}$

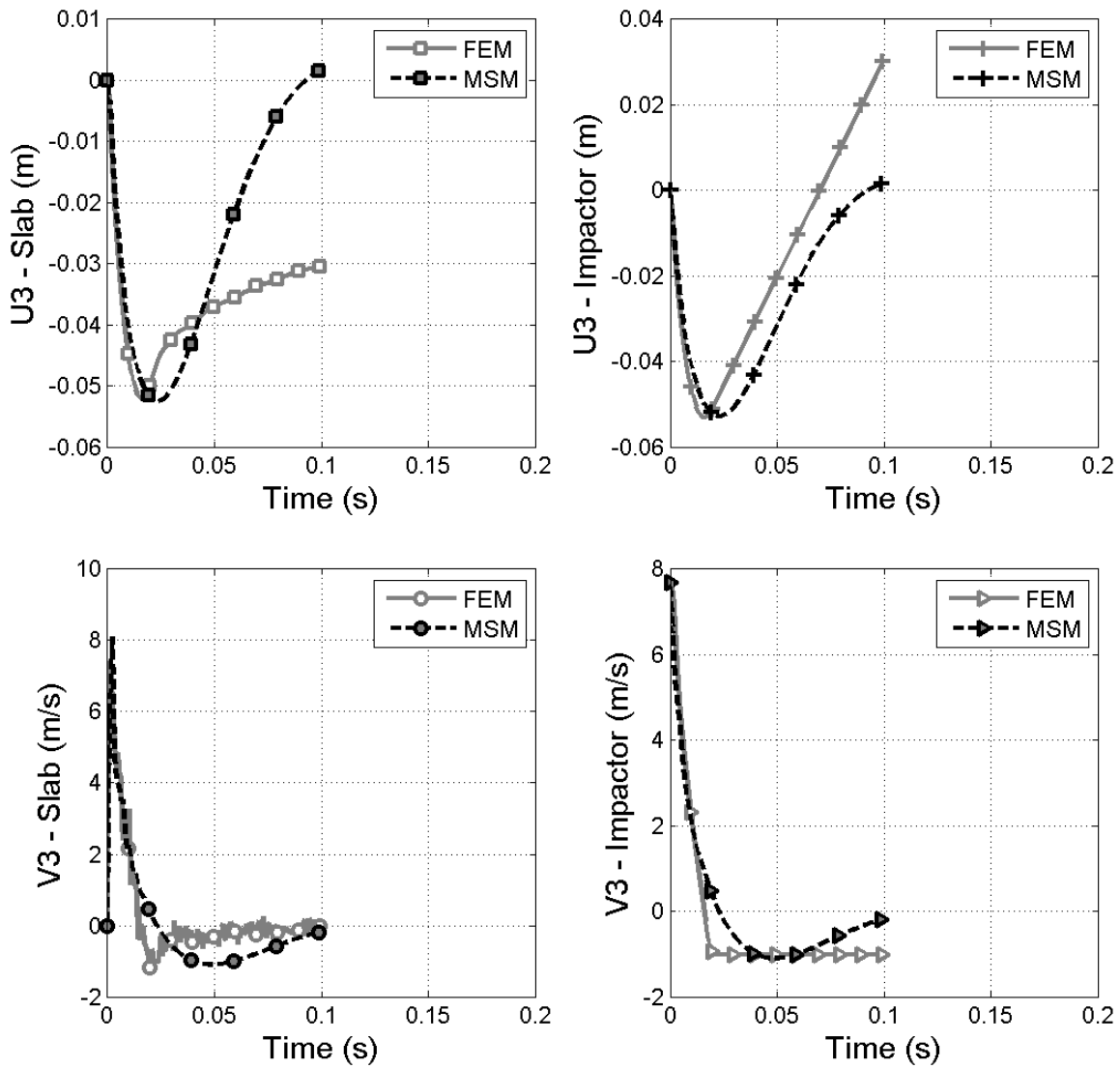


Figure B.20: Displacement and velocity of slab and impactor:  $m = 5000 \text{ kg}$

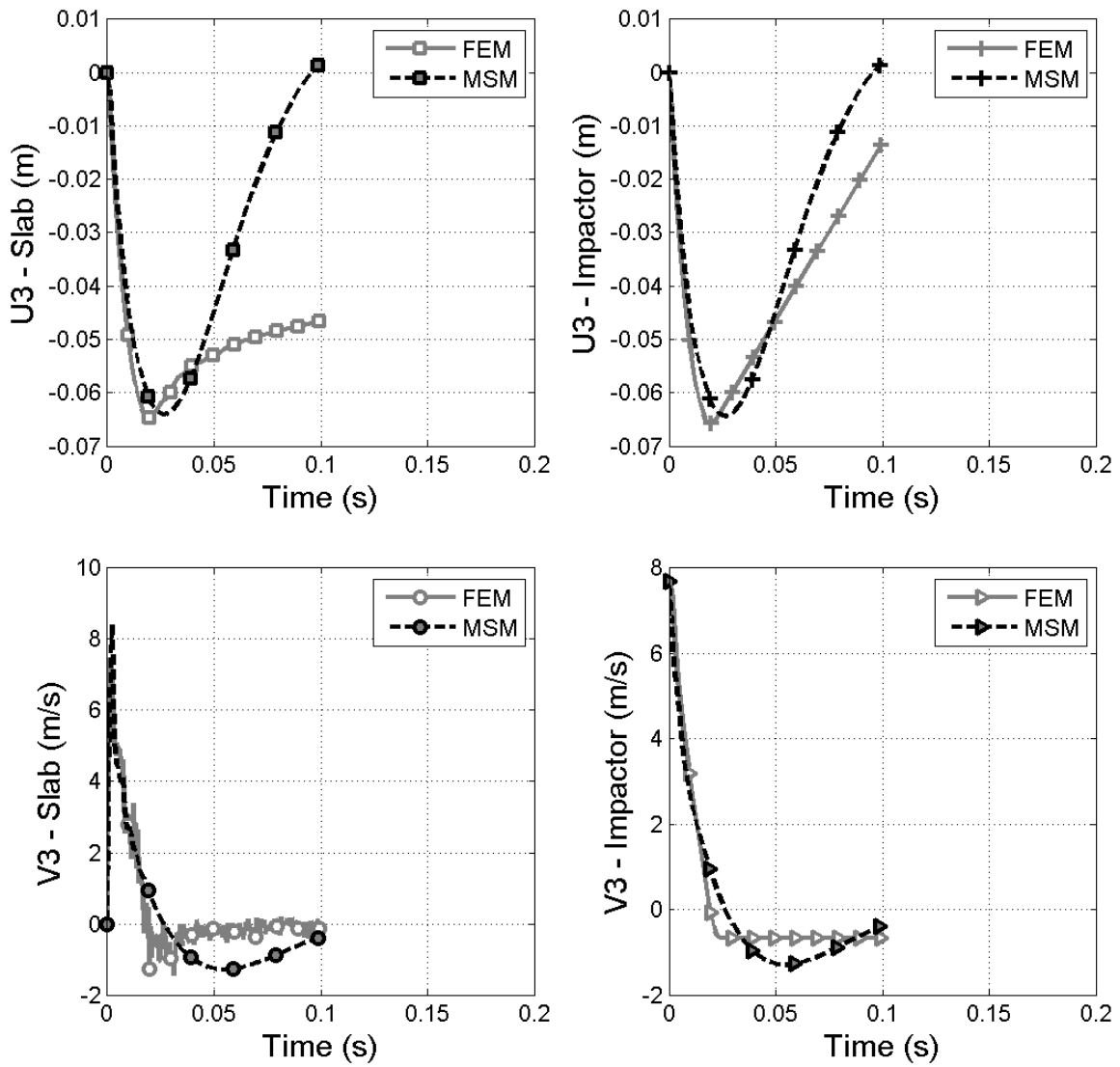


Figure B.21: Displacement and velocity of slab and impactor:  $m = 6000 \text{ kg}$

## B.4 Steel diameter

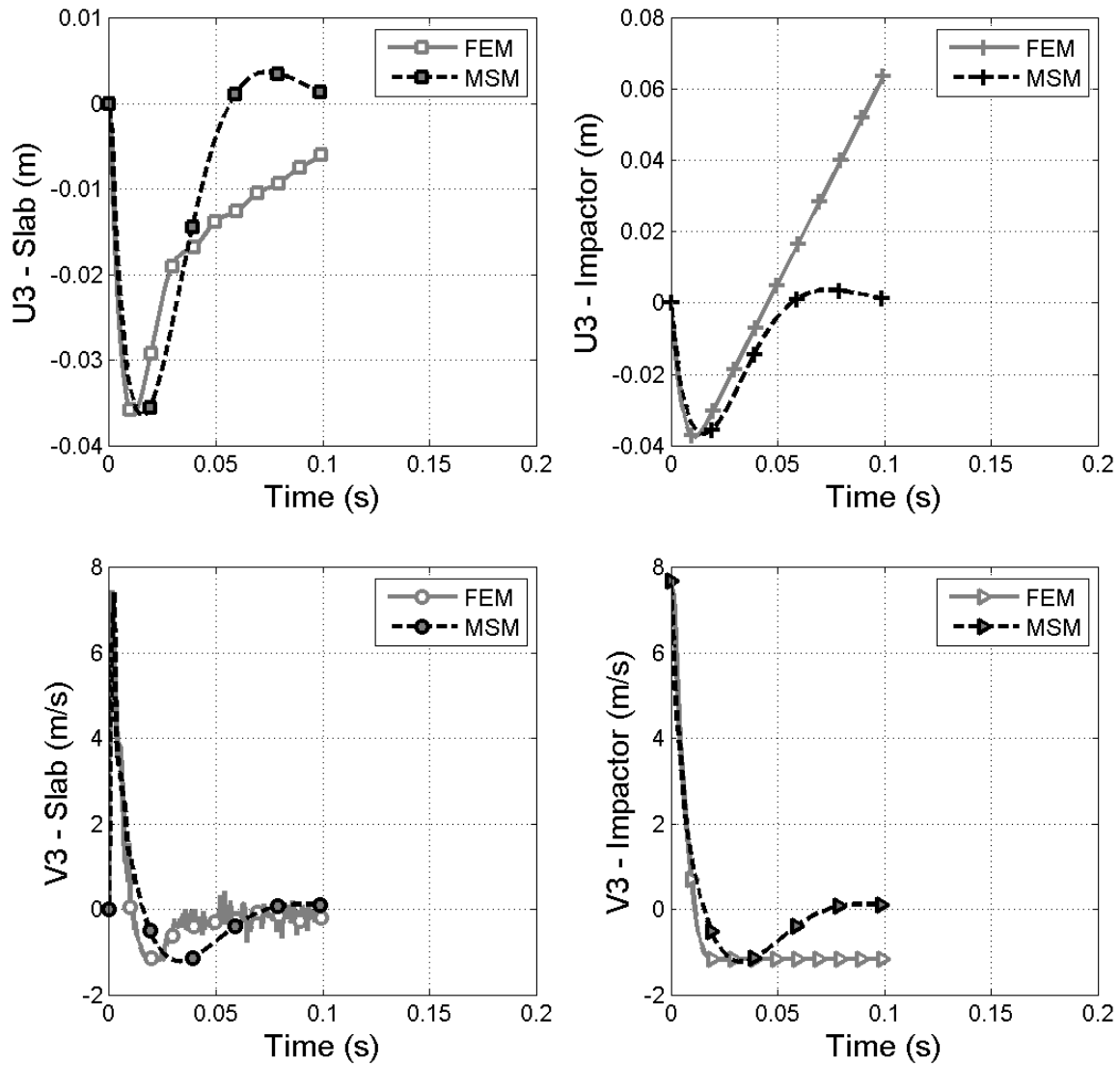


Figure B.22: Displacement and velocity of slab and impactor:  $d_A = 0.006 m$

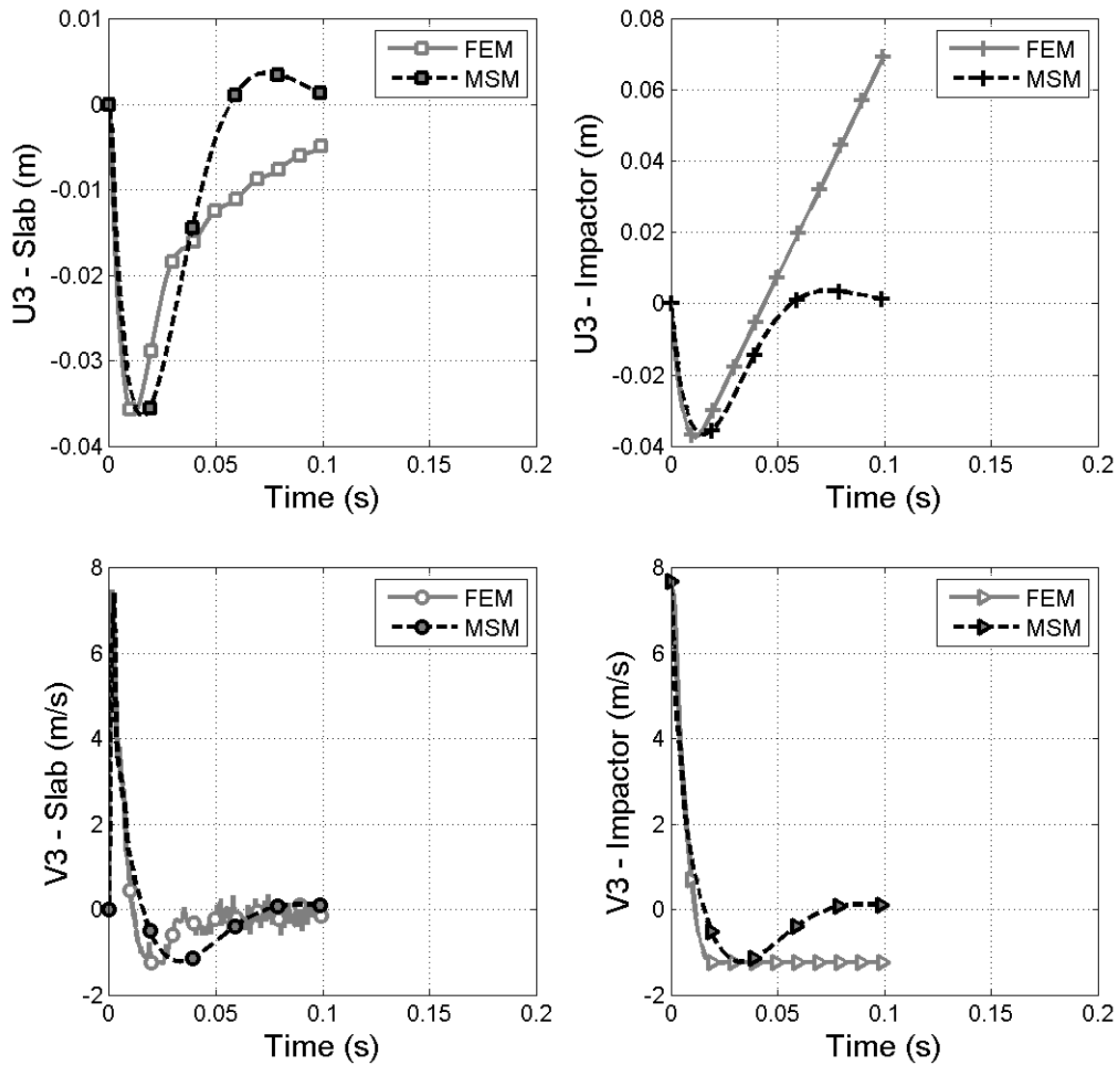


Figure B.23: Displacement and velocity of slab and impactor:  $d_A = 0.008\text{ m}$

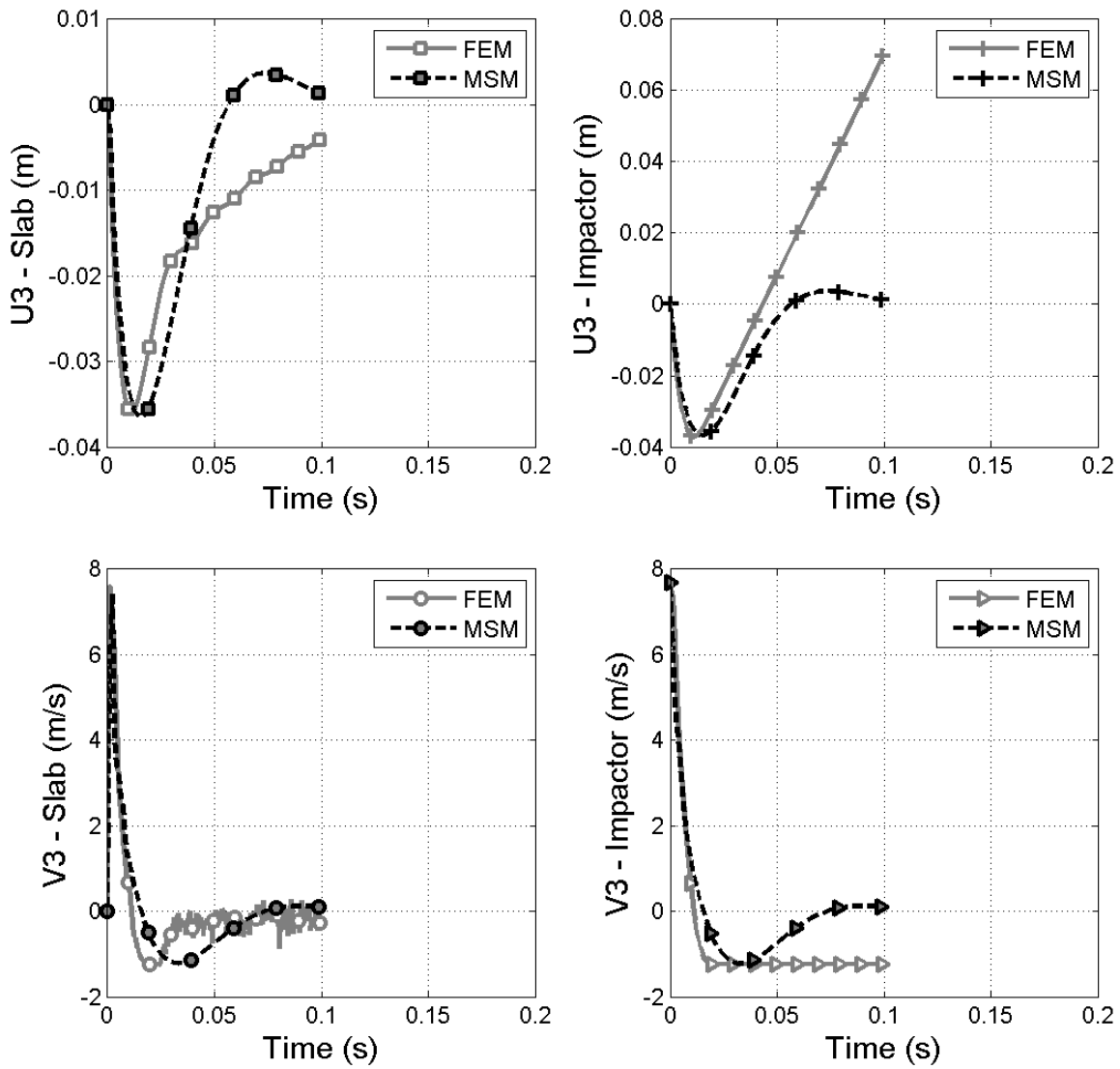


Figure B.24: Displacement and velocity of slab and impactor:  $d_A = 0.01\text{ m}$

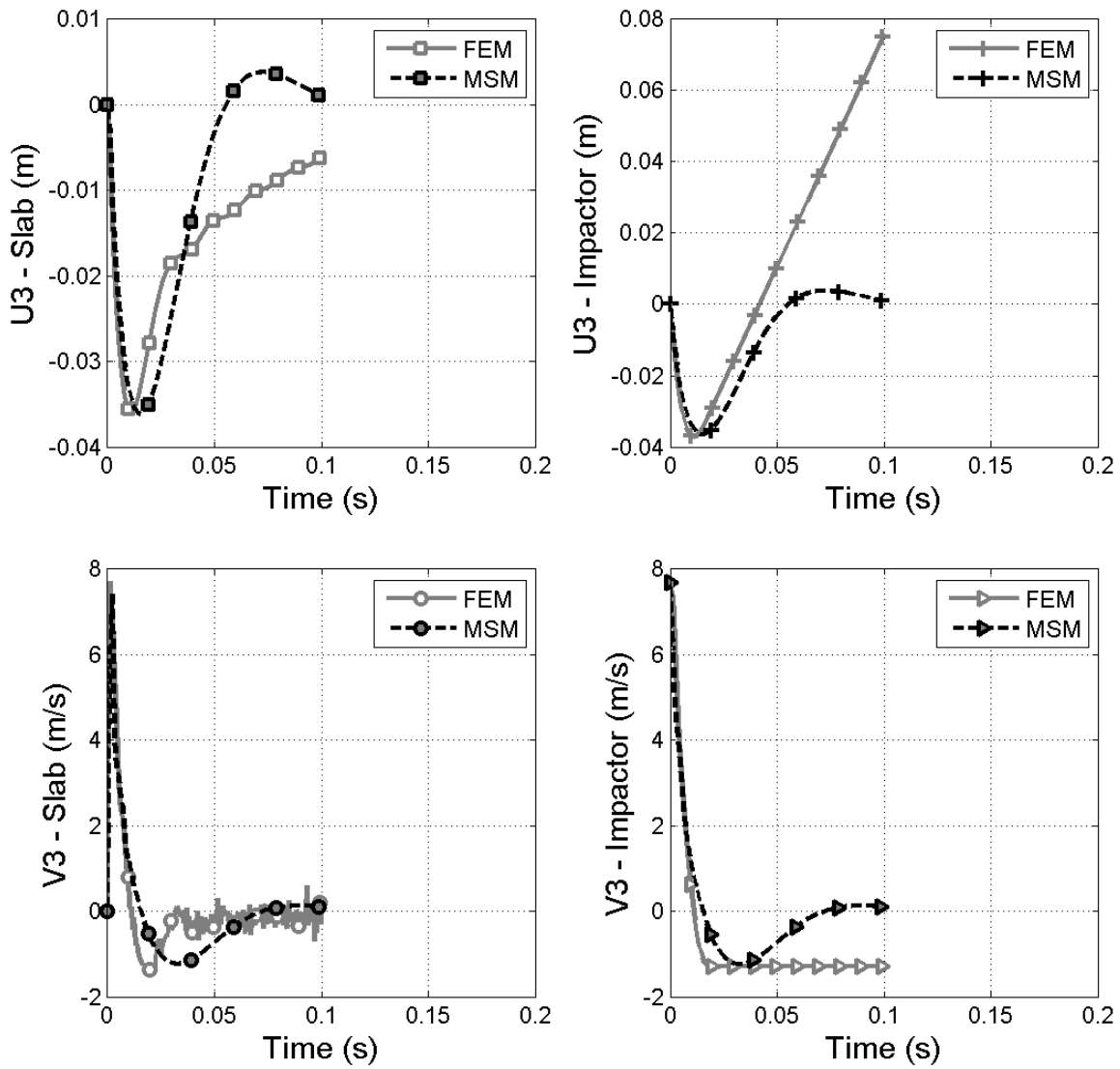


Figure B.25: Displacement and velocity of slab and impactor:  $d_A = 0.012\text{ m}$

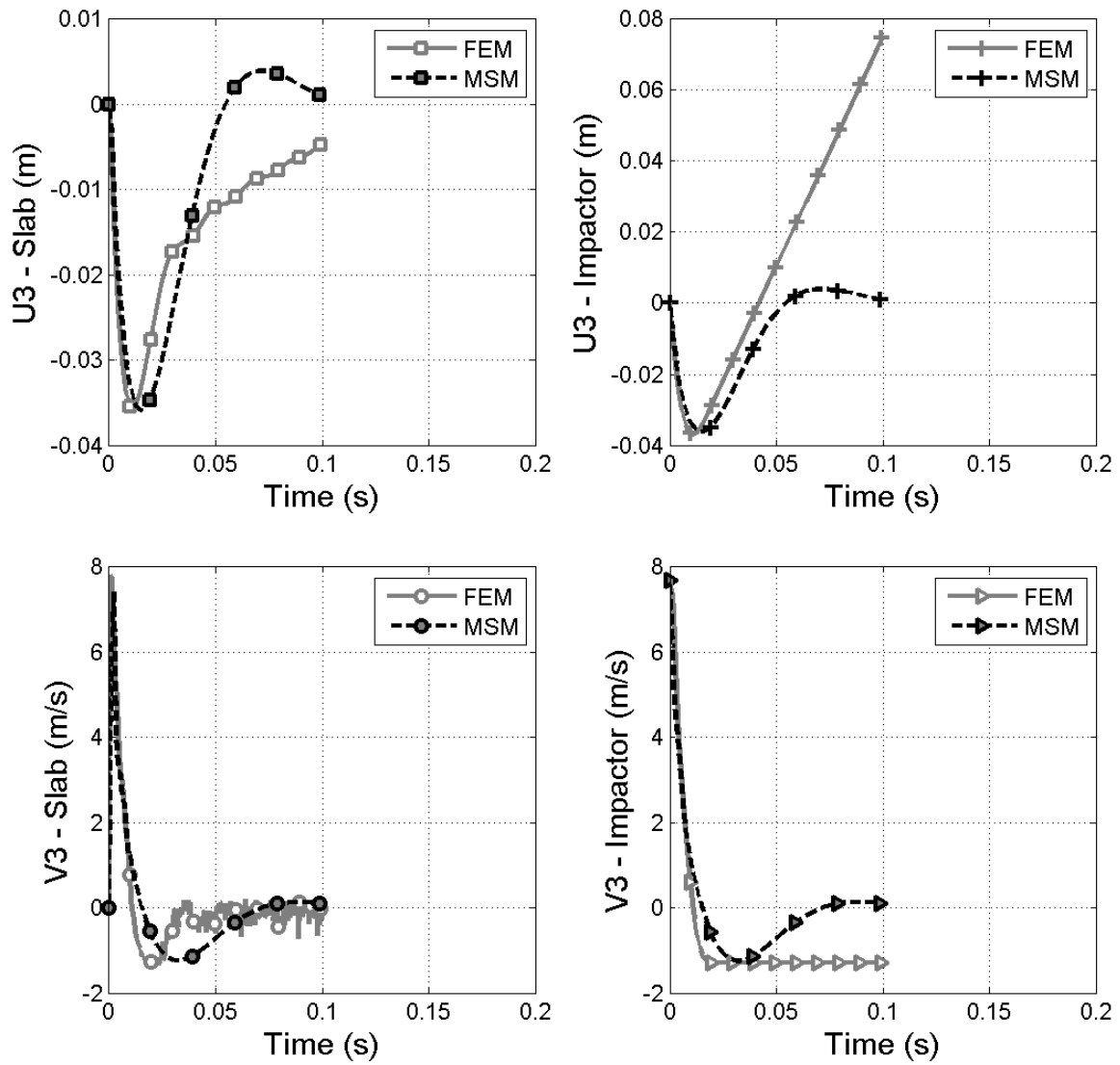


Figure B.26: Displacement and velocity of slab and impactor:  $d_A = 0.014\text{ m}$

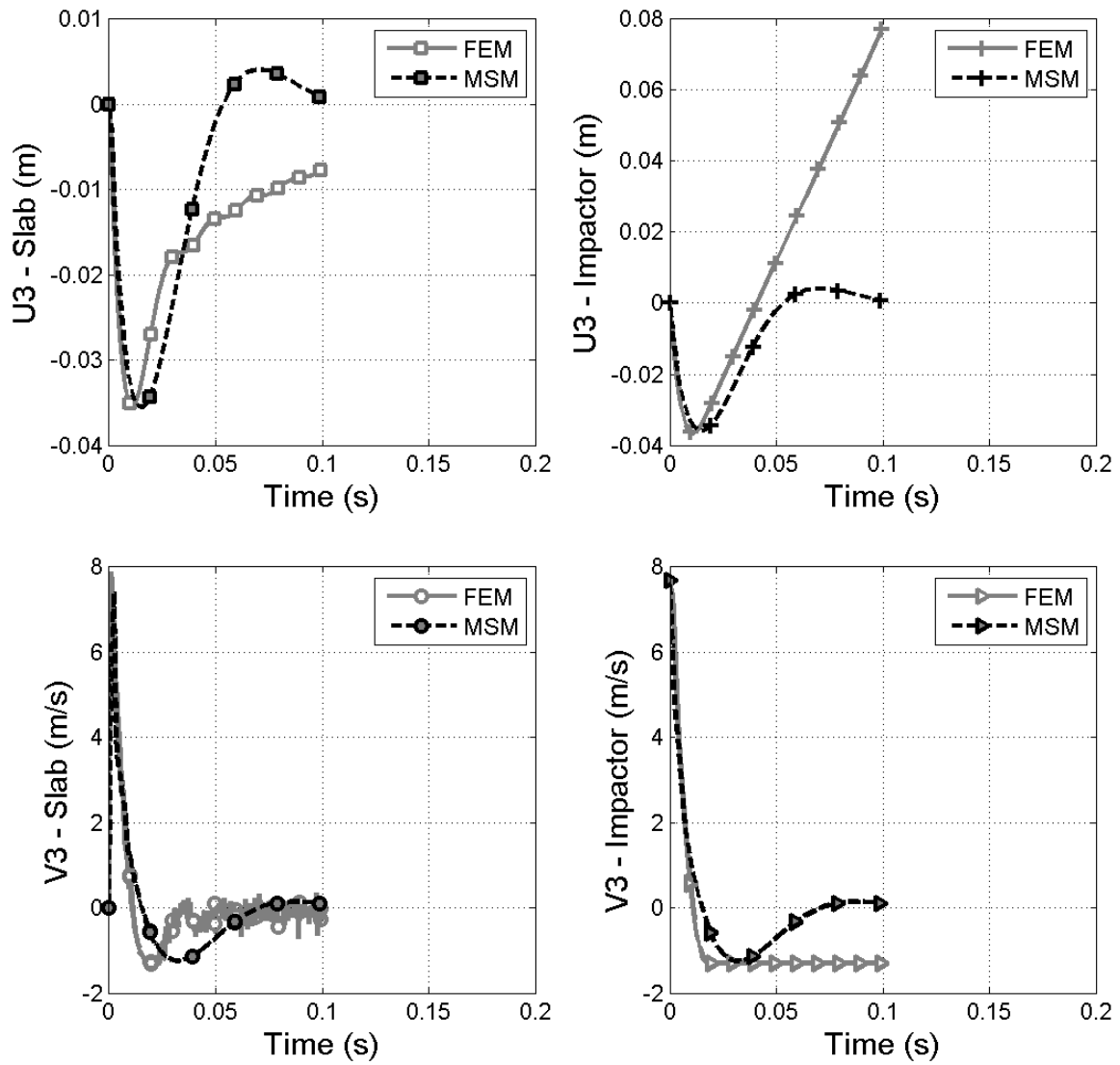


Figure B.27: Displacement and velocity of slab and impactor:  $d_A = 0.016\text{ m}$

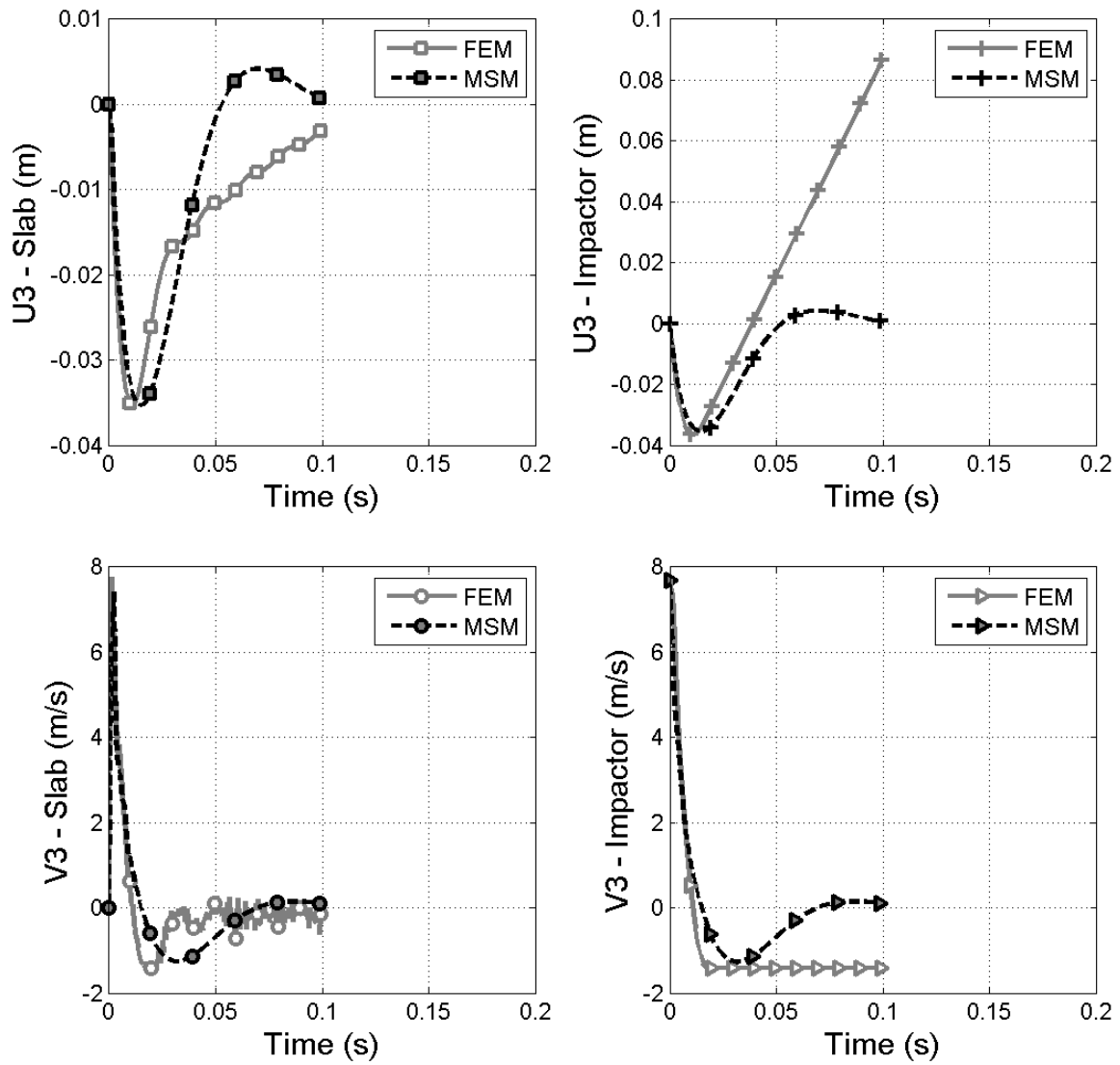


Figure B.28: Displacement and velocity of slab and impactor:  $d_A = 0.02\text{ m}$

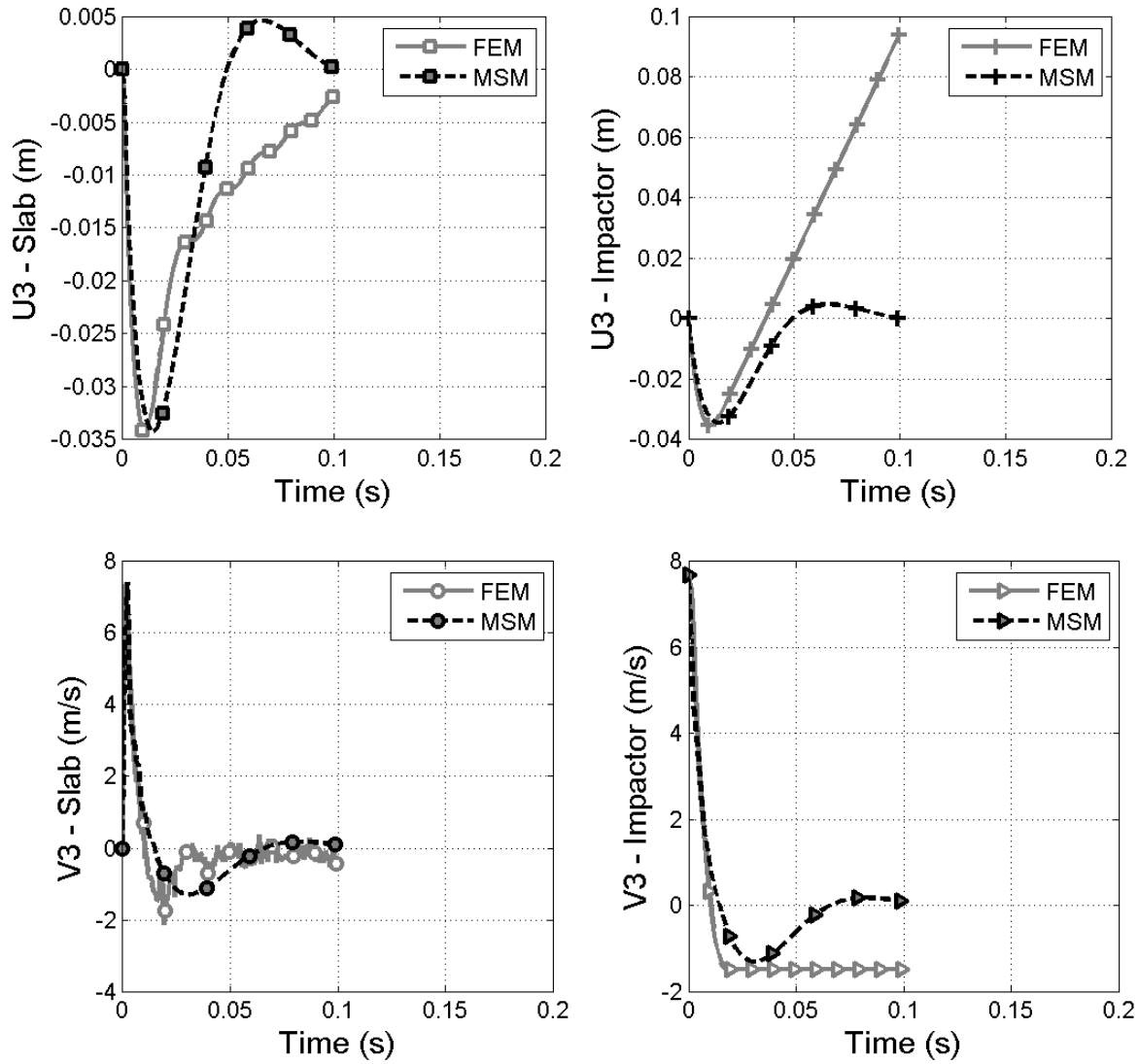


Figure B.29: Displacement and velocity of slab and impactor:  $d_A = 0.03 \text{ m}$

## B.5 Concrete density

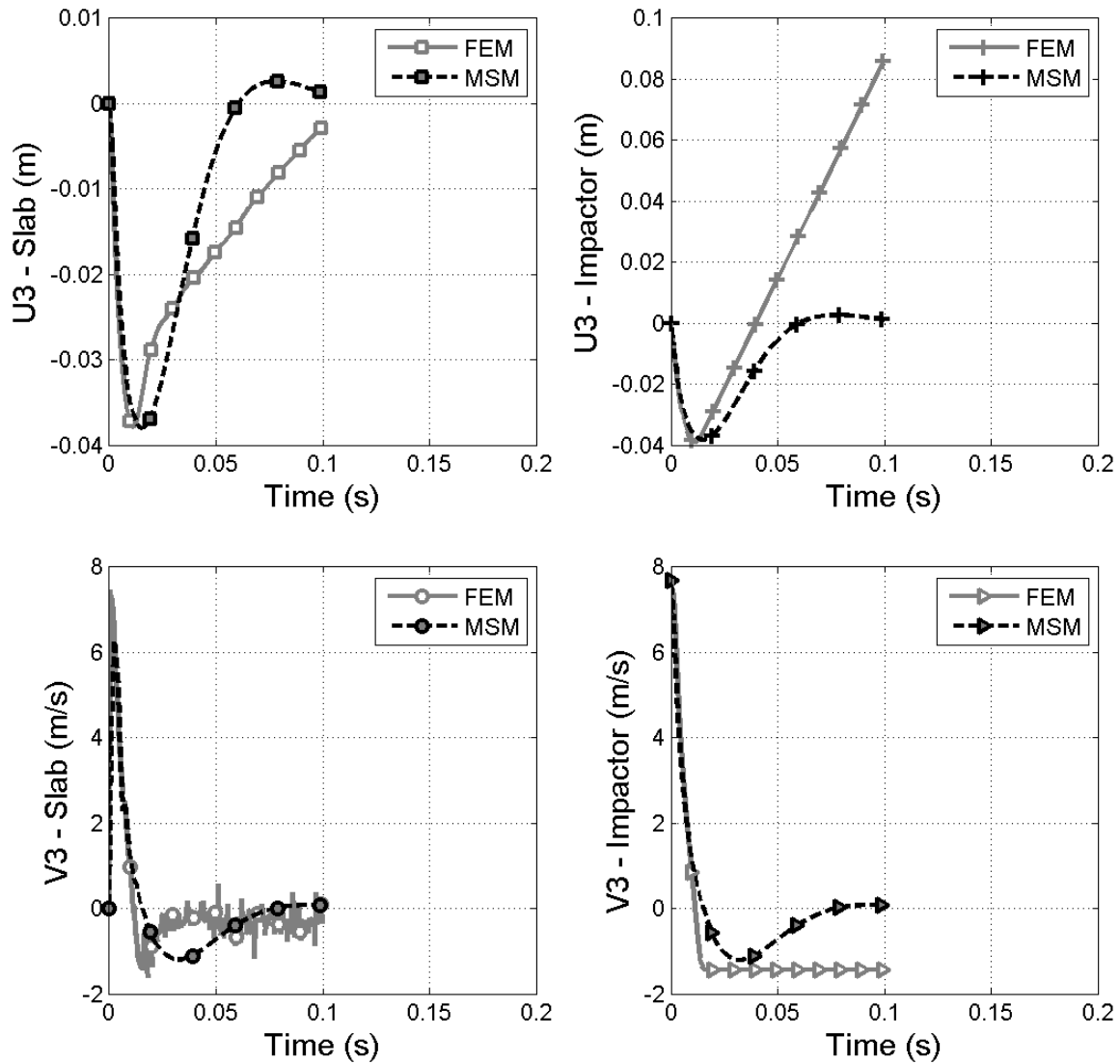


Figure B.30: Displacement and velocity of slab and impactor:  $\rho_c = 1200 \text{ kg/m}^3$

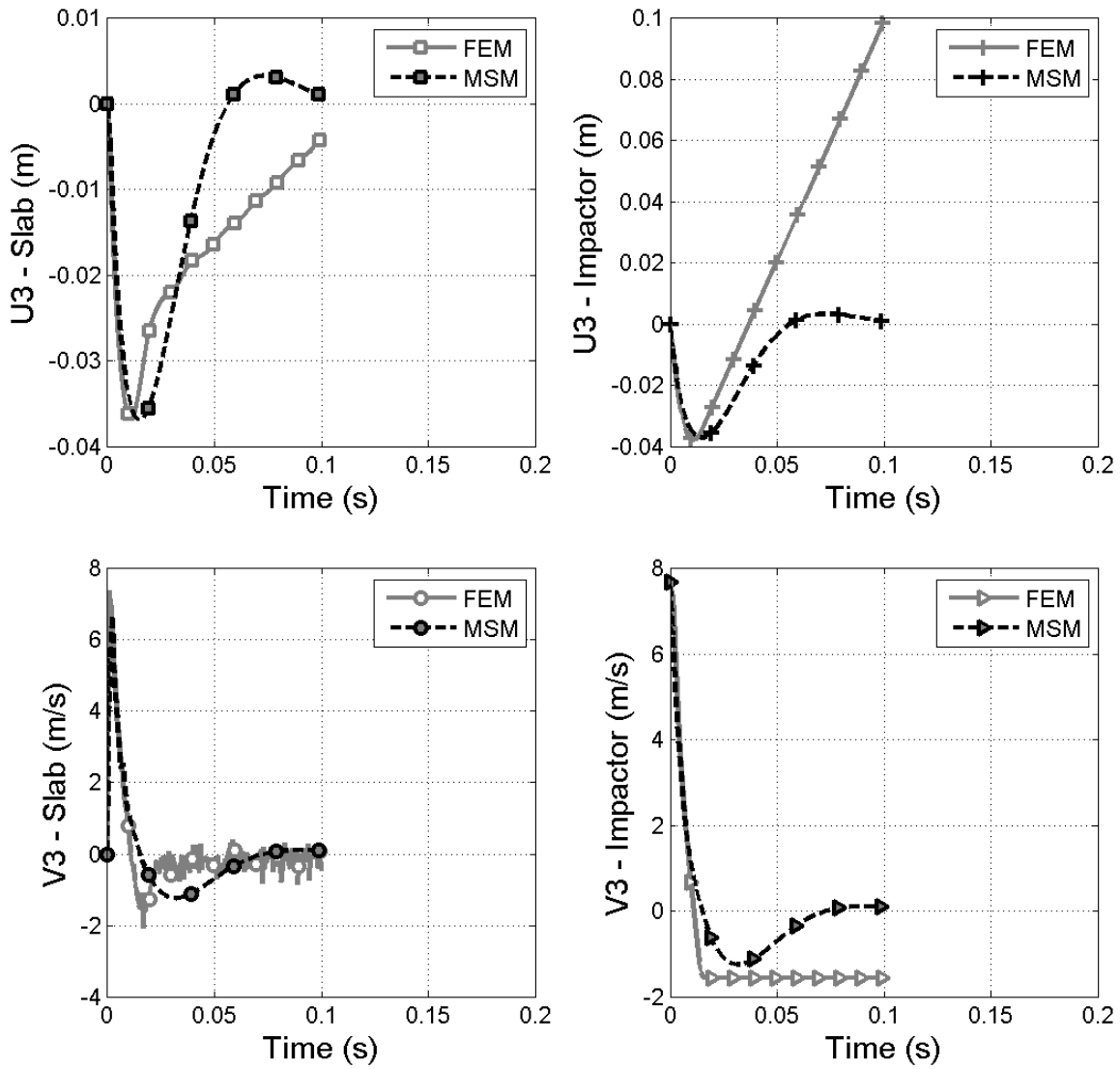


Figure B.31: Displacement and velocity of slab and impactor:  $\rho_c = 1600 \text{ kg/m}^3$

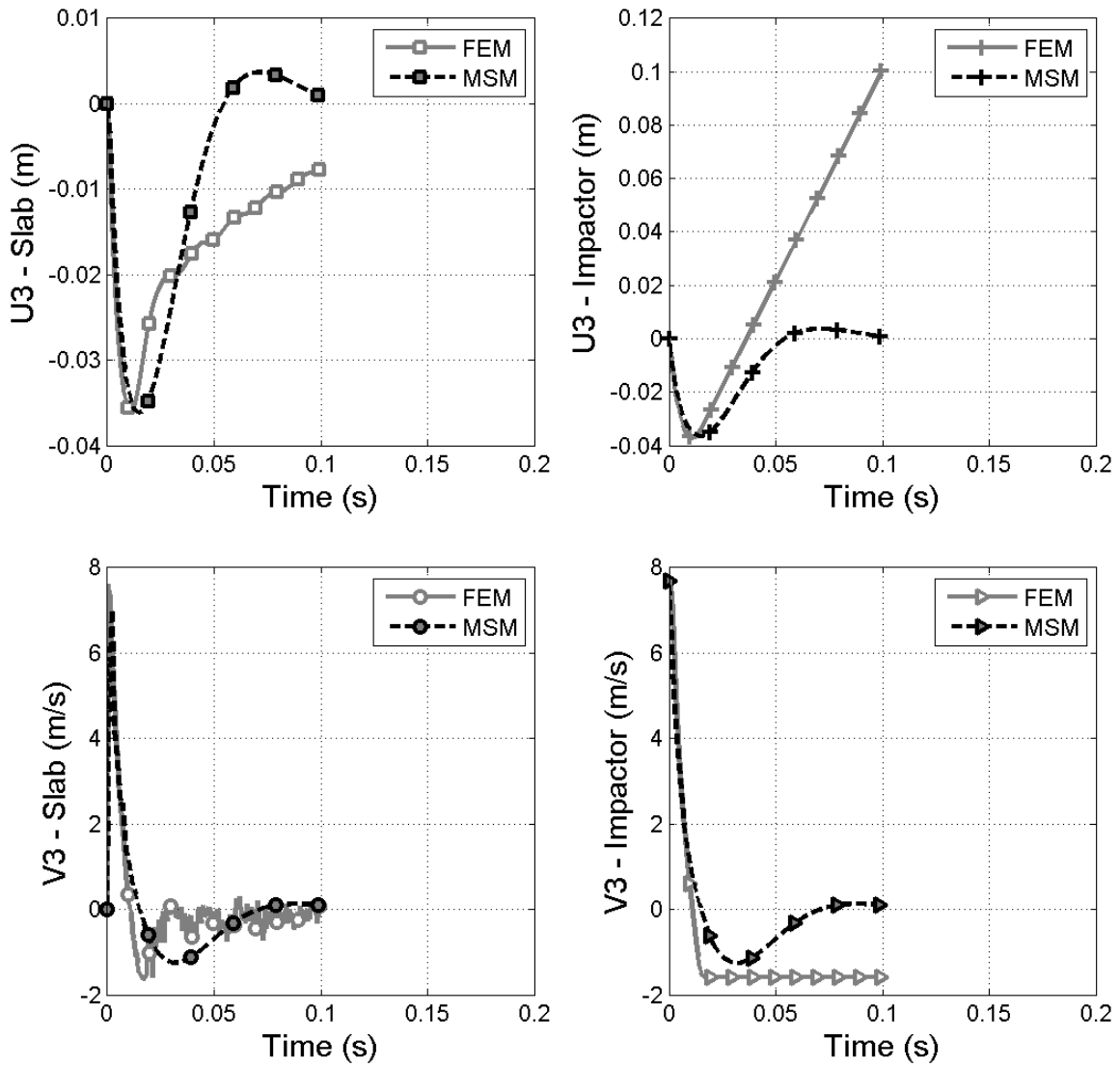


Figure B.32: Displacement and velocity of slab and impactor:  $\rho_c = 2000 \text{ kg/m}^3$

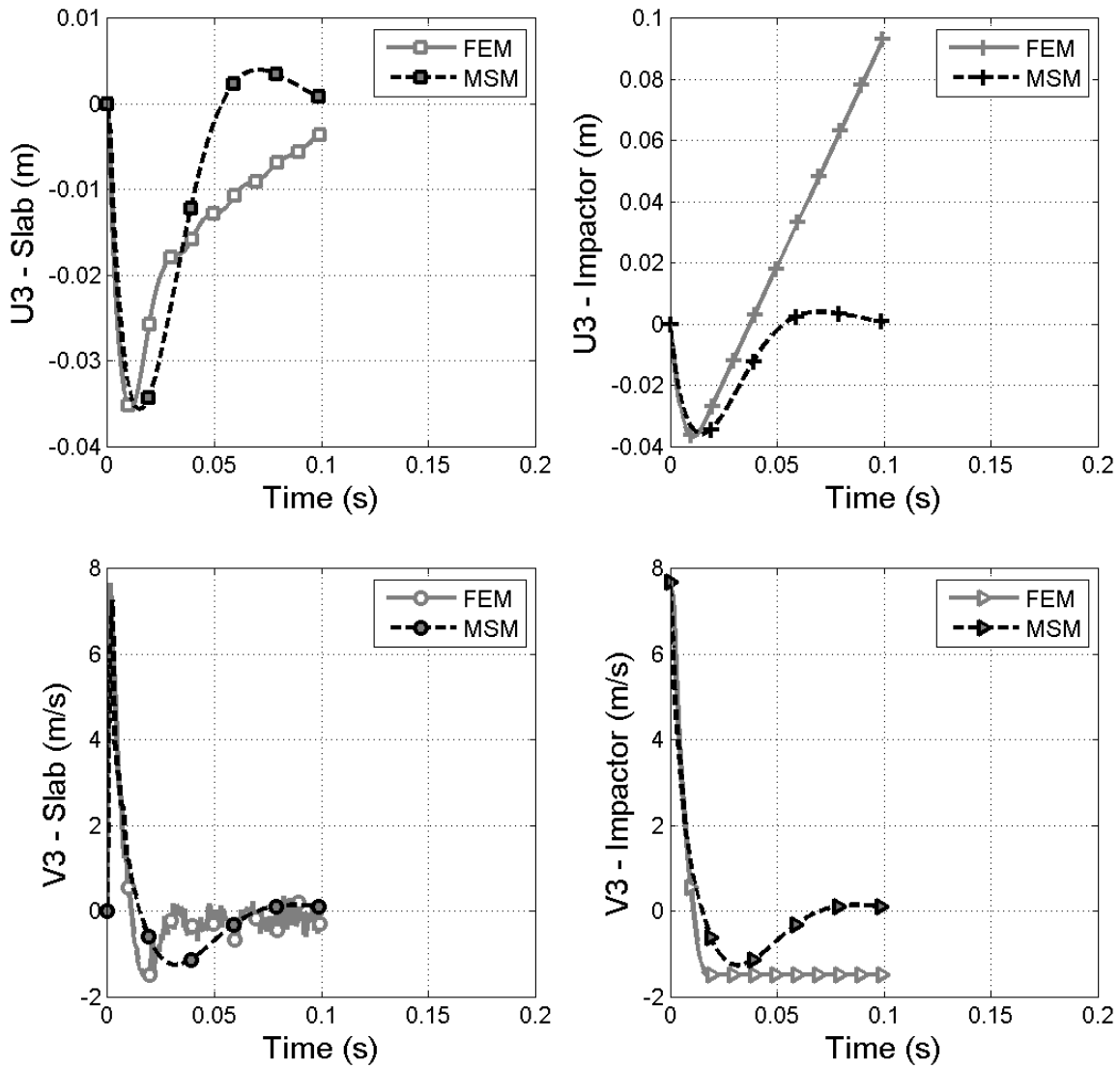


Figure B.33: Displacement and velocity of slab and impactor:  $\rho_c = 2300 \text{ kg/m}^3$

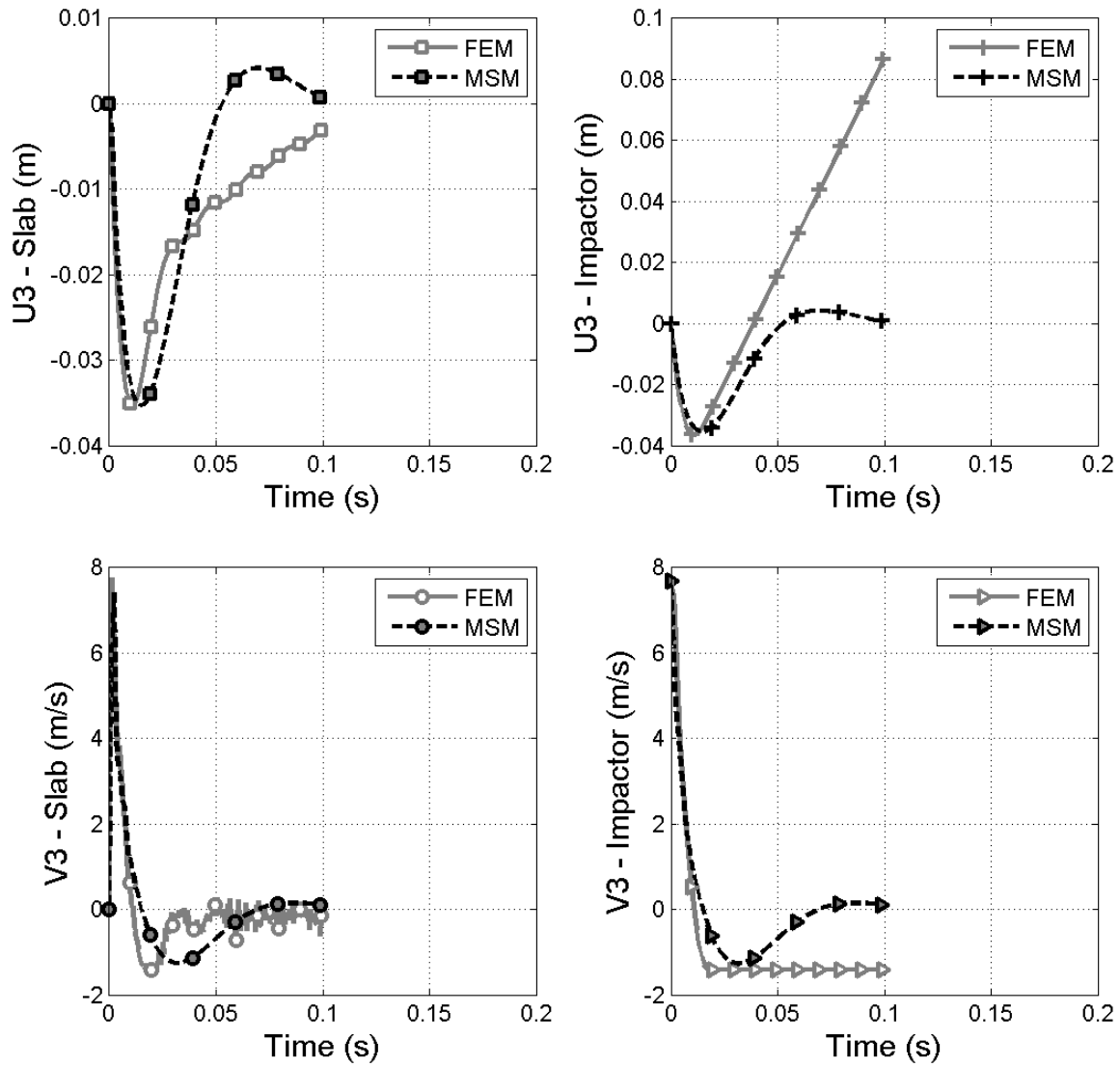


Figure B.34: Displacement and velocity of slab and impactor:  $\rho_c = 2500 \text{ kg/m}^3$

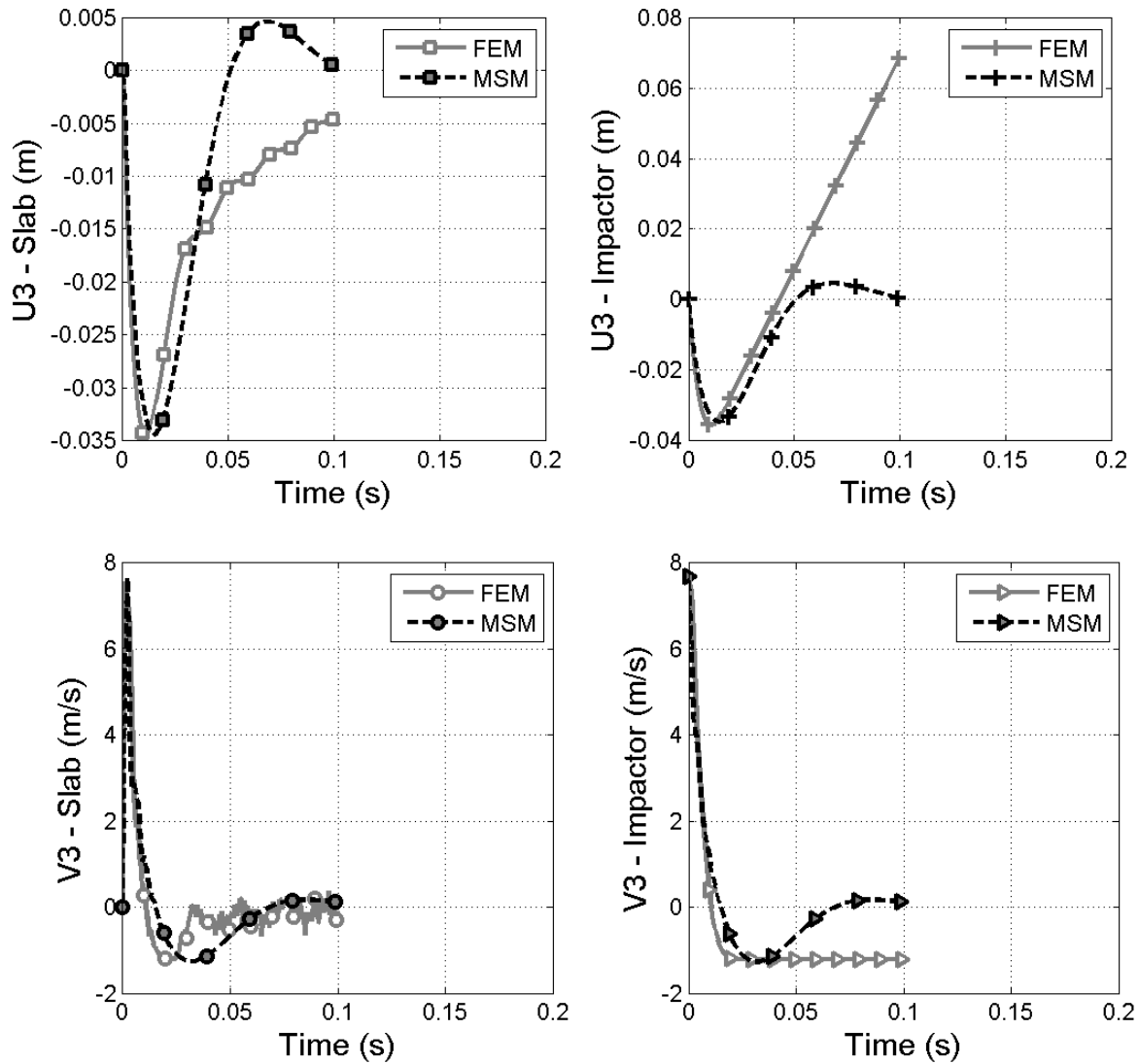


Figure B.35: Displacement and velocity of slab and impactor:  $\rho_c = 3000 \text{ kg/m}^3$

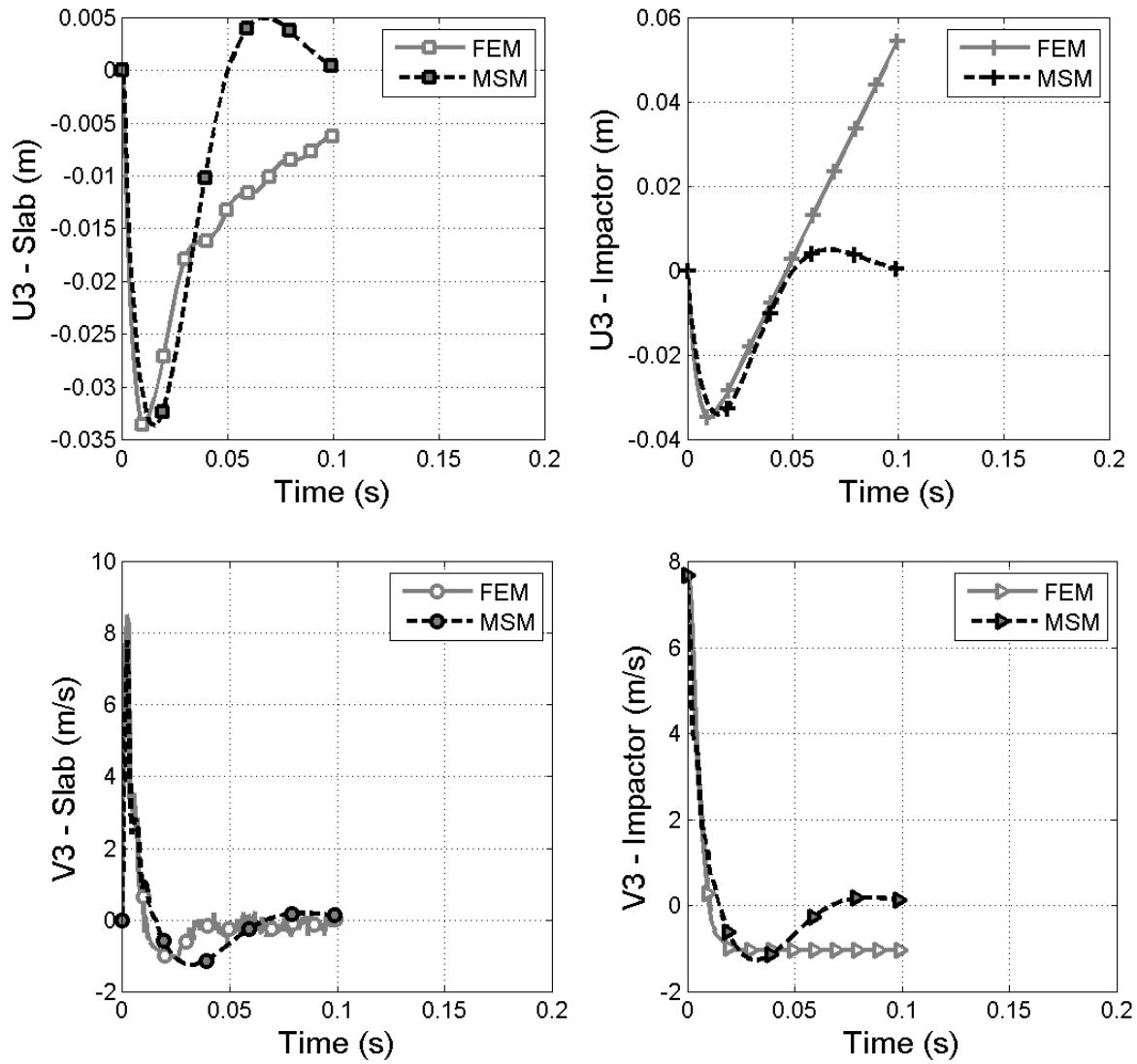


Figure B.36: Displacement and velocity of slab and impactor:  $\rho_c = 3500 \text{ kg/m}^3$

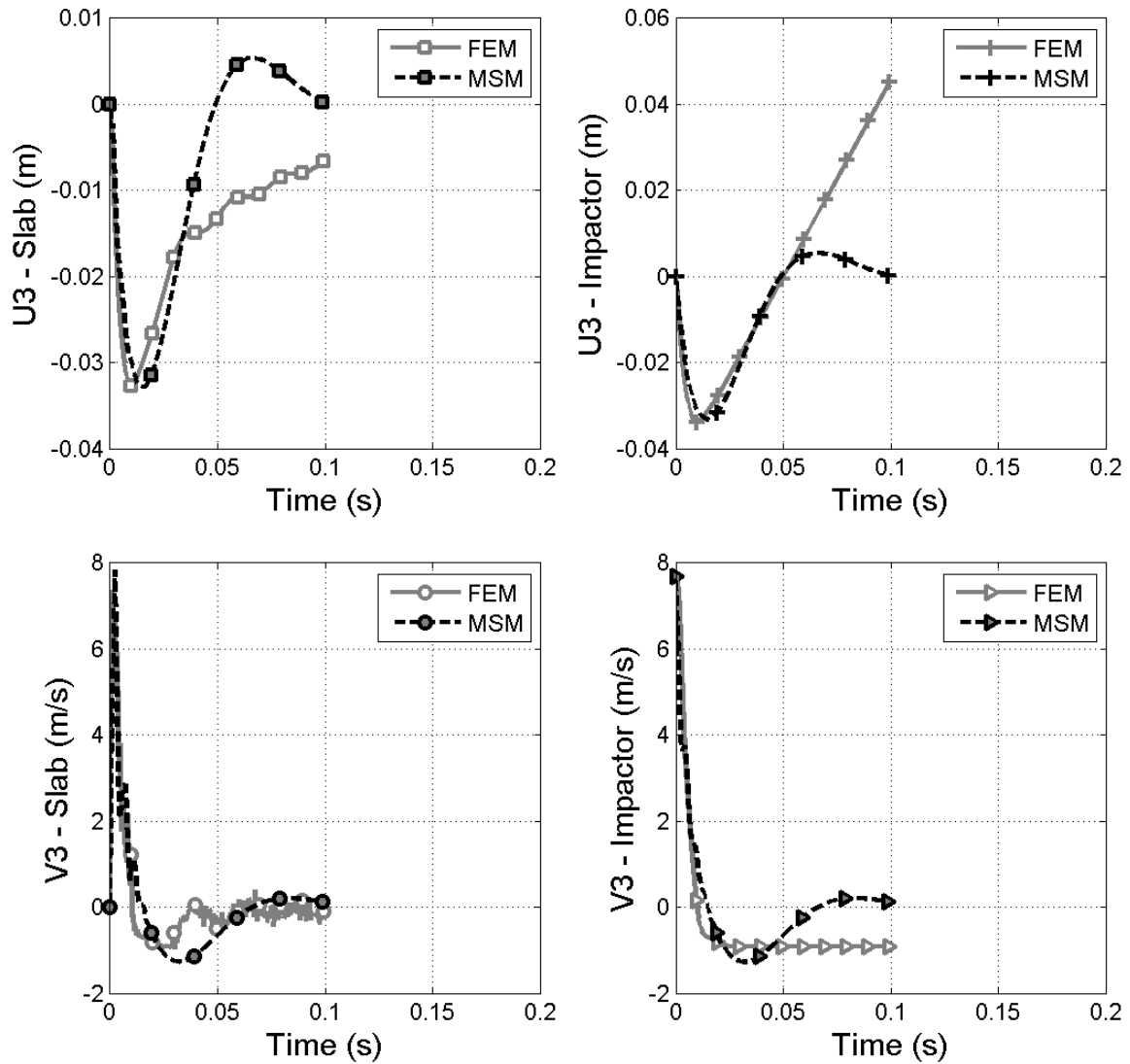


Figure B.37: Displacement and velocity of slab and impactor:  $\rho_c = 4000 \text{ kg/m}^3$

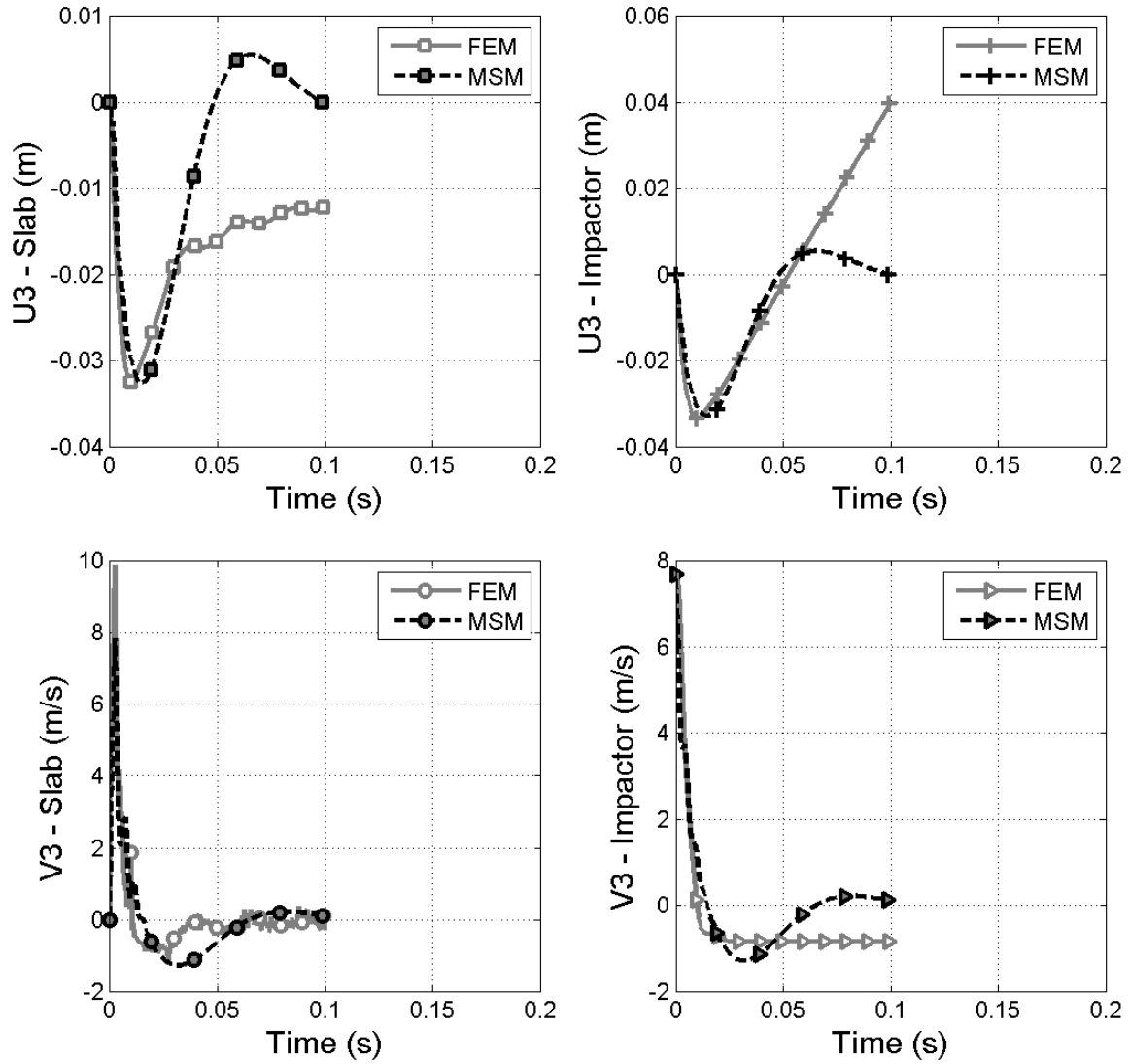


Figure B.38: Displacement and velocity of slab and impactor:  $\rho_c = 4500 \text{ kg/m}^3$

## B.6 Slab thickness

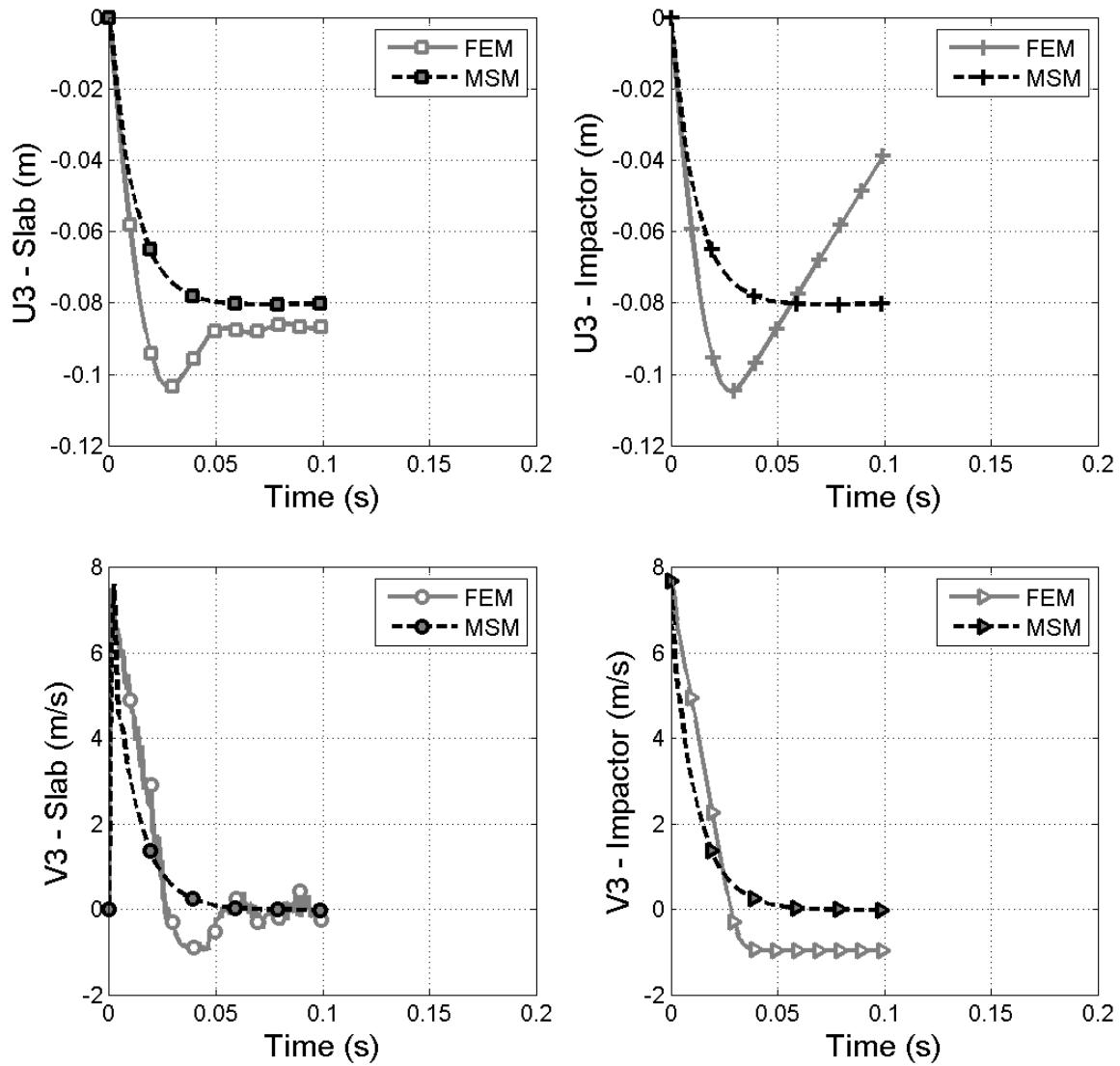


Figure B.39: Displacement and velocity of slab and impactor:  $e = 0.3 m$

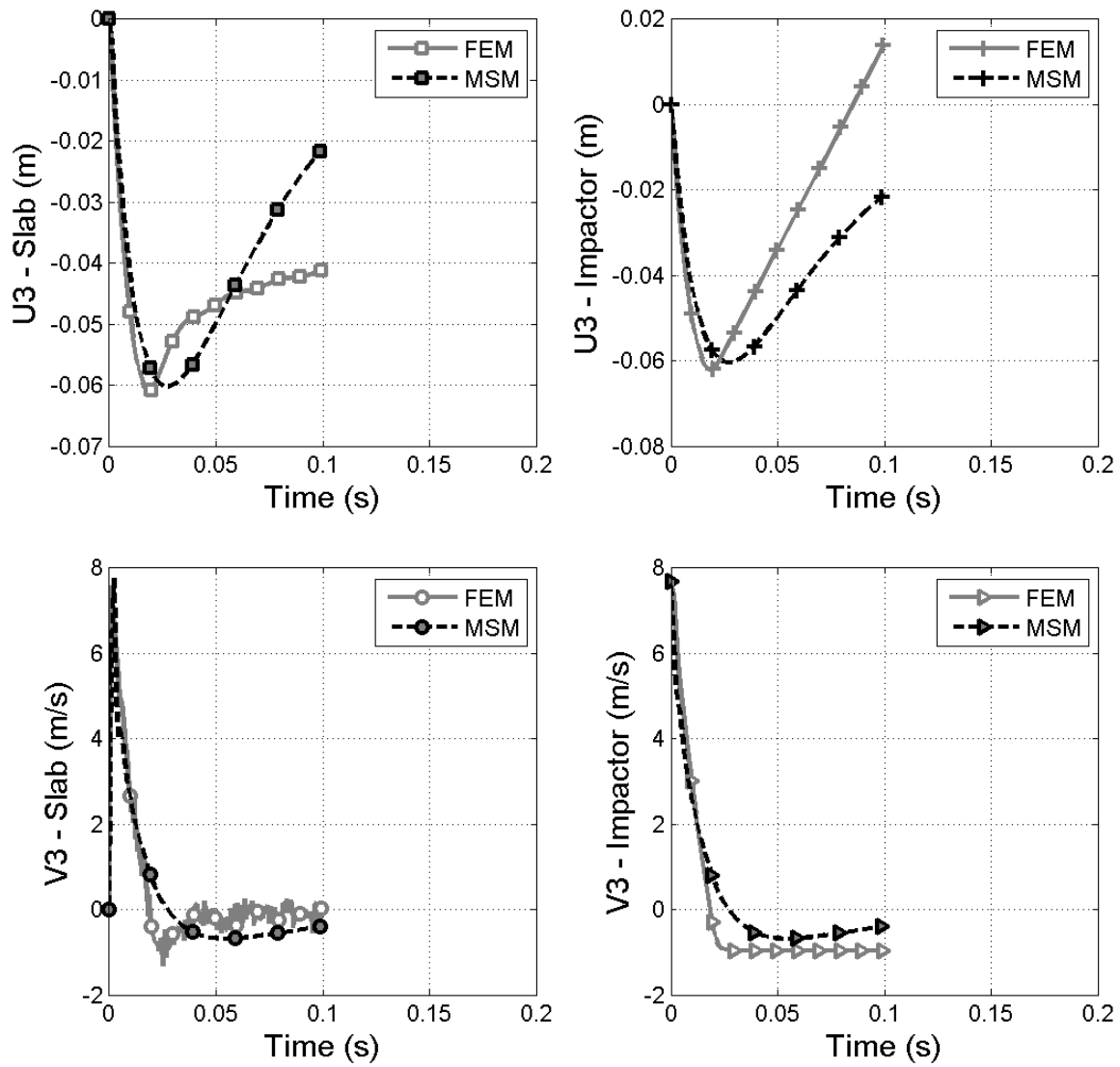


Figure B.40: Displacement and velocity of slab and impactor:  $e = 0.4 m$

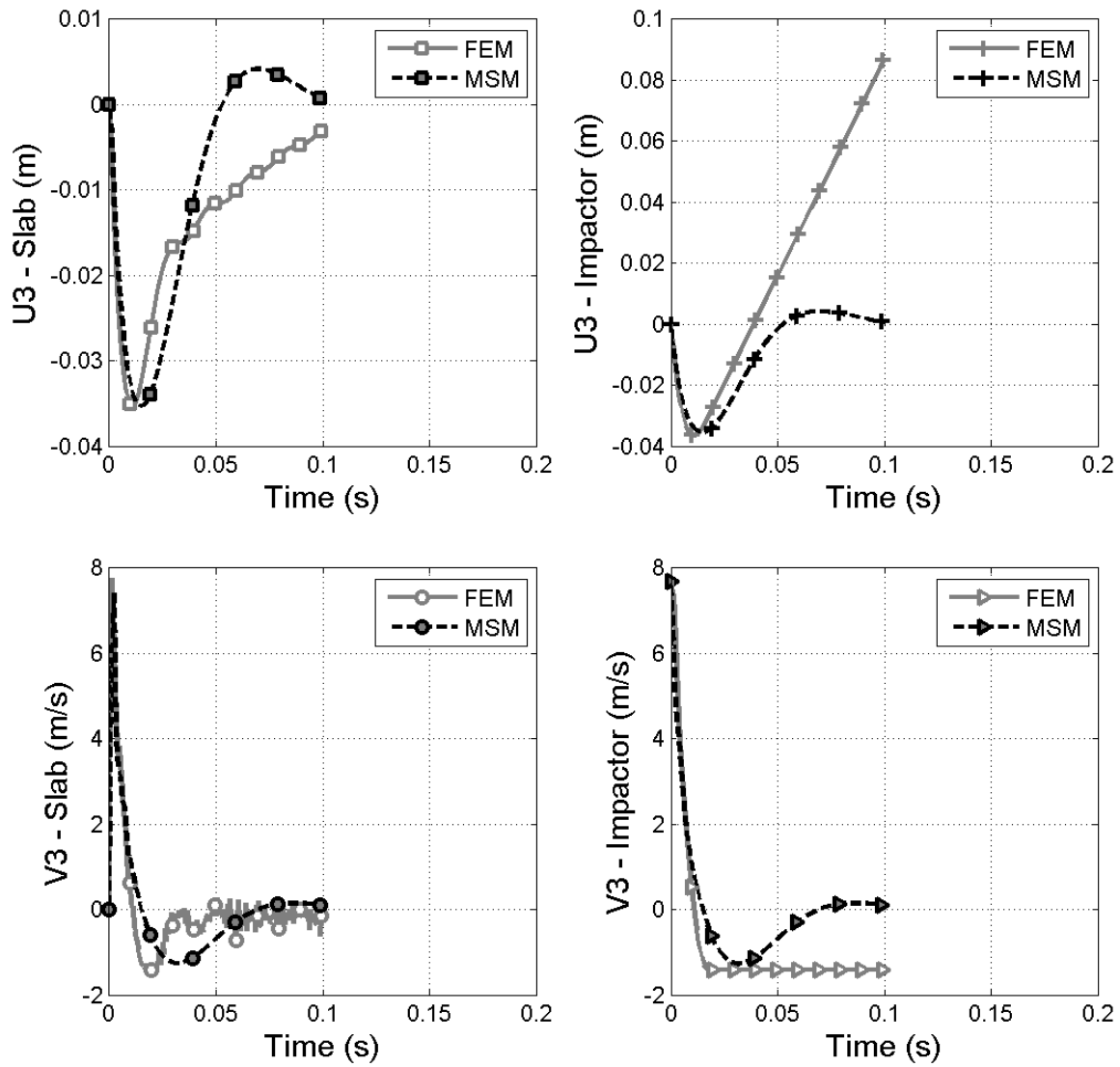


Figure B.41: Displacement and velocity of slab and impactor:  $e = 0.5 m$

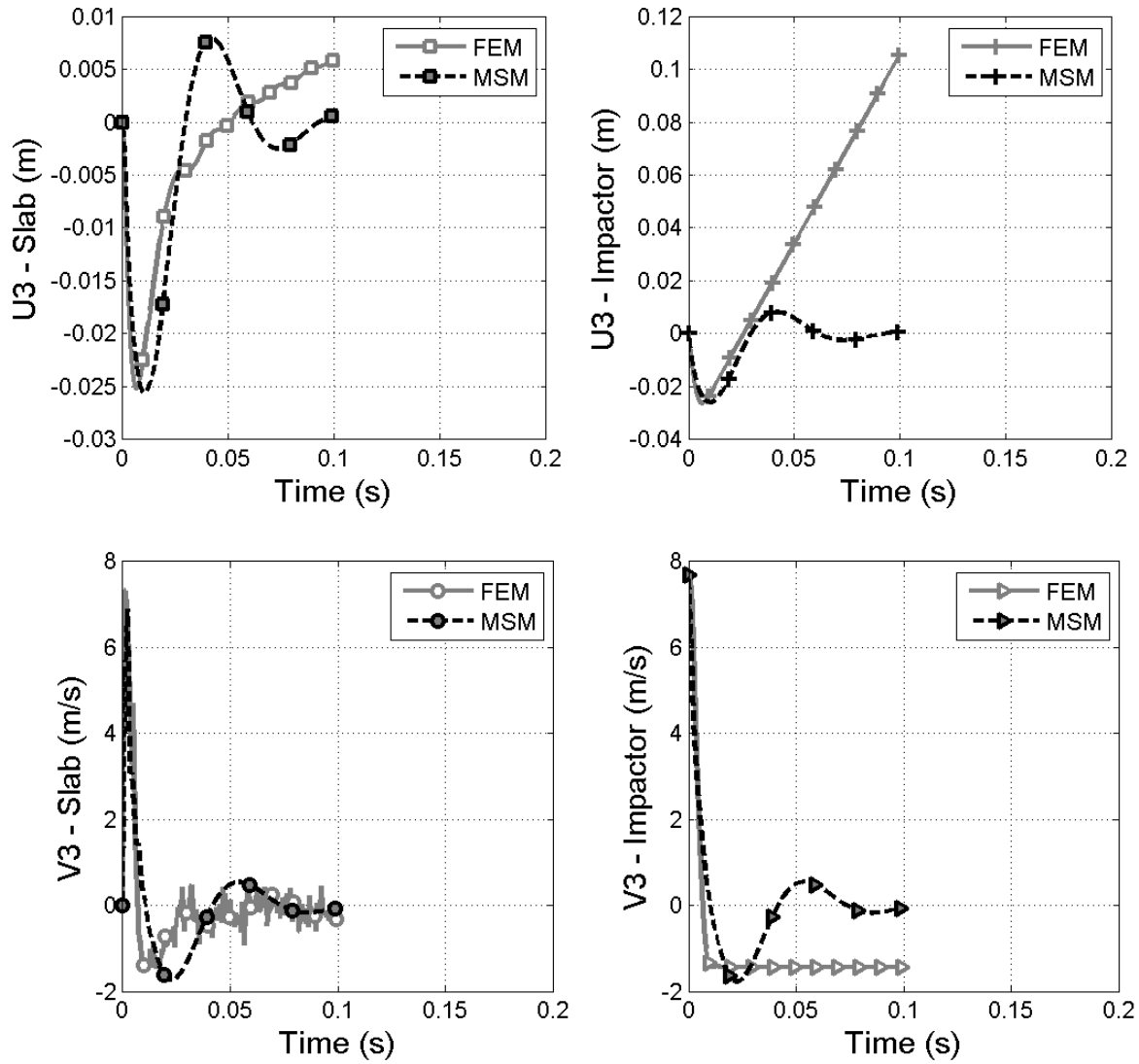


Figure B.42: Displacement and velocity of slab and impactor:  $e = 0.6 m$

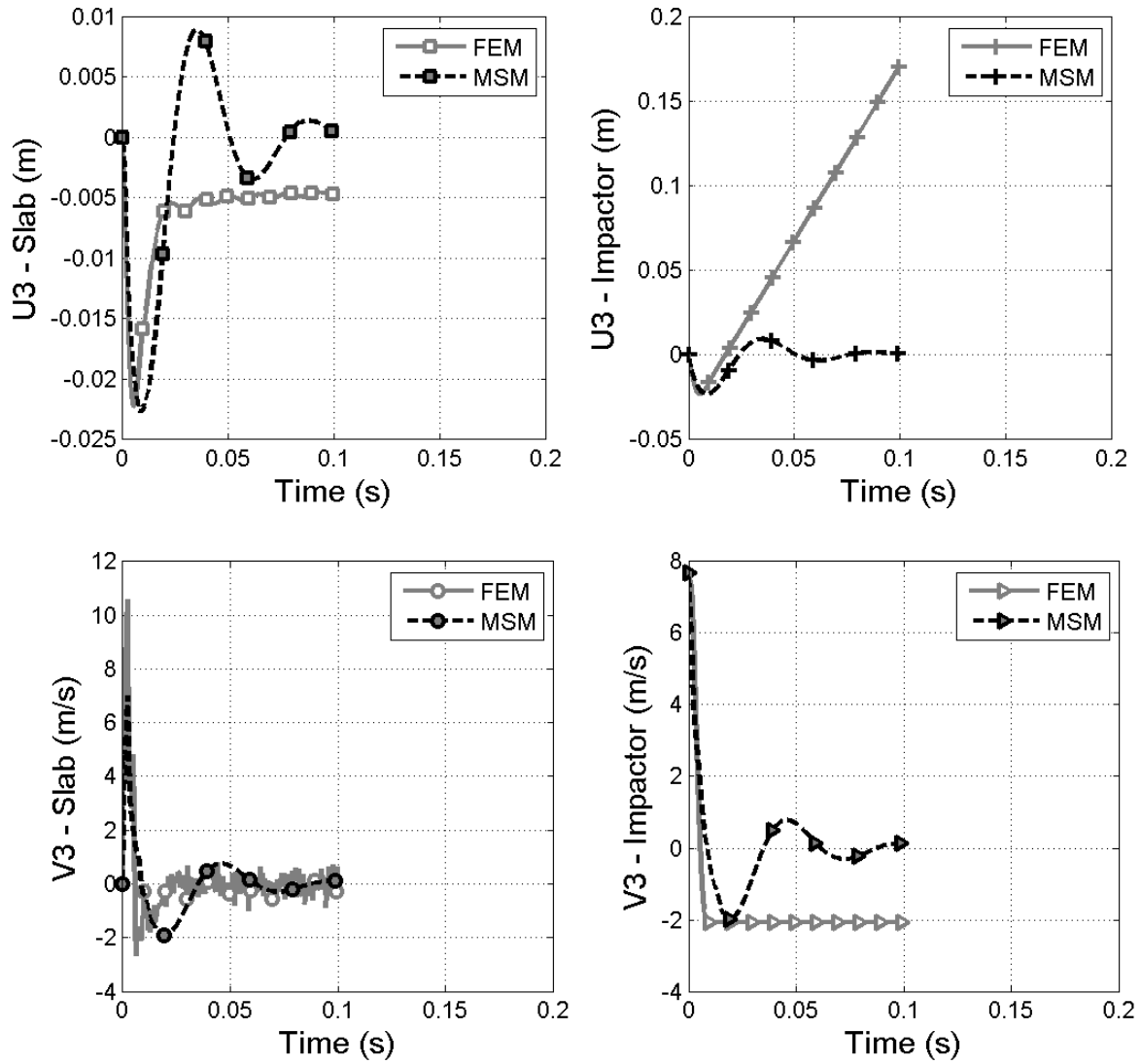


Figure B.43: Displacement and velocity of slab and impactor:  $e = 0.7 m$

FOLIO ADMINISTRATIF

THÈSE SOUTENUE DEVANT L'INSTITUT NATIONAL  
DES SCIENCES APPLIQUÉES DE LYON

NOM : **KASSEM**

DATE de SOUTENANCE : **04/11/2015**

Prénom : **Fidaa**

TITRE : **Reliability of reinforced concrete structures : Case of slabs subjected to impact**

NATURE : **Doctorat**

Numéro d'ordre : **2015ISAL0096**

Ecole doctorale : **MEGA - Mécanique, Energétique, Génie Civil, Acoustique**

Spécialité : **Génie Civil**

RESUME: An optimal design of reinforced concrete structures requires to take into account the potential development of nonlinearities due to materials damage (concrete cracking, steel yielding, etc.). In addition, the lack of knowledge on the potential load, as well as the uncertainties related to the features of the structure (geometry, mechanical properties) shows that the design of RC structures could be made in a reliability framework. This latter allows propagating uncertainties in the deterministic analysis. However, in order to compute failure probability for one or several criteria, mechanical and stochastic models have to be coupled which can be very time consuming and in some cases impossible. Indeed, either the complexity of the deterministic model considered implies important computing times (from minutes to hours) or reliability methods evaluating the failure probability require a too large number of simulations of the deterministic model.

The platform OpenTURNS is used to study the reliability of a RC multifiber cantilever beam, a RC slabs subjected to low impact velocities, and a prestressed concrete containment building. Only the physical problem of RC slabs subjected to impact is investigated in detail in this study. This study focuses on RC slabs which are subjected to accidental dropped object impact during handling operations within nuclear plant buildings. In this case, dropped objects are characterized by small impact velocities and damage can arise at the impact zone depending on the impact energy and the relative masses of the colliding bodies.

The aim of this study is to address the issue of computational cost of reliability analysis and to propose computational strategies allowing the accurate assessment of the failure probability for minimum computational time. The first strategy consists in using deterministic analytical models involving low computational time. The second one consists in choosing an appropriate probabilistic method where the failure probability is assessed from a small number of simulations. The first part of this study describes the behavior and the failure modes of RC slabs subjected to impact. Then two deterministic models are used and evaluated. The first model consists of a 3D finite element model simulated with ABAQUS/Explicit. The steel is modeled as an elasto-plastic material with hardening and, the behavior of concrete is described by the damaged plasticity model. The model is validated with experiments from the literature. A simplified analytical model is also used, it consists in a two degrees of freedom mass-spring system which accounts for potential viscous damping. A frequency decrease approach is used to describe the degradation of the slab. This study includes a reliability analysis of RC slabs under low velocity impact. Firstly, the choices of random variables inputs and their distributions, failure criteria and probabilistic methods are discussed. In the case where materials have nonlinear behavior, the failure criterion is defined according to the maximum displacement of the slab at the impact point. The two strategies used to reduce the computational cost of a reliability analysis are compared in order to verify their efficiency to calculate the probability of failure. Finally, a parametric study is performed to identify the influence of deterministic model parameters on the calculation of failure probability.

MOTS-CLÉS: **RC structures, RC slabs, impact at low velocity, dynamic, material nonlinear behaviors, deterministic approaches, reliability approaches, failure probability**

Laboratoire de recherche : **LGCIE - Laboratoire de Génie Civil et Ingénierie Environnementale**

Directeur de thèse: **Ali LIMAM**

Président de jury :

Composition du jury : **Laurence CURTIL, Fabrice GATUIN, Abdellatif KHAMLICHI, Elias BOU-SAID, David BERTRAND, Ali LIMAM**